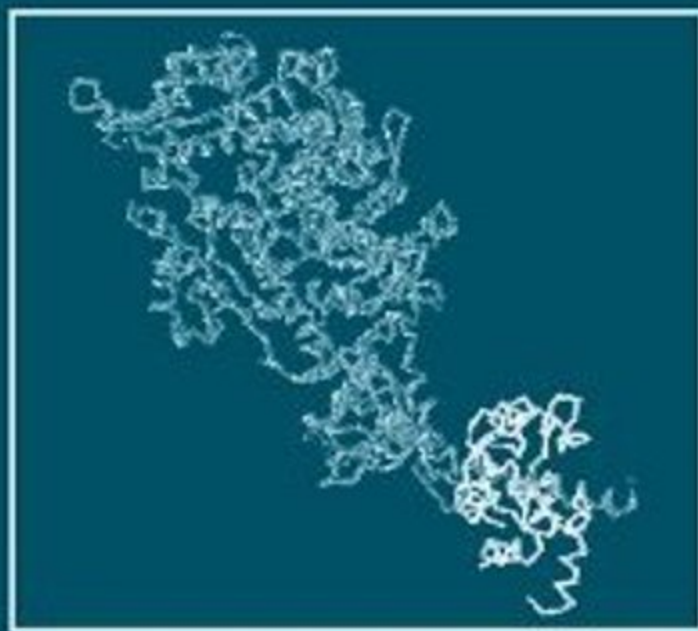


INTERNATIONAL
REVIEW OF CELL AND
MOLECULAR BIOLOGY

Edited by
Kwang W. Jeon



Volume 276



INTERNATIONAL REVIEW OF CELL AND MOLECULAR BIOLOGY

Series Editors

GEOFFREY H. BOURNE 1949–1988
JAMES F. DANIELLI 1949–1984
KWANG W. JEON 1967–
MARTIN FRIEDLANDER 1984–1992
JONATHAN JARVIK 1993–1995

Editorial Advisory Board

ISAIAH ARKIN	WALLACE F. MARSHALL
PETER L. BEECH	BRUCE D. MCKEE
HOWARD A. BERN	MICHAEL MELKONIAN
ROBERT A. BLOODGOOD	KEITH E. MOSTOV
DEAN BOK	ANDREAS OKSCHE
HIROO FUKUDA	THORU PEDERSON
RAY H. GAVIN	MANFRED SCHLIWA
MAY GRIFFITH	TERUO SHIMMEN
WILLIAM R. JEFFERY	ROBERT A. SMITH
KEITH LATHAM	NIKOLAI TOMILIN

Academic Press is an imprint of Elsevier
525 B Street, Suite 1900, San Diego, CA 92101-4495, USA
30 Corporate Drive, Suite 400, Burlington, MA 01803, USA
32 Jamestown Road, London NW1 7BY, UK
Radarweg 29, PO Box 211, 1000 AE Amsterdam, The Netherlands

First edition 2009

Copyright © 2009, Elsevier Inc. All Rights Reserved.

No part of this publication may be reproduced, stored in a retrieval system or transmitted in any form or by any means electronic, mechanical, photocopying, recording or otherwise without the prior written permission of the publisher

Permissions may be sought directly from Elsevier's Science & Technology Rights Department in Oxford, UK: phone (+44) (0) 1865 843830; fax (+44) (0) 1865 853333; email: permissions@elsevier.com. Alternatively you can submit your request online by visiting the Elsevier web site at <http://elsevier.com/locate/permissions>, and selecting *Obtaining permission to use Elsevier material*.

Notice

No responsibility is assumed by the publisher for any injury and/or damage to persons or property as a matter of products liability, negligence or otherwise, or from any use or operation of any methods, products, instructions or ideas contained in the material herein. Because of rapid advances in the medical sciences, in particular, independent verification of diagnoses and drug dosages should be made.

British Library Cataloguing in Publication Data

A catalogue record for this book is available from the British Library

Library of Congress Cataloging-in-Publication Data

A catalog record for this book is available from the Library of Congress

For information on all Academic Press publications
visit our website at elsevierdirect.com

ISBN: 978-0-12-374807-2

PRINTED AND BOUND IN USA

09 10 11 12 10 9 8 7 6 5 4 3 2 1

**Working together to grow
libraries in developing countries**

www.elsevier.com | www.bookaid.org | www.sabre.org

ELSEVIER	BOOK AID International	Sabre Foundation
-----------------	----------------------------------	-------------------------

CONTRIBUTORS

Lidia Bakota

Department of Neurobiology, University of Osnabrück, 49076 Osnabrück, Germany

Anthony Bishopp

Plant Molecular Biology Laboratory, Institute of Biotechnology, University of Helsinki, FIN-00014 Helsinki, Finland

Roland Brandt

Department of Neurobiology, University of Osnabrück, 49076 Osnabrück, Germany

Arnold I. Caplan

Department of Biology, Skeletal Research Center, Case Western Reserve University, Cleveland, Ohio 44106

Ykä Helariutta

Department of Forest Genetics and Plant Physiology, Umeå Plant Science Centre, Swedish University of Agricultural Sciences, SE-901 83 Umeå, Sweden; and Plant Molecular Biology Laboratory, Institute of Biotechnology, University of Helsinki, FIN-00014 Helsinki, Finland

Hanna Help

Plant Molecular Biology Laboratory, Institute of Biotechnology, University of Helsinki, FIN-00014 Helsinki, Finland

Sugie Higashi-Fujime

Department of Molecular and Cellular Pharmacology, Faculty of Medicine, Gunma University Graduate School of Medicine, Maebashi, Gunma 371-8511, Japan

Jin-ping Li

Department of Medical Biochemistry and Microbiology, University of Uppsala, SE-751 23 Uppsala, Sweden

Ulf Lindahl

Department of Medical Biochemistry and Microbiology, University of Uppsala, SE-751 23 Uppsala, Sweden

Kamelia Miri

Department of Cell and Systems Biology, University of Toronto, Toronto, Ont.,
Canada M5S 3G5

Akio Nakamura

Department of Molecular and Cellular Pharmacology, Faculty of Medicine,
Gunma University Graduate School of Medicine, Maebashi, Gunma 371-8511,
Japan

Nobukazu Shitan

Research Institute for Sustainable Humanosphere, Kyoto University, Uji
611-0011, Japan

J. Michael Sorrell

Department of Biology, Skeletal Research Center, Case Western Reserve
University, Cleveland, Ohio 44106

Akifumi Sugiyama

Research Institute for Sustainable Humanosphere, Kyoto University, Uji
611-0011, Japan

Kojiro Takanashi

Research Institute for Sustainable Humanosphere, Kyoto University, Uji
611-0011, Japan

Susannah Varmuza

Department of Cell and Systems Biology, University of Toronto, Toronto, Ont.,
Canada M5S 3G5

Kazufumi Yazaki

Research Institute for Sustainable Humanosphere, Kyoto University, Uji
611-0011, Japan

CYTOKININ SIGNALING DURING ROOT DEVELOPMENT

Anthony Bishopp,^{*} Hanna Help,^{*} and Ykä Helariutta^{*,†}

Contents

1. Introduction	2
2. The Two-Component Signal Transduction Pathway	4
2.1. Cytokinin perception via the receptors	5
2.2. Relaying the message: The histidine-containing phosphotransfer proteins (HPT)	11
2.3. Transcriptional control of target genes	14
3. The Role of Cytokinin Signaling Specific to Certain Developmental Pathways	22
3.1. Asymmetric patterning of cytokinin signaling defines the root stem cell niche	22
3.2. Cytokinins control root meristem size	24
3.3. Primary vascular development	28
3.4. Secondary vascular development	31
3.5. Cytokinin regulates root architecture	32
3.6. Cytokinin control the process of root nodulation	36
4. Concluding Remarks	38
References	39

Abstract

The cytokinin class of phytohormones regulates division and differentiation of plant cells. They are perceived and signaled by a phosphorelay mechanism similar to those observed in prokaryotes. Research into the components of phosphorelay had previously been marred by genetic redundancy. However, recent studies have addressed this with the creation of high-order mutants. In addition, several new elements regulating cytokinin signaling have been identified. This has uncovered many roles in diverse developmental and physiological processes. In this review, we look at these processes specifically in the

^{*} Plant Molecular Biology Laboratory, Institute of Biotechnology, University of Helsinki, FIN-00014 Helsinki, Finland

[†] Department of Forest Genetics and Plant Physiology, Umeå Plant Science Centre, Swedish University of Agricultural Sciences, SE-901 83 Umeå, Sweden

context of root development. We focus on the formation and maintenance of the root apical meristem, primary and secondary vascular development, lateral root emergence and development, and root nodulation. We believe that the root is an ideal organ with which to investigate cytokinin signaling in a wider context.

Key Words: Plant hormone, Root meristem, Root architecture, Hormone interactions, *Arabidopsis*. © 2009 Elsevier Inc.

1. INTRODUCTION

Cytokinin phytohormones (ck) form a group of adenine derivatives which promote cell division and differentiation in plants. In 1913, Haberlandt observed that diffusates from phloem could stimulate cell division in potato parenchyma cells. This led him to propose that certain chemical factors were able to promote cell division (Haberlandt, 1913). More than 40 years later, such a compound was identified from herring sperm, and was named kinetin (Miller et al., 1956). During subsequent decades, many similar compounds were identified which occurred naturally in plants. Together, they were termed cytokinins for their ability to promote cytokinesis in plant cells (Mok and Mok, 1994).

Although cytokinins were identified by their effects on cell cultures, more recent studies using *Arabidopsis* have focused on their effects on whole plants or plant calli. Cytokinins normally inhibit root growth (Miller et al., 1956). This effect has been exploited by researchers who have based an assay around comparing the inhibition of root growth of plants germinated on cytokinin media. Those plants with impaired ck signaling or reduced ck content are less sensitive to ck, therefore producing longer roots; whereas, those which have elevated ck signaling or levels with increased ck sensitivity produce shorter roots. Similar assays have been based around the formation of adventitious roots, shoot formation, and the greening of calli. Cytokinins stimulate cell division and the greening of calli (Miller et al., 1956) and inhibit the formation of adventitious roots near the cut end of hypocotyls (Kuroha et al., 2002).

The naturally occurring cytokinins identified in plants and microbes fall into two groups—those adenine derivatives with isoprene-derived side chains and those with aromatic side chains. In plants, the first group predominates. Isopentyl-adenine (iP) and *trans*-zeatin (*t-z*) are most prevalent in *Arabidopsis*, while *cis*-zeatin (*c-z*) is abundant in other species such as rice and maize (Sakakibara, 2006).

Cytokinin synthesis generally requires several steps; modification of an adenine moiety, modification of a side chain, and fusing of these two components. This occurs through multistep processes. Although there are many possible ways to synthesize ck species, they generally fall into two

pathways, the IPT-dependent MEP pathway and the IPT-independent MVA pathway. Both *t-z* and *iP* forms of cytokinin (which predominate in *Arabidopsis*) are preferentially formed by the IPT-dependent pathway. It is believed that the IPT enzymes act as a rate-limiting step in the synthesis of ck. Consistently, *Arabidopsis* plants lacking four of the seven *IPT* genes show considerable reductions in levels of *t-zs* and *iPs* (Miyawaki et al., 2006).

There is still some debate as to whether cytokinins are produced and act locally or if they are transported. In *Arabidopsis*, *IPT* genes are expressed ubiquitously throughout the root. However, expression levels are the highest in proliferating tissues (Miyawaki et al., 2004). Within the root, some *IPTs* have specific expression patterns, such as *IPT1* (expressed in xylem precursors), *IPT2* (expressed in phloem tissues), *IPT5* (expressed in root primordia and columella root caps), and *IPT7* (expressed in endodermal cells at the elongation zone (EZ)) (Miyawaki et al., 2004). The identification of ck species in xylem and phloem sap suggests a long distance systematic transport (Kamboj et al., 1998). However, grafts between plants with manipulated *IPT* levels and wild type in tobacco (Bohner and Gatz, 2001; Faiss et al., 1997) and *Arabidopsis* (Matsumoto-Kitano et al., 2008) reveal that the effect of altered *IPT* levels is only seen in the mutant tissues. If cytokinins can also act as local signals, this relinquishes the need for long distance transport for the regulation of specific developmental processes. Cytokinins also exist in abundant inactive forms. This creates a storage reserve which can later be metabolized into the active form in the tissue, in which it is required. For example, in rice the *LOG* gene codes for an enzyme LONELY GUY, which is able to convert inactive cytokinin species to active forms in meristems (Kurakawa et al., 2007). The movement of ck across plant tissues can happen either via diffusion or specific transporters. So far, at least two purine permease cotransporters have been identified in *Arabidopsis*, *AtPUP1* and *AtPUP2*. The proteins have broad substrate specificity and can transport several cytokinin species, as well as adenine and other adenine derivatives (Bürkle et al., 2003).

Cytokinin oxidases were identified over 35 years ago as compounds which catalyze the irreversible degradation of ck into inactive products that lack the adenine side chain (Paces et al., 1971). The first gene encoding one of these loci was identified in maize (Houba-Hérin et al., 1999; Morris et al., 1999) and since then, homologs have been identified in many plants including *Arabidopsis* and orchids (Schmülling et al., 2003; Yang et al., 2003). In *Arabidopsis*, there is a family of seven *CKX* genes (Schmülling et al., 2003). Like the *IPTs* described earlier, the *CKX* genes are expressed widely throughout the plant, although some members show spatial specificities. For example, *CKX1,5*, and *6* are all expressed at high levels in the vascular cylinder, *CKX1* is also high in lateral roots (LRs) and *CKX4* and *5* are strong in the root cap and root apical meristem (Werner et al., 2003). It has been shown for six of the seven members that overexpression in *Arabidopsis* leads to decreased cytokinin levels, decreased transcription of

ck response genes, and developmental defects associated with decreased cytokinin (Werner et al., 2003).

2. THE TWO-COMPONENT SIGNAL TRANSDUCTION PATHWAY

The identification of key molecules involved in cytokinin signal transduction has allowed researchers to produce a model for cytokinin perception and response. This model is similar to the two-component signaling systems through which bacteria sense and respond to environmental stimuli. Typically, such two-component signaling systems are based around a histidine protein kinase (HK) and a response regulator (RR). Extracellular stimuli are perceived by the HK and modulate the activity of the HK by allowing it to transfer a phosphoryl group from a phospho-accepting histidine residue in the kinase domain of the HK to an aspartate residue on the receiver domain of the RR. This activates downstream processes enabling a specific response.

The sequencing of various eukaryotic genomes has revealed that, while two-component signaling molecules were absent from organisms such as *Drosophila melanogaster* and the nematode *Caenorhabditis elegans*, they were prevalent in fungal and plant genomes (Saito, 2001). In all the eukaryotic two-component systems, and some more complex prokaryotic two-component systems, phosphotransfer from the HK to the RR occurs via a multistep phosphorelay. In this case, the transfer of the phosphoryl group from the phospho-donating histidine residue of the HK involves, an autophosphorylation of a phospho-accepting aspartate residue on the HK, followed by the phosphorylation of a phospho-accepting histidine residue on an intermediate His-containing phosphotransfer protein (HPt), before the final phosphorylation of a phospho-accepting aspartate residue on the RR. This always occurs via a multistep His→Asp→His→Asp system. In higher plants, these two-component systems can be divided into three functional subgroups based on the input stimulus: cytokinin, ethylene, and osmoregulation.

The elements involved in cytokinin signaling via two-component signaling are encoded by multigene families. In *Arabidopsis*, cytokinin is perceived by three receptors, *Arabidopsis* histidine kinases (AHKs) 2, 3, and 4—AHK4 was originally isolated through the *woodenleg* (*wol*) and *cytokinin response 1* (*cre1*) mutations. The phosphoryl transfer occurs via five true *Arabidopsis* phosphotransfer proteins (AHPs 1–5), while a pseudo AHP (AHP6) acts as an inhibitor of phosphotransfer. The phosphomessage is then relayed to members of the large *Arabidopsis* response regulator (ARRs) family members, which contains approximately 32 members. The type-B

ARRs are then able to initiate transcription of certain response genes including the six-member cytokinin response factors (CRF) family and the type-A ARRs. The type-A ARRs act as inhibitors of cytokinin signaling. Phosphorylation of AHPs also triggers the relocalization of CRFs to the nucleus, where they initiate transcription of cytokinin-induced target genes. Interactions between the components of the *Arabidopsis* cytokinin signaling network are shown in Fig. 1.1.

Although much of the pioneering work in understanding the cytokinin signaling network was done in the model plant *Arabidopsis*, recent research has shown that the processes are likely to be conserved in diverse plant species including legumes and monocots. Additionally, research using such species has indicated roles for cytokinin signaling in processes that are not possible to investigate in *Arabidopsis*, such as root nodulation.

2.1. Cytokinin perception via the receptors

In the early part of this decade, there were several important papers which identified key components and led to an understanding of cytokinin signaling in plants. It was previously believed that a two-component signaling system was responsible for detecting cytokinin as, when a histidine kinase gene homologous to those in bacterial two-component systems (CKI) was overexpressed, plants exhibited responses similar to those produced by cytokinin application (Kakimoto, 1996). However in 2001, Tatsuo Kakimoto's lab proved this by identifying *CRE1* as a cytokinin receptor. They showed that mutants lacking *CRE1* were less responsive to cytokinin in both tissue culture and root elongation assays. More importantly, they showed that expression of *CRE1* in a heterologous yeast system could complement a histidine kinase mutant in a cytokinin-dependent manner (Inoue et al., 2001). At about the same time, two other groups published descriptions of mutations in this gene. Ykä Helariutta's lab cloned the *WOL* gene, and the locus was found to be allelic to *CRE1* (Mähönen et al., 2000). Chiharu Ueguchi and colleagues published a description of a small gene family of histidine kinases which they proposed to be acted in a single biological signaling pathway (Ueguchi et al., 2001a). In the same year they demonstrated that histidine kinase activity of one of the members, *AHK4*, was dependent on ck, and that *ahk4* loss-of-function mutants displayed cytokinin insensitivity in various assays (Ueguchi et al., 2001b). Almost simultaneously, Takeshi Mizuno's group published similar data that *AHK4* could act as a ck sensor in bacteria (Suzuki et al., 2001a). The gene that both groups described as *AHK4* was again allelic to *CRE1*. For the purpose of this review, we will refer to this gene as *CRE1*.

The year 2001 proved to be fruitful for cytokinin signaling as a number of papers were published demonstrating that not only *CRE1* was the ck receptor, but that it also bound cytokinin and initiated phosphorelay.

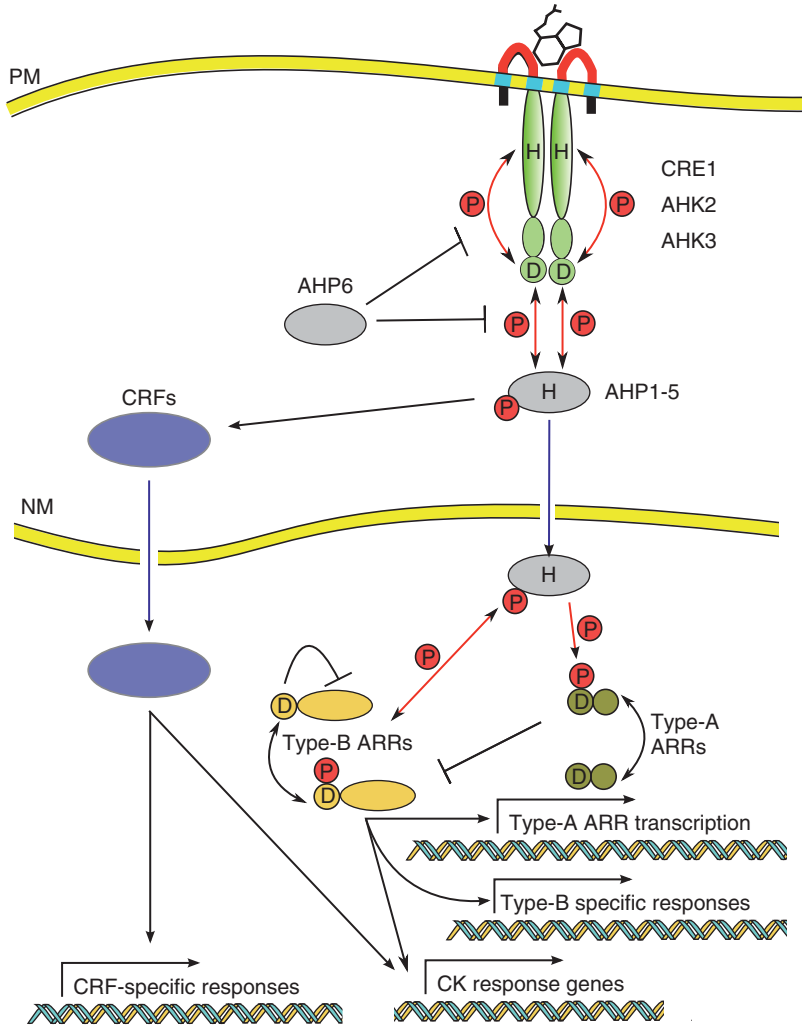


Figure 1.1 Model showing phosphorelay mechanism. The cytokinin receptors form dimers which are localized on the plasma membrane (PM) by their transmembrane domains (shown in blue). The CHASE domain (shown in red) is located outside the PM and binds cytokinin. Binding of cytokinin stimulates conformational changes within the proteins which initiate phosphorelay. Phosphorelay involves the transfer of a phosphoryl group (shown in red) from conserved phospho-accepting His and Asp residues (shown as H and D, respectively). The first step involves an autophosphorylation of the receptor, and the second step involves transfer of the phosphoryl group to AHP1–5. When the AHPs are phosphorylated, they are transported through the nuclear membrane (NM) to the nucleus (shown with a blue arrow). In the nucleus, the AHPs phosphorylate the type-A and the type-B ARRs. Without phosphorylation the type-B ARRs are unable to act as transcription factors due to strong repression by the phospho-receiving domain. However, when these proteins are phosphorylated they

Tatsuo Kakimoto's group had already created a yeast-based system in which *CRE1* could complement in a ck-dependent manner a yeast strain lacking the osmosensing histidine kinase *SLN1*. They went on to show that this complementation required the conserved phospho-accepting and donating histidine and aspartate residues in the transmitter and receiver domains (Inoue et al., 2001). Takeshi Mizuno's group created *Escherichia coli* and yeast-based systems, which they used to demonstrate that phosphotransfer to endogenous *E. coli* HPTs could be severely reduced if *Arabidopsis* HPTs were cointroduced. This suggested that the *Arabidopsis* HPTs were capable of receiving phosphoryl groups from *CRE1* (Suzuki et al., 2001a). They then went on to demonstrate direct *in vitro* binding of *CRE1* to a variety of cytokinin species (Yamada et al., 2001). *In planta* evidence for cytokinin two-component signaling came later that year when Hwang and Sheen demonstrated that ectopic expression of *CRE1* in leaf mesophyll cells could activate transcription of an *ARR6* in a cytokinin-dependent manner (Hwang and Sheen, 2001).

Complete sequencing of the *Arabidopsis* genome has shown that there are 16 proteins encoding putative HKs. Of these only eight contain all the conserved motifs from within the His kinase domain and are therefore likely to possess His kinase activity (Hwang et al., 2002). Within this remaining group, *AHK2*, *AHK3*, and *AHK4/CRE1/WOL* form a distinct CRE-family, based not only on sequence similarity but also because they contain both a receiver and a receiver-like domain (Fig. 1.2A and Table 1.1).

Since the discovery of the CRE-family as cytokinin receptors, researchers have simultaneously followed two avenues towards a greater understanding of how these receptors operate. One approach has been via genetics, with detailed descriptions of mutants lacking one, two, or all of the ck receptors. The other approach has used computational and biochemical methods to understand how these molecules function. We are now entering an exciting point where these methods can be combined.

are relieved from this repressive force and can initiate transcription of target genes. These target genes include the CRF genes and the type-A ARR. The type-A ARR acts as a negative inhibitor of cytokinin signaling. They receive phosphoryl groups from the AHPs which stabilize these otherwise rapidly degraded proteins. These phosphorylated proteins then exert an inhibitory effect on cytokinin by an as yet unknown mechanism. The pseudo AHP, *AHP6*, can inhibit phosphorelay at multiple stages including the autophosphorylation of the receptor and phosphorylation of other true AHPs. In addition to relaying phosphoryl groups to the ARRs, phosphorylated AHPs have a second effect of promoting the relocalization of CRFs to the nucleus. The mechanism by which this is achieved is unknown. Once relocalized within the nucleus, the CRFs initiate the transcription of ck response genes. Many targets of the CRFs and type-B ARRs are shared, while some are specific to the CRFs. Likewise, the type-B ARRs also contain a set of targets which are specific to them (including the type-A ARRs and the CRFs).

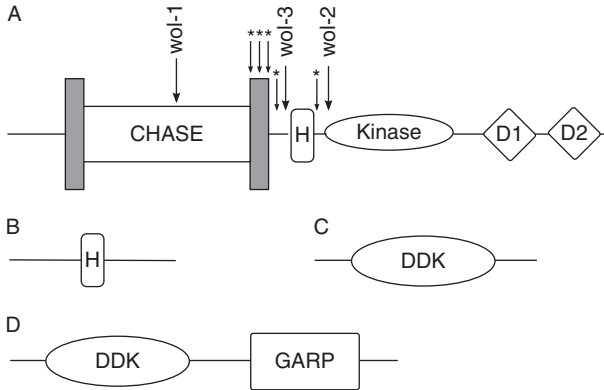


Figure 1.2 Schematic diagrams representing phosphorelay components. (A) Typical CRE-family histidine kinase (in this case *CRE1*). The transmembrane domains are shown in gray and span the CHASE domain. The conserved phospho-donating histidine residue is labeled H. This is followed by a kinase domain. The receiver-like domain is marked D1 and the phospho-accepting receiver domain is marked D2. The location of the mutations in the three *wol* alleles are marked and the changes reported by [Miwa et al. \(2007\)](#) which confer constitutively active kinase activity are marked with an asterisk. (B) Typical AHP. The conserved phospho-accepting histidine residue is shown. This is absent in AHP6. (C) Typical type-A ARR. (D) Typical type-B ARR. Both of these classes of proteins contain a DDK phospho-receiving domain. Type-B ARRs contain an additional C-terminal DNA-binding GARP motif.

Detailed genetic studies of single mutants in all three CRE-family genes have shown only subtle phenotypes revealed by careful analysis (certain exceptions exist, which will be discussed later). For example, *cre1* mutants show reduced sensitivity to cytokinin-mediated inhibition of root growth, but without *ck* the root length is not differentiable from wild type ([Higuchi et al., 2004](#); [Inoue et al., 2001](#)). Analysis of gene expression showed considerable overlap in the expression domains of the three receptors, although *CRE1* was more highly expressed in the root as opposed to the shoot, while *AHK3* was higher in the shoot ([Higuchi et al., 2004](#); [Mähönen et al., 2000](#); [Nishimura et al., 2004](#); [Ueguchi et al., 2001a](#)). The overlapping expression and the high level of conservation in protein structure have led to considerable genetic redundancy between these loci. Triple mutant combinations lacking all three CRE-family receptors show strong phenotypes producing small infertile plants, which have a reduction in meristem size but possess all the basic plant organs ([Higuchi et al., 2004](#); [Nishimura et al., 2004](#); [Riefler et al., 2006](#)). These plants do not show any response to *ck* in a variety of assays, including root elongation, inhibition of adventitious root formation, and induction of *ck* response genes ([Higuchi et al., 2004](#); [Nishimura et al., 2004](#)). The number of vascular cells is decreased and all vascular cells differentiate as protoxylem ([Mähönen et al., 2006a](#)). These

Table 1.1 Properties of *Arabidopsis* CRE-family receptors

	Expression in the root		Subcellular localization	Ck binding demonstrated <i>in vitro</i>	Phosphorelay to AHPs demonstrated <i>in vitro</i>	Loss-of-function phenotype
	By RT-PCR/ RNA blot	By reporter construct				
AHK2	Equal in root and shoot (Higuchi et al., 2004)	Ubiquitous—but highest in meristematic region (Higuchi et al., 2004; Nishimura et al., 2004)	–	–	–	No discernable phenotype in single mutant
AHK3	Lower in root than shoot (Higuchi et al., 2004)	Ubiquitous—but highest at TZ (Higuchi et al., 2004; Nishimura et al., 2004)	PM (Kim et al., 2006)	Yes (Romanov et al., 2006)	Indirectly (Kim et al., 2006)	Slightly reduced ck sensitivity (Higuchi et al., 2004; Nishimura et al., 2004)
<i>CRE1</i> /WOL/ AHK4	Higher than in shoot (Higuchi et al., 2004)	Ubiquitous—but highest in vascular tissue (Higuchi et al., 2004; Nishimura et al., 2004)	–	Yes (Yamada et al., 2001)	Yes (Suzuki et al., 2002)	Reduced ck sensitivity (Inoue et al., 2001; Ueguchi et al., 2001b) Occasional ectopic xylem files

results demonstrated that ck and the CRE-family receptors are key regulators of plant growth and development. However, in each case, the triple cytokinin receptor mutant could be recovered. This questions the requirement for ck signaling during embryo development, although it cannot be ruled out that an additional receptor may be active during embryogenesis.

The cytokinin binding site has been mapped, first computationally (Pas et al., 2004) and later confirmed experimentally (Heyl et al., 2007) to the extracytoplasmic CHASE domain at the N-terminus of the protein. This CHASE domain is not unique to the AHK family; it occurs in other eukaryotic His kinases, adenylyl cyclases, and diguanylate cyclases. It always occurs at the N-terminus and is flanked by two transmembrane domains (Anantharaman and Aravind, 2001; Mougél and Zhulin, 2001). Although it has not been shown experimentally that the CHASE domain of the CRE-family proteins lies outside the cell, it is incredibly likely based on protein structure and homology with other CHASE domain proteins.

Comparison between *CRE1* and AHK3 showed both were sensitive *t-z*. However, they differed in sensitivity towards other cytokinins; AHK3 was more sensitive towards *c-z* and dihydrozeatin and was activated by cytokinin ribosides and ribotides, whereas *CRE1* was more sensitive to isopentyladenine (iP) (Romanov et al., 2006; Spíchal et al., 2004). This suggests that different cytokinin responses can be modulated by differences in receptor specificity. However, this has been challenging to assess, as physiological cytokinin responses tend to be slow, while changes in cytokinin conformation occur rapidly and RRs are frequently targeted by multiple receptors (Spíchal et al., 2004). However, there is the possibility that different plant species favor different ck species. This cytokinin specificity appears to be conserved to some extent among the CRE-family receptors in maize, as ZmHK1 (*CRE1* homologue) responds more strongly to iP than *t-Z*, whereas ZmHK2 (AHK3 homologue) responds more strongly to *t-Z*, although all receptors responded strongly to *c-z* (Yonekura-Sakakibara et al., 2004).

Although loss-of-function mutants in any of the *CRE1* family genes exhibit only subtle phenotypes, alleles do exist which show strong phenotypes. For example, the *wol*, *wol-2*, and *wol-3* mutants have short determinate root growth, fewer cells within the vascular bundle and all vascular cells differentiate as protoxylem (de Leon et al., 2004; Kuroha et al., 2006; Mähönen et al., 2000; Scheres et al., 1995). The *wol-1* mutation lies within the CHASE domain and abolishes cytokinin binding (Mähönen et al., 2000; Yamada et al., 2001). Comparative analysis of *wol*, *cre1* loss-of-function alleles and *trans*-heterozygotes revealed that *wol* exerts a dose-dependent negative activity on ck signaling (Mähönen et al., 2006b). It has been demonstrated, both in *in vitro* assays and using a heterologous yeast system, that *CRE1* not only acts as a kinase that phosphorylates HPTs in the presence of ck but also acts as a phosphatase which dephosphorylates HPTs in the

absence of ck. The *wol* mutation mimics the ck-unbound state and confers constitutive phosphatase activity, removing phosphate from the HPTs and decreasing the total phosphoload (Mähönen et al., 2006b). Bidirectional phosphorelay may be unique to *CRE1*, as neither AHK2 nor AHK3 demonstrated any significant phosphatase activity in yeast assays (Mähönen et al., 2006b).

Several other mutations have been identified in the second transmembrane domain and around the histidine kinase domain which render *CRE1* constitutively active in a heterologous bacterial system (Miwa et al., 2007). The changes in the transmembrane domain are proposed to mimic the conformational changes caused by ck binding, therefore causing constitutive ck phenotypes. Interestingly, similar mutations in AHK2 or AHK3 can also cause the same constitutive phenotypes (Miwa et al., 2007). So far, these phenotypes have not been investigated *in planta*, although the *wol-2* mutation lies within the histidine kinase domain, and the *wol-3* mutation slightly upstream; both of these are close to some of the mutations reported by Miwa et al. (de Leon et al., 2004; Kuroha et al., 2006). It has also been shown that in yeast assays the ck receptors are able to form dimers, either with themselves or other members of the CRE-family (Dortay et al., 2006). This occurs through a region in the N-terminal part of the His kinase domain, in a similar manner to that observed in bacterial sensor His kinases (Marina et al., 2005; Stock et al., 2000).

2.2. Relaying the message: The histidine-containing phosphotransfer proteins (HPT)

While the pioneering research with the ck receptors was underway, work was ongoing with another class of cytokinin signaling related molecules, the HPTs (Fig. 1.2B and Table 1.2). Before the turn of the millennium, two-component signaling had been well documented in prokaryotic species (Wurgler-Murphy and Saito, 1997), and various components including HPTs had been identified in *Arabidopsis* and maize (Imamura et al., 1999; Miyata et al., 1998; Sakakibara et al., 1999; Suzuki et al., 1998). It had also been shown that certain *Arabidopsis* and maize HPTs were able to be dephosphorylated by downstream RRs (Imamura et al., 1999; Sakakibara et al., 1999).

At this stage there was no confirmed link between ck and two-component signaling downstream of the receptors. In 2001, Hwang and Sheen changed this. They used a transient expression assay, based on transcription of *ARR6* to demonstrate that the HPTs integrate multiple histidine kinase activities and shuttle the phosphomessage from the cytoplasm to the nucleus. They observed the localization of AHP1-GFP and AHP2-GFP, which rapidly shifted from the cytoplasm to the nucleus on the application of ck (Hwang and Sheen, 2001). AHP2 was shown to interact

Table 1.2 Properties of *Arabidopsis* Hpts

	Expression in the root		Subcellular localization		Phosphorelay from receptors demonstrated <i>in vitro</i>	Phosphorelay to type-B ARRs demonstrated <i>in vitro</i>	Loss-of-function phenotype	Constitutive expression
	By RT-PCR	By reporter construct	Without ck	With ck				
AHP1	Yes (Suzuki et al., 1998)	–	Cytoplasmic (Hwang and Sheen, 2001)	Nucleus (Hwang and Sheen, 2001)	Indirectly (Miyata et al., 1998)	Yes (Suzuki et al., 1998)	No (Hutchison et al., 2006)	–
AHP2	Yes (Suzuki et al., 1998)	–	Cytoplasmic (Hwang and Sheen, 2001)	Nucleus (Hwang and Sheen, 2001)	Yes (Suzuki et al., 2002)	Yes (Imamura et al., 2001; Suzuki 2001b)	No (Hutchison et al., 2006)	CK hypersensitivity (Suzuki et al., 2002)
AHP3	Yes (Suzuki et al., 1998)	–	Cytoplasmic (Tanaka et al., 2004)	–	Yes (Miyata et al., 1998)	–	No (Hutchison et al., 2006)	–
AHP4	Weak (Tanaka et al., 2004)	–	Throughout (Yamada et al., 2004)	Nuclear (Yamada et al., 2004)	Yes (Tanaka et al., 2004)	–	No (Hutchison et al., 2006)	–
AHP5	Yes (Tanaka et al., 2004)	–	Nucleus (Hwang and Sheen, 2001)	Nucleus (Hwang and Sheen, 2001)	Yes (Tanaka et al., 2004)	–	No (Hutchison et al., 2006)	–
AHP6	Yes (Mahonen et al., 2006a)	Protoxylem and associated pericycle cells (Mahonen et al., 2006a)	–	–	Does not accept phosphoryl group (Mahonen et al., 2006a)	Not applicable	Loss of protoxylem identity (Mahonen et al., 2006a)	–

with *CRE1* in *E. coli* to activate bacterial RRs, and this interaction is dependent on the conserved phospho-accepting histidine residue in AHP2 (Suzuki et al., 2001b). Furthermore, it was shown that overexpression of AHP2 renders plants hypersensitive to exogenous cytokinin in several physiological assays (Suzuki et al., 2002). However, the first data showing either loss or reduction of HPt function came from an unlikely source. In *Catharanthus roseus* (Madagascar periwinkle) cell cultures, silencing of the HPt *CsHPt1* by RNA interference (RNAi), abolished the ck inductive effect on the expression of the endogenous RR *CsRR1* (Papon et al., 2004). The delay for similar studies to be performed in *Arabidopsis* was most likely because any single loss-of-function HPt mutant was indistinguishable from wild type, and it took the creation of high-order mutant combinations for a phenotype to be revealed. Hutchison et al. (2006) created a quintuple mutant with almost complete loss of activity of all the true AHPs (AHP1–5). This mutant showed compromised expression of many type-A ARRs, as well as growth abnormalities consistent with reduced ck signaling. The phenotype was not as severe as that of the triple ck receptor mutant. This is likely to be due to the partial activity of certain AHPs, but could theoretically indicate other molecules in relaying the message from the receptors to the regulators.

While the five true AHPs behave in a manner consistent with two-component phosphorelay, the pseudo AHP, AHP6, does not. The *ahp6* mutant was identified in a genetic screen for suppressors of *wol* (Mähönen et al., 2006a). The all-protoxylem phenotype seen in *wol* is suppressed in *wol ahp6*, suggesting that AHP6 might modify ck signaling status. AHP6 differs from the true AHPs as it lacks the conserved phospho-accepting histidine residue necessary for phosphorelay. Using an *in vitro* system, the authors showed that while AHP1–3 and AHP5 could receive a phosphoryl group from a histidine kinase, AHP6 could not. When AHP6 was engineered, so that the conserved phospho-accepting histidine residue was added, it was able to receive the phosphoryl group. Using a similar *in vitro* assay, it was shown that not only does AHP6 not function as a phosphotransfer protein, but inhibits phosphotransfer between the receptor and other AHPs and between AHPs and ARRs. Consistent with the idea of inhibition of ck signaling, *ahp6* mutants resemble plants treated with ck in that they lose protoxylem identity and show ectopic expression of the response regulator *ARR15* (Mähönen et al., 2006a). This will be discussed in Section 3.5.

Analysis of the relative contribution of each AHP in the quintuple mutant *ahp* mutant, suggests that in contrast to the other AHPs, AHP4 may also play a negative role in some processes (Hutchison et al., 2006). However, no phenotype has either been observed in the loss-of-function mutant, or in the double *ahp6 ahp4* mutant (Bishopp and Help, unpublished data).

2.3. Transcriptional control of target genes

The *Arabidopsis* genome contains 32 genes encoding putative RR proteins that are not fused to histidine kinase domains. There is some discrepancy in this number depending on how tight the description of RR is. All of these RRs contain a DDK RR domain which is homologous to those in prokaryotes and yeast (Hwang et al., 2002). These can be divided into several groups, based on similarity of the receiver domain and the C-terminal region (Sakai et al., 1998, 2000, 2002). The first type-A ARR contains only the receiver domain (Fig. 1.2C and Table 1.3), whereas the type-B ARR, in addition to the receiver domain, has C-terminal domains containing a GARP family myb-like DNA-binding domain, nuclear localization signal, and transcription activator domains (Fig. 1.2D and Table 1.4). The GARP family of DNA-binding domains is plant specific, named after its founding members—GOLDEN2 from maize, ARR from *Arabidopsis*, and Psr1 from *Chlamydomonas* (Hosoda et al., 2002).

The number of type-A ARRs varies in different analyses, but for the purpose of this review, we follow the recent description from the Kieber group, which describes the family as containing *ARR3, 4, 5, 6, 7, 8, 9, 15, 16*, and *17* (To et al., 2004). *ARR22* and *ARR24* differ from the type-A ARRs as their receiver domains have higher similarity to the receiver domains of hybrid histidine kinases (Kiba et al., 2004) and these have been proposed to form a distinct type-C ARR class (To and Kieber, 2008).

The type-B AARs family is widely accepted as containing 11 members, *ARR1, 2, 10, 11, 12, 13, 14, 18, 19, 20*, and *22*. However, this can be further split up into three distinct subfamilies based on sequence similarity of the receiver domain (Mason et al., 2004). Subfamily I comprises the members *ARR1, 2, 10, 11, 12, 14*, and *18*. There is strong evidence that members of this subfamily are involved in cytokinin responses (Argyros et al., 2008; Hwang and Sheen, 2001; Imamura et al., 2003; Ishida et al., 2008; Mason et al., 2004, 2005; Sakai et al., 2000, 2002; Yokoyama et al., 2007). There is no direct evidence that members of the other subgroups have any involvement. It has been noted that constitutive expression of a version of *ARR21* where the C-terminal domain has been engineered to remove the N-terminal receiver, leads to miss-expression of certain type-A ARRs (Tajima et al., 2004). However, as yet there is no evidence to suggest a ck-related role for the endogenous gene.

The remainder of the putative RRs has been termed pseudo RRs as they have atypical receiver domains. There is no data to suggest that these molecules are involved in cytokinin response; however, an increasing amount of evidence supports roles in other processes, such as the measurement of circadian period (Mizuno and Nakamichi, 2005).

Table 1.3 Properties of *Arabidopsis* type-A ARR8s

	Expression levels (RT-PCR)		Expression pattern by reporter gene	Subcellular localization	Phosphorelay from AHPs demonstrated <i>in vitro</i>	Loss-of-function phenotype	Constitutive expression phenotype
	Without ck	With ck					
ARR3	Expressed (To et al., 2004)	No/marginal induction (D'Agostino et al., 2000; Rashotte et al., 2003)	Root vasculature (To et al., 2004)	–	Yes (Imamura et al., 1999)	None (To et al., 2004)	–
ARR4	Moderate basal expression (D'Agostino et al., 2000)	Rapidly induced (Brandstatter and Kieber, 1998)	Root vasculature (To et al., 2004)	–	Yes (Imamura et al., 1999)	None (To et al., 2004)	Increased ck sensitivity (Osakabe et al., 2002)
ARR5	Low basal expression (D'Agostino et al., 2000)	Rapidly induced (Brandstatter and Kieber, 1998)	Root tip, LRs, vasculature (D'Agostino et al., 2000)	–	No, but phosphoreceiving site essential (To et al., 2007)	None (To et al., 2004)	–
ARR6	Low basal expression (D'Agostino et al., 2000)	Rapidly induced (D'Agostino et al., 2000)	Not seen in root without ck (To et al., 2004)	Mainly nuclear (Imamura et al., 2001)	Yes (Imamura et al., 1999)	None (To et al., 2004)	–
ARR7	Low basal expression (D'Agostino et al., 2000)	Rapidly induced (D'Agostino et al., 2000)	Examined in embryogenesis (Muller and Sheen, 2008)	Mainly nuclear (Imamura et al., 2001)	No, but protein can be phosphorylated (Lee et al., 2008)	No phenotype observed (Leibfried et al., 2005)	Decreased ck sensitivity (Lee et al., 2007)
ARR8	Moderate basal expression (D'Agostino et al., 2000)	Little/no induction (D'Agostino et al., 2000)	Throughout root (To et al., 2004)	–	–	None (To et al., 2004)	Decreased ck sensitivity (Kiba et al., 2003)

(continued)

Table 1.3 (continued)

	Expression levels (RT-PCR)		Expression pattern by reporter gene	Subcellular localization	Phosphorelay from AHPs demonstrated <i>in vitro</i>	Loss-of-function phenotype	Constitutive expression phenotype
	Without ck	With ck					
ARR9	Moderate basal expression (D'Agostino et al., 2000)	Little/no induction (D'Agostino et al., 2000)	Throughout root (To et al., 2004)	–	–	None (To et al., 2004)	–
ARR15	Low basal expression (D'Agostino et al., 2000)	Rapidly induced (D'Agostino et al., 2000)	Procambial cells (Kiba et al., 2002; Mahonen et al., 2006a)	Predominantly nuclear (Kiba et al., 2002)	–	No phenotype (Kiba et al., 2003)	Decreased ck sensitivity (Kiba et al., 2003)
ARR16	Low basal expression (D'Agostino et al., 2000)	Rapidly induced (D'Agostino et al., 2000)	Mostly endodermis (Kiba et al., 2002)	Predominantly cytoplasmic (Kiba et al., 2002)	–	–	–
ARR17	Weak/absent (D'Agostino et al., 2000; Rashotte et al., 2003)	No/marginal induction (D'Agostino et al., 2000; Rashotte et al., 2003)	–	–	–	–	–

Table 1.4 Properties of *Arabidopsis* type-B ARRs

	Expression in the root		Subcellular localization	Phosphorelay from AHPs demonstrated <i>in vitro</i>	Transcriptional activity demonstrated	Loss-of-function phenotype	Constitutive expression phenotype	
	By RT-PCR	By reporter construct						
ARR1	Strong (Mason et al., 2004)	EZ (Mason et al., 2004)	Nuclear (Sakai et al., 2000)	Yes (Mahonen et al., 2006a)	Yes (Sakai et al., 2000)	Longer roots (Sakai et al., 2002)	Shorter roots (Sakai et al., 2002)	
ARR2	Strong (Mason et al., 2004)	EZ, LRs (Mason et al., 2004)	Nuclear (Sakai et al., 2000; Lohrmann et al., 2001)	–	Yes (Sakai et al., 2000; Lohrmann et al., 2001)	None (Mason et al., 2005)	Cytokinin-like responses (Hwang and Sheen, 2001)	Nucleus (Hwang and Sheen, 2001)
ARR10	Strong (Mason et al., 2004)	EZ, LRs (Mason et al., 2004)	Nuclear (Hosoda et al., 2002)	Yes (Imamura et al., 2001)	Yes (Hosoda et al., 2002)	None (Yokoyama et al., 2007)	–	
ARR11	Strong (Mason et al., 2004)	Root–shoot junction (Mason et al., 2004)	Nuclear (Lohrmann et al., 1999)	Yes (Imamura et al., 2003)	Yes (Lohrmann et al., 1999)	None (Mason et al., 2005)	–	
ARR12	Strong (Mason et al., 2004)	EZ, LRs (Mason et al., 2004)	Nuclear (Mason et al., 2004)	–	–	None (Mason et al., 2005)	–	
ARR14	Not detected (Mason et al., 2004)	Not in roots (Mason et al., 2004)	–	–	–	–	–	
ARR18	Not detected (Mason et al., 2004)	Not in roots (Mason et al., 2004)	–	–	–	None (Mason et al., 2005)	–	

2.3.1. Type-B ARR_s relay the cytokinin signal

Even as the link between cytokinin signaling and two-component signaling was being established, work was already progressing on the downstream RR_s. By 1999, 14 ARR_s have been identified and divided into the two classes, type-A and type-B. The same year it was shown that expression of type-A, but not type-B RR_s, was induced by cytokinin (Brandstatter and Kieber, 1998; Kiba et al., 1999; Taniguchi et al., 1998).

The following year revealed that two of the type-B ARR_s, *ARR1* and *ARR2*, act as transcription factors. They bind DNA in a sequence-specific manner and their C-terminal halves could function as a transactivation domain in bombarded plant cells when fused to the GAL4 DNA-binding domain (Sakai et al., 2000). Lohrmann et al. (1999, 2001) showed that *ARR2* could bind to the promoter of genes controlling the mitochondrial respiratory complex and that *ARR11* could activate transcription when fused to the yeast GAL4 DNA-binding domain. However, 2001 proved to be a golden year for ck signaling research in which many key discoveries were made. Hwang and Sheen (2001) separated the roles of the two types of RR_s. They showed that the type-B ARR_s acted as positive regulators of ck signaling, whereas the type-A ARR_s act as negative repressors forming a negative feed back loop. They cloned four type-A ARR_s and three type-B ARR_s into their leaf mesophyll system (see Section 2.1) and reported that type-A ARR_s could repress the expression of the type-A ARR, *ARR6*, whereas the type-B ARR_s increased the expression of *ARR6*. Finally, Hwang and Sheen constitutively expressed *ARR2* and this was sufficient to mimic cytokinin treatments in certain developmental processes.

In the same year, Atsuhiro Oka's group provided genetic evidence for the role of the type-B ARR, *ARR1*, by investigating the cytokinin sensitivity of *arr1* mutant lines and constitutively expressing *ARR1* (Sakai et al., 2002). The constitutively expressing lines showed greater sensitivity to ck and increased expression of the type-A ARR, *ARR6*, whereas *arr1* showed slightly reduced sensitivity to ck and slightly reduced expression of *ARR6*. The authors also expressed an engineered version of *ARR1* lacking the DDK signal receiver (*ARR1*ΔDDK) which mimicked constitutively active ck signaling and rapidly induced type-A ARR expression without the need for *de novo* protein synthesis.

It had already been shown that *ARR10* and several other type-B ARR_s localize either predominantly or exclusively to the nuclei (Hwang and Sheen, 2001; Imamura et al., 2001; Lohrmann et al., 2001; Sakai et al., 2000). However, detailed analysis of the DNA-binding B motif of *ARR10* revealed that the NLS was located in this region (Hosoda et al., 2002). Analysis of this domain including resolution of the 3D structure was able to propose specific residues which interact with DNA and suggested that in contrast to the other GARP proteins, that *ARR10* bound DNA as a monomer (Hosoda et al., 2002).

Slowly the remaining type-B ARR_s were investigated, *ARR11* was shown to accept phosphoryl groups from an AHP and bind DNA with the same sequence as *ARR1*, *2*, and *10*. Constitutive expression of a version lacking the DDK signal receiver (*ARR11*ΔDDK) led to growth abnormalities consistent with cytokinin treatments, although the roots were unaffected (Imamura et al., 2003). Due to the lack of phenotypes in the single type-B mutants or the subtle nature of *arr1*, a more systematic approach was needed. This began with analysis of gene expression of all type-B ARR_s. RT-PCR revealed that members of subfamily I were expressed in all tissues, and that *ARR1,2,10,11*, and *12* were expressed highly in roots (Mason et al., 2004; Tajima et al., 2004). Analysis of translational fusions between type-B ARR_s and the GUS reporter gene showed considerable overlap in expression within the root, as *ARR1,2,10*, and *12* were all strongly expressed close to the root tip and *ARR2,10*, and *12* were expressed in LR_s (Mason et al., 2004). Analysis of single loss-of-function mutants in six of the seven members from the type-B ARR subfamily I revealed only subtle effects in cytokinin assays (Mason et al., 2005). It took the construction of higher order mutants to significantly decrease the sensitivity towards cytokinin, including effects on root elongation, LR formation, and induction of cytokinin primary response genes. In particular the *arr1,10,12* triple and *arr10,12* double mutant showed a great reduction in cytokinin sensitivity (Argyros et al., 2008; Ishida et al., 2008; Mason et al., 2005; Yokoyama et al., 2007). The phenotypes of these plants will be discussed in subsequent chapters relating to the biological processes in which they are involved.

2.3.2. The type-A ARR_s act through negative regulation

The type-A ARR_s were first identified as two-component signaling components which were rapidly induced by cytokinin (Brandstatter and Kieber, 1998; D'Agostino et al., 2000; Imamura et al., 1998; Kiba et al., 1999). However, there are some differences in the basal expression levels of these genes; *ARR4,8*, and *9* have relatively high-basal levels of expression and *ARR5,6,7*, and *15* show the greatest induction in response to cytokinin (D'Agostino et al., 2000; Rashotte et al., 2003).

ARR15 was shown to be a nuclear localized protein; its expression was significantly decreased in *cre1* mutants, but accumulated rapidly in the roots of wild-type seedlings when treated with cytokinin (Kiba et al., 2002). Although the loss-of-function *arr15* mutant did not show any discernable phenotype, the constitutive expression of *ARR15* lead to reduced sensitivity to cytokinin in various assays and a decrease in expression of a selection of other type-A ARR_s (Kiba et al., 2003). These results were similar to those from overexpression studies of *ARR8*, which was also proposed to be a negative regulator of cytokinin signaling, but was unlike *ARR4* which promoted cytokinin responses when constitutively expressed (Osakabe et al., 2002).

Analyses of single loss-of-function mutants in *arr3*, *arr6*, *arr8*, and *arr9* were unable to show any phenotype, and only mild rosette phenotypes were visible in *arr4* and *arr5* when grown under specific conditions (To et al., 2004). It took the construction of higher order mutants to display increasing sensitivity to ck both in physiological assays and in assays measuring the transcription of *ARR7*. The greatest sensitivity was observed in the hextuple mutant. This is likely to suggest significant functional redundancy between the type-A ARRs. Consistent with this, analysis of transcriptional fusions with the GUS reporter revealed that after ck treatment, there is considerable overlap between expression of these six type-A ARRs, especially within the root (To et al., 2004). Although there have been no reports of a loss-of-function phenotype in *arr7* mutants, based on transcriptional analysis of plants constitutively expressing *ARR7*, it is likely, that it also acts as a negative repressor (Lee et al., 2007).

Recent investigations into the cytokinin regulation of ARR activity have revealed that cytokinins directly regulate the stability of a selection of type-A ARRs through phosphorelay. It was shown that the aspartate phospho-accepting domain in *ARR5* and *ARR7* is necessary for receiver domain phosphorylation (Lee et al., 2008; To et al., 2007). Both studies showed that this residue was necessary for function of the relevant ARR. While constitutive expression of *ARR7* leads to decreased root growth inhibition by cytokinin, constitutive expression of a version where the phospho-accepting aspartate residue is mutated has no phenotype (Lee et al., 2007, 2008). Equally, when expressed under its own promoter, a version of *ARR5* in which this residue is mutated to an alanine was unable to rescue the *arr3,4,5,6* phenotype (To et al., 2007). However, a version where this residue was mutated to a glutamic acid (which mimics the phosphorylated active protein form) was able to rescue the *arr3,4,5,6* phenotype, suggesting that *ARR5* does not function entirely by acting as a phosphate sink. Investigations into the stability of *ARR5* and *ARR7* showed it to be stabilized in the presence of cytokinin, and this is reliant on the phospho-accepting aspartate residue (To et al., 2007). These results suggest that the type-A ARRs may be regulated by phosphorylation, and that the active phosphorylated form would reinforce the negative feedback loop. In addition to ck signaling molecules, type-A ARRs have been shown to have distinct developmental targets (although none have been identified in the root thus far) in controlling the regulation of circadian rhythms (*ARR3,4,8*, and *9*) and in controlling phytochrome function (*ARR4*) (Hanano et al., 2006; Salomé et al., 2006; To et al., 2004).

RRs have been identified in a number of other plant species including rice and maize. In these species type-A RR have also been shown to be upregulated by ck (Asakura et al., 2003; Du et al., 2007; Hirose et al., 2007; Ito and Kurata 2006; Pareek et al., 2006). It was shown that constitutive expression of the type-A RR *OsRR6* in rice led to plants with a dwarf

phenotype, small roots, and elevated ck levels (Hirose et al., 2007). This is consistent with a role for *OsRR6* as a negative regulator of ck signaling.

2.3.3. Newly identified components of cytokinin response

There have been several approaches towards identifying target genes downstream of cytokinin signaling based on microarray analyses. These have involved cytokinin treatments, analyses of lines with reduced cytokinin (*wol* and a transgenic line constitutively expressing *CKX1*) and analysis of lines with enhanced cytokinin signaling based on the constitutive expression of *ARR21* and *22* (Brenner et al., 2005; Kiba et al., 2005; Rashotte et al., 2003). These have resulted in the discovery of many genes whose expression is upregulated by cytokinin, including type-A ARRs, cytokinin oxidases, and various transcription factors. This includes several members of the AP2/ERF family of transcription factors, which lies within the ethylene response factor (ERF) family (Rashotte et al., 2006). These fall into a small subfamily and the six members were termed CRF1–6. The CRF1–6 proteins have uniform localization throughout the cell; however, when treated with cytokinin they move rapidly into the nucleus (Rashotte et al., 2006). This process is dependent on both the ck receptors and the AHPs but independent of the type-A or type-B ARRs. The relocalization of CRFs to the nucleus does not occur in triple cytokinin receptor mutants or quintuple *ahp* mutant protoplasts but can occur in high-order type-A or type-B *arr* mutant combinations. Analysis of single *arf* mutants showed weak phenotypes; however, double and triple mutant combinations had much stronger phenotypes, including, in some combinations, embryo lethality. Comparisons between the target genes of *arf* and type-B *arr* mutants revealed substantial overlap, with approximately two-thirds of the genes affected in the type-B *arr1,12* double mutant effected in triple *arf* mutants. However, cytokinin induction of type-A ARRs was not affected in *arf* mutants. This data suggests a model where the phosphorylated AHPs can directly induce CRFs to relocalize to the nucleus where they can activate cytokinin-mediated gene expression. This provides a branching point in the cytokinin signaling pathway. It is also distinctly possible that the CRFs receive input from unidentified cytokinin receptors or other signals, as the phenotype of the *arf* mutants is stronger than that observed for any of the combinations of cytokinin signaling mutants observed so far.

A new class of molecules has recently been identified which are likely to have a role in cytokinin signaling by antagonizing the negative regulation through the type-A ARRs. GLABROUS1 ENHANCER BINDING PROTEIN (GeBP) was identified through a yeast one hybrid screen as it bound to the promoter of the cytokinin-induced *myb* gene *GLABROUS1* (Curaba et al., 2003). It is a member of a small family of leucine zipper proteins called, GeBP-like proteins (GPLs). Analysis of a triple loss-of-function mutant of GPL members showed reduced sensitivity to ck and

increased transcription of type-A ARR. Whereas expression of a GPL variant showing constitutive transcriptional activity showed increased ck sensitivity and reduced ARR expression (Chevalier et al., 2008). It is not yet known whether these proteins have a role in the context of root development, but based on expression patterns this remains a possibility.

3. THE ROLE OF CYTOKININ SIGNALING SPECIFIC TO CERTAIN DEVELOPMENTAL PATHWAYS

3.1. Asymmetric patterning of cytokinin signaling defines the root stem cell niche

After the two haploid nuclei of pollen and egg cell fuse, the newly formed diploid cell undergoes several rounds of cellular divisions, and the daughter cells form a nonsymmetric embryo. When the embryo reaches the 16-cell globular stage, the uppermost of the basal cells forms the hypophysis. This will later become the root apical meristem. The cells in the 16-cell embryo divide further, forming a globular embryo. When the hypophysis cell divides, it gives rise to two distinctly identified cells. The upper, lens shaped cell will form the stem cell niche also known as the quiescent centre (QC) (Dolan et al., 1993; Friml et al., 2002, 2003; Scheres et al., 1994). In root meristems, the QC cells are generally regarded as plant stem cells based on their position, role, and behavior (Sabatini et al., 2003; van den Berg et al., 1997). The cells on the apical side of the globular embryo continue to proliferate and the embryo gains bilateral symmetry as it reaches the heart stage. By now, the root stem cell niche has already been positioned to the basal side of the embryo. These root apical meristematic cells divide and the root primordium becomes enlarged and elongated.

Until recently, the role of cytokinin signaling during embryogenesis was unclear. Indeed the triple cytokinin receptor mutant did not show embryonic defects, raising the suggestion that ck signaling was not required during the specification of the basic body plan. However, recently Müller and Sheen (2008) have shown that this is not the case. There is an absolute requirement for differential ck output in controlling the specification of the root stem cell niche, and that the interplay between auxin and cytokinin is critical for this.

Müller and Sheen generated a synthetic promoter, TCS, based around a target sequence known to be bound by diverse type-B RRs (Hosoda et al., 2002; Imamura et al., 2003; Sakai et al., 2000) and enriched in the *cis*-regulatory regions upstream of early ck target genes (Rashotte et al., 2003). This synthetic promoter was capable of reporting ck phosphorelay output, triggered through any of the three cytokinin receptors, and relayed to any RR that they tested. They used this promoter to drive GFP, enabling them

to follow ck signaling during embryogenesis (Fig. 1.3A–D). They first observed ck signaling output in the hypophysis during the 16-cell stage embryo. As the hypophysis underwent asymmetric division, ck signaling was repressed in the basal daughter cell and its decedents, but was retained in the apical daughter cell. They showed that ck signaling was required to ensure that cells divided correctly to form the root apical meristem, by inducing a dominant-acting transcriptional repressor of type-B ARR targets. In embryos without ck signaling output, there were strong patterning defects, resulting in failure to make a root apical meristem.

After division of the hypophysis, the domain of cytokinin signaling output is restricted to the apical cell as the negative type-A ck RRs *ARR15* and *7* are expressed at high levels in the basal cell. It has been

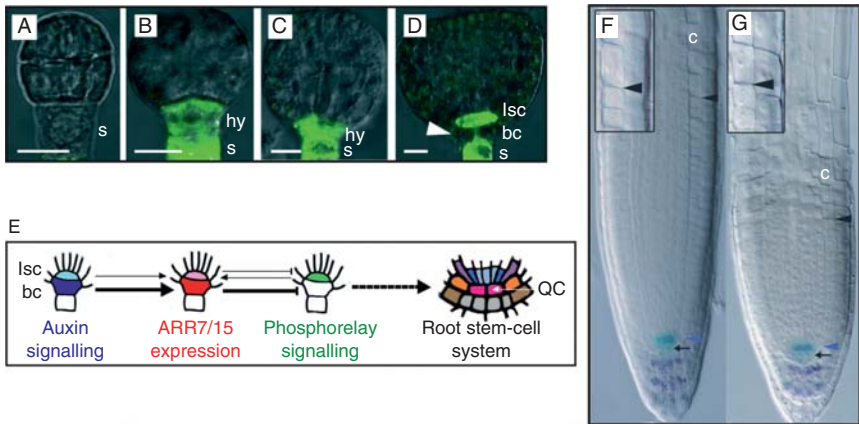


Figure 1.3 Cytokinin regulates the formation and the size of the root apical meristem. Panels (A)–(D) follow the expression of *TCS::GFP* expression during early embryogenesis. The signal was first detected in the founder of the root stem cells, the hypophysis, at the 16-cell stage (B). By the transition stage, the hypophysis has undergone asymmetrical cell division (compare panel (C) with panel (D)). *TCS::GFP* expression is repressed in the resulting large basal daughter cell but maintained in the apical lens-shaped cell. An arrowhead points to the location where *TCS::GFP* is downregulated in the basal cell lineage. bc, basal cell lineage; hy, hypophysis; lsc, lens shaped cell; s, suspensor. Panel (E) shows a schematic model showing the auxin-dependent downregulation of phosphorelay in the lens-shaped cell. Reprinted from Nature (Müller and Sheen, 2008) (Copyright 1998), with permission from Macmillan Publishers Ltd. Panels (F) and (G) represent wild-type *Arabidopsis* roots. The QC cells are stained blue and the starch granules in columella cell are stained purple. The cortical cells are marked with c. The root on the left (F) is an untreated control plant showing a normal meristematic zone (MZ) region and cell elongation (black arrowhead marks the first elongating cortical cell). The root on the right (G) was treated with ck and shows a reduction in the size of the meristematic region and premature cell differentiation (black arrowhead). Reprinted from *Current Biology* (Dello Ioio et al., 2007) (Copyright 2007), with permission from Elsevier.

known for several years that correct asymmetric distribution of auxin is required to specify the root apical meristem, and that auxin signaling is active in this basal cell (Friml et al., 2003; Sabatini et al., 1999). Using a combination of hormonal treatments, Müller and Sheen were able to show that expression of *ARR7* and *15* was promoted by both auxin and cytokinin. They also created modified reporter constructs for both ARRs which lacked auxin-binding sites (Ulmasov et al., 1999). These were unresponsive to auxin, while retaining ck response, and showed strongly reduced expression in the basal cells of the hypophysis, indicating that auxin was able to directly regulate the cytokinin response elements.

To demonstrate that *ARR7* and *15* have a role in the formation of the root meristem, Müller and Sheen employed an inducible RNAi-based system to create a double *arr7 arr15* mutant. Soon after induction, ectopic cytokinin signaling could be seen in the basal cell. This resulted in defects in cell division and arrangement. In turn, this led to embryos in which root stem cell niche identity became ambiguous, expression of key transcription factors involved in root stem cell specification was abolished or severely reduced, and finally the embryos finally aborted. These phenotypes could be phenocopied by the ubiquitous expression of a dominant-acting transcriptional repressor domain fused to a type-B ARR under the control of the synthetic auxin promoter.

Based on these results, Müller and Sheen were able to produce a model in which ck signaling output could be regulated by auxin-mediated expression of type-A RRs (summarized in Fig. 1.3E). This is able to nullify ck signaling output in the basal cell and allow the formation of the root apical meristem. Interestingly, they found that this targeting of *ARR7* and *15* by auxin only occurred early during embryogenesis and manipulation of ck signaling at the heart stage and later had no effect on the organization of the root apical meristem.

3.2. Cytokinins control root meristem size

As discussed above, the root QC is established during embryogenesis in *Arabidopsis*. In young roots, the QC cells seldom divide. They are thought to function as structural initial cells that, while being sessile themselves, act as a steady point of active signaling to their neighboring cells (Jiang and Feldman, 2005; van den Berg et al., 1997). Cells in cell-to-cell contact with the QC cells are regarded as functional initial cells. These give rise to cell lineages comprising distinct cell types, via tightly regulated periclinal cell divisions (Fig. 1.4B) (Sabatini et al., 2003; van den Berg et al., 1995). The QC cells and neighboring initial cells are often referred to as meristematic cells. It has been observed, that these cells divide at different rates, depending on the number of cells in the meristematic stem cell niche as well as their position. The cells closest to the convergence point of different initial cell lines in the

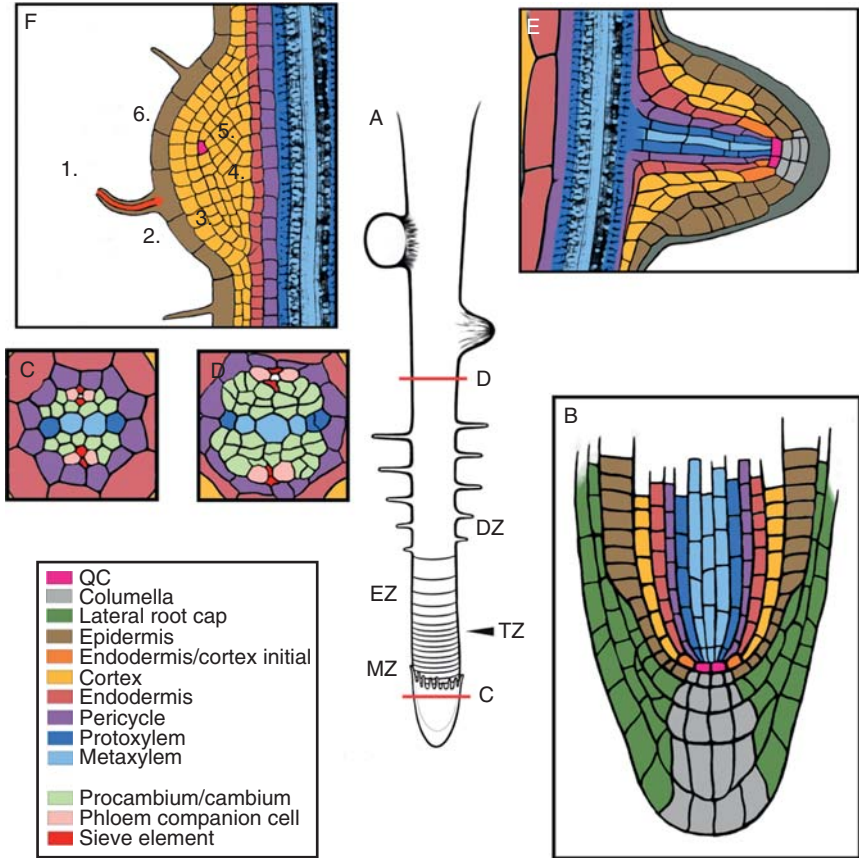


Figure 1.4 The anatomy of the root. In the center of the image is an illustration of a root (A); MZ and EZ are marked at their respective positions. The LR cap which offers protection to the growing root is drawn at the tip of the root. The horizontal bands on the root (MZ + EZ) illustrate epidermal cell lengths, which increase as the root matures. The region where cells leave the meristematic phase and enter the elongation phase is called TZ, as it presents the border between proliferating and elongating/differentiating cells. Root hairs indicate the differentiation zone (DZ). A LRP (top right), a root nodule (top left), a detailed image of the root tip (bottom left), and cross sections through the stele during primary (C) and secondary development (D) are included in the image. For identifying different cell types, see the key at the bottom left. The relative positions of these cross sections are shown by the red lines, labeled (C) and (D). Notice the cambial cell divisions during secondary development. Nodule formation follows the following stages: 1. release of exogenous ck/elicitor from soil rhizobia, 2. IT formation, 3. ck signaling and gene activation, 4. cortical cell proliferation, 5. nodule meristem formation, and 6. nodule growth.

niche are usually the most infrequent proliferators (Dello Ioio et al., 2007). If a cell is in cell-to-cell contact with a QC cell, it will only seldom divide, while its distal daughter cells will proliferate actively (Baum et al., 2002).

The identity of a certain cell or initial cell line is also determined by its position in the stem cell niche. The precisely positioned cell initials proliferate into daughter cells which subsequently differentiate as various cell types in the root, including epidermis, endodermis, cortex, pericycle, and vascular cell tissues (Dolan et al., 1993). The combination of maintaining the identity of initial cells in the correct position and inhibiting them from proliferating, while at the same time allowing daughter cells to proliferate and differentiate into different cell types, maintains the autonomous growth of the root apical meristem. It also allows growth to be flexible enabling it to respond to the internal and environmental stimuli.

Root meristems continuously produce new cells. So, with steadily increasing cell numbers, it is critical to maintain a balance between the proliferation of the meristematic cells and the differentiation of the newly formed daughter cells. If the proliferation of the daughter cells is not rapid enough, the root meristem can grow out of proportion. In contrast, if cell proliferation is somehow protracted, disrupted, or the differentiation of the daughter cells is too rapid, the meristematic region can shrink in size longitudinally. In the most severe cases the root meristem might even cease to grow altogether (as seen in triple cytokinin receptor mutants and *wol* mutants (Higuchi et al., 2004; Nishimura et al., 2004)). When the newly formed daughter cells of different cell types leave the actively dividing meristematic region, they enter the transition zone (TZ) (Dello Ioio et al., 2007) (Fig. 1.4A). Soon after this, cell types elongate to their characteristic lengths, which is visible in the EZ. This is followed by the differentiation zone (DZ) in which cells assume their final identity (Fig. 1.4A). In *Arabidopsis*, the DZ is easily distinguishable by root hair formation. The proliferative activity of the meristematic cells and their differentiation and elongation rates define the ultimate size of a root meristem. To maintain balanced growth, roots must have a finely tuned mechanism to control the balance between cell division and differentiation.

Complete loss of cytokinin perception leads to a decrease in meristem size and root length (Higuchi et al., 2004; Nishimura et al., 2004). Similarly, primary growth is arrested in the *arr1,10,12* triple mutant (Ishida et al., 2008; Yokoyama et al., 2007). Furthermore, Hutchison et al. (2006) showed that the primary root elongation rate of *ahp1,2,3,4,5* quintuple mutants was significantly reduced when compared with wild type. Based on analysis of cell cycle markers, in various cases it has been suggested that the severe reduction in root growth was due to decreased cell divisions in root meristem. It is unclear whether this is due to a direct effect of loss of ck on the meristematic size, or whether it is the result of vascular defects (discussed in Section 3.5).

Exogenous ck reduces the number of meristematic cells and leads to a decrease in the size of meristematic region (Fig. 1.3F and G) (Dello Ioio et al., 2007). The *stunted plant1* mutant was identified due to defective cell

expansion in the root EZ and this phenotype resembled plants which had been treated with ck (Baskin et al., 1995). When the *stp1* mutants were treated with various plant hormones, they responded normally to auxin, ethylene, gibberellins, and abscisic acid, but only weakly to cytokinin in a root length assay (Beemster and Baskin, 2000). Beemster and Baskin postulated that STP1 controls cytokinin-mediated meristematic cell division and elongation in the root meristem and EZ and that the *STP1* expression is downregulated by cytokinin. In combinations of multiple type-A ARR mutants, plants treated with ck show increased sensitivity to ck-mediated reduction in primary root elongation compared to wild type (To et al., 2004). Contrastingly, plants lacking multiple type-B ARRs are less sensitive to exogenously applied cytokinins in regard to root elongation than wild type (Argyros et al., 2008; Ishida et al., 2008; Mason et al., 2005; Sakai et al., 2002).

Even though meristem elongation is suppressed by cytokinins, there is evidence that exogenous cytokinins do not actually affect the meristematic stem cells, but only the dividing and maturing daughter cells (Fig. 1.3F and G) (Dello Ioio et al., 2007). Consistently, the expression of QC markers, stem cell regulatory genes, and cell-specific marker genes remain unaltered after ck treatments, although meristems were reduced in size and columella markers were absent (Dello Ioio et al., 2007).

In contrast to plants treated with exogenous cytokinins, mutants with reduced cytokinin biosynthesis (such as *ipt3,5,7*) or cytokinin perception (*ahk3*) have larger meristems than wild type (Dello Ioio et al., 2007). It has also been shown, that the *ipt3,5,7* triple and *ipt1,3,5,7* quadruple mutants, *cre1*, *ahk3*, and *ahk2 ahk3* mutant plants grow longer roots when compared with wild-type plants (Dello Ioio et al., 2007; Miyawaki et al., 2006; Riefler et al., 2006). The meristematic phenotype of the *ipt3,5,7* mutants can be partially suppressed by the application of exogenous ck (Dello Ioio et al., 2007). Spíchal et al. (2009) published the effects of a purine derivative with anticytokinin properties named PI-55. The compound had high affinity to the *CRE1* receptor, reducing the binding of natural ligands and inhibiting the transcription of *ARRs*. Application of PI-55 increased primary root length in *ahk2 ahk3* double mutants and it also increased LR numbers in both wild-type and ck-receptor mutant backgrounds. Even though the *cre1* mutation increases root length (Riefler et al., 2006), it does not affect meristem size (Dello Ioio et al., 2007). It has been suggested that *AHK3*, *ARR1*, and *ARR12* are key components in regulating cell differentiation at the TZ and in timing the maturation of the meristem (Dello Ioio et al., 2007). The *AHK3* expression pattern is strongest in the TZ between the root meristem and the EZ. Both *ahk3* and *arr1* and *arr12* (single and double) mutants phenocopy the cytokinin biosynthesis mutants (*ipt3,5,7* mutants) producing enlarged meristems and longer roots. Unlike *AHK3*, expression of *AHK2* and *CRE1* was not detected in the root TZ. Consistently, *ahk2*

mutants showed no increase in root meristem size and only a small increase was observed in *cre1* mutants (Dello Ioio et al., 2007). These results indicate that AHK2 and *CRE1* only have a minor role—and that the AHK3 is the main receptor—in controlling root meristem size and root elongation (Dello Ioio et al., 2007, 2008). Constitutive expression of *ARR1*ΔDDK showed a significant reduction in plant meristem size (Dello Ioio et al., 2008).

Taniguchi et al. (2007) have studied the targets of *ARR1*, and amid a spectrum of direct and indirect targets identified the AP2-like gene, *IAA3*/*SHY2* as a direct target of *ARR1* and primarily responsive to cytokinins. Dello Ioio et al. (2008) confirmed that *IAA3*/*SHY2* acted downstream of *ARR1* and also showed that *SHY2* expression is induced by cytokinins in the stele in wild-type but not in *arr1* mutant plants. *SHY2* is a member of the *Aux/IAA* family. The *Aux/IAA* proteins are auxin responsive inhibitors of auxin signaling. They can hybridize with the auxin response factors, ARFs, which in turn can bind into the auxin responsive elements in DNA. On application of auxin the *Aux/IAAs* are rapidly degraded (Mockaitis and Estelle, 2008). The *shy2* loss-of-function mutants have abnormally large meristems, whereas *SHY2* overexpression leads to a decrease in meristem size. *SHY2* is a repressor of auxin signaling and it negatively regulates auxin transport mediated by the PIN proteins. Based on these observations, it has been postulated that cytokinin signaling and auxin jointly regulate the processes of cell division and differentiation in the root meristem by an interaction which converges on *SHY2* (Dello Ioio et al., 2008).

It has been demonstrated that cytokinin-mediated two-component signaling is involved in controlling the size of the root meristem by regulating cell differentiation rates at the TZ. However, controlling root apical meristem size (root meristem stem cell numbers and proliferation) involves the interactions with other plant hormones, such as auxin.

3.3. Primary vascular development

Root growth can be separated into two phases. During the primary phase, the identity of all major cell types is established, at least in the form of initial cells. In the secondary phase (discussed later) some of these cells proliferate radially, which results in thickening of the root. The vascular cylinder is surrounded by a pericycle which separates it from the cortex. The cells in the stele are classified into protoxylem, metaxylem, phloem, and procambial cells (see Fig. 1.4C). The vascular cell types can be distinguished from another firstly by their position and secondly by their appearance, even before they reach the EZ. In the primary roots of *Arabidopsis* the xylem axis is comprised by two protoxylem cell files at the marginal position. Each touch two pericyclic cells. The central part of the axis is occupied by two to three metaxylem cell files. Xylem cells transport water, nutrients, and

signaling molecules from the roots to the areal parts of the plant. Two phloem poles are located at 90° to the protoxylem cell files. Phloem cells transport photosynthetic assimilates, metabolites, and hormones from the shoot to the root system. The xylem and phloem are separated by procambial cells which remain undifferentiated. Later, these procambial cells divide and are responsible for secondary growth via formation of cambium (see below).

The requirement of ck signaling for correct vascular development has been shown at multiple stages of phosphorelay including the receptors (Mähönen et al., 2006a), the HPts (Hutchison et al., 2006), and the RRs (Yokoyama et al., 2007). The first indication that ck played a role in vascular development was when it was realized that the *wol* mutant encoded a ck receptor. As described above, the recessive *wol* mutant displays a short root phenotype, the number of vascular cell files is decreased and all vascular cells differentiate as protoxylem (Fig. 1.5C) (Mähönen et al., 2000; Scheres et al., 1995).

A publication by Takeshi Mizuno's lab in 2004 also suggested that two-component signaling downstream of the receptors was involved in vascular development. They analyzed the biochemistry of the type-C *ARR22* (Kiba et al., 2004). They demonstrated that expression of this gene is not induced by cytokinin treatments, but that can be phosphorylated by AHP5 *in vitro*, for which the phospho-accepting aspartate residue is vital. Constitutive expression of *ARR22* led to a phenotype similar to *wol*, where all vascular cells differentiate as protoxylem, whereas a mutant version lacking the phospho-accepting aspartate residue had no phenotype. Together, these results suggest that a reduction in two-component signaling can affect the differentiation of xylem, but it is unclear whether *ARR22* itself has any role in this process.

The role of ck in vascular development was confirmed genetically in 2006, when it was shown that plants lacking all three ck receptors displayed a *wol*-like vascular phenotype with fewer cell files within the vascular bundle, all of which differentiate as protoxylem (Mähönen et al., 2006a). Equally, the same effect could be observed when ck levels were depleted from root vascular tissues, by ectopically expressing *CKX2*. While, if plants are germinated on media supplemented with cytokinin, cells fail to differentiate as protoxylem (Mähönen et al., 2006a).

These data led to the proposal that cytokinin signaling was required within the vasculature to promote the identity of cell types other than protoxylem (Mähönen et al., 2006a). The pseudo HPt, AHP6, is expressed specifically within the protoxylem and protoxylem-associated pericycle cells where it acts as an inhibitor of cytokinin signaling. In wild-type plants, cytokinin signaling is most active in the procambial cells flanking the xylem axis, where expression of the response regulator *ARR15* is highest. In *ahp6* mutant plants, the *ARR15* expression domain extends into the region in

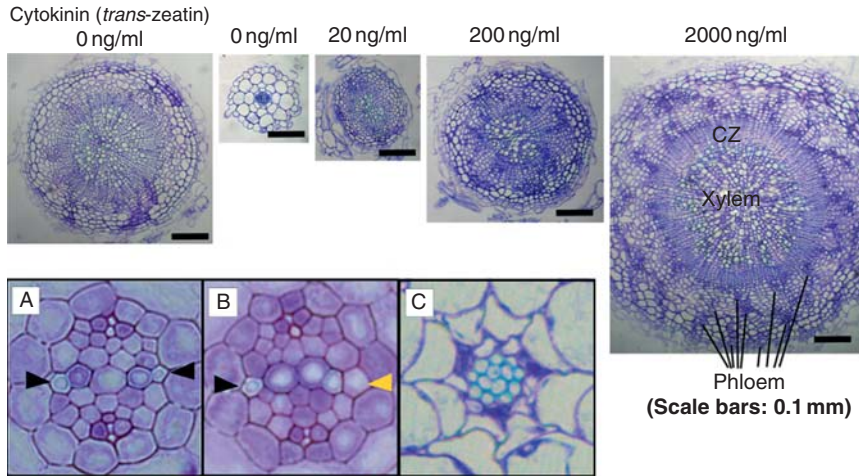


Figure 1.5 Primary and secondary vascular development. The top row shows cross sections from 25-day-old *Arabidopsis* roots. On the left is wild type; note the thickness and the existence of a considerable number of cell files. Next is the *ipt1,3,5,7* mutants, with a significantly thinner root and fewer vascular cells. The following panels show that this phenotype can be suppressed by growth on an increasing amount of cytokinin. These images are reproduced with permission from Matsumoto-Kitano et al. (2008). Copyright (2008) National Academy of Sciences, USA. Panel (A) shows a cross section through a 5-day-old *Arabidopsis* root, showing normal vascular composition. The protoxylem cell files are marked with black arrowheads. Panel (B) shows a similar cross section through *ahp6* where protoxylem identity is missing. A yellow arrowhead denotes the site where protoxylem would normally occur. Panel (C) shows *wol*, where there are fewer cell files in the vascular bundle, all of which differentiate as protoxylem.

which protoxylem would normally form and these cells retain properties typical of procambial cells and do not differentiate as protoxylem (Fig. 1.5B). The expression of AHP6 is inhibited by cytokinin; in *wol* or the triple cytokinin receptor mutant AHP6 expression expands to all vascular cells, whereas when roots are treated with cytokinin AHP6 expression is abolished. This interaction between ck signaling and AHP6 is able to specify the exact boundary within which protoxylem may differentiate.

Although any of three ck receptors is sufficient to maintain identity of cell lines other than protoxylem, there is data suggesting that the relative contribution of each receptor is not equal. Without the addition of exogenous ck the *ahk2 ahk3* double mutant does not display abnormalities in the number of xylem files (Mähönen et al., 2006a; Yokoyama et al., 2007). However, either the *cre1 ahk2*, or the *cre1 ahk3* mutant combinations frequently display at least one file of ectopic protoxylem. This phenotype can be suppressed when combined with *ahp6* (Mähönen et al., 2006a).

Similar vascular phenotypes have also been reported in the quintuple *ahp1,2,3,4,5* mutant which has a narrow vascular cylinder with ectopic

protoxylem and neither metaxylem or phloem (Hutchison et al., 2006). Analysis of the expression of type-B ARRs had suggested that there was likely to be redundancy within the root as *ARR1,2,10*, and *12* all showed strong expression in primary and LR tips (Mason et al., 2004). Initial analysis of multiple triple mutant combinations showed reduced ck response in various assays, including effects on root elongation, LR formation, and induction of cytokinin primary response genes (Mason et al., 2005). However, the construction of a new allelic combination of *arr10 arr12* mutants, combined with careful analysis of the vascular phenotype revealed that protoxylem was resistant to ck treatment in this line (Yokoyama et al., 2007). The revised *arr1 arr10 arr12* triple mutant showed strong ck-related phenotypes in multiple pathways, and an all-protoxylem phenotype similar to that of the *wol* mutant (Argyros et al., 2008; Ishida et al., 2008; Yokoyama et al., 2007).

Taken together, this data offers perhaps the most complete understanding of ck signaling in any developmental process. Work from labs in Europe, Japan, and the USA has enabled us to understand the components involved at each level of phosphorelay from the receptors to the RRs, and the mechanism of negative regulation. However, as the phenotype of *ahp6* is relatively weak, and can be enhanced by the addition of ck, it is likely that there are additional negatively acting elements.

3.4. Secondary vascular development

In roots, secondary vascular development involves root thickening growth via secondary xylem (and phloem) formation. Secondary vascular development begins when the cambial cells start to proliferate and divide in an organized manner (Chaffey et al., 2002; Dolan et al., 1993). These cambial cells are considered to be a secondary meristem inside the stele (Hertzberg et al., 2001; Schrader et al., 2004). The anticlinal cell divisions (Fig. 1.4D) form either new xylem or phloem cells, depending on their position in the root. The cells produced by the cambial meristem can move either in a centripetal direction (towards the center of the root) and differentiate into xylem, or in a centrifugal direction (towards the epidermis) and differentiate into phloem (Matsumoto-Kitano et al., 2008). In addition, *Arabidopsis* secondary vascular development can be divided into two phases based on the cell types that differentiate from the cambial daughter cells. During the first phase, roots produce only vessel elements and parenchyma cells. After a while, the plants switch into the second phase producing vessel elements and lignified fiber cells (Chaffey et al., 2002).

Recently, there has been a report demonstrating that cytokinins also play a role in the regulation of cambial development during root development. The first indication that cytokinin might regulate secondary development came from the analysis of the ectopic expression of the *AHK2* under the

promoter of *CRE1* (Mähönen et al., 2006b). When expressing this cytokinin receptor isoform with no apparent phosphatase function in *cre1* knock-out background, a proliferation pattern of vascular tissue indicative for enhanced secondary development was observed. The *Arabidopsis* quadruple mutant lacking *IPT1,3,5,7* has decreased levels of isopentyladenine and *t-z* and has increased elongation of both the primary and LRs (Miyawaki et al., 2006). This mutant also shows a severe defect in root thickening, lacks vascular cambium in the root and shows considerably delayed secondary growth (Matsumoto-Kitano et al., 2008). This effect can be restored by the application of exogenous *t-z* or by the grafting of a wild-type stock on to a *ipt1,3,5,7* root (Fig. 1.5) (Matsumoto-Kitano et al., 2008). This shows not only a role for cytokinin in the regulation of cambial activity, but also demonstrated that ck species are able to move between the root and the shoot. Secondary development is a less significant process in *Arabidopsis* than it is in woody species, but data from Poplar also shows that cytokinins can also regulate cambial activity in a tree, as transgenic trees with decreased cytokinin produce thinner stems (Nieminen et al., 2008).

3.5. Cytokinin regulates root architecture

Plasticity in root architecture allows plants to adapt to their continuously changing environment. Root branching via the formation of lateral root primordia (LRP) and elongation of the LR are two of the most important processes controlling root architecture. In *Arabidopsis*, LR formation is initiated at the pericycle from the cells in contact with the xylem cell files. These pericyclic cells are referred to as LR founder cells (Dubrovsky et al., 2000; Malamy and Benfey, 1997; Smet et al., 2006). The founder cells function as extended meristems that are able to dedifferentiate at both environmental and endogenous cues, and to initiate the development of LRP at discrete locations (Celenza et al., 1995; Laskowski et al., 1995, 2008; Malamy and Ryan, 2001; Parizot et al., 2008). LR development can be divided into different stages; initiation, primordium formation, meristem organization, LR emergence, and LR elongation (Laskowski et al., 1995; Malamy and Benfey, 1997; Nibau et al., 2008). The initiation stage includes stimulation of pericyclic cell divisions and dedifferentiation of these cells. Hormones such as cytokinin and auxin induce LR formation. After initiation, the founder cells divide asymmetrically in a periclinal direction (Fig. 1.6A). Daughter cells divide anticlinally, towards the epidermis and form a LRP. After this, the primordium enlarges, forming a bump inside the root (Fig. 1.6B). Already at this stage the meristem QC cells can be detected in young LRP (Figs. 1.4E and 1.6B). Having formed a meristem of its own, and reached a critical size, the LRP functions autonomously and emerges from the root through the epidermis. After emergence, the LR meristem

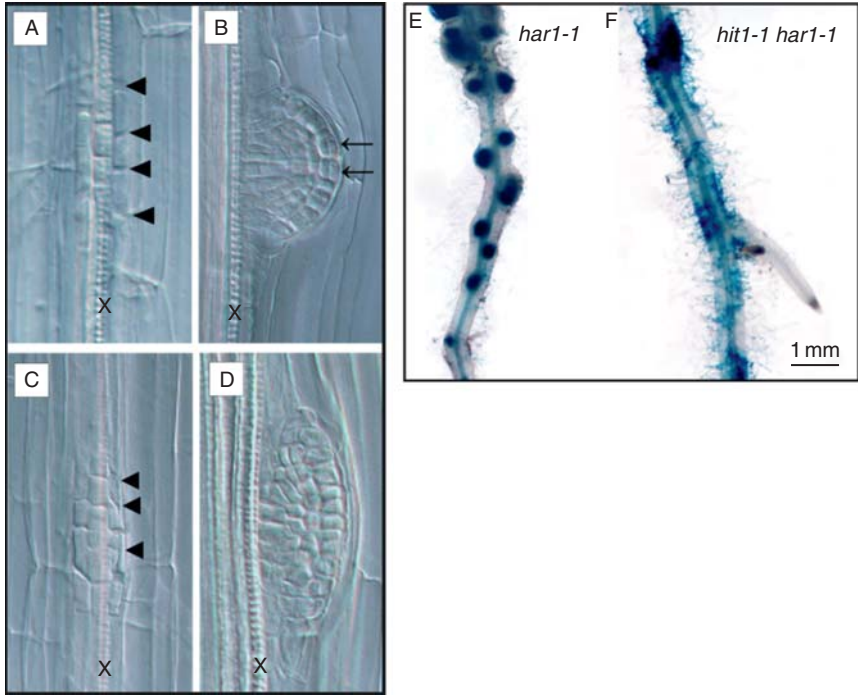


Figure 1.6 Cytokinin regulates LR and nodule development. Panels on the left show pericyclic cell divisions (arrowheads) during LR initiation. Nontreated plants show organized periclinal cell divisions during LR initiation (A), marked by black arrowheads. Cytokinin-treated plants at the same phase show disorganized cell division (C) pointed out by arrows. Panels (B) and (D) show LR development at a later stage, after the primordium has formed. Nontreated plants (B) have organized cell proliferation and formation of meristematic cells (arrows), whereas ck-treated plants exhibit no such pattern of organization (D). LRP development arrests at this stage in ck-treated plants. Protoxylem cell files are marked with X in all of the images. Reprinted from [Laplaze et al. \(2007\)](#), with permission from American Society of Plant Biologists. Panels (E) and (F) show root segments from *har1* and *hit1 har1* double mutants. Images have been taken 10 days after inoculation with *Mesorhizobium loti* bacteria. The bacteria carry a *lacZ* reporter gene. Note the lack of nodule primordia in the *hit har* double mutant. Reprinted from [Murray et al. \(2007\)](#), with permission from AAAS.

controls the growth of the LR by promoting cell proliferation and elongation ([Nibau et al., 2008](#); [Smet et al., 2006](#)).

This section will focus on the emergence of LRs in respect to cytokinin signaling, and describe which components of the ck signaling pathway are most relevant. Also, similarities and differences between different plant species will be discussed briefly.

Cytokinin, auxin, and ethylene all regulate the establishment and development of LRs ([Aloni et al., 2006](#)). However, it has been suggested that

they can act through separate pathways in some stages of LR development, but there is likely to be some crosstalk between these pathways (Kuderova et al., 2008; Laplaze et al., 2007).

The application of exogenous cytokinin inhibits LR formation (Kuderova et al., 2008; Laplaze et al., 2007; Li et al., 2006). Analysis of the cell division marker, *CYCB1;1::GUS*, revealed that in the pericycle founder cells of ck-treated lines, fewer pericycle divisions occur (Li et al., 2006). This ck-mediated inhibition of cell division affects the LR founder cells and perturbs the first initial anticlinal cell division (Laplaze et al., 2007). Exogenous cytokinin causes LR development to arrest soon after the primordium has formed (Laplaze et al., 2007). Similarly, if the endogenous cytokinin levels of roots are elevated, via increased expression of *IPT* genes (Kuderova et al., 2008), there is a significant decrease in LR numbers. The cytokinin-mediated growth inhibition of LRs seems to be dose-dependent in both ck-treated and ck-overproducing lines. The total number of LR meristems was significantly reduced in cytokinin overproducing plants, although the number of LRPs in these plants was close to normal, or even higher than in wild type. This led to an abnormally high density of LRPs (Kuderova et al., 2008). Based on these observations, Kuderova et al. (2008) and Laplaze et al. (2007) showed that high-ck levels have a deleterious impact on LR development, firstly by inhibiting LRP formation, secondly by disrupting cellular division leading to formation of disfigured primordia, and thirdly, arresting the growth before the lateral root meristem forms (Fig. 1.6C and D). It seems that LRP development is sensitive to exogenous/elevated ck levels at early stages, before root emergence. Contrastingly, depleting cytokinin has been shown to lead to an increase in LR numbers (Laplaze et al., 2007) and their elongation (Miyawaki et al., 2006). For instance, when a cytokinin degrading enzyme (*CKX1*) was expressed in xylem-pole pericyclic cells, LRs developed normally but their density was increased (Laplaze et al., 2007). Additionally, *ipt1,3,5,7* quadruple mutants have longer LRs than wild type (Miyawaki et al., 2006).

The inhibitory role of cytokinin on root elongation differs between primary and LRs. For instance, treating roots with exogenous ck does not inhibit the growth of the LRPs, nor does it reduce LR elongation (Li et al., 2006). This is in contrast to the inhibitory effect of cytokinin on primary root growth (see previous chapter). In addition, Laplaze and colleagues claim that LR development is more sensitive to exogenously applied ck than primary roots. They showed that the young primordia arrested development after ck application. Following on from this, Laplaze et al. (2007) showed that indeed, LR founder cells and young primordia are sensitive to exogenous cytokinin, but once the LR meristems are established, LRP are not suppressed by ck and are able to elongate. This would indicate that ck is able to inhibit LR formation only when applied before the LRPs had established their own meristems (making them cytokinin synthesis tissues and thus insensitive to exogenous cks).

It is likely that the different receptors display different relative requirements in controlling LRP initiation and LR formation. For example, Riefler et al. (2006) showed that *ahk2 ahk3* mutants produce more LRs than wild type. In their assay, the *cre1*, *cre1 ahk2*, and *cre1 ahk3* mutants showed no differences in LR number. However, in a ck assay for inhibition of LRs, both Nishimura et al. (2004) and Li et al. (2006) showed that *ahk2 ahk3* mutants behave as wild type and produce no LRs, while double mutants involving *cre1* showed the greatest ck insensitivity.

Based on these reports with the cytokinin receptor mutants (Dello Ioio et al., 2007, 2008; Li et al., 2006; Nishimura et al., 2004; Riefler et al., 2006), it can be concluded that in *Arabidopsis*, reduced cytokinin signaling by knocking out (one or both) AHK2 and AHK3 receptors, stimulates the growth of both primary and LRs. Similarly, knocking out the CRE1 receptor leads to an increased number of LRs, when plants are treated with exogenous cytokinins. Thus, depending on the developmental process and endo/exogenous ck levels, different receptors are required in controlling LRP initiation and LR formation.

Recent studies performed with *Medicago truncatula* (Gonzalez-Rizzo et al., 2006) and *Oryza sativa* (Rani Debi et al., 2005) have yielded similar results to *Arabidopsis*, but the developmental processes regulated by the ck receptors may vary between different plant species. It is clear; however, that the effect of ck in controlling the emergence of LRs is likely to be widely conserved. Some of the differences in LR formation can be explained by the deviating regulatory pathways between nodulating (i.e., *M. truncatula* and *O. sativa*) and nonnodulating (*Arabidopsis thaliana*) species. For example, in rice, the effect of cytokinin inhibition on LRP initiation appears to resemble *Arabidopsis*, but contrastingly the emergence of the LR is not inhibited by cytokinins. Also in rice, cytokinins seem to stimulate LR elongation—an opposite effect to *Arabidopsis* root system (Rani Debi et al., 2005). Likewise, in *M. truncatula* and *Lotus japonicus*, the *Arabidopsis* CRE1 orthologs, named MtCRE1 and LHK1, respectively, have key roles in LR formation. In these two root nodule forming species, CRE1 orthologs are involved both in regulating nodulation and LR formation (Gonzalez-Rizzo et al., 2006; Murray et al., 2007). It has however been shown, that when grown in nonsymbiotic conditions, *M. truncatula* MtCRE1 RNAi plants with downregulated MtCRE1 signaling and *L. japonicus* plants constitutively expressing the ck degrading enzyme CKX3 showed increased LR formation (Gonzalez-Rizzo et al., 2006; Lohar et al., 2004). *L. japonicus* plants with either *lhk1* loss-of-function mutation or with constitutive CKX3 activity showed increased insensitivity to ck and dramatically inhibited nodulation (Lohar et al., 2004; Murray et al., 2007).

Arabidopsis plants with mutations in the type-B ARRs also show decreased sensitivity to ck inhibition in LR formation. Mason et al. (2005) analyzed all combinations of the *arr1*, *arr10*, and *arr12* mutants and observed an additive effect on LR numbers in ck-treated plants. When single

mutants were treated with cytokinin, plants showed almost equal loss of LR_s to wild-type plants. However, *arr1,12* double mutants and *arr1,10,12* triple mutants were much more resistant to ck applications (Mason et al., 2005). It was later shown that this mutant combination does not confer complete loss-of-function. However, when these genes are knocked out, primary root growth terminates prematurely, preventing analysis of LR_s (Ishida et al., 2008). Type-A *arr* mutants show greater sensitivity towards ck treatments than wild type (To et al., 2004). In the absence of exogenous cytokinin, the hextuple *arr3,4,5,6,8,9* mutant has significantly fewer LR_s than wild-type. In this mutant LR formation can also be inhibited with much lower concentrations of cytokinin than is needed in wild-type.

3.6. Cytokinin control the process of root nodulation

Root nodulation involves several steps. Firstly, the root must be in contact with soil microbes, for example, rhizobial bacteria, which sense compounds excreted by the plant. The microbes must respond by eliciting nodulation factors (such as cytokinin like compounds) into the soil rhizosphere. The plant receives these factors and triggers root hair curling and infection thread (IT) formation inside the root hair. As the IT elongates, it activates signal cascades (e.g., calcium pulse and cytokinin signaling) in the epidermis and cortex, leading to the production of early nodulation-related genes in these tissues (Bauer et al., 1996; Crespi and Frugier, 2008; Marsh et al., 2007; Oldroyd and Downie, 2008; Schauser et al., 1999; Schultze and Kondorosi, 1998) (Fig. 1.4F). As a result of increased cytokinin signaling and expression of several nodulation promoting genes, cell proliferation initiating factors are activated. This leads to cortical cell divisions and formation of nodule primordia. With some input from the *Rhizobium* symbiotic bacteria, this nodule will form a functional meristem. This provides the nodule with proliferating cells and produces a niche for the nitrogen-fixing symbiotic microbes. The pericyclic cells divide and eventually form vascular tissue which sustains the nodule (Crespi and Frugier, 2008; Hirsch et al., 1989; Oldroyd and Downie, 2008; Pate et al., 1969; Sprent and Embrapa, 1979).

Research on root nodule formation is extremely important not only agriculturally, but also for understanding plant developmental processes such as organogenesis and plant-microbe interactions. Cytokinin-induced stimulation of cortical cell proliferation has been observed in many plant species, such as alfalfa (*Medicago sativa*), *M. truncatula*, white clover (*Trifolium repens*), pea (*Pisum sativum*), and lotus (*L. japonicus*). When alfalfa (*M. sativa*) plants were inoculated with zeatin producing bacterial strains, normal nodules expressing early nodulation-related genes were formed (Cooper and Long, 1994). A few years later Bauer et al. (1996) showed that cytokinins induced plant responses that were similar to those caused by the microbial symbiont infection. The effect of cytokinin induction on

promoting the expression of early nodulation-related genes was confirmed in alfalfa by van Rhijn et al. (1998). They proposed that cytokinins can act as “the trigger for early nodulin gene induction in both nitrogen-fixing and mycorrhizal interactions.” Experiments with other leguminous plants yielded similar results. For instance, when white clover (*T. repens*) roots were treated with low concentrations of cytokinin, this was enough to induce cortical cell divisions, leading to nodule primordia formation in some plants (Mathesius et al., 2000). Lorteau et al. (2001) showed that low concentrations of exogenously applied cytokinin stimulated nodulation in peas (*P. sativum*). However, high-ck concentrations had the opposite effect and also reduced the LR numbers. The authors concluded that the inhibition of nodule and LR organogenesis happened due to stimulation of ethylene, a known inhibitor of nodulation. *L. japonicus* roots expressing *Arabidopsis* and *Zea mays* cytokinin degrading enzymes (*AtCKX2* and *ZmCKX1*, respectively) had significantly reduced numbers of root nodules (Lohar et al., 2004). Some plants failed to produce nodules altogether. Similarly, *M. truncatula* plants in which expression of the *CRE1* homologue *MtCRE1* was reduced using *RNAi* were impaired in both root nodule formation and frequency (Gonzalez-Rizzo et al., 2006). Reduction in cytokinin perception seemed to affect both IT progression and nodule formation. Even though the initiation of ITs was normal, growth terminated in the *RNAi* silenced root hairs and epidermis cells. Some trees such as alder (*Alnus glutinosa*) can also form nitrogen-fixing nodules. Rodriguez-Barrueco and Bermudez de Castro (1973) grew young alder roots *in vitro* and subjected them to exogenous cytokinin. Cytokinin-treated alders formed pseudonodules in their roots, indicating that ck can regulate nodule initiation and formation also in tree species.

In 2007 two labs published genetic evidence confirming the role of ck-mediated two-component signaling in controlling root nodulation in *L. japonicus*. Tirichine et al. (2007) isolated the *spontaneous nodule formation2* (*snf2*) mutant which displayed spontaneous nodule organogenesis. The mutation was cloned and shown to cause a dominant mutation in the *CRE1* homologue, *LHK1*. Murray et al. (2006) had already performed a genetic screen for suppressors of *har1*, a mutation which results in an excessive number of root nodules, and identified the *hyperinfected1* (*hit1*) mutant as a suppressor with low nodule number (Fig. 1.6E and F). In 2007, they demonstrated that *hit1* was a loss-of-function allele of *Lhk1* (Murray et al., 2007).

In the absence of a suitable microbe, *snf2* mutants develop rhizobia-free nodules which in terms of ontogeny and physiology, resemble normal rhizobia-induced nodules (Tirichine et al., 2007). When inoculated with a suitable microbe, the mutant plants were able to produce normal nitrogen-fixing nodules. The *snf2* mutation was located in the CHASE domain of the ck receptor *LHK1*. Using a similar *in vitro* assay that had

previously been used by Suzuki et al. (2001a) to confirm that *Arabidopsis* *CRE1* could act as a ck receptor, Tirichine and colleagues demonstrated that LHK1 was indeed a ck receptor, and that the *snf2* mutation caused two-component output at a level comparable to ck-induced LHK1.

The *hit1* mutants were susceptible to hyperinfection by the rhizobia but their progression was blocked between the epidermis and cortex resulting in significantly reduced nodulation (Murray et al., 2007). These phenotypes were striking when combined with the *har1* mutant, but fairly subtle in *hit1* alone. The authors employed a homologous yeast-based system (previously used by Inoue et al. (2001) and Maeda et al. (1994)) to show that LHK4 was a ck receptor, but when the *hit1* mutation was introduced it conferred cytokinin insensitivity. Consistent with this *hit1* mutant roots showed reduced sensitivity to exogenously applied cytokinin. The LHK1 homologues, LHK2 and LHK3, are also likely to act as ck receptors, which would explain the moderate phenotype of the *hit1* mutants. This idea is supported by data from Coba de la Peña et al. (2008) who showed that in lupin, expression of the *LaHK1* gene, homologous to *Arabidopsis* *AHK3*, is enriched in young root nodules.

It appears that an antagonistic relationship exists between nodule formation and LR initiation. Both of these processes involve initiation and formation of a meristem (from differentiated root cells), and thus require a dedifferentiation event to take place in specific tissues. Both pathways utilize the same components of the cytokinin signaling pathway. The evolutionary history between the nodule forming ability of plants and their interaction with nitrogenous soil rhizobia is still under investigation. It will be interesting to understand how the ck signaling pathway has been recruited to this role.

4. CONCLUDING REMARKS

Our knowledge of the core ck signaling pathway is fairly advanced based on numerous genetic and biochemical studies. However, some elements remain poorly understood. For some time, it was believed that the type-A ARRs acted as negative regulators of phosphorelay purely by competing with type-B ARRs to receive phospho groups. To et al. (2007) showed that this is not true. A version of *ARR7* in which the phospho-receiving site has been modified, such that it cannot be phosphorylated but mimics the phosphorylated form, is partially active. This suggests that phosphorylated type-A ARRs can regulate phosphorelay. This would involve an interaction either with other two-component signaling proteins or components as yet to be identified.

Genetic studies of the receptors, AHPs or ARRs have revealed that genetic redundancy is a common phenomenon. Large scale yeast-based

studies of the interactions between two-component proteins have shown that there is very little specificity between components (Dortay et al., 2006, 2008). For example, in yeast two-hybrid assays, any of the three receptors can interact with any of the AHPs tested (AHP1, 2, 3, and 5) (Dortay et al., 2006).

Cytokinin regulates many processes. In addition to those involved in development, it also regulates physiological responses, and is not only active in the root but in vegetative and reproductive tissues. One of the outstanding mysteries is how the specificity of cytokinin responses is determined. We have discussed how different receptors display different affinities to certain ck species. There is also evidence that certain type-A ARR_s execute tissue-specific roles, such as controlling circadian period and regulating the size of the shoot apical meristem (Leibfried et al., 2005; Salomé et al., 2006). One possibility is that this effect could be modulated by certain interactions being more preferable *in planta* due to specific cellular conditions. It could also be related to kinetics in a system where multiple components are competing for a limited number of phospho groups. Another possibility would be that auxiliary proteins are modulating cytokinin responses. This could potentially include integration with other hormonal signaling pathways, as shown by Dello Ioio et al. (2008) and Müller and Sheen (2008). Many of the processes described such as LR development, vascular development, and root nodulation are not only regulated by cytokinin, but also by other hormones.

An attractive challenge facing researchers is how to apply this knowledge into tangible improvements which can be made to crop plants. Our understanding of not only ck signaling but also biosynthesis and metabolism can provide several ways in which ck responses can be modified. Werner et al. (2008) have used grafting experiments to fuse a root stock constitutively expressing a cytokinin degrading enzyme and displaying increased root growth to a wild-type stock. They show that the increased root growth does not occur at the expense of shoot growth. This presents possibilities of generating crops with enhanced root networks. Such crops would offer environmental benefits such as greater fixation of carbon dioxide to the soil and resistance to drought and winds. Manipulation of secondary vascular growth offers possible improvements for root crops and forestry.

REFERENCES

- Aida, M., Beis, D., Heidstra, R., Willemsen, V., Blilou, I., Galinha, C., et al., 2004. The PLETHORA genes mediate patterning of the *Arabidopsis* root stem cell niche. *Cell* 119, 109–120.
- Aloni, R., Aloni, E., Langhans, M., Ullrich, C.I., 2006. Role of cytokinin and auxin in shaping root architecture: regulating vascular differentiation, lateral root initiation, root apical dominance and root gravitropism. *Ann. Bot. (Lond.)* 97, 883–893.

- Anantharaman, V., Aravind, L., 2001. The CHASE domain: a predicted ligand-binding module in plant cytokinin receptors and other eukaryotic and bacterial receptors. *Trends Biochem. Sci.* 26, 579–582.
- Argyros, R.D., Mathews, D.E., Chiang, Y.H., Palmer, C.M., Thibault, D.M., Etheridge, N., et al., 2008. Type B response regulators of *Arabidopsis* play key roles in cytokinin signaling and plant development. *Plant Cell* 20, 2102–2116.
- Asakura, Y., Hagino, T., Ohta, Y., Aoki, K., Yonekura-Sakakibara, K., Deji, A., et al., 2003. Molecular characterization of His-Asp phosphorelay signaling factors in maize leaves: implications of the signal divergence by cytokinin-inducible response regulators in the cytosol and the nuclei. *Plant Mol. Biol.* 52, 331–341.
- Baskin, T.I., Cork, A., Williamson, R.E., Gorst, J.R., 1995. STUNTED PLANT 1, a gene required for expansion in rapidly elongating but not in dividing cells and mediating root growth responses to applied cytokinin. *Plant Physiol.* 107, 233–243.
- Bauer, P., Ratet, P., Crespi, M.D., Schultze, M., Kondorosi, A., 1996. Nod factors and cytokinins induce similar cortical cell division, amyloplast deposition and msenod12a expression patterns in alfalfa roots. *Plant J.* 10, 91–105.
- Baum, S.F., Dubrovsky, J.G., Rost, T.L., 2002. Apical organization and maturation of the cortex and vascular cylinder in *Arabidopsis thaliana* (Brassicaceae) roots. *Am. J. Bot.* 89, 908–920.
- Beemster, G.T., Baskin, T.I., 2000. Stunted plant 1 mediates effects of cytokinin, but not of auxin, on cell division and expansion in the root of *Arabidopsis*. *Plant Physiol.* 124, 1718–1727.
- Bohner, S., Gatz, C., 2001. Characterisation of novel target promoters for the dexamethasone-inducible/tetracycline-repressible regulator TGV using luciferase and isopentenyl transferase as sensitive reporter genes. *Mol. Gen. Genet.* 264, 860–870.
- Brandstatter, I., Kieber, J.J., 1998. Two genes with similarity to bacterial response regulators are rapidly and specifically induced by cytokinin in *Arabidopsis*. *Plant Cell* 10, 1009–1019.
- Brenner, W.G., Romanov, G.A., Kollmer, I., Burkle, L., Schmullig, T., 2005. Immediate-early and delayed cytokinin response genes of *Arabidopsis thaliana* identified by genome-wide expression profiling reveal novel cytokinin-sensitive processes and suggest cytokinin action through transcriptional cascades. *Plant J.* 44, 314–333.
- Bürkle, L., Cedzich, A., Dopke, C., Stransky, H., Okumoto, S., Gillissen, B., et al., 2003. Transport of cytokinins mediated by purine transporters of the PUP family expressed in phloem, hydathodes, and pollen of *Arabidopsis*. *Plant J.* 34, 13–26.
- Celenza, J.L. Jr., Grisafi, P.L., Fink, G.R., 1995. A pathway for lateral root formation in *Arabidopsis thaliana*. *Genes Dev.* 9, 2131–2142.
- Chaffey, N., Cholewa, E., Regan, S., Sundberg, B., 2002. Secondary xylem development in *Arabidopsis*: a model for wood formation. *Physiol. Plant* 114, 594–600.
- Chevalier, F., Perazza, D., Laporte, F., Le Henanff, G., Hornitschek, P., Bonneville, J.M., et al., 2008. Gebp and gebp-like proteins are noncanonical leucine-zipper transcription factors that regulate cytokinin response in *Arabidopsis*. *Plant Physiol.* 146, 1142–1154.
- Coba de la Pena, T., Carcamo, C.B., Almonacid, L., Zaballos, A., Lucas, M.M., Balomenos, D., et al., 2008. A cytokinin receptor homologue is induced during root nodule organogenesis and senescence in *Lupinus albus* L. *Plant Physiol. Biochem.* 46, 219–225.
- Cooper, J.B., Long, S.R., 1994. Morphogenetic rescue of *Rhizobium meliloti* nodulation mutants by *trans*-zeatin secretion. *Plant Cell* 6, 215–225.
- Crespi, M., Frugier, F., 2008. *De novo* organ formation from differentiated cells: root nodule organogenesis. *Sci. Signal.* 1, re11.
- Curaba, J., Herzog, M., Vachon, G., 2003. Gebp, the first member of a new gene family in *Arabidopsis*, encodes a nuclear protein with DNA-binding activity and is regulated by KNAT1. *Plant J.* 33, 305–317.

- D'Agostino, I.B., Deruere, J., Kieber, J.J., 2000. Characterization of the response of the *Arabidopsis* response regulator gene family to cytokinin. *Plant Physiol.* 124, 1706–1717.
- de Leon, B.G., Zorrilla, J.M., Rubio, V., Dahiya, P., Paz-Ares, J., Leyva, A., 2004. Interallelic complementation at the *Arabidopsis* *CRE1* locus uncovers independent pathways for the proliferation of vascular initials and canonical cytokinin signalling. *Plant J.* 38, 70–79.
- Dello Ioio, R., Linhares, F.S., Scacchi, E., Casamitjana-Martinez, E., Heidstra, R., Costantino, P., et al., 2007. Cytokinins determine *Arabidopsis* root-meristem size by controlling cell differentiation. *Curr. Biol.* 17, 678–682.
- Dello Ioio, R., Nakamura, K., Moubayidin, L., Perilli, S., Taniguchi, M., Morita, M.T., et al., 2008. A genetic framework for the control of cell division and differentiation in the root meristem. *Science* 322, 1380–1384.
- Dolan, L., Janmaat, K., Willemsen, V., Linstead, P., Poethig, S., Roberts, K., et al., 1993. Cellular organisation of the *Arabidopsis thaliana* root. *Development* 119, 71–84.
- Dortay, H., Mehnert, N., Burkle, L., Schmulling, T., Heyl, A., 2006. Analysis of protein interactions within the cytokinin-signaling pathway of *Arabidopsis thaliana*. *FEBS J.* 273, 4631–4644.
- Dortay, H., Gruhn, N., Pfeifer, A., Schwerdtner, M., Schmulling, T., Heyl, A., 2008. Toward an interaction map of the two-component signaling pathway of *Arabidopsis thaliana*. *J. Proteome Res.* 7, 3649–3660.
- Du, L., Jiao, F., Chu, J., Jin, G., Chen, M., Wu, P., 2007. The two-component signal system in rice (*Oryza sativa* L.): a genome-wide study of cytokinin signal perception and transduction. *Genomics* 89, 697–707.
- Dubrovsky, J.G., Doerner, P.W., Colon-Carmona, A., Rost, T.L., 2000. Pericycle cell proliferation and lateral root initiation in *Arabidopsis*. *Plant Physiol.* 124, 1648–1657.
- Faiss, M., Zalubilova, J., Strnad, M., Schmulling, T., 1997. Conditional transgenic expression of the *ipt* gene indicates a function for cytokinins in paracrine signaling in whole tobacco plants. *Plant J.* 12, 401–415.
- Friml, J., Benkova, E., Blilou, I., Wisniewska, J., Hamann, T., Ljung, K., et al., 2002. Atpin4 mediates sink-driven auxin gradients and root patterning in *Arabidopsis*. *Cell* 108, 661–673.
- Friml, J., Vieten, A., Sauer, M., Weijers, D., Schwarz, H., Hamann, T., et al., 2003. Efflux-dependent auxin gradients establish the apical-basal axis of *Arabidopsis*. *Nature* 426, 147–153.
- Gonzalez-Rizzo, S., Crespi, M., Frugier, F., 2006. The *Medicago truncatula* *CRE1* cytokinin receptor regulates lateral root development and early symbiotic interaction with *Sinorhizobium meliloti*. *Plant Cell* 18, 2680–2693.
- Haberlandt, G., 1913. Zur Physiologie der Zellteilungen. *Sitzungsber. K. Preuss Akad. Wiss.* 318–345.
- Hanano, S., Domagalska, M.A., Nagy, F., Davis, S.J., 2006. Multiple phytohormones influence distinct parameters of the plant circadian clock. *Genes Cells* 11, 1381–1392.
- Hertzberg, M., Aspeborg, H., Schrader, J., Andersson, A., Erlandsson, R., Blomqvist, K., et al., 2001. A transcriptional roadmap to wood formation. *Proc. Natl. Acad. Sci. USA* 98, 14732–14737.
- Heyl, A., Wulfetange, K., Pils, B., Nielsen, N., Romanov, G.A., Schmulling, T., 2007. Evolutionary proteomics identifies amino acids essential for ligand-binding of the cytokinin receptor CHASE domain. *BMC Evol. Biol.* 7, 62.
- Higuchi, M., Pischke, M.S., Mähönen, A.P., Miyawaki, K., Hashimoto, Y., Seki, M., et al., 2004. *In planta* functions of the *Arabidopsis* cytokinin receptor family. *Proc. Natl. Acad. Sci. USA* 101, 8821–8826.
- Hirose, N., Makita, N., Kojima, M., Kamada-Nobusada, T., Sakakibara, H., 2007. Overexpression of a type-A response regulator alters rice morphology and cytokinin metabolism. *Plant Cell Physiol.* 48, 523–539.

- Hirsch, M., Bhuvaneswari, T.V., Torrey, J.G., Bisseling, T., 1989. Early nodulin genes are induced in alfalfa root outgrowths elicited by auxin transport inhibitors. *Proc. Natl. Acad. Sci. USA* 86, 1244–1248.
- Hosoda, K., Imamura, A., Katoh, E., Hatta, T., Tachiki, M., Yamada, H., et al., 2002. Molecular structure of the GARP family of plant Myb-related DNA binding motifs of the *Arabidopsis* response regulators. *Plant Cell* 14, 2015–2029.
- Houba-Hérin, N., Pethe, C., d'Alayer, J., Laloue, M., 1999. Cytokinin oxidase from *Zea mays*: purification, cDNA cloning and expression in moss protoplasts. *Plant J.* 17, 615–626.
- Hutchison, C.E., Li, J., Argueso, C., Gonzalez, M., Lee, E., Lewis, M.W., et al., 2006. The *Arabidopsis* histidine phosphotransfer proteins are redundant positive regulators of cytokinin signaling. *Plant Cell* 18, 3073–3087.
- Hwang, I., Sheen, J., 2001. Two-component circuitry in *Arabidopsis* cytokinin signal transduction. *Nature* 413, 383–389.
- Hwang, I., Chen, H.C., Sheen, J., 2002. Two-component signal transduction pathways in *Arabidopsis*. *Plant Physiol.* 129, 500–515.
- Imamura, A., Hanaki, N., Umeda, H., Nakamura, A., Suzuki, T., Ueguchi, C., et al., 1998. Response regulators implicated in His-to-Asp phosphotransfer signaling in *Arabidopsis*. *Proc. Natl. Acad. Sci. USA* 95, 2691–2696.
- Imamura, A., Hanaki, N., Nakamura, A., Suzuki, T., Taniguchi, M., Kiba, T., et al., 1999. Compilation and characterization of *Arabidopsis thaliana* response regulators implicated in His-Asp phosphorelay signal transduction. *Plant Cell Physiol.* 40, 733–742.
- Imamura, A., Yoshino, Y., Mizuno, T., 2001. Cellular localization of the signaling components of *Arabidopsis* His-to-Asp phosphorelay. *Biosci. Biotechnol. Biochem.* 65, 2113–2117.
- Imamura, A., Kiba, T., Tajima, Y., Yamashino, T., Mizuno, T., 2003. *In vivo* and *in vitro* characterization of the ARR11 response regulator implicated in the His-to-Asp phosphorelay signal transduction in *Arabidopsis thaliana*. *Plant Cell Physiol.* 44, 122–131.
- Inoue, T., Higuchi, M., Hashimoto, Y., Seki, M., Kobayashi, M., Kato, T., et al., 2001. Identification of *CRE1* as a cytokinin receptor from *Arabidopsis*. *Nature* 409, 1060–1063.
- Ishida, K., Yamashino, T., Yokoyama, A., Mizuno, T., 2008. Three type-B response regulators, ARR1, ARR10 and ARR12, play essential but redundant roles in cytokinin signal transduction throughout the life cycle of *Arabidopsis thaliana*. *Plant Cell Physiol.* 49, 47–57.
- Ito, Y., Kurata, N., 2006. Identification and characterization of cytokinin-signalling gene families in rice. *Gene* 382, 57–65.
- Jiang, K., Feldman, L.J., 2005. Regulation of root apical meristem development. *Annu. Rev. Cell Dev. Biol.* 21, 485–509.
- Kakimoto, T., 1996. CKI1, a histidine kinase homolog implicated in cytokinin signal transduction. *Science* 274, 982–985.
- Kamboj, J.S., Blake, P.S., Baker, D.A., 1998. Cytokinins in the vascular saps of *Ricinus communis*. *Plant Growth Regul.* 25, 123–126.
- Kiba, T., Taniguchi, M., Imamura, A., Ueguchi, C., Mizuno, T., Sugiyama, T., 1999. Differential expression of genes for response regulators in response to cytokinins and nitrate in *Arabidopsis thaliana*. *Plant Cell Physiol.* 40, 767–771.
- Kiba, T., Yamada, H., Mizuno, T., 2002. Characterization of the ARR15 and ARR16 response regulators with special reference to the cytokinin signaling pathway mediated by the AHK4 histidine kinase in roots of *Arabidopsis thaliana*. *Plant Cell Physiol.* 43, 1059–1066.
- Kiba, T., Yamada, H., Sato, S., Kato, T., Tabata, S., Yamashino, T., et al., 2003. The type-A response regulator, ARR15, acts as a negative regulator in the cytokinin-mediated signal transduction in *Arabidopsis thaliana*. *Plant Cell Physiol.* 44, 868–874.
- Kiba, T., Aoki, K., Sakakibara, H., Mizuno, T., 2004. *Arabidopsis* response regulator, ARR22, ectopic expression of which results in phenotypes similar to the wol cytokinin-receptor mutant. *Plant Cell Physiol.* 45, 1063–1077.

- Kiba, T., Naitou, T., Koizumi, N., Yamashino, T., Sakakibara, H., Mizuno, T., 2005. Combinatorial microarray analysis revealing *Arabidopsis* genes implicated in cytokinin responses through the His \rightarrow Asp phosphorelay circuitry. *Plant Cell Physiol.* 46, 339–355.
- Kim, H.J., Ryu, H., Hong, S.H., Woo, H.R., Lim, P.O., Lee, I.C., et al., 2006. Cytokinin-mediated control of leaf longevity by AHK3 through phosphorylation of ARR2 in *Arabidopsis*. *Proc. Natl. Acad. Sci. USA* 103, 814–819.
- Kuderova, A., Urbankova, I., Valkova, M., Malbeck, J., Brzobohaty, B., Nemethova, D., et al., 2008. Effects of conditional IPT-dependent cytokinin overproduction on root architecture of *Arabidopsis* seedlings. *Plant Cell Physiol.* 49, 570–582.
- Kurakawa, T., Ueda, N., Maekawa, M., Kobayashi, K., Kojima, M., Nagato, Y., et al., 2007. Direct control of shoot meristem activity by a cytokinin-activating enzyme. *Nature* 445, 652–655.
- Kuroha, T., Kato, H., Asami, T., Yoshida, S., Kamada, H., Satoh, S., 2002. A *trans*-zeatin riboside in root xylem sap negatively regulates adventitious root formation on cucumber hypocotyls. *J. Exp. Bot.* 53, 2193–2200.
- Kuroha, T., Ueguchi, C., Sakakibara, H., Satoh, S., 2006. Cytokinin receptors are required for normal development of auxin-transporting vascular tissues in the hypocotyl but not in adventitious roots. *Plant Cell Physiol.* 47, 234–243.
- Laplaze, L., Benkova, E., Casimiro, I., Maes, L., Vanneste, S., Swarup, R., et al., 2007. Cytokinins act directly on lateral root founder cells to inhibit root initiation. *Plant Cell* 19, 3889–3900.
- Laskowski, M.J., Williams, M.E., Nusbaum, H.C., Sussex, I.M., 1995. Formation of lateral root meristems is a two-stage process. *Development* 121, 3303–3310.
- Laskowski, M., Grieneisen, V.A., Hofhuis, H., Hove, C.A., Hogeweg, P., Maree, A.F., et al., 2008. Root system architecture from coupling cell shape to auxin transport. *PLoS Biol.* 6, e307.
- Laux, T., 2003. The stem cell concept in plants: a matter of debate. *Cell* 113, 281–283.
- Lee, D.J., Park, J.Y., Ku, S.J., Ha, Y.M., Kim, S., Kim, M.D., et al., 2007. Genome-wide expression profiling of *Arabidopsis* response regulator 7 (ARR7) overexpression in cytokinin response. *Mol. Genet. Genomics* 277, 115–137.
- Lee, D.J., Kim, S., Ha, Y.M., Kim, J., 2008. Phosphorylation of *Arabidopsis* response regulator 7 (ARR7) at the putative phospho-accepting site is required for ARR7 to act as a negative regulator of cytokinin signaling. *Planta* 227, 577–587.
- Leibfried, A., To, J.P., Busch, W., Stehling, S., Kehle, A., Demar, M., et al., 2005. WUSCHEL controls meristem function by direct regulation of cytokinin-inducible response regulators. *Nature* 438, 1172–1175.
- Li, X., Mo, X., Shou, H., Wu, P., 2006. Cytokinin-mediated cell cycling arrest of pericycle founder cells in lateral root initiation of *Arabidopsis*. *Plant Cell Physiol.* 47, 1112–1123.
- Lohar, D.P., Schaff, J.E., Laskey, J.G., Kieber, J.J., Bilyeu, K.D., Bird, D.M., 2004. Cytokinins play opposite roles in lateral root formation, and nematode and Rhizobial symbioses. *Plant J.* 38, 203–214.
- Lohrmann, J., Buchholz, G., Keitel, C., Sweere, U., Kircher, S., Bäurle, I., et al., 1999. Differential expression and nuclear localization of response regulator-like proteins from *Arabidopsis thaliana*. *Plant Biol.* 1, 495–505.
- Lohrmann, J., Sweere, U., Zabaleta, E., Bäurle, I., Keitel, C., Kozma-Bognar, L., et al., 2001. The response regulator ARR2: a pollen-specific transcription factor involved in the expression of nuclear genes for components of mitochondrial complex I in *Arabidopsis*. *Mol. Genet. Genomics* 265, 2–13.
- Lorteau, M.A., Ferguson, B.J., Guinel, F.C., 2001. Effects of cytokinin on ethylene production and nodulation in pea (*Pisum sativum*) cv. Sparkle. *Physiol. Plant* 112, 421–428.
- Maeda, T., Wurgler-Murphy, S.M., Saito, H., 1994. A two-component system that regulates an osmosensing MAP kinase cascade in yeast. *Nature* 369, 242–245.

- Mähönen, A.P., Bonke, M., Kauppinen, L., Riikonen, M., Benfey, P.N., Helariutta, Y., 2000. A novel two-component hybrid molecule regulates vascular morphogenesis of the *Arabidopsis* root. *Genes Dev.* 14, 2938–2943.
- Mähönen, A.P., Bishopp, A., Higuchi, M., Nieminen, K.M., Kinoshita, K., Tormakangas, K., et al., 2006a. Cytokinin signaling and its inhibitor AHP6 regulate cell fate during vascular development. *Science* 311, 94–98.
- Mähönen, A.P., Higuchi, M., Törmäkangas, K., Miyawaki, K., Pischke, M.S., Sussman, M.R., et al., 2006b. Cytokinins regulate a bidirectional phosphorelay network in *Arabidopsis*. *Curr. Biol.* 16, 1116–1122.
- Malamy, J.E., Benfey, P.N., 1997. Organization and cell differentiation in lateral roots of *Arabidopsis thaliana*. *Development* 124, 33–44.
- Malamy, J.E., Ryan, K.S., 2001. Environmental regulation of lateral root initiation in *Arabidopsis*. *Plant Physiol.* 127, 899–909.
- Marina, A., Waldburger, C.D., Hendrickson, W.A., 2005. Structure of the entire cytoplasmic portion of a sensor histidine-kinase protein. *EMBO J.* 24, 4247–4259.
- Marsh, J.F., Rakocevic, A., Mitra, R.M., Brocard, L., Sun, J., Eschstruth, A., et al., 2007. *Medicago truncatula* NIN is essential for Rhizobial-independent nodule organogenesis induced by autoactive calcium/calmodulin-dependent protein kinase1. *Plant Physiol.* 144, 324–335.
- Mason, M.G., Li, J., Mathews, D.E., Kieber, J.J., Schaller, G.E., 2004. Type-B response regulators display overlapping expression patterns in *Arabidopsis*. *Plant Physiol.* 135, 927–937.
- Mason, M.G., Mathews, D.E., Argyros, D.A., Maxwell, B.B., Kieber, J.J., Alonso, J.M., et al., 2005. Multiple type-B response regulators mediate cytokinin signal transduction in *Arabidopsis*. *Plant Cell* 17, 3007–3018.
- Mathesius, U., Charon, C., Rolfe, B.G., Kondorosi, A., Crespi, M., 2000. Temporal and spatial order of events during the induction of cortical cell divisions in white clover by *Rhizobium leguminosarum* bv. *Trifolii* inoculation or localized cytokinin addition. *Mol. Plant Microbe Interact.* 13, 617–628.
- Matsumoto-Kitano, M., Kusumoto, T., Tarkowski, P., Kinoshita-Tsujimura, K., Vaclavikova, K., Miyawaki, K., et al., 2008. Cytokinins are central regulators of cambial activity. *Proc. Natl. Acad. Sci. USA* 105, 20027–20031.
- Miller, C., Skoog, F., von Saltza, M.H., Strong, F.M., 1956. Kinetin, a cell division factor from deoxyribonucleic acid. *J. Am. Chem. Soc.* 77, 1392.
- Miwa, K., Ishikawa, K., Terada, K., Yamada, H., Suzuki, T., Yamashino, T., et al., 2007. Identification of amino acid substitutions that render the *Arabidopsis* cytokinin receptor histidine kinase AHK4 constitutively active. *Plant Cell Physiol.* 48, 1809–1814.
- Miyata, S., Urao, T., Yamaguchi-Shinozaki, K., Shinozaki, K., 1998. Characterization of genes for two-component phosphorelay mediators with a single hpt domain in *Arabidopsis thaliana*. *FEBS Lett.* 437, 11–14.
- Miyawaki, K., Matsumoto-Kitano, M., Kakimoto, T., 2004. Expression of cytokinin biosynthetic isopentenyltransferase genes in *Arabidopsis*: tissue specificity and regulation by auxin, cytokinin, and nitrate. *Plant J.* 37, 128–138.
- Miyawaki, K., Tarkowski, P., Matsumoto-Kitano, M., Kato, T., Sato, S., Tarkowska, D., et al., 2006. Roles of *Arabidopsis* ATP/ADP isopentenyltransferases and trna isopentenyltransferases in cytokinin biosynthesis. *Proc. Natl. Acad. Sci. USA* 103, 16598–16603.
- Mizuno, T., Nakamichi, N., 2005. Pseudo-response regulators (prrs) or true oscillator components (tocs). *Plant Cell Physiol.* 46, 677–685.
- Mockaitis, K., Estelle, M., 2008. Auxin receptors and plant development: a new signaling paradigm. *Annu. Rev. Cell Dev. Biol.* 24, 55–80.
- Mok, W.S., Mok, M.C., 1994. *Cytokinins: Chemistry, Activity and Function*. CRC Press, Boca Raton, Florida.

- Morris, R.O., Bilyeu, K.D., Laskey, J.G., Cheikh, N.N., 1999. Isolation of a gene encoding a glycosylated cytokinin oxidase from maize. *Biochem. Biophys. Res. Commun.* 255, 328–333.
- Mougel, C., Zhulin, I.B., 2001. CHASE: an extracellular sensing domain common to transmembrane receptors from prokaryotes, lower eukaryotes and plants. *Trends Biochem. Sci.* 26, 582–584.
- Müller, B., Sheen, J., 2008. Cytokinin and auxin interaction in root stem-cell specification during early embryogenesis. *Nature* 453, 1094–1097.
- Murray, J., Karas, B., Ross, L., Brachmann, A., Wagg, C., Geil, R., et al., 2006. Genetic suppressors of the *Lotus japonicus* har1–1 hypermodulation phenotype. *Mol. Plant Microbe Interact.* 19, 1082–1091.
- Murray, J.D., Karas, B.J., Sato, S., Tabata, S., Amyot, L., Szczygłowski, K., 2007. A cytokinin perception mutant colonized by *Rhizobium* in the absence of nodule organogenesis. *Science* 315, 101–104.
- Nibau, C., Gibbs, D.J., Coates, J.C., 2008. Branching out in new directions: the control of root architecture by lateral root formation. *New Phytol.* 179, 595–614.
- Nieminen, K., Immanen, J., Laxell, M., Kauppinen, L., Tarkowski, P., Dolezal, K., et al., 2008. Cytokinin signaling regulates cambial development in poplar. *Proc. Natl. Acad. Sci. USA* 105, 20032–20037.
- Nishimura, C., Ohashi, Y., Sato, S., Kato, T., Tabata, S., Ueguchi, C., 2004. Histidine kinase homologs that act as cytokinin receptors possess overlapping functions in the regulation of shoot and root growth in *Arabidopsis*. *Plant Cell* 16, 1365–1377.
- Oldroyd, G.E., Downie, J.A., 2008. Coordinating nodule morphogenesis with rhizobial infection in legumes. *Annu. Rev. Plant Biol.* 59, 519–546.
- Osakabe, Y., Miyata, S., Urao, T., Seki, M., Shinozaki, K., Yamaguchi-Shinozaki, K., 2002. Overexpression of *Arabidopsis* response regulators, ARR4/ATRR1/IBC7 and ARR8/ATRR3, alters cytokinin responses differentially in the shoot and in callus formation. *Biochem. Biophys. Res. Commun.* 293, 806–815.
- Paces, V., Werstiuk, E., Hall, R.H., 1971. Conversion of N⁶-(2-isopentenyl) adenoside to adenosine by enzyme activity in tobacco tissue. *Plant Physiol.* 48, 775–778.
- Papon, N., Vansiri, A., Gantet, P., Chenieux, J.C., Rideau, M., Creche, J., 2004. Histidine-containing phosphotransfer domain extinction by RNA interference turns off a cytokinin signalling circuitry in *Catharanthus roseus* suspension cells. *FEBS Lett.* 558, 85–88.
- Pareek, A., Singh, A., Kumar, M., Kushwaha, H.R., Lynn, A.M., Singla-Pareek, S.L., 2006. Whole-genome analysis of *Oryza sativa* reveals similar architecture of two-component signaling machinery with *Arabidopsis*. *Plant Physiol.* 142, 380–397.
- Parizot, B., Laplace, L., Boucheron-Dubuisson, E., Bayle, V., Bonke, M., De Smet, I., et al., 2008. Diarch symmetry of the vascular bundle in *Arabidopsis* root encompasses the pericycle and is reflected in distich lateral root initiation. *Plant Physiol.* 146, 140–148.
- Pas, J., von Grotthuss, M., Wyrwicz, L.S., Rychlewski, L., Barciszewski, J., 2004. Structure prediction, evolution and ligand interaction of CHASE domain. *FEBS Lett.* 576, 287–290.
- Pate, J.S., Gunning, B.E.S., Briarty, L.G., 1969. Ultrastructure and functioning of the transport system of the leguminous root nodule. *Planta* 85, 11–34.
- Rani Debi, B., Taketa, S., Ichii, M., 2005. Cytokinin inhibits lateral root initiation but stimulates lateral root elongation in rice (*Oryza sativa*). *J. Plant Physiol.* 162, 507–515.
- Rashotte, A.M., Carson, S.D., To, J.P., Kieber, J.J., 2003. Expression profiling of cytokinin action in *Arabidopsis*. *Plant Physiol.* 132, 1998–2011.
- Rashotte, A.M., Mason, M.G., Hutchison, C.E., Ferreira, F.J., Schaller, G.E., Kieber, J.J., 2006. A subset of *Arabidopsis* AP2 transcription factors mediates cytokinin responses in concert with a two-component pathway. *Proc. Natl. Acad. Sci. USA* 103, 11081–11085.
- Rhijn, P., Goldberg, R.B., Hirsch, A.M., 1998. *Lotus corniculatus* nodulation specificity is changed by the presence of a soybean lectin gene. *Plant Cell* 10, 1233–1250.

- Riefler, M., Novak, O., Strnad, M., Schmulling, T., 2006. *Arabidopsis* cytokinin receptor mutants reveal functions in shoot growth, leaf senescence, seed size, germination, root development, and cytokinin metabolism. *Plant Cell* 18, 40–54.
- Rodriguez-Barrueco, C., Bermudez de Castro, F., 1973. Cytokinin-induced pseudonodules on *Alnus glutinosa*. *Physiol. Plant.* 29, 277–280.
- Romanov, G.A., Lomin, S.N., Schmulling, T., 2006. Biochemical characteristics and ligand-binding properties of *Arabidopsis* cytokinin receptor AHK3 compared to *CRE1/AHK4* as revealed by a direct binding assay. *J. Exp. Bot.* 57, 4051–4058.
- Sabatini, S., Beis, D., Wolkenfelt, H., Murfett, J., Guilfoyle, T., Malamy, J., et al., 1999. An auxin-dependent distal organizer of pattern and polarity in the *Arabidopsis* root. *Cell* 99, 463–472.
- Sabatini, S., Heidstra, R., Wildwater, M., Scheres, B., 2003. SCARECROW is involved in positioning the stem cell niche in the *Arabidopsis* root meristem. *Genes Dev.* 17, 354–358.
- Saito, H., 2001. Histidine phosphorylation and two-component signaling in eukaryotic cells. *Chem. Rev.* 101, 2497–2509.
- Sakai, H., Aoyama, T., Bono, H., Oka, A., 1998. Two-component response regulators from *Arabidopsis thaliana* contain a putative DNA-binding motif. *Plant Cell Physiol.* 39, 1232–1239.
- Sakai, H., Aoyama, T., Oka, A., 2000. *Arabidopsis* ARR1 and ARR2 response regulators operate as transcriptional activators. *Plant J.* 24, 703–711.
- Sakai, H., Honma, T., Aoyama, T., Sato, S., Kato, T., Tabata, S., et al., 2002. ARR1, a transcription factor for genes immediately responsive to cytokinins. *Science* 16, 1519–1521.
- Sakakibara, H., Hayakawa, A., Deji, A., Gawronski, S.W., Sugiyama, T., 1999. His-Asp phosphotransfer possibly involved in the nitrogen signal transduction mediated by cytokinin in maize: molecular cloning of cdnas for two-component regulatory factors and demonstration of phosphotransfer activity *in vitro*. *Plant Mol. Biol.* 41, 563–573.
- Sakakibara, H., 2006. Cytokinins: activity, biosynthesis, and translocation. *Ann. Rev. Plant Biol.* 57, 431–449.
- Salomé, P.A., To, J.P., Kieber, J.J., McClung, C.R., 2006. *Arabidopsis* response regulators ARR3 and ARR4 play cytokinin-independent roles in the control of circadian period. *Plant Cell* 18, 55–69.
- Schauser, L., Roussis, A., Stiller, J., Stougaard, J., 1999. A plant regulator controlling development of symbiotic root nodules. *Nature* 402, 191–195.
- Scheres, B., Wolkenfelt, H., Willemsen, V., Terlouw, M., Lawson, E., Dean, C., et al., 1994. Embryonic origin of the *Arabidopsis* primary root and root meristem initials. *Development* 120, 2475–2477.
- Scheres, B., Di Laurenzio, L., Willemsen, V., Hauser, M.T., Janmaat, K., Weisbeek, P., et al., 1995. Mutations affecting the radial organisation of the *Arabidopsis* root display specific defects throughout the embryonic axis. *Development* 121, 53–62.
- Schmülling, T., Werner, T., Riefler, M., Krupkova, E., Bartrina, Y., Manns, I., 2003. Structure and function of cytokinin oxidase/dehydrogenase genes of maize, rice, *Arabidopsis* and other species. *J. Plant Res.* 116, 241–252.
- Schrader, J., Moyle, R., Bhalerao, R., Hertzberg, M., Lundeberg, J., Nilsson, P., et al., 2004. Cambial meristem dormancy in trees involves extensive remodelling of the transcriptome. *Plant J.* 40, 173–187.
- Schultze, M., Kondorosí, A., 1998. Regulation of symbiotic root nodule development. *Annu. Rev. Genet.* 32, 33–57.
- Smet, I., Vanneste, S., Inzé, D., Beeckman, T., 2006. Lateral root initiation or the birth of a new meristem. *Plant Mol. Biol.* 60, 871–887.

- Spíchal, L., Rakova, N.Y., Riefler, M., Mizuno, T., Romanov, G.A., Strnad, M., et al., 2004. Two cytokinin receptors of *Arabidopsis thaliana*, *CRE1/AHK4* and *AHK3*, differ in their ligand specificity in a bacterial assay. *Plant Cell Physiol.* 45, 1299–1305.
- Spíchal, L., Werner, T., Popa, I., Riefler, M., Schmullig, T., Strnad, M., 2009. The purine derivative PI-55 blocks cytokinin action via receptor inhibition. *FEBS J.* 276, 244–253.
- Sprent, J.I., Embrapa, J.I., 1979. Root nodule anatomy, type of export product and evolutionary origin in some Leguminosae. *Plant Cell Environ.* 3, 35–43.
- Stock, A.M., Robinson, V.L., Goudreau, P.N., 2000. Two-component signal transduction. *Annu. Rev. Biochem.* 69, 183–215.
- Suzuki, T., Imamura, A., Ueguchi, C., Mizuno, T., 1998. Histidine-containing phosphotransfer (hpt) signal transducers implicated in His-to-Asp phosphorelay in *Arabidopsis*. *Plant Cell Physiol.* 39, 1258–1268.
- Suzuki, T., Miwa, K., Ishikawa, K., Yamada, H., Aiba, H., Mizuno, T., 2001a. The *Arabidopsis* sensor His-kinase, *ahk4*, can respond to cytokinins. *Plant Cell Physiol.* 42, 107–113.
- Suzuki, T., Sakurai, K., Ueguchi, C., Mizuno, T., 2001b. Two types of putative nuclear factors that physically interact with histidine-containing phosphotransfer (Hpt) domains, signaling mediators in His-to-Asp phosphorelay, in *Arabidopsis thaliana*. *Plant Cell Physiol.* 42, 37–45.
- Suzuki, T., Ishikawa, K., Yamashino, T., Mizuno, T., 2002. An *Arabidopsis* histidine-containing phosphotransfer (hpt) factor implicated in phosphorelay signal transduction: overexpression of AHP2 in plants results in hypersensitiveness to cytokinin. *Plant Cell Physiol.* 43, 123–129.
- Tajima, Y., Imamura, A., Kiba, T., Amano, Y., Yamashino, T., Mizuno, T., 2004. Comparative studies on the type-B response regulators revealing their distinctive properties in the His-to-Asp phosphorelay signal transduction of *Arabidopsis thaliana*. *Plant Cell Physiol.* 45, 28–39.
- Tanaka, Y., Suzuki, T., Yamashino, T., Mizuno, T., 2004. Comparative studies of the AHP histidine-containing phosphotransmitters implicated in His-to-Asp phosphorelay in *Arabidopsis thaliana*. *Biosci. Biotechnol. Biochem.* 68, 462–465.
- Taniguchi, M., Kiba, T., Sakakibara, H., Ueguchi, C., Mizuno, T., Sugiyama, T., 1998. Expression of *Arabidopsis* response regulator homologs is induced by cytokinins and nitrate. *FEBS Lett.* 429, 259–262.
- Taniguchi, M., Sasaki, N., Tsuge, T., Aoyama, T., Oka, A., 2007. ARR1 directly activates cytokinin response genes that encode proteins with diverse regulatory functions. *Plant Cell Physiol.* 48, 263–277.
- Tirichine, L., Sandal, N., Madsen, L.H., Radutoiu, S., Albrektsen, A.S., Sato, S., et al., 2007. A gain-of-function mutation in a cytokinin receptor triggers spontaneous root nodule organogenesis. *Science* 315, 104–107.
- To, J.P., Kieber, J.J., 2008. Cytokinin signaling: two-components and more. *Trends Plant Sci.* 13, 85–92.
- To, J.P., Haberer, G., Ferreira, F.J., Deruere, J., Mason, M.G., Schaller, G.E., et al., 2004. Type-A *Arabidopsis* response regulators are partially redundant negative regulators of cytokinin signaling. *Plant Cell* 16, 658–671.
- To, J.P., Deruere, J., Maxwell, B.B., Morris, V.F., Hutchison, C.E., Ferreira, F.J., et al., 2007. Cytokinin regulates type-A *Arabidopsis* response regulator activity and protein stability via two-component phosphorelay. *Plant Cell* 19, 3901–3914.
- Ueguchi, C., Koizumi, H., Suzuki, T., Mizuno, T., 2001a. Novel family of sensor histidine kinase genes in *Arabidopsis thaliana*. *Plant Cell Physiol.* 42, 231–235.
- Ueguchi, C., Sato, S., Kato, T., Tabata, S., 2001b. The *AHK4* gene involved in the cytokinin-signaling pathway as a direct receptor molecule in *Arabidopsis thaliana*. *Plant Cell Physiol.* 42, 751–755.

- Ulmasov, T., Hagen, G., Guilfoyle, T.J., 1999. Dimerization and DNA binding of auxin response factors. *Plant J.* 19, 309–319.
- van den Berg, C., Willemsen, V., Hage, W., Weisbeek, P., Scheres, B., 1995. Cell fate in the *Arabidopsis* root meristem determined by directional signalling. *Nature* 378, 62–65.
- van den Berg, C., Willemsen, V., Hendriks, G., Weisbeek, P., Scheres, B., 1997. Short-range control of cell differentiation in the *Arabidopsis* root meristem. *Nature* 390, 287–289.
- Werner, T., Motyka, V., Lancou, L., Smets, R., van Onckelen, H., Schmülling, T., 2003. Cytokinin-deficient transgenic *Arabidopsis* plants show multiple developmental alterations indicating opposite functions of cytokinins in the regulation of shoot and root meristem activity. *Plant Cell* 15, 2532–2550.
- Werner, T., Holst, K., Pors, Y., Guivarc'h, A., Mustroph, A., Chriqui, D., et al., 2008. Cytokinin deficiency causes distinct changes of sink and source parameters in tobacco shoots and roots. *J. Exp. Bot.* 59, 2659–2672.
- Wurgler-Murphy, S.M., Saito, H., 1997. Two-component signal transducers and MAPK cascades. *Trends Biochem. Sci.* 22, 172–176.
- Yamada, H., Suzuki, T., Terada, K., Takei, K., Ishikawa, K., Miwa, K., et al., 2001. The *Arabidopsis* AHK4 histidine kinase is a cytokinin-binding receptor that transduces cytokinin signals across the membrane. *Plant Cell Physiol.* 42, 1017–1023.
- Yamada, H., Koizumi, N., Nakamichi, N., Kiba, T., Yamashino, T., Mizuno, T., 2004. Rapid response of *Arabidopsis* T87 cultured cells to cytokinin through His-to-Asp phosphorelay signal transduction. *Biosci. Biotechnol. Biochem.* 68, 1966–1976.
- Yang, S.H., Yu, H., Goh, C.J., 2003. Functional characterisation of a cytokinin oxidase gene DSCCKX1 in *Dendrobium* orchid. *Plant Mol. Biol.* 51, 237–248.
- Yokoyama, A., Yamashino, T., Amano, Y., Tajima, Y., Imamura, A., Sakakibara, H., et al., 2007. Type-B ARR transcription factors, ARR10 and ARR12, are implicated in cytokinin-mediated regulation of protoxylem differentiation in roots of *Arabidopsis thaliana*. *Plant Cell Physiol.* 48, 84–96.
- Yonekura-Sakakibara, K., Kojima, M., Yamaya, T., Sakakibara, H., 2004. Molecular characterization of cytokinin-responsive histidine kinases in maize. Differential ligand preferences and response to cis-zeatin. *Plant Physiol.* 134, 1654–1661.

LIVE-CELL IMAGING IN THE STUDY OF NEURODEGENERATION

Lidia Bakota *and* Roland Brandt

Contents

1. Introduction	51
2. Live Imaging of Cell Lines	54
2.1. Cultures and gene delivery	54
2.2. Time-lapse microscopy and fluorescence-protein tracking to study neurite outgrowth and transport of granules	55
2.3. Photobleaching (FRAP, FLIP) and photoactivation to study protein aggregation and mobility	56
2.4. Fluorescence correlation spectroscopy (FCS) for studying molecular dynamics	58
2.5. Fluorescence lifetime imaging microscopy (FLIM)/ Förster (or fluorescence) resonance energy transfer (FRET) and fluorescence cross-correlation spectroscopy (FCCS) for studying interactions of molecules	58
2.6. Bimolecular fluorescence complementation (BiFC) for analyzing protein interactions	59
2.7. Total internal reflection fluorescence microscopy (TIRFM) for analyzing events near cell membrane	61
2.8. Organelle-specific dyes for tracking mobility of mitochondria	61
2.9. Ion-sensitive dyes for studying neuronal function	62
2.10. Potential and limitation	63
3. Live Imaging of Primary Neurons	64
3.1. Cultures and gene delivery	64
3.2. Time-lapse microscopy and fluorescence-protein tracking to study transport in axons	65
3.3. Photobleaching and photoactivation for analyzing protein diffusion	66
3.4. FCS for studying membrane binding	67
3.5. Use of organelle-specific dyes to determine axonal transport of mitochondria	68

Department of Neurobiology, University of Osnabrück, 49076 Osnabrück, Germany

International Review of Cell and Molecular Biology, Volume 276
ISSN 1937-6448, DOI: 10.1016/S1937-6448(09)76002-2

© 2009 Elsevier Inc.
All rights reserved.

3.6. Fluorescent speckle microscopy (FSM) for visualizing movement of cytoskeletal polymer	68
3.7. Chromophore-assisted laser inactivation (CALI) and fluorophore-assisted light inactivation (FALI) for studying cell and process motility	69
3.8. Ion-sensitive dyes for imaging Ca^{2+} concentrations in primary neurons	69
3.9. Potential and limitation	70
4. Live Imaging of Organotypic Cultures	71
4.1. Cultures and gene delivery	71
4.2. Imaging of neurons to study neuronal fate <i>in vivo</i>	76
4.3. Imaging of dendritic arborization, spines, and synapses to study neuronal connectivity	77
4.4. Photobleaching (FRAP, FLIP) and photoactivation to study molecular dynamics	79
4.5. Ion-sensitive dyes for studying neuronal function	81
4.6. Coculture experiments for studying axonal outgrowth and pathfinding	82
4.7. Live imaging of RNA translation	83
4.8. Potential and limitation	83
5. Live Imaging of Animals	84
5.1. Transgenic animals	84
5.2. Live imaging of invertebrate models to study network development and degeneration	86
5.3. Live imaging of vertebrate models to study cell function in intact brain	87
5.4. Potential and limitation	90
6. Multiphoton Versus One-Photon Microscopy—Potential and Limitation	91
7. Combined Approaches	92
7.1. Live imaging and matrix-assisted laser desorption/ionization (MALDI) to correlate functional states with degeneration	92
7.2. Live imaging and electron microscopy to correlate ultrastructure with degeneration	93
7.3. Live imaging and electrophysiology to correlate cell signaling and morphology with function	93
8. Concluding Remarks	94
Acknowledgment	95
References	95

Abstract

The development of vital fluorescent synthetic dyes and the generation of a myriad of genetically encoded fluorescent proteins permit sensitive visualization of a broad range of dynamic features in living cells with fluorescence microscopy. Many neurodegenerative diseases such as Alzheimer's disease

(AD), amyotrophic lateral sclerosis (ALS), Creutzfeld–Jacob disease (CJD), Huntington’s disease (HD), multiple sclerosis (MS), and Parkinson’s disease (PD) share common aspects on a cellular level that are associated with a change in the dynamic behavior of the whole cell, cell compartments, or single proteins. These include disturbances of transport mechanisms or protein turnover, mis-sorting and aggregation of proteins, and changes in the structural plasticity of neurons. In this chapter, we describe different live-cell-imaging techniques, present representative examples, and discuss the current and potentially future use of live-cell-imaging approaches to answer key questions regarding the mechanisms or potential treatments of neurodegenerative diseases.

Key Words: Neurodegeneration, Fluorescent proteins, Disease models, Time-lapse microscopy, Protein dynamics. © 2009 Elsevier Inc.

1. INTRODUCTION

Neurodegenerative disease is a condition in which neurons progressively degenerate in a region-specific manner, causing neuronal dysfunction, loss of connectivity, and cell death. The disease may have quite different symptoms dependent on the brain region and time course of degeneration of neurons. It may cause movement problems or memory deficits and dementia, and include quite diverse disorders such as Alzheimer’s disease (AD), amyotrophic lateral sclerosis (ALS), Creutzfeld–Jacob disease (CJD), Huntington’s disease (HD), multiple sclerosis (MS), or Parkinson’s disease (PD) (see [Table 2.1](#) for symptoms and cellular mechanisms). Some of the neurodegenerative diseases affect many patients as in the two most common diseases, AD and PD. Others occur rarely such as CJD, the most common human prion disease.

Despite the different symptoms, most of the neurodegenerative diseases share common aspects on a cellular level. Often, neurodegenerative diseases are associated with an aggregation of misfolded or pathologically modified proteins. Examples include AD, where the two aggregates, amyloid plaques and neurofibrillary tangles, represent major histopathological hallmarks, and PD in which α -synuclein aggregates into Lewy bodies. In many cases, the formation of protein aggregates causes disturbances of transport mechanisms, as it becomes most evident in the long axons of motor neurons in ALS. Aggregates can in turn be the result of disturbances in protein turnover, pathological changes in protein folding, or missorting of proteins. In many cases, neurodegenerative diseases are also characterized by the loss of neuronal connections or by changes in the structural plasticity of neurons, for example, loss of synapses and changes in spine morphology as an early event in the progression of AD. In some cases, mitochondrial dysfunction or calcium dishomeostasis is involved, both of which may have a variety of diverse consequences.

Table 2.1 Symptoms and cellular mechanisms of representative neurodegenerative diseases

Disease	Symptoms	Cellular mechanisms	References
Alzheimer's disease (AD)	Memory loss, confusion, irritability and aggression, language breakdown	Aggregation of $A\beta$ in amyloid plaques and tau in neurofibrillary tangles, hyperphosphorylation of tau, cytoskeletal breakdown, mitochondrial dysfunction, calcium dishomeostasis, synaptic failure	Ballatore et al. (2007), Chaturvedi and Beal (2008), Haass and Selkoe (2007), Mattson (2007), Skovronsky et al. (2006)
Amyotrophic lateral sclerosis (ALS)	Muscle weakness and atrophy throughout the body, loss of the ability to initiate and control voluntary movement except for the eyes	Degeneration of motor neurons, aggregation of neurofilaments in cell body and axon, axonal transport defect, mitochondrial dysfunction	Chaturvedi and Beal (2008), Fischer and Glass (2007)
Creutzfeldt–Jacob disease (CJD)	Progressive dementia, leading to memory loss and personality changes, speech impairment, balance, and coordination dysfunction	Aggregation of prion protein, protein misfolding	Aguzzi et al. (2007), Skovronsky et al. (2006)
Huntington's disease (HD)	Uncoordinated body movements, decline in some mental abilities, especially executive functions	Neuronal aggregation of mutated huntingtin, transcriptional dysregulation, excitotoxicity, altered energy metabolism, impaired axonal transport, and altered synaptic transmission, mitochondrial dysfunction, calcium dishomeostasis	Chaturvedi and Beal (2008), Mattson (2007), Roze et al. (2008)

Multiple sclerosis (MS)

Neurological symptoms that often progresses to physical and cognitive disability

Thinning or complete loss of myelin, transection of axons, chronic necrosis, mitochondrial dysfunction

[Chaturvedi and Beal \(2008\)](#), [Trapp and Stys \(2009\)](#)

Parkinson's disease (PD)

Muscle rigidity, tremor, slowing of physical movement

Abnormal accumulation of ubiquitinated α -synuclein (Lewy bodies), intracellular transport deficit, mitochondrial dysfunction, calcium dishomeostasis, synaptic failure

[Chaturvedi and Beal \(2008\)](#), [Schapira \(2009\)](#), [Skovronsky et al. \(2006\)](#)

Thus, many cellular aspects of neurodegenerative diseases are associated with a change in the dynamic behavior of cell compartments or proteins. Therefore, focusing on analyzing the dynamics of disease-relevant processes could provide relevant information for a better understanding of the cellular mechanisms that underlay neurodegenerative disorders. Many of these aspects would be concealed by analysis of protein distribution and cell morphology in fixed tissue. Furthermore, analysis of protein dynamics could provide information about changes which occur already in an early, presymptomatic state of the disorder. The focus on cellular mechanisms also implies that live-imaging studies with the aim to analyze the behavior of single cells rather than imaging of cellular assemblies (as is the case in positron emission tomography (PET) or fMRI scans) is required.

With the availability of genetically encoded fluorescent proteins such as green fluorescent protein (GFP) and its derivatives, new live-cell-imaging techniques have been developed to study different aspects of cell physiology. Live-cell-imaging techniques can be applied to dissociated cells, organotypic cultures, or animals *in vivo*. The aim of this review is to describe the different approaches, present representative examples, and discuss the current and potentially future use of live-cell imaging to answer key questions related to the analysis of the mechanisms of neurodegenerative diseases.



2. LIVE IMAGING OF CELL LINES

Neurodegeneration is associated with some general features, which can be studied on the level of isolated cells that serve as a model for neurons. These include the induction of apoptotic events, the retraction of processes, disturbances of cellular transport mechanisms, changes in the interaction of proteins, the formation of protein aggregates, and malfunction of organelles. The study of cell lines provides the advantage that the cells can be cultured as homogenous material in relative large quantities. Thus, cell lines can be efficiently used for screening applications that require a high throughput at defined conditions. Many cell lines can be efficiently transfected by standard techniques to express an exogenous gene thus allowing the introduction of genetic fluorescence probes and fusion constructs into a cellular context. The generation of lines that stably express the exogenous genes provides the further advantage that a defined amount of the fluorescence probe is synthesized. This also permits the determination of gene dosage effects.

2.1. Cultures and gene delivery

Numerous cell lines have been produced from different tissues of diverse species. Many of them can be used for live-cell imaging. With respect to the study of neurodegeneration, cell lines that establish characteristic properties

of neurons appear to be the most appropriate. A basic feature of neurons is the formation of one or several processes (neurites) that emanate from the cell body and which can become quite long. Since neurites represent a typical compartment that differs from the cell soma in several aspects such as protein composition and cytoskeletal organization, cells where process formation can be induced appear to be the most suited. An example for frequently used cells in this context is the neural rat PC12 cell line. PC12 cells had been established from a transplantable rat adrenal pheochromocytoma, and show features of peripheral neurons after treatment with nerve growth factor (NGF) such as the development of neurites that extend hundreds of micrometer (Greene and Tischler, 1976). As an alternative cell line, differentiated P19 cells have been used as a model for neurons. P19 cells are pluripotent murine embryonal carcinoma cells that differentiate into neuron-like and glial cells after treatment with retinoic acid (Jones-Villeneuve et al., 1982; McBurney, 1993). Both PC12 and P19 cells can be efficiently transfected with DNA encoding recombinant genes. Stable lines expressing these genes can be isolated according to standard protocols. Also for specialized applications, human cell lines can be useful—in particular, for the study of human genes in a cellular context of the same species. Cell lines that have been frequently used as models include the neuroblastoma cell lines, SK-N-SH-SY5Y and SK-N-BE2 cells (Biedler et al., 1973, 1978). A very interesting system with characteristics of human central nervous system (CNS) neurons provides the teratocarcinoma cell line NTera 2. These cells can be induced by treatment with retinoic acid to develop into terminally differentiated neurons, so-called human model neurons (NT2-N cells) with a polar cytoskeletal organization (Pleasure et al., 1992). While the NT2-N cells are no longer susceptible for efficient transfections by standard techniques, they can be infected with several viral vectors including herpes simplex virus (HSV) with minimal neurotoxicity (Fath et al., 2000).

2.2. Time-lapse microscopy and fluorescence-protein tracking to study neurite outgrowth and transport of granules

Several neurodegenerative diseases are associated with a change in neuronal morphology including a retraction of processes and alterations of intracellular structures and transport mechanisms. Analysis of the time sequence of these events by live-cell imaging could provide important information about the factors and molecular cascades involved. In addition, time-lapse microscopy-based screening approaches could help to identify factors that affect neurodegeneration in cellular model systems.

Fluorescence protein tracking has been used in PC12 cells to determine the movement of granules containing fragile X mental retardation protein (FMRP) (De Diego Otero et al., 2002). A lack of FMRP causes fragile

X syndrome, a common form of inherited mental retardation. In this study, PC12 cell lines have been generated which express enhanced green fluorescent protein (EGFP)-tagged FMRP with an inducible expression system (Tet-On). After induction of expression with doxycycline, trafficking of FMRP-EGFP granules into the neurites of PC12 cells was determined. In a follow-up study, a missense mutation (I304N) of FMRP was analyzed. It was shown that FMRP I304N-EGFP does not form visible granules but still was transported into neurites indicating that the disease-related mutations affect transport features (Schrier et al., 2004). Using this method, it would also be possible to systematically identify and analyze effectors of the transport of ribonucleoprotein granules that may have an important role for the localized expression of the tau proteins that are known to play a key role in tauopathies such as AD.

Recently a time-lapse microscopy-based approach has been developed to discriminate between early and late effector proteins of neurite outgrowth in a cell line model (Laketa et al., 2007). GFP-tagged open reading frames were transfected in PC12 cells. Differentiation was then induced with NGF. The localization of the synthesized fluorescent proteins during neurite development and process outgrowth was determined by time-lapse microscopy. The cells were classified into groups where a change of neurite length, a change in the number of neurites, and a blockage of neurite outgrowth were observed. Using this approach, several proteins that affected neurite development and outgrowth could be identified, and the functional interactions with known regulators was determined by coexpression experiments. It would be informative to use a similar systematic time-lapse microscopy-based screening approach to identify disease-related factors which are involved in process retraction and to determine their functional interaction with known neurite outgrowth regulators.

2.3. Photobleaching (FRAP, FLIP) and photoactivation to study protein aggregation and mobility

A change in the intracellular dynamics of proteins, for example, as a result of protein aggregation, is a characteristic feature in several neurodegenerative diseases. For example, protein misfolding and aggregation are central features of polyglutamine neurodegenerative disorders such as HD. Also, PD is characterized by the formation of Lewy bodies as a result of pathological aggregation of α -synuclein or NFTs are formed in AD from aggregated tau proteins. The understanding of aggregate formation in cells in a spatio-temporal manner could provide important information on the mechanism of this pathological process. Molecular dynamics such as aggregate formation could be analyzed by FRAP (fluorescence recovery after photobleaching) technique, which is a powerful tool to study the mobility of fluorescently labeled molecules in living cells. In a typical FRAP

experiment, a population of fluorescent protein is bleached within a small region of interest (ROI) using a high-intensity laser, and the recovery of fluorescence within this area is subsequently monitored (Lippincott-Schwartz and Patterson, 2003). The recorded fluorescence recovery reflects the replacement of bleached protein in the ROI with unbleached protein from outside the region. Thus, a change in the time of fluorescence recovery could give information about immobilization due to protein interactions, as well as about reduced apparent diffusion constants which are affected by the size of the oligomers. Closely related are fluorescence loss in photobleaching (FLIP) experiments in which a region of the cell is repeatedly bleached and loss of fluorescence in the surrounding area is followed over time. FRAP and FLIP experiments have been used to analyze the dynamics of the formation of nuclear inclusions from an expanded polyglutamine protein, ataxin-3 (Chai et al., 2002). It could be shown that the nuclear inclusions are aggregates of this protein that the dynamics of aggregate formation are heterogenous with respect to different polyglutamine disease proteins and that coaggregation with transcriptional components may contribute to the disease process. FRAP experiments have also been performed in neural PC12 cell lines. For example, FRAP in combination with other techniques has been used to analyze the organization and dynamics of membrane protein clusters in PC12 cells (Sieber et al., 2007). In similar studies, the anatomy and the formation of intracellular protein clusters in neurodegenerative disease such as the formation of NFTs or Lewy bodies could be analyzed. FRAP-based assays in cell line models may also be useful to screen for drugs that modify or prevent aggregate formation.

A problem that is associated with carrying out FRAP or FLIP experiments is that bleaching with a high-intensity laser may introduce artifacts as a result of phototoxicity. In addition, bleaching-based methods are often not sensitive enough to determine the motion of a small subpopulation of molecules in a spatiotemporal manner. An attractive alternative method has become available with the development of GFP variants that can be photoactivated (Patterson and Lippincott-Schwartz, 2002). Usually, photoactivation requires a lower energy and allows focal activation of a subpopulation of fluorescence-tagged molecules and to follow their distribution in unprecedented sensitivity and over longer times. This technique has, for example, been used to analyze the flux of microtubule subpopulations during chromosome segregation (Ferenz and Wadsworth, 2007). We have recently used a fluorescence photoactivation approach to analyze the determinants of the motion of the tau protein in processes of differentiated PC12 cells. We could show that AD-relevant factors such as experimentally induced hyperphosphorylation and addition of preaggregated amyloid β peptides ($A\beta$) increased tau's diffusion providing a screening method for factors that influence tau distribution in neurites (Weissmann et al., in revision).

2.4. Fluorescence correlation spectroscopy (FCS) for studying molecular dynamics

Changes in the molecular dynamics of proteins or lipids are a characteristic feature of several neurodegenerative diseases. For example, evidence exists that membrane properties and the fluidity of membrane components is changed in AD and affected by $A\beta$ (Eckert et al., 2005). FCS provides a sensitive optical method with which diffusion and fluid flow can be measured in the microsecond range. Fluorophores within a defined volume are illuminated by laser light and fluctuations of fluorescence emission are recorded. Recently, Chen et al. (2008) described *in vivo* applications of FCS. In PC12 cells, FCS has, for example, been used to determine the lateral mobility of the μ -opioid receptor in the plasma membrane. For that, the receptor had been coupled with EGFP and stable lines were produced (Vukojevic et al., 2008). It is also possible to determine the aggregation state of proteins by FCS. An example is given by a study where cytotoxicity was related to the course of aggregation of huntingtin-polyQ proteins in mammalian cells, and the effect of a particular chaperonin was determined (Kitamura et al., 2006).

2.5. Fluorescence lifetime imaging microscopy (FLIM)/ Förster (or fluorescence) resonance energy transfer (FRET) and fluorescence cross-correlation spectroscopy (FCCS) for studying interactions of molecules

Neurodegeneration is associated with a change in the interactions of molecules which may affect signaling events in the neurons. In cell-free experiments, many factors that interact with proteins, which are of relevance in the disease process, have been identified. An example presents the microtubule-associated protein tau that is involved in tauopathies. Tau is known to interact with many neuronal proteins in addition to its binding to microtubules (Brandt and Leschik, 2004). With respect to the functional relevance of tau's interactions, it would be important to determine the potential binding partners and disease-related changes also in a cellular context.

One technique that is suitable for live-cell-imaging applications is FRET. FRET exploits a nonradiative energy transfer mechanism between two chromophores, which are in close proximity: FRET is exquisitely sensitive to the nanometer-range proximity and orientation between fluorophores. With the development of different genetically encoded fluorescence proteins, FRET analysis became more popular, and the most frequently used FRET pair for biological use is a cyan fluorescent protein (CFP) and yellow-fluorescent protein (YFP) pair, both of which are genetic variants of GFP. Precise measurements and quantitative *in vivo* imaging is

increasingly provided by the advances of FLIM of FRET-based molecular biosensors. For a recent description of the method see [Kalab and Pralle \(2008\)](#). In FLIM, the lifetime of the fluorophore signal rather than its intensity is used to create the image. This has the advantage of minimizing the effect of photon scattering.

Several studies have been performed to analyze interactions between proteins in PC12 cells by FRET or FLIM/FRET analysis. In particular, in many studies the interaction between proteins of the SNARE complex, which is central to the fast neurotransmitter release at the presynapse, has been analyzed by FRET ([An and Almers, 2004](#); [Liu et al., 2006](#)). An interesting application provides a study in which FRET imaging has been performed during NGF-induced PC12 cell differentiation to analyze the occurrence and extent of protein interactions during neurite formation ([Nakamura et al., 2008](#)). In this study, positive and negative signaling feedback loops have been reported, and it was suggested that these feedback loops determine neurite-budding sites. FLIM/FRET analyses would also be informative to determine the intracellular events that accompany neurite retraction during neurodegenerative conditions.

Another technique that provides the possibility to determine interactions of molecules in living cells is fluorescence cross-correlation spectroscopy (FCCS). FCCS detects the synchronous movement of two biomolecules with different fluorescence labels. This allows one to determine a potential interaction of the molecules under study. By extracting information from molecular dynamics, FCCS permits access to processes on a molecular scale. For a discussion of *in vivo* applications of FCCS, see [Bacia et al. \(2006\)](#). FCCS has, for example, been used to analyze the size and organization of an RNA-induced silencing complex in the cytoplasm and the nucleus of human cells ([Ohrt et al., 2008](#)). In a similar line, FCCS experiments may be helpful to analyze the formation and organization of pathologic cytosolic protein aggregates in neuronal cells.

2.6. Bimolecular fluorescence complementation (BiFC) for analyzing protein interactions

An additional method to visualize interactions between proteins in a cellular context became possible with the development of BiFC. BiFC as well as other complementation techniques have the advantage that they can also capture transient interactions as they may occur during signaling events. BiFC is based on complementation between two nonfluorescent fragments of a fluorescent protein. Fluorescence starts when the two fragments are brought in proximity to each other by an interaction between proteins fused to the fragments. Also a multicolor BiFC approach has been developed for simultaneous visualization of interactions with multiple alternative partners

in the same cell, based on complementation between fragments of engineered fluorescent proteins that produce bimolecular fluorescent complexes with distinct spectral characteristics. For an overview about the method, see [Hu et al. \(2005\)](#).

BiFC has been used in a neuroglioma cell line to directly visualize the oligomerization of α -synuclein in living cells. Oligomerization of α -synuclein is thought to be a central event in the progression of PD and related disorders. Prefibrillar α -synuclein oligomers rather than aggregates may induce neurodegeneration. In the study, several fusion constructs of α -synuclein containing nonfluorescent GFP fragments were produced, and it was shown that protein complementation (i.e., the generation of a fluorescence signal) only occurred when α -synuclein was fused to both fragments of GFP. Visualization of oligomer formation was combined with a cytotoxicity assay. It could be shown that stabilization of α -synuclein oligomers resulted in an increased cytotoxicity. Thus, this assay may provide a useful tool to search for therapeutics for synucleinopathies by a microscope-based high-throughput screening approach.

A similar approach was taken to visualize aggregation of the microtubule-associated protein tau in human embryonic kidney cells ([Chun et al., 2007](#)). In this assay, higher amounts of aggregated tau protein were evident by lower GFP fluorescence as was validated using aggregation-prone tau constructs. The assay was used to determine the role of glycogen synthase kinase 3β (GSK3 β) activity on tau aggregation. GSK3 β has previously been implicated to have a role in disease-relevant tau modifications. In fact, increased GSK3 β -mediated phosphorylation of a pseudophosphorylated tau construct resulted in decreased GFP fluorescence, that is, in increased aggregation. Thus, this assay may allow to untangle the complex regulation of tau phosphorylation and its effect on tau aggregation. It would be of high interest to combine this assay with measurements of cytotoxicity as the relation between tau aggregation and cell death is unclear.

In another study, the interaction of the amyloid precursor protein (APP) with Notch receptors was analyzed in nonneuronal cells using BiFC ([Chen et al., 2006](#)). BiFC was accomplished by fusing the N-terminal fragment or the C-terminal fragment of YFP to APP and the Notch receptor, respectively. A strong fluorescent signal was obtained with coexpression of the fragment of C-terminal YFP fused to APP and the N-terminal fragment of YFP fused to a truncated form of the Notch receptor. Fluorescence was detected at the plasma membrane and the endoplasmic reticulum indicating formation of a heterodimer between APP and the receptor at these positions. Thus, the method may be useful to study APP and Notch signaling and interaction during development and neurodegeneration. It should, however, be noted that in all of these applications the interaction between proteins may be hindered by the presence of the fluorescent protein sequence. Furthermore, fluorescence may not be detected if the orientation

of the fragments does not permit complementation. Thus, false-negative results cannot be excluded and other methods need to be used to confirm the absence of interaction between the molecules under study.

2.7. Total internal reflection fluorescence microscopy (TIRFM) for analyzing events near cell membrane

TIRFM, also called evanescent wave microscopy, can be used to analyze cellular processes taking place near the plasma membrane. TIRFM uses evanescent wave to selectively illuminate and excite fluorophores in a restricted region of the specimen immediately adjacent to a glass–water interface. The evanescent wave is generated only when the incident light is totally reflected at the glass–water interface. Using this method, cellular events within the small evanescent range (<200 nm) near the plasma membrane can be detected. For a description of TIRFM and other laser-based measurements see [Botvinick and Shah \(2007\)](#). Thus, TIRFM provides an effective optical method to trace and analyze events and vesicles near a cell membrane without interference of signals from other parts of the cell.

TIRFM has been used in many studies to investigate the behavior of secretory granules adjacent to the plasma membrane such as docking and fusion. The neuroendocrine PC12 cells are a common model to study these processes. An example presents a study where secretory vesicles of PC12 cells have been labeled by GFP-tagged Rab3A, a small G protein involved in the fusion of secretory vesicles to plasma membranes ([Yang et al., 2003](#)). Movements of the secretory vesicles before and after stimulation by high K^+ were examined. In another study, TIRF was used to determine actin and dynamin recruitment in PC12 cells at sites of endo- and exocytosis ([Felmy, 2009](#)). Since changes in synaptic transmission appear to be an early event in several neurodegenerative diseases, it would be very interesting to analyze endo- and exocytosis in a PC12 neurodegeneration model in order to identify molecular events that may be disturbed already in a presymptomatic state of the disease.

2.8. Organelle-specific dyes for tracking mobility of mitochondria

A typical feature of many neurodegenerative diseases is an impairment of axonal transport processes, in particular an impairment of fast axonal transport on microtubule tracks. Organelles such as mitochondria and lysosomes are transported along microtubules. Commercially available fluorescent probes that specifically label mitochondria or lysosomes (e.g., MitoTracker, LysoTracker, or rhodamine 123) have become common tools to determine the distribution of these organelles. Sufficient transport and function of mitochondria appears to be of particular importance for neuronal

maintenance due to the high energy consumption of neurons (Mattson et al., 2008).

Mitochondria-specific staining followed by live imaging has, for example, been used to determine the effect of kinases on microtubule-dependent transport. In a study by Mandelkow et al. (2004), CHO cells have been stably transfected with microtubule-associated proteins. Expression of the neuronal tau protein resulted in an inhibition of transport on microtubules. In these experiments, mitochondria were stained with MitoTracker and the movement of the fluorescent mitochondria was followed over time. Whether an overexpression of microtubule-associated protein (MAPs) such as tau protein has a role during neurodegeneration is a matter of debate. However, tracking of mitochondria by live-imaging techniques could help to correlate the impairment of transport mechanisms with other features of neurodegeneration to determine the time sequence and potential functional relation between the different hallmarks of neurodegenerative processes. In particular, it would be very informative to analyze the effect of the formation of oligomers or higher aggregates of tau protein as it occurs in AD on transport features.

2.9. Ion-sensitive dyes for studying neuronal function

The intracellular concentration of calcium is closely correlated with the activity state of a neuron. Calcium has an important role as a second messenger in many processes including neurotransmitter release, long-term potentiation, and protein degradation. In age-associated neurodegenerative diseases such as AD and PD, the impairment of calcium homeostasis is considered to be a key pathological event leading to neuronal dysfunction and cell death. In addition, evidence exists that calcium oscillations can trigger apoptosis under certain conditions indicating a role of calcium elevations in neuronal cell death.

Calcium imaging permits to visualize the calcium status in a cell in a spatiotemporal manner. The technique takes advantage of the use of calcium indicators, which respond to the binding of Ca^{2+} ions by changing their spectral properties. Calcium indicators can be small molecules that specifically chelate calcium ions. Many of the small-molecule indicators are esters in which the chelator carboxyl groups are modified to render the molecules lipophilic in order to make them cell permeable (e.g., calcium green, fura-2). For a recent overview about the properties and use of the chemical calcium indicators see Paredes et al. (2008). In addition, genetically encoded calcium indicators derived from GFP (e.g., Cameleons) have been generated, which can be transfected in cell lines according to standard procedures (McCombs and Palmer, 2008). Cells with the indicator can then be analyzed by fluorescence microscopy and analyzed according to the change in the fluorescence reflecting the Ca^{2+} status.

Genetically encoded calcium indicators can also be targeted to specific cellular compartments through the generation of fusion constructs. An interesting example presents a study where Cameleon was fused to phogrin, a protein that is localized to secretory granule membranes to monitor changes in Ca^{2+} concentration at the secretory vesicle surface (Emmanouilidou et al., 1999). With a similar method, it may become possible to generate a calcium-monitoring cell line model of neurodegeneration by combining a targeted genetically encoded calcium sensor with the expression of aggregation-prone proteins derived from tau or α -synuclein sequence.

It should be noted that also other indicators of potential relevance for neurodegeneration-associated events can be produced. An interesting example is given by the development of a genetically encoded fluorescent reporter of the ATP:ADP ratio (Berg et al., 2009). The sensor was constructed by combining a GFP variant with the bacterial regulator protein GlnK1 that binds Mg-ATP and ADP by producing different changes in fluorescence. Since mitochondrial dysfunction is a characteristic feature of several neurodegenerative diseases, imaging the ATP:ADP level may be an important read out for neurodegenerative processes in cell line models.

2.10. Potential and limitation

Models based on cell lines have the advantage of providing homogenous material that can be efficiently used for screening purposes with high content microscopy. The combination with genetic methods allows to produce genetically modified cells that stably express a reproducible amount of the protein of interest, for example, fluorescent-tagged proteins. It should, however, be noted that most of the cell lines do not develop into a polar and terminally differentiated state with defined axonal and dendritic compartments. Furthermore, cell-cell contacts that may modify functional properties of the neurons are missing. Thus, while it may be possible to analyze fundamental mechanisms of neurodegeneration, cell line-based methods are not appropriate to determine pathological mechanisms that require the presence of structural and functional polarity.

In addition, overexpression of proteins may cause artifacts and the absence of the effect need to be controlled in mock transfected cells. Furthermore, the inclusion of the relative large GFP (or GFP variant) moiety to a protein of interest in fusion experiments may change the properties of the protein under interest in an unpredictable manner. Thus, care in the interpretation of the results is required, and performing similar experiments in other systems is needed to confirm the results.

3. LIVE IMAGING OF PRIMARY NEURONS

In many diseases, changes occur in a compartment-specific manner. For example, AD is associated with a redistribution of tau protein, which is normally enriched in the axon, to the somatodendritic compartment where it forms aggregates. ALS is associated with a transport deficit which occurs mainly in the axon, and also MS is characterized by a compartment-specific change in the cytoskeletal organization of the axon. Thus, aspects that require a compartment-specific analysis can only be studied in an experimental model that develops axonal-somatodendritic polarity. While many cell lines such as the commonly used PC12 cells develop neurites, they do not develop into a true polar state as would, for example, be evident by an axon-specific localization of the microtubule-associated protein tau. In contrast, neurons from primary cultures, that is, from cultures started from material taken directly from a part of the nervous system of an organism, develop polarity. Primary neurons from different organisms and different parts of the nervous system have been prepared for live-imaging applications. These include chick neurons for the study of axonal growth, cultures of *Aplysia* neurons, rat dorsal root ganglion neurons, and mouse as well as rat hippocampal cultures. All of these cultures have in common that the material is very limited and that the neurons are generally not efficiently transfectable by standard gene transfer techniques.

3.1. Cultures and gene delivery

One of the first and since often used *in vitro* systems for the study of isolated neurons represents the culture of hippocampal neurons from 18- or 19-day rat fetuses (Banker and Cowan, 1977). Following trypsinization, the cells are plated out at low density and can be followed for several days during which they establish a single axon and several dendrites (Dotti et al., 1988). Primary cultures of fetal rat hippocampal neurons have, for example, been used to study the effect of $A\beta$ on phosphorylation and distribution of endogenous tau protein (Busciglio et al., 1995). The same system has also been used to test the effect of kinase inhibitors during $A\beta$ -induced neurodegeneration (Rapoport and Ferreira, 2000). Hippocampal neurons can also be isolated from mouse brain. This provides the advantage that transgenic, knock-in or knockout mice can be used for the experiments. By using hippocampal neurons that have been prepared from wild type, tau knockout, and human tau transgenic mice, it could, for example, be shown that the presence of tau protein is essential for $A\beta$ -induced neurotoxicity (Rapoport et al., 2002). As an alternative and technically easier to prepare system, rat, mouse, or even human cortical cultures are used.

For example, it has been shown that fibrillar but not soluble A β induces the phosphorylation of tau at selected residues in human cortical neurons (Busciglio et al., 1995).

It is not easy to transfect primary neurons, and care has to be taken that the neurons do not degenerate. However, in the last years, several methods based on the use of gene guns, new transfection reagents and nucleofection have been developed which allow the transfer and analysis of exogenous genes in hippocampal and cortical neurons for some applications. More efficacious and better to control is viral vector-mediated gene transfer, and several vectors have been used to efficiently express foreign genes in primary neurons. This includes a defective HSV vector system that permits the introduction of genes into mammalian CNS neurons. With this virus, infection of rat neurons in primary culture derived from different regions such as spinal cord, cerebellum, thalamus, basal ganglia, and hippocampus has been demonstrated (Geller and Freese, 1990). HSV-mediated gene transfer has been used to express APP or presenilin in cortical neurons to test the effect of AD-relevant mutations on neuronal apoptosis (Bursztajn et al., 1998). HSV-mediated expression as well as expression using Semliki forest virus (SFV) is useful for transient expression for up to 1 week. For long-term expression, adenoviral and lentiviral expression systems have been developed. Lentivirus-mediated gene transfer allows, for example, the delivery of RNAi in hippocampal neurons for long-term silencing of genes (Janas et al., 2006). Lentiviral vectors are also of particular interest for gene therapeutic applications since they have several advantages over other methods. These include a high efficiency of infection also of nondividing cells, long-term stable expression of the transgene, and low immunogenicity.

3.2. Time-lapse microscopy and fluorescence-protein tracking to study transport in axons

Time-lapse video recording was used to follow the early stages of process formation in cultured hippocampal neurons. Here, it has been shown that the neurons acquired their characteristic shape by a stereotyped sequence of developmental events (Dotti et al., 1988). Time-lapse imaging has also been used to directly follow organelle transport in developing hippocampal neurons using light and video microscopy (Bradke and Dotti, 1997). Thus, events that accompany neuronal degeneration in cellular disease models could be imaged by similar approaches. This could give important information about when and how disease-relevant conditions affect fundamental processes in a neuron such as axonal vesicle transport.

Transport features have also been analyzed using fluorescence-tagged membrane proteins in hippocampal neurons. Among others, the APP has been tagged with GFP variants, and cells were imaged by video microscopy

(Kaether et al., 2000). It was reported that APP-YFP was transported very fast ($4.5 \mu\text{m/s}$) and over long distances. Other membrane proteins moved much slower and over shorter distances only. Using two-color video microscopy, it was shown that the different proteins were sorted to different carriers along axons of doubly transfected neurons. During AD, APP is cleaved to generate $A\beta$ which aggregates into senile plaques as a characteristic hallmark of the disease. Thus, the transport characteristics of APP could be of importance for the place and extent of $A\beta$ formation.

In addition, mechanisms of cell death could be visualized in real time. An example presents a study from our lab where live imaging has been used to determine the mode of cell death in primary neurons. Here, cortical neurons that have been infected with a HSV vector coding for a hyperphosphorylation-mimicking tau construct were imaged over a period of 48 h. We could show that expression of a disease-relevant tau variant (pseudohyperphosphorylated (PHP) tau) was associated with increased perikarya suggesting the development of a ballooned phenotype as a specific feature of tau-mediated cell death (Leschik et al., 2007). Interestingly, the development of a ballooned phenotype did not result in a selective loss of neurites suggesting that tau-dependent neurodegeneration develops in the absence of changes in neuritic morphology. It should also be noted that the “ballooned” neurons could not be conserved by standard-fixation protocols, probably due to a breakdown of cytoskeletal structure. Thus, detection and observation of “ballooning” was only possible by live-imaging approaches.

3.3. Photobleaching and photoactivation for analyzing protein diffusion

Neurodegenerative diseases are often associated with a missorting or relocalization of proteins. An example presents the microtubule-associated tau protein which is normally enriched in the axon and which gets redistributed to the somatodendritic compartment in tauopathies such as AD. Photobleaching and photoactivation approaches allow to analyze protein diffusion and effects of disease-relevant factors on the mobility of proteins. For example, the movement of the microtubule-associated protein tau in axons has been analyzed by FRAP in chicken retinal ganglion neurons, which had been transfected with EGFP-tau constructs (Konzack et al., 2007). With this approach, it was possible to determine the apparent diffusion constants. Using this method, it would also be possible to analyze the effect of disease-relevant conditions on tau movement and distribution. An alternative to photobleaching would be the use of a photoactivation approach employing recently developed photoactivatable or photoconvertible GFP variants. Photoactivation has the advantage that the energy that is required for activation is much lower than the energy which is needed for

photobleaching. Thus, the risk of damage to the cells is lower with a photoactivation approach. Photoactivatable tau constructs have been used in our lab to determine the diffusion of tau constructs and fragments of tau in processes of cortical neurons (Weissmann et al., in revision). We could show that tau's aminoterminal projection domain-mediated binding and enrichment of tau at distal neurites indicating that the tip of a neurite acts as an adsorber, trapping tau protein. Furthermore, addition of preaggregated $A\beta$ increased tau's diffusion compatible with a decreased binding to microtubules. Several neurodegenerative diseases, including ALS, are associated with transport defects. It would be informative to study the effect of neurodegenerative conditions on slow axonal transport, which could, for example, be followed by photoactivation of neurofilament proteins in which fusion proteins of photoactivatable GFP with neurofilament subunits have been incorporated.

Photoactivation experiments can also be performed with caged fluorescence probes. Caged fluorescein-labeled tubulin has been previously used to determine slow axonal transport in *Xenopus* neurons and mouse sensory neurons (Okabe and Hirokawa, 1992). In these experiments, the probe was microinjected and after incorporation into the microtubule array, a narrow region of the axon was illuminated with a 365-nm microbeam. The photoactivated microtubule segment was then followed over time. However, caged compounds have to be microinjected in the cells which is much less effective and more labor intensive than using genetically encoded fluorescence probes.

3.4. FCS for studying membrane binding

The functional interaction between extracellular amyloid plaques and intracellular neurofibrillary tangles in AD requires a communication between these two components, probably via a transmembrane protein. For a better understanding of pathological processes and for the development of therapeutic strategies, information about the identity and the function of a putative receptor would be very important.

FCS has been used to study the existence of a target molecule for $A\beta$ in the plasma membrane of cultured human cerebral cortical neurons (Hossain et al., 2007). Using $A\beta$ that had been labeled with the fluorophore rhodamine, slowly diffusing complexes of bound $A\beta$ were observed indicating the presence of a receptor or target molecule in the membrane. Competition experiments indicated specificity of the binding. Thus, this technique could be used to screen for drugs that suppress binding of $A\beta$ to the membrane providing candidate factors that reduce $A\beta$ -mediated toxicity.

3.5. Use of organelle-specific dyes to determine axonal transport of mitochondria

Mitochondrial pathologies are a common feature in several neurodegenerative diseases. A malfunction of mitochondria and a depletion in ATP could also be caused by a defective transport of mitochondria within neurons. This can be analyzed by using dye labeling of mitochondria and following their transport and distribution in primary neurons. Transport occurs mainly on microtubules, and the presence of microtubule-associated proteins may affect mitochondrial transport. To address this issue, axonal transport of mitochondria has been analyzed in primary retinal ganglion cells (Mandelkow et al., 2004). Mitochondria have been labeled with the fluorescent dye MitoTracker and followed over time to determine their velocity. The neurons have been infected with adenovirus to express tau which leads to the inhibition of the axonal transport of mitochondria. Interestingly, transport could be rescued by phosphorylating tau with microtubule affinity regulating kinase (MARK)/Par-1, a family of kinases that is known for its involvement in establishing cell polarity and in phosphorylating tau protein during AD.

3.6. Fluorescent speckle microscopy (FSM) for visualizing movement of cytoskeletal polymer

Most neurodegenerative diseases are associated with a change in the organization and the dynamics of cytoskeletal filament systems. Thus, a direct observation of the behavior of the filamentous cytoskeleton by live-imaging approaches could be useful to determine the factors that influence cytoskeletal dynamics.

FSM is a technique for visualizing the movement, assembly, and turnover of cytoskeletal components in living cells. In FSM, a nonuniform “speckle” pattern is created by coassembly of a small fraction of fluorescent subunits in a pool of unlabeled subunits, thus, generating random variations in fluorescence. Movements of the “speckle” pattern can then be analyzed in time-lapse recordings using a conventional wide-field epi-fluorescence light microscope and digital imaging. A nonuniform “speckle” pattern can be obtained with microinjection of fluorescently labeled cytoskeletal subunits, for example, fluorescent-tagged tubulin dimers, or with expression of EGFP-fusion of subunits (Waterman-Storer and Salmon, 1999). FSM has been used to analyze the movement of microtubules and actin filaments during adhesion-mediated neuronal growth cone guidance in *Aplysia* (Lee and Suter, 2008). Using this method, microtubule rearrangements and microtubule-actin filament coupling could be visualized in subcellular regions. It would be interesting to use FSM also to determine the effect of disease-relevant changes on actin and microtubule dynamics in relevant subcompartments such as dendritic spines or the presynaptic terminal.

3.7. Chromophore-assisted laser inactivation (CALI) and fluorophore-assisted light inactivation (FALI) for studying cell and process motility

CALI and FALI are techniques that induce a specific loss of protein function with high spatial and temporal resolution in order to follow the effect of such a functional knockout. Originally, the CALI method used laser light of 620 nm, which was focused through microscope optics onto a 10 μm spot. Within the spot, the laser energy is targeted via specific Malachite green-labeled, nonfunction-blocking antibodies, that generate short-lived protein-damaging reactive oxygen species, thus inactivating proteins in close proximity. FALI uses fluorophores such as fluorescein conjugates as a target with the same intent. Combined with time-lapse video microscopy, CALI and FALI offer the possibility to induce and observe, for example, changes in growth cone dynamics and the contribution of selected proteins on growth cone motility and neurite outgrowth (Buchstaller and Jay, 2000; Jacobson et al., 2008).

CALI has been used to determine the role of the MAP tau during axon growth (Liu et al., 1999). Tau has been inactivated either in whole chick dorsal root ganglion neurons or in a region of the growth cone. Complete inactivation reduced neurite number and length. Inactivation in a growth cone region decreased neurite extension rate and lamellipodial size, suggesting a specific role of tau in growth cone steering. It would be interesting to use CALI or FALI to test the effect of disease-relevant tau modifications such as hyperphosphorylation or mutations that are associated with FTDP-17 cases.

3.8. Ion-sensitive dyes for imaging Ca^{2+} concentrations in primary neurons

Neuronal Ca^{2+} homeostasis is important for vital functions of a neuron (see Section 2.9). Oxidative stress impairs Ca^{2+} homeostasis making neurons more vulnerable to degeneration. In fact, aging-related neurodegenerative diseases such as AD, PD, or HD are characterized by feedback between Ca^{2+} dyshomeostasis and the aggregation of disease-related proteins such as A β , α -synuclein, or huntingtin (Wojda et al., 2008).

Intracellular calcium levels have been determined, for example, in a cellular aging model, based on the culture of hippocampal neurons from young (2 months) and aged (24 months) rat brains (Hajieva et al., 2009). To induce stress, neurons were treated with glutamate or hydrogen peroxide and were imaged with calcium green to record intracellular Ca^{2+} levels. It was found that Ca^{2+} levels were increased in aged neurons at stress conditions. Similar experiments could be performed to dissect the connection between the aggregation of disease-relevant proteins such as tau,

α -synuclein, or huntingtin and disturbed Ca^{2+} homeostasis. It would also be informative to know about any compartment-specific differences and about the kinetics of Ca^{2+} changes in response to external stimuli. In some cases, neurodegeneration appears to be associated with a disturbed balance of the action of kinases and phosphatases leading to the hyperphosphorylation of cellular proteins. Thus, determining the effect of a disturbed phosphorylation on Ca^{2+} levels could be informative with respect to a crosstalk between different signal transduction mechanisms during diseases. As a first experiment in this direction, cultured hippocampal neurons have been treated with phosphatase inhibitors okadaic acid (OA) and cantharidin and Ca^{2+} levels have been imaged with Fura-2. It was reported that OA and higher concentrations of cantharidin reduced NMDA receptor-mediated Ca^{2+} responses. Changes in Ca^{2+} signaling were accompanied by increased phosphorylation of cytoskeletal proteins. Pharmacological treatments that alter phosphorylation can have many side effects. It would be interesting to determine the effect of specific kinases in similar experiments using neurons that have been prepared from mice with a knockout of individual kinases.

3.9. Potential and limitation

Primary neuronal cultures have the advantage that the neurons have a polar cytoarchitecture with distinct axonal and somatodendritic compartments. Thus, compartment-specific mechanisms or events that are associated with a missorting of proteins, as they occur during neurodegenerative conditions, can be studied in such a model. Different primary culture models have been used for live-imaging approaches and each has its advantages and limitations. One of the most studied models are hippocampal neurons from mouse and rat since they provide a relative uniform population of cells in which the neurons develop through a stereotypic and endogenously controlled series of events. A limitation of this culture system is that the axons are relatively short and growth cones are small thus limiting studies on mechanisms of axon elongation or growth cone mobility. In this case, dorsal root ganglion neurons from chick or other species have been proven to be more appropriate.

One of the major limitations of using dissociated primary neurons is due to the fact that *in vivo* neurons are embedded in an authentic three-dimensional (3D) environment with contacts to neurons, glia cells and extracellular matrix proteins. These interactions are lost when cells are placed on a coverslip which may substantially change their properties. As an example, synapses degenerated and the density of dendritic spines was strongly reduced after tau expression in cultures of dissociated hippocampal neurons (Thies and Mandelkow, 2007). In contrast, when tau was expressed in neurons of organotypic slices of the hippocampus, spines were largely unaffected (Shahani et al., 2006). Such differences may be very relevant

when neurodegenerative processes are analyzed and results that have been obtained using dissociated cultures should be confirmed in more complex culture models or in living animals.

4. LIVE IMAGING OF ORGANOTYPIC CULTURES

4.1. Cultures and gene delivery

Cultured brain tissue derived from late embryonic, newborn, or early postnatal animals develops in much the same way as if it had remained *in situ* in the intact animal. This provides the major advantage over cell lines or dissociated primary cultures, because cells exhibit preserved tissue-specific organization *in vitro* by which they can replicate many aspects of the *in vivo* context. Thus, brain slices are physiologically more relevant preparations compared to cell cultures.

Over the years, slice culture systems have been successfully established from a variety of different brain regions including hippocampus, cortex, striatum, ventral mesencephalon, hypothalamic paraventricular nucleus, spinal cord, and cerebellum (Bali et al., 2008; Krassioukov et al., 2002; Lonchamp et al., 2006; Snyder-Keller et al., 2008). All of these tissue explants are suitable for imaging studies. While nonhuman cultures are more widely used, since most of the cultured explants originate from rat or mouse CNS, human brain tissue culture techniques had also been developed. A comprehensive review surveying the history of human CNS tissue culture as well as discussing tissue sources and culturing options is given by Walsh et al. (2005).

4.1.1. Differences between acute and organotypic slices

Organotypic cultures can be sustained up to several months, ensuring long-term possibility for experimental approaches. In contrast, acute slices are maintained and visualized only for a few hours but have the advantage that they can be derived from adult animals as well. Although in both slice types some local circuitry remains intact, the slices develop subsequently in isolation from the animal. Therefore, the absence of extrinsic afferent fibers and efferent targets might induce a reorganization of the intrinsic explant connections. To address these questions, De Simoni et al. (2003) applied patch-clamp techniques and confocal microscopy in the CA1 region of the rat hippocampus to compare acute slices from the third postnatal week, in which development occurred *in vivo*, with various stages of organotypic slices. The organotypic slice sample was taken out after postnatal day 5, allowing development of neuronal circuits in intact brain until a certain level. During slicing, axons of many CA3 cells and all CA1 cells are cut from their input and output connections. This will occur in both preparations but

as acute slices are used within the following 8 h, they have little chance for remodeling. In organotypic slices, however, cutting of axons inevitably leads to a rearrangement of connectivity over the following days. However, the comparison of organotypic cultures with acute slices suggested that the main difference between development *in vitro* and *in vivo* occurs within the first week after preparation of the cultures. Thus, although connectivity was greater in organotypic slices, once this was established, development continued in both preparations at a remarkably similar rate. Therefore, they concluded that, for the parameters studied, changes seem to be preprogrammed by 5 days and their subsequent development is largely independent of environment (De Simoni et al., 2003).

4.1.2. Culturing techniques

Several methods have been developed to maintain thin slices of brain alive in a short (several hours) or long-term (up to several months) culture. The culturing techniques provide a milieu that maintain viability of the cells and preserve much of the 3D cytoarchitecture, meaning a distinct organotypic organization of the main neuronal cell and neurophil layers as well as afferent fiber patterns. The two most widely used tissue culture techniques are the roller-tube and the membrane interface culture methods (Gähwiler et al., 1997, 2001).

The roller-tube or also called roller drum technique for culturing nervous tissue was primarily introduced by Hogue (1947) and later modified by many others. However, the most widely used protocol is the one described by Gähwiler (1981). During the roller-tube procedure explants or slices are embedded in either a blood clot or collagen gel attached to a flying coverslips and cultivated for weeks in roller-tubes, while rotating at a specific speed and with an appropriate angle to alternatively dip the slice into culture medium or bring it into the air. After 2–3 weeks in culture, the majority of damaged cells on both cut sides and the afferent fibers disappear. The remaining culture is spread, over a much greater area. Due to the flattening of the tissue, individual nerve cells are often arranged in monolayer thickness and can, therefore, be viewed with phase-contrast microscopy. The degree of organotypic organization depends on the age of the animals used for culturing. In view of the accessibility of individual living cells, this approach seems to be particularly well suited for physiological and pharmacological studies on morphologically identified nerve cells (Gähwiler, 1981). Notwithstanding, due to the intense thinning of the tissue, these explants might bear a large experimental variability.

The membrane interface method, also called the membrane insert culture or membrane filter method, originally was presented by Stoppini and co-workers in 1991 and modified by others. In contrast to the roller-tube culture procedure, the membrane interface culture method maintains a thickness of slices at $\sim 100\text{--}150\ \mu\text{m}$ during the cultivation period, and this makes it more suitable for the study of 3D patterns within the regions of interest.

The principle of membrane interface culture methods is to maintain brain slices on a semiporous membrane insert at the interface between medium and a humidified atmosphere. The medium provides adequate nutrition to tissues through the membrane via capillary action, while the thin sheath of medium covering the tissue allows sufficient oxygen flow to the cells.

Several detailed procedure descriptions for slice preparations and culturing tips have been elaborated (Bergold and Casaccia-Bonnel, 1997; De Simoni and Yu, 2006). Furthermore, profound descriptions of protocols for preparation of organotypic hippocampal slice cultures that can be readily adapted for live-imaging studies are also available. These protocols specify not only culture procedure but also provide an overview about long-term live-imaging methods that are based on transgenes expressed in the mice, or on constructs introduced through transfection or viral vectors (Gogolla et al., 2006a,b).

4.1.3. Slice cultures on multielectrode arrays

Firing patterns of spontaneous or stimulated neuronal activity from the neuronal microenvironment play an important role in neuronal development and plasticity during physiological and disease conditions. Therefore, electrophysiological recordings parallel to neuron imaging provides further possibilities to investigate the functional state of the neuronal network. One approach is the conventional patch-clamp procedure, where single cells are under observation. As an alternative, a noninvasive recording from several tens of cells can be achieved by cultivating cells or tissue slices on substrates containing multielectrode array (MEA). Although culturing dissociated cells from different brain regions on MEA had long been developed, maintaining tissue slices on MEA fields brings further challenge, due to the need of special nourishing conditions. The existing culture methods for organotypic slice cultures have limitations on the types of culture substrates that can be used, because brain slices need to be kept at the liquid–air interface to ensure oxygen availability for the tissue cells and avoid hypoxia and necrosis. Therefore, both of the existing methods mentioned above are not directly compatible with the long-term use of organotypic cultures on substrates containing microfabricated structures such as substrate-integrated electrodes or microchannels for microenvironment control. Nevertheless, multielectrode array for extracellular recording had been applied to hippocampal acute slices (Steidl et al., 2006) and several groups have published methods for culturing long-term organotypic cultures on MEAs, that are fabricated on porous substrates to emulate the “Stoppini” method (Kristensen et al., 2001; Thiebaud et al., 1997), or with the MEAs rocked in the culture incubator to replicate the conditions of the roller-tube method (Egert et al., 1998).

Furthermore, a novel method to maintain organotypic cultures of rodent hippocampus for several weeks on stationary MEAs and glass surfaces had been reported by [Berdichevsky et al. \(2009\)](#). The organotypic culture platform described is modular, consisting of three components: PDMS miniwell for slice culture on stationary, solid substrate, microchannels that are integrated into the PDMS well for axon guidance, and the MEA integrated into the culture substrate. This cultivation method allowed the first use of microchannels with organotypic slices. Since different combinations of modules can be used for a variety of experiments, this method can serve a number of potential applications, in particular the selective fluid delivery to the organotypic slice or extended processes for studies of axonal sprouting, and long-term studies of the developing neural activity in the compartmented slices and extended axons with MEAs.

4.1.4. Labeling samples for live imaging

4.1.4.1. Staining with lipophilic dyes One option for the live study of the CNS connections in slice preparations is to use a fluorescent, long-chain lipidsoluble carbocyanine perchlorate dye. Several different versions of the carbocyanine dyes are available. The most extensively used are the 1,1'-dioctadecyl-3,3,3',3'-tetramethylindocarbocyanine perchlorate, (DiI), which fluoresces bright red when viewed with a filter set appropriate for rhodamine and 3,3'-dioladecyloxacarbocyanine perchlorate (DiO), which fluoresces orange/yellow. These dyes readily become incorporated into the plasma membranes of neurons exposed to them. Since they can diffuse within the plane of the membrane to label the neurons retrogradely and anterogradely, they are well suitable for tracing axonal pathways as well.

The dyes can be applied by passive incubation, as it was used, for example, in the study of [Miyata et al. \(2002\)](#), where fine crystals of DiI were placed onto the surface of cerebral hemispheres taken from E12–14 mouse embryos using a fine brush. To achieve region-specific staining of the tissue or labeling cells in deeper layers, direct injection ([Deng and Dunaevsky, 2005](#); [Dickson et al., 2007](#)), or gene gun-mediated ballistic delivery of lipophilic dyes (DiOlistics) ([Benediktsson et al., 2005](#)) is applicable. Following these methods, neurons can be visualized within minutes.

4.1.4.2. Gene delivery Live cells can also be lightened up utilizing expression of fluorescent proteins, however, in contrast to dissociated cell cultures conventional transfection techniques have been of limited effectiveness in neural tissues. A higher likelihood that the cells are being transfected by a genetically encoded fluorescent probe is ensured by ballistic delivery (biolistics) by which the DNA is brought close to cells in tissue. The use of particle-mediated gene transfer on slice explants had been extensively elaborated by several groups ([Lo, 2001](#); [O'Brien and Lummis, 2006](#)).

The principle of biolistics is to accelerate micrometer-sized gold or tungsten particles, called microcarriers, which are coated with cDNAs towards the target tissue, cells, or organelles. Following these methods, neurons can be visualized after 24–48 h.

Several types of viruses can also be used to effectively accomplish the expression of the desired fluorescent protein. Diverse viruses have different biological profiles with respect to the cloning capacity, host range, duration of expression, level of expression, and effects on neuronal viability. Therefore, the choice of vector depends on both the gene of interest and the application target. The vectors have been modified in order to overcome limitations of the parent viruses from which they were derived and to rule out the possibility of a pathogenic effect.

SFV and Sindbis (SIN) virus vectors are widely used in neurobiological studies because they efficiently infect neurons, albeit they possess a limited cloning capacity and mediate only transient expression (Rhême et al., 2005). In contrast, gene delivery to neurons based on replication-incompetent lentiviruses provides stable expression of the transgenes, since the lentiviral genome integrates into the host cell genome. These vectors exhibit increased cellular tropism as they express on their surface the vesicular stomatitis virus G glycoprotein that promotes nonspecific membrane fusion. Therefore, neuron specificity can be achieved by coupling the expression of the gene of interest to a neuron-specific promoter (Dittgen et al., 2004). Engineered adenovirus, adeno-associated virus (AAV), and measles virus are also used for viral gene expression. A nice comparative study of GFP expression in rat hippocampal slices was done with these recombinant viruses as well as the ones mentioned above (Ehrenguber et al., 2001).

4.1.4.3. Transgenic animals As an alternative to the above-mentioned methods for “introducing the color” to live cells within the slice preparation, it is also possible to use transgenic animals with intrinsic fluorescent labeling. From the dozens of spectral and photophysical fluorescent protein variants (XFPs) available, some have been introduced as a transgene to allow long-term visualization of cells *in vivo* or *ex vivo*. In some mice, only subsets of neurons or glial cells are expressing the fluorescent protein, whereas in other mice, the transgenic element is designed to randomly express different colors or color sets in distinct neuron populations. Furthermore, several strains were generated to express the fluorescence protein after induction (Lichtman et al., 2008). Some of the XFP modifications are directly applicable for visualizing the cell function as well. Towards that, for example, transgenic mice expressing a pH or Cl-sensing fluorescent proteins are employed (Metzger et al., 2002).

4.2. Imaging of neurons to study neuronal fate *in vivo*

A progressive loss of structure or function of neurons occurs during several neurodegenerative diseases including PD, AD, and HD, or following severe mechanical damage affecting the whole cell or its processes. Although there are many approaches available to analyze diverse aspect of cell degeneration in fixed samples, spatiotemporal dynamics during the course of neurodegeneration can be captured only by live imaging. Since slice cultures combine the accessibility and control of extracellular environment with the presence of an authentic CNS environment, it is feasible to follow the neuronal fate step by step with a live-imaging approach.

Employing slice imaging, the alterations of the whole cell or cell domains can be analyzed after damage or applying disease-relevant substances. A study by [Dickson et al. \(2007\)](#) utilized acute slice preparations of the adult rodent neocortex and live-imaging techniques to visualize the response of discretely injured neuronal processes up to 8 h. Their approach allowed them to follow DiI-labeled neurons after transection injury that was performed on cells sufficiently deep to the cut surface to avoid visualization of reactive injury owing to the initial slice preparation. The authors could observe the highly dynamic behavior of axonal sprouts in contrast to other *in vivo* experimental studies that interpreted static observations of histochemically or immunohistochemically prepared tissue. The data indicate that axons possess cellular features that enable substantial adaptive responses to damage and live imaging could identify a time window when, possibly through manipulation of cytoskeletal elements, appropriate regeneration of local and long projections can be achieved.

In a study from our lab, [Shahani et al. \(2006\)](#) investigated the role of tau during neurodegeneration, since tau alteration and dysfunction and extensive neuron loss has long been associated with tauopathies such as AD. Different EGFP-tagged human tau constructs were introduced in mouse hippocampal slices by SIN virus infection and EGFP-positive neurons in the CA1, CA3, and DG regions were imaged over a period of 4 days. This method provided a possibility to monitor the alteration of cells upon tau expression. In the study, a time-dependent loss of individual neurons in all hippocampal regions was observed, which was highly significant when PHP tau, which mimics a highly phosphorylated, disease-relevant tau species, was utilized. Tracking the fate of neurons in live samples revealed a “ballooned” phenotype of cells, which is not possible to preserve by standard-fixation procedures. This feature pointed out that tau-induced cell death involves not only apoptotic, but nonapoptotic mechanisms as well.

Further studies could address the interplay between $A\beta$ and tau during neurodegeneration on the basis of experimental conditions where both disease-relevant proteins are combined. This could, for example, be done by expressing EGFP-tau constructs in slices from APP transgenic mice that

have previously been developed as models for the amyloid pathology of AD. Moreover, additional players in signal transduction mechanisms during neurodegenerative disease conditions could be identified and characterized by a similar approach.

4.3. Imaging of dendritic arborization, spines, and synapses to study neuronal connectivity

Changes in synaptic connectivity may precede neurodegeneration during the course of disease and may also be involved in potentially compensatory mechanisms. In order to ameliorate therapeutic solutions, the understanding of the background of disease development is required. Therefore, a robust focus has also to be implemented on studies tracing changes of neuronal morphology on the level of dendritic arborization, spines, and synapses. In many studies, dendritic spines, which present the postsynaptic site where most excitatory input is received by neurons, were analyzed (Tackenberg et al., 2009). Some studies explored these aspects in dissociated cultures (Thies and Mandelkow, 2007); however, analyses in a 3D context, that mimics the authentic environment brings the knowledge to a further level.

Dendritic spines vary greatly in their morphology, and the spine size and strength of the synapses correlate. Impairments in synaptic function due to elevated levels of $A\beta$ have been shown by electrophysiological recordings performed through a hole drilled on the skull of rats in a study in which rats were injected intracerebroventricularly with $A\beta$ -fragments (Freir et al., 2001). However, the dynamics of morphological changes in the presence of $A\beta$, which reflects the development and plasticity of synaptic structures could only be evaluated after live imaging of spine motility measurements. In the context of synaptic plasticity, a nice study was exploring the effects of $A\beta$, a peptide, which levels are elevated in AD as well as in Down's syndrome patients (Shrestha et al., 2006). The authors analyzed the elongation and retraction of spines by time-lapse image recordings over a period of 15 min with two-photon microscopy. For the experiments, mouse hippocampal slice cultures, which were transfected biolistically with a GFP encoding plasmid, were used. They found that sublethal levels of $A\beta$ alter dendritic spine number and that the effect on spine density was blocked by rolipram, a phosphodiesterase type IV inhibitor, suggesting the involvement of a cAMP-dependent pathway. Furthermore, shape and dynamics of spines in developing hippocampal neurons was also altered after $A\beta$ exposure. Although no change in spine formation or turnover, that would explain the $A\beta$ -induced reduction in spine density was detected, spine motility was reduced in $A\beta$ -treated neurons, which might be a cause for the reduction of the synaptic contacts. Spine density was restored after a brief withdrawal of $A\beta$, underlining that therapeutic approaches which reduce levels of $A\beta$ might mediate their effect through the restoration of lost dendritic spines

leading to improved cognitive abilities. A longer time-lapse imaging study with two-photon laser scanning microscopy performed on cultivated rat hippocampal slices was done by [Shankar et al. \(2007\)](#). The authors followed spine alteration on apical dendrites of biolistically transfected cells for a total of 75–90 min after introduction of a natural A β oligomer fraction via perfusion. Thus, by this method A β was applied acutely, in contrast to the previously described study, where A β oligomers were present from the start of the culture. The authors observed that 1 h after first exposure to the oligomers, dendritic morphology and spine density were qualitatively similar to those before A β exposure, which suggests that the decrease in spine number is not due to immediate toxic effects of A β . Further studies revealed that spine loss occurred progressively over a period of 5–15 days. These alterations were induced by physiological concentrations of naturally secreted A β dimers and trimers, but not monomers, and were reversible or could be prevented by A β -specific antibodies or a small-molecule modulator of A β aggregation ([Shankar et al., 2007](#)).

Both studies utilized techniques with which changes in spine motility can be analyzed for minutes or even hours during treatment with disease-relevant substances. Similar approaches might uncover specific effects on synapse structure and number and their correlation with spine shape alterations.

4.3.1. Imaging dendritic spines by stimulated emission depletion (STED) microscopy

Specialized fluorescence imaging methods such as STED microscopy can also be utilized in live studies of spine morphology changes. The development and use of STED microscopy was driven to step through the diffraction-limited resolution of conventional light microscopy ([Hell and Wichmann, 1994](#)). Among other biological approaches applying STED microscopy, a recent study describes the advantages of this technique in imaging dendritic spines ([Nägerl et al., 2008](#)). The authors prepared and cultivated with roller-tube method hippocampal slices from YFP-transgenic animals. In these animals, CA1 pyramidal neurons, which were in this study in the focus, were strongly but sparsely labeled. STED microscopy permitted the imaging of activity-driven structural changes of spines during a period of 1 h in a resolution that revealed more precise structural details, than a conventional fluorescent laser scanning microscope is able to provide. However, a strong limitation of STED microscopy comes from the fact, that this technical approach is highly limited in imaging in depth. The images were acquired in the range of 0–10 μm from the surface of the coverslip, which is far from the thickness of an organotypic slice. Therefore, this approach could be useful by its ability to provide improved quantification of morphological parameters of spines, such as the neck width and the curvature of the heads of spines, but it compromises the collection of data from 3D aspects of the neuron and its connections.

4.4. Photobleaching (FRAP, FLIP) and photoactivation to study molecular dynamics

Time-lapse morphological analyses can give information about the motility of single spines. However, it is also necessary to determine how much the structure of individual spines influence the compartmentalization and hence the trafficking and interaction of membrane-associated or soluble proteins, which might play a role in synaptic plasticity. The alterations in spine structure are region and time dependent and entail functional consequences, which might be altered during neurodegenerative processes. An approach to examine whether variability in the shape of dendritic spines affects protein movement within the plasma membrane is to utilize membrane anchored enhanced GFP (mGFP) and the FLIP technique (see [Section 2.3](#)). [Hugel et al. \(2009\)](#) established mice expressing EGFP fused to the membrane-anchoring domain of a palmitoylated mutant of MARCKS29. Expression was mediated by the Thy1 promoter, which resulted in generation of various mice lines expressing the fluorescent protein in hippocampus CA1 region with different patterns. Prior to FLIP analysis, the authors performed 3D image reconstruction of the shape of spines on the respective dendritic segment. During FLIP experiments, the decrease in fluorescence during repeated bleaching of the dendritic shaft was measured in the spine head. Comparing the membrane-associated protein flux between dendritic shafts and spine heads revealed a progressive loss of fluorescence in neighboring dendritic spines. The rate of decrease in fluorescence corresponded to the kinetics of mGFP exchange between the dendritic shaft and the spine head compartment. The FLIP kinetic parameters varied considerably between different spine shapes, and the differences in mGFP exchange between dendritic shaft and spine head compartments were even more obvious when the same analyses were performed after induction of epileptiform activity to explore the changes of FLIP kinetic parameters while topological changes of spines occurred. Dendritic spines with long necks or voluminous heads exhibited slower membrane kinetics than those with short necks or small heads ([Hugel et al., 2009](#)). Synapses are dynamic structures and the removal and incorporation of proteins in the synaptic field is continuous according to request. Therefore, studying the parameters that might affect dynamic rearrangement of synaptic proteins, involving lateral diffusion within the plasma membrane, is essential for understanding structure-dependent functional activity of spines.

The compartmentalization of spines is not restricted on the level of the membrane. However, to what extent the spines isolate the signaling elements and, by that, the propagation of excitatory input towards the dendritic shaft or neighboring spines still needs to be explored. Several papers from the group of Svoboda deal with this question in the context of signal transduction events evoked by activation of *N*-methyl-D-aspartate

receptors (NMDARs). Activity of NMDARs brings a whole chain of signaling molecules into active state including the small guanosine triphosphatase (GTPase) Ras. Furthermore, Ras activates the extracellular signal-related kinase (ERK), which is involved in several signaling processes affecting synaptic plasticity. While Ras is membrane bound and can change its position via diffusion in the plasma membrane, ERK dissipates through different compartments, including spines, dendrites, and the nucleus after activation. Therefore, the spatial and temporal dynamics of Ras-ERK signaling are important for understanding the downstream effects governing morphological and functional alterations of spines. To investigate Ras activation in microcompartments of the cell such as spines, [Yasuda et al. \(2006\)](#) generated a FRET-based indicator of Ras activation, FRas-F, which is rapidly reversible and reports the time course of endogenous Ras activation (see [Section 2.5](#) for the features of FRET). Applying this method protein-protein interactions or activity-driven conformational changes of a protein can be imaged in cells. The two elements of FRas-F were constructed by tagging Ras with monomeric enhanced green fluorescent protein (mEGFP) and tagging the Ras-binding domain (RBD) with two monomeric red fluorescent proteins (mRFPs). FRET was determined in transfected pyramidal neurons of organotypic hippocampal slices using two-photon fluorescence lifetime imaging (2pFLIM), and Ras activation was quantified calculating the fraction of Ras molecules bound to RBD. After the development and characterization of FRas-F, [Harvey et al. \(2008b\)](#) continued to analyze the temporal and spatial modality of Ras. To induce synapse-specific plasticity, a train of two-photon glutamate uncaging pulses were applied that led to a robust Ras activation in the stimulated spine. Ras was active for minutes, and the activity spread over several micrometers in both directions along the parent dendrite and invaded nearby spines prior to inactivation. To investigate whether Ras mobility could affect the spread of Ras activity, Ras tagged with photoactivatable GFP (paGFP-Ras) was expressed. The photoactivation approach provided direct observation and measurement of protein dissipation, in contrast to indirect mobility measurements that could be achieved with the FLIP technique discussed above ([Hugel et al., 2009](#)). The data suggest that Ras diffuses relatively freely within the plasma membrane, and using a constitutively active Ras, that the diffusion is not related to the activity state of the protein. Therefore, it is likely that Ras-dependent signaling is necessary for crosstalk between neighboring spines, which might act as functional units. Whether this implies that spines are affected in similar units during disease-relevant conditions, still needs to be demonstrated.

[Harvey et al. \(2008a\)](#) also developed a FRET-based sensor of ERK activity (the extracellular signal-regulated kinase activity reporter, EKAR) to address the question of spatiotemporal ERK signaling dynamics in living cells. EKAR was constructed as a single molecule that was composed of

several modules, including an ERK docking domain, a substrate peptide and a phospho-binding domain. The donor (EGFP) was tagged to the ERK docking domain and the acceptor (mRFP1) was tagged to the phospho-binding domain. ERK activation leads to phosphorylation of the substrate peptide that in turn binds to the phospho-binding domain resulting in a conformational change of the molecule, thereby triggering FRET between the fluorophores. The authors reported that EKAR's signal is smaller than Ras sensors; however, it is sufficient to examine the spatial and temporal dynamics of ERK signaling under biologically relevant conditions in living cells. Utilizing these genetically encoded FRET-based sensors changes in signal transduction leading to neurodegenerative dénouement may be revealed.

4.5. Ion-sensitive dyes for studying neuronal function

Exploration of cell signaling processes also involves measurement of extracellular or intracellular changes in the concentration of ions involved. There are well-established methods for utilizing ion-sensitive dyes in dissociated cell cultures (see [Section 3.8](#)). Furthermore, there are several studies, which describe analyses of movement and changes in the concentration of ions in tissue slices, as well as newly developed tools with which long-term live imaging of ion dynamics in organotypic slices can be performed.

Several fluorescent dyes can be utilized to visualize the change in the intracellular concentration of Ca^{2+} , the ubiquitous second messenger. [Petrozzino et al. \(1995\)](#) were applying a low affinity fluorescent indicator, mag-Fura 5, that is sensitive to Ca^{2+} in the micromolar range to investigate the magnitude and dynamics of changes in the Ca^{2+} concentration in spines and dendrites of hippocampal CA1 pyramidal neurons, in acute as well as in organotypic slices. Mag-Fura 5 was introduced to the cells via a patch-clamp pipette and the Ca^{2+} increase during synaptic stimulation was traced in time range of seconds. Using this approach, low affinity Ca^{2+} -dependent biochemical processes could be followed during stimulation. Another low affinity calcium-sensitive dye, fluo-4FF AM was utilized on rat cerebellar slices to measure the effects of cannabinoid receptor CB1 inhibition on a presynaptic Ca^{2+} influx after stimulation of parallel fibers ([Daniel et al., 2004](#)). The Griesbeck group developed several genetically encoded calcium indicators. One example is TN-XXL, which is a modification of a troponin C-based calcium biosensor. TN-XXL showed enhanced fluorescence changes in neurons *in vivo* in mouse cortex with two-photon ratiometric imaging. This approach provides a new field for imaging long-term changes of ion concentration, since it was shown to be applicable for imaging for several weeks ([Mank et al., 2008](#)). Transgenic approaches were also utilized to generate mice expressing genetically encodable fluorescent probes. An example are mice that express the enhanced yellow-fluorescent protein

(EYFP) that is able to monitor intracellular changes in pH and Cl^- concentration. Metzger et al. (2002) constructed the transgene, to have the expression under control of the Kv3.1 K^+ channel promoter (pKv3.1). This drives EYFP expression in specific subsets of neurons, namely the cerebellar granule cells, interneurons of the cerebral cortex, and in neurons of hippocampus and thalamus. This promoter also provides high enough levels of expression of the fluorescent protein to be used to monitor the intracellular microenvironment in brain slices and eventually in the live animal.

All of these fluorescence probes can readily be exploited in physiological experiments using brain slices and can also provide an opportunity to visualize an impairment of neuronal function upon neurodegenerative insult. To exploit the mechanism how $\text{A}\beta$ oligomers influence signaling through NMDARs, Ca^{2+} transients were measured in the spine head using 2PLSM in CA1 pyramidal neurons in acute rat hippocampal slices. Cells were filled through the patch pipette with the Ca^{2+} -sensitive, green-fluorescing Fluo-5F, and changes in Ca^{2+} -concentration were monitored after stimulation with local two-photon laser photoactivation of MNI-glutamate (4-methoxy-7-nitroindolyl-caged L-glutamate). After glutamate uncaging, a partial reduction of NMDAR-mediated Ca^{2+} influx was observed into active spines in the presence of acute administration of $\text{A}\beta$ oligomers, while $\text{A}\beta$ monomers did not influence Ca^{2+} influx compared to control conditions. The results suggest that $\text{A}\beta$ oligomer application mimics a state of partial NMDAR blockade that can lead to the progressive loss of dendritic spines (Shankar et al., 2007).

4.6. Coculture experiments for studying axonal outgrowth and pathfinding

Damaged axons of higher vertebrates are unable to regenerate in the adult CNS due to an active suppression of neuroregeneration. CNS lesions or neurodegenerative disease can be causative for axonal damage; therefore, it is important to investigate the underlying mechanisms or possible trains of repair processes. Several coculture experiments have been developed to exploit the inhibitory signals, mechanism of axonal outgrowth and pathfinding, or developmental alterations if a certain brain region lacks proper input or output connections (Li et al., 1994; Ohshima et al., 2008; Snyder-Keller et al., 2008; Wu et al., 2008). Most of the questions addressing these issues can only be answered in an organotypic environment. However, the majority of data have been extracted from histochemically or immunohistochemically prepared tissue. Thus, they do not provide information about dynamic features.

Organotypic hippocampal–entorhinal brain slices are the most abundantly employed due to the differentiated termination of distinct synaptic inputs in the hippocampal formation (Del Turco and Deller, 2007). One of

the tracers that can be efficiently applied is a biotinylated dextrane amine (BDA). BDA is applicable for following the extensions of single or multiple neurons; however, the number of stained neurons is limited because extensive labeling procedure might lead to mechanical damage. For the study of a higher number of cells and their processes labeled in a noninvasive way, a transgenic approach can be utilized. [Hechler et al. \(2006\)](#) reported generation of several EGFP-expressing mice, which can be used in an EGFP/wild-type coculture system. Since EGFP expression is driven by different promoters assigning the expression to various subpopulations or subdomains of cells, each strain is suitable as a model for investigations of different aspects of growth and remodeling of axons. Furthermore, transgenic GFP-expressing rats are also available and utilized for GFP/wild-type coculture experiments, as described in an elegant approach by [Koyama et al. \(2004\)](#). In this study, the different cues that contribute to mossy fiber pathfinding during several developmental stages have been investigated.

4.7. Live imaging of RNA translation

Local protein synthesis regulates many aspects of neuronal function, for example, axonal growth and cell signaling. The amount and distribution of mRNA or respective proteins can be analyzed by biochemical or microscopic approaches. However, due to the development of photoconvertible fluorescent proteins, *de novo* protein synthesis can also be followed live in space and time. An exciting study by [Leung et al. \(2006\)](#) describes utilization of the photoconvertible fluorescent protein Kaede linked to the β -actin 3' UTR (Kaede- β -actin 3' UTR). Kaede protein is originally green but can be irreversibly converted to a red form by UV illumination, thereby permitting the detection of newly synthesized protein by visualizing newly occurring green fluorescence. Time-lapse imaging showed that after conversion of Kaede from green to red in *Xenopus* retinal growth cones and stimulation with netrin-1, *de novo* protein synthesis could be observed in Kaede- β -actin 3' UTR expressing growth cones even when axons were severed from their cell bodies. This demonstrates that mRNA translation occurs locally in the growth cone without the need for protein transport from the soma. Impairment of local protein synthesis may contribute to degenerative processes. Similar experiments could reveal disease-associated disturbances in cell compartment-specific mRNA translation.

4.8. Potential and limitation

Slice-based assay systems are important tools to exploit physiological and disease-related aspects of neuronal morphology and function in an organotypic environment. Slice models provide good experimental access to individual neurons, especially in cultures prepared with roller-tube method,

during which cells flatten to a monolayer. The major advantage in contrast to dissociated cells is that neurons in slices retain their authentic connections. For brain slices cultivated on a membrane interface, a 3D tissue-specific organization of synaptic connections is even more pronounced. Therefore, physiological and disease-related molecular mechanisms might be unraveled and possible routes for treatments could be efficiently evaluated in an authentic environment. However, it should be noted that only acute slices might be obtained from adult animals, facilitating the understanding of age-related processes. In contrast, organotypic slices that allow long-term culturing and imaging are retrieved from embryonic or newborn animals, excluding the opportunity for imaging alterations related to ageing.

5. LIVE IMAGING OF ANIMALS

5.1. Transgenic animals

Considerable effort has been made in the past years to develop novel experimental animal models that manifest many of the characteristic neuropathological and behavioral features of human neurodegenerative diseases. This has been in part driven by the identification of genetic mutations associated with familial forms of these conditions and gene polymorphisms associated with the more common sporadic variants of these diseases. Transgenic animals provide the possibility for long-term imaging of cells in *ex vivo* slice models as well as *in vivo*. This is due to the expression of genetically encoded fluorescent proteins that are introduced to animals via transgenic approaches (Araki et al., 2005; Feng et al., 2000; Hutter, 2004; Sun et al., 1999). However, in contrast to tissue explants, where the surrounding milieu can readily be modified, *in vivo* experiments require the use of animals carrying a disease-relevant transgene or treatments with disease-relevant substances. Since during evolution many processes have been preserved across species, fundamental mechanisms of human neurodegenerative diseases can be studied in different animal models.

Caenorhabditis elegans and *Drosophila melanogaster* are commonly used invertebrate genetic model organisms. For example, tauopathy models have been developed in *C. elegans* based on the overexpression of human tau and disease-related tau mutants. In one study, it was shown that pan-neuronal expression of tau caused progressive uncoordinated locomotion (Unc), tau aggregation, phosphorylation of tau at several disease-related sites, and loss of neurons (Kraemer et al., 2003). Neurons showed signs of axonal degeneration including the formation of vacuoles and membranous infoldings. Mutant tau expressing worms exhibited a more severe phenotype. In a study from our lab, it was shown that human tau in *C. elegans*

becomes highly phosphorylated and exhibits conformational changes similar to human PHF tau (Brandt et al., 2009). However, in these animals, no neuronal degeneration but a defective pattern of motor neuron development was observed as a result of the expression of tau with disease-related mutations. A model for tauopathies has also been generated in *Drosophila* by expressing wild-type and mutant forms of human tau in the fly (Wittmann et al., 2001). The transgenic flies exhibited several features that are typical for the human disease including progressive neurodegeneration and accumulation of tau protein. However, there were also differences. Using *Drosophila*, it was reported that flies exhibited neurodegeneration in the absence of the formation of neurofibrillary tangles. Whether these findings may give new insights into the sequence of events that occur also in the human disease or whether these represent features that are specific for *C. elegans* or *Drosophila* remains to be shown.

A *Drosophila* model for PD has been generated by expression of normal and mutant forms of α -synuclein in the fly (Feany and Bender, 2000). Adult-onset loss of dopaminergic neurons, intraneuronal inclusions containing α -synuclein and locomotor dysfunction were observed thus recapitulating some of the features of the human disorder. Also a *Drosophila* model for ALS has been developed based on the observation that some inherited cases of ALS have a mutation in the gene for zinc-superoxide dismutase (SOD1). Transgenic expression of wild-type or disease-linked mutants of human SOD1 in motor neurons induced progressive movement deficits (Watson et al., 2008). However, no oligomerization of SOD1 or neuronal loss was observed. A *Drosophila* models for human neurodegenerative diseases were reviewed by Bilen and Bonini (2005).

Several disease models have also been developed in the zebrafish (*Danio rerio*), which has become a well-used model organism for studies of vertebrate development. Disease models in zebrafish include a model for ALS, which has been generated by overexpression of mutant SOD1 (Lemmens et al., 2007). Similar to ALS patients, the mutation induces a motor axonopathy in the fish. Also a model for PD based on inactivation of DJ-1 has been developed. Mutations in DJ-1 lead to early onset of PD in patients and caused a loss of dopaminergic neurons after exposure to hydrogen peroxide and proteasome inhibition in the fish (Breitaud et al., 2007).

Genetic model organisms such as *C. elegans*, *Drosophila*, and zebrafish also allow to perform genetic interaction screens to identify mutations that effect degenerative phenotypes. This has, for example, been performed using a transgenic *Drosophila* model that expressed A β and mutations that affect A β metabolism and toxicity have been identified (Cao et al., 2008).

Most of the rodent transgenic animals are mice, nevertheless the number of rats carrying disease-related genes is also increasing (Bugos et al., 2009). Murine models have been designed to better understand diverse aspects of molecular and systemic events occurring during the decay of cognitive

capabilities or neurodegenerative processes. Several mouse models have been developed dealing with the amyloid pathogenesis of AD by encoding human APP or presenilin protein with different familial mutations that were identified in AD patients (Dodart et al., 2002; Higgins and Jacobsen, 2003; Spiess and Hyman, 2005). With respect to tau pathology, transgenic mice expressing human wild-type tau or tau protein with different mutations to achieve the formation of NFTs have been constructed. The latter models can facilitate the understanding of some aspects of other neurodegenerative diseases as well, that are collectively named as tauopathies (Götz, 2001). Janus (2008) summarized the information about conditionally inducible tau mice, in which the temporal regulation of the expression of the transgene enables studying the mechanisms underlying tau pathology from another perspective. Transgenic mouse models representing various features of PD (Fillon and Kahle, 2005) and HD (Lin et al., 2001; Sipione and Cattaneo, 2001) have also been developed. In addition, transgenic animals that are of assistance to unravel the molecular mechanisms of ALS (Jackson et al., 2002) or the prion disease (Scott et al., 2000) were described, and a transgenic mouse strain with GFP-tagged mutant prion, which provides direct visualization of affected cells, had also been utilized (Medrano et al., 2008).

5.2. Live imaging of invertebrate models to study network development and degeneration

C. elegans and *Drosophila* embryos are transparent organisms, which facilitates imaging studies. The construction of transgenic *Drosophila* lines that express GFP in the nervous system of embryos, larvae, pupae, and adults makes it also a useful model to study nervous system degeneration by live-imaging approaches (Sun et al., 1999). This approach has even been taken further in *C. elegans*. Using variants of GFP with different spectral properties and other fluorescent proteins and dyes, a total of five different colors were used simultaneously to analyze the *C. elegans* nervous system *in vivo* (Hutter, 2004).

Although it is not completely clear in how far the pathological features that have been observed in vertebrate disease models reflect the human disease, it could be very informative to use the different disease models also for live-cell imaging to follow, for example, axonal transport deficits. However, except few studies, that has not been done yet. One example is a study with *Drosophila* strains that have mutations in the blue cheese (bchs) gene. A loss-of-function mutation of the bchs gene leads to insoluble CNS protein aggregates, reduced adult life span, and neuronal apoptosis (Finley et al., 2003). These mutants could therefore be a model to analyze impaired axonal transport, which is one of the earliest pathological manifestations of

several neurodegenerative diseases. Using live fluorescence imaging of individual motor neurons in intact *Drosophila* larvae, it could be shown that lysosomal vesicles fail to be transported toward motor neuron termini in *bchs* mutant larvae (Lim and Kraut, 2009).

5.3. Live imaging of vertebrate models to study cell function in intact brain

5.3.1. Zebrafish

Similar to *Drosophila*, also the zebrafish embryo is transparent which facilitates imaging studies. In addition, small animal models as an alternative to more difficult to keep vertebrates as the rat or mouse have a potential in large-scale chemical and genetic screening. By injection of different fluorescent protein expression cassettes, single-, double-, or triple-labeled embryos have been developed (Finley et al., 2001). The animals express, besides GFP, blue fluorescent protein (BFP) and red fluorescent protein (DsRed). The fluorescent proteins can be independently detected which opens the possibility to analyze different aspects of neuronal degeneration at the same time and in parallel.

Zebrafish larvae have also been used to analyze dendrite growth and synaptogenesis during development by long-term imaging of dendritic arbors expressing a fluorescent postsynaptic marker protein (Niell et al., 2004). Based on this study, a “synaptotropic model” has been concluded postulating that synapse formation can direct dendrite arborization. Several mental disorders including AD are associated with spine pathology suggesting that spine alterations play a central role in mental deficits. Thus, it could be informative to study changes of dendritic arbors as a result of neurodegenerative conditions in a zebrafish model.

An exciting application of the zebrafish model is presented in a study by Peri and Nüsslein-Volhard (2008) where the mechanism of degradation of neurons by microglia has been studied by *in vivo* imaging. Microglial-mediated neuronal degeneration may have an important role in many neuronal diseases.

5.3.2. Live imaging mouse neocortex *in vivo*

Spine loss, dendritic alterations, or neuronal cell death represent common hallmarks of neurodegenerative diseases. However, little is known about the underlying mechanisms or relationship between the processes leading to morphological or behavioral changes. Moreover, none of the previously discussed methods can enable scrutinizing these aspects in an *in vivo* ageing environment. Thus, the establishment of long-term *in vivo* imaging techniques provided an important approach to study morphological alterations of neurons or glial cells over extended periods of time during the course of degeneration.

Through a cranial window, [Fuhrmann et al. \(2007\)](#) could visualize cortical dendrites of Thy-1 YFP-H line mice that were inoculated intracerebrally with the prion strain RML (Rocky Mountain Laboratory, Ft. Collins, CO) to model scrapie. Pathological features of prion diseases also include extensive neuronal loss and synaptic alterations. However, the temporal and spatial relationship of these events is not well known. Two-photon imaging over a time period of 3 h was utilized to analyze possible short-term structural plasticity modifications of spines in presymptomatic and symptomatic scrapie-infected mice. In general, the authors observed that the spine density per dendrite length was significantly reduced in symptomatic compared with presymptomatic mice, whereas varicosities significantly increased in symptomatic mice. Regarding plasticity, however, no changes were observed in spine density or morphology, during the 3 h observation time. In order to gain information about the long-term kinetics same dendritic segments were repeatedly visualized up to 2 months. The authors observed that the daily turnover ratio was already higher during the presymptomatic time compared to controls and it even increased later on accompanied by a linear decrease of spine density, mainly affecting persistent spines. Interestingly, at the beginning of the symptomatic phase the fraction of newly formed spines showed an increase. This indicates that the onset of the symptomatic phase of the disease is a critical time point of when neurons react to increasing spine loss by enhanced formation of new spines. These results also implicate that mechanisms regarding the development of new spines are not impaired at the onset of the disease.

[Zeng et al. \(2007\)](#) were exploiting short-term changes of dendrites as a result of kainate-induced seizure. To elucidate the acute changes occurring after a seizure of the highest stage according to a five point modified Racine scale ([Racine, 1972](#)), cortical neurons from GFP-M mice were examined with two-photon imaging. Same dendritic segments were imaged preexposure to kainate injection and up to 2 h after allowing mice to remain in stage 5 seizures for 30 min. Kainate-induced seizure led to immediate mild or severe dendritic beading accompanied by a loss of spines. The dendritic beading usually recovered almost completely within 1–2 h, but the recovery of spines was only partial and this loss of spines remained even during imaging up to 24 h. Severe blebbing of dendrites accompanied by loss of spines were reported by [Takano et al. \(2007\)](#) as well. They were visualizing same dendritic segments of cortical neurons in a time period of minutes. Thy-1 YFP-H line mice were utilized in order to elucidate the morphological consequences of cortical spreading depression (CSD) that has been implicated in migraine and in progressive neuronal injury after stroke and head trauma. In their study the changes in volume of the neuronal somas was also quantified, which showed an increase in parallel to structural changes of the dendrites. However, the morphological alterations appeared

to be transient in this case, since the morphology of most dendrites returned to normal after CSD, and neuronal cell bodies assumed their pre-CSD volumes within 8–10 min.

Spires et al. (2005) examined the alterations in morphology and synaptic connections *in vivo* in an AD mouse model. For visualization of neurons, enhanced GFP containing AAV was intracortically injected. To achieve simultaneous imaging of A β plaques and vessels, mice were injected with methoxy-XO4 and Texas Red dextran, respectively. This approach provided the possibility to examine the effects of dense-cored amyloid plaques on spines, since the number and morphology of spines on dendritic segments were analyzed at different distances from plaques. Two-photon imaging revealed disrupted neurite trajectories and reductions in dendritic spine density in plaque-forming mice compared with age-matched control mice. This feature was more profound in the vicinity of plaques, however, a robust decrease of spines was also reported on dendrites, which were not associated with plaques. Interestingly, the authors found, that despite massive spine loss, amyloid plaques had no influence on the spine morphology and length. Furthermore, the same group was examining plaque formation and their growth pattern by reimaging the same cortical region of a plaque-forming and YFP-expressing mouse over days to weeks. Plaques and vessels were identified the same way as described above. The authors reported that senile plaque formation was a very rapid event occurring within 24 h. Crossing plaque-forming mice with a line that expresses EGFP in microglia showed that microglia were attracted to the site within a day after plaque formation. Further investigations revealed progressive neuritic changes over the next days to weeks (Meyer-Luehmann et al., 2008).

Several studies utilizing cultured cells or organotypic slices couple changes in number and shape of spines occurring during A β treatment to altered calcium handling, for example, Ca²⁺ overload, reduction, or activation of Ca²⁺-dependent degenerative processes (Canzoniero and Snider, 2005; Shankar et al., 2007). Recent experimental approaches exploited this issue *in vivo*. Busche et al. (2008) examined the activity level of neurons in plaque-forming and wild-type mice *in vivo*. The Ca²⁺ indicator dye Oregon Green 488 BAPTA-1 AM (OGB-1) and a fluorescent marker of plaques (thioflavin S) were sequentially injected into the layer 2/3 of the cortex. The authors observed an increased number of silent as well as hyperactive cells in plaque-forming mice. The hyperactive neurons were found exclusively near the plaques of A β -depositing mice, which fits nicely with the observation of Ca²⁺ overload in the study by Kuchibhotla et al., (2008). The authors were employing a yellowameleon 3.6 FRET-based probe, packed in an AAV2, which they injected into the region of cortical cells of adult mice. Quantitative imaging revealed elevated Ca²⁺ level in 20% of neurites in plaque-forming mice compared to transgenic or nontransgenic mice with no plaque formation.

Data demonstrated that A β plaques are focal sources leading to Ca²⁺ overload. This functional abnormality led to morphological changes, for example, beading, which was coupled to calcineurin activation.

Dysfunction of the nervous system includes alterations of glial cells as well. In a follow-up study [Kuchibhotla et al. \(2009\)](#) investigated Ca²⁺ handling of astrocytes in AD mouse models. In this case, they were using OGB-1 to visualize Ca²⁺ levels. Time-lapse imaging revealed that calcium transients in astrocytes were more frequent, synchronously coordinated across long distances, and uncoupled from neuronal activity. Furthermore, rare intercellular calcium waves were observed, but only in mice with A β plaques, originating near plaques and spreading radially at least 200 μ m.

In all of these studies, live time-lapse imaging directly revealed long-term or rapid neuronal alterations on the level of morphology as well as function of cells *in vivo*. It became obvious that different environmental conditions leading to neurodegeneration have diverse spatial and temporal dynamics. From these studies important data yields to a better understanding where, when, and how morphological alterations occur *in vivo*, whether they are reversible, and if so until which level. These kinds of experiments could also reveal the effect of potential drugs, and the time scale of their administration, which might protect neurons or enhance the regeneration processes.

5.4. Potential and limitation

Invertebrate and lower vertebrate models allow systematic screening for drugs that reduce neurodegeneration. However, most neurodegenerative diseases exhibit brain region-specific functional impairments and cell death. Thus, since the anatomy of the brain of *C. elegans*, *Drosophila*, and zebrafish is quite different from the human brain, conclusions with respect to brain region-specific disease-related changes are limited. Live imaging of neurons in rodents allows an analysis of disease processes in a way that is closest to the course of neurodegeneration that takes place in humans. In case of the mouse model, many papers address these issues, albeit in most cases data are drawn from fixed tissues and therefore dynamic features of the disease are missing. With the development of a technique that allows short-term or long-term imaging of neurons even on the level of individual dendritic spines in the living mouse cortex or hippocampus dynamic aspects of changes are revealed during physiological as well as disease-related conditions ([Grutzendler et al., 2002](#); [Mizrahi et al., 2004](#)). This allows following up the evolution of alterations more accurately in time, even up to months, and in space.

It should be noted, however, that a complex interplay of various factors is a common property of several neurodegenerative diseases. This requires diverse transgenic animal approaches, or treatment of animals, which may

address different but in most cases not all aspects of neurodegenerative processes. It is laborious to generate double transgenic animals, which carry a relevant gene that leads to disease development as well as a gene that encodes a fluorescence protein for visualization. Furthermore, there are fewer options to modify the extracellular environment compared to organotypic slices, which limits the experimental repertoire that can be used.

6. MULTIPHOTON VERSUS ONE-PHOTON MICROSCOPY—POTENTIAL AND LIMITATION

The development of vital fluorescent synthetic dyes and a myriad of genetically encoded fluorescent proteins enabled sensitive visualization of a vast range of features in living cells and tissue samples with fluorescence microscopy. However, standard fluorescence microscopy can give only a 2D view of a specimen and to achieve 3D resolution optical sectioning needs to be applied. One highly efficient way of optical sectioning is to utilize confocal microscopy; however, it has some limitation when long-term live imaging or greater imaging in depths has to be achieved. In both cases a nonlinear microscopy technique, the multiphoton imaging has a significant advantage over one-photon excitation. Denk (1994) developed the first biological application of multiphoton excitation, by the invention of a two-photon laser scanning microscope. Two-photon microscopy provides high-resolution images from deep within living tissue, due to the relatively deep penetration of IR excitation light into biological specimens. This is the only method by which imaging of cellular and subcellular processes at a level down to individual dendritic spines can be achieved in the *in vivo* mouse cortex or organotypic cultures (e.g., see Fig. 2.1).

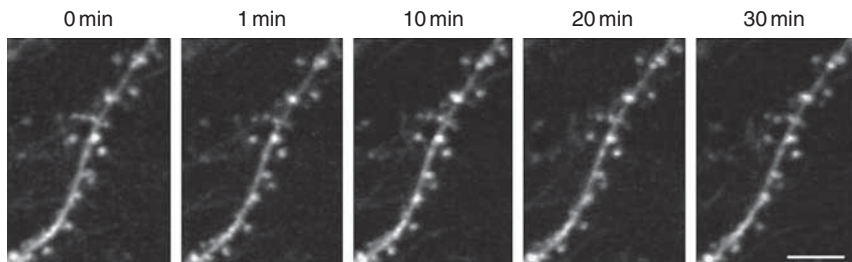


Figure 2.1 Time-lapse images of a representative dendritic segment of a CA1 pyramidal neuron. EGFP-tau was introduced in the mouse organotypic hippocampal slice culture by Sindbis virus. Repetitive imaging with 2PLSM could follow the same apical dendritic segment of an EGFP-positive neuron in CA1 region. The excitatory wavelength was 910 nm. Scale bar, 5 μm .

Furthermore, since potential photobleaching and phototoxicity related to fluorescence excitation is restricted to the focal point, multiphoton imaging results in less damage to the specimen especially during longer, repetitive imaging. Several specialized techniques utilized in research employing one-photon excitation have already been adapted to two-photon microscopy as well. Therefore the distribution, behavior, and interactions of labeled molecules in individual cells of the nervous tissue can be determined *in vivo* or *ex vivo* under physiological and experimental conditions (Benninger et al., 2008; Helmchen and Denk, 2002; Svoboda and Yasuda, 2006).

7. COMBINED APPROACHES

One limitation of live-imaging approaches is that they depend on light microscopic techniques which provide limited data acquisition. Thus, combined approaches have been developed to complement data from live-imaging studies with other techniques such as mass spectroscopy to identify proteins and protein modifications on a molecular level, or electron microscopy for structural analysis, and electrophysiology to follow cell function.

7.1. Live imaging and matrix-assisted laser desorption/ionization (MALDI) to correlate functional states with degeneration

Combination of cellular live imaging with mass spectroscopic techniques allows to correlate functional states as determined by live imaging with local expression profiles. An example presents the application of MALDI MS technique directly to tissue sections to create maps of selected molecules on a cellular level (Wisztorski et al., 2008). A typical experiment involves performing a live-imaging study on a tissue slice, freezing the slice at a selected time point, and analyzing the distribution and posttranslational modifications of proteins from the frozen tissue. The application of such a combined approach could allow to correlate stages of neuronal degeneration as determined by live imaging with the phosphorylation pattern of selected proteins, for example, phosphorylation of tau protein which is involved in tauopathies. It may also be possible to identify additional protein modifications which may be of relevance for the disease process and to analyze for the molecular determinants of protein redistribution during pathological processes.

7.2. Live imaging and electron microscopy to correlate ultrastructure with degeneration

Correlative light-electron microscopy (CLEM) allows to combine live imaging with the high resolution provided by electron microscopic techniques. One approach is to use GFP-tagged proteins for live imaging followed by performing high-resolution scanning electron microscopy to determine localization of GFP at the nanometer level (Drummond and Allen, 2008). Correlative light and electron microscopy after live-cell imaging was, for example, used to analyze the complex in which microtubules are associated to chromosomes (Haraguchi et al., 2008). In this approach, cells expressing a GFP fusion protein were cultured on a gridded coverslip, live imaged, and fixed with glutaraldehyde at specific time points during mitosis. After postfixation cells were processed for electron microscopy, embedded and the block trimmed according to the grid reference on the coverslip and sliced in ultrathin sections. Sections were then stained and analyzed by electron microscopy. Such an approach could be very useful to correlate neurodegenerative processes, for example, spine shapes, with an ultrastructural analysis of individual spines or to determine cytoskeletal changes on a nanometer level at distinct steps of axonopathy.

7.3. Live imaging and electrophysiology to correlate cell signaling and morphology with function

Combination of live-cell imaging and electrophysiology provides an approach to understand the function of neural networks. This requires the ability to monitor action potentials and synaptic activity in populations of identified neurons within tissue explants or animals *in vivo*. A nice study by Mao et al. (2008) describes whole-cell recordings from pyramidal neurons in acute hippocampal culture, together with imaging action potential or synaptically evoked calcium transients by visualizing Ca^{2+} levels with a genetically encoded calcium indicator (GCaMP). Furthermore, diverse GCaMP constructs were engineered to target the expression of the calcium sensor to the membrane or to dendritic spines. Whole-cell voltage-clamp recordings were obtained from pyramidal neurons of rat hippocampal organotypic cultures in the study by Shankar et al. (2007) to investigate the effect of $\text{A}\beta$ oligomers on cell function. Thus, Ca^{2+} imaging and simultaneous electrophysiological recording permit to follow the functional state of cells and their connections at physiological or disease-relevant conditions.

8. CONCLUDING REMARKS

Neurodegenerative diseases represent a large human, societal, and economic burden, which is continually growing as the elderly population increases worldwide. A better understanding of the disease mechanisms underlying neurodegenerative disorders is required if new treatments are to be developed. Toward this goal, many *in vitro* and *in vivo* models, which develop aspects of different neurodegenerative disorders, have been developed.

Many aspects of degeneration are associated with dynamic changes in the behavior of cells, cell compartments, or proteins. Thus, live-cell-imaging approaches could contribute to a better understanding of dynamic features of neurodegenerative diseases. In fact, several basic mechanisms and processes have already been uncovered and characterized by live-cell-imaging approaches of neurodegeneration models. These include a detailed analysis of the dynamics of the formation of protein inclusions in cell models of HD by FRAP and FLIP methods, or the determination of diffusion constants for disease-relevant proteins in axons of primary neurons. However, it appears that until now the full potential of live-imaging approaches has not yet been exploited for questions related to the development and treatment of neurodegenerative disorders. In particular, it would be very informative to improve and apply live-imaging techniques for the analysis of more complex culture models or animals *in vivo* since it became more and more evident that disease-related changes involve also cell-cell contacts and the presence of extracellular factors. With respect to the study of animals, it has become evident that even other body systems such as the immune system can have an important role that is relevant for the development of therapeutic strategies. An example presents the observation that approaches that are based on immunization against disease-relevant proteins such as A β in AD cannot be readily transferred from the mouse model to human patients due to the development of complications related to inflammatory reactions (Lichtlen and Mohajeri, 2008). In addition, combined approaches, for example, by correlating live-imaging results with mass spectroscopic data, will provide the possibility to determine changes of many proteins using proteomic methods thereby opening a systems biology perspective for the analysis of disease-related mechanisms.

Epifluorescence, confocal laser scanning microscopy (LSM), or multiphoton microscopy is limited due to the need to use fluorophores or fluorescent proteins. The way of their application, the amount of expression, and their illumination can lead to a damage of the biological sample. Furthermore, all of these techniques have a limited resolution due to diffraction of light. Therefore, broadening the borders requires further

development in several directions. Transparent species like *C. elegans* provide the possibility to use the endogenous higher harmonic generation, such as third harmonic generation microscopy. This nonlinear imaging methodology does not require application of a fluorescent probe; nevertheless, it is possible to observe neurodegeneration within *C. elegans* up to several hours (Gualda et al., 2008). With respect to gain higher resolution, extensive development was starting in early 1990s and is still taking place. Hell (2009) recently summarized novel techniques by which a nanoscale spatial resolution can be achieved.

Thus, in the future, live-cell imaging of neurodegenerative diseases will go in different directions with the potential to provide complementary data to more standard approaches based on analysis of fixed tissue or biochemical techniques.

ACKNOWLEDGMENT

Funds have been provided by the Deutsche Forschungsgemeinschaft (DFG BR1192/11–1).

REFERENCES

- Aguzzi, A., Heikenwalder, M., Polymenidou, M., 2007. Insights into prion strains and neurotoxicity. *Nat. Rev. Mol. Cell Biol.* 8, 552–561.
- An, S.J., Almers, W., 2004. Tracking SNARE complex formation in live endocrine cells. *Science* 306, 1042–1046.
- Araki, R., Sakagami, H., Yanagawa, Y., Hikima, T., Ishizuka, T., Yawo, H., 2005. Transgenic mouse lines expressing synaptophluorin in hippocampus and cerebellar cortex. *Genesis* 42, 53–60.
- Bacia, K., Kim, S.A., Schwille, P., 2006. Fluorescence cross-correlation spectroscopy in living cells. *Nat. Methods* 3, 83–89.
- Bali, B., Ferenczi, S., Kovács, K., 2008. Direct inhibitory effect of glucocorticoids on corticotrophin-releasing hormone gene expression in neurones of the paraventricular nucleus in rat hypothalamic organotypic cultures. *J. Neuroendocrinol.* 20, 1045–1051.
- Ballatore, C., Lee, V.M., Trojanowski, J.Q., 2007. Tau-mediated neurodegeneration in Alzheimer's disease and related disorders. *Nat. Rev. Neurosci.* 8, 663–672.
- Banker, G.A., Cowan, W.M., 1977. Rat hippocampal neurons in dispersed cell culture. *Brain Res.* 126, 397–442.
- Benediktsson, A., Schachtele, S., Green, S., Dailey, M., 2005. Ballistic labeling and dynamic imaging of astrocytes in organotypic hippocampal slice cultures. *J. Neurosci. Methods* 141, 41–53.
- Benninger, R., Hao, M., Piston, D., 2008. Multi-photon excitation imaging of dynamic processes in living cells and tissues. *Rev. Physiol. Biochem. Pharmacol.* 160, 71–92.
- Berdichevsky, Y., Sabolek, H., Levine, J., Staley, K., Yarmush, M., 2009. Microfluidics and multielectrode array-compatible organotypic slice culture method. *J. Neurosci. Methods* 178, 59–64.
- Berg, J., Hung, Y.P., Yellen, G., 2009. A genetically encoded fluorescent reporter of ATP:ADP ratio. *Nat. Methods* 6(2), 161–166.

- Bergold, P., Casaccia-Bonnel, P., 1997. Preparation of organotypic hippocampal slice cultures using the membrane filter method. *Methods Mol. Biol.* 72, 15–22.
- Biedler, J.L., Helson, L., Spengler, B.A., 1973. Morphology and growth, tumorigenicity, and cytogenetics of human neuroblastoma cells in continuous culture. *Cancer Res.* 33, 2643–2652.
- Biedler, J.L., Roffler-Tarlov, S., Schachner, M., Freedman, L.S., 1978. Multiple neurotransmitter synthesis by human neuroblastoma cell lines and clones. *Cancer Res.* 38, 3751–3757.
- Bilen, J., Bonini, N.M., 2005. *Drosophila* as a model for human neurodegenerative disease. *Annu. Rev. Genet.* 39, 153–171.
- Botvinick, E.L., Shah, J.V., 2007. Laser-based measurements in cell biology. *Methods Cell Biol.* 82, 81–109.
- Bradke, F., Dotti, C.G., 1997. Neuronal polarity: vectorial cytoplasmic flow precedes axon formation. *Neuron* 19, 1175–1186.
- Brandt, R., Leschik, J., 2004. Functional interactions of tau and their relevance for Alzheimer's disease. *Curr. Alzheimer Res.* 1, 255–269.
- Brandt, R., Gergou, A., Wacker, I., Fath, T., Hutter, H., 2009. A *Caenorhabditis elegans* model of tau hyperphosphorylation: induction of developmental defects by transgenic overexpression of Alzheimer's disease-like modified tau. *Neurobiol. Aging* 30, 22–33.
- Bretaud, S., Allen, C., Ingham, P.W., Bandmann, O., 2007. P53-dependent neuronal cell death in a DJ-1-deficient zebrafish model of Parkinson's disease. *J. Neurochem.* 100, 1626–1635.
- Buchstaller, A., Jay, D.G., 2000. Micro-scale chromophore-assisted laser inactivation of nerve growth cone proteins. *Microsc. Res. Tech.* 48, 97–106.
- Bugos, O., Bhide, M., Zilka, N., 2009. Beyond the rat models of human neurodegenerative disorders. *Cell Mol. Neurobiol.* [Epub ahead of print].
- Bursztajn, S., DeSouza, R., McPhie, D.L., Berman, S.A., Shioi, J., Robakis, N.K., et al., 1998. Overexpression in neurons of human presenilin-1 or a presenilin-1 familial Alzheimer disease mutant does not enhance apoptosis. *J. Neurosci.* 18, 9790–9799.
- Busche, M., Eichhoff, G., Adelsberger, H., Abramowski, D., Wiederhold, K., Haass, C., et al., 2008. Clusters of hyperactive neurons near amyloid plaques in a mouse model of Alzheimer's disease. *Science* 321, 1686–1689.
- Busciglio, J., Lorenzo, A., Yeh, J., Yankner, B.A., 1995. Beta-amyloid fibrils induce tau phosphorylation and loss of microtubule binding. *Neuron* 14, 879–888.
- Canzoniero, L.M., Snider, B.J., 2005. Calcium in Alzheimer's disease pathogenesis: too much, too little or in the wrong place? *J. Alzheimers Dis.* 8, 147–154.
- Cao, W., Song, H.J., Gangi, T., Kelkar, A., Antani, I., Garza, D., et al., 2008. Identification of novel genes that modify phenotypes induced by Alzheimer's beta-amyloid overexpression in *Drosophila*. *Genetics* 178, 1457–1471.
- Chai, Y., Shao, J., Miller, V.M., Williams, A., Paulson, H.L., 2002. Live-cell imaging reveals divergent intracellular dynamics of polyglutamine disease proteins and supports a sequestration model of pathogenesis. *Proc. Natl. Acad. Sci. USA* 99, 9310–9315.
- Chaturvedi, R.K., Beal, M.F., 2008. Mitochondrial approaches for neuroprotection. *Ann. N. Y. Acad. Sci.* 1147, 395–412.
- Chen, C.D., Oh, S.Y., Hinman, J.D., Abraham, C.R., 2006. Visualization of APP dimerization and APP-Notch2 heterodimerization in living cells using bimolecular fluorescence complementation. *J. Neurochem.* 97, 30–43.
- Chen, H., Farkas, E.R., Webb, W.W., 2008. *In vivo* applications of fluorescence correlation spectroscopy. *Methods Cell Biol.* 89, 3–35.
- Chun, W., Waldo, G.S., Johnson, G.V., 2007. Split GFP complementation assay: a novel approach to quantitatively measure aggregation of tau *in situ*: effects of GSK3beta activation and caspase 3 cleavage. *J. Neurochem.* 103, 2529–2539.

- Daniel, H., Rancillac, A., Crepel, F., 2004. Mechanisms underlying cannabinoid inhibition of presynaptic Ca^{2+} influx at parallel fibre synapses of the rat cerebellum. *J. Physiol.* 557, 159–174.
- De Diego Otero, Y., Severijnen, L.A., van Cappellen, G., Schrier, M., Oostra, B., Willemsen, R., 2002. Transport of fragile X mental retardation protein via granules in neurites of PC12 cells. *Mol. Cell Biol.* 22, 8332–8341.
- De Simoni, A., Yu, L., 2006. Preparation of organotypic hippocampal slice cultures: interface method. *Nat. Protoc.* 1, 1439–1445.
- De Simoni, A., Griesinger, C., Edwards, F., 2003. Development of rat CA1 neurones in acute versus organotypic slices: role of experience in synaptic morphology and activity. *J. Physiol.* 550, 135–147.
- Del Turco, D., Deller, T., 2007. Organotypic entorhino-hippocampal slice cultures—a tool to study the molecular and cellular regulation of axonal regeneration and collateral sprouting *in vitro*. *Methods Mol. Biol.* 399, 55–66.
- Deng, J., Dunaevsky, A., 2005. Dynamics of dendritic spines and their afferent terminals: spines are more motile than presynaptic boutons. *Dev. Biol.* 277, 366–377.
- Denk, W., 1994. Two-photon scanning photochemical microscopy: mapping ligand-gated ion channel distributions. *Proc. Natl. Acad. Sci. USA* 91, 6629–6633.
- Dickson, T., Chung, R., McCormack, G., Staal, J., Vickers, J., 2007. Acute reactive and regenerative changes in mature cortical axons following injury. *Neuroreport* 18, 283–288.
- Dittgen, T., Nimmerjahn, A., Komai, S., Licznarski, P., Waters, J., Margrie, T., et al., 2004. Lentivirus-based genetic manipulations of cortical neurons and their optical and electrophysiological monitoring *in vivo*. *Proc. Natl. Acad. Sci. USA* 101, 18206–18211.
- Dodart, J., Mathis, C., Bales, K., Paul, S., 2002. Does my mouse have Alzheimer's disease? *Genes Brain Behav.* 1, 142–155.
- Dotti, C.G., Sullivan, C.A., Banker, G.A., 1988. The establishment of polarity by hippocampal neurons in culture. *J. Neurosci.* 8, 1454–1468.
- Drummond, S.P., Allen, T.D., 2008. From live-cell imaging to scanning electron microscopy (SEM): the use of green fluorescent protein (GFP) as a common label. *Methods Cell Biol.* 88, 97–108.
- Eckert, G.P., Wood, W.G., Müller, W.E., 2005. Membrane disordering effects of beta-amyloid peptides. *Subcell Biochem.* 38, 319–337.
- Egert, U., Schlosshauer, B., Fennrich, S., Nisch, W., Fejtl, M., Knott, T., et al., 1998. A novel organotypic long-term culture of the rat hippocampus on substrate-integrated multielectrode arrays. *Brain Res. Brain Res. Protoc.* 2, 229–242.
- Ehrengruber, M., Hennou, S., Büeler, H., Naim, H., Déglon, N., Lundstrom, K., 2001. Gene transfer into neurons from hippocampal slices: comparison of recombinant Semliki Forest Virus, adenovirus, adeno-associated virus, lentivirus, and measles virus. *Mol. Cell Neurosci.* 17, 855–871.
- Emmanouilidou, E., Teschemacher, A.G., Pouli, A.E., Nicholls, L.I., Seward, E.P., Rutter, G., 1999. Imaging Ca^{2+} concentration changes at the secretory vesicle surface with a recombinant targeted cameleon. *Curr. Biol.* 9, 915–918.
- Fath, T., Eidenmüller, J., Maas, T., Brandt, R., 2000. Herpes simplex virus-mediated expression of the axonal protein tau in human model neurons (NT2-N cells). *Microsc. Res. Tech.* 48, 85–96.
- Feany, M.B., Bender, W.W., 2000. A *Drosophila* model of Parkinson's disease. *Nature* 404, 394–398.
- Felmy, F., 2009. Actin and dynamin recruitment and the lack thereof at exo- and endocytotic sites in PC12 cells. *Pflügers Arch.* 458(2), 403–417.

- Feng, G., Mellor, R., Bernstein, M., Keller-Peck, C., Nguyen, Q., Wallace, M., et al., 2000. Imaging neuronal subsets in transgenic mice expressing multiple spectral variants of GFP. *Neuron* 28, 41–51.
- Ferenz, N.P., Wadsworth, P., 2007. Prophase microtubule arrays undergo flux-like behavior in mammalian cells. *Mol. Biol. Cell* 18, 3993–4002.
- Fillon, G., Kahle, P., 2005. Alpha-synuclein transgenic mice: relevance to multiple system atrophy. *Mov. Disord.* 20 (Suppl. 12), S64–S66.
- Finley, K.R., Davidson, A.E., Ekker, S.C., 2001. Three-color imaging using fluorescent proteins in living zebrafish embryos. *Biotechniques* 31, 66–70.
- Finley, K.D., Edeen, P.T., Cumming, R.C., Mardahl-Dumesnil, M.D., Taylor, B.J., Rodriguez, M.H., et al., 2003. Blue cheese mutations define a novel, conserved gene involved in progressive neural degeneration. *J. Neurosci.* 23, 1254–1264.
- Fischer, L.R., Glass, J.D., 2007. Axonal degeneration in motor neuron disease. *Neurodegener. Dis.* 4, 431–442.
- Freir, D., Holscher, C., Herron, C., 2001. Blockade of long-term potentiation by beta-amyloid peptides in the CA1 region of the rat hippocampus *in vivo*. *J. Neurophysiol.* 85, 708–713.
- Fuhrmann, M., Mitteregger, G., Kretschmar, H., Herms, J., 2007. Dendritic pathology in prion disease starts at the synaptic spine. *J. Neurosci.* 27, 6224–6233.
- Gähwiler, B., 1981. Organotypic monolayer cultures of nervous tissue. *J. Neurosci. Methods* 4, 329–342.
- Gähwiler, B., Capogna, M., Debanne, D., McKinney, R., Thompson, S., 1997. Organotypic slice cultures: a technique has come of age. *Trends Neurosci.* 20, 471–477.
- Gähwiler, B., Thompson, S., Muller, D., 2001. Preparation and maintenance of organotypic slice cultures of CNS tissue. *Curr. Protoc. Neurosci.* Chapter 6: Unit 6.11.
- Geller, A.I., Freese, A., 1990. Infection of cultured central nervous system neurons with a defective herpes simplex virus 1 vector results in stable expression of *Escherichia coli* beta-galactosidase. *Proc. Natl. Acad. Sci. USA* 87, 1149–1153.
- Gogolla, N., Galimberti, I., DePaola, V., Caroni, P., 2006a. Long-term live imaging of neuronal circuits in organotypic hippocampal slice cultures. *Nat. Protoc.* 1, 1223–1226.
- Gogolla, N., Galimberti, I., DePaola, V., Caroni, P., 2006b. Preparation of organotypic hippocampal slice cultures for long-term live imaging. *Nat. Protoc.* 1, 1165–1171.
- Götz, J., 2001. Tau and transgenic animal models. *Brain Res. Brain Res. Rev.* 35, 266–286.
- Greene, L.A., Tischler, A.S., 1976. Establishment of a noradrenergic clonal line of rat adrenal pheochromocytoma cells which respond to nerve growth factor. *Proc. Natl. Acad. Sci. USA* 73, 2424–2428.
- Grutzendler, J., Kasthuri, N., Gan, W., 2002. Long-term dendritic spine stability in the adult cortex. *Nature* 420, 812–816.
- Gualda, E.J., Filippidis, G., Mari, M., Voglis, G., Vlachos, M., Fotakis, C., et al., 2008. *In vivo* imaging of neurodegeneration in *Caenorhabditis elegans* by third harmonic generation microscopy. *J. Microsc.* 232, 270–275.
- Haass, C., Selkoe, D.J., 2007. Soluble protein oligomers in neurodegeneration: lessons from the Alzheimer's amyloid beta-peptide. *Nat. Rev. Mol. Cell Biol.* 8, 101–112.
- Hajjeva, P., Kuhlmann, C., Luhmann, H.J., Behl, C., 2009. Impaired calcium homeostasis in aged hippocampal neurons. *Neurosci. Lett.* 451, 119–123.
- Haraguchi, T., Kojidani, T., Koujin, T., Shimi, T., Osakada, H., Mori, C., et al., 2008. Live cell imaging and electron microscopy reveal dynamic processes of BAF-directed nuclear envelope assembly. *J. Cell Sci.* 121, 2540–2554.
- Harvey, C., Ehrhardt, A., Cellurale, C., Zhong, H., Yasuda, R., Davis, R., et al., 2008a. A genetically encoded fluorescent sensor of ERK activity. *Proc. Natl. Acad. Sci. USA* 105, 19264–19269.

- Harvey, C., Yasuda, R., Zhong, H., Svoboda, K., 2008b. The spread of Ras activity triggered by activation of a single dendritic spine. *Science* 321, 136–140.
- Hechler, D., Nitsch, R., Hendrix, S., 2006. Green-fluorescent-protein-expressing mice as models for the study of axonal growth and regeneration *in vitro*. *Brain Res. Rev.* 52, 160–169.
- Hell, S., 2009. Microscopy and its focal switch. *Nat. Methods* 6, 24–32.
- Hell, S., Wichmann, J., 1994. Breaking the diffraction resolution limit by stimulated emission: stimulated emission depletion microscopy. *Opt. Lett.* 19, 780–782.
- Helmchen, F., Denk, W., 2002. New developments in multiphoton microscopy. *Curr. Opin. Neurobiol.* 12, 593–601.
- Higgins, G., Jacobsen, H., 2003. Transgenic mouse models of Alzheimer's disease: phenotype and application. *Behav. Pharmacol.* 14, 419–438.
- Hogue, M., 1947. Human fetal ependymal cells in tissue cultures. *Anat. Rec.* 99, 642.
- Hossain, S., Grande, M., Ahmadvanov, G., Pramanik, A., 2007. Binding of the Alzheimer amyloid beta-peptide to neuronal cell membranes by fluorescence correlation spectroscopy. *Exp. Mol. Pathol.* 82, 169–174.
- Hu, C.D., Grinberg, A.V., Kerppola, T.K., 2005. Visualization of protein interactions in living cells using bimolecular fluorescence complementation (BiFC) analysis. *Curr. Protoc. Protein Sci.* Chapter 19:Unit 19.10.
- Hugel, S., Abegg, M., de Paola, V., Caroni, P., Gähwiler, B., McKinney, R., 2009. Dendritic spine morphology determines membrane-associated protein exchange between dendritic shafts and spine heads. *Cereb. Cortex* 19, 697–702.
- Hutter, H., 2004. Five-colour *in vivo* imaging of neurons in *Caenorhabditis elegans*. *J. Microsc.* 215, 213–218.
- Jackson, M., Ganel, R., Rothstein, J., 2002. Models of amyotrophic lateral sclerosis. *Curr. Protoc. Neurosci.* Chapter 9:Unit 9.13. Review.
- Jacobson, K., Rajfur, Z., Vitriol, E., Hahn, K., 2008. Chromophore-assisted laser inactivation in cell biology. *Trends Cell Biol.* 18, 443–450.
- Janas, J., Skowronski, J., Van Aelst, L., 2006. Lentiviral delivery of rai in hippocampal neurons. *Methods Enzymol.* 406, 593–605.
- Janus, C., 2008. Conditionally inducible tau mice—designing a better mouse model of neurodegenerative diseases. *Genes Brain Behav.* 7 (Suppl. 1), 12–27.
- Jones-Villeneuve, E.M., McBurney, M.W., Rogers, K.A., Kalnins, V.I., 1982. Retinoic acid induces embryonal carcinoma cells to differentiate into neurons and glial cells. *J. Cell Biol.* 94, 253–262.
- Kaether, C., Skehel, P., Dotti, C.G., 2000. Axonal membrane proteins are transported in distinct carriers: a two-color video microscopy study in cultured hippocampal neurons. *Mol. Biol. Cell* 11, 1213–1224.
- Kalab, P., Pralle, A., 2008. Quantitative fluorescence lifetime imaging in cells as a tool to design computational models of ran-regulated reaction networks. *Methods Cell Biol.* 89, 541–568.
- Kitamura, A., Kubota, H., Pack, C.G., Matsumoto, G., Hirayama, S., Takahashi, Y., et al., 2006. Cytosolic chaperonin prevents polyglutamine toxicity with altering the aggregation state. *Nat. Cell Biol.* 8, 1163–1170.
- Konzack, S., Thies, E., Marx, A., Mandelkow, E.M., Mandelkow, E., 2007. Swimming against the tide: mobility of the microtubule-associated protein tau in neurons. *J. Neurosci.* 27, 9916–9927.
- Koyama, R., Yamada, M., Nishiyama, N., Matsuki, N., Ikegaya, Y., 2004. Developmental switch in axon guidance modes of hippocampal mossy fibers *in vitro*. *Dev. Biol.* 267, 29–42.
- Kraemer, B.C., Zhang, B., Leverenz, J.B., Thomas, J.H., Trojanowski, J.Q., Schellenberg, G.D., 2003. Neurodegeneration and defective neurotransmission in a *Caenorhabditis elegans* model of tauopathy. *Proc. Natl. Acad. Sci. USA* 100, 9653–9655.

- Krassioukov, A., Ackery, A., Schwartz, G., Adamchik, Y., Liu, Y., Fehlings, M., 2002. An *in vitro* model of neurotrauma in organotypic spinal cord cultures from adult mice. *Brain Res. Brain Res. Protoc.* 10, 60–68.
- Kristensen, B., Noraberg, J., Thiébaud, P., Koudelka-Hep, M., Zimmer, J., 2001. Biocompatibility of silicon-based arrays of electrodes coupled to organotypic hippocampal brain slice cultures. *Brain Res.* 896, 1–17.
- Kuchibhotla, K., Goldman, S., Lattarulo, C., Wu, H., Hyman, B., Bacskai, B., 2008. Abeta plaques lead to aberrant regulation of calcium homeostasis *in vivo* resulting in structural and functional disruption of neuronal networks. *Neuron* 59, 214–225.
- Kuchibhotla, K., Lattarulo, C., Hyman, B., Bacskai, B., 2009. Synchronous hyperactivity and intercellular calcium waves in astrocytes in Alzheimer mice. *Science* 323, 1211–1215.
- Laketa, V., Simpson, J.C., Bechtel, S., Wiemann, S., Pepperkok, R., 2007. High-content microscopy identifies new neurite outgrowth regulators. *Mol. Biol. Cell* 18, 242–252.
- Lee, A.C., Suter, D.M., 2008. Quantitative analysis of microtubule dynamics during adhesion-mediated growth cone guidance. *Dev. Neurobiol.* 68, 1363–1377.
- Lemmens, R., Van Hoecke, A., Hersmus, N., Geelen, V., D'Hollander, I., Thijs, V., et al., 2007. Overexpression of mutant superoxide dismutase 1 causes a motor axonopathy in the zebrafish. *Hum. Mol. Genet.* 16, 2359–2365.
- Leschik, J., Welzel, A., Weissmann, C., Eckert, A., Brandt, R., 2007. Inverse and distinct modulation of tau-dependent neurodegeneration by presenilin 1 and amyloid-beta in cultured cortical neurons: evidence that tau phosphorylation is the limiting factor in amyloid-beta-induced cell death. *J. Neurochem.* 101, 1303–1315.
- Leung, K.M., van Horck, F.P., Lin, A.C., Allison, R., Standart, N., Holt, C.E., et al., 2006. Asymmetrical beta-actin mRNA translation in growth cones mediates attractive turning to netrin-1. *Nat. Neurosci.* 9, 1247–1256.
- Li, D., Field, P., Yoshioka, N., Raisman, G., 1994. Axons regenerate with correct specificity in horizontal slice culture of the postnatal rat entorhino-hippocampal system. *Eur. J. Neurosci.* 6, 1026–1037.
- Lichtlen, P., Mohajeri, M.H., 2008. Antibody-based approaches in Alzheimer's research: safety, pharmacokinetics, metabolism, and analytical tools. *J. Neurochem.* 104, 859–874.
- Lichtman, J., Livet, J., Sanes, J., 2008. A technicolour approach to the connectome. *Nat. Rev. Neurosci.* 9, 417–422.
- Lim, A., Kraut, R., 2009. The *Drosophila* BEACH family protein, blue cheese, links lysosomal axon transport with motor neuron degeneration. *J. Neurosci.* 29, 951–963.
- Lin, C., Tallaksen-Greene, S., Chien, W., 2001. Neurological abnormalities in a knock-in mouse model of Huntington's disease. *Hum. Mol. Genet.* 10, 137–144.
- Lippincott-Schwartz, J., Patterson, G.H., 2003. Development and use of fluorescent protein markers in living cells. *Science* 300, 87–91.
- Liu, C.W., Lee, G., Jay, D.G., 1999. Tau is required for neurite outgrowth and growth cone motility of chick sensory neurons. *Cell Motil. Cytoskeleton* 43, 232–242.
- Liu, J., Guo, T., Wei, Y., Liu, M., Sui, S.F., 2006. Complexin is able to bind to SNARE core complexes in different assembled states with distinct affinity. *Biochem. Biophys. Res. Commun.* 347, 413–419.
- Lo, D.C., 2001. Neuronal transfection using particle-mediated gene transfer. *Curr. Protoc. Neurosci.* Chapter 3:Unit 3.15.
- Lonchamp, E., Dupont, J., Beekenkamp, H., Poulain, B., Bossu, J., 2006. The mouse cerebellar cortex in organotypic slice cultures: an *in vitro* model to analyze the consequences of mutations and pathologies on neuronal survival, development, and function. *Crit. Rev. Neurobiol.* 18, 179–186.
- Mandelkow, E.M., Thies, E., Trinczek, B., Biernat, J., Mandelkow, E., 2004. MARK/PAR1 kinase is a regulator of microtubule-dependent transport in axons. *J. Cell Biol.* 167, 99–110.

- Mank, M., Santos, A., Direnberger, S., Mrcic-Flogel, T., Hofer, S., Stein, V., et al., 2008. A genetically encoded calcium indicator for chronic *in vivo* two-photon imaging. *Nat. Methods* 5, 805–811.
- Mao, T., O'Connor, D.H., Scheuss, V., Nakai, J., Svoboda, K., 2008. Characterization and subcellular targeting of gcamp-type genetically-encoded calcium indicators. *PLoS ONE* 3, 1796.
- Mattson, M.P., 2007. Calcium and neurodegeneration. *Aging Cell* 6, 337–350.
- Mattson, M.P., Gleichmann, M., Cheng, A., 2008. Mitochondria in neuroplasticity and neurological disorders. *Neuron* 60, 748–766.
- McBurney, M.W., 1993. P19 embryonal carcinoma cells. *Int. J. Dev. Biol.* 37, 135–140.
- McCombs, J.E., Palmer, A.E., 2008. Measuring calcium dynamics in living cells with genetically encodable calcium indicators. *Methods* 46, 152–159.
- Medrano, A., Barmada, S., Biasini, E., Harris, D., 2008. GFP-tagged mutant prion protein forms intra-axonal aggregates in transgenic mice. *Neurobiol. Dis.* 31, 20–32.
- Metzger, F., Repunte-Canonigo, V., Matsushita, S., Akemann, W., Diez-Garcia, J., Ho, C., et al., 2002. Transgenic mice expressing a pH and Cl⁻ sensing yellow-fluorescent protein under the control of a potassium channel promoter. *Eur. J. Neurosci.* 15, 40–50.
- Meyer-Luehmann, M., Spires-Jones, T., Prada, C., Garcia-Alloza, M., de Calignon, A., Rozkalne, A., et al., 2008. Rapid appearance and local toxicity of amyloid-beta plaques in a mouse model of Alzheimer's disease. *Nature* 451, 720–724.
- Miyata, T., Kawaguchi, A., Saito, K., Kuramochi, H., Ogawa, M., 2002. Visualization of cell cycling by an improvement in slice culture methods. *J. Neurosci. Res.* 69, 861–868.
- Mizrahi, A., Crowley, J., Shtoyerman, E., Katz, L., 2004. High-resolution *in vivo* imaging of hippocampal dendrites and spines. *J. Neurosci.* 24, 3147–3151.
- Nägerl, U., Willig, K., Hein, B., Hell, S., Bonhoeffer, T., 2008. Live-cell imaging of dendritic spines by STED microscopy. *Proc. Natl. Acad. Sci. USA* 105, 18982–18987.
- Nakamura, T., Aoki, K., Matsuda, M., 2008. FRET imaging and *in silico* simulation: analysis of the signaling network of nerve growth factor-induced neurite outgrowth. *Brain Cell Biol.* 36, 19–30.
- Niell, C.M., Meyer, M.P., Smith, S.J., 2004. *In vivo* imaging of synapse formation on a growing dendritic arbor. *Nat. Neurosci.* 7, 254–260.
- O'Brien, J., Lummis, S., 2006. Biolistic transfection of neuronal cultures using a hand-held gene gun. *Nat. Protoc.* 1, 977–981.
- Ohr, T., Mütze, J., Staroske, W., Weinmann, L., Höck, J., Crell, K., et al., 2008. Fluorescence correlation spectroscopy and fluorescence cross-correlation spectroscopy reveal the cytoplasmic origination of loaded nuclear RISC *in vivo* in human cells. *Nucleic Acids Res.* 36, 6439–6449.
- Ohshima, Y., Kubo, T., Koyama, R., Ueno, M., Nakagawa, M., Yamashita, T., 2008. Regulation of axonal elongation and pathfinding from the entorhinal cortex to the dentate gyrus in the hippocampus by the chemokine stromal cell-derived factor 1 alpha. *J. Neurosci.* 28, 8344–8353.
- Okabe, S., Hirokawa, N., 1992. Differential behavior of photoactivated microtubules in growing axons of mouse and frog neurons. *J. Cell Biol.* 117, 105–120.
- Paredes, R.M., Etzler, J.C., Watts, L.T., Zheng, W., Lechleiter, J.D., 2008. Chemical calcium indicators. *Methods* 46, 143–151.
- Patterson, G.H., Lippincott-Schwartz, J., 2002. A photoactivatable GFP for selective photolabeling of proteins and cells. *Science* 297, 1873–1877.
- Peri, F., Nüsslein-Volhard, C., 2008. Live imaging of neuronal degradation by microglia reveals a role for v0-atpase a1 in phagosomal fusion *in vivo*. *Cell* 133, 916–927.
- Petrozzino, J., Pozzo Miller, L., Connor, J., 1995. Micromolar Ca²⁺ transients in dendritic spines of hippocampal pyramidal neurons in brain slice. *Neuron* 14, 1223–1231.

- Pleasure, S.J., Page, C., Lee, V.M., 1992. Pure, postmitotic, polarized human neurons derived from ntera 2 cells provide a system for expressing exogenous proteins in terminally differentiated neurons. *J. Neurosci.* 12, 1802–1815.
- Racine, R., 1972. Modification of seizure activity by electrical stimulation. II. Motor seizure. *Electroencephalogr. Clin. Neurophysiol.* 32, 281–294.
- Rapoport, M., Dawson, H.N., Binder, L.I., Vitek, M.P., Ferreira, A., 2002. Tau is essential to beta -amyloid-induced neurotoxicity. *Proc. Natl. Acad. Sci. USA* 99, 6364–6369.
- Rapoport, M., Ferreira, A., 2000. PD98059 prevents neurite degeneration induced by fibrillar beta-amyloid in mature hippocampal neurons. *J. Neurochem.* 74, 125–133.
- Rhème, C., Ehrenguber, M., Grandgirard, D., 2005. Alphaviral cytotoxicity and its implication in vector development. *Exp. Physiol.* 90, 45–52.
- Roze, E., Saudou, F., Caboche, J., 2008. Pathophysiology of Huntington's disease: from huntingtin functions to potential treatments. *Curr. Opin. Neurol.* 21, 497–503.
- Schapira, A.H., 2009. Neurobiology and treatment of Parkinson's disease. *Trends Pharmacol. Sci.* 30, 41–47.
- Schrier, M., Severijnen, L.A., Reis, S., Rife, M., van't Padje, S., van Cappellen, G., et al., 2004. Transport kinetics of FMRP containing the I304N mutation of severe fragile X syndrome in neurites of living rat PC12 cells. *Exp. Neurol.* 189, 343–353.
- Scott, M., Supattapone, S., Nguyen, H., DeArmond, S., Prusiner, S., 2000. Transgenic models of prion disease. *Arch. Virol.* 16(Suppl.), 113–124.
- Shahani, N., Subramaniam, S., Wolf, T., Tackenberg, C., Brandt, R., 2006. Tau aggregation and progressive neuronal degeneration in the absence of changes in spine density and morphology after targeted expression of Alzheimer's disease-relevant tau constructs in organotypic hippocampal slices. *J. Neurosci.* 26, 6103–6114.
- Shankar, G., Bloodgood, B., Townsend, M., Walsh, D., Selkoe, D., Sabatini, B., 2007. Natural oligomers of the Alzheimer amyloid-beta protein induce reversible synapse loss by modulating an NMDA-type glutamate receptor-dependent signaling pathway. *J. Neurosci.* 27, 2866–2875.
- Shrestha, B., Vitolo, O., Joshi, P., Lordkipanidze, T., Shelanski, M., Dunaevsky, A., 2006. Amyloid beta peptide adversely affects spine number and motility in hippocampal neurons. *Mol. Cell Neurosci.* 33, 274–282.
- Sieber, J.J., Willig, K.I., Kutzner, C., Gerding-Reimers, C., Harke, B., Donnert, G., et al., 2007. Anatomy and dynamics of a supramolecular membrane protein cluster. *Science* 317, 1072–1076.
- Sipione, S., Cattaneo, E., 2001. Modeling Huntington's disease in cells, flies, and mice. *Mol. Neurobiol.* 23, 21–51.
- Skovronsky, D.M., Lee, V.M., Trojanowski, J.Q., 2006. Neurodegenerative diseases: new concepts of pathogenesis and their therapeutic implications. *Annu. Rev. Pathol.* 1, 151–170.
- Snyder-Keller, A., Tseng, K., Lyng, G., Graber, D., O'Donnell, P., 2008. Afferent influences on striatal development in organotypic cocultures. *Synapse* 62, 487–500.
- Spires, T., Hyman, B., 2005. Transgenic models of Alzheimer's disease: learning from animals. *NeuroRx* 2, 423–437.
- Spires, T., Meyer-Luehmann, M., Stern, E., McLean, P., Kocho, J., Nguyen, P., et al., 2005. Dendritic spine abnormalities in amyloid precursor protein transgenic mice demonstrated by gene transfer and intravital multiphoton microscopy. *J. Neurosci.* 25, 7278–7287.
- Steidl, E., Neveu, E., Bertrand, D., Buisson, B., 2006. The adult rat hippocampal slice revisited with multi-electrode arrays. *Brain Res.* 1096, 70–84.
- Sun, B., Xu, P., Salvaterra, P.M., 1999. Dynamic visualization of nervous system in live *Drosophila*. *Proc. Natl. Acad. Sci. USA* 96, 10438–10443.
- Svoboda, K., Yasuda, R., 2006. Principles of two-photon excitation microscopy and its applications to neuroscience. *Neuron* 50, 823–839.

- Tackenberg, C., Ghori, A., Brandt, R., 2009. Thin, stubby or mushroom: spine pathology in Alzheimer's disease. *Curr. Alzheimer Res.* In press.
- Takano, T., Tian, G., Peng, W., Lou, N., Lovatt, D., Hansen, A., et al., 2007. Cortical spreading depression causes and coincides with tissue hypoxia. *Nat. Neurosci.* 754–762.
- Thiebaud, P., de Rooij, N., Koudelka-Hep, M., Stoppini, L., 1997. Microelectrode arrays for electrophysiological monitoring of hippocampal organotypic slice cultures. *IEEE Trans. Biomed. Eng.* 44, 1159–1163.
- Thies, E., Mandelkow, E.M., 2007. Missorting of tau in neurons causes degeneration of synapses that can be rescued by the kinase MARK2/Par-1. *J. Neurosci.* 27, 2896–2907.
- Trapp, B.D., Stys, P.K., 2009. Virtual hypoxia and chronic necrosis of demyelinated axons in multiple sclerosis. *Lancet Neurol.* 8, 280–291.
- Vukojevic, V., Ming, Y., D'Addario, C., Hansen, M., Langel, U., Schulz, R., et al., 2008. Mu-opioid receptor activation in live cells. *FASEB J.* 22, 3537–3548.
- Walsh, K., Megyesi, J., Hammond, R., 2005. Human central nervous system tissue culture: a historical review and examination of recent advances. *Neurobiol. Dis.* 18, 2–18.
- Waterman-Storer, C.M., Salmon, E.D., 1999. Fluorescent speckle microscopy of microtubules: how low can you go? *FASEB J.* 13, S225–S230.
- Watson, M.R., Lagow, R.D., Xu, K., Zhang, B., Bonini, N.M., 2008. A *Drosophila* model for amyotrophic lateral sclerosis reveals motor neuron damage by human SOD1. *J. Biol. Chem.* 283, 24972–24981.
- Weissmann, C., Reyher, H. J., Gauthier, A., Steinhoff, H. J., Junge, W., Brandt, R. Microtubule binding and trapping at the tip of neurites regulate tau motion in living neurons. *Traffic* (in revision).
- Wisztorski, M., Croix, D., Macagno, E., Fournier, I., Salzet, M., 2008. Molecular MALDI imaging: an emerging technology for neuroscience studies. *Dev. Neurobiol.* 68, 845–858.
- Wittmann, C.W., Wszolek, M.F., Shulman, J.M., Salvaterra, P.M., Lewis, J., Hutton, M., et al., 2001. Tauopathy in *Drosophila*: neurodegeneration without neurofibrillary tangles. *Science* 293, 711–714.
- Wojda, U., Salinska, E., Kuznicki, J., 2008. Calcium ions in neuronal degeneration. *IUBMB Life* 60, 575–590.
- Wu, P., Li, M., Yu, D., Deng, J., 2008. Reelin, a guidance signal for the regeneration of the entorhino-hippocampal path. *Brain Res.* 1208, 1–7.
- Yang, D.M., Huang, C.C., Lin, H.Y., Tsai, D.P., Kao, L.S., Chi, C.W., et al., 2003. Tracking of secretory vesicles of PC12 cells by total internal reflection fluorescence microscopy. *J. Microsc.* 209, 223–227.
- Yasuda, R., Harvey, C., Zhong, H., Sobczyk, A., van Aelst, L., Svoboda, K., 2006. Supersensitive Ras activation in dendrites and spines revealed by two-photon fluorescence lifetime imaging. *Nat. Neurosci.* 9, 283–291.
- Zeng, L., Xu, L., Rensing, N., Sinatra, P., Rothman, S., Wong, M., 2007. Kainate seizures cause acute dendritic injury and actin depolymerization *in vivo*. *J. Neurosci.* 27, 11604–11613.

INTERACTIONS BETWEEN HEPARAN SULFATE AND PROTEINS—DESIGN AND FUNCTIONAL IMPLICATIONS

Ulf Lindahl *and* Jin-ping Li

Contents

1. Introduction	106
2. HS Proteoglycans	107
2.1. Syndecans	107
2.2. Glypicans	108
2.3. Secreted HS proteoglycans	108
3. Structure and Biosynthesis of HS	109
3.1. Formation of linkage region	111
3.2. Chain assembly	115
3.3. Chain modification	115
3.4. Regulation of biosynthesis	117
4. Interactions of HS with Proteins	120
4.1. Topology of protein-binding domains in HS	122
4.2. Functional implications	123
4.3. Aspects of specificity	126
5. Interference with HS Function	129
5.1. Perturbation of core proteins	130
5.2. Perturbation of HS-binding protein domains	131
5.3. Perturbation of polysaccharide structure	131
6. Is There a “Sulfation Code”?	134
7. HS and Disease	136
7.1. Amyloid diseases	136
7.2. Tumor development and metastasis	139
7.3. Inflammatory and repair reactions	140
7.4. Infection	141
8. Concluding Remarks	142
References	143

Department of Medical Biochemistry and Microbiology, University of Uppsala, SE-751 23 Uppsala, Sweden

International Review of Cell and Molecular Biology, Volume 276
ISSN 1937-6448, DOI: 10.1016/S1937-6448(09)76003-4

© 2009 Elsevier Inc.
All rights reserved.

Abstract

Heparan sulfate (HS) proteoglycans at cell surfaces and in the extracellular matrix of most animal tissues are essential in development and homeostasis, and variously implicated in disease processes. Functions of HS polysaccharide chains depend on ionic interactions with a variety of proteins including growth factors and their receptors. Negatively charged sulfate and carboxylate groups are arranged in various types of domains, generated through strictly regulated biosynthetic reactions and with enormous potential for structural variability. The level of specificity of HS–protein interactions is assessed through binding experiments *in vitro* using saccharides of defined composition, signaling assays in cell culture, and targeted disruption of genes for biosynthetic enzymes followed by phenotype analysis. While some protein ligands appear to require strictly defined HS structure, others bind to variable saccharide domains without any apparent dependence on distinct saccharide sequence. These findings raise intriguing questions concerning the functional significance of regulation in HS biosynthesis.

Key Words: Heparan Sulfate, Heparin, Sulfate groups, Iduronic acid, Protein binding, Growth factors, Proteoglycan. © 2009 Elsevier Inc.

1. INTRODUCTION

Heparan sulfate (HS) was recognized as a polysaccharide, “heparin monosulfuric acid,” related to but less sulfated than heparin, that was eliminated in side fractions of heparin manufacture. While HS was defined as a distinct molecular entity more than 60 years ago, by [Jorpes and Gardell \(1948\)](#), the elucidation of its structure has been a slow, painstaking process that is still underway. Owing to its structural heterogeneity and variability, HS cannot be considered a single compound but rather a family of related polymers. In fact, current distinction between heparin and HS is not based primarily on carbohydrate structure but rather on proteoglycan (PG) type and cellular distribution. In contrast to heparin that occurs exclusively in connective-tissue type mast cells, HS is produced by most cells in the body. It occurs, largely in PG form, at cell surfaces and in the extracellular matrix. The diverse and fundamental roles of HS in development and homeostasis are reflected by the occurrence of HSPGs throughout the evolutionary system, from *Cnidaria* onwards ([Medeiros et al., 2000](#)). Most physiological—and pathophysiological—effects of HS are due to interactions, more-or-less electrostatic in nature, with various proteins. Reviews dealing with structural, metabolic, and functional aspects of HSPGs have been published ([Bernfield et al., 1999](#); [Bishop et al., 2007](#); [Casu and Lindahl, 2001](#); [Esko and Lindahl, 2001](#); [Esko and Selleck, 2002](#); [Gallagher, 2001](#); [Lindahl et al., 1998](#); [Salmivirta et al., 1996](#); [Sugahara and Kitagawa, 2002](#)).

The aim of the present review is to pursue significant long-term trends in HS research, with particular emphasis on structure–function relations. Given the dramatic expansion of the field, we do not endeavor to cover all aspects of this development comprehensively, but will emphasize, in particular the structural diversity of HS with two major questions in mind: “How is it regulated?” and “Why is it needed?” A detailed account of methodological progress regarding HS compositional and sequence analysis, conformational aspects, and HS–protein interactions falls outside the scope of this review, and the reader is referred to several recent papers/reviews in the area (Guerrini et al., 2002, 2007; Korir and Larive, 2009; Mulloy and Forster, 2000; Powell et al., 2004; Volpi et al., 2008; Wu et al., 2002).

2. HS PROTEOGLYCANs

HS chains generally occur in tissues covalently attached to core proteins in PG structures (Bulow and Hobert, 2006). Apart from some minor or “part-time” species, the various HSPGs fall within one of four major categories characterized by different core protein structures. Two of these families, the syndecans and glypicans, involve HSPG species that are associated with the plasma membrane of cells. A third group comprises various secreted forms, including perlecan, agrin, and collagen XVIII. Finally, serglycin in intracellular storage granules carries heparin chains, which may be considered a special form of HS (Section 3.3). Current information suggests that HS structure is cell- but not PG type-specific, such that all HS chains synthesized by a given cell are similar although they may be linked to different core proteins (Kramer and Yost, 2003). Nevertheless, because of the spatial and temporal constraints caused by such association, the chains may differ in functional regards (Ding et al., 2005; Kirkpatrick and Selleck, 2007). Given the topic of the present review, HS–protein interactions, the various types of HSPGs will be discussed in rather cursory terms, largely relating to studies in mammals.

2.1. Syndecans

The syndecan (Sdc) cell-surface HSPGs have common structural organization, involving discrete cytoplasmic, transmembrane, and NH₂-terminal extracellular domains. The four core proteins of the vertebrate Sdc family range in molecular size from 22 to 45 kDa, largely due to the distinct extracellular domains (Oh and Couchman, 2004). These domains show limited peptide sequence homology and may carry both HS and chondroitin sulfate (CS) chains (Carey, 1997). The cytoplasmic domains are small, but functionally important as they interact with PDZ domains in the adaptor protein syntenin, and with the phosphoinositide PIP(2) and thus regulate dynamics of the actin

cytoskeleton and membrane trafficking (Alexopoulou et al., 2007; Woods and Couchman, 2001; Zimmermann et al., 2005). This interaction system controls syndecan recycling through endosomal compartments, promotes internalization of accompanying protein cargo, and regulates cell adhesion and signaling systems. Importantly, Sdc1 and Sdc4 contain extracellular target sequences for protease cleavage, prerequisite for shedding of Sdc “ectodomains” with special functional and pathophysiological properties (Brule et al., 2006; Hayashida et al., 2008; Rodriguez-Manzaneque et al., 2008).

Expression of various syndecans in tissues is regulated during development (Rapraeger, 2001). Although most adult tissues express more than one Sdc form, Sdc1 is the major species in epithelial cells and is involved in angiogenesis, wound healing, and leukocyte–endothelial interactions (Stepp et al., 2002). Sdc2 is abundantly expressed in cells of mesenchymal origin in kidney, lung, and stomach, as well as in cells forming cartilage and bone, with potential roles in left–right axis patterning during development (Essner et al., 2006). Sdc3 dominates in neuronal cells, and was implicated as a potential coreceptor for agouti-related protein that modulates feeding behavior through binding to a melanocortin receptor (Reizes et al., 2001) (see Section 5.1). Sdc4 is widely expressed through all stages of embryonic development and in most adult tissues, though generally at relatively low levels. A major function of Sdc4 is regulation of matrix structure, and modulation of cell adhesion and migration via interactions provided by the syntenin–PIP(2) system (Woods and Couchman, 2001).

2.2. Glypicans

Members of the glypican (Gpc) family are glycosylphosphatidylinositol (GPI)-anchored membrane HSPGs that were first discovered in human lung fibroblasts (David et al., 1990). To date, six Gpc isoforms have been identified in mammalia. Mature Gpc core proteins of ~60 kDa generally carry three to four HS chains. Fourteen conserved cysteine residues account for the formation of a compact, globular, N-terminal distal portion of the core proteins (Bernfield et al., 1999; Filmus and Selleck, 2001). The various Gpc isoforms are by and large expressed in all tissues, with some notable specific characteristics during development (Fransson et al., 2004). Gpc1 occurs mainly not only in the embryonic central nervous and skeletal systems but also in other adult tissues (Litwack et al., 1998). Gpc2 occurs more specifically in axons and growth cones of the developing brain, and appears not to be present in the adult (Ivins et al., 1997). Gpc3–6 are widely expressed during development, to a lesser extent in adult tissues (Fransson et al., 2004).

2.3. Secreted HS proteoglycans

The two major secreted HSPG species are perlecan (Knox and Whitelock, 2006) and agrin (Bezakova and Ruegg, 2003). Perlecan is a large (>400 kDa) multidomain HSPG in the extracellular matrix. Originally isolated

from a mouse Engelbreth–Holm–Swarm tumor (Hassell et al., 1980), it is now recognized as a ubiquitous component of basement membranes, and is generally found in mesenchymal organs and connective tissues (Handler et al., 1997). The core protein, of which only a single form has been identified, contains five distinct polypeptide domains, with three potential attachment sites for HS or CS chains in domain I and one in domain V.

Due to its abundant occurrence in the extracellular matrix, perlecan is important to a wide range of developmental and homeostatic processes, from establishment of cartilage to regulation of wound healing. For detailed accounts of structural characteristics, expression patterns, and functions of perlecan, see Handler et al. (1997), Iozzo (2005), and Knox and Whitelock (2006). Disruption of the perlecan gene in mice results in embryonic or early neonatal death, with multiple skeletal abnormalities and overall fragile basement membranes (Bulow and Hobert, 2006). Direct interactions of perlecan core protein with growth factors (Mongiati et al., 2000) have been demonstrated. Agrin, along with perlecan and collagen XVIII, is a major basement membrane HSPG (Iozzo, 2005). It was cloned as a 220 kDa extracellular-matrix polypeptide comprised of multiple domains (Hoch et al., 1994; Rupp et al., 1991) and recognized as a HSPG in a study of chick brain development (Tsen et al., 1995). Agrin transcripts are highly homologous in all species, but multiple isoforms of the protein are generated by alternative splicing at several positions. The central rod-like domain of agrin carries the HS chains, resulting in a >500 kDa macromolecule (Kroger and Schroder, 2002). Agrin has been primarily considered a neuronal PG, although it is widely expressed in various tissues during development. In particular, agrin is recognized as a key player in formation, maintenance, and regeneration of neuromuscular junctions (Bezakova and Ruegg, 2003). Collagen XVIII occurs in basement membranes of various tissues together with other PGs, but may be selectively involved in protein binding, as shown for L-selectin in mouse kidney (Celie et al., 2005).

3. STRUCTURE AND BIOSYNTHESIS OF HS

Current knowledge predicts that the polysaccharide chains of all known HSPGs are generated according to the same general mechanism (Fig. 3.1A,B) (Esko and Lindahl, 2001; Esko and Selleck, 2002; Lindahl et al., 1998). The process involves a series of initial glycosylation reactions that generate a glucuronosyl–galactosyl–galactosyl–xylosyl (GlcA β 1,3Gal β 1,3Gal β 1,4Xyl) tetrasaccharide substituent on core-protein serine residues to be substituted with glycosaminoglycan (GAG) chains. This carbohydrate–protein linkage sequence is identical for PGs carrying glucosaminoglycan (heparin, HS) and galactosaminoglycan (CS, dermatan

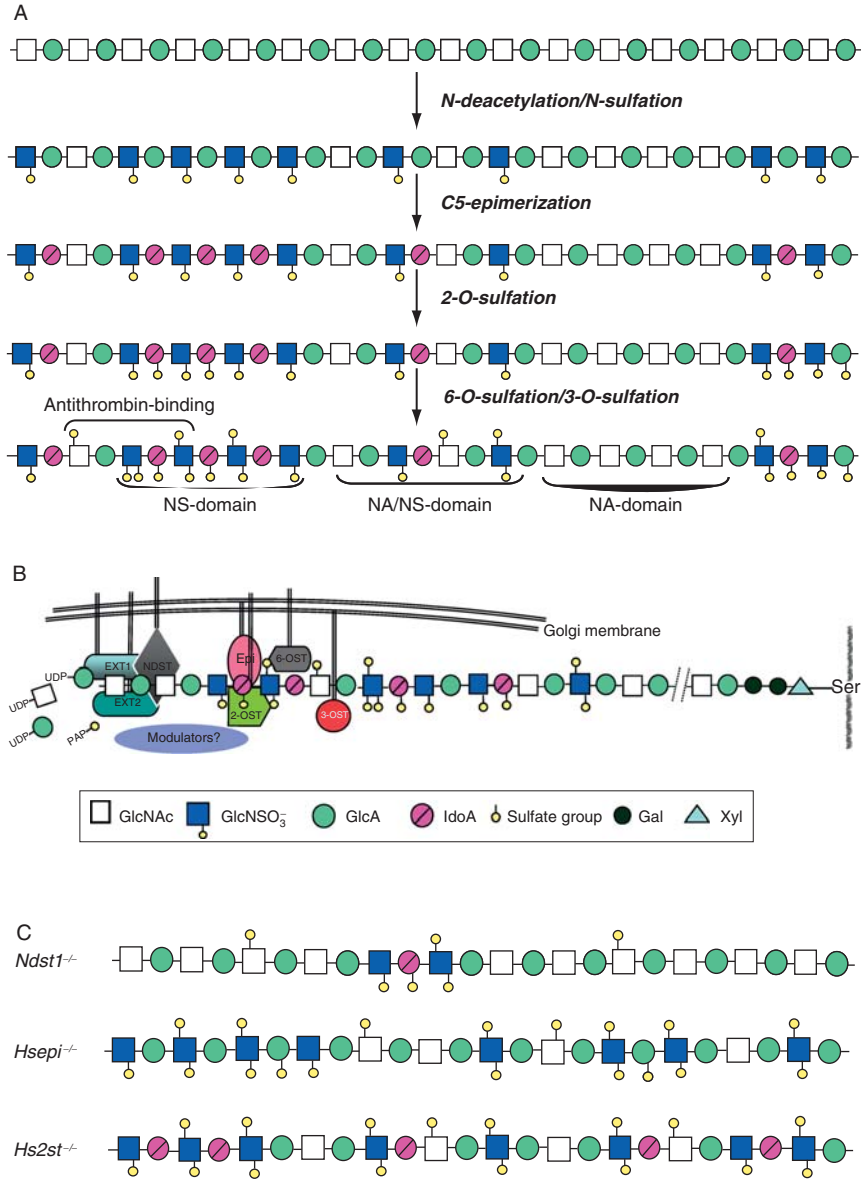


Figure 3.1 Biosynthesis of HS. (A) Polymer-modification reactions in HS biosynthesis. The order of reactions is dictated by substrate specificity (Table 3.1), possibly also by topology of enzymes in the GAGosome (panel B). For clarity, the action of each enzyme is separately depicted along the entire length of a hypothetical polysaccharide sequence, whereas the reactions in the cell are presumably concerted (panel B). Structure symbols are defined under the schemes. (B) Conjectured GAGosome, showing consecutive action of enzymes acting on a nascent HS chain. The involvement






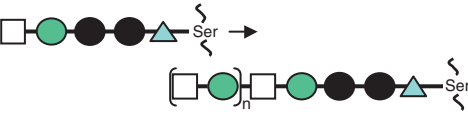
sulfate [DS]) chains. The type of GAG chain to be formed is determined through the next glycosylation step, which will add either a β 1,4-linked *N*-acetylgalactosamine (GalNAc) or an α 1,4-linked *N*-acetylglucosamine (GlcNAc) residue to the nonreducing terminal GlcA unit of the linkage sequence. This step commits the process toward generation of CS/DS- or HS/heparin-type chains, respectively. GlcNAc substitution is followed by polymerization of alternating GlcA and GlcNAc residues, yielding a $(\text{GlcA}\beta 1,4\text{GlcNAc}\alpha 1,4)_n$ HS precursor polysaccharide. The resultant polymer is modified through a complex series of reactions, involving *N*-deacetylation/*N*-sulfation of GlcNAc (yielding GlcNS) residues, C5-epimerization of GlcA to iduronic acid (IdoA) units, and *O*-sulfation of hexuronic acids at C2 and glucosamine residues at C3 and C6. Because most of these reactions will engage only a fraction of potentially available sugar units, the final products have heterogeneous structures that vary with tissue source. However, due to the sequential nature of the process, and the substrate specificities of the enzymes involved, the structural variability is nonrandom and expressed through the occurrence of more-or-less modified saccharide domains. In all, 11 different enzymes (excluding isoforms) have been implicated in HS biosynthesis, and some of their properties are summarized in [Table 3.1](#). Some of the enzymes occur as multiple isoforms whereas others are single entities. The following sections describe the process in more detail, and raise some questions regarding its subcellular organization and regulation. All known HS biosynthesis enzymes have been molecularly cloned, and most of them are expressed in recombinant form ([Table 3.1](#)).



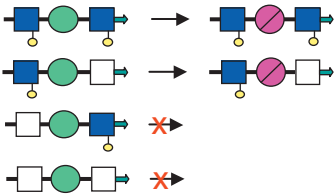
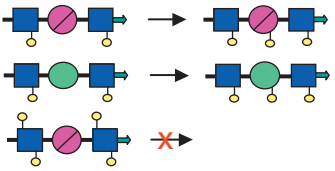
3.1. Formation of linkage region

Xylosyltransferase (XylT) initiates the process using UDP-Xyl as donor and PG core protein as acceptor. No defined consensus amino acid sequence for xylosylation exists, except that a glycine residue is generally located immediately carboxy terminal to target serine residues. Usually at least two acidic residues occur in the vicinity. Two XylT isoforms have been found in mammals, and both have been implicated with PG biosynthesis ([Ponighaus et al., 2007](#)). The subsequent addition of two galactose residues is catalyzed by distinct galactosyltransferases (GalTs). Formation of the linkage region is completed by glucuronyltransferase I (GlcATI) that is distinct from the enzymes committed to formation of the actual polysaccharide chain ([Sugahara and Kitagawa, 2000](#); [Wei et al., 1999](#)). Xyl residues

of protein “modulators” is purely speculative ([Section 3.4.2](#)). (C) Effects of deletions of genes encoding specific enzymes on HS structure. The sequences shown are arbitrarily designed, but are based on composition data deduced from structural analysis of HS generated by mutant embryos ([Li et al., 2003](#); [Merry et al., 2001](#); [Ringvall et al., 2000](#)).


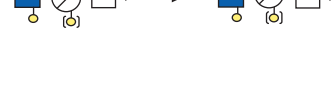
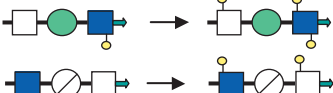
Table 3.1 Enzymes involved in mammalian HS biosynthesis





Enzyme	Gene	Substrate ^a → product	Loss-of-function phenotypes	Key references ^b
Xylosyltransferase 1 (XylT1)	<i>Xylt1</i>		N.r. ^c	1–4
Xylosyltransferase 2 (XylT2)	<i>Xylt2</i>		Biliary epithelial cysts, renal defects	
Galactosyltransferase 1 (GalT1)	<i>B4galt7</i>		Progeroid form of Ehlers-Danlos syndrome	5, 6
Galactosyltransferase 2 (GalT2)	<i>B3galt6</i>		N.r.	7
Glucuronyltransferase (GlcAT1)	<i>B3gat3</i>		N.r.	8, 9
N-acetylglucosaminyltransferase (EXTL2)	<i>Extl2</i>		N.r.	10
Polymerase 1 (EXT1) Polymerase 2 (EXT2)	<i>Ext1</i> <i>Ext2</i>	 (joint EXT1/EXT2 action)	Homozygous—early embryonic lethality, heterozygous—hereditary multiple exostoses (HME)	11–17

<i>N</i> -deacetylase/ <i>N</i> -sulfotransferase 1 (NDST1)	<i>Ndst1</i>		Prenatal/neonatal lethality, lung defect, skeletal malformations	18–19
<i>N</i> -deacetylase/ <i>N</i> -sulfotransferase 2 (NDST2)	<i>Ndst2</i>		Abnormal mast cells lacking heparin	20–25
<i>N</i> -deacetylase/ <i>N</i> -sulfotransferase 3 (NDST3)	<i>Ndst3</i>		Subtle hematological and behavioral abnormalities	26–27
<i>N</i> -deacetylase/ <i>N</i> -sulfotransferase 4 (NDST4)	<i>Ndst4</i>		N.r.	28
Glucuronyl C5-epimerase (Hsepi)	<i>Glee</i>		Neonatal lethality, lung defect, renal agenesis, skeletal malformations	29–32
Hexuronyl 2- <i>O</i> -sulfotransferase (2-OST)	<i>Hs2st</i>		Neonatal lethality, renal agenesis, skeletal malformations	33–37

(continued)

Table 3.1 (continued)

Enzyme	Gene	Substrate ^a → product	Loss-of-function phenotypes	Key references ^b
Glucosaminyl 6- <i>O</i> -sulfotransferase 1 (6-OST1)	<i>Hs6st1</i>		Various developmental defects	33, 38–41
Glucosaminyl 6- <i>O</i> -sulfotransferase 2–3 (6-OST2–3)	<i>Hs6st2–3</i>		N.r.	
Glucosaminyl 3- <i>O</i> -sulfotransferase 1–6 (3-OST1–6)	<i>Hs3st1–6</i>		Intrauterine growth retardation (3-OST1)	42–44

^a See Fig. 3.1A for explanation of symbols.  , *N*-unsubstituted glucosamine;  , GlcA or IdoA with or without 2-*O*-sulfation; X, rejected by enzyme.

^b References concerning discovery of reaction, demonstrated effect on exogenous substrate, cloning, and knockout of gene. 1, Stoolmiller et al. (1972); 2, Campbell et al. (1984); 3, Gotting et al. (2000); 4, Condac et al. (2007); 5, Almeida et al. (1999); 6, Gotte et al. (2008); 7, Bai et al. (2001); 8, Kitagawa et al. (1998); 9, Wei et al. (1999); 10, Kitagawa et al. (1999); 11, Silbert (1963); 12, Helting and Lindahl (1971); 13, Lidholt and Lindahl (1992); 14, Lind et al. (1998); 15, McCormick et al. (2000); 16, Lin et al. (2000); 17, Stickens et al. (2005); 18, Wei et al. (1993); 19, Ringvall et al. (2000); 20, Silbert (1967); 21, Lindahl et al. (1973); 22, Riesenfeld et al. (1982); 23, Navia et al. (1983); 24, Eriksson et al. (1994); 25, Forsberg et al. (1999); 26, Aikawa and Esko (1999); 27, Pallerla et al. (2008); 28, Aikawa Ji et al. (2001); 29, Höök et al. (1974); 30, Jacobsson et al. (1979); 31, Li et al. (1997); 32, Li et al. (2003); 33, Jacobsson and Lindahl (1980); 34, Kobayashi et al. (1997); 35, Bullock et al. (1998); 36, Merry et al. (2001); 37, Rong et al. (2001); 38, Habuchi et al. (1998); 39, Habuchi et al. (2000); 40, Habuchi et al. (2007); 41, Smeds et al. (2003); 42, Kusche et al. (1988); 43, Shworak et al. (1997); 44, HajMohammadi et al. (2003).

^c N.r., not reported (to our knowledge).

in CS/DS- and HSPGs may be 2-*O*-phosphorylated, Gal residues in CS/DS (but not HS) PGs also 6-*O*-sulfated, and recent findings suggest that these substituents may be involved in regulation of GlcAT1 activity (Tone et al., 2008).

3.2. Chain assembly

Addition of the first hexosamine residue onto the linkage tetrasaccharide marks a bifurcation in the biosynthetic pathway. A GlcNAc residue initiates formation of a heparin/HS precursor chain, and is incorporated by EXTL2/EXTL3, members of the exostosin (EXT) family of enzymes (Busse et al., 2007; Kim et al., 2001, 2002). Addition of GalNAc commits the process toward chondroitin formation (Uyama et al., 2003). The mode of control over the addition of α 1,4GlcNAc versus β 1,4GalNAc remains unclear, but depends on enzyme recognition of the PG polypeptide portion. In HS formation, acidic as well as hydrophobic amino acid residues close to the serine attachment site in the PG core protein appear to promote GlcNAc substitution (Lugemwa and Esko, 1991; Zhang and Esko, 1994). Also distant effects of polypeptide structure have been demonstrated (Chen and Lander, 2001). Subsequent formation of the actual (GlcA β 1,4GlcNAc α 1,4)_{*n*} copolymer is catalyzed by a Golgi-located heterodimeric complex of two other EXTs, EXT1 and EXT2 (Busse et al., 2007; Kim et al., 2003; Lind et al., 1993, 1998; McCormick et al., 2000; Senay et al., 2000).

3.3. Chain modification

The distinctive structural features of HS chains are established through the series of polymer-modification reactions outlined in Fig. 3.1A. The process is initiated by removal of *N*-acetyl groups from subsets of GlcNAc residues followed by sulfation of the free amino groups, catalyzed by one or more of the four NDST isoenzymes (Aikawa and Esko, 1999; Aikawa Ji et al., 2001; Kusche-Gullberg et al., 1998). In vertebrates, NDST1 and NDST2 are expressed in most tissues examined, whereas NDST3 and NDST4 occur predominantly during embryonic development and in the adult brain. Due to selective NDST action, HS chains consist of domains of consecutive *N*-sulfated disaccharide units (NS-domains), alternating *N*-acetylated and *N*-sulfated units (NA/NS-domains), and essentially unmodified *N*-acetylated sequences (NA-domains) (Esko and Lindahl, 2001; Gallagher, 2001; Maccarana et al., 1996). The roles of individual NDST isoforms in generating overall *N*-sulfation, as well as the *N*-substituent domain patterns are still poorly understood. Differences in relative *N*-deacetylation and *N*-sulfation activities (Aikawa and Esko, 1999; Aikawa Ji et al., 2001) and selectively regulated translation (Grobe and Esko, 2002)

of NDST isoforms hint at functional distinctions yet to be discovered. Notably, the mechanism behind the restricted formation of *N*-unsubstituted GlcN residues in HS (Westling and Lindahl, 2002) remains to be resolved. NDST1 deficiency consistently results in undersulfation, whereas lack of other isoforms appears to be largely, albeit not completely compensated for (Grobe et al., 2002; Ledin et al., 2006; Pallerla et al., 2008). Mice lacking NDST2 were unable to synthesize the highly sulfated heparin, but then heparin-producing mast cells are exceptional in expressing the NDST2 isoform alone, whereas most tissues contain NDST1 as well (Forsberg et al., 1999). Heparin may be considered an unusually extended and highly sulfated NS-domain.

The NDST enzymes have a key role in the overall polymer-modification process, since most subsequent modifications of the HS chain, by GlcA C5-epimerization and various *O*-sulfation reactions depend on the presence of GlcNS residues (Esko and Lindahl, 2001; Esko and Selleck, 2002; Gallagher, 2001; Lindahl et al., 1998). The sequential order of the reactions reflects the substrate specificities of the corresponding enzymes (Table 3.1). Hsepi, only a single form occurring in mammals (Li et al., 2003), requires an adjacent GlcNS unit for substrate recognition, but will not attack GlcA residues that are 2-*O*-sulfated or located next to a 6-*O*-sulfated GlcN unit (Jacobsson et al., 1984). Likewise, 2-*O*-sulfation is precluded by adjacent 6-*O*-sulfation, whereas 2-*O*-sulfated sequences are readily 6-*O*-sulfated (Jacobsson and Lindahl, 1980; Kobayashi et al., 1996). Also finer structural features may be ascribed to substrate preferences by the enzymes. An adjacent GlcNS substituent thus is required only at C4 of the potential Hsepi target GlcA residue, whereas the C1 substituent may be either *N*-acetylated or *N*-sulfated (Jacobsson et al., 1984). IdoA residues therefore occur both in NS- and in NA/NS-, but not in NA-domains (Fig. 3.1A). The 2-OST, again only a single form (Kobayashi et al., 1997), shows strong preference for IdoA over GlcA targets; hence IdoA residues are commonly 2-*O*-sulfated, whereas GlcA2S units are rare (Rong et al., 2001). The three known 6-OST isoforms differ somewhat regarding sequence preference around target GlcN residues (Habuchi et al., 2000), but can all substitute both GlcNS and GlcNAc units in various sequence settings (Jemth et al., 2003; Smeds et al., 2003). 6-*O*-Sulfation of GlcNAc residues occurs preferentially, but not exclusively adjacent to *N*-sulfated disaccharide units (Holmborn et al., 2004). 6-OST1 rather than the other two recognized isoforms appears to be principally responsible for 6-*O*-sulfation of HS in most tissues (Habuchi et al., 2007). Early studies revealed a mastocytoma 3-OST activity required to generate a functional antithrombin-binding region (Kusche et al., 1988). Subsequently, as many as six 3-OST isoforms (and an additional splice variant) have been molecularly cloned, and their acceptor structure preferences can now be approached in molecular terms at the active site level (Rosenberg et al., 1997; Xu et al., 2008).

Regulatory factors apart from substrate specificity remain to be elucidated. For instance, we cannot explain why 2-*O*-sulfation is almost exclusively restricted to NS-domains whereas both NS- and NA/NS-domains are subject to 6-*O*-sulfation (Maccarana et al., 1996) (Fig. 3.1A). That *O*-sulfation reactions generally do not go to completion (i.e., do not involve all potentially available acceptor sites) is a major cause of the structural variability of HS species (Esko and Lindahl, 2001; Esko and Selleck, 2002; Lindahl et al., 1998). In addition to the commonly occurring monosaccharide units (GlcNAc, GlcNS, GlcNAc6S, GlcNS6S, GlcA, IdoA, IdoA2S, in the following referred to as “common”) that constitute most of the saccharide chains, three unusual units (GlcN (with unsubstituted amino group), GlcN(S)3S (with sulfated or unsubstituted amino group), GlcA2S; in the following referred to as “rare”) have been identified. In all, about 20 different –HexA–GlcNR– and at least 12 –GlcNR–HexA– disaccharide sequences (R = –SO₃[–] or –COCH₃) have been demonstrated (or in a few cases inferred) in heparin/HS (Casu and Lindahl, 2001; Lindahl et al., 1994; Mochizuki et al., 2008); if we account also for the occurrence of *N*-unsubstituted GlcN units (Norgard-Sumnicht and Varki, 1995; van den Born et al., 1995; Westling and Lindahl, 2002), these numbers are further increased. The potential structural variability of HS chains is enormous.

HS chains may be further modified subsequent to completion of the *bona fide* biosynthetic process, by action of two Sulf endo-6-*O*-sulfatases that catalyze limited release of GlcNS 6-*O*-sulfate groups preferentially from heavily sulfated NS-domains (Ai et al., 2003, 2006; Uchimura et al., 2006b). The Sulf enzymes strongly associate with the cell membrane and are enzymatically active on the cell surface to desulfate both cell-surface and extracellular matrix HS.

3.4. Regulation of biosynthesis

3.4.1. Evidence for regulated HS biosynthesis

HS biosynthesis is strictly regulated (Esko and Lindahl, 2001; Esko and Selleck, 2002; Sugahara and Kitagawa, 2002). Whereas oligosaccharides from various sources show extensive structural variability (Casu and Lindahl, 2001; Warda et al., 2006), analysis of HS from various mammalian organs thus revealed organ-specific differences in HS composition that appeared reproducible within a given species. In a systematic approach, HS was isolated from multiple organs of an inbred mouse strain, and subjected to compositional analysis based on anion-exchange HPLC of products obtained after selective chemical or enzymatic depolymerization. Strikingly similar chromatograms were obtained from HS species derived from the same organ of different mice, whereas the corresponding patterns relating to different organs were distinct (Ledin et al., 2004). The interpretation of these findings, in terms of defined patterns of variously substituted

monosaccharide residues along HS chains remains elusive. There is no current technology for sequence analysis of extended stretches of HS polymer. Moreover, even highly purified HS preparations appear polydisperse with regard to chain length, and “sequencing” does not seem really meaningful.

Another approach toward assessing the structural diversity of HS chains involved immunohistochemical analysis of tissues using monoclonal antibodies generated either by conventional approach (van den Born et al., 1995) or through application of phage-display libraries (Smits et al., 2004; van den Born et al., 2005; van Kuppevelt et al., 1998). A variety of tissues showed remarkably selective expression of multiple HS-based epitopes of apparently different structures, some of which have been at least partly identified (Kurup et al., 2007; Ten Dam et al., 2006; van den Born et al., 2005). Tissue-specific changes in HS epitope expression during mouse embryonic development was revealed using a “ligand and carbohydrate engagement” assay (Allen and Rapraeger, 2003). These results suggest that, for instance, the “kidney HS” often used to study interactions with various proteins actually consists of several distinct HS subspecies, derived from vascular walls, glomerular basement membrane, tubular basement membrane, etc. The remarkably reproducible composition of oligosaccharides obtained upon selective degradation of HS from a given organ (Ledin et al., 2004) would therefore reflect structures of HS subspecies that occur in constant relative amounts, each with distinct molecular-weight distribution and regulated level of polymer modification. We surmise that HS chains within the same biosynthetic pool show similar distribution of NA-, NS-, and NA/NS-domains, and that each domain type retains a typical substitution pattern. Such patterns would presumably be characterized by defined GlcA/IdoA ratios and levels of different (*N*-, 2-*O*-, 3-*O*-, 6-*O*-) sulfate groups, but there is no evidence for the generation of predetermined sequences of variously modified/substituted monosaccharide units.

3.4.2. The GAGosome concept

Virtually all multicellular organisms, from ancient cnidarians to modern mammals produce HSPGs. While we believe that the basic mechanisms of chain assembly and modification are similar in various organisms little is known about the actual design of the biosynthetic apparatus. Studies on heparin biosynthesis in a cell-free microsomal system revealed a rapid process, a fully modified heparin chain being completed in less than 30 s (Höök et al., 1975). We therefore surmise that the chain elongation and modification reactions in heparin/HS biosynthesis are confined to a single Golgi compartment. The enzymes implicated show the type II transmembrane topology typical of Golgi enzymes, and there is evidence for close functional, even physical interactions between pairs of enzyme proteins, including EXT1/EXT2 (Busse et al., 2007; McCormick et al., 2000; Senay

et al., 2000), EXT2/NDST1 (Esko and Selleck, 2002; Presto et al., 2008), and Hsepi/2-OST (Hagner-McWhirter et al., 2004; Pinhal et al., 2001). The GAGosome concept was coined to denote a biosynthetic apparatus of assembled enzymes (Esko and Selleck, 2002; Presto et al., 2008), ready to accommodate the appropriate core protein (presumably previously subjected to upstream substitution by linkage-region oligosaccharide). We can still only speculate regarding the actual mode of GAGosome function, especially concerning the various stages of polymer modification. We proposed a model based on more-or-less processive, albeit interrupted, action of enzymes or enzyme pairs along a (still nascent) precursor polymer (Salmivirta et al., 1996) (shown in modified form in Fig. 3.1B). The model, while conjectural, accounts for the order and concerted mode of action of some of the enzymes, including the promoting effect of *N*-sulfation on chain elongation (Lidholt and Lindahl, 1992) and the coupling between C5-epimerization and 2-*O*-sulfation (Hagner-McWhirter et al., 2004). In accord with the model, recent experiments showed seemingly processive *N*-sulfation of a $(\text{GlcA}\beta 1,4\text{GlcNAc}\alpha 1,4)_n$ polysaccharide substrate *in vitro*, catalyzed by either NDST1 or NDST2 in the presence of PAPS (Carlsson et al., 2008). “Modulators?” are arbitrarily introduced (Fig. 3.1B) to account for features of the biosynthetic process not readily explained by the topology of catalytically active enzymes, such as the domain organization of substituents along the HS chain and the distinctly regulated composition of HS produced by different cells. Other findings to accommodate include the “recycling” of PG core proteins carrying truncated HS chains followed by renewed chain elongation and modification (Fransson et al., 2004).

The complexity of GAGosome function is underpinned by the variety of manipulations of cells and animals found to result in changes in HS structure. A typical HS was thus generated by rat hepatocytes, whereas a microsomal fraction derived from the same cells instead produced a more extensively *N*-sulfated, heparin-like polysaccharide (Riesenfeld et al., 1982). While this discrepancy is still not explained, factors such as PAPS and UDP-sugar concentrations may well be involved, hence the regulation of the “antiporters” that control the flux of various nucleotides across the Golgi membrane (Hirschberg et al., 1998). Inhibition of PAPS biosynthesis, by addition of chlorate to cultured Madin-Darby canine kidney cells was in fact found to differentially affect *N*- and *O*-sulfation of HS (Safaiyan et al., 1999). Moreover, inactivation in mice of a recently discovered, Golgi-resident PAP 3'-phosphatase implicated in PAPS metabolism led to decreased proportions of sulfated versus nonsulfated HS disaccharides (Frederick et al., 2008). Transgenic overexpression in mice of heparanase (Zcharia et al., 2004), an endoglucuronidase originally detected due to its ability to degrade macromolecular heparin (Gong et al., 2003; Ögren and Lindahl, 1975), resulted in accelerated HSPG turnover, but also to unexpected upregulation of HS sulfation, particularly 6-*O*-sulfation (Escobar

Galvis et al., 2007). Upregulation of *N*- and 6-*O*-sulfation, sometimes referred to as “compensatory,” were noted in mice depleted of *Hsepi* (Li et al., 2003) or *Hs2st* (Merry et al., 2001) genes and therefore devoid of HSPGs with IdoA2S residues.

Further complex regulatory phenomena appear linked to the postbiosynthetic-“editing” Sulf endo-6-*O*-sulfatases, committed to selective release of 6-*O*-sulfate groups from, in particular, -IdoA2S-GlcNS6S-sequences within NS-domains (Ai et al., 2003, 2006). Targeted disruption of the *Sulf1* and *Sulf2* genes led to some functional consequences, but also to perturbations of HS structure beyond the predicted loss of -IdoA2S-GlcNS6S- and corresponding increase in -Ido2S-GlcNS- sequences (Ai et al., 2007; Lamanna et al., 2007, 2008; Langsdorf et al., 2007).

4. INTERACTIONS OF HS WITH PROTEINS

The biological functions of HSPGs appear to be exerted almost exclusively through interactions with proteins. Protein binding is generally mediated by the HS chains, but may also involve interactions of core proteins. The cytoplasmic domains of syndecans thus interact with intracellular components to control cellular adhesion or motility, modulated by matrix proteins such as fibronectin that bind both extracellular HS substituents and integrins (Alexopoulou et al., 2007; Couchman et al., 2001; Mahalingam et al., 2007). Also extracellular domains of PG core proteins may directly bind protein ligands, thereby affecting signaling functions (Kirkpatrick et al., 2006; Whitelock et al., 2008). The vast majority of protein ligands, however, interact with sulfated domains of HS chains. These ligands, often referred to as “heparin-binding proteins,” are highly diverse and include enzymes and enzyme inhibitors, cytokines, morphogens, growth factors, matrix proteins, lipoproteins, various proteins associated with disease, etc. (Bernfield et al., 1999; Bishop et al., 2007; Kjellén and Lindahl, 1991). Ionic attraction between negatively charged groups in HS/heparin chains and basic amino acid residues in the protein ligands is a prominent feature, although nonionic interactions may also contribute to binding (Jairajpuri et al., 2003).

Comparison of “heparin-binding” and “nonbinding” proteins led to postulation of “consensus sequences” for GAG binding based on clustered basic amino acid residues (Cardin and Weintraub, 1989). However, the concept appeared biased through somewhat preconceived notions of peptide secondary structure, assuming helical shape where β -strand or irregular conformation might also apply. Moreover, the key amino acid residues comprising heparin-binding domains may actually be located in distinct albeit juxtapositioned loops (Spillmann and Lindahl, 1994) (Section 4.1; Fig. 3.2).

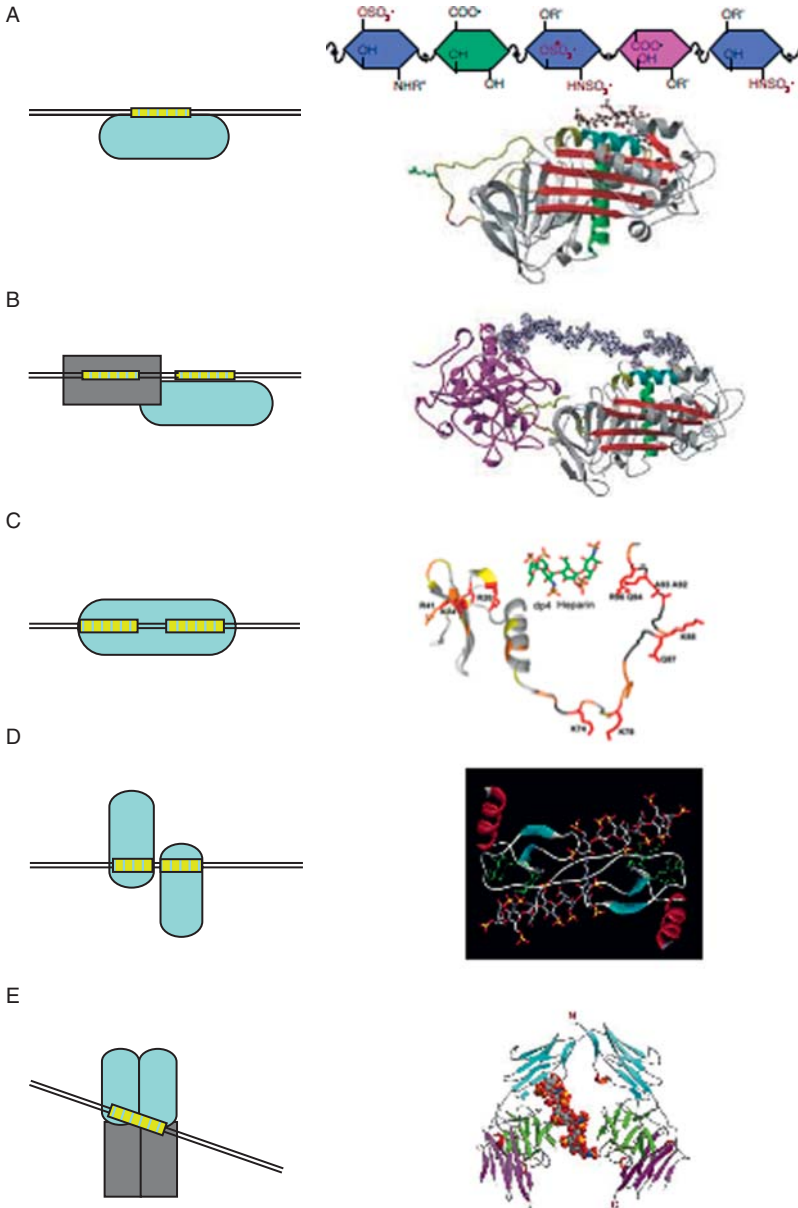


Figure 3.2 Examples of HS–protein interactions selected to illustrate the role of saccharide domain organization (Section 4.1). (A) Single HS domain binding to a single protein, illustrated by interaction of antithrombin with specific pentasaccharide sequence. Structure of the pentasaccharide (R' , optional $-H$ or $-SO_3^-$; R'' , $-SO_3^-$ or $-COCH_3$) pinpoints the four sulfate groups essential to the interaction; the 3-O-sulfate group on the internal GlcNS residue is a rare constituent (Section 4.3.1). The conformational change induced by pentasaccharide-binding results in exposure of

4.1. Topology of protein-binding domains in HS

On the carbohydrate side, the protein-binding regions may range in size from a few disaccharide units to 12-mers, or even larger (Gallagher, 2001). Contiguous NS-domains of >8-mer size are generally rare in HS, that instead may contain composite binding sites involving short NS-domains separated by one or more *N*-acetylated disaccharide units (*N*-sulfated/acetylated/sulfated [SAS] domains) (Kreuger et al., 2002). Interactions with the protein ligands shown in Fig. 3.2 were selected to illustrate some variations on this theme. The pentasaccharide sequence required to activate antithrombin was identified in heparin (Casu et al., 1981; Thunberg et al., 1982) but is also contained within single domains of some HS species (de Agostini et al., 2008; Rosenberg et al., 1997) (Fig. 3.2A). SAS domains may bridge HS-binding sites located in different proteins (exemplified by antithrombin and thrombin in Fig. 3.2B), but also sites composed of widely separated clusters of basic amino acid residues within a single polypeptide, as in CXCL12gamma chemokine (Laguri et al., 2007) (Fig. 3.2C) or endostatin (Kreuger et al., 2002). Single HS chains may join homodimeric proteins, such as various chemokines (Proudfoot, 2006; Spillmann et al., 1998; Vives et al., 2002) (illustrated by RANTES in Fig. 3.2D), VEGF-AA (Robinson et al., 2006), PDGF-BB (Abramsson et al., 2007), interferon- γ (Lortat-Jacob et al., 1995), but also higher oligomers such as platelet factor 4 (Stringer and Gallagher, 1997). The HS domain requirement for complex formation is not readily deduced from the number of interacting polypeptides. Whereas an ≥ 18 -mer, clearly involving SAS-domain arrangement, is needed to span the HS-binding sites of an IL-8 dimer (Spillmann et al., 1998), oligosaccharides as small as 4-mers were shown to promote formation of ternary complex with fibroblast growth factor 1 (FGF1) and fibroblast growth factor receptor 1 (FGFR1) (Wu et al., 2002). The actual stoichiometry of FGF-HS-FGFR complexes (Fig. 3.2E) remains a matter of debate (Section 4.2.2).

the “bait” loop (left extreme of polypeptide) targeting serine proteases. Reproduced from *Nat. Struct. Mol. Biol.* (Li et al., 2004) with permission. (B) SAS domains required to bind two distinct proteins, here antithrombin and thrombin (may also bind to contiguous *N*-sulfated sequence in heparin). Reproduced from *Nat. Struct. Mol. Biol.* (Li et al., 2004) with permission. (C) SAS domains required to span two binding sites in a single protein, illustrated by the chemokine CXCL12alpha. Reproduced from *PLoS ONE* (Laguri et al., 2007). (D) SAS domains binding a homodimer, the chemokine RANTES. Reproduced from *Biochemistry* (Vives et al., 2002) with permission. (E) Single domain (but possibly also SAS type) stabilizing a heterooligomeric complex of FGF1 and FGFR2 ectodomain (Section 4.2.2). Reproduced from *Nature* (Pellegrini et al., 2000) with permission.

4.2. Functional implications

“Heparin-binding proteins” have been identified by the hundreds, often without any clue to functional significance. Most of the functionally relevant interactions recognized involve HS rather than heparin, and many such interactions have now been ascribed functions and physiological roles (Bishop et al., 2007; Conrad, 1998) (Fig. 3.3).

From a mechanistic standpoint, most HS–protein interactions studied fall into either of two categories.

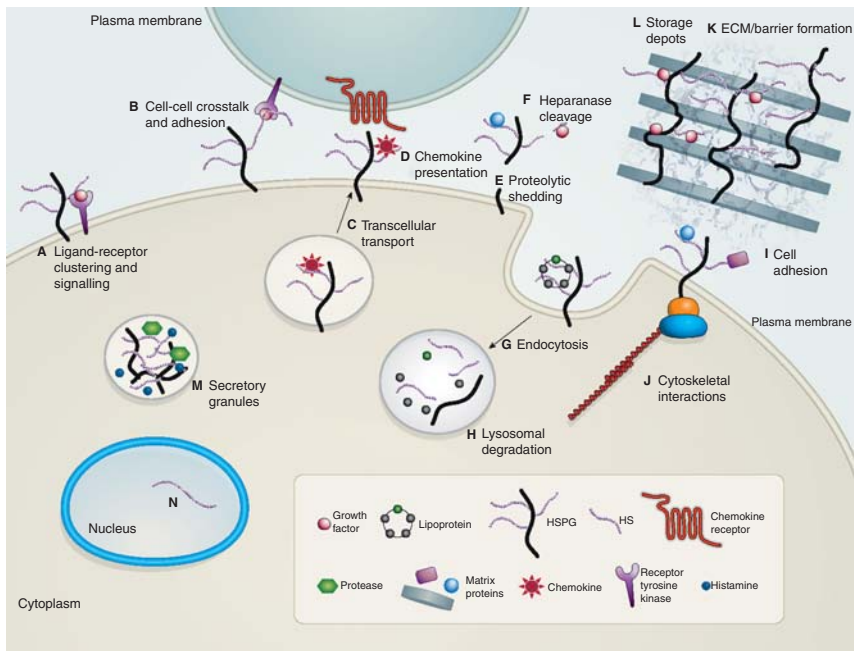


Figure 3.3 HS–protein interactions in various functional settings. (A, B) HSPGs present growth factors to their receptors, on the same or an adjacent cell, and may form part of signalling complexes. Chemokines are bound to HS chains for transcytosis (C) and presentation at cell surfaces (D). Truncation of HSPGs by proteolytic shedding of ectodomains (E) and cleavage of HS chains by heparanase (F). Uptake of cell-surface HSPGs by endocytosis (G) for degradation in lysosomes (H) or recycling back to the surface. HSPGs facilitate cell adhesion by interacting with extracellular-matrix proteins through their HS chains (I) and with the cytoskeleton via cytoplasmic core-protein domains (J). HSPGs in extracellular matrices contribute to physiological barriers (K) and provide storage of growth factors and morphogens (L). Serglycin carrying heparin chains are required for storage of proteases and histamine in secretory granules of mast cells (M). Experiments suggest that HS chains with special structural features may be located in the nucleus, although with so far unknown function (N). Reproduced from *Nature* (Bishop et al., 2007) with permission. For additional references see the text.

4.2.1. HS as scaffold or protein carrier

Numerous processes in development and homeostasis require proteins to be presented at a given site and time in the body. Such positioning may be achieved by interaction of proteins with the polysaccharide chains of HSPGs, at cell surfaces or in the extracellular matrix (Fig. 3.3). The diversity of protein ligands is striking. HSPGs at cell surfaces (or in the extracellular matrix) serve as carriers for lipases (Mahley and Ji, 1999; Spillmann et al., 2006), chemokines (Parish, 2006; Wang et al., 2005) (Fig. 3.3D), and growth factors (Abramsson et al., 2007; Jakobsson et al., 2006; Robinson et al., 2006) (Fig. 3.3A and B) with important roles in lipid metabolism, inflammatory processes, and angiogenesis, respectively. HSPGs that transiently capture growth factors or morphogens may help to stabilize protein gradients (Guimond and Turnbull, 2004; Kirkpatrick and Selleck, 2007; Lander et al., 2002), to control the range of signaling (Koziel et al., 2004), or simply to protect the proteins against degradation. Capturing may result in endocytosis of a protein ligand, possibly along with bound HSPG (MacArthur et al., 2007; Spijkers et al., 2008) (Fig. 3.3G) or in transcytosis of, for instance, a chemokine (Wang et al., 2005) (Fig. 3.3C) or lipoprotein lipase enzyme (Obunike et al., 2001). HSPGs (perlecan, agrin, collagen XVIII) in basement membrane interact with matrix proteins, such as fibronectin and laminin, and thus provide support, resistance to mechanical stress, and filtration barrier properties (Iozzo, 2005) (Fig. 3.3K). Proteins bound to HSPGs may be mobilized through protease-mediated shedding of PG ectodomains (Fig. 3.3E) or through cleavage of HS chains by heparanase (Fig. 3.3F). Protein carrier functions of HSPGs may extend from one cell harboring the core protein to a “receptor” located on another cell (Fig. 3.3B and D). There are now many examples of such “*trans* actions,” the HS chains serving either as mere carriers or in actual coreceptor functions (Section 4.2.2). Endothelial HSPG may directly bind leukocyte L-selectin (Wang et al., 2005), or provide a scaffold for presentation of chemokines to leukocyte receptors (Proudfoot, 2006; Proudfoot et al., 2003) (Section 7.3). VEGF signaling in endothelial cells during angiogenesis may be supported by HS expressed by adjacent perivascular smooth muscle cells (Jakobsson et al., 2006). Ectodermal syndecan-2 is required to establish left–right axis during visceral development in *Xenopus* (Kramer and Yost, 2002). HSPGs secreted by one type of cell often modulate processes in other cells. For example, agrin is released by motor neurons into the synaptic cleft, where it induces clustering of acetylcholine receptors on the sarcolemma (Gautam et al., 1996, 1999).

4.2.2. HS in activation and coreceptor functions

In many interactions, HS chains serve active functions and directly contribute to biological activities or signaling processes. A well-studied example is the anticoagulant activity of heparin (and some HSs; Section 4.3.1)

mediated by binding of a specific pentasaccharide sequence to antithrombin. Binding induces a subtle conformational change of the antithrombin molecule, which thereby turns into a more efficient inhibitor of procoagulant serine proteases (Bjork and Olson, 1997; Bourin and Lindahl, 1993; Jin et al., 1997) (Fig. 3.2A and B).

Mechanisms by which cell-surface HSPGs modulate formation of signaling complexes between various growth factors/morphogens and their receptors (Fig. 3.3A) have received much recent attention. Whereas a few of these effects appear to be mediated by the core proteins rather than the HS substituents (Kirkpatrick et al., 2006; Kramer and Yost, 2003; Ohkawara et al., 2003), most studies revealed a dependence on HS saccharide. Hedgehog, BMP, and Wnt signaling in *Drosophila* thus were all affected by impeded HS chain formation due to loss of EXT function (Bornemann et al., 2004; Han et al., 2004; The et al., 1999). HSPGs could variously serve to sustain morphogen gradients, deliver the signaling protein to the *bona fide* receptor, or directly participate in formation of a signaling complex. For most signaling pathways, the precise nature of HS involvement remains unclear. Complex structure-function relations may apply, as illustrated by the “catch or present” model for HS involvement in Wnt signaling (Ai et al., 2003). This morphogen is sequestered by HS chains at the cell surface, and becomes available for receptor activation only following Sulf-catalyzed release of 6-*O*-sulfate groups. The resultant low-affinity HS-Wnt complexes can functionally interact with Frizzled receptors to initiate Wnt signal transduction.

The role of HS in growth factor signaling has been most thoroughly studied in relation to the FGF family. Of the 22 FGF members identified 21 show significant affinity for HS (Asada et al., 2008), generally implicated with signaling through cognate high-affinity tyrosine-kinase receptors (FGFRs) (Eswarakumar et al., 2005). In particular, studies of signaling pathways induced by FGF1 and FGF2 provide models for “coreceptor” functions of HS that presumably apply also to several other growth factors. FGF2 was the first growth factor shown to depend on HS for interaction with its receptor (Rapraeger et al., 1991; Yayon et al., 1993). Exogenous heparin, either full-length chains or oligosaccharides above a certain minimal size could serve as coreceptors when added along with FGF2 to HS-deficient fibroblasts. Saccharide interaction with both the growth factor and its receptor in signaling complexes was inferred from the finding that receptor activation leading to mitogenesis required 6-*O*-sulfate in addition to *N*- and 2-*O*-sulfate groups, whereas *N*- and 2-*O*-sulfate groups sufficed for binding of FGF2 alone (Guimond et al., 1993). More detailed information regarding interaction of heparin/HS with FGF/FGFR was obtained through crystallization of ternary complexes of growth factor, receptor ectodomain, and heparin oligosaccharides. Two distinct types of complexes were discerned, both containing two molecules each of FGF and FGFR.

In one structure the two FGF–FGFR pairs interact in symmetrical mode with two oligosaccharides (2:2:2 complex), each thought to represent the nonreducing terminus of a native polysaccharide chain (Schlessinger et al., 2000). The other, asymmetrical, model features a single saccharide sequence that interacts with both FGFs but only one of the two FGFR molecules (2:2:1 complex), thus enabling assembly of a putative signaling complex along a single polysaccharide chain (Pellegrini et al., 2000) (Fig. 3.2E). The controversy over these models (Harmer et al., 2004; Mohammadi et al., 2005) is still unresolved. However, recent studies using carefully selected heparin oligosaccharides suggested that, depending on oligosaccharide size various types of complexes could be generated in solution (Delehedde et al., 2002; Wu et al., 2003) and, further, that mitogenic activity would be primarily associated with asymmetric ternary complex formation (Goodger et al., 2008). Notably, heparin ≥ 8 -mers showed striking ability to *trans*-dimerize FGF2 in apparently cooperative manner, generating an asymmetric complex with potent mitogenic activity. These findings raise intriguing questions regarding FGF–FGFR complex assembly along variously sized NS-domains in authentic HS chains.

4.3. Aspects of specificity

The strict regulation of HS biosynthesis, as reflected by the distinct composition (Ledin et al., 2004) and immune recognition properties (Kurup et al., 2007; van Kuppevelt et al., 1998) of HSs from different tissues (Section 3.4.1), suggests a high degree of specificity and selectivity in interactions of HS with proteins. This notion has been underpinned by the marked specificity of the interaction between heparin/HS and antithrombin (Fig. 3.2A, Section 4.3.1), and is variously referred to in terms of “sulfation patterns,” “sequence specificity,” “sulfation code” (Bulow and Hobert, 2006; Gallagher, 2006; Guimond and Turnbull, 1999; Patel et al., 2008; Salmivirta et al., 1996). There are, however, reasons for a nuanced view of the matter (Kreuger et al., 2006; Rudd et al., 2007; Skidmore et al., 2008). Interactions may be modulated by factors such as conformational flexibility (primarily of IdoA residues) (Casu et al., 1986; Mulloy and Forster, 2000), selective effects of counteractions (Powell et al., 2004; Rudd et al., 2007), influences of residues adjacent to the actual protein-binding domain (Guerrini et al., 2008), and domain organization within the HS chain (Kreuger et al., 2002). What is the role of carbohydrate structure in terms of actual sequence dependence? We approach this question by separately considering interactions involving rare as opposed to exclusively common HS constituents.

4.3.1. Interactions involving rare HS constituents

The occurrence *per se* of a rare unit in a protein-binding domain signals some degree of interactive specificity. The number of identified protein ligands within this category is still low, but likely to increase. The antithrombin case remains the epitome of a highly selective, sequence-dependent HS-protein interaction. The rare 3-*O*-sulfated glucosamine unit was first identified as an essential component of the antithrombin-binding pentasaccharide sequence implicated with the blood anticoagulant activity of heparin (Petitou et al., 2003), and currently used in the clinic as a synthetic antithrombotic oligosaccharide (Petitou and van Boeckel, 2004). Loss of either one of the four essential sulfate groups (Fig. 3.2A) will increase the k_d for antithrombin by 2–3 orders of magnitude (Bourin and Lindahl, 1993; Petitou et al., 1988). Notably, three of these groups are common *N*- and 6-*O*-sulfates. Only about one-third of the chains in typical heparin preparations contain the 3-*O*-sulfate group (hence show anticoagulant activity), and we still cannot explain the functional significance of anticoagulant heparin in (the extravascular) mast cells. The same structure was found, albeit in much lower abundance also in certain vascular HS species (de Agostini et al., 1990; Marcum et al., 1983), suggesting a role in regulation of blood coagulation. Recombinant 3-OST1 was found to catalyze incorporation of the 3-*O*-sulfate group into the appropriate acceptor structure (Rosenberg et al., 1997). Surprisingly, *Hs3st1*^{-/-} mice did not show any obvious procoagulant phenotype (HajMohammadi et al., 2003). Instead, 3-*O*-sulfated HS with anticoagulant activity was found also at extravascular sites, particularly in the ovary, potentially involved in regulation of protease action at ovulation (de Agostini et al., 2008). Furthermore, HS chains that did not bind antithrombin also contained abundant 3-*O*-sulfated glucosamine residues, hinting at interactions with other unidentified proteins. Indeed, various 3-*O*-sulfated saccharide sequences have been identified (Edge and Spiro, 1990; Pejler et al., 1987; Shukla et al., 1999), and shown to be generated by some of the many 3-OST isoforms (Liu et al., 1999). The 3-*O*-sulfate group was identified as part of an epitope, different from the antithrombin-binding pentasaccharide, that promoted interaction of cell-surface HS with the Herpes simplex gD glycoprotein, an essential step in viral invasion of the target cell (Shukla et al., 1999). Recently, a phage-display antibody recognizing 3-*O*-sulfated oligosaccharide structures (Ten Dam et al., 2006) implicated a unique HS epitope with differentiation of embryonic stem cells along the mesodermal lineage to the hemangioblast stage (Baldwin et al., 2008). A surprising link of 3-*O*-sulfation to circadian rhythm was revealed by the finding of light-induced 3-OST expression in the pineal gland and associated changes in pineal HS fine structure (Kuberan et al., 2004). Finally, 3-*O*-sulfated HS was recently associated with submandibular gland morphogenesis in mice. The polysaccharide was found to bind FGFR-2b and increase FGF10-dependent epithelial proliferation and branching (M.P. Hoffman, personal communication).

The 3-*O*-sulfated glucosamine component of the epitope recognized by the viral gD glycoprotein is unusual also by lacking *N*-substituent. A corresponding 3-OST was implicated with regulation of Notch signaling in *Drosophila* (Kamimura et al., 2004). *N*-Unsubstituted glucosamine residues in HS have further been associated with recognition by L-selectin (Norgard-Sumnicht and Varki, 1995).

Whereas IdoA is the major 2-*O*-sulfated hexuronic acid, most HS preparations contain minor proportions of 2-*O*-sulfated GlcA. The same 2-OST catalyzes sulfation of the two uronic acids, although with marked preference for IdoA (Rong et al., 2001). Still the ratio of GlcA2S/IdoA2S may vary considerably. HS isolated from adult human brain thus showed appreciable proportions of –GlcA2S–GlcNS– disaccharide unit, whereas the same component was virtually absent from a neonatal brain specimen (Lindahl et al., 1995). No protein ligand has yet been found to require 2-*O*-sulfated GlcA for binding to HS. Remarkably, however, a HS fraction isolated from nuclei of rat hepatocytes was strikingly enriched in –GlcA2S–GlcNS6S– disaccharide units (Fedarko and Conrad, 1986).

4.3.2. Interactions based on common HS constituents

Beyond the few known examples of protein-binding HS epitopes containing rare sugar residues, there is no clear indication of distinct sequence specificity based on the precise distribution of the common sulfate groups that constitute binding motifs for the great majority of protein ligands. On the contrary, extensive sharing of binding sites on HS chains between proteins has been observed, for instance, for different members of the FGF family (Jemth et al., 2002; Kreuger et al., 2005). By and large, binding strength has been found to correlate with the overall degree of saccharide sulfation. On the other hand, several examples of HS–protein interaction have been described where a particular kind of sulfate group (*N*-, 2-*O*-, or 6-*O*-sulfate) appears to contribute more to interaction than others. This applies, for instance, to FGF2, FGF10 (Ashikari-Hada et al., 2004; Jemth et al., 2002), human papilloma virus-type 16 L1 capsid protein (Knappe et al., 2007), and the angiogenic growth factor VEGF-A₁₆₅ (Robinson et al., 2006). Recent findings implicate different structural components of HS chains in selective projection of motor axons in *Caenorhabditis elegans*, dependent on interactions with both the axon guidance cue *slt-1*/Slit and its receptor *eva-1* (Bulow et al., 2008). Other protein ligands such as the pleiotropic hepatocyte growth factor (Catlow et al., 2008) and the neuritogenic growth factor, pleiotrophin (Bao et al., 2005) are markedly nonselective and bind a variety of GAG structures containing sequences with clustered sulfate groups.

Recent studies of FGF action provide further insight into HS structure–function relations, as well as potential clues to the role of HS biosynthesis regulation (Section 6). The ability of HS-related oligo- and polysaccharides

to induce complex formation with FGF1 or FGF2 and various FGFRs was promoted by increasing overall sulfate content, in apparently nonspecific fashion (Jastrebova et al., 2006). Likewise, FGF2-induced FGFR-1c signaling, measured as phosphorylation of either Erk1/2 or Akt in CHO cells devoid of endogenous HS, was more intensely stimulated by highly N-, 2-O-, and 6-O-sulfated deca-saccharides than by deca-saccharides lacking some 2-O- or 6-O-sulfate groups. Notably, addition of FGF2 alone in the absence of oligosaccharides led to appreciable but transient signals. Low-sulfated deca-saccharides were able to variously prolong the signals, whereas fully sulfated deca-saccharide, equivalent to “heparin-like” NS-domains increased not only the duration but also the intensity of signaling (Jastrebova et al., unpublished results). Such variability may correlate to differential induction of signaling pathways and functional effects (Delehedde et al., 2000). Selectively 6-O-desulfated heparin, capable of FGF2-binding but unable to support FGF2-signaling in HS-deficient cells, efficiently inhibited the signal-promoting effect of fully sulfated heparin, presumably by sequestering the growth factor (Guimond et al., 1993). Overall, it is too early to define the role of GAG structure in FGF signaling in generalizing terms; in particular, more information is needed regarding different members of the FGF family. For instance, a fraction of relatively low-sulfated, heparin-derived octa-saccharide showed higher ability to support FGF7-stimulated DNA synthesis in chlorate-treated mouse keratinocytes, than fully sulfated octa-saccharide (Luo et al., 2006). Contrary to this hint of selectivity, not only HS but also CS/DS-containing PGs participated in FGF2-induced mitogenic response of metastatic melanoma cells (Nikitovic et al., 2008).

5. INTERFERENCE WITH HS FUNCTION

Most information available on roles of HS in development and homeostasis derives from genetic manipulation of the common model organisms, that is, mouse (*Mus musculus*), fruit fly (*Drosophila melanogaster*), zebra fish (*Danio rerio*), nematode (*C. elegans*), and frog (*Xenopus laevis*). Transgenic overexpression of genes has been used to study the effects of increasing abundance of defined core proteins or biosynthetic enzymes. Conversely, gene expression has been obliterated or attenuated through a variety of techniques, including targeted gene disruption, gene trap mutations, and RNAi- or morpholino-mediated knockdown. The present discussion is primarily aimed at processes directly related to HS-protein interactions, and studies of core proteins will therefore be considered only when they have apparent bearing on this theme. Some information has been obtained from studies of human disease (Section 7). For more comprehensive accounts, the reader is referred to several recent reviews on HS in

embryonic development (Bulow and Hobert, 2006; Hacker et al., 2005; Haltiwanger and Lowe, 2004) and homeostasis (Bernfield et al., 1999; Bishop et al., 2007).

Mutations causing overall disruption of HS biosynthesis, as seen for example following elimination of *EXT* polymerase genes led to early embryonic lethality (Bulow and Hobert, 2006), as did deletion of the secreted HSPG perlecan (Iozzo, 2005). However, many mutants with defective HSPG core proteins or HS biosynthetic enzymes survive the embryonic stage and show unexpectedly mild or highly specific phenotypes that may pinpoint particular aspects of HS biology. To avoid the systemic effects of potentially lethal mutations, conditional knockouts of selected genes have been induced in specific tissues or cell types. Other ways to define HS function involve deletion of HS-substituted portions of core proteins, or modification of HS-binding motifs in protein ligands. Selected examples of these approaches are given below.

5.1. Perturbation of core proteins

Deletion of genes for various HSPGs results in highly variable phenotypes (Bulow and Hobert, 2006) that do not, however, necessarily reflect lack of the constituent HS chains. For example, whereas elimination of the matrix HSPG, perlecan, caused early embryonic lethality (Iozzo, 2005), mice expressing perlecan devoid of the HS-substituted domain I appeared normal apart from a defective lens capsule phenotype (Rossi et al., 2003) (notably, though, the mutant perlecan still contained domain V, potentially carrying a HS chain). Conversely, the stimulation of Wnt/JNK signaling activity observed upon ectopic overexpression of glypican-3 in mesothelioma cells was independent of HS chains (Song et al., 2005). Loss-of-function phenotypes following deletion of *Sdc* genes in vertebrates showed surprisingly mild defects (Bulow and Hobert, 2006). Whereas members of the *Sdc* family are assumed to act in partially redundant manner, specific functions have been ascribed to individual species. *Sdc3* in hypothalamus was found to have an important regulatory role in feeding behavior of mice. This function was accidentally discovered following ectopic overexpression of *Sdc1* in hypothalamic nuclei (Reizes et al., 2001). The resultant “syndrophin” mice showed lack of normal appetite regulation and developed maturity-onset obesity, similar to mice lacking α -melanocyte-stimulating hormone (MSH). Appetite depression due to activation of the melanocortin MSH receptor is reversed by agouti-related protein, an MSH antagonist proposed to block receptor activation in HS-dependent manner. HS chains provided by *Sdc3* are shed from the neuronal cell surface in response to a period of feeding, allowing MSH to interact with the receptor and depress appetite. Ectopic *Sdc1* expression was not similarly modulated, hence the obese phenotype. In accord with this hypothesis, mice lacking the *Sdc3* gene

(Strader et al., 2004), or overexpressing HS-degrading heparanase (Zcharia et al., 2004), showed decreased food intake and low body weight. It was further proposed that the role of Sdc3 in regulating energy balance is not restricted to direct effects on melanocortin signaling but also involves hypothalamic neuronal plasticity (Reizes et al., 2006, 2008). Protease-mediated shedding of Sdc ectodomains is frequently implicated with regulation of various cell functions, PGs switching from promoter to inhibitor activities (Alexopoulou et al., 2007).

5.2. Perturbation of HS-binding protein domains

The functional significance of HS–protein interactions may be assessed by changing polypeptide structure in a way predicted to modulate, usually preclude, HS binding. Mutations may be introduced by transgenic technique *in vivo*, or through expression of recombinant proteins for test *in vitro* or administration *in vivo*. Among several examples to illustrate this approach, we note that deletion of only three basic amino acid residues from the N-terminal region of BMP-4 perturbed the distribution of the morphogen in the developing *Xenopus* embryo, resulting in aberrant long-range receptor activation and associated patterning defect (Ohkawara et al., 2002).

Spatially restricted patterning cues provided by VEGF-A control blood vessel branching morphogenesis, and chemotaxis of vascular endothelial cells is dictated by VEGF gradients (Barkefors et al., 2008; Ruhrberg et al., 2002). Mouse embryos, engineered to express solely an isoform of VEGF-A that lacks the HS-binding motif, showed decreased capillary branch formation. The changes in extracellular localization of VEGF-A in the mutant embryos resulted in an altered distribution of endothelial cells within the growing vasculature (Ruhrberg et al., 2002). Similarly, deletion *in vivo* of the basic “retention motif” from PDGF-B resulted in defective investment of pericytes in the microvessel wall, indicating that HS-mediated retention of PDGF-B in microvessels is essential for proper recruitment and organization of these support cells (Lindblom et al., 2003).

Selective recruitment of leukocytes, important in various pathophysiological settings, is controlled by chemokine-mediated activation of seven-transmembrane-spanning receptors. Essential to this process is the formation of haptotactic gradients by immobilization of chemokines on cell-surface HSPGs (Proudfoot, 2006; Proudfoot et al., 2003). Chemokines, mutated in their GAG-binding sites retained chemotactic activity *in vitro* but were unable to recruit cells when administered intraperitoneally.

5.3. Perturbation of polysaccharide structure

In general terms, disruption of HS synthesis in vertebrate development causes malformations that are composites of those caused by mutations of multiple HS-dependent growth factors and morphogens (Table 3.1).

Complete inhibition of HS biosynthesis, as seen following homozygous obliteration of *Ext1* (Lin et al., 2000) or *Ext2* (Stickens et al., 2005) genes, led to early termination of mouse embryonic development. Conditional, cell-selective deletion of the *Ext1* gene showed that HS-dependent protein interactions are essential in brain patterning (Inatani et al., 2003; Matsumoto et al., 2007). Similar techniques involving one or more of the NDST isoforms revealed regulatory roles of HS in T-cell reactivity (Garner et al., 2008), lacrimal gland development (Pan et al., 2008), and chemokine/L-selectin-mediated neutrophil trafficking during inflammatory responses (Wang et al., 2005).

Phenotypes due to interference with biosynthetic polymer modification were generally less severe though highly variable, in reflection of the diverse effects on cellular signaling mechanisms and other HS-dependent processes (Bulow and Hobert, 2006; Gorsi and Stringer, 2007) (Table 3.1). In mice, inhibition of *N*-sulfation, by knockout of *Ndst1*, resulted in overall down-regulation of subsequent modification reactions, hence in generation of HS with greatly reduced charge density (Fig. 3.1C). The *Ndst1*^{-/-} mice showed severe defects of multiple organs, including skeleton, brain, and lungs, and died shortly after birth due to respiratory failure (Ringvall et al., 2000). The *Hsepi*^{-/-} and *Hs2st*^{-/-} phenotypes were partly similar, with neonatal lethality but differed from the *Ndst1*^{-/-} pattern, in particular by lacking kidneys, whereas the brains appeared grossly normal (Bullock et al., 1998; Li et al., 2003). Most *Hs6st1* knockout embryos died during late gestation, and those that survived were smaller than wild-type littermates, with various developmental abnormalities (Habuchi et al., 2007). 3-OST function and deficiency were discussed in Section 4.3.1.

Comparing selected mutant phenotypes (Table 3.1) with the corresponding HS structures (Fig. 3.1C) enables correlation of structural features with specific patterning events in organogenesis. Thus, both *Hsepi*^{-/-} and *Hs2st*^{-/-} mice lacked kidneys, contrary to *Ndst1*^{-/-} mice that produced an overall poorly sulfated HS, still with some IdoA2S units. Taken together, these findings suggest a key role for IdoA2S units in kidney induction (presumably through GDNF signaling) (Li et al., 2003; Merry et al., 2001).

The relatively modest effects of deletion of certain steps in HS biosynthesis on developmental processes have bearing on the question of specificity in HS-protein interactions (Section 4.3). Mutant mice thus displayed organ systems, potential targets of HS-dependent signaling, that appeared unexpectedly normal, for example, the intestinal, central nervous, and vascular systems in *Hsepi*^{-/-} and *Hs2st*^{-/-} mice (Bullock et al., 1998; Li et al., 2003). These findings could reflect various kinds of redundancy. Signaling systems activated by growth factors/morphogens not dependent on HSPGs could be recruited to promote essential responses such as selective cell proliferation, migration, etc. Alternatively, essential signaling events critically reliant

on participation of HS chains could be less dependent on detailed polysaccharide structure. Discriminating these alternatives requires information regarding the corresponding HS-deficient target system, that is, the phenotype obtained when HS is either completely absent or else unable to participate in a given signaling function. The severe cerebral patterning defects following conditional *Ext1* knockout in mice thus clearly implicated HS in fundamental steps of brain development (Inatani et al., 2003), yet brains of *Hsepi* mutant mice appeared macroscopically normal (Li et al., 2003) (Yamaguchi et al., unpublished results). Furthermore, deletion of the C-terminal, HS-binding motif of PDGF-B led to impaired growth factor retention and pericyte recruitment in vascular development *in vivo*, suggesting an important role for HS in PDGF-BB function. The nearly normal vascular development in *Hsepi*^{-/-} embryos again argues against any critical constraint of HS structure in this context (Abramsson et al., 2007). Indeed, binding of HS-related oligosaccharides to PDGF-BB was found to depend on overall degree of sulfation, without any apparent requirement for specific sequence. The more severe vascular phenotype of *Ndst1*^{-/-} embryos is in accordance with the overall reduction in sulfation level of *Ndst1*^{-/-} HS (Abramsson et al., 2007; Ringvall et al., 2000). We therefore conclude that the severely perturbed HS generated by the *Hsepi*^{-/-} mutant (Fig. 3.1C) could satisfy at least some essential HS-dependent signaling steps in cerebral patterning and vasculogenesis. An interesting question is to what extent this unexpected functional potential relies on the “compensatory” upregulation of N- and 6-O-sulfation observed for both *Hsepi*^{-/-} (Li et al., 2003) and *Hs2st*^{-/-} (Merry et al., 2001) mutant HS.

These and other findings highlight the need for more detailed information regarding the molecular interactions of wild-type and genetically manipulated HS chains with growth factors/morphogens and their receptors in various settings of cellular signaling. So far, such information has been restricted to a few members of the FGF family and their receptors, involving heparin oligosaccharides rather than authentic HS structures (Section 4.2.2). Recent experiments based on nitrocellulose-filter trapping of radiolabeled HS with growth factors showed aberrant binding of FGF2 to *Hsepi*^{-/-} compared to wild-type HS (Jia et al., 2009). Even more pronounced difference between wild-type and IdoA-free HS was noted in binding to GDNF, implicated with the kidney agenesis observed in both *Hsepi*^{-/-} and *Hs2st*^{-/-} mice (Bullock et al., 1998; Li et al., 2003). Anomalous growth factor binding is not, however, predictably linked to functional shortcomings of mutant HS species, as illustrated by seemingly normal FGF2 signaling properties in spite of poor growth factor binding of *Hs2st*^{-/-} HS (Merry et al., 2001). An intriguing question relating to each distinct mutant HS in defined functional settings is whether an observed signaling failure is due

primarily to lack of a structural component, such as IdoA in *Hsepi*^{-/-} HS, or to secondary perturbation of domain organization along the HS chain.

6. IS THERE A “SULFATION CODE”?

We still lack a clear picture of structure–function relations in HS biology. Figure 3.4 is an attempt to unify the scattered pieces of information, as reviewed in previous sections, into a coherent albeit somewhat speculative pattern. Can we envisage a “sulfation code,” in terms of predetermined saccharide sequences, tailor-made to suit individual protein ligands? The antithrombin-binding region with its rare 3-*O*-sulfate group (Fig. 3.2A) provides a near fit to this concept. We speculate that HS domains containing rare groups generally mediate highly selective interactions that rely heavily on the presence of the rare unit (Fig. 3.4A). Other interactions, based exclusively on common units may be largely nonspecific as illustrated by several previous examples, protein binding increasing in strength with increasing level of sulfation (Fig. 3.4B). The general lack of specificity does not exclude that a certain type (*N*-, 2-*O*-, 6-*O*-) of sulfate substituent may contribute more to a particular interaction than other groups. A functional consequence of this model is the potential for modulated response, in broad sense, which could cover anything from simple ligand affinity and morphogen gradient shape to receptor activation and intracellular signaling. There is no reason to rule out; however, that yet other interactions may critically depend on combinations of (common) sulfate groups that are located in defined positions in relation to key basic amino acid residues. Such critical sulfate groups, indicated in *red* in Fig. 3.4C may of course be conceived in terms of specific sequences, although they are rarely created as such. Instead, the probability of generating a particular constellation of sulfate groups through a process of essentially stochastic 2-*O*- and 6-*O*-sulfation within a NS-domain will increase, for statistical reason, with increasing levels of sulfate substitution. Notably, this model will enable modulation of, say, intracellular signaling through sets of cell-surface receptors, through regulation of overall sulfation levels of HS coreceptors. The 2-*O*- and 6-*O*-sulfation reactions may again be independently adjusted to accommodate the relative importance of 2-*O*- versus 6-*O*-sulfate groups. In this way, protein-binding domains containing specific combinations of sulfate groups may be generated in regulated fashion, but without any requirement for synthesis of predetermined sequences. Whether such arrangement should be understood in terms of “sequence specificity” appears essentially a semantic question. Intermixed (B) and (C) mechanisms are clearly feasible. The significance of model (C)

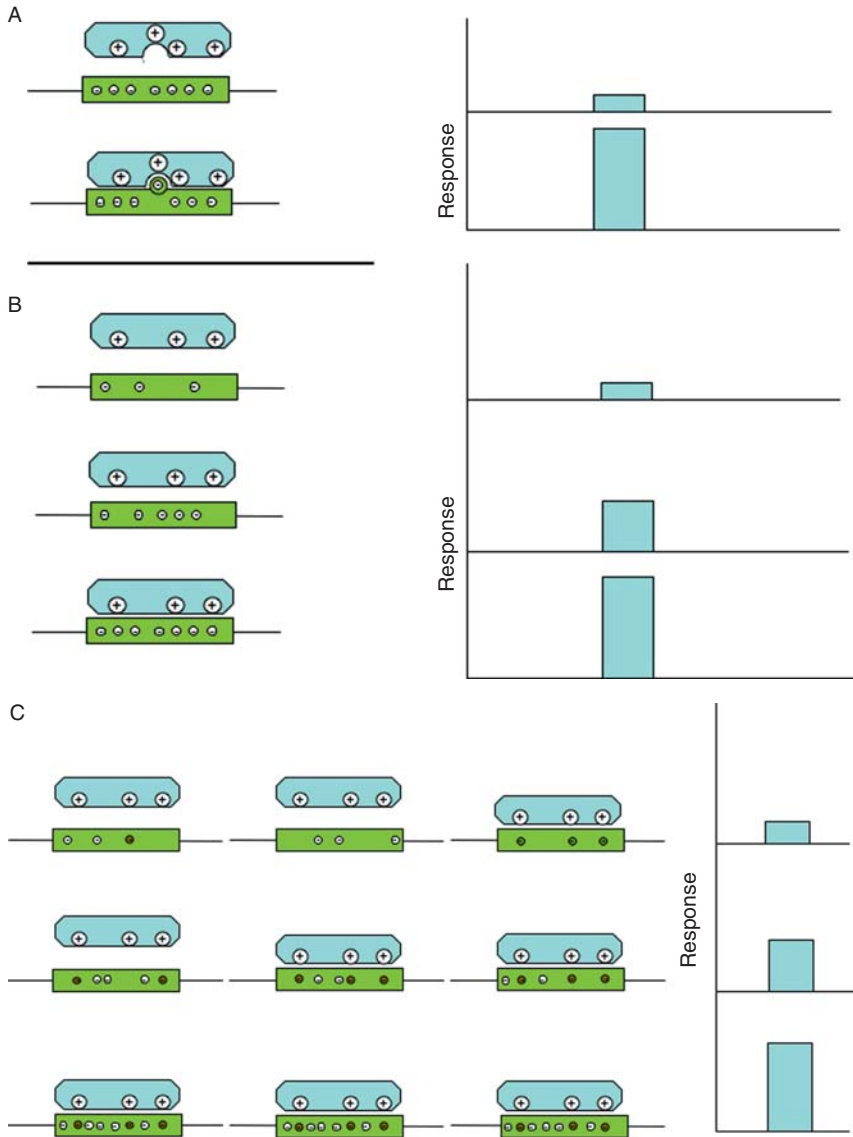


Figure 3.4 Levels of specificity in HS-protein interactions. (A) Interactions involving rare constituents (such as the GlcN 3-O-sulfate group). We hypothesize that the resultant all-or-nothing type response generally depends on the presence or absence of the rare unit (as in the antithrombin case; Fig. 3.2A). (B) Interactions based on exclusively common components, that depend on overall negative charge density rather than specific location of critical sulfate groups. Variations in sulfation level translate into modulated functional response. (C) Interactions involving “hidden sequence specificity,” that depend on defined location of critical sulfate groups

would be particularly apparent in relation to development of HS-based, selective drugs.

7. HS AND DISEASE

In addition to their crucial roles in development and homeostasis, HSPGs also contribute to pathophysiology, by interacting with proteins involved in diverse disease processes.

7.1. Amyloid diseases

Amyloidosis constitutes a heterogeneous group of diseases characterized by organ-selective deposition of proteins and peptides, in all 22 different types, that adopt non-native conformations and assemble into fibrils of highly regular structure (Ancsin, 2003; Kisilevsky, 2000; van Horsen et al., 2003). Virtually all types of amyloid deposits contain HS, that is believed to promote fibrillogenesis by associating with the amyloid precursors, potentially contributing to the conformational change required for their assembly into fibrils (Fig. 3.5A). The codeposition with HSPG also protects the amyloidogenic peptides against proteolytic degradation. Two common amyloid diseases with major clinical and social impact are Alzheimer's disease (AD) and type-2 diabetes. Other amyloidoses are relatively rare but often severe.

7.1.1. Alzheimer's disease

AD is characterized by progressive decline in cognitive function, mostly in elderly individuals, associated with profuse accumulation of amyloid β -peptide ($A\beta$) in neuritic plaques or in more diffuse deposits in the brain parenchyma and the walls of cerebral and leptomeningeal vessels. The 40–42 amino-acid residue $A\beta$ peptides are generated through posttranslational proteolytic modification of a larger amyloid-precursor protein. Early findings of HS in amyloid deposits of the AD brain (Snow et al., 1987) have been extended to include more than one type of HSPG (van Horsen et al., 2003). However, the precise role of HS chains in $A\beta$ aggregation remains unclear, as does the mechanism behind the neurotoxic action of aggregates. Binding of $A\beta$ to membrane-associated HS of microglia cells, mediated by a

(indicated in *red*). Only those HS domains that accommodate the critical sulfate constellation promote a functional response. The probability of generating such assemblage increases with increasing level of (stochastic) sulfation; with fully sulfated (“heparin-like”) structures (bottom models) all interactions are productive. The combined output of multiple interactions enables graded modulation of functional response.

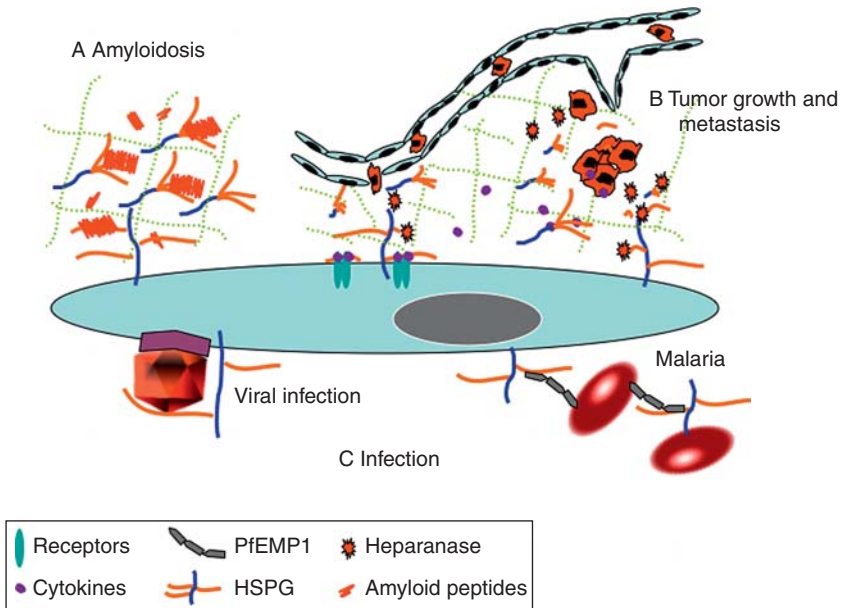


Figure 3.5 HS–protein interactions in disease conditions. (A) The polymerization of amyloidogenic peptides is facilitated by HS that is codeposited with the resultant fibrils. (B) Upregulation of heparanase, typically seen in cancer cells with high metastatic capacity, results in degradation of HSPGs in extracellular-matrix/basement membrane, facilitating mobilization of the cells and penetration of the vascular wall. Cleavage of the HS chains also releases growth factors that promote angiogenesis, cell proliferation, and tissue remodeling. (C) HSPGs are involved in various infectious processes. Illustrated here is the coreceptor function of cell-surface HSPG in viral invasion, and the role of HS chains, immobilized on vascular endothelium and at the erythrocyte membrane in promoting cytoadherence and “rosetting,” respectively, of erythrocytes in severe malaria. These adhesive phenomena are due to the plasmodium-encoded PfEMP1 protein that is exposed at the erythrocyte surface and binds to HS. Also note the role of HSPGs as carrier of chemokines and as selectin ligand in inflammatory conditions (Section 7.3).

specific peptide sequence, was implicated in $A\beta$ -induced killing of neurons (Giulian et al., 1998), and recent findings point to microglia as a source of HS in $A\beta$ deposits (O’Callaghan et al., 2008). Toxic effects of $A\beta$ are mediated by peptide oligomers, protofibrils, rather than full-grown fibrils (Walsh et al., 2002), in agreement with a mechanism based on molecular interaction with cell-surface HS. In fact, demonstration of common binding sites for aggregated $A\beta$ and FGF2 in HS from human cerebral cortex suggested that $A\beta$ might impair essential cellular functions by displacing growth factors from cell-surface HSPGs (Lindahl et al., 1999).

The roles of HS in AD pathophysiology are complex and partly contradictory. One of the key enzymes, β secretase-1 (BACE1), required to cleave

out A β peptide from its precursor protein is inhibited by HS (Scholefield et al., 2003), pointing toward prospects of drugs based on structural modification of heparin (Patey et al., 2008). In fact, treatment of AD model mice with low-molecular weight heparin inhibited A β deposition (Bergamaschini et al., 2004). Moreover, transgenic mice overexpressing heparanase that truncates HS chains (Zcharia et al., 2004) were found unable to mount the inflammatory response elicited in wild-type control mice upon intracerebral injection of aggregated A β . The injected A β aggregates were rapidly eliminated in wild-type mice but not in the heparanase transgenes (Zhang et al., unpublished results). HS therefore may not only promote A β fibrillization and toxicity, but also prevent A β generation and facilitate clearance of established A β aggregates.

7.1.2. Diabetes

Type-2 diabetes is the most common form of diabetes, characterized by peripheral insulin resistance and defective islet B-cells. A majority (>95%) of afflicted individuals exhibit amyloid deposits in the islets of Langerhans along with the progressive loss of beta-cell function (Hull et al., 2004). The amyloid fibril is composed of islet amyloid polypeptide (IAPP) that is stored together with insulin. IAPP, generated through anomalous processing of pro-IAPP (Betsholtz et al., 1989) binds heparin and interacts with HSPGs in the extracellular-matrix and basement membrane (Abedini et al., 2006). Whereas the pathophysiological role of HS-IAPP interaction is unclear, inhibition of HS biosynthesis in mouse islets transfected with human IAPP led to decreased amyloid deposition (Hull et al., 2007).

HS has also been ascribed a pathophysiological role in diabetic nephropathy, as glomerular protein leakage has been associated with loss of HS or of sulfated HS domains. Interestingly, such loss was observed along with upregulation of heparanase in response to increased glucose concentration *in vitro* (Lewis and Xu, 2008) and in diseased kidney biopsies (Wijnhoven et al., 2008).

7.1.3. Rare forms of amyloidosis

With the exception of AD and type-2 diabetes amyloid diseases are relatively rare, expressed through deposition of amyloid in different organs depending on type of causative amyloidogenic peptide. Involvement of HSPGs is amply documented in AA amyloidosis, in which the acute-phase protein, serum amyloid A (SAA) is deposited in major internal organs (liver, spleen, and kidneys) with resulting tissue damage and functional impairment. Early studies revealed codeposition of amyloid (Congo-red staining) and GAGs (Alcian-blue staining) in an animal model (Snow and Kisilevsky, 1985). HS was identified as the major GAG in amyloid-laden organs (Kisilevsky and Fraser, 1996), and analysis of HS isolated from different organs suggested amyloid-specific structural features (Lindahl and

Lindahl, 1997). Several reports proposed a role for HS in pathophysiology of AA amyloidosis, and also pointed to prospects for drug development. Low-molecular weight heparin (Zhu et al., 2001) as well as compounds that mimic sulfated GAGs (Kisilevsky et al., 1995) thus attenuate disease progress in a mouse model. Treatment of mice with a glucosamine analog that interrupts HS biosynthesis led to inhibition of AA amyloid deposition, as did a HS-binding SAA-derived peptide in a cell culture-based amyloidogenesis model (Elimova et al., 2004). Moreover, organs accumulating HS-derived oligosaccharides due to selective heparanase overexpression resisted experimentally induced AA amyloidosis in mice (Li et al., 2005). Taken together, these results suggest that HS chains exceeding a critical length are required for aggregation and deposition of AA peptide.

Transthyretin-related amyloidosis occurs in various clinical settings. Analysis of amyloid fibrils from a case of familial amyloid polyneuropathy revealed transthyretin associated with both HS- and CSPGs (Inoue et al., 1998). Several other potentially amyloidogenic peptides associate with heparin/HS, including β 2-microglobulin (Relini et al., 2008), gelsolin fragments (Suk et al., 2006), α -synuclein (Cohlberg et al., 2002), and cellular prion protein (Warner et al., 2002). Again, these data collectively suggest that HS polymers above a certain minimal length (that may vary for different amyloid species) template fibril formation by promoting aggregation of peptide monomers, whereas GAGs/mimetics below critical size may inhibit this process. Characterization of HS-binding peptide domains, as well as peptide-binding HS regions is important ongoing projects in this area.

7.2. Tumor development and metastasis

Tumor-related morbidity and mortality depend on cell transformation, and on the capacity of tumor cells to invade and metastasize. HSPGs, both on the tumor cells and in surrounding cells and tissues influence the process at various levels (Fig. 3.5B). The unrestricted proliferation of tumor cells, their increased mobility and penetration of boundaries such as basement membrane, and the stimulated angiogenesis around developing tumors are all phenomena amenable to regulation through HS-protein interactions (Fuster and Esko, 2005). The pathophysiological roles of HS depend on type of PG core protein (Aikawa et al., 2008; Langford et al., 2005; Whitelock et al., 2008b), and may be modulated through proteolytic release of PG “ectodomain” (Sanderson et al., 2005). Protein interactions of relevance to tumor biology depend on structural properties of HS, on tumor and adjacent cells. Increased as well as decreased levels of HS sulfation due to cell transformation have been reported (Escobar Galvis et al., 2007; Nackaerts et al., 1997; Robinson et al., 1984; Winterbourne and Mora, 1981). However, such information is not readily interpretable in terms of

tumor promotor or repressor functions for HSPGs, which presumably depend on arrays of growth factors and signaling mechanisms. Tumor repressor properties were early ascribed to *Ext1* and *Ext2*, encoding the HS copolymerase. Partial, selective loss of expression of these genes results in hereditary multiple exostoses (HME), a condition characterized by development (through still unclear mechanism) of essentially benign skeletal tumors (Stickens et al., 2005).

Enzymes involved in postbiosynthetic modification of HS have been implicated with tumor pathophysiology. Heparanase was found to be over-expressed by tumor cells, with strong correlation to malignancy (Parish et al., 2001; Sanderson et al., 2005; Vlodaysky et al., 2008). Cleavage of HS chains disrupts the architecture of basement membranes, thus facilitating entry of tumor cells into circulation and further dissemination. Degradation of basement membrane is also essential to angiogenesis, required for the pathological growth of primary tumors and metastases. Cytokines and growth factors bound to HSPGs in the extracellular matrix are mobilized through cleavage of HS chains, catalyzed by heparanase (Fig. 3.3F) and become accessible for stimulation of tumor growth, stromal development, or angiogenesis. Growth factors promoting angiogenesis, such as VEGF-A, PDGF-B, and FGF2 all depend, in various ways, on interactions with HS (Abramsson et al., 2007; Whitelock et al., 2008). Finally, heparanase over-expression in transgenic mice not only stimulates HSPG turnover, but also increases HS sulfation (Escobar Galvis et al., 2007) (Section 3.4.2). Tumors with increased expression of heparanase contained HS with higher content of, in particular, 6-*O*-sulfate groups compared to HS from the corresponding healthy tissues. The change in sulfation pattern may influence signaling pathways of importance to tumor development.

The two endo-6-*O*-sulfatases, Sulf-1 and -2, have been implicated also in tumor pathophysiology. Whereas the partial release of GlcN 6-*O*-sulfate groups from HS, catalyzed by these enzymes affects action of several growth factors potentially involved in cancer development (Ai et al., 2007; Lamanna et al., 2008; Uchimura et al., 2006a), attempts to directly associate Sulfs with neoplasia have yielded contradictory results. Although some tumor types showed marked upregulation of the enzymes (Backen et al., 2007; Morimoto-Tomita et al., 2005), transfection of a human myeloma cell line with human Sulf-1 and Sulf-2 resulted in potent inhibition of tumor growth following implantation into SCID mice (Dai et al., 2005).

7.3. Inflammatory and repair reactions

A key element of the inflammatory response to tissue injury is the recruitment of leukocytes into damaged areas, which is followed by various repair processes (Bishop et al., 2007; Parish, 2006). Briefly, vascular endothelial cells are stimulated to express P-selectin that induces rolling of leukocytes

along vessel walls. Encounter with chemokines at the endothelial surface leads to activation of leukocyte integrin receptors, firm adhesion to the endothelium, and finally leukocyte extravasation. Endothelial HSPG serves as scaffold for presentation of chemokines to leukocyte receptors (Proudfoot, 2006; Proudfoot et al., 2003). Chemokines bind weakly to HS and therefore need to oligomerize in order to remain immobilized, with special requirements for domain organization (see SAS domains, Section 4.1) along the HS chain (Imberly et al., 2007; Spillmann et al., 1998). Endothelial HSPG has potential additional role in neutrophil recruitment, as a ligand for leukocyte L-selectin that promotes adhesion to the endothelium (Wang et al., 2005). The potent anti-inflammatory effects of heparin are due primarily to blockade of L- and P-selectins (Wang et al., 2002), but may also reflect disruption of HS–chemokine interaction or heparanase inhibition.

Mast cells degranulate after certain types of injury, releasing histamine and proteases with important functions in tissue repair. These components of storage granules occur normally bound to serglycin PG substituted with highly sulfated heparin chains. Elimination of heparin, by deletion of either serglycin (Abrink et al., 2004) or NDST2, critical in heparin biosynthesis (Forsberg et al., 1999), severely decreased granule contents.

Release of heparanase, from leukocytes, endothelium, or activated platelets, is commonly observed in inflammation and may promote the process in various ways (Parish, 2006). Cleavage of HS chains in vascular basement membrane is believed to facilitate extravasation of leukocytes. Release of HS fragments carrying growth factors such as VEGF or FGF2 may stimulate angiogenesis and various tissue repair processes. However, the potential roles of heparanase in inflammation add up to a more complex picture. Cleavage of endothelial HS could actually interfere with presentation of chemokines or interaction with neutrophil L-selectin, hence attenuate the extravasation process. In fact, peritoneal recruitment of neutrophils in LPS-stimulated transgenic heparanase-overexpressing mice was significantly reduced compared to wild-type controls (Li et al., unpublished results).

7.4. Infection

Surface proteins of many pathogenic microorganisms (viruses, bacteria, and parasites) interact with HS. Experiments in cell culture point to roles for HSPGs as coreceptors in viral invasion of target cells (Vives et al., 2005; WuDunn and Spear, 1989; and others; Fig. 3.5C). A sequence containing a 3-*O*-sulfated, *N*-unsubstituted glucosamine unit was implicated with the HS coreceptor function in Herpes simplex (HSV-1) infection (Shukla et al., 1999), and this unexpected specificity could be exploited in design of an inhibitory oligosaccharide (Copeland et al., 2008). With few exceptions, however, there is little evidence for obligatory coreceptor functions of

HSPGs *in vivo* (Bishop et al., 2007). Strains of *Plasmodium falciparum* associated with development of severe forms of malaria employ HS as a host receptor, and a HS-binding protein encoded by the parasite was implicated with the “rosetting” and endothelial binding of infected erythrocytes typical for the disease (Vogt et al., 2006) (Fig. 3.5C). The resultant sequestration of malaria parasites *in vivo* was efficiently blocked by administration of a heparin derivative lacking anticoagulant activity.

8. CONCLUDING REMARKS

Functionally important processes in development and homeostasis that depend on HS–protein interactions impress by their number (which is likely to further increase as the research area expands), as well as by the structural diversity of HS species involved. This diversity is not readily rationalized in terms of stringent requirement for particular HS sequences in interactions with given proteins. Many interacting proteins seem able to accommodate a variety of HS structures in ways that remain at least in part compatible with functional demands. This conclusion is based on *in vitro* binding and signaling experiments, and on studies with genetically manipulated organisms that lack one or more of the enzymes involved in HS biosynthesis (Section 5.3). Distinct patterning steps have been identified, of critical importance to embryonic development, that depend on HS involvement but not on strict saccharide sequence. Other events appear more stringent, and fail when the HS at hand is perturbed beyond a critical level. Moreover, “hidden sequence specificity” (Fig. 3.4C) may apply—a particular constellation of sulfate substituents that is required but not readily discernible in cognate HS structure. Ultimate assessment of structural requirements will rely on availability of synthetic saccharides of systematically varied composition and sequence, to be tested in relevant assay systems *in vitro*. Such compounds are within reach (Noti et al., 2006), though not yet routinely available, and will be essential in development of HS-based carbohydrate (or mimetic) drugs.

The diverse structure–function relations in HS–protein interactions call for intensified efforts to understand the mechanisms of regulation in HS biosynthesis. The evidence for such regulation, while compelling, does not—in our opinion—reflect strict sequence control, but rather modulated levels of modification (sulfation, epimerization, etc.), possibly also controlled size and distribution of various types of saccharide domains along the HS chain (Section 3). How are graded modification levels translated into modulated response of signaling mechanisms and/or controlled shifts in morphogen/growth factor gradients (Fig. 3.4)? Ultimate answers to these questions will require further refined techniques for structural

characterization (at times referred to as “sequencing”) of extended polysaccharide stretches. A promising early approach to this challenge involved separation by gel electrophoresis of oligosaccharides obtained by partial endoglycosidase digestion of terminally labeled DS (Cheng et al., 1994). Principally similar methods could conceivably be applied to HS, along with novel variants of capillary electrophoresis and mass spectrometry for analysis of complex saccharide mixtures (Volpi et al., 2008). Such endeavors should parallel efforts to elucidate the nature and mode of action of the GAGosome, the membrane-bound complex of proteins committed to HS biosynthesis (Fig. 3.1B).

Finally, a deeper insight into structure–function relationships in HS-related biology requires further refined genetic approach. In particular, tissue-specific conditional knockout of selected biosynthetic enzymes will enable assessment of subtle functional defects of selected organ systems that remain seemingly unaffected within an otherwise lethal phenotype. For example, *Hsepi*^{-/-} mice die shortly after birth due to respiratory failure and kidney agenesis, but the gross morphology of their brains does not differ markedly from that of wild-type littermates (Section 5.3). What is the cognitive capacity of a mouse with cerebral HS devoid of IdoA units?

REFERENCES

- Abedini, A., Tracz, S.M., Cho, J.H., Raleigh, D.P., 2006. Characterization of the heparin binding site in the N-terminus of human pro-islet amyloid polypeptide: implications for amyloid formation. *Biochemistry* 45, 9228–9237.
- Abramsson, A., Kurup, S., Busse, M., Yamada, S., Lindblom, P., Schallmeiner, E., et al., 2007. Defective N-sulfation of heparan sulfate proteoglycans limits PDGF-BB binding and pericyte recruitment in vascular development. *Genes Dev.* 21, 316–331.
- Abrink, M., Grujic, M., Pejler, G., 2004. Serglycin is essential for maturation of mast cell secretory granule. *J. Biol. Chem.* 279, 40897–40905.
- Ai, X., Do, A.T., Lozynska, O., Kusche-Gullberg, M., Lindahl, U., Emerson, Jr., C.P., 2003. Qsulf1 remodels the 6-O sulfation states of cell surface heparan sulfate proteoglycans to promote Wnt signaling. *J. Cell Biol.* 162, 341–351.
- Ai, X., Do, A.T., Kusche-Gullberg, M., Lindahl, U., Lu, K., Emerson, Jr., C.P., 2006. Substrate specificity and domain functions of extracellular heparan sulfate 6-O-endosulfatases, Qsulf1 and Qsulf2. *J. Biol. Chem.* 281, 4969–4976.
- Ai, X., Kitazawa, T., Do, A.T., Kusche-Gullberg, M., Labosky, P.A., Emerson, Jr., C.P., 2007. SULF1 and SULF2 regulate heparan sulfate-mediated GDNF signaling for esophageal innervation. *Development* 134, 3327–3338.
- Aikawa, J., Esko, J.D., 1999. Molecular cloning and expression of a third member of the heparan sulfate/heparin GlcNAc N-deacetylase/N-sulfotransferase family. *J. Biol. Chem.* 274, 2690–2695.
- Aikawa Ji, J., Grobe, K., Tsujimoto, M., Esko, J.D., 2001. Multiple isozymes of heparan sulfate/heparin GlcNAc N-deacetylase/GlcN N-sulfotransferase. Structure and activity of the fourth member, NDST4. *J. Biol. Chem.* 276, 5876–5882.
- Aikawa, T., Whipple, C.A., Lopez, M.E., Gunn, J., Young, A., Lander, A.D., et al., 2008. Glypican-1 modulates the angiogenic and metastatic potential of human and mouse cancer cells. *J. Clin. Invest.* 118, 89–99.

- Alexopoulou, A.N., Mulhaupt, H.A., Couchman, J.R., 2007. Syndecans in wound healing, inflammation and vascular biology. *Int. J. Biochem. Cell Biol.* 39, 505–528.
- Allen, B.L., Rapraeger, A.C., 2003. Spatial and temporal expression of heparan sulfate in mouse development regulates FGF and FGF receptor assembly. *J. Cell Biol.* 163, 637–648.
- Almeida, R., Levery, S.B., Mandel, U., Kresse, H., Schwientek, T., Bennett, E.P., et al., 1999. Cloning and expression of a proteoglycan UDP-galactose beta-xylose beta 1,4-galactosyltransferase I. A seventh member of the human beta4-galactosyltransferase gene family. *J. Biol. Chem.* 274, 26155–26171.
- Ancsin, J.B., 2003. Amyloidogenesis: historical and modern observations point to heparan sulfate proteoglycans as a major culprit. *Amyloid* 10, 67–79.
- Asada, M., Shinomiya, M., Suzuki, M., Honda, E., Sugimoto, R., Ikekita, M., Imamura, T., 2009. Glycosaminoglycan affinity of the complete fibroblast growth factor family. *Biochim. Biophys. Acta* 1790, 40–48.
- Ashikari-Hada, S., Habuchi, H., Kariya, Y., Itoh, N., Reddi, A.H., Kimata, K., 2004. Characterization of growth factor-binding structures in heparin/heparan sulfate using an octasaccharide library. *J. Biol. Chem.* 279, 12346–12354.
- Backen, A.C., Cole, C.L., Lau, S.C., Clamp, A.R., McVey, R., Gallagher, J.T., et al., 2007. Heparan sulphate synthetic and editing enzymes in ovarian cancer. *Br. J. Cancer* 96, 1544–1548.
- Bai, X., Zhou, D., Brown, J.R., Crawford, B.E., Hennet, T., Esko, J.D., 2001. Biosynthesis of the linkage region of glycosaminoglycans: cloning and activity of galactosyltransferase II, the sixth member of the beta 1,3-galactosyltransferase family (beta 3GalT6). *J. Biol. Chem.* 276, 48189–48195.
- Baldwin, R.J., ten Dam, G.B., van Kuppevelt, T.H., Lacaud, G., Gallagher, J.T., Kouskoff, V., et al., 2008. A developmentally regulated heparan sulfate epitope defines a subpopulation with increased blood potential during mesodermal differentiation. *Stem Cells* 26, 3108–3118.
- Bao, X., Mikami, T., Yamada, S., Faissner, A., Muramatsu, T., Sugahara, K., 2005. Heparin-binding growth factor, pleiotrophin, mediates neuritogenic activity of embryonic pig brain-derived chondroitin sulfate/dermatan sulfate hybrid chains. *J. Biol. Chem.* 280, 9180–9191.
- Barkefors, I., Le Jan, S., Jakobsson, L., Hejll, E., Carlson, G., Johansson, H., et al., 2008. Endothelial cell migration in stable gradients of vascular endothelial growth factor A and fibroblast growth factor 2: effects on chemotaxis and chemokinesis. *J. Biol. Chem.* 283, 13905–13912.
- Bergamaschini, L., Rossi, E., Storini, C., Pizzimenti, S., Distaso, M., Perego, C., et al., 2004. Peripheral treatment with enoxaparin, a low molecular weight heparin, reduces plaques and beta-amyloid accumulation in a mouse model of Alzheimer's disease. *J. Neurosci.* 24, 4181–4186.
- Bernfield, M., Götte, M., Park, P.W., Reizes, O., Fitzgerald, M.L., Lincecum, J., et al., 1999. Functions of cell surface heparan sulfate proteoglycans. *Annu. Rev. Biochem.* 68, 729–777.
- Betsholtz, C., Svensson, V., Rorsman, F., Engstrom, U., Westermark, G.T., Wilander, E., et al., 1989. Islet amyloid polypeptide (IAPP): cDNA cloning and identification of an amyloidogenic region associated with the species-specific occurrence of age-related diabetes mellitus. *Exp. Cell Res.* 183, 484–493.
- Bezakova, G., Ruegg, M.A., 2003. New insights into the roles of agrin. *Nat. Rev. Mol. Cell Biol.* 4, 295–308.
- Bishop, J.R., Schuksz, M., Esko, J.D., 2007. Heparan sulphate proteoglycans fine-tune mammalian physiology. *Nature* 446, 1030–1037.
- Bjork, I., Olson, S.T., 1997. Antithrombin. A bloody important serpin. *Adv. Exp. Med. Biol.* 425, 17–33.

- Bornemann, D.J., Duncan, J.E., Staatz, W., Selleck, S., Warrior, R., 2004. Abrogation of heparan sulfate synthesis in *Drosophila* disrupts the Wingless, Hedgehog and Decapentaplegic signaling pathways. *Development* 131, 1927–1938.
- Bourin, M.C., Lindahl, U., 1993. Glycosaminoglycans and the regulation of blood coagulation. *Biochem. J.* 289, 313–330.
- Brule, S., Charnaux, N., Sutton, A., Ledoux, D., Chaigneau, T., Saffar, L., et al., 2006. The shedding of syndecan-4 and syndecan-1 from hela cells and human primary macrophages is accelerated by SDF-1/CXCL12 and mediated by the matrix metalloproteinase-9. *Glycobiology* 16, 488–501.
- Bullock, S.L., Fletcher, J.M., Beddington, R.S., Wilson, V.A., 1998. Renal agenesis in mice homozygous for a gene trap mutation in the gene encoding heparan sulfate 2-sulfotransferase. *Genes Dev.* 12, 1894–1906.
- Bulow, H.E., Hobert, O., 2006. The molecular diversity of glycosaminoglycans shapes animal development. *Annu. Rev. Cell Dev. Biol.* 22, 375–407.
- Bulow, H.E., Tjoe, N., Townley, R.A., Didiano, D., van Kuppevelt, T.H., Hobert, O., 2008. Extracellular sugar modifications provide instructive and cell-specific information for axon-guidance choices. *Curr. Biol.* 18, 1978–1985.
- Busse, M., Feta, A., Presto, J., Wilen, M., Gronning, M., Kjellen, L., et al., 2007. Contribution of EXT1, EXT2, and EXTL3 to heparan sulfate chain elongation. *J. Biol. Chem.* 282, 32802–32810.
- Campbell, P., Jacobsson, I., Benzing-Purdie, L., Rodén, L., Fessler, J.H., 1984. Silk—a new substrate for UDP-D-xylose: proteoglycan core protein beta-D-xylosyltransferase. *Anal Biochem.* 137, 505–516.
- Cardin, A.D., Weintraub, H.J.R., 1989. Molecular modeling of protein-glycosaminoglycan interactions. *Atherosclerosis* 9, 21–32.
- Carey, D.J., 1997. Syndecans: multifunctional cell-surface co-receptors. *Biochem. J.* 327 (Pt. 1), 1–16.
- Carlsson, P., Presto, J., Spillmann, D., Lindahl, U., Kjellen, L., 2008. Heparin/heparan sulfate biosynthesis: processive formation of N-sulfated domains. *J. Biol. Chem.* 283, 20008–20014.
- Casu, B., Oreste, P., Torri, G., Zoppetti, G., Choay, J., Lormeau, J.-C., et al., 1981. The structure of heparin oligosaccharide fragments with high anti-(factor Xa) activity containing the minimal antithrombin III-binding sequence. *Biochem. J.* 197, 599–609.
- Casu, B., Lindahl, U., 2001. Structure and biological interactions of heparin and heparan sulfate. *Adv. Carbohydr. Chem. Biochem.* 57, 159–206.
- Casu, B., Choay, J., Ferro, D.R., Gatti, G., Jacquinet, J.C., Petitou, M., et al., 1986. Controversial glycosaminoglycan conformations. *Nature* 322, 215–216.
- Catlow, K.R., Deakin, J.A., Wei, Z., Delehedde, M., Fernig, D.G., Gherardi, E., et al., 2008. Interactions of hepatocyte growth factor/scatter factor with various glycosaminoglycans reveal an important interplay between the presence of iduronate and sulfate density. *J. Biol. Chem.* 283, 5235–5248.
- Celie, J.W., Keuning, E.D., Beelen, R.H., Drager, A.M., Zweegman, S., Kessler, F.L., et al., 2005. Identification of L-selectin binding heparan sulfates attached to collagen type XVIII. *J. Biol. Chem.* 280, 26965–26973.
- Chen, R.L., Lander, A.D., 2001. Mechanisms underlying preferential assembly of heparan sulfate on glypican-1. *J. Biol. Chem.* 276, 7507–7517.
- Cheng, F., Heinegard, D., Malmstrom, A., Schmidchen, A., Yoshida, K., Fransson, L.A., 1994. Patterns of uronosyl epimerization and 4-/6-O-sulphation in chondroitin/dermatan sulphate from decorin and biglycan of various bovine tissues. *Glycobiology* 4, 685–696.
- Cohlberg, J.A., Li, J., Uversky, V.N., Fink, A.L., 2002. Heparin and other glycosaminoglycans stimulate the formation of amyloid fibrils from alpha-synuclein *in vitro*. *Biochemistry* 41, 1502–1511.

- Condac, E., Silasi-Mansat, R., Kosanke, S., Schoeb, T., Towner, R., Lupu, F., et al., 2007. Polycystic disease caused by deficiency in xylosyltransferase 2, an initiating enzyme of glycosaminoglycan biosynthesis. *Proc. Natl. Acad. Sci. USA* 104, 9416–9421.
- Conrad, H.E., 1998. Heparin-Binding Proteins. Academic Press, San Diego.
- Copeland, R., Balasubramaniam, A., Tiwari, V., Zhang, F., Bridges, A., Linhardt, R.J., et al., 2008. Using a 3-*O*-sulfated heparin octasaccharide to inhibit the entry of herpes simplex virus type 1. *Biochemistry* 47, 5774–5783.
- Couchman, J.R., Chen, L., Woods, A., 2001. Syndecans and cell adhesion. *Int. Rev. Cytol.* 207, 113–150.
- Dai, Y., Yang, Y., MacLeod, V., Yue, X., Rapraeger, A.C., Shriver, Z., et al., 2005. Hsulf-1 and hsulf-2 are potent inhibitors of myeloma tumor growth *in vivo*. *J. Biol. Chem.* 280, 40066–40073.
- David, G., Lories, V., Decock, B., Marynen, P., Cassiman, J.J., Van den Berghe, H., 1990. Molecular cloning of a phosphatidylinositol-anchored membrane heparan sulfate proteoglycan from human lung fibroblasts. *J. Cell Biol.* 111, 3165–3176.
- de Agostini, A.I., Watkins, S.C., Slayter, H.S., Youssoufian, H., Rosenberg, R.D., 1990. Localization of anticoagulant active heparan sulfate proteoglycans in vascular endothelium: antithrombin binding on cultured endothelial cells and perfused rat aorta. *J. Cell Biol.* 111, 1293–1304.
- de Agostini, A.I., Dong, J.C., de Vantery Arrighi, C., Ramus, M.A., Dentand-Quadri, I., Thalmann, S., et al., 2008. Human follicular fluid heparan sulfate contains abundant 3-*O*-sulfated chains with anticoagulant activity. *J. Biol. Chem.* 283, 28115–28124.
- Delehedde, M., Seve, M., Sergeant, N., Wartelle, I., Lyon, M., Rudland, P.S., et al., 2000. Fibroblast growth factor-2 stimulation of p42/44MAPK phosphorylation and ikappab degradation is regulated by heparan sulfate/heparin in rat mammary fibroblasts. *J. Biol. Chem.* 275, 33905–33910.
- Delehedde, M., Lyon, M., Gallagher, J.T., Rudland, P.S., Fernig, D.G., 2002. Fibroblast growth factor-2 binds to small heparin-derived oligosaccharides and stimulates a sustained phosphorylation of p42/44 mitogen-activated protein kinase and proliferation of rat mammary fibroblasts. *Biochem. J.* 366, 235–244.
- Ding, K., Lopez-Burks, M., Sanchez-Duran, J.A., Korc, M., Lander, A.D., 2005. Growth factor-induced shedding of syndecan-1 confers glypican-1 dependence on mitogenic responses of cancer cells. *J. Cell Biol.* 171, 729–738.
- Edge, A.S.B., Spiro, R.G., 1990. Characterization of novel sequences containing 3-*O*-sulfated glucosamine in glomerular basement membrane heparan sulfate and localization of sulfated disaccharides to a peripheral domain. *J. Biol. Chem.* 265, 15874–15881.
- Elimova, E., Kisilevsky, R., Szarek, W.A., Ancsin, J.B., 2004. Amyloidogenesis recapitulated in cell culture: a peptide inhibitor provides direct evidence for the role of heparan sulfate and suggests a new treatment strategy. *FASEB J.* 18, 1749–1751.
- Eriksson, I., Sandbäck, D., Ek, B., Lindahl, U., Kjellén, L., 1994. cDNA cloning and sequencing of mouse mastocytoma glucosaminyl N-deacetylase/N-sulfotransferase, an enzyme involved in the biosynthesis of heparin. *J. Biol. Chem.* 269, 10438–10443.
- Escobar Galvis, M.L., Jia, J., Zhang, X., Jastrebova, N., Spillmann, D., Gottfridsson, E., et al., 2007. Transgenic or tumor-induced expression of heparanase upregulates sulfation of heparan sulfate. *Nat. Chem. Biol.* 3, 773–778.
- Esko, J.D., Lindahl, U., 2001. Molecular diversity of heparan sulfate. *J. Clin. Invest.* 108, 169–173.
- Esko, J.D., Selleck, S.B., 2002. Order out of chaos: assembly of ligand binding sites in heparan sulfate. *Annu. Rev. Biochem.* 71, 435–471.
- Essner, J.J., Chen, E., Ekker, S.C., 2006. Syndecan-2. *Int. J. Biochem. Cell Biol.* 38, 152–156.
- Eswarakumar, V.P., Lax, I., Schlessinger, J., 2005. Cellular signaling by fibroblast growth factor receptors. *Cytokine Growth Factor Rev.* 16, 139–149.

- Fedarko, N.S., Conrad, H.E., 1986. A unique heparan sulfate in the nuclei of hepatocytes: structural changes with the growth state of the cells. *J. Cell Biol.* 102, 587–599.
- Filmus, J., Selleck, S.B., 2001. Glypicans: proteoglycans with a surprise. *J. Clin. Invest.* 108, 497–501.
- Forsberg, E., Pejler, G., Ringvall, M., Lunderius, C., Tomasini-Johansson, B., Kusche-Gullberg, M., et al., 1999. Abnormal mast cells in mice deficient in a heparin-synthesizing enzyme. *Nature* 400, 773–776.
- Fransson, L.A., Belting, M., Cheng, F., Jonsson, M., Mani, K., Sandgren, S., 2004. Novel aspects of glypican glycobiochemistry. *Cell. Mol. Life Sci.* 61, 1016–1024.
- Frederick, J.P., Tafari, A.T., Wu, S.M., Megosh, L.C., Chiou, S.T., Irving, R.P., et al., 2008. A role for a lithium-inhibited Golgi nucleotidase in skeletal development and sulfation. *Proc. Natl. Acad. Sci. USA* 105, 11605–11612.
- Fuster, M.M., Esko, J.D., 2005. The sweet and sour of cancer: glycans as novel therapeutic targets. *Nat. Rev. Cancer* 5, 526–542.
- Gallagher, J.T., 2001. Heparan sulfate: growth control with a restricted sequence menu. *J. Clin. Invest.* 108, 357–361.
- Gallagher, J.T., 2006. Multiprotein signalling complexes: regional assembly on heparan sulphate. *Biochem. Soc. Trans.* 34, 438–441.
- Garner, O.B., Yamaguchi, Y., Esko, J.D., Videm, V., 2008. Small changes in lymphocyte development and activation in mice through tissue-specific alteration of heparan sulphate. *Immunology* 125, 420–429.
- Gautam, M., Noakes, P.G., Moscoso, L., Rupp, F., Scheller, R.H., Merlie, J.P., et al., 1996. Defective neuromuscular synaptogenesis in agrin-deficient mutant mice. *Cell* 85, 525–535.
- Gautam, M., DeChiara, T.M., Glass, D.J., Yancopoulos, G.D., Sanes, J.R., 1999. Distinct phenotypes of mutant mice lacking agrin, musk, or rapsyn. *Brain Res. Dev. Brain Res.* 114, 171–178.
- Giulian, D., Haverkamp, L.J., Yu, J., Karshin, W., Tom, D., Li, J., et al., 1998. The HHQK domain of beta-amyloid provides a structural basis for the immunopathology of Alzheimer's disease. *J. Biol. Chem.* 273, 29719–29726.
- Gong, F., Jemth, P., Escobar Galvis, M.L., Vlodavsky, I., Horner, A., Lindahl, U., et al., 2003. Processing of macromolecular heparin by heparanase. *J. Biol. Chem.* 278, 35152–35158.
- Goodger, S.J., Robinson, C.J., Murphy, K.J., Gasiunas, N., Harmer, N.J., Blundell, T.L., et al., 2008. Evidence that heparin saccharides promote FGF2 mitogenesis through two distinct mechanisms. *J. Biol. Chem.* 283, 13001–13008.
- Gorsi, B., Stringer, S.E., 2007. Tinkering with heparan sulfate sulfation to steer development. *Trends Cell Biol.* 17, 173–177.
- Gotte, M., Spillmann, D., Yip, G.W., Versteeg, E., Echtermeyer, F.G., van Kuppevelt, T.H., et al., 2008. Changes in heparan sulfate are associated with delayed wound repair, altered cell migration, adhesion and contractility in the galactosyltransferase I (beta4GalT-7) deficient form of Ehlers-Danlos syndrome. *Hum. Mol. Genet.* 17, 996–1009.
- Gotting, C., Kuhn, J., Zahn, R., Brinkmann, T., Kleesiek, K., 2000. Molecular cloning and expression of human UDP-D-xylose: proteoglycan core protein beta-D-xylosyltransferase and its first isoform XT-II. *J. Mol. Biol.* 304, 517–528.
- Grobe, K., Esko, J.D., 2002. Regulated translation of heparan sulfate *N*-acetylglucosamine *N*-deacetylase/*n*-sulfotransferase isozymes by structured 5'-untranslated regions and internal ribosome entry sites. *J. Biol. Chem.* 277, 30699–30706.
- Grobe, K., Ledin, J., Ringvall, M., Holmborn, K., Forsberg, E., Esko, J.D., et al., 2002. Heparan sulfate and development: differential roles of the *N*-acetylglucosamine *N*-deacetylase/*N*-sulfotransferase isozymes. *Biochim. Biophys. Acta* 1573, 209–215.
- Guerrini, M., Raman, R., Venkataraman, G., Torri, G., Sasisekharan, R., Casu, B., 2002. A novel computational approach to integrate NMR spectroscopy and capillary

- electrophoresis for structure assignment of heparin and heparan sulfate oligosaccharides. *Glycobiology* 12, 713–719.
- Guerrini, M., Guglieri, S., Naggi, A., Sasisekharan, R., Torri, G., 2007. Low molecular weight heparins: structural differentiation by bidimensional nuclear magnetic resonance spectroscopy. *Semin. Thromb. Hemost.* 33, 478–487.
- Guerrini, M., Guglieri, S., Casu, B., Torri, G., Mourier, P., Boudier, C., et al., 2008. Antithrombin-binding octasaccharides and role of extensions of the active pentasaccharide sequence in the specificity and strength of interaction: evidence for very high affinity induced by an unusual glucuronic acid residue. *J. Biol. Chem.* 283, 26662–26675.
- Guimond, S.E., Turnbull, J.E., 1999. Fibroblast growth factor receptor signalling is dictated by specific heparan sulphate saccharides. *Curr. Biol.* 9, 1343–1346.
- Guimond, S., Turnbull, J.E., 2004. Proteoglycans make the grade-ient. *Mol. Cell* 16, 159–160.
- Guimond, S., Maccarana, M., Olwin, B.B., Lindahl, U., Rapraeger, A.C., 1993. Activating and inhibitory heparin sequences for FGF-2 (basic FGF). Distinct requirements for FGF-1, FGF-2, and FGF-4. *J. Biol. Chem.* 268, 23906–23914.
- Habuchi, H., Kobayashi, M., Kimata, K., 1998. Molecular characterization and expression of heparan-sulfate 6-O-sulfotransferase. *J. Biol. Chem.* 273, 9208–9213.
- Habuchi, H., Tanaka, M., Habuchi, O., Yoshida, K., Suzuki, H., Ban, K., et al., 2000. The occurrence of three isoforms of heparan sulfate 6-O-sulfotransferase having different specificities for hexuronic acid adjacent to the targeted N-sulfoglucosamine. *J. Biol. Chem.* 275, 2859–2868.
- Habuchi, H., Nagai, N., Sugaya, N., Atsumi, F., Stevens, R.L., Kimata, K., 2007. Mice deficient in heparan sulfate 6-O-sulfotransferase-1 exhibit defective heparan sulfate biosynthesis, abnormal placentation, and late embryonic lethality. *J. Biol. Chem.* 282, 15578–15588.
- Hacker, U., Nybakken, K., Perrimon, N., 2005. Heparan sulphate proteoglycans: the sweet side of development. *Nat. Rev. Mol. Cell Biol.* 6, 530–541.
- Hagner-McWhirter, A., Li, J.P., Oscarson, S., Lindahl, U., 2004. Irreversible glucuronyl C5-epimerization in the biosynthesis of heparan sulfate. *J. Biol. Chem.* 279, 14631–14638.
- HajMohammadi, S., Enjyoji, K., Princivale, M., Christi, P., Lech, M., Beeler, D., et al., 2003. Normal levels of anticoagulant heparan sulfate are not essential for normal hemostasis. *J. Clin. Invest.* 111, 989–999.
- Haltiwanger, R.S., Lowe, J.B., 2004. Role of glycosylation in development. *Annu. Rev. Biochem.* 73, 491–537.
- Han, C., Belenkaya, T.Y., Khodoun, M., Tauchi, M., Lin, X., 2004. Distinct and collaborative roles of *Drosophila* EXT family proteins in morphogen signalling and gradient formation. *Development* 131, 1563–1575.
- Handler, M., Yurchenco, P.D., Iozzo, R.V., 1997. Developmental expression of perlecan during murine embryogenesis. *Dev. Dyn.* 210, 130–145.
- Harmer, N.J., Ilag, L.L., Mulloy, B., Pellegrini, L., Robinson, C.V., Blundell, T.L., 2004. Towards a resolution of the stoichiometry of the fibroblast growth factor (FGF)-FGF receptor-heparin complex. *J. Mol. Biol.* 339, 821–834.
- Hassell, J.R., Robey, P.G.R., Barrach, H.J., Wilczek, J., Rennard, S.I., Martin, G.R., 1980. Isolation of a heparan sulfate-containing proteoglycan from basement membrane. *Proc. Natl. Acad. Sci. USA* 77, 4494–4498.
- Hayashida, K., Stahl, P.D., Park, P.W., 2008. Syndecan-1 ectodomain shedding is regulated by the small gtpase Rab5. *J. Biol. Chem.* 283, 35435–35444.
- Helting, T., Lindahl, U., 1971. Occurrence and biosynthesis of beta-glucuronidic linkages in heparin. *J. Biol. Chem.* 246, 5442–5447.
- Hirschberg, C.B., Robbins, P.W., Abejón, C., 1998. Transporters of nucleotide sugars, ATP, and nucleotide sulfate in the endoplasmic reticulum and Golgi apparatus. *Annu. Rev. Biochem.* 67, 49–69.

- Hoch, W., Campanelli, J.T., Harrison, S., Scheller, R.H., 1994. Structural domains of agrin required for clustering of nicotinic acetylcholine receptors. *EMBO J.* 13, 2814–2821.
- Holmborn, K., Ledin, J., Smeds, E., Eriksson, I., Kusche-Gullberg, M., Kjellen, L., 2004. Heparan sulfate synthesized by mouse embryonic stem cells deficient in NDST1 and NDST2 is 6-O-sulfated but contains no N-sulfate groups. *J. Biol. Chem.* 279, 42355–42358.
- Höök, M., Lindahl, U., Backstrom, G., Malmstrom, A., Fransson, L.-Å., 1974. Biosynthesis of heparin. Formation of iduronic acid residues. *J. Biol. Chem.* 249, 3908–3915.
- Höök, M., Lindahl, U., Hallén, A., Bäckström, G., 1975. Biosynthesis of heparin. Studies on the microsomal sulfation process. *J. Biol. Chem.* 250, 6065–6071.
- Hull, R.L., Westermarck, G.T., Westermarck, P., Kahn, S.E., 2004. Islet amyloid: a critical entity in the pathogenesis of type 2 diabetes. *J. Clin. Endocrinol. Metab.* 89, 3629–3643.
- Hull, R.L., Zraika, S., Udayasankar, J., Kisilevsky, R., Szarek, W.A., Wight, T.N., et al., 2007. Inhibition of glycosaminoglycan synthesis and protein glycosylation with WAS-406 and azaserine result in reduced islet amyloid formation *in vitro*. *Am. J. Physiol. Cell Physiol.* 293, C1586–C1593.
- Imberty, A., Lortat-Jacob, H., Perez, S., 2007. Structural view of glycosaminoglycan-protein interactions. *Carbohydr. Res.* 342, 430–439.
- Inatani, M., Irie, F., Plump, A., Tessier-Lavigne, M., Yamagata, Y., 2003. Mammalian brain morphogenesis and midline axon guidance require heparan sulfate. *Science* 302, 1044–1046.
- Inoue, S., Kuroiwa, M., Saraiva, M.J., Guimaraes, A., Kisilevsky, R., 1998. Ultrastructure of familial amyloid polyneuropathy amyloid fibrils: examination with high-resolution electron microscopy. *J. Struct. Biol.* 124, 1–12.
- Iozzo, R.V., 2005. Basement membrane proteoglycans: from cellar to ceiling. *Nat. Rev. Mol. Cell Biol.* 6, 646–656.
- Ivins, J.K., Litwack, E.D., Kumbasar, A., Stipp, C.S., Lander, A.D., 1997. Cerebroglycan, a developmentally regulated cell-surface heparan sulfate proteoglycan, is expressed on developing axons and growth cones. *Dev. Biol.* 184, 320–332.
- Jacobson, I., Bäckström, G., Höök, M., Lindahl, U., Feingold, D.S., Malmström, A., Rodén, L., 1979. Biosynthesis of heparin. Assay and properties of the microsomal uronosyl C-5 epimerase. *J. Biol. Chem.* 254, 2975–2982.
- Jacobson, I., Lindahl, U., 1980. Biosynthesis of heparin. Concerted action of late polymer-modification reactions. *J. Biol. Chem.* 255, 5094–5100.
- Jacobson, I., Lindahl, U., Jensen, J.W., Rodén, L., Prihar, H., Feingold, D.S., 1984. Biosynthesis of heparin. Substrate specificity of heparosan N-sulfate D-glucuronosyl 5-epimerase. *J. Biol. Chem.* 259, 1056–1063.
- Jairajpuri, M.A., Lu, A., Desai, U., Olson, S.T., Bjork, I., Bock, S.C., 2003. Antithrombin III phenylalanines 122 and 121 contribute to its high affinity for heparin and its conformational activation. *J. Biol. Chem.* 278, 15941–15950.
- Jakobsson, L., Kreuger, J., Holmborn, K., Lundin, L., Eriksson, I., Kjellen, L., et al., 2006. Heparan sulfate in trans potentiates VEGFR-mediated angiogenesis. *Dev. Cell* 10, 625–634.
- Jastrebova, N., Vanwildemeersch, M., Rapraeger, A.C., Gimenez-Gallego, G., Lindahl, U., Spillmann, D., 2006. Heparan sulfate-related oligosaccharides in ternary complex formation with fibroblast growth factors 1 and 2 and their receptors. *J. Biol. Chem.* 281, 26884–26892.
- Jemth, P., Kreuger, J., Kusche-Gullberg, M., Sturiale, L., Gimenez-Gallego, G., Lindahl, U., 2002. Biosynthetic oligosaccharide libraries for identification of protein-binding heparan sulfate motifs. Exploring the structural diversity by screening for fibroblast growth factor (FGF)1 and FGF2 binding. *J. Biol. Chem.* 277, 30567–30573.
- Jemth, P., Smeds, E., Do, A.T., Habuchi, H., Kimata, K., Lindahl, U., et al., 2003. Oligosaccharide library-based assessment of heparan sulfate 6-O-sulfotransferase substrate specificity. *J. Biol. Chem.* 278, 24371–24376.

- Jia, J., Maccarana, M., Zhang, X., Bespalov, M., Lindahl, U., Li, J.-P., 2009. Lack of L-iduronic acid in heparan sulfate affects interaction with growth factors and cell signaling. *J. Biol. Chem.* E-PUB.
- Jin, L., Abrahams, J.P., Skinner, R., Petitou, M., Pike, R.N., Carrell, R.W., 1997. The anticoagulant activation of antithrombin by heparin. *Proc. Natl. Acad. Sci. USA* 94, 14683–14688.
- Jorpes, J.E., Gardell, S., 1948. On heparin monosulfuric acid. *J. Biol. Chem.* 176, 267–275.
- Kamimura, K., Rhodes, J.M., Ueda, R., McNeely, M., Shukla, D., Kimata, K., et al., 2004. Regulation of Notch signaling by *Drosophila* heparan sulfate 3-*O* sulfotransferase. *J. Cell Biol.* 166, 1069–1079.
- Kim, B.T., Kitagawa, H., Tamura, J., Saito, T., Kusche-Gullberg, M., Lindahl, U., et al., 2001. Human tumor suppressor EXT gene family members EXTL1 and EXTL3 encode alpha 1,4-*N*-acetylglucosaminyltransferases that likely are involved in heparan sulfate/heparin biosynthesis. *Proc. Natl. Acad. Sci. USA* 98, 7176–7181.
- Kim, B.T., Kitagawa, H., Tamura, J., Kusche-Gullberg, M., Lindahl, U., Sugahara, K., 2002. Demonstration of a novel gene DEXT3 of *Drosophila melanogaster* as the essential *N*-acetylglucosamine transferase in the heparan sulfate biosynthesis: chain initiation and elongation. *J. Biol. Chem.* 277, 13659–13665.
- Kim, B.T., Kitagawa, H., Tanaka, J., Tamura, J., Sugahara, K., 2003. *In vitro* heparan sulfate polymerization: crucial roles of core protein moieties of primer substrates in addition to the EXT1-EXT2 interaction. *J. Biol. Chem.* 278, 41618–41623.
- Kirkpatrick, C.A., Selleck, S.B., 2007. Heparan sulfate proteoglycans at a glance. *J. Cell Sci.* 120, 1829–1832.
- Kirkpatrick, C.A., Knox, S.M., Staatz, W.D., Fox, B., Lercher, D.M., Selleck, S.B., 2006. The function of a *Drosophila* glypican does not depend entirely on heparan sulfate modification. *Dev. Biol.* 300, 570–582.
- Kisilevsky, R., 2000. Review: amyloidogenesis—unquestioned answers and unanswered questions. *J. Struct. Biol.* 130, 99–108.
- Kisilevsky, R., Fraser, P., 1996. Proteoglycans and amyloid fibrillogenesis. *Ciba Found. Symp.* 199, 58–67; discussion 68–72, 90–103.
- Kisilevsky, R., Lemieux, L.J., Fraser, P.E., Kong, X., Hultin, P.G., Szarek, W.A., 1995. Arresting amyloidosis *in vivo* using small-molecule anionic sulphonates or sulphates: implications for Alzheimer's disease. *Nat. Med.* 1, 143–148.
- Kitagawa, H., Tone, Y., Tamura, J., Neumann, K.W., Ogawa, T., Oka, S., et al., 1998. Molecular cloning and expression of glucuronyltransferase I involved in the biosynthesis of the glycosaminoglycan-protein linkage region of proteoglycans. *J. Biol. Chem.* 273, 6615–6618.
- Kitagawa, H., Shimakawa, H., Sugahara, K., 1999. The tumor suppressor EXT-like gene EXTL2 encodes an alpha 1,4-*N*-acetylhexosaminyltransferase that transfers *N*-acetylgalactosamine and *N*-acetylglucosamine to the common glycosaminoglycan-protein linkage region. The key enzyme for the chain initiation of heparan sulfate. *J. Biol. Chem.* 274, 13933–13937.
- Kjellén, L., Lindahl, U., 1991. Proteoglycans: structures and interactions. *Annu. Rev. Biochem.* 60, 443–475.
- Knappe, M., Bodevin, S., Selinka, H.C., Spillmann, D., Streeck, R.E., Chen, X.S., et al., 2007. Surface-exposed amino acid residues of HPV16 L1 protein mediating interaction with cell surface heparan sulfate. *J. Biol. Chem.* 282, 27913–27922.
- Knox, S.M., Whitelock, J.M., 2006. Perlecan: how does one molecule do so many things? *Cell. Mol. Life Sci.* 63, 2435–2445.
- Kobayashi, M., Habuchi, H., Habuchi, O., Saito, M., Kimata, K., 1996. Purification and characterization of heparan sulfate 2-sulfotransferase from cultured Chinese hamster ovary cells. *J. Biol. Chem.* 271, 7645–7653.

- Kobayashi, M., Habuchi, H., Yoneda, M., Habuchi, O., Kimata, K., 1997. Molecular cloning and expression of Chinese hamster ovary cell heparan-sulfate 2-sulfotransferase. *J. Biol. Chem.* 272, 13980–13985.
- Korir, A.K., Larive, C.K., 2009. Advances in the separation, sensitive detection, and characterization of heparin and heparan sulfate. *Anal. Bioanal. Chem.* 393, 155–169.
- Koziel, L., Kunath, M., Kelly, O.G., Vortkamp, A., 2004. Ext1-dependent heparan sulfate regulates the range of Ihh signaling during endochondral ossification. *Dev. Cell* 6, 801–813.
- Kramer, K.L., Yost, H.J., 2002. Ectodermal syndecan-2 mediates left-right axis formation in migrating mesoderm as a cell-nonautonomous Vg1 cofactor. *Dev. Cell* 2, 115–124.
- Kramer, K.L., Yost, H.J., 2003. Heparan sulfate core proteins in cell-cell signaling. *Annu. Rev. Genet.* 37, 461–484.
- Kreuger, J., Matsumoto, T., Vanwildemeersch, M., Sasaki, T., Timpl, R., Claesson-Welsh, L., et al., 2002. Role of heparan sulfate domain organization in endostatin inhibition of endothelial cell function. *EMBO J.* 21, 6303–6311.
- Kreuger, J., Jemth, P., Sanders-Lindberg, E., Eliahu, L., Ron, D., Basilico, C., et al., 2005. Fibroblast growth factors share binding sites in heparan sulphate. *Biochem. J.* 389, 145–150.
- Kreuger, J., Spillmann, D., Li, J.P., Lindahl, U., 2006. Interactions between heparan sulfate and proteins: the concept of specificity. *J. Cell Biol.* 174, 323–327.
- Kroger, S., Schroder, J.E., 2002. Agrin in the developing CNS: new roles for a synapse organizer. *News Physiol. Sci.* 17, 207–212.
- Kuberan, B., Lech, M., Borjigin, J., Rosenberg, R.D., 2004. Light-induced 3-O-sulfotransferase expression alters pineal heparan sulfate fine structure. A surprising link to circadian rhythm. *J. Biol. Chem.* 279, 5053–5054.
- Kurup, S., Wijnhoven, T.J., Jenniskens, G.J., Kimata, K., Habuchi, H., Li, J.P., et al., 2007. Characterization of anti-heparan sulfate phage display antibodies AO4B08 and HS4E4. *J. Biol. Chem.* 282, 21032–21042.
- Kusche, M., Bäckström, G., Riesenfeld, J., Petitou, M., Choay, J., Lindahl, U., 1988. Biosynthesis of heparin. O-Sulfation of the antithrombin-binding region. *J. Biol. Chem.* 263, 15474–15484.
- Kusche-Gullberg, M., Eriksson, I., Sandbäck Pikas, D., Kjellén, L., 1998. Identification and expression in mouse of two heparan sulfate glucosaminyl N-deacetylase/N-sulfotransferase genes. *J. Biol. Chem.* 273, 119027–119029.
- Laguri, C., Sadir, R., Rueda, P., Baleux, F., Gans, P., Arenzana-Seisdedos, F., et al., 2007. The novel CXCL12 γ isoform encodes an unstructured cationic domain which regulates bioactivity and interaction with both glycosaminoglycans and CXCR4. *PLoS ONE* 2, e1110.
- Lamanna, W.C., Kalus, I., Padva, M., Baldwin, R.J., Merry, C.L., Dierks, T., 2007. The heparanome—the enigma of encoding and decoding heparan sulfate sulfation. *J. Biotechnol.* 129, 290–307.
- Lamanna, W.C., Frese, M.A., Balleininger, M., Dierks, T., 2008. Sulf loss influences N-, 2O-, and 6O-sulfation of multiple heparan sulfate proteoglycans and modulates FGF signaling. *J. Biol. Chem.* 283, 27724–27735.
- Lander, A.D., Nie, Q., Wan, F.Y., 2002. Do morphogen gradients arise by diffusion? *Dev. Cell* 2, 785–796.
- Langford, J.K., Yang, Y., Kieber-Emmons, T., Sanderson, R.D., 2005. Identification of an invasion regulatory domain within the core protein of syndecan-1. *J. Biol. Chem.* 280, 3467–3473.
- Langsdorf, A., Do, A.T., Kusche-Gullberg, M., Emerson, Jr., C.P., Ai, X., 2007. Sulf α s are regulators of growth factor signaling for satellite cell differentiation and muscle regeneration. *Dev. Biol.* 311, 464–477.
- Ledin, J., Staatz, W., Li, J.P., Gotte, M., Selleck, S., Kjellen, L., et al., 2004. Heparan sulfate structure in mice with genetically modified heparan sulfate production. *J. Biol. Chem.* 279, 42732–42741.

- Ledin, J., Ringvall, M., Thuveson, M., Eriksson, I., Wilen, M., Kusche-Gullberg, M., et al., 2006. Enzymatically active *N*-deacetylase/*N*-sulfotransferase-2 is present in liver but does not contribute to heparan sulfate *N*-sulfation. *J. Biol. Chem.* 281, 35727–35734.
- Lewis, E.J., Xu, X., 2008. Abnormal glomerular permeability characteristics in diabetic nephropathy: implications for the therapeutic use of low-molecular weight heparin. *Diabetes Care* 31 (Suppl. 2), S202–S207.
- Li, J.-P., Hagner-McWhirter, Å, Kjellén, L., Palgi, J., Jalkanen, M., Lindahl, U., 1997. Biosynthesis of heparin/heparan sulfate. cDNA cloning and expression of D-glucuronyl C5-epimerase from bovine lung. *J. Biol. Chem.* 272, 28158–28163.
- Li, J.P., Gong, F., Hagner-McWhirter, A., Forsberg, E., Abrink, M., Kisilevsky, R., et al., 2003. Targeted disruption of a murine glucuronyl C5-epimerase gene results in heparan sulfate lacking L-iduronic acid and in neonatal lethality. *J. Biol. Chem.* 278, 28363–28366.
- Li, W., Johnson, D.J., Esmon, C.T., Huntington, J.A., 2004. Structure of the antithrombin-thrombin-heparin ternary complex reveals the antithrombotic mechanism of heparin. *Nat. Struct. Mol. Biol.* 11, 857–862.
- Li, J.P., Galvis, M.L., Gong, F., Zhang, X., Zcharia, E., Metzger, S., et al., 2005. *In vivo* fragmentation of heparan sulfate by heparanase overexpression renders mice resistant to amyloid protein A amyloidosis. *Proc. Natl. Acad. Sci. USA* 102, 6473–6477.
- Lidholt, K., Lindahl, U., 1992. Biosynthesis of heparin. The D-glucuronosyl- and *N*-acetyl-D-glucosaminyltransferase reactions and their relation to polymer modification. *Biochem. J.* 287, 21–29.
- Lin, X., Wei, G., Shi, Z., Dryer, L., Esko, J.D., Wells, D.E., et al., 2000. Disruption of gastrulation and heparan sulfate biosynthesis in EXT1-deficient mice. *Dev. Biol.* 224, 299–311.
- Lind, T., Lindahl, U., Lidholt, K., 1993. Biosynthesis of heparin/heparan sulfate. Identification of a 70-kDa protein catalyzing both the D-glucuronosyl- and the *N*-acetyl-D-glucosaminyltransferase reactions. *J. Biol. Chem.* 268, 20705–20708.
- Lind, T., Tufaro, F., McCormick, C., Lindahl, U., Lidholt, K., 1998. The putative tumor suppressors EXT1 and EXT2 are glycosyltransferases required for the biosynthesis of heparan sulfate. *J. Biol. Chem.* 273, 26265–26268.
- Lindahl, U., Bäckström, G., Jansson, L., Hallén, A., 1973. Biosynthesis of heparin. Formation of sulfamino groups. *J. Biol. Chem.* 248, 7234–7241.
- Lindahl, B., Lindahl, U., 1997. Amyloid-specific heparan sulfate from human liver and spleen. *J. Biol. Chem.* 272, 26091–26094.
- Lindahl, U., Lidholt, K., Spillmann, D., Kjellén, L., 1994. More to “heparin” than anticoagulation. *Thromb. Res.* 75, 1–32.
- Lindahl, B., Eriksson, L., Lindahl, U., 1995. Structure of heparan sulphate from human brain, with special regard to Alzheimer’s disease. *Biochem. J.* 306, 177–184.
- Lindahl, U., Kusche-Gullberg, M., Kjellen, L., 1998. Regulated diversity of heparan sulfate. *J. Biol. Chem.* 273, 24979–24982.
- Lindahl, B., Westling, C., Gimenez-Gallego, G., Lindahl, U., Salmivirta, M., 1999. Common binding sites for beta-amyloid fibrils and fibroblast growth factor-2 in heparan sulfate from human cerebral cortex. *J. Biol. Chem.* 274, 30631–30635.
- Lindblom, P., Gerhardt, H., Liebner, S., Abramsson, A., Enge, M., Hellstrom, M., et al., 2003. Endothelial PDGF-B retention is required for proper investment of pericytes in the microvessel wall. *Genes Dev.* 17, 1835–1840.
- Litwack, E.D., Ivins, J.K., Kumbasar, A., Paine-Saunders, S., Stipp, C.S., Lander, A.D., 1998. Expression of the heparan sulfate proteoglycan glypican-1 in the developing rodent. *Dev. Dyn.* 211, 72–87.
- Liu, J., Shworak, N.W., Sinay, P., Schwartz, J.J., Zhang, L., Fritze, L.M., et al., 1999. Expression of heparan sulfate D-glucosaminyl 3-O-sulfotransferase isoforms reveals novel substrate specificities. *J. Biol. Chem.* 274, 5185–5192.

- Lortat-Jacob, H., Turnbull, J.E., Grimaud, J.A., 1995. Molecular organization of the interferon γ -binding domain in heparan sulphate. *Biochem. J.* 310, 497–505.
- Lugemwa, F.N., Esko, J.D., 1991. Estradiol beta-D-xyloside, an efficient primer for heparan sulfate biosynthesis. *J. Biol. Chem.* 266, 6674–6677.
- Luo, Y., Ye, S., Kan, M., McKeehan, W.L., 2006. Control of fibroblast growth factor (FGF) 7- and FGF1-induced mitogenesis and downstream signaling by distinct heparin octasaccharide motifs. *J. Biol. Chem.* 281, 21052–21061.
- MacArthur, J.M., Bishop, J.R., Stanford, K.I., Wang, L., Bensadoun, A., Witztum, J.L., et al., 2007. Liver heparan sulfate proteoglycans mediate clearance of triglyceride-rich lipoproteins independently of LDL receptor family members. *J. Clin. Invest.* 117, 153–164.
- Maccarana, M., Sakura, Y., Tawada, A., Yoshida, K., Lindahl, U., 1996. Domain structure of heparan sulfates from bovine organs. *J. Biol. Chem.* 271, 17804–17810.
- Mahalingam, Y., Gallagher, J.T., Couchman, J.R., 2007. Cellular adhesion responses to the heparin-binding (hepi) domain of fibronectin require heparan sulfate with specific properties. *J. Biol. Chem.* 282, 3221–3230.
- Mahley, R.W., Ji, Z.S., 1999. Remnant lipoprotein metabolism: key pathways involving cell-surface heparan sulfate proteoglycans and apolipoprotein E. *J. Lipid Res.* 40, 1–16.
- Marcum, J.A., Fritze, L., Galli, S.J., Karp, G., Rosenberg, R.D., 1983. Microvascular heparinlike species with anticoagulant activity. *Am. J. Physiol.* 245, H725–H733.
- Matsumoto, Y., Irie, F., Inatani, M., Tessier-Lavigne, M., Yamaguchi, Y., 2007. Netrin-1/DCC signaling in commissural axon guidance requires cell-autonomous expression of heparan sulfate. *J. Neurosci.* 27, 4342–4350.
- McCormick, C., Duncan, G., Goutsos, K.T., Tufaro, F., 2000. The putative tumor suppressors EXT1 and EXT2 form a stable complex that accumulates in the Golgi apparatus and catalyzes the synthesis of heparan sulfate. *Proc. Natl. Acad. Sci. USA* 97, 668–673.
- Medeiros, G.F., Mendes, A., Castro, R.A., Bau, E.C., Nader, H.B., Dietrich, C.P., 2000. Distribution of sulfated glycosaminoglycans in the animal kingdom: widespread occurrence of heparin-like compounds in invertebrates. *Biochim. Biophys. Acta* 1475, 287–294.
- Merry, C.L., Bullock, S.L., Swan, D.C., Backen, A.C., Lyon, M., Beddington, R.S., et al., 2001. The molecular phenotype of heparan sulfate in the *Hs2st*^{-/-} mutant mouse. *J. Biol. Chem.* 276, 35429–35434.
- Mochizuki, H., Yoshida, K., Shibata, Y., Kimata, K., 2008. Tetrasulfated disaccharide unit in heparan sulfate: enzymatic formation and tissue distribution. *J. Biol. Chem.* 283, 31237–31245.
- Mohammadi, M., Olsen, S.K., Ibrahimi, O.A., 2005. Structural basis for fibroblast growth factor receptor activation. *Cytokine Growth Factor Rev.* 16, 107–137.
- Mongiat, M., Taylor, K., Otto, J., Aho, S., Uitto, J., Whitelock, J.M., et al., 2000. The protein core of the proteoglycan perlecan binds specifically to fibroblast growth factor-7. *J. Biol. Chem.* 275, 7095–7100.
- Morimoto-Tomita, M., Uchimura, K., Bistrup, A., Lum, D.H., Egeblad, M., Boudreau, N., et al., 2005. Sulf-2, a proangiogenic heparan sulfate endosulfatase, is upregulated in breast cancer. *Neoplasia* 7, 1001–1010.
- Mulloy, B., Forster, M.J., 2000. Conformation and dynamics of heparin and heparan sulfate. *Glycobiology* 10, 1147–1156.
- Nackaerts, K., Verbeken, E., Deneffe, G., Vanderschueren, B., Demedts, M., David, G., 1997. Heparan sulfate proteoglycan expression in human lung-cancer cells. *Int. J. Cancer* 74, 335–345.
- Navia, J.L., Riesenfeld, J., Vann, W.F., Lindahl, U., Rodén, L., 1983. Assay of N-acetylheparosan deacetylase with a capsular polysaccharide from *Escherichia coli* K5 as substrate. *Anal. Biochem.* 135, 134–140.

- Nikitovic, D., Assouti, M., Sifaki, M., Katonis, P., Krasagakis, K., Karamanos, N.K., et al., 2008. Chondroitin sulfate and heparan sulfate-containing proteoglycans are both partners and targets of basic fibroblast growth factor-mediated proliferation in human metastatic melanoma cell lines. *Int. J. Biochem. Cell Biol.* 40, 72–83.
- Norgard-Sumnicht, K., Varki, A., 1995. Endothelial heparan sulfate proteoglycans that bind to L-selectin have glucosamine residues with unsubstituted amino groups. *J. Biol. Chem.* 270, 12012–12024.
- Noti, C., de Paz, J.L., Polito, L., Seeberger, P.H., 2006. Preparation and use of microarrays containing synthetic heparin oligosaccharides for the rapid analysis of heparin–protein interactions. *Chemistry* 12, 8664–8686.
- Obunike, J.C., Lutz, E.P., Li, Z., Paka, L., Katopodis, T., Strickland, D.K., et al., 2001. Transcytosis of lipoprotein lipase across cultured endothelial cells requires both heparan sulfate proteoglycans and the very low density lipoprotein receptor. *J. Biol. Chem.* 276, 8934–8941.
- O’Callaghan, P., Sandwall, E., Li, J.P., Yu, H., Ravid, R., Guan, Z.Z., et al., 2008. Heparan sulfate accumulation with Abeta deposits in Alzheimer’s disease and Tg2576 mice is contributed by glial cells. *Brain Pathol.* 18, 548–561.
- Ögren, S., Lindahl, U., 1975. Cleavage of macromolecular heparin by an enzyme from mouse mastocytoma. *J. Biol. Chem.* 250, 2690–2697.
- Oh, E.S., Couchman, J.R., 2004. Syndecans-2 and -4; close cousins, but not identical twins. *Mol. Cells* 17, 181–187.
- Ohkawara, B., Iemura, S., ten Dijke, P., Ueno, N., 2002. Action range of BMP is defined by its N-terminal basic amino acid core. *Curr. Biol.* 12, 205–209.
- Ohkawara, B., Yamamoto, T.S., Tada, M., Ueno, N., 2003. Role of glypican 4 in the regulation of convergent extension movements during gastrulation in *Xenopus laevis*. *Development* 130, 2129–2138.
- Pallerla, S.R., Lawrence, R., Lewejohann, L., Pan, Y., Fischer, T., Schlomann, U., et al., 2008. Altered heparan sulfate structure in mice with deleted NDST3 gene function. *J. Biol. Chem.* 283, 16885–16894.
- Pan, Y., Carbe, C., Powers, A., Zhang, E.E., Esko, J.D., Grobe, K., et al., 2008. Bud specific N-sulfation of heparan sulfate regulates Shp2-dependent FGF signaling during lacrimal gland induction. *Development* 135, 301–310.
- Parish, C.R., 2006. The role of heparan sulphate in inflammation. *Nat. Rev. Immunol.* 6, 633–643.
- Parish, C.R., Freeman, C., Hulett, M.D., 2001. Heparanase: a key enzyme involved in cell invasion. *Biochim. Biophys. Acta* 1471, M99–M108.
- Patel, V.N., Likar, K.M., Zisman-Rozen, S., Cowherd, S.N., Lassiter, K.S., Sher, I., et al., 2008. Specific heparan sulfate structures modulate FGF10-mediated submandibular gland epithelial morphogenesis and differentiation. *J. Biol. Chem.* 283, 9308–9317.
- Patey, S.J., Edwards, E.A., Yates, E.A., Turnbull, J.E., 2008. Engineered heparins: novel beta-secretase inhibitors as potential Alzheimer’s disease therapeutics. *Neurodegener. Dis.* 5, 197–199.
- Pejler, G., Danielsson, Å., Björk, I., Lindahl, U., Nader, H.B., Dietrich, C.P., 1987. Structure and antithrombin-binding properties of heparin isolated from the clams *Anomalocardia brasiliensis* and *Tivela mactroides*. *J. Biol. Chem.* 262, 11413–11421.
- Pellegrini, L., Burke, D.F., von Delft, F., Mulloy, B., Blundell, T.L., 2000. Crystal structure of fibroblast growth factor receptor ectodomain bound to ligand and heparin. *Nature* 407, 1029–1034.
- Petitou, M., van Boeckel, C.A., 2004. A synthetic antithrombin III binding pentasaccharide is now a drug! What comes next? *Angew. Chem. Int. Ed. Engl.* 43, 3118–3133.
- Petitou, M., Lormeau, J.C., Choay, J., 1988. Interaction of heparin and antithrombin III. The role of O-sulfate groups. *Eur. J. Biochem.* 176, 637–640.

- Petitou, M., Casu, B., Lindahl, U., 2003. 1976–1983, a critical period in the history of heparin: the discovery of the antithrombin binding site. *Biochimie* 85, 83–89.
- Pinhal, M.A., Smith, B., Olson, S., Aikawa, J., Kimata, K., Esko, J.D., 2001. Enzyme interactions in heparan sulfate biosynthesis: uronosyl 5-epimerase and 2-O-sulfotransferase interact *in vivo*. *Proc. Natl. Acad. Sci. USA* 98, 12984–12989.
- Ponighaus, C., Ambrosius, M., Casanova, J.C., Prante, C., Kuhn, J., Esko, J.D., et al., 2007. Human xylosyltransferase II is involved in the biosynthesis of the uniform tetrasaccharide linkage region in chondroitin sulfate and heparan sulfate proteoglycans. *J. Biol. Chem.* 282, 5201–5206.
- Powell, A.K., Yates, E.A., Fernig, D.G., Turnbull, J.E., 2004. Interactions of heparin/heparan sulfate with proteins: appraisal of structural factors and experimental approaches. *Glycobiology* 14, 17R–30R.
- Presto, J., Thuveson, M., Carlsson, P., Busse, M., Wilen, M., Eriksson, I., et al., 2008. Heparan sulfate biosynthesis enzymes EXT1 and EXT2 affect NDST1 expression and heparan sulfate sulfation. *Proc. Natl. Acad. Sci. USA* 105, 4751–4756.
- Proudfoot, A.E., 2006. The biological relevance of chemokine-proteoglycan interactions. *Biochem. Soc. Trans.* 34, 422–426.
- Proudfoot, A.E., Handel, T.M., Johnson, Z., Lau, E.K., LiWang, P., Clark-Lewis, I., et al., 2003. Glycosaminoglycan binding and oligomerization are essential for the *in vivo* activity of certain chemokines. *Proc. Natl. Acad. Sci. USA* 100, 1885–1890.
- Rapraeger, A.C., 2001. Molecular interactions of syndecans during development. *Semin. Cell Dev. Biol.* 12, 107–116.
- Rapraeger, A.C., Krufka, A., Olwin, B.B., 1991. Requirement of heparan sulfate for bfgf-mediated fibroblast growth and myoblast differentiation. *Science* 252, 1705–1708.
- Reizes, O., Lincecum, J., Wang, Z., Goldberger, O., Huang, L., Kaksonen, M., et al., 2001. Transgenic expression of syndecan-1 uncovers a physiological control of feeding behavior by syndecan-3. *Cell* 106, 105–116.
- Reizes, O., Clegg, D.J., Strader, A.D., Benoit, S.C., 2006. A role for syndecan-3 in the melanocortin regulation of energy balance. *Peptides* 27, 274–280.
- Reizes, O., Benoit, S.C., Clegg, D.J., 2008. The role of syndecans in the regulation of body weight and synaptic plasticity. *Int. J. Biochem. Cell Biol.* 40, 28–45.
- Relini, A., De Stefano, S., Torrassa, S., Cavalleri, O., Rolandi, R., Gliozzi, A., et al., 2008. Heparin strongly enhances the formation of beta2-microglobulin amyloid fibrils in the presence of type I collagen. *J. Biol. Chem.* 283, 4912–4920.
- Riesenfeld, J., Höök, M., Lindahl, U., 1982. Biosynthesis of heparan sulfate in rat liver. Characterization of polysaccharides obtained with intact cells and with a cell-free system. *J. Biol. Chem.* 257, 7050–7055.
- Ringvall, M., Ledin, J., Holmborn, K., van Kuppevelt, T., Ellin, F., Eriksson, I., et al., 2000. Defective heparan sulfate biosynthesis and neonatal lethality in mice lacking N-deacetylase/N-sulfotransferase-1. *J. Biol. Chem.* 275, 25926–25930.
- Robinson, J., Viti, M., Hook, M., 1984. Structure and properties of an under-sulfated heparan sulfate proteoglycan synthesized by a rat hepatoma cell line. *J. Cell Biol.* 98, 946–953.
- Robinson, C.J., Mulloy, B., Gallagher, J.T., Stringer, S.E., 2006. VEGF165-binding sites within heparan sulfate encompass two highly sulfated domains and can be liberated by K5 lyase. *J. Biol. Chem.* 281, 1731–1740.
- Rodriguez-Manzaneque, J.C., Carpizo, D., Plaza-Calonge, M.D., Torres-Collado, A.X., Thai, S.N., Simons, M., et al., 2009. Cleavage of syndecan-4 by ADAMTS1 provokes defects in adhesion. *Int. J. Biochem. Cell Biol.* 41, 800–810.
- Rong, J., Habuchi, H., Kimata, K., Lindahl, U., Kusche-Gullberg, M., 2001. Substrate specificity of the heparan sulfate hexuronic acid 2-O-sulfotransferase. *Biochemistry* 40, 5548–5555.

- Rosenberg, R.D., Shworak, N.W., Liu, J., Schwartz, J.J., Zhang, L., 1997. Heparan sulfate proteoglycans of the cardiovascular system. Specific structures emerge but how is synthesis regulated? *J. Clin. Invest.* 100, S67–S75.
- Rossi, M., Morita, H., Sormunen, R., Airenne, S., Kreivi, M., Wang, L., et al., 2003. Heparan sulfate chains of perlecan are indispensable in the lens capsule but not in the kidney. *EMBO J.* 22, 236–245.
- Rudd, T.R., Guimond, S.E., Skidmore, M.A., Duchesne, L., Guerrini, M., Torri, G., et al., 2007. Influence of substitution pattern and cation binding on conformation and activity in heparin derivatives. *Glycobiology* 17, 983–993.
- Ruhrberg, C., Gerhardt, H., Golding, M., Watson, R., Ioannidou, S., Fujisawa, H., et al., 2002. Spatially restricted patterning cues provided by heparin-binding VEGF-A control blood vessel branching morphogenesis. *Genes Dev.* 16, 2684–2698.
- Rupp, F., Payan, D.G., Magill-Solc, C., Cowan, D.M., Scheller, R.H., 1991. Structure and expression of a rat agrin. *Neuron* 6, 811–823.
- Safaiyan, F., Kolset, S.O., Prydz, K., Gottfridsson, E., Lindahl, U., Salmivirta, M., 1999. Selective effects of sodium chlorate treatment on the sulfation of heparan sulfate. *J. Biol. Chem.* 274, 36267–36273.
- Salmivirta, M., Lidholt, K., Lindahl, U., 1996. Heparan sulfate—a piece of information. *FASEB J.* 10, 1270–1279.
- Sanderson, R.D., Yang, Y., Kelly, T., MacLeod, V., Dai, Y., Theus, A., 2005. Enzymatic remodeling of heparan sulfate proteoglycans within the tumor microenvironment: growth regulation and the prospect of new cancer therapies. *J. Cell Biochem.* 96, 897–905.
- Schlessinger, J., Plotnikov, A.N., Ibrahim, O.A., Eliseenkova, A.V., Yeh, B.K., Yayon, A., et al., 2000. Crystal structure of a ternary FGF–FGFR–heparin complex reveals a dual role for heparin in FGFR binding and dimerization. *Mol. Cell* 6, 743–750.
- Scholefield, Z., Yates, E.A., Wayne, G., Amour, A., McDowell, W., Turnbull, J.E., 2003. Heparan sulfate regulates amyloid precursor protein processing by BACE1, the Alzheimer's beta-secretase. *J. Cell Biol.* 163, 97–107.
- Senay, C., Lind, T., Mugeruma, K., Tone, Y., Kitagawa, H., Sugahara, K., et al., 2000. The EXT1/EXT2 tumor suppressors; catalytic activities and role in heparan sulfate biosynthesis. *EMBO Rep.* 1, 282–286.
- Shukla, D., Liu, J., Blaiklock, P., Shworak, N.W., Bai, X., Esko, J.D., et al., 1999. A novel role for 3-O-sulfated heparan sulfate in herpes simplex virus 1 entry. *Cell* 99, 13–22.
- Shworak, N.W., Liu, J., Fritze, L.M.S., Schwartz, J.J., Zhang, L., Logeart, D., et al., 1997. Molecular cloning and expression of mouse and human cDNAs encoding heparan sulfate D-glucosaminyl 3-O-sulfotransferase. *J. Biol. Chem.* 272, 28008–28019.
- Silbert, J.E., 1963. Incorporation of C14 and H3 from nucleotide sugars into a polysaccharide in the presence of a cell-free preparation from mouse mast cell tumours. *J. Biol. Chem.* 238, 3542–3546.
- Silbert, J.E., 1967. Biosynthesis of heparin. IV. N-deacetylation of a precursor glycosaminoglycan. *J. Biol. Chem.* 242, 5153–5157.
- Skidmore, M.A., Guimond, S.E., Rudd, T.R., Fernig, D.G., Turnbull, J.E., Yates, E.A., 2008. The activities of heparan sulfate and its analogue heparin are dictated by biosynthesis, sequence, and conformation. *Connect Tissue Res.* 49, 140–144.
- Smeds, E., Hauchi, H., Do, A.T., Hjertson, E., Grundberg, H., Kimata, K., et al., 2003. Substrate specificities of mouse heparan sulphate glucosaminyl 6-O-sulphotransferases. *Biochem. J.* 372, 371–380.
- Smits, N.C., Robbesom, A.A., Versteeg, E.M., van de Westerlo, E.M., Dekhuijzen, P.N., van Kuppevelt, T.H., 2004. Heterogeneity of heparan sulfates in human lung. *Am. J. Respir. Cell Mol. Biol.* 30, 166–173.

- Snow, A.D., Kisilevsky, R., 1985. Temporal relationship between glycosaminoglycan accumulation and amyloid deposition during experimental amyloidosis. A histochemical study. *Lab. Invest.* 53, 37–44.
- Snow, A.D., Willmer, J.P., Kisilevsky, R., 1987. Sulfated glycosaminoglycans in Alzheimer's disease. *Hum. Pathol.* 18, 506–510.
- Song, H.H., Shi, W., Xiang, Y.Y., Filmus, J., 2005. The loss of glypican-3 induces alterations in Wnt signaling. *J. Biol. Chem.* 280, 2116–2125.
- Spijkers, P.P., Denis, C.V., Blom, A.M., Lenting, P.J., 2008. Cellular uptake of c4b-binding protein is mediated by heparan sulfate proteoglycans and CD91/LDL receptor-related protein. *Eur. J. Immunol.* 38, 809–817.
- Spillmann, D., Lindahl, U., 1994. Glycosaminoglycan-protein interactions: a question of specificity. *Curr. Opin. Struct. Biol.* 4, 677–682.
- Spillmann, D., Witt, D., Lindahl, U., 1998. Defining the interleukin-8-binding domain of heparan sulfate. *J. Biol. Chem.* 273, 15487–15493.
- Spillmann, D., Lookene, A., Olivecrona, G., 2006. Isolation and characterization of low sulfated heparan sulfate sequences with affinity for lipoprotein lipase. *J. Biol. Chem.* 281, 23405–23413.
- Stepp, M.A., Gibson, H.E., Gala, P.H., Iglesia, D.D., Pajooheh-Ganji, A., Pal-Ghosh, S., et al., 2002. Defects in keratinocyte activation during wound healing in the syndecan-1-deficient mouse. *J. Cell Sci.* 115, 4517–4531.
- Stickens, D., Zak, B.M., Rougier, N., Esko, J.D., Werb, Z., 2005. Mice deficient in Ext2 lack heparan sulfate and develop exostoses. *Development* 132, 5055–5068.
- Stoolmiller, A.C., Horwitz, A.L., Dorfman, A., 1972. Biosynthesis of the chondroitin sulfate proteoglycan. Purification and properties of xylosyltransferase. *J. Biol. Chem.* 247, 3525–3532.
- Strader, A.D., Reizes, O., Woods, S.C., Benoit, S.C., Seeley, R.J., 2004. Mice lacking the syndecan-3 gene are resistant to diet-induced obesity. *J. Clin. Invest.* 114, 1354–1360.
- Stringer, S.E., Gallagher, J.T., 1997. Specific binding of the chemokine platelet factor 4 to heparan sulfate. *J. Biol. Chem.* 272, 20508–20514.
- Sugahara, K., Kitagawa, H., 2000. Recent advances in the study of the biosynthesis and functions of sulfated glycosaminoglycans. *Curr. Opin. Struct. Biol.* 10, 518–527.
- Sugahara, K., Kitagawa, H., 2002. Heparin and heparan sulfate biosynthesis. *IUBMB Life* 54, 163–175.
- Suk, J.Y., Zhang, F., Balch, W.E., Linhardt, R.J., Kelly, J.W., 2006. Heparin accelerates gelsolin amyloidogenesis. *Biochemistry* 45, 2234–2242.
- Ten Dam, G.B., Kurup, S., van de Westerlo, E.M., Versteeg, E.M., Lindahl, U., Spillmann, D., et al., 2006. 3-O-sulfated oligosaccharide structures are recognized by anti-heparan sulfate antibody HS4C3. *J. Biol. Chem.* 281, 4654–4662.
- The, I., Bellaiche, Y., Perrimon, N., 1999. Hedgehog movement is regulated through tout velu-dependent synthesis of a heparan sulfate proteoglycan. *Mol. Cell* 4, 633–639.
- Thunberg, L., Bäckström, G., Lindahl, U., 1982. Further characterization of the antithrombin-binding sequence in heparin. *Carbohydr. Res.* 100, 393–410.
- Tone, Y., Pedersen, L.C., Yamamoto, T., Izumikawa, T., Kitagawa, H., Nishihara, J., et al., 2008. 2-O-Phosphorylation of xylose and 6-O-sulfation of galactose in the protein linkage region of glycosaminoglycans influence the glucuronyltransferase-I activity involved in the linkage region synthesis. *J. Biol. Chem.* 283, 16801–16807.
- Tsen, G., Halfter, W., Kroger, S., Cole, G.J., 1995. Agrin is a heparan sulfate proteoglycan. *J. Biol. Chem.* 270, 3392–3399.
- Uchimura, K., Morimoto-Tomita, M., Bistrup, A., Li, J., Lyon, M., Gallagher, J., et al., 2006a. Hsulf-2, an extracellular endoglucosamine-6-sulfatase, selectively mobilizes heparin-bound growth factors and chemokines: effects on VEGF, FGF-1, and SDF-1. *BMC Biochem.* 7, 2.

- Uchimura, K., Morimoto-Tomita, M., Rosen, S.D., 2006b. Measuring the activities of the Sulfis: two novel heparin/heparan sulfate endosulfatases. *Methods Enzymol.* 416, 243–253.
- Uyama, T., Kitagawa, H., Tanaka, J., Tamura, J., Ogawa, T., Sugahara, K., 2003. Molecular cloning and expression of a second chondroitin *N*-acetylgalactosaminyltransferase involved in the initiation and elongation of chondroitin/dermatan sulfate. *J. Biol. Chem.* 278, 3072–3078.
- van den Born, J., Gunnarsson, K., Bakker, M.A.H., Kjellén, L., Kusche-Gullberg, M., Maccarana, M., et al., 1995. Presence of *N*-unsubstituted glucosamine units in native heparan sulfate revealed by a monoclonal antibody. *Curr. Opin. Struct. Biol.* 270, 31303–31309.
- van den Born, J., Salmivirta, K., Henttinen, T., Ostman, N., Ishimaru, T., Miyaura, S., et al., 2005. Novel heparan sulfate structures revealed by monoclonal antibodies. *J. Biol. Chem.* 280, 20516–20523.
- van Horsen, J., Wesseling, P., van den Heuvel, L.P., de Waal, R.M., Verbeek, M.M., 2003. Heparan sulphate proteoglycans in Alzheimer's disease and amyloid-related disorders. *Lancet Neurol.* 2, 482–492.
- van Kuppevelt, T.H., Dennissen, M.A., van Venrooij, W.J., Hoet, R.M., Veerkamp, J.H., 1998. Generation and application of type-specific anti-heparan sulfate antibodies using phage display technology. Further evidence for heparan sulfate heterogeneity in the kidney. *J. Biol. Chem.* 273, 12960–12966.
- Vives, R.R., Sadir, R., Imberty, A., Rencurosi, A., Lortat-Jacob, H., 2002. A kinetics and modeling study of RANTES(9–68) binding to heparin reveals a mechanism of cooperative oligomerization. *Biochemistry* 41, 14779–14789.
- Vives, R.R., Imberty, A., Sattentau, Q.J., Lortat-Jacob, H., 2005. Heparan sulfate targets the HIV-1 envelope glycoprotein gp120 coreceptor binding site. *J. Biol. Chem.* 280, 21353–21357.
- Vlodavsky, I., Elkin, M., Abboud-Jarrous, G., Levi-Adam, F., Fuks, L., Shafat, I., et al., 2008. Heparanase: one molecule with multiple functions in cancer progression. *Connect Tissue Res.* 49, 207–210.
- Vogt, A.M., Pettersson, F., Moll, K., Jonsson, C., Normark, J., Ribacke, U., et al., 2006. Release of sequestered malaria parasites upon injection of a glycosaminoglycan. *PLoS Pathog.* 2, e100.
- Volpi, N., Maccari, F., Linhardt, R.J., 2008. Capillary electrophoresis of complex natural polysaccharides. *Electrophoresis* 29, 3095–3106.
- Walsh, D.M., Klyubin, I., Fadeeva, J.V., Cullen, W.K., Anwyl, R., Wolfe, M.S., et al., 2002. Naturally secreted oligomers of amyloid beta protein potently inhibit hippocampal longterm potentiation *in vivo*. *Nature* 416, 535–539.
- Wang, L., Brown, J.R., Varki, A., Esko, J.D., 2002. Heparin's anti-inflammatory effects require glucosamine 6-*O*-sulfation and are mediated by blockade of L- and P-selectins. *J. Clin. Invest.* 110, 127–136.
- Wang, L., Fuster, M., Sriramarao, P., Esko, J.D., 2005. Endothelial heparan sulfate deficiency impairs L-selectin- and chemokine-mediated neutrophil trafficking during inflammatory responses. *Nat. Immunol.* 6, 902–910.
- Warda, M., Toida, T., Zhang, F., Sun, P., Munoz, E., Xie, J., et al., 2006. Isolation and characterization of heparan sulfate from various murine tissues. *Glycoconj. J.* 23, 555–563.
- Warner, R.G., Hundt, C., Weiss, S., Turnbull, J.E., 2002. Identification of the heparan sulfate binding sites in the cellular prion protein. *J. Biol. Chem.* 277, 18421–18430.
- Wei, Z., Swiedler, S.J., Ishihara, M., Orellana, A., Hirschberg, C.B., 1993. A single protein catalyzes both *N*-deacetylation and *N*-sulfation during the biosynthesis of heparan sulfate. *Proc. Natl. Acad. Sci. USA* 90, 3885–3888.

- Wei, G., Bai, X., Sarkar, A.K., Esko, J.D., 1999. Formation of HNK-1 determinants and the glycosaminoglycan tetrasaccharide linkage region by UDP-glcua:Galactose beta1, 3-galacturonosyltransferases. *J. Biol. Chem.* 274, 7857–7864.
- Westling, C., Lindahl, U., 2002. Location of N-unsubstituted glucosamine residues in heparan sulfate. *J. Biol. Chem.* 277, 49247–49255.
- Whitelock, J.M., Melrose, J., Iozzo, R.V., 2008. Diverse cell signaling events modulated by perlecan. *Biochemistry* 47, 11174–11183.
- Wijnhoven, T.J., van den Hoven, M.J., Ding, H., van Kuppevelt, T.H., van der Vlag, J., Berden, J.H., et al., 2008. Heparanase induces a differential loss of heparan sulphate domains in overt diabetic nephropathy. *Diabetologia* 51, 372–382.
- Winterbourne, D.J., Mora, P.T., 1981. Cells selected for high tumorigenicity or transformed by simian virus 40 synthesize heparan sulfate with reduced degree of sulfation. *J. Biol. Chem.* 256, 4310–4320.
- Woods, A., Couchman, J.R., 2001. Syndecan-4 and focal adhesion function. *Curr. Opin. Cell Biol.* 13, 578–583.
- Wu, Z.L., Zhang, L., Beeler, D.L., Kuberan, B., Rosenberg, R.D., 2002. A new strategy for defining critical functional groups on heparan sulfate. *FASEB J.* 16, 539–545.
- Wu, Z.L., Zhang, L., Yabe, T., Kuberan, B., Beeler, D.L., Love, A., et al., 2003. The involvement of heparan sulfate (HS) in FGF1/HS/FGFR1 signaling complex. *J. Biol. Chem.* 278, 17121–17129.
- WuDunn, D., Spear, P.G., 1989. Initial interaction of Herpes simplex virus with cells is binding to heparan sulfate. *J. Virol.* 63, 52–58.
- Xu, D., Moon, A.F., Song, D., Pedersen, L.C., Liu, J., 2008. Engineering sulfotransferases to modify heparan sulfate. *Nat. Chem. Biol.* 4, 200–202.
- Yayon, A., Aviezer, D., Safran, M., Gross, J.L., Heldman, Y., Cabilly, S., et al., 1993. Isolation of peptides that inhibit binding of basic fibroblast growth factor to its receptor from a random phage-epitope library. *Proc. Natl. Acad. Sci. USA* 90, 10643–10647.
- Zcharia, E., Metzger, S., Chajek-Shaul, T., Aingorn, H., Elkin, M., Friedmann, Y., et al., 2004. Transgenic expression of mammalian heparanase uncovers physiological functions of heparan sulfate in tissue morphogenesis, vascularization, and feeding behavior. *FASEB J.* 18, 252–263.
- Zhang, L., Esko, J.D., 1994. Amino acid determinants that drive heparan sulfate assembly in a proteoglycan. *J. Biol. Chem.* 269, 19295–19299.
- Zhu, H., Yu, J., Kindy, M.S., 2001. Inhibition of amyloidosis using low-molecular-weight heparins. *Mol. Med.* 7, 517–522.
- Zimmermann, P., Zhang, Z., Degeest, G., Mortier, E., Leenaerts, I., Coomans, C., et al., 2005. Syndecan recycling [corrected] is controlled by syntenin-PIP2 interaction and Arf6. *Dev. Cell* 9, 377–388.

FIBROBLASTS—A DIVERSE POPULATION AT THE CENTER OF IT ALL

J. Michael Sorrell *and* Arnold I. Caplan

Contents

1. Introduction	162
2. General Characteristics of Fibroblasts	163
2.1. The fibroblast, a working definition	163
2.2. Fibroblast-related populations	165
2.3. Fibroblast-related cells of bone marrow origin	168
3. Fibroblast Diversity	169
3.1. Methods for establishing fibroblast cultures	170
3.2. Dermal fibroblast subpopulations	171
3.3. Fibroblast separation using cell surface markers	175
3.4. Phenotypic markers for fibroblasts and fibroblast-related cells	175
4. Functional Significance of Fibroblast Heterogeneity	176
5. Fibroblast Interactions with Epithelial Cells	179
5.1. Fibroblast interactions with keratinocytes	179
5.2. Fibroblast–keratinocyte interactions for basement membrane formation	182
5.3. Fibroblasts regulate epidermal cell differentiation	183
5.4. Fibroblasts associated with hair follicle epithelium	184
5.5. Fibroblast interactions with vascular endothelial cells	185
6. Fibroblasts, the Architects of Tissues	189
6.1. Fibroblasts, producers of the ECM	189
6.2. Human dermal fibroblasts in tissue engineering	192
7. Thy-1 ⁺ and Thy-1 [−] Subpopulations of Fibroblasts	194
8. Fibroblasts as Sentinel Cells	196
8.1. Fibroblast interactions with immunocompetent cells	196
8.2. Fibroblast regulation of neuropeptides	196
9. Fibroblasts in Aging	198
10. Concluding Remarks	202
Acknowledgments	202
References	202

Department of Biology, Skeletal Research Center, Case Western Reserve University, Cleveland, Ohio 44106

International Review of Cell and Molecular Biology, Volume 276
ISSN 1937-6448, DOI: 10.1016/S1937-6448(09)76004-6

© 2009 Elsevier Inc.
All rights reserved.

Abstract

The capacity of fibroblasts to produce and organize the extracellular matrix and to communicate with other cells makes them a central component of tissue biology. Even so, fibroblasts remain a somewhat enigmatic population. Our inability to fully comprehend these cells is in large part due to the paucity of unique cellular markers and to their pervasive diversity. Much of our understanding of fibroblast diversity has evolved from studies where subpopulations of these cells have been produced without resorting to cell surface markers. In this regard, cloning and mechanical separation of tissues prior to establishing cultures has provided multiple subpopulations. Nonetheless, in isolated situations, the expression or lack of expression of Thy-1/CD90 has been used to separate fibroblast subsets. The role of fibroblasts in intercellular communication is emerging through the implementation of organotypic studies in which three-dimensional fibroblast culture are combined with other populations of cells. Such studies have revealed critical paracrine loops that are essential for organ development and for wound repair. These studies also provide a backdrop for the emerging field of tissue engineering. The participation of fibroblasts in the regulation of tissue homeostasis and their contribution to the aging process are emerging issues that require better understanding. In short, fibroblasts represent a multifaceted, complex group of cells.

Key Words: Fibroblasts, Cloning, Cell Culture, Extracellular matrix, Growth factors/cytokines organotypic cultures. © 2009 Elsevier Inc.

1. INTRODUCTION

Fibroblasts constitute a pervasive but diverse population of cells whose primary function is to establish, maintain, and modify connective tissue stromas. These connective tissue stromas functionally interact with other tissues, such as epithelial tissues, starting with embryonic development and concluding with aging of the individual. This review examines fibroblasts from the perspective of their phenotypic and functional diversity. Such an analysis requires methods to identify and separate distinct subpopulations of cells. It also requires experimental studies to demonstrate that subpopulations of fibroblasts functionally interact with other cells such as epidermal cells, vascular endothelial cells, and immunocompetent cells in varied ways. The production of the extracellular matrix (ECM) is critical for both organ development and maintenance *in vivo* as well as in the emerging field of tissue engineering. Fibroblasts play an integrative role at sites of wounds and inflammation through their interactions with immunocompetent cells and through their regulation of neuropeptides at these sites. Here again, differences in matrix production by diverse subpopulations of fibroblasts may affect the outcome of specific cellular interactions. Finally, fibroblasts serve

as a window into the aging of specific organs as well as a window into the aging of the individual. Thus, fibroblasts, despite their diversity, are a vibrant and central cellular component of tissue biology.

2. GENERAL CHARACTERISTICS OF FIBROBLASTS

2.1. The fibroblast, a working definition

Fibroblasts are the principal cellular constituents of connective tissues. As such, they appear in virtually every tissue and organ of the body. However, this ubiquity generates problems in understanding the functions of these cells, particularly since fibroblasts have been shown to constitute a heterogeneous population of cells (Azzarone and Macieira-Coelho, 1982; Bahar et al., 2004; Fritsch et al., 1999; Harper and Grove, 1979; Nolte et al., 2008; Parker, 1932; Schafer et al., 1985; Sempowski et al., 1995; Sorrell and Caplan, 2004). In classical cell biology, fibroblasts were often considered to be an uninteresting and relatively inert population of cells. This view has radically changed and now they are considered to be a central and vibrant component of tissue biology. Their diversity in phenotypic expression meets the demands of a multifold of tissues and specific subregions within tissues.

Fibroblasts are often defined morphologically as elongated, spindle-shaped cells that readily adhere to tissue culture substrates and migrate over these substrates (Conrad et al., 1977b; Garrett and Conrad, 1979; Parker, 1932). However, fibroblasts may exhibit a variety of shapes and sizes in culture. Indeed, morphological variations have been used as a basis for selecting subpopulations for cloning and other studies (Bayreuther et al., 1988, 1991; Rodemann et al., 1989; Sorrell et al., 2007a). The functional definition of fibroblasts can be further expanded by describing a population of cells that (1) synthesize and secrete a complex array of structural (e.g., collagens and fibronectin) and nonstructural (e.g., matricellular family of molecules such as thrombospondins and osteopontin) ECM molecules, (2) actively organize and remodel ECM through the production of proteinases, (3) converse with nearby cells through paracrine, autocrine, and other forms of communication. As such, this places fibroblasts at the center of tissue and organ physiology (Fig. 4.1). Fibroblasts, through intrinsic and extrinsic aging contribute to the aging of tissues and the individual (Gilchrest, 1996). Finally, fibroblasts, through various manifestations, participate directly or indirectly in fibrotic diseases and nonhealing wounds (Ågren and Werthén, 2007; Darby and Hewitson, 2007; Hasan et al., 1997). Because of these diverse properties, fibroblasts defy a concise definition.

Fibroblasts have multiple embryonic origins, a feature that complicates our understanding of these cells and which contributes to their diversity. Much of our information about the origin of the dermis derives from

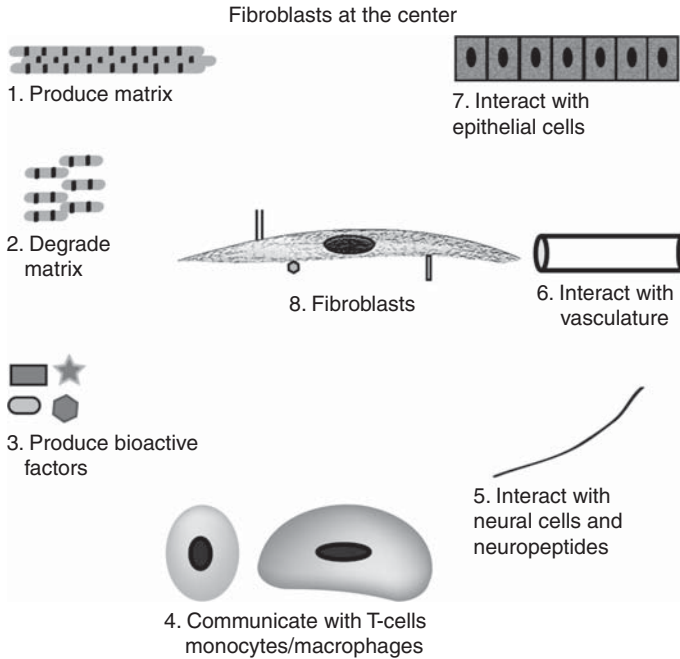


Figure 4.1 The fibroblast at the center. Fibroblasts have multiple functions that are central to tissue biology. (1) They produce and organize structural elements of the ECM. (2) They degrade structural elements of the ECM. (3) They secrete a complex mixture of growth factors, cytokines, and chemokines. (4) They communicate with cells of hematopoietic origin that reside in tissue stromas. (5) They interact with neural cells and neuropeptides. (6) They interact with vascular tissue. (7) They interact with epithelial tissues. (8) Fibroblasts express a variety of cell surface receptors that enable them to respond to bioactive factors released by other cells.

experimental embryological studies of avian and murine embryos which leave some question as to its relevance to human development. Dermal fibroblasts in the dorsal region arise developmentally from the dermo-myotome (Christ and Scaal, 2009; Houzelstein et al., 2000; Scaal and Christ, 2004). This embryonic tissue gives rise to the dermis, hypodermis (i.e., subcutaneous adipose tissue), and underlying musculature. The somatopleure provides cells that migrate and differentiate into the ventral dermis. In contrast, fibroblasts in the scalp and facial skin originate from the neural crest as do other mesenchymal tissues in this region, such as cartilage and bone (Le Lièvre and Le Douarin, 1975).

Signals from the neural crest, such as Wnt-1, are critical for the differentiation of cells into the dermal lineage. In addition, undefined factors released from the ectoderm also appear to play a role in this differentiation process (Christ and Scaal, 2009). One of the earliest markers for dermal cell differentiation is the homeobox gene *Msx-1* (Christ and Scaal, 2009). Other homeobox genes play a role in specifying dermal fibroblast subsets in a

cranial to caudal axis (Chang et al., 2002). Thus, fibroblasts possess positional information that may have physiological consequences with respect to their interactions with other cell types.

In skin, as in other organs, a fetal population of fibroblasts arises from an undifferentiated mesenchyme (Smith and Holbrook, 1986). Fetal dermal fibroblasts are physiologically distinct from their adult descendents. For example, fetal fibroblasts are responsible for scar-free wound repair, a feature not shared by their descendents (Adzick and Lorenz, 1994). Human fetal dermal fibroblasts ultimately differentiate into multiple subpopulations of fibroblasts at any given anatomic site (Sorrell and Caplan, 2004). The timing and molecular cues for fibroblast differentiation into adult phenotypes is currently not understood except for the subset of fibroblasts associated with hair and feather follicles (Botchkarev, 2003; Millar, 2002).

It has been proposed that fibroblasts may arise from epithelial cells at sites of local injury. This proposition is based upon the acquisition of the fibroblast-specific protein-1 (FSP-1) marker by local epithelial cells as they undergo a transition to a mesenchymal phenotype (Strutz et al., 1995).

Small populations of fibroblast-like cells have been shown to circulate via the vascular system. In the adult, these cells arise in the bone marrow and possibly other sites such as adipose tissue (Bianco et al., 2001; Caplan, 2005). One of these populations has been shown to differentiate into multiple types of mesenchymal cells and to play other facilitative functions in wound repair. These cells have been termed mesenchymal stem cells (MSCs). A second population also arises from adult bone and circulates as a monocyte-like cell that continues to express hematopoietic antigens such as CD34 and CD45. These cells also home to wound sites where they assume a fibroblast-like phenotype. These cells have been termed fibrocytes (Quan et al., 2004).

Thus, fibroblasts have a varied origin which may account, at least partially, for their diversity. Nonetheless, much more information is required to understand the origin of these cells. The paucity of specific markers for these varied subpopulations complicates this task.

The principal defining characteristics of fibroblasts are their shape and their ability to secrete ECM molecules such as type I collagen. This broad definition encompasses cells that are not the major constituents of interstitial stromas. Specific subsets of cells that either arise from stromal fibroblasts or which reside along with stromal fibroblasts are listed below. [Figure 4.2A and B](#) summarizes some of the molecular markers that are used to identify fibroblasts and fibroblast-related populations.

2.2. Fibroblast-related populations

2.2.1. Myofibroblasts

This is a differentiated subpopulation of fibroblasts that is found throughout the body in limited quantities ([Fig. 4.2A](#)). The principal characteristic that distinguishes these cells from other populations of fibroblasts is the presence

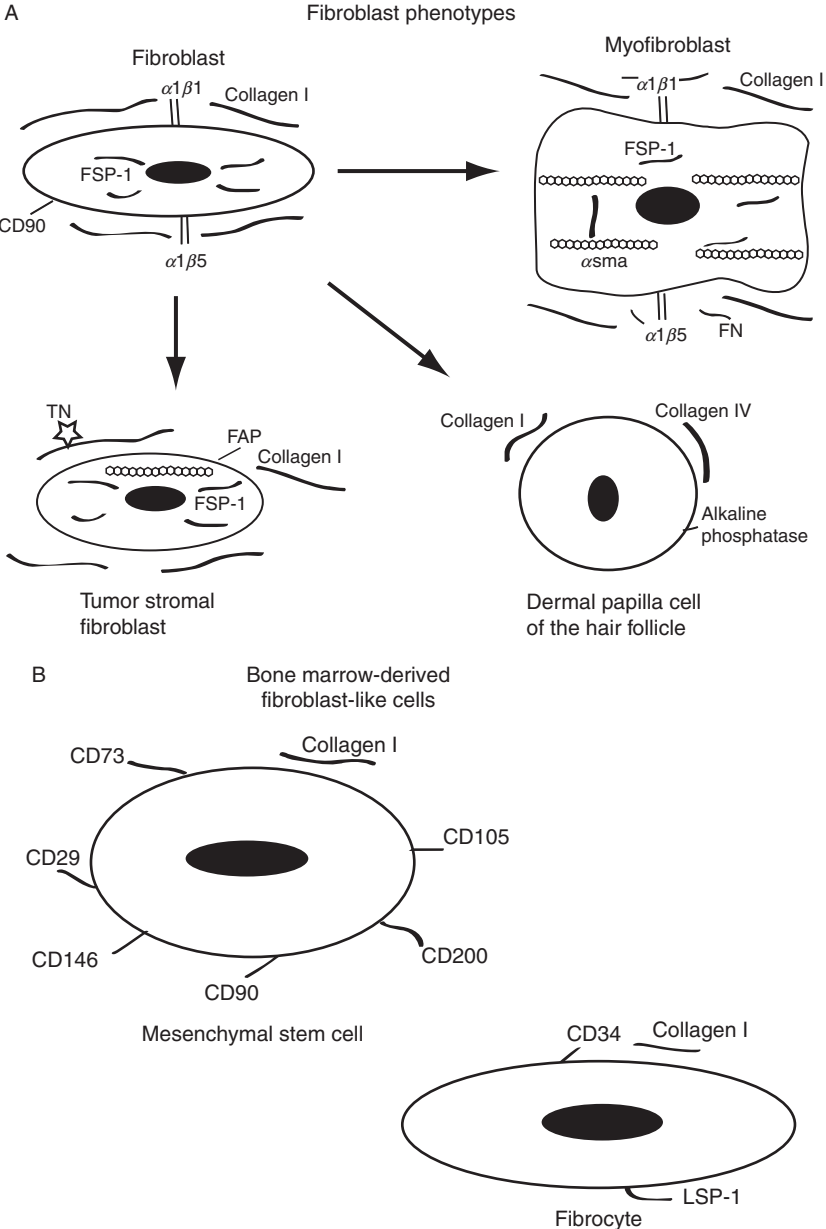


Figure 4.2 Schematic diagrams to show fibroblast diversity. (A) Fibroblast phenotypes. Human dermal fibroblasts differentiate into the cellular populations shown here. Examples of cellular and ECM molecules that characterize these cells are shown: $\alpha_1\beta_1$ integrin (binds collagen type I), $\alpha_1\beta_5$ integrin (binds fibronectin), FN (fibronectin), TN (tenascin-C), FSP-1 (fibroblast-specific protein-1), α sma (α -smooth muscle actin),

of organized α -smooth muscle actin cytoplasmic filaments (Darby and Hewitson, 2007; Gabbiani, 2003). This feature imbues these cells with contractile characteristics that exceed that of most other fibroblasts (Germain et al., 1994; Grinnell, 1994; Moulin et al., 2001). These cells have been termed wound and tumor cells because of their prevalence in these situations (Amadeu et al., 2003; Ronnov-Jessen et al., 1995). A small number of myofibroblasts, or at least myofibroblast-like cells, have been identified in normal skin that contains relatively few hair follicles (Desmoulière et al., 1992; Sorrell et al., 2007a). The connective tissue sheath that surrounds hair follicles consists of myofibroblasts, and is thus a major source of these cells in normal, noninjured skin (Jahoda and Reynolds, 2001).

In vitro studies have shown that normal fibroblasts can be induced to acquire the myofibroblast phenotype by exposing these cells to the fetal form of fibronectin, which is highly expressed at wound sites, and to transforming growth factor- β 1 (TGF- β 1) (Serini et al., 1998). This suggests that myofibroblasts at wound sites may originate from normal interstitial fibroblasts that differentiate and migrate into granulation tissue, although other sources for these cells have also been proposed (Jahoda et al., 1991). Once in granulation tissue, myofibroblasts produce the provisional matrix that is rich in fibronectin and hyaluronan that supports initial vascular restoration and also actively contract wounds. Subsequently, the myofibroblast population at wound sites disappears, apparently through apoptosis. Granulation tissue is then repopulated with fibroblasts that produce a more densely collagenous ECM which is more akin to the matrix found in interstitial stroma.

2.2.2. Differentiated fibroblasts associated with hair follicles

These cells appear in skin at the beginning of fetal development as a condensed mesenchymal population that lies immediately beneath the epidermis (Fig. 4.2A; Millar, 2002). Local epidermal cells communicate with these condensed populations of cells and begin to differentiate, proliferate, and invaginate to ultimately form hair follicles (Botchkarev, 2003; Holbrook and Minami, 1991; Millar 2002). Dermal papillae cells are retained at the base of hair follicles and continue throughout life to direct the cyclic process of hair growth. A second population differentiates into connective tissue sheath cells that encase the length of the hair follicle.

FAP (fibroblast activation protein), CD90 (Thy-1/CD90), alkaline phosphatase (non-specific alkaline phosphatase), collagen type I, and collagen type IV. (B) Bone marrow-derived fibroblast-like cells. Two types of bone marrow-derived fibroblast-like cells have been identified in connective tissues outside the marrow. These are MSCs and fibrocytes. Examples of cellular and ECM molecules that characterize these cells are shown: Collagen I, CD29, CD73, CD90, CD105, CD146, CD200, CD34, and LSP-1 (leukocyte-specific protein-1).

Jahoda and Reynolds (2001) have determined that these sheath cells exhibit characteristics of myofibroblasts. Some dermal papillae cells, such as those found in male facial skin, express androgen receptors (Itami et al., 1995). This enables sex hormones to regulate the growth of hair in regions of the body where this receptor is expressed.

2.2.3. Tumor stromal cells

Tumor stromal cells are a specialized population of connective tissue fibroblasts that are activated and differentiated through contact with tumor cells (Fig. 4.2A; Dicker et al., 2002; Kalluri and Zeisberg, 2006; Lacina et al., 2007; Ronnov-Jessen et al., 1995, 1996). It is assumed that most of these cells arise from nearby connective tissue stroma; however, at least a portion of these cells may originate from alternate sources. One of the markers for tumor stromal fibroblasts is fibroblast activation protein (FAP). This is a cell surface ectopeptidase that shares structural homology with dipeptidylpeptidase IV (DPP-IV), also known as CD26 (De Meester et al., 1999; Park et al., 1999). Tumor stromal cells modify their production of ECM molecules and provide essential support for the increased vascularization of the tumor (Adany et al., 1990). They are nonmalignant cells; however, upon separation from tumor cells, cultured tumor stromal cells can, unlike normal fibroblasts, support tumor formation under *in vitro* conditions (Bissell et al., 2002). The mechanisms by which normal fibroblasts are induced to differentiate into tumor stromal cells are not well established. However, there is some evidence that these events share some similarities of those events that induce fetal dermal mesenchymal cells to differentiate into dermal papillae cells of hair follicles (Dicker et al., 2002).

2.3. Fibroblast-related cells of bone marrow origin

The bone marrow is a primary site for the origin of most blood-borne cells (except for T cells) (Fig. 4.2B). These blood-borne cells include cells that can take residence in connective tissues and express fibroblast-like characteristics. These include cells that have been termed MSCs and fibrocytes. MSCs have been defined as “adult stem cells” since they retain sufficient phenotypic plasticity to develop into differentiated and functional bone, cartilage, adipose, and tendon cells upon receiving proper stimulation (Bianco et al., 2001; Caplan, 2005). Significant MSC populations have been identified in the hematopoietic bone marrow and in subcutaneous adipose tissue (Caplan, 2007; Guilak et al., 2006). Specific methods have been developed to isolate and culture these cells from the indicated sources (Lennon et al., 2000). In addition, there is now increasing evidence that these cells may circulate through the vasculature in order to home to sites of wounds (Badvias et al., 2003). These cells adhere to tissue culture plastic, exhibit fibroblast morphology, and produce ECM molecules, hence their

inclusion as a fibroblast-like population (Sorrell et al., 2009). However, their ability to circulate and differentiate into multiple phenotypes distinguishes them from traditional fibroblasts. Covas et al. (2008), using global gene arrays and real-time polymerase chain reaction (PCR) technology, demonstrated that MSCs did not express FSP-1 as did authentic fibroblasts. Thus, MSCs share many characteristic markers with fibroblasts, but they are a distinct subpopulation of cells.

The fibrocyte is a population of bone marrow-derived, blood-borne cells that populate extracellular matrices (Chesney et al., 1997; Metcalf and Ferguson, 2007; Quan et al., 2004). These cells exhibit monocytes-like characteristics in blood. However, once resident in ECM they assume the spindle cell shape characteristic of fibroblasts and they produce collagens, contain vimentin cytoplasmic filaments. Thus, they bear a superficial resemblance to fibroblasts; however, these cells also express the CD34 and CD45 hematopoietic cell markers that are absent from authentic fibroblasts. These cells also express the class II major histocompatibility antigens and other adhesion markers that enable them to functionally interact with T cell populations (Quan et al., 2004). These cells may also exit connective tissue to travel to proximal lymph node where they may prime naïve T cells. Thus, the fibrocyte has basic fibroblast characteristics, but it functions as a dendritic cell. The presence of higher than normal fibrocytes in connective tissue has been associated with fibrotic lesions such as hypertrophic scars and with extensive burn sites (Wang et al., 2006; Yang et al., 2005). At present, this is a population of cells that is poorly characterized and not well understood.

3. FIBROBLAST DIVERSITY

Fibroblasts are a diverse group of cells with an equally diverse set of functions. This translates into localized sets of connective tissues that are equally dissimilar in their fibroblast populations. At one level, this diversity is organ/tissue dependent. For example, fibroblasts derived from the dermis, cornea, heart, and tendons differ in their cellular orientation and ECM organization (Doane and Birk, 1991). Equally of interest is phenotypic diversity within a given organ or tissue. In skin, fibroblasts from the head, trunk, and legs exhibit diversity in their expression of *hox* genes in a cranial to caudal axis (Chang et al., 2002; Rinn et al., 2006, 2008). Superimposed upon this is layer-specific fibroblast diversity at the same anatomical site in skin (Harper and Grove, 1979; Schafer et al., 1985; Sorrell and Caplan, 2004). Fibroblast diversity is not restricted to skin. Extensive studies of rodent lung fibroblasts by Phipps and others (Fries et al., 1994; Sempowski et al., 1995) have shown that at least two subsets of pulmonary

fibroblasts exist, and similar subsets have been found elsewhere. The functional significance for these multiple levels of fibroblast diversity within one organ, skin, are not yet fully understood. This raises the issue of how to obtain diverse subpopulations of fibroblasts.

The functional significance of diverse fibroblast subpopulations within the given tissues is best studied by isolating specific subpopulations, characterizing these populations, recombining these populations with other relevant cells in coculture studies, and wherever possible, integrating the above with *in vivo* studies. This leads to the next section which discusses approaches to separate functional fibroblast subpopulations from a given tissue. Due to the paucity of specific markers for fibroblasts in general and subsets in particular, a variety of separation techniques must be explored. In this regard, it is helpful to understand the basic methods that have been employed to establish fibroblast cultures, since these methods also provide a means for separating subpopulations.

3.1. Methods for establishing fibroblast cultures

The two basic methods for establishing primary fibroblast cultures from tissues are the explant method and the tissue dissociation method. The methods discussed here is for skin, but these methods can be adapted for any organ or tissue. Human skin specimens are clean but not necessarily sterile. Therefore, the first step is to cut the specimens into small pieces and to “sterilize” the pieces by incubating them in culture media that contains high levels of antibiotics and antimycotics (Sorrell et al., 2007a). The small pieces of skin are then treated with enzymes such as trypsin-ethylenediaminetetraacetic acid (EDTA), dispase, or thermolysin to detach the epidermis (Sorrell et al., 2004, 2007a; Wang et al., 2004). The epidermal sheets obtained in this manner can then be either discarded or used to establish keratinocyte cultures. The remaining dermal pieces are used to establish primary fibroblast cultures by one of the two methods described in Sections 3.2 and 3.3.

The traditional and most commonly used method to establish primary fibroblast cultures is the explant culture method (Balin et al., 2002). The small pieces of dermis that have been stripped of the epidermis are placed onto the surfaces of plastic tissue culture dishes. It is essential that the pieces remain in contact with the plastic as the fibroblasts must crawl from the tissue pieces over the plastic surfaces. Emergence of fibroblasts begins after about 2 days in culture and continues for several additional days. Brief treatment of dermal pieces with trypsin-EDTA usually increases the rate at which fibroblasts emerge from the tissue. Once sufficient numbers of fibroblasts have crawled onto the culture plate, they are detached with trypsin-EDTA and filtered to remove the remnants of the dermal pieces.

The primary advantage of the explant culture method is its simplicity; however, investigators who use this method should realize that the explant procedure provides a level of fibroblast selection (Balin et al., 2002). One study has shown that the fibroblasts that exit dermal pieces early differ from those fibroblasts that exit later. Thus, the length of time that the explanted dermis remains attached to the culture may affect the degree of fibroblast diversity.

The alternate approach is to treat small dermal pieces extensively with proteinases that attack a wide spectrum of ECM proteins. Cocktails containing trypsin-EDTA and collagenase typically release larger numbers and greater varieties of cells than are typically obtained by the explant method (Wang et al., 2004). However, care must be taken to use small pieces of tissue and not to compromise cellular viability by an overly extensive incubation with enzymes. This method also releases nonfibroblastic cells from the dermis. Many of these extraneous cells will be lost upon subculture of the fibroblasts; nonetheless, the possibility that nonfibroblastic cells might remain in fibroblast cultures should be remembered. One of the nonfibroblastic populations that are released in this manner are microvascular endothelial cells. These endothelial cells can be separated from the fibroblasts using immunological panning or microbeads that have been coated with antibodies that are specific for vascular endothelial cell surface markers (Gupta et al., 1997; Kraling et al., 1994; Richard et al., 1998).

3.2. Dermal fibroblast subpopulations

Dermal fibroblast subpopulations may be established either by sampling skin at different anatomic sites (Fig. 4.3A) or by mechanically separating single-site biopsies into defined layers (Fig. 4.3B). Resident fibroblasts in scalp, facial, trunk, and extremity skin differ in terms of homeobox gene expression, which means that there is the potential for phenotypic variability among fibroblasts from various anatomic sites (Chang et al., 2002; Rinn et al., 2006, 2008). Furthermore, fibroblasts from these regions may also differ in the amounts of environmental exposure to which they have been subjected (Fisher et al., 2008; Varani et al., 2004, 2006). Thus, most direct comparisons of fibroblast function should be made using cells from a given anatomic site. Fibroblast subpopulations have also been obtained from the same anatomic site by mechanically separating skin into as many as five defined layers before placing tissues into culture (Bahar et al., 2004; Sorrell and Caplan, 2004). The logic behind this method can be best explained by outlining the histological structure of adult human skin.

Adult human skin consists of three primary layers: the avascular epidermis; the thin, highly vascular papillary dermis; and the much thicker, highly collagenous reticular layer (Cormack, 1987; Sorrell and Caplan, 2004). These three layers of skin rest upon a hypodermis consisting primarily of

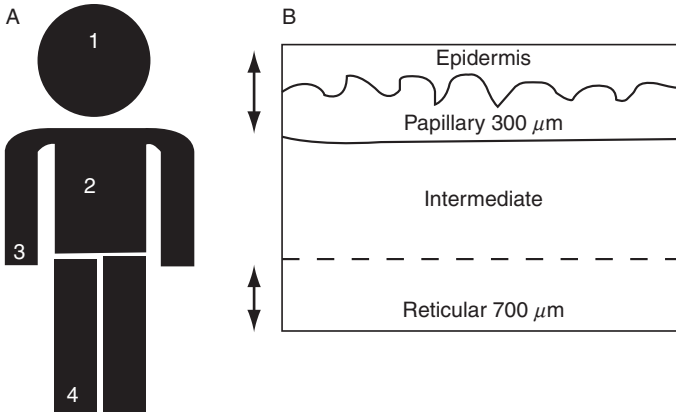


Figure 4.3 Dermal fibroblast diversity. Adult human dermal fibroblast diversity develops from (A) anatomical diversity and (B) layer-specific diversity. (A) Fibroblasts in anatomical regions 1–4 (head, trunk, and extremities) show differences in homeobox gene expression (Chang et al., 2002). (B) Fibroblasts at a given anatomic site show diversity that depends upon their depth within the dermis (Sorrell and Caplan, 2004). Layers of skin harvested at a depth of 300 μm contain cells of the epidermis and papillary dermis; layers harvested at a depth of 700 μm or lower contain cells of the deep dermis. Intermediate dermal cells have also been shown to be different from the upper and lower layers.

adipose cells. The epidermis and papillary dermis combined has a depth of approximately 300–400 μm . However, the depth of this region is variable and depends upon such factors as donor age and anatomical location of the biopsy sample. Skin becomes substantially thinner in elderly individuals. This results from the loss of the dermal papillae at the base of the epidermis and the reduced thickness of the papillary dermis (Gilchrest, 1996; Montagna and Carlisle, 1979). In some regions of the body, such as the palmoplantar regions, the epidermis is substantially thicker (Cormack, 1987).

Typically, the superficial portion of the papillary dermis is arranged into ridge-like structures, the dermal papillae, which contain microvascular and neural components that sustain the epidermis. These dermal papillae greatly extend the surface area for epithelial–mesenchymal interactions and delivery of soluble molecules to the epidermis. A vascular plexus, the rete subpapillare, demarcates the lower limit of the papillary dermis. The reticular layer of the dermis extends from this superficial vascular plexus to a deeper vascular plexus, the rete cutaneum, which serves as the boundary between the dermis and hypodermis. Hair follicles and their associated dermal cells extend into and often through the reticular dermis to terminate in the hypodermis, a tissue rich in adipocytes. Human skin is substantially thicker than that of most experimental animals (particularly rodents). This feature, combined with the structure of skin, lends itself to separation of the dermis by layers.

3.2.1. Culture of fibroblasts from dermal layers

Layers of skin have been obtained by shaving the skin at defined depths using a dermatome (Bahar et al., 2004; Harper and Grove, 1979; Schafer et al., 1985). For trunk and buttocks skin, the epidermis and underlying papillary dermis can be shaved at a depth of 300–400 μm . Skin dermatomed at this depth does not leave a scar; thus, samples can be obtained from live donors. Once dermatomed, the epidermis is detached enzymatically and the remaining dermis can be placed into culture using either explant procedures or enzymatic disaggregation procedures (Sections 2.2.1 and 2.2.2). However, dermatomed layers from deeper regions of the dermis can only be obtained from cadavers (Schafer et al., 1985) or from large pieces of skin removed as a consequence of esthetic surgical procedures (Sorrell et al., 2004). Breast and abdominal skin are the primary types of skin that are used for this application. Standard 4–6 mm punch biopsies are difficult to separate into defined layers, but are useful to establish full-thickness fibroblast cultures.

A variation of this method is to strip the epidermis from the dermis using trypsin-EDTA or other enzyme such as dispase (Wang et al., 2004). Single cell suspensions of primary epidermal cells are cultured according to the Rheinwald/Green method should these cells be required for coculture work (Rheinwald and Green, 1975). However, primary keratinocytes placed into culture and fed with fibroblast medium do not grow well. Instead, small clusters of fibroblast appear among the epidermal cells. Further culture with fibroblast medium allows the fibroblast population to expand at the expense of the keratinocyte population. Fibroblasts that grow out the epidermal layer can be harvested by differential trypsin-EDTA treatment or they can be selected using cloning rings. Presumably, the fibroblasts grown out of the epidermal layer represent a subpopulation of fibroblasts that are closely associated with the epidermis *in vivo*. Most of the populations obtained in this manner express characteristics of papillary dermal fibroblasts.

3.2.2. Clonal separation of fibroblast subpopulations by limiting dilution

Fibroblast cultures that have been established by any of the methods described above can be subjected to cloning procedures to further isolate unique subsets of fibroblasts (Falanga et al., 1995; Fritsch et al., 1999; Ko et al., 1977; Korn et al., 1984; Limeback et al., 1982; Rodemann et al., 1989; Smith and Hayflick, 1974; Sorrell et al., 2007a). The most common method is to clone by limiting dilution. Here, fibroblasts are suspended in medium that contains high serum levels (10–20%) at a low density and are then plated into wells of 96-well culture plates so that there is a high probability that wells will contain only a single cell. Falanga et al. (1995) modified this approach by culturing 96-well plates at low oxygen levels where fibroblast proliferation was enhanced. Ideally, a concentration of

7–8 cells/ml is prepared and 0.1 ml of this suspension is plated into each of the 96 wells. This means that a significant number of wells should contain only a single fibroblast. This is determined through microscopic examination of individual wells. Proliferating cell populations, as determined microscopically, are then transferred to wells of either 48- or 24-well culture plates for further expansion (Sorrell et al., 2007a). There are typically sufficient numbers of cells in this format so that morphological determinations can be made. Also, the rapidity with which wells become confluent provides information about comparative proliferation kinetics. Thus, the first level of selection in the cloning process is made at this point. The rapidity of current PCR methods makes it possible to use this approach to obtain a limited number of gene expression profiles for relatively small numbers of cells. If specific target genes are known, this approach could be used in early screening assays. A final round of expansion is achieved by transferring cells to 35-mm dishes or 6-well culture dishes. At this point, cells can be divided into 4–6 aliquots and seeded onto 100-mm dishes or T75 culture flasks. The cells from one of the dishes/flasks are kept growing for studies and the remainder of the cells are frozen for future studies.

An alternate approach to cloning is the use of cloning rings as a means of removing small clusters of cells from a 35- or 100-mm culture dish. However, this is not a reliable method to obtain clones since fibroblasts on tissue culture surfaces actively migrate and seek out other fibroblasts in low-density cultures. Thus, the probability that small cluster of fibroblasts arose from a single cell is small. Nonetheless, it is possible to obtain moderately homogeneous populations of cells using this approach. Once identified, a cloning ring is placed around the cellular cluster and trypsin-EDTA is added inside the ring to detach the cells. Cells acquired in this manner can then be plated into wells of either a 48- or 24-well culture plate for initial expansion in cell numbers.

Not every fibroblast will proliferate under these conditions. Some fibroblasts in normal skin are postmitotic and thus cannot be used to establish populations (Nolte et al., 2008; Rodemann et al., 1989). Other cells may not grow well in the absence of nearby fibroblasts with those they would normally communicate. This indicates that the cloning procedure selects for fibroblasts that possess mitotic capacity under these limiting culture conditions. Another problem related to cloning results from the large number of enforced population doublings that are required to achieve a sufficiently large population of cell so that studies can be performed. Thus, fibroblasts must be assayed to assure phenotypic stability before they are employed in studies. It also means that there will be only a limited population that can be attained from each clone prior to the cells attaining replicative senescence. Nonetheless, studies have shown that multiple subpopulations of dermal fibroblasts can be obtained using cloning by limiting dilution (Nolte et al., 2008; Rodemann et al., 1989; Sorrell et al., 2007a).

3.3. Fibroblast separation using cell surface markers

The separation of distinct subpopulations using cell surface markers was originally developed by hematologists to identify and separate hematopoietic cells in the bone marrow with respect to defined lineage markers. This technique has also been used to separate diverse cell types from many different complex mixtures of cells. In skin, this method has been employed for the isolation of dermal microvascular endothelial cells from dermal digests (Gupta et al., 1997). Endothelial cells express a set of cell surface markers, such as PECAM-1/CD31, that set these cells apart from the larger dermal fibroblast population. However, the absence of unique cell surface markers to distinguish subpopulations of adult human dermal fibroblasts means that this procedure has not been successful for this population of cells (Sorrell et al., 2003a). This does not necessarily mean that this approach is totally ineffective for all types of fibroblasts. As discussed in Section 7, Thy-1/CD90 has been successfully used to separate fibroblast subset in lung and other tissues (Fries et al., 1994).

There is a twofold advantage in the immunological separation of fibroblasts. First, this approach eliminates the necessity of the large number of enforced population doublings that is required for cloning. Second, the antibody used for separation can also be employed for immunohistological analyses of tissues to determine whether there is an organized distribution of immunoreactive cells. Such information can provide important background information regarding the function of these cells *in vivo*.

3.4. Phenotypic markers for fibroblasts and fibroblast-related cells

Fibroblasts and fibroblast-related cells express a large number of cellular markers (Fig. 4.2). Expression of the cytoplasmic filament vimentin has been one of the most reliable markers for fibroblasts (Sorrell et al., 2007a). Another cytoplasmic marker is FSP-1, also known as S100A4, a member of the S100 superfamily of intracellular proteins (Strutz et al., 1995). The antibody directed to this protein has been primarily used in studies of pathological fibrotic conditions, and has not been extensively applied to fibroblasts in normal tissue settings. The contractile filament α -smooth muscle actin appears in a subset of fibroblasts that are found throughout the body. The presence of this marker is shared with smooth muscle cells and has led to the term myofibroblast, which has been applied to these cells (Amadeu et al., 2003; Darby and Hewitson, 2007; Gabbiani, 2003). Cytoplasmic markers are effective for analytical studies, but are not suitable for isolating and sorting live cells.

The expression of unique cell surface markers is essential for the identification and separation of live cells. Unfortunately, there are few relevant

cell surface markers for the isolation of fibroblast subpopulations. The best characterized cell surface marker for this purpose is Thy-1/CD90 (Fries et al., 1994). However, the intraorgan distribution of Thy-1⁺ and Thy-1⁻ fibroblasts is limited (Section 7). Skin is an organ in which all fibroblasts express this antigen (Saalbach et al., 1996, 1997, 1998). Aminopeptidase N/CD13 (APN/CD13) is an ectopeptidase that is highly expressed at sites of epithelial/mesenchymal interactions in human skin and in developing human breast tissue (Atherton et al., 1992, 1994; Sorrell et al., 2003a). However, all subpopulations express this antigen when human dermal fibroblasts are placed onto culture (Sorrell et al., 2003a). Thus, antibodies to this marker have not proven to be successful in separating dermal fibroblast subpopulations.

Another group of cytoplasmic markers for fibroblasts are receptors for sex hormones. Androgen receptors are present in the dermal papilla fibroblasts of hair follicles in male facial skin (Itami et al., 1995). Subsets of fibroblasts in females contain estrogen receptors (Pugliese, 2007). Such fibroblasts are located in the uterine connective tissue (Malmstrom et al., 2007). These fibroblasts participate in the cycle of events associated with the menstrual cycle. There are also reports of fibroblasts in the upper legs and buttocks of human females that express estrogen receptors. It has been hypothesized that activation of these cells may contribute to the formation of cellulite (Pugliese, 2007).

Phenotypic stability is a major concern for cultured cells. Cells in culture do not always express specific antigen in the same manner as they do *in vivo*. Loss of some antigens and/or acquisition of other antigens can complicate cell selection protocols. Also, cloned fibroblasts have been shown to express phenotypic variability in specific situations. For example, Falanga et al. (1995) found that human dermal fibroblasts which were cloned from a single cell were heterogeneous for message expression for collagen and TGF- β 1. Thus, it is imperative that assays are performed to assess phenotypic stability after multiple cell passages. The proliferative life span of fibroblasts can vary significantly (Cristofalo et al., 1998; Balin et al., 2002). Fibroblasts that undergo proliferative senescence after a low number of population doublings generally modify their physiology in a significant manner (Smith and Hayflick, 1974).

4. FUNCTIONAL SIGNIFICANCE OF FIBROBLAST HETEROGENEITY

Pioneering *in vitro* studies of fibroblasts date to the early 1900s when Carrel established a line of embryonic chick heart cells that served as a standard fibroblast line for decades. Parker (1932) became one of the first

investigators to note fibroblast heterogeneity when he established nine stable populations from different embryonic chick tissues. Conrad's group (Conrad et al., 1977b; Garrett and Conrad, 1979) cultured fibroblasts from the cornea, heart, and skin of chick embryos and found significant differences in terms of both morphology and growth kinetics. This group also found that the glycosaminoglycans produced by these different populations of fibroblasts could be reproducibly differentiated in both the medium and cell layer fractions (Conrad et al., 1977a). This was one of the first documentations that fibroblasts differed in their production of ECM molecules. Doane and Birk (1991) cultured fibroblasts isolated from tendon, cornea, and skin and found that each of these populations retain characteristics of their tissue phenotype in culture.

Much of the evidence for fibroblast diversity depends upon *in vitro* data. Consequently, whenever possible, it is important to correlate *in vitro* studies with *in vivo* functional information. This requires understanding of the histological architecture of the target organ and stably expressed antigens that permit localization of target cells *in vivo*. Skin, because of its accessibility, is one of the best studied organs with respect to fibroblast positioning. However, other organs and tissues have also been studied in this respect (Fries et al., 1994; Koumas et al., 2001; Stenmark et al., 2006).

Fritsch et al. (1999) isolated fibroblast clones from adult duodenal tissue and characterized three clones that displayed individual characteristics. Their clones C9 and C11 exhibited a large, highly spread epithelioid morphology in contrast to clone C20 which exhibited a more typical spindle-shape morphology. All three clones contained vimentin cytoplasmic filaments, but only clone C20 contain organized α -smooth muscle actin filaments. Cell growth was stimulated by tumor necrosis factor- α (TNF- α) for clones C9 and C11, but only C9 growth was stimulated by hepatocyte growth factor/scatter factor (HGF/SF). Clone C20 produced more HGF/SF than the other two cell lines and it interacted with HT29 tumor cells to induce them to grow as a layer in coculture. When mixed with epithelial cells and implanted in rodent intestine, clone C9 gave rise to villus-like structures whereas the other two lines gave rise to glandular structures. C20 cells and HT29 cell cocultures produce a basement membrane. Thus, the authors concluded that the intestine contained physiological diverse subpopulations of fibroblasts that produced and responded differently to growth factors and cytokines.

Bayreuther and colleagues (Bayreuther et al., 1988, 1991; Nolte et al., 2008; Rodemann et al., 1989) in a series of reports cloned human dermal fibroblasts from the same piece of skin and identified morphologically distinct subpopulations which they grouped into a replicative subset and a postmitotic subset. The postmitotic subset expressed high levels of low pH β -galactosidase activity, which has been proposed to be a marker for cellular senescence (Dimiri et al., 1995). This group (Nolte et al., 2008) also

proposed that fibroblasts undergo a differentiation and aging process *in vivo* that accounts, at least partially, for *in vivo* fibroblast diversity.

Fibroblasts cultured separately from the papillary and reticular dermal layers are physiologically distinct subsets of cells (Harper and Grove, 1979; Schafer et al., 1985; Sorrell and Caplan, 2004). This, however, raises the issue of whether these two subpopulations of fibroblasts are themselves homogeneous or heterogeneous. Our group obtained the dermatomed superficial layer of skin from live donors, detached the epidermis, and enzymatically disassociated the dermal component. This procedure maximized potential cellular diversity for cloning studies. First passage cells were cloned by limiting dilution in 96-well culture plates and were selected for further study on the basis of cellular morphology and growth kinetics.

Once selected, stable clones were interrogated for the presence of organized α -smooth muscle actin filaments, relative ability to contract type I collagen gels, ability to organize insoluble fibronectin fibrils, and their production and response to selected growth factors and cytokines. Distinct characteristics emerged that resulted in the allocation of clones into three groups. (1) One set of clones expressed characteristics typical of papillary dermal fibroblasts. (2) Another set expressed characteristics more typical of reticular dermal fibroblasts. (3) The third set of clones expressed α -smooth muscle actin filaments, a characteristic of myofibroblasts.

As will be discussed in more detail in Section 5.3, papillary and reticular dermal fibroblasts differed in their release of two essential growth factors used in the paracrine communication between fibroblasts and keratinocytes, keratinocyte growth factor-1 (KGF-1), and granulocyte/macrophage colony-stimulating factor (GM-CSF) (Sorrell et al., 2004). Clones with papillary characteristics produced less KGF-1 and more GM-CSF than did the clones with reticular characteristics. Thus, cloned subsets from the papillary dermis conformed to characteristics of fibroblast subpopulations created by mechanical separation of skin. Dermal fibroblasts release inflammatory factors such as interleukin-6 (IL-6). Two of the clones derived from the papillary dermis released significantly elevated levels of IL-6, both on a constitutive level and following exposure of the cells to IL-1 α . This is an indication that these cellular subsets might play a dominant role in inflammatory responses.

Thus, cloning studies indicated that the papillary dermal fibroblast population which was created by dermatoming the superficial layer of skin was itself heterogeneous. Physiological differences between the papillary dermal population and other dermal subpopulations resulted from the presence of a dominant cell type that could be isolated by cloning. In a similar manner, reticular dermal subpopulations contained a dominant cell type (unpublished data). These results further suggest that the characteristics of connective tissues can be substantially altered should a new subpopulation become dominant. Fibroblasts located in the central region of the dermis have been

shown to differ from those located in the superficial and basal layers of the dermis (Bahar et al., 2004; Tajima and Izumi, 1996; Wang et al., 2008). Thus, the full extent of fibroblast diversity in the normal adult dermis is not yet fully established.

5. FIBROBLAST INTERACTIONS WITH EPITHELIAL CELLS

5.1. Fibroblast interactions with keratinocytes

Coculture studies with human dermal fibroblasts and human keratinocytes evolved from the pioneering work of Rheinwald and Green (1975) who developed a method to culture-expand keratinocytes on an irradiated 3T3 fibroblast feeder layer. Their work emphasized the sustaining effects of fibroblasts for keratinocyte growth and it ultimately resulted in the discovery that fibroblasts were releasing soluble growth factors such as KGF-1 and KGF-2 (Igarashi et al., 1996; Rubin et al., 1995).

Fibroblasts secrete KGFs, but do not directly respond to these factors since they lack the requisite receptors. Keratinocytes possess KGF receptors and respond to these factors in part by releasing soluble factors that induce fibroblasts to upregulate their production of KGF message and protein (Werner and Smola, 2001; Werner et al., 2007). This was first demonstrated in a coculture system (Maas-Szabowski and Fusenig, 1996; Smola et al., 1993) and was later established *in vivo* to be a part of the wound response (Werner, 1998). The cytokine IL-1 α was identified as one of the principal factors released by stimulated keratinocytes that induced the upregulated KGF production by fibroblasts (Maas-Szabowski and Fusenig, 1996). Thus, these studies revealed the existence of a paracrine loop that regulated fibroblast and keratinocyte functions as a consequence to wounding.

Nowinski et al. (2004) modified their approach in order to better define the fibroblast genes that responded to soluble keratinocyte signals. They set up cocultures of human dermal fibroblasts and keratinocytes where these two populations were physically separated by a membrane that prevented cellular transmigration. Global gene microarrays for the cocultured fibroblasts revealed that 243 mRNAs were upregulated by twofold or more and 100 mRNAs were downregulated by half or more compared with control fibroblasts that were cultured alone. Thus, the physiology of the fibroblasts was substantially modified by signals derived from keratinocytes. Of the affected genes, 69 coded for growth factors, cytokines, chemokines, and their receptors. ECM molecules, adhesion receptors, and proteinases were also significantly affected by coculture. Exposure of fibroblasts to recombinant IL-1 α exerted a similar effect as did coculture with keratinocytes. This provided additional evidence for the role of IL-1 α in paracrine interactions between keratinocytes and fibroblasts. However, IL-1 exposure alone did

not elicit a response that fully matched that of coculture. This suggests that keratinocytes release other factors that regulate fibroblast physiology. Other fibroblast-activating factors that have been shown to be released by keratinocytes are activin A, a member of the TGF superfamily (Werner and Smola, 2001) and parathyroid-related protein (Blomme et al., 1999a,b). Ghahary and others (Ghahary and Ghaffari, 2007; Ghahary et al., 2004) discovered that keratinocytes at sites of hypertrophic scars released a factor identified as stratifin which stimulated matrix metalloproteinase-1 (MMP-1) collagenase expression by dermal fibroblasts. Longaker's group (Lim et al., 2002), in a similar manner, found that keratinocytes obtained from keloid lesions induced normal dermal fibroblasts to produce collagen in a keloid-like manner. Thus, the epidermis at pathologic sites may influence the physiology of the underlying dermal cells.

Interestingly, keratinocyte stimulation of fibroblasts also upregulate factors such as vascular endothelial growth factor-A (VEGF-A) and insulin-like growth factor-1 (IGF-1) that affect fibroblast interactions with vascular endothelial cells (Jain, 2003). This suggests that the high microvascular density in the superficial dermis may result from the combined interactions of vascular cells with stimulated fibroblasts and with keratinocytes that also produce proangiogenic factors (Detmar, 2000).

Stimulated dermal fibroblasts produce other factors that regulate keratinocyte physiology. One of these additional factors is GM-CSF. Unlike KGF-1, dermal fibroblasts do not produce this factor on a constitutive basis (Sorrell et al., 2004). However, coculture with keratinocytes or exposure of these cells to IL-1 induces the production and release of this factor. The effects of GM-CSF on epidermal development are clearly different from that of KGF-1 (Maas-Szabowski et al., 2001). In an elegant set of studies, it was shown that KGF-1 alone produced a hyperproliferative epidermis in skin equivalents, while GM-CSF alone produced a hypoplastic epidermis that expressed terminally differentiated characteristics. However, in combination, both factors produced a more normal epidermis. These results suggested that multiple bioactive factors presented in an appropriately balanced mixture were essential for the proper development of the epidermis (Hughes and Chuong, 2003).

The studies described earlier raise the issue of whether all dermal fibroblasts responded to keratinocyte stimuli in the same manner. Papillary and reticular dermal fibroblasts cultured from the same piece of skin both upregulated their production of KGF-1 and GM-CSF. However, the degree of upregulation varied significantly and consistently for these two subpopulations of cells. This was best described by comparing the ratios of KGF-1 and GM-CSF released by these cells. Papillary dermal fibroblasts consistently released less KGF-1 and more GM-CSF than did their reticular dermal fibroblast counterparts (Sorrell et al., 2004). The molecular profile for site-matched papillary and reticular dermal fibroblasts is demonstrated in

Fig. 4.4 for papillary and reticular fibroblast couples from different aged donors. The data in Fig. 4.4 also emphasizes the importance of selecting fibroblast subsets. The consistent pattern of ratios for KGF and GM-CSF were not evident for nonselected fibroblasts cultured from the same pieces of skin. The nonselected fibroblasts were developed as explant cultures from full-thickness dermal pieces. Phenotypically, the nonselected fibroblasts rarely matched papillary fibroblasts, and were often intermediate in characteristics. Thus, selected subpopulations of fibroblasts would be expected

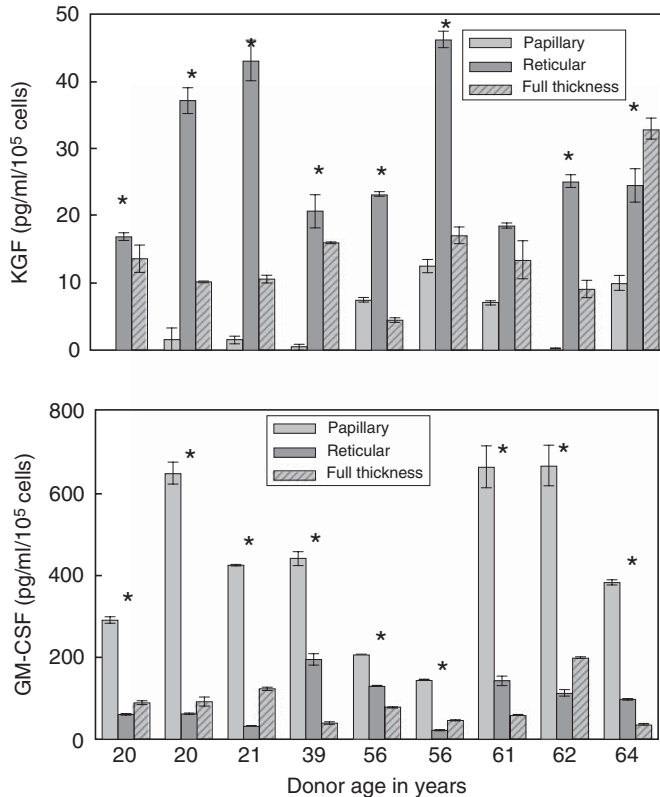


Figure 4.4 Molecular profiles of dermal fibroblasts. Dermal fibroblasts cultured from the papillary and deep reticular layers of the same piece of skin express unique patterns in their release of the two growth factors KGF-1 and GM-CSF (Sorrell et al., 2004). Papillary fibroblasts release low levels of KGF-1 and elevated levels of GM-CSF compared with matched reticular fibroblasts. This characteristic is not age dependent. In contrast, nonselected fibroblasts cultured from full-thickness skin from the same sites do not display any recognizable pattern. The asterisk (*) indicates that the levels of the indicated factor were significantly different for papillary and reticular fibroblasts using the paired *t*-test, $p < 0.05$.

to behave differently from nonselected cells in their interactions with other types of cells due to variations in growth factor/cytokine output (Sorrell et al., 2004, 2008).

The downstream influence of keratinocyte-derived bioactive factors on dermal fibroblasts appears to be mediated by AP-1 target genes. Szabowski et al. (2000) examined fibroblasts from Jun-knockout and Jun-B-knockout mouse embryos and found that the Jun^{-/-} cells produced very low levels of KGF-1 and GM-CSF, whereas Jun-B^{-/-} cells produced elevated levels of these factors. Incorporation of these fibroblasts into bilayered skin equivalents with normal human keratinocytes led to strikingly different results. Epidermal layers on skin equivalents containing Jun^{-/-} fibroblasts were atrophic, basal cell proliferation was reduced, and terminal differentiation was delayed. IL-1 and other inflammatory factors, such as TNF- α , activate AP-1-mediated transcription and enhance the activity of NF- κ B (Angel and Szabowski, 2002). Differences in the phenotypes of fibroblasts in skin might be related to how these cells respond to external signals and modulate the diverse group of genes regulated by AP-1 transcription factors.

5.2. Fibroblast-keratinocyte interactions for basement membrane formation

The epidermis of the skin is firmly attached to the underlying dermis by a complex multimolecular structure, the basement membrane (Aumailley and Rousselle, 1999; Burgeson and Christiano, 1997). The organization of basement membrane to form a morphologically identifiable structure results from a cooperative effort of both keratinocytes and fibroblasts (Fleischmajer et al., 1993; Marinkovich et al., 1993; Moulin et al., 2000; Smola et al., 1998). This cooperation is based upon both communication between cell types and colateral deposition of ECM molecules.

Marinkovich et al. (1993) studied the cellular origin of various basement membrane molecules by probing skin equivalents constructed with bovine keratinocytes and human dermal fibroblasts with species-specific antibodies. Their conclusion was that major molecular species found in the basement membrane were contributed by both epidermal cells and adjacent fibroblasts. However, other studies have shown that specific molecular components of the basement membrane may be primarily produced by one or the other of these cell types. For example, the nidogen/entactin component of the basement membrane appears to be produced primarily by dermal fibroblasts (Contard et al., 1993; Fleischmajer et al., 1995). Fibroblast communication with epidermal cells also appears to play a role in basement membrane fabrication. Smola et al. (1994) found that keratinocytes induced the expression of TGF- β 2 by dermal fibroblasts and that this factor in turn regulated the production of laminins and type VII collagen by keratinocytes. Others (König and Bruckner-Tuderman, 1991, 1994; Monical and

Kefalides, 1994) have also provided evidence that fibroblasts, possibly through TGF- β signaling, regulate the production of type VII collagen by epidermal cells in coculture situations. The kinetics of basement membrane formation in coculture situations also appears to be defined by fibroblasts (Smola et al., 1998). Thus, paracrine communication between fibroblasts and epidermal cells appears to play a role in the construction and organization of the basement membrane (Marinkovich et al., 1993).

Fibroblast interaction with epidermal cells with respect to basement membrane formation may be variable. Moulin et al. (2000) showed that myofibroblasts obtained from wound sites did not support keratinocyte differentiation and basement membrane formation to the same extent as did normal dermal fibroblasts. Consequently, the ability was compared for site-matched papillary and reticular dermal fibroblasts to support basement membrane formation (Sorrell et al., 2004). Papillary dermal fibroblasts appeared to induce basement membrane formation faster when reticular fibroblasts were present. Therefore, fibroblasts adjacent to the epidermis might either produce more ECM components of the basement membrane and/or produce soluble factors that influence keratinocytes to reestablish a basement membrane.

5.3. Fibroblasts regulate epidermal cell differentiation

Fibroblast diversity in skin depends upon both anatomic positioning and upon intrasite positioning (Fig. 4.3A). This implies that dermal fibroblasts located at different anatomic sites may differentially interact with other cell types. Proof of this concept has been demonstrated in studies where epidermal cells and dermal cells from different anatomic sites have been combined. The now classic example of this type of recombination was performed on avian embryos where the feather-producing wing epidermis was grafted onto the dermis of the scale-producing leg and foot region (Dhouailly, 1973). The characteristics of the epidermis were modified so that scales were produced by the epidermis. This indicated that differentiated dermal fibroblasts instructed the epidermis to reprogram its epigenetic profile. Thus, fibroblast differentiation plays a major role in tissue development and differentiation.

This characteristic is not limited to avian embryos. Human scalp skin, which contains a high density of hair follicles, is fundamentally different from palmoplantar skin where hair follicles are completely absent (Cormack, 1987). Furthermore, the epidermis at palmoplantar sites is thicker and it contains keratins not expressed elsewhere. Thus, human skin exhibits variability in the expression of epidermal appendages in much the same manner as does avian skin. Yamaguchi et al. (1999) demonstrated in a skin equivalent model that dermal fibroblasts from human palmoplantar skin induced the formation of an epidermis with a palmoplantar phenotype even when nonpalmoplantar epidermal cells were used. As in the avian study, this

indicates that site-specific differentiation of fibroblasts influences the differentiation of overlying epidermal cells. The identities of the molecular cues that regulate these events are not well understood except in situations that involve the formation of hair follicles (Section 5.4).

Gingival tissue in the oral cavity has a histological structure that is similar to that of dermis. However, the gingival epidermis does not have a stratum corneum and there are different keratins expressed in the oral epidermis than in the skin epidermis. Gingival fibroblasts bear a striking morphological resemblance to dermal fibroblasts. Nonetheless, studies have shown that there are phenotypic differences between these two populations of fibroblasts with respect to growth factor production of KGF-1 and HGF/SF (Grøn et al., 2002; Shannon et al., 2006). Gingival tissue heals in an accelerated scar-free manner similar to that observed in the early fetal dermis (Enoch et al., 2008). This suggests that gingival fibroblasts share essential characteristics with fetal fibroblasts. One feature of similarity is that both populations contract collagenous matrices faster than do adult dermal fibroblasts (Shannon et al., 2006). This contractile ability exists even without the expression of organized α -smooth muscle actin filament that is a characteristic of myofibroblasts.

Fibroblasts cultured from the oral cavity have been shown to support the differentiation of oral epithelial cells into an oral epidermis using bilayered skin equivalents (Costea et al., 2003). Chinnathambi et al. (2003) constructed bilayered skin equivalents using heterotypic mixtures of human dermal and oral fibroblasts and skin and oral keratinocytes. They found that the oral fibroblast population directed development of an oral epidermis.

The studies reported in this section provide evidence that fibroblasts are imbued with an epigenetic program that reflects their anatomical location. Chang's group has demonstrated that homeobox gene expression is dependent upon anatomical location of fibroblasts (Chang et al., 2002; Rinn et al., 2006, 2008). However, interactions between fibroblasts and other cells depend upon the expression of cellular signaling molecules and ECM molecules. Our understanding of these factors remains rudimentary.

5.4. Fibroblasts associated with hair follicle epithelium

Hair is a product of mesenchymal-epithelial interactions that occur early in fetal development (Botchkarev, 2003; Millar, 2002). Two differentiated fibroblast populations arise from these interactions. The first differentiated population to appear is condensed mesenchymal cells that arise at the base of the fetal epidermis. These cells induce the proliferation, differentiation, and invagination of the epidermis to form hair follicles (Holbrook and Minami, 1991). The condensed dermal cells ultimately give rise to two distinct fibroblast subpopulations that are both associated with hair follicles. A condensed population of cells is retained at the base of the hair follicle. These dermal papillae cells, characterized from other dermal fibroblasts by

their expression of nonspecific alkaline phosphatase, are retained throughout life (Kopf, 1957). These cells during adult life undergo cyclic physiological changes that direct the cyclic growth and regression of hair follicles (Botchkarev, 2003; Millar, 2002). These dermal papillae fibroblasts are also differentiated from other dermal fibroblasts through their elevated production of ECM molecules that are characteristic of basement membranes (Couchman, 1986). Immunohistochemical analyses of proteoglycans and glycosaminoglycans associated with adult human hair follicles indicate that the chondroitin sulfate proteoglycan versican and the heparan sulfate proteoglycan perlecan are highly expressed along with the cell surface heparan sulfate proteoglycans syndecan-1 and CD44. This emphasizes the point of differences in the composition of ECM between the hair follicle and the interfollicular dermis. The glycosaminoglycan chains found in this region are known to bind and sequester bioactive factors that are important for hair follicle growth regulation: FGFs, VEGF-A₁₆₅, sonic hedgehog, bone matrix proteins, Wnt-factors, and HGF/SF (Malgouries et al., 2008). It seems likely that a physiological interplay between dermal papillae cells and follicular epidermal cells is important since changes in the amounts and composition of proteoglycans/glycosaminoglycan was noted during the different stages of the hair follicle. Relatively little information is currently available about the production of these ECM molecules by culture dermal papillae cells since it is difficult to culture these cells and maintain their differentiated status.

A second subpopulation forms the connective tissue sheath that surrounds the hair follicle and which separates it from the surrounding interfollicular dermis (Jahoda and Reynolds, 2001). These sheath fibroblasts express α -smooth muscle actin, a feature that differentiates these cells from the fibroblasts of the normal interfollicular dermis. Hair follicles are present in most regions of human skin; however, these cells do not contribute significantly to fibroblast cultures. Special conditions are required for the isolation and culture of these cells (Jahoda and Reynolds, 2001).

5.5. Fibroblast interactions with vascular endothelial cells

Physiological interactions between human dermal fibroblasts and epidermal cells have been extensively, although not exhaustively characterized. In contrast, much less is known about physiological interactions between fibroblasts and another type of epithelial cell, vascular endothelial cells. Interactions between these two cellular populations are highly relevant for early stages of wound repair when a rich vascular network is established in granulation tissue (Singer and Clark, 1999). Also, these interactions are becoming more relevant with the increased implementation of tissue of engineered implants. These implants, to maintain their effectiveness, require vascular continuity with host vasculature and fibroblasts play a

major role in the attraction and stabilization of host vasculature (Démarchez et al., 1992; Pinney et al., 2000).

Our current understanding of fibroblast–vascular endothelial cell interactions is primarily based upon coculture studies using both cell types. In aggregate, these studies have shown that fibroblasts produce a variety of proangiogenic factors that induce endothelial cell differentiation, migration, tubule formation, and tubule stabilization (Bishop et al., 1999; Black et al., 1999; Davie et al., 2006; Hudon et al., 2003; Martin et al., 1999; Montesano et al., 1993; Sorrell et al., 2007b, 2008; Supp et al., 2002; Velasquez et al., 2002). The molecular mechanisms by which fibroblasts achieve these events are not yet fully understood. Fibroblasts produce and secrete a variety of potent proangiogenic factors, such as VEGFs, FGFs, TGF- β 1, HGF/SF, and angiopoietin-1 (Jain, 2003), that play critical roles in these events. Paracrine loops similar to those defined for interactions between fibroblasts and keratinocytes likely exist, but have yet to be well characterized. The ECM elaborated by fibroblasts is also necessary for interactions with vascular endothelial cells. Structural matrix molecules such as fibrillar collagens, tenascin-C, and fibronectin interact with specific integrin receptors expressed by endothelial cells (Ballard et al., 2006; Sottile, 2004). Enzymatic degradation products of ECM molecule may also have either pro- or antiangiogenic characteristics (Iozzo, 2005). Matricellular molecules such as osteopontin and thrombospondins also modulate endothelial cell physiology (Detmar, 2000; Puolakkainen et al., 2005). Thus, multiple and varied interactions occur between fibroblasts and vascular endothelial cells.

Bishop et al. (1999) developed an *in vitro* coculture system in which adult human dermal fibroblasts create thin three-dimensional lawns onto which human umbilical vein endothelial cells (HUVECs) were seeded. These fibroblastic lawns thus contain a complex array of fibroblast-derived ECM molecules and fibroblast-derived proangiogenic factors.

Consequently, HUVECs seeded onto these lawns differentiate, migrate, and form tube-like structures in the absence of exogenous proangiogenic factors. However, vascular endothelial cells vary in their physiological requirements. Human dermal microvascular endothelial cells, unlike HUVECs, require the addition of exogenous proangiogenic factors to the culture medium in order for them to respond in a similar manner (Sorrell et al., 2007b). HUVECs seeded onto permissive dermal fibroblast lawn begin to migrate and align end to end within hours of seeding. Tubules that form under these conditions remain stable for well in excess of 2 weeks in culture. These events can be modulated by the addition of pro- and antiangiogenic factors to the culture medium (Bishop et al., 1999; Sorrell et al., 2008). Thus, these cocultures can be used to study vascular behavior and fibroblast–vascular endothelial cell interactions.

Fibroblast diversity may influence interactions with vascular endothelial cells as it influences interactions with epidermal cells (Sorrell et al., 2004).

Montesano et al. (1993) discovered that genetically different murine fibroblast populations interacted variably with HUVECs in coculture; some populations supported tubule formation, while other populations failed to support these events. With fibroblast subpopulation derived from the same piece of skin available, it was possible to determine whether these subpopulations could differentially interact with HUVECs in coculture (Sorrell et al., 2008). Dermal fibroblasts cultured from the same piece of skin were found to act as either permissive or nonpermissive in their interactions. Permissive populations of fibroblasts, which were located primarily in the papillary dermis, supported a rapid and robust level of tubule formation by HUVECs. In contrast, nonpermissive fibroblasts, primarily located in the reticular dermis, failed to support these events. The nonpermissive characteristics were partially modulated by the combined addition of exogenous proangiogenic factors VEGF-A and HGF/SF to the culture medium. The inability to completely relieve the block suggested that other factors were critical in defining the permissive environment. This was partially supported by discovery that permissive and nonpermissive fibroblasts produced nearly equivalent amounts of the major proangiogenic factors VEGF-A and FGF-2. Only HGF/SF production was limited for nonpermissive cells.

Permissive and nonpermissive fibroblast lawns were set up on opposite sides of a single culture dish. Cellular tracing studies indicated that there was only marginal mixing of these two subpopulations of fibroblasts at the midline. Therefore, it was possible to seed HUVECs over these two lawns in a situation where there was a common culture medium. If soluble factors released into the medium defined permissive and nonpermissive environments, the level of tubule formation should have occurred uniformly across the entire culture dish. Instead, tubules formed only over the permissive fibroblast lawn. These results suggest that nonsoluble factors in ECM generated by dermal fibroblasts play a significant role in regulation of tubule formation (Ruhrberg et al., 2002; Sottile, 2004). The identity of these nonsoluble factors is not currently known.

Cloning studies revealed diversity among fibroblasts in the papillary dermal region (Sorrell et al., 2007a). Subpopulations of cells that were identified as either papillary- or reticular-like were used to establish fibroblast lawns for coculture studies with HUVECs. As shown in Fig. 4.5, the noncloned parent population of fibroblasts supported a robust level of tubule formation as did the cloned subpopulation 9B7, which expressed papillary-like characteristics. In contrast, reticular-like clone 14D7 failed to support tubule formation. In the absence of specific molecular markers for fibroblast subpopulations, it is not possible to ascertain the *in vivo* locations of specific subpopulations. Helmbold et al. (2001) identified cells positive for the human vascular pericyte marker 3G5 in neonatal human foreskin. They isolated 3G5-positive cells from dermal tissue digests and reported the positive cells to coexpress α -smooth muscle actin.

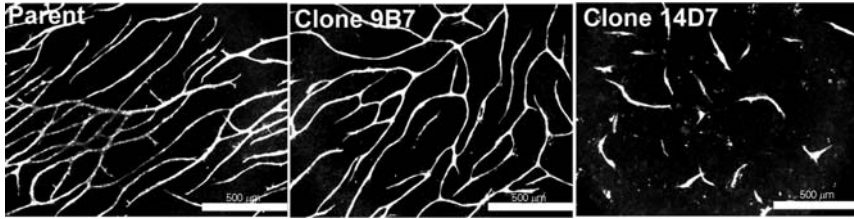


Figure 4.5 Fibroblast interactions with vascular endothelial cells *in vitro*. The papillary dermis of adult human skin contains multiple subpopulations of fibroblasts. (A) The uncloned parent papillary dermal fibroblast population supports the formation of a complex tube-like network. (B) Clone 9B7 also supports the formation of a complex tube-like network. (C) However, clone 14D7 fails to support the formation of a complex tube-like network. Bars = 500 μm .

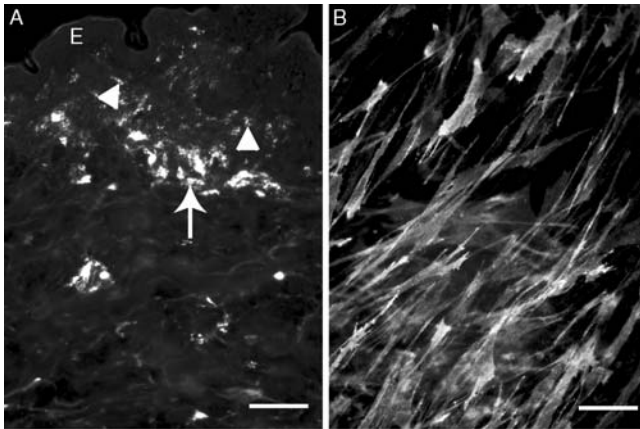


Figure 4.6 Cells reactive to the pericyte marker 3G5. (A) The vascular plexus (arrow) that separates the papillary and reticular dermis contains cells immunostained by the 3G5 pericyte marker (American Type Tissue Collection, Bethesda, MD). Other immunoreactive cells are present in the papillary dermis (arrowheads) adjacent to the epidermis (E). (B) Papillary dermal fibroblasts in high-density lawns that support vascular tubule formation (present but not visible) are immunoreactive for the 3G5 antibody. Bars = 300 μm (A) and 25 μm (B).

The papillary dermis of adult human skin also contained 3G5-positive cells (Fig. 4.6A). Fibroblasts cultured from this region were found to express this antigen in contrast with fibroblasts cultured from the reticular dermis; however, these 3G5-positive fibroblasts did not express the α -smooth muscle actin marker (Sorrell et al., 2007a). In coculture situations, 3G5-positive cells appeared to account for the major population in the fibroblast lawn (Fig. 4.6B). These results suggest that the 3G5 antibody might be

used to select cultured fibroblasts that support vascular endothelial cells in culture. However, these results are preliminary and require further critical evaluation.

6. FIBROBLASTS, THE ARCHITECTS OF TISSUES

6.1. Fibroblasts, producers of the ECM

The ECM profoundly influences both fibroblast function and the function of adjacent epithelial tissues. During embryonic and fetal development, these epithelial/mesenchymal interactions are responsible for tissue and organ development. Basement membranes that are produced at intersects between fibroblasts and epithelial tissues bind, protect, and concentrate critical bioactive factors on the basis of interactions with heparan sulfate glycosaminoglycan chains (Iozzo, 2005; Ramirez and Rifkin, 2003). In skin, ECM defines the overall architecture of the organ. The histological patterns that demarcate the papillary and reticular dermis in adult human skin are defined by the differential production, deposition, and organization of ECM molecules (Cormack, 1987; Sorrell and Caplan, 2004).

ECM production by fibroblasts is a complex process. Fibroblasts produce a wide range of matrix molecules, but the relative amounts of individual molecules may vary significantly. Major structural elements of tissues, such as collagenous fiber bundles and elastic fibers, owe their existence to multiple classes of ECM molecules. Proteoglycans play an essential role in the organizational events for these structures. The small proteoglycan decorin plays an essential role in the organization of collagenous fibers, while the large proteoglycan versican plays an equally important role in the development of elastic fibers.

Proteoglycans are complex macromolecules that are composed of a core protein to which complex carbohydrate glycosaminoglycan chains are covalently attached (Heinegård and Oldberg, 1993). Their high anionic charge maintains tissue hydration; however, it is their ability to interact with other matrix molecules makes them a multifunctional set of molecules. In many proteoglycans, both the protein and carbohydrate components exhibit variability that is developmentally and tissue specific. For example, the large chondroitin sulfate proteoglycan produced by fibroblasts, versican, is characterized by different splice-variants of the core protein that increase complexity. Also, proteoglycan core proteins *in vivo* are subject to proteolytic attack so that fragmented proteoglycans may be found in pathological and even normal situations (Sandy et al., 2001).

The relative composition and structure of proteoglycans are modified during development. Carrino et al. (2000) demonstrated that intact decorin and biglycan proteoglycans extracted from human fetal skin were smaller

than the same molecules that were extracted from adult human skin. The deglycosylated core proteins were the same size, thus, indicating the presence of longer glycosaminoglycan chains. The ECM of fetal dermal tissue also contains a relatively higher content of the nonsulfated glycosaminoglycan hyaluronan (Adzick and Lorenz, 1994). Versican, the large chondroitin sulfate proteoglycan that is produced by fibroblasts is also relatively more abundant in fetal skin (Carrino et al, 2000; Sorrell et al., 1999b). This proteoglycan possesses a hyaluronan-binding domain that allows this proteoglycan to anchor hyaluronan in tissues (Heinegård and Oldberg, 1993). Tumor stromas contain activated fibroblasts that produce an ECM that differs from that of normal tissue. Adany et al. (1990) used monoclonal antibodies specific for discrete glycosaminoglycan epitopes to demonstrate that the composition of these molecules changed in the tumor stroma. Regional distribution of glycosaminoglycan epitopes were also found during human skin development and in adult human skin (Sorrell et al., 1990). Thus, fibroblasts regulate their microenvironments through the production of ECM molecules such as proteoglycans.

Fibroblast diversity also affects proteoglycan production. Decorin is differentially expressed by site-matched papillary and reticular dermal fibroblasts both at the protein and message levels (Schonherr et al., 1993). Cultured papillary and reticular dermal fibroblasts apportion decorin into both the medium and cell layer fractions (Fig. 4.7). Papillary fibroblasts release more decorin into the conditioned medium than do equivalent numbers of reticular fibroblasts. However, the differences in the amounts of decorin in the cell layer fractions are even more striking. The decorin produced by adult dermal fibroblasts is larger than the molecule extracted from adult skin, but is approximately the same size as the molecule extracted from fetal skin. The larger size is primarily due to a longer dermatan sulfate glycosaminoglycan chain. Reticular fibroblasts also appear to produce proportionally more versican than do papillary fibroblasts (Wang et al., 2008). Thus, the overall composition of ECM produced by these two subpopulations is different.

The production of ECM and proteinases has been assessed in multiple layers of the adult human dermis. Fibroblasts in the upper, middle, and lower thirds of the dermis produced significantly different amounts of mRNA for the α (XVI) of type XVI collagen (Akagi et al., 1999). Tajima and Pinnell (1981) quantified the amounts of type I and type III collagens produced by monolayer cultures, but found no differences to account for *in vivo* variations. In contrast, Bahar et al. (2004) extracted mRNA from multiple layers of the dermis and found differences in message levels for collagenase and for pro α 1 and pro α III collagens for the different layers. The highest levels of collagenase were found in the superficial papillary dermis. These studies provide evidence that extracellular matrices produced by subpopulations of fibroblasts vary, not only the compositions of

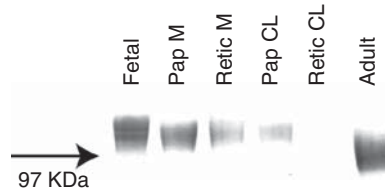


Figure 4.7 Differential decorin production by papillary and reticular dermal fibroblasts. Proteoglycans were extracted from the cell layer fraction and medium fraction of high-density papillary and reticular dermal fibroblast cultures. The extracts were electrophoresed on a 5–17.5% linear gradient sodium dodecyl sulfate-polyacrylamide gel under reducing conditions and were then transferred to a blotting membrane (Carrino et al., 2000, 2003). The blotting membrane was immunostained with decorin-specific antibody 6B6 (Seikagaku America, Falmouth, MA). Proteoglycans extracted from fetal and adult human skin are shown for comparison. The medium fraction for papillary cultures (Pap M) contains more decorin than the corresponding medium fraction for reticular cultures (Retic M). The cell layer fraction for papillary cultures (Pap CL) contains significantly more decorin than does the corresponding reticular cell layer fraction (Retic CL). Decorin produced by cultured dermal fibroblasts is slightly larger than that found in adult human skin. It is approximately the same size as the molecules found in fetal skin.

proteoglycans that they produced, but also differ in the compositions of other matrix molecules that interact with these proteoglycans.

Decorin binds and sequesters TGF- β 1 and interacts with type I collagen (Iozzo, 1997, 1998, 1999). Decorin knockout mice have a thin, fragile dermis in which collagen fiber bundles vary extensively in size and organization, a distinctly abnormal situation when compared with wild-type mice (Danielson et al., 1997). Thus, decorin has multiple functions in ECM that include direction of tissue organization and interactions with growth factors.

The papillary dermis and reticular dermis differ in both the composition and organization of their respective extracellular matrices. The papillary dermis is characterized by thin, poorly organized collagen fiber bundles, consisting primarily of type I and type III collagens, which contrast with the thick, well-organized fiber bundles in the reticular dermis (Cormack, 1987). Collagen fiber bundles in the papillary dermis contain more type III collagen than do those in the reticular dermis (Meigel et al., 1977). Other matrix molecules are also differentially apportioned between the papillary and reticular dermis. Immunohistochemical studies of normal adult skin highlight structural and compositional differences in proteoglycan deposition. The proteoglycan decorin is intensely expressed in the papillary dermis, but is otherwise dispersed between collagen fiber bundles in the reticular dermis. By contrast, versican associates with microfibrils in the papillary dermis, but is more extensively expressed in elastic fibers of the reticular dermis (Sorrell et al., 1999b; Zimmermann et al., 1994). The nonfibrillar collagen types XII

and XVI, along with tenascin-C, are characteristically found in the papillary dermis; whereas, collagen type IV and tenascin-X are primarily restricted to the reticular dermis (Akagi et al., 1999; Berthod et al., 1997; Grassel et al., 1999; Lethias et al., 1996; Lightner et al., 1993; Wälchli et al., 1994).

Human dermal fibroblasts are highly antigenic when injected into mice for the production of monoclonal antibodies. This laboratory made several attempts to produce cell-specific antibodies. Out of nearly 10,000 hybridoma clones that were analyzed for this project, nearly half of the clones produced antibodies that recognized various ECM molecules (unpublished results). Many of these antigens were common ECM molecules such as fibronectin and tenascin-C. Nonetheless, monoclonal antibodies were also produced that recognized unique components of ECM. One such antibody, termed PG-4, was found to recognize an epitope present on both chondroitin sulfate and dermatan sulfate glycosaminoglycan chains (Sorrell et al., 1999a). As such, this PG-4 antibody recognized all of the major interstitial proteoglycans produced by dermal fibroblasts: versican, decorin, and biglycan. The epitope was found to be highly expressed in chondroitin sulfate glycosaminoglycan chains that contained high levels of the rare oversulfated disaccharide known as chondroitin sulfate-D.

ECM molecules can delineate cellular subpopulations in tissues. One of the monoclonal antibodies produced against human dermal fibroblasts, termed BV-3, identified antigen localized around larger blood vessels of the dermis and it also identified antigen in the papillary dermal region (Fig. 4.8A and B). This antigen has yet to be fully characterized; however, it is produced by dermal fibroblasts (Fig. 4.8C). At low cellular density, the antigen is localized to intracellular vesicles; however, at high density, the antigen is released into ECM. This characteristic makes this antibody unsuitable for cellular separation studies, but it does help to define functional zones within tissues. Stenmark et al. (2006) have shown that adventitial region of pulmonary blood vessels contain discrete subpopulations of fibroblasts. Thus, the restricted presence of ECM molecules may identify another fibroblast subpopulation in the dermis.

6.2. Human dermal fibroblasts in tissue engineering

The ability of fibroblasts to generate and organize extracellular matrices and to produce growth factors/cytokines/chemokines makes these cells an essential component of tissue-engineered organs. In this regard, it is important to understand that fibroblasts cultured in typical monolayer fashion are physiologically different from fibroblasts that have been placed in a three-dimensional context (Geesin et al., 1993; Grinnell, 2003; Pinney et al., 2000). Fibroblasts in three-dimensional context produce a matrix that is more typical of that found *in vivo* and they interact more effectively with other cell types.

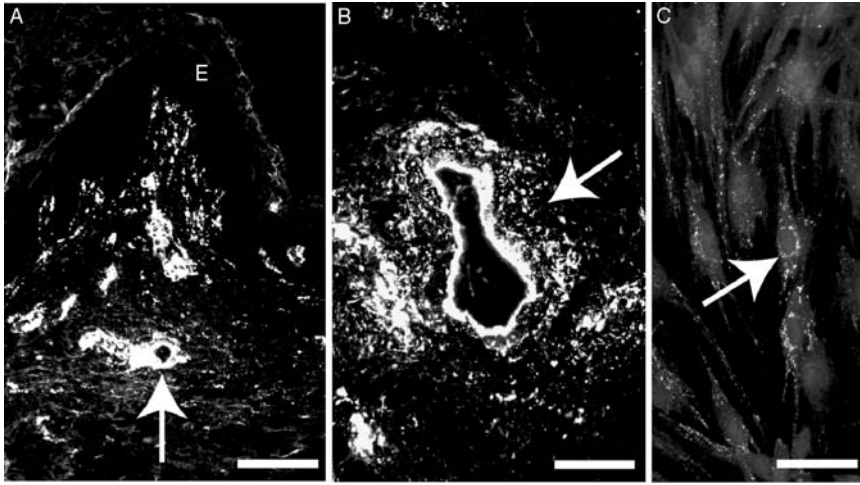


Figure 4.8 Vascular-associated fibroblast antigen. Monoclonal antibodies produced against human dermal fibroblasts (Sorrell et al., 2003a) recognize cellular subpopulations in skin. (A) Antibody BV-3 recognizes antigen in the regions around larger blood vessels (arrow) and in the papillary dermis adjacent to the epidermis (E). (B) At higher magnification, antigen is present in the fibroblast dominated adventitial layer surrounding larger blood vessels (arrow). (C) Cultured human dermal fibroblasts express the antigen in intracellular sites (arrow). Bars = 500 μm (A), 100 μm (B), and 50 μm (C).

The first example of a tissue-engineered organ was a bilayered skin equivalent. Bell and coworkers (Bell et al., 1979, 1983) fabricated a three-dimensional dermal equivalent by encasing dermal fibroblasts in a type I collagen matrix. Once the matrix gelled, fibroblasts actively began to contract the matrix to create a more solid structure. It was found that partially contracted collagen gels provided a superior substrate on which keratinocytes attached, proliferated, and differentiated into a multilayered epidermal-like structure. Asselineau et al. (1986) found that elevation of this bilayered structure to the air-liquid interface enabled the epidermis to undergo its full repertoire of differentiation.

Once constructed, bilayered skin equivalents can be subjected to experimental manipulations as a means to better understand epithelial/mesenchymal interactions that occur during wound repair (Section 5.1). In addition to their use in basic biological studies, skin equivalents have proven to be useful as a full-thickness skin replacement in situations where large areas of skin have been lost (Boyce, 1996; Boyce and Warden, 2002). The dermal component of these skin equivalents is also essential for facilitating the ingrowth of host vasculature in grafting situations (Démarchez et al., 1992). Fibroblasts that have been placed in a three-dimensional context produced elevated levels of proangiogenic factors compared with the same

fibroblasts cultured as monolayers (Pinney et al., 2000). Thus, the presence of fibroblasts in tissue-engineered constructs may facilitate their vascularization. In order to enhance vascularization, methods are being developed to generate vascular structures in the dermal equivalent prior to grafting (Black et al., 1999; Hudon et al., 2003; Supp et al., 2002). Ideally, this would greatly increase the rate at which the graft becomes vascularized by the host. Tremblay et al. (2005) demonstrated that such engineered vasculature could connect with host vasculature through the process of inosculation. The use of fibroblasts in tissue-engineered constructs raises the issue of whether selected subpopulations of these cells might perform more effectively in specific situations. Currently, little is known on this topic; therefore, it is an area of research interest in the future.

7. THY-1⁺ AND THY-1⁻ SUBPOPULATIONS OF FIBROBLASTS

Fibroblast diversity exists in organs other than skin. As discussed above (Section 4), Fritsch et al. (1999) cloned physiologically functionally distinct subpopulations of fibroblasts from human small intestinal tissue. Others have shown that various organs, such as the lungs (Fries et al., 1994; Rege and Hagood, 2006), spleen (Borrello and Phipps, 1996), liver (Dudas et al., 2007), and female reproductive system (Koumas et al., 2001; Malmstrom et al., 2007) contain at least two subpopulations of fibroblasts based either upon the expression of Thy-1 (Thy-1⁺) or lack of expression of this antigen (Thy-1⁻). Thy-1, also known as CD90, is a glycoposphatidylinositol-linked glycoprotein of the cell surface that is differentially expressed on neurons, lymphocytes, and fibroblasts (Barker et al., 2004; Rege and Hagood, 2006). The differential expression of Thy-1/CD90 positive and negative cells is not a uniform characteristic of all tissues. All dermal fibroblasts express this antigen; consequently, the use of this cell surface marker to separate subpopulations of dermal fibroblasts is not effective.

Much of our understanding of the differences between Thy-1⁺ and Thy-1⁻ fibroblasts has been based on studies of rodent lungs (Fries et al., 1994; Rege and Hagood, 2006; Sempowski et al., 1995). Normal fibroblasts from rodent lungs exhibit differences in size, shape, production, and response to cytokines, and the ability to accumulate lipids. Thus, these fibroblasts can potentially be identified and separated on the basis of these characteristics. However, Phipp's group found that it was possible to separate these cells by fluorescence-activated cell sorting using the expression or lack of expression of Thy-1 as a cellular marker (Fries et al., 1994; Penney et al., 1992; Sempowski et al., 1996).

Thy-1⁺ fibroblasts isolated from rat lungs accumulated Oil Red O positive lipid droplets in culture in contrast with Thy-1⁻ cells. TNF- α stimulation resulted in the upregulation of IL-1 α message and protein in Thy-1⁻ cells, but not Thy-1⁺ cells (Fries et al., 1994). However, both populations produced equivalent amounts of another potent inflammatory factor, IL-6. This implied that these cells might differentially respond to pulmonary inflammation. This became more evident as it was shown that Thy-1⁻ fibroblasts secreted more latent TGF- β 1 and were more efficient in activating this latent TGF- β 1 in response to fibrogenic stimuli (Silvera et al., 1994). These cells also expressed platelet-derived growth factor- α receptor at higher levels than do Thy-1⁺ cells and proliferated more extensively in response to platelet-derived growth factor-AA (Zhou et al., 2004). Also, Thy-1⁻ pulmonary cells alone could be induced to differentiate into myofibroblasts.

Cumulatively, these characteristics indicate that the Thy-1⁻ subpopulation represents a fibrogenic phenotype that appears to be responsible for fibrosis in lung pathologies. Interferon- γ , which is secreted by T-helper cells, induced increased expression of MHC class II antigens on the surfaces of these Thy-1⁻ cells. Further, Thy-1^(-/-) mice exhibited more severe lung fibrosis than did wild-type control mice, all of which provides further evidence for a fibrogenic role for a select subpopulation of pulmonary fibroblasts (Hagood et al., 2005). Thus, pathological tissue fibrosis may result in the activation or hyperproliferation of a specific fibroblast subpopulation. In contrast, pulmonary Thy-1⁺ fibroblasts expressed characteristics in terms of their size, shape, and ECM production that were more typical of traditional fibroblasts.

The fibrocyte is a fibroblast-like cell (Section 2.3) that originates in bone marrow and circulates as a monocytes-like cell (Chesny et al., 1997). These cells, like the pulmonary Thy-1⁻ cells, express MHC class II antigens and appear to be present in higher than normal levels in fibrotic situations. Thus, it is essential that present and future studies take into account the origin of fibroblasts in a particular tissue to determine whether it is an innate cell of that organ, or whether it is an immigrant.

Koumas et al. (2001, 2003) found that Thy-1/CD90 was differentially expressed by fibroblasts in the adult human female reproductive tract and that this marker could be used to separate myofibroblastic and lipofibroblastic phenotypes from this organ. Dudas et al. (2007) found that Thy-1⁺ was an *in vivo* and *in vitro* marker for normal rat hepatic myofibroblasts. As such, the Thy-1⁺ cells were confined to perivascular regions of the liver. Thus, these cells might conform to either pericytes and/or smooth muscle cells. The function of Thy-1/CD90 on the surfaces of fibroblasts is not well understood. It has been proposed that it might regulate cellular adhesions, cytoskeletal organization, and cellular migration.

8. FIBROBLASTS AS SENTINEL CELLS

8.1. Fibroblast interactions with immunocompetent cells

Phipps and coworkers (Cao et al., 1998; Fries et al., 1995) noted that subsets of fibroblasts from various tissues expressed CD40, an antigen that participates in communication of stromal cells with T cells. Further, they developed the concept that subsets of fibroblasts actively participated in inflammatory responses, thus serving as sentinel cells which interact with dendritic cells and other immunocompetent cells (Silzle et al., 2004; Smith et al., 1997). In this regard, Parsonage et al. (2005) proposed that fibroblastic conversations with inflammatory cells may either temper or promote inflammatory interactions. In such interactions, fibroblasts respond to multiple factors such as IL-1, IL-6, and TNF- α by modifying their own output of immunoregulatory factors. These include both inflammatory cytokines and chemokines. In this manner, fibroblasts integrate inflammatory signals in order to modulate various aspects of wound repair.

The mechanism by which fibroblasts functionally interact with T cells is not well understood. However, coculture models have begun to shed light on this issue. Normal adult skin contains resident T cells that are thought to participate in immunosurveillance of this organ. Clark et al. (2006) discovered that they could establish three-dimensional cultures when skin explants were seated onto acellular scaffolding material. Fibroblast invasion of the scaffolding preceded the ingress of resident T cells from the skin explant. Invasive T cells expressed CD45RO, an indication that they were memory T cells. Dermal fibroblast that had established themselves in the three-dimensional scaffolding attracted the T cells from the explant through the release of cytokines and chemokines. These factors included: IL-8, interferon-inducible protein-10, monocyte chemoattractant protein-1, -3, and macrophage inflammatory protein-3 α . In a subsequent study (Clark and Kupper, 2007), it was found that cultured human dermal fibroblasts supported the proliferation of this T cell population in a manner that did not require antigen recognition when IL-15 was added to the coculture medium. These results further emphasize the fibroblast partnership with immunocompetent cellular populations in both normal and pathological situations.

8.2. Fibroblast regulation of neuropeptides

Terminal nerve endings in the highly innervated superficial dermis and the epidermis of skin release neuropeptides, such as substance P, neurokinin A, vasoactive intestinal polypeptide, and α calcitonin gene-related peptide into this region (Wallengren, 1999). These neuropeptides promote cellular

proliferation of both fibroblasts and keratinocytes (Nilsson et al., 1985; Scholzen et al., 1998) and to stimulate fibroblast migration (Kahler et al., 1993). As such, they may play a role in hyperproliferative disorders of the epidermis and dermal pathologies such as scleroderma (Peters et al., 2006), and they help to mediate events during contact allergic reactions in this region (Wallengren, 1999). Terminal nerve endings release neuropeptides into the dermal papillae of hair follicles, thus helping to regulate hair growth (Paus et al., 1999).

Neuropeptide function depends upon their strict regulation. This regulation in large part depends upon a limited lifespan for these factors. This is regulated by extracellular peptidases that are situated at sites of neuropeptide release (Scholzen et al., 1998). Fibroblast- and keratinocyte-associated ectopeptidases play an important role in this process. Ectopeptidases are integral membrane cell surface proteins that regulate the cleavage of either terminal amino acids from peptides or regulate internal cleavage of specific peptides (De Meester et al., 1999; Riemann et al., 1999). Functional ectopeptidases that have been identified in skin include: aminopeptidase N/CD13, dipeptidyl peptidase IV/CD26, FAP, and neutral endopeptidase/CD10 (Olerud et al., 1999; Sorrell et al., 2003a).

Monoclonal antibodies raised against human dermal fibroblasts recognize APN/CD13 as a cell surface antigen (Piela-Smith et al., 1995; Sorrell et al., 2003a). The functional activity of ectopeptidases has been demonstrated by cultured human dermal fibroblasts (Raynaud et al., 1992; Sorrell et al., 2003b). Ectopeptidase activity on live dermal fibroblasts is regulated by inflammatory cytokines and glucocorticoids, which is to be expected given their role in wound repair, inflammation, and allergic reactions. Studies have shown that the activity of APN/CD13 peptidase is upregulated by exposing cells to IL-4, interferon- γ , and dexamethasone (Sorrell et al., 2003b; Stefanović et al., 1998). This enzyme catalyzes the removal of an N-terminal alanine, although other amino acids such as arginine can also be removed. Neurokinin A and IL-8 have been shown to be natural substrates for this enzyme (Hoffmann et al., 1993; Kanayama et al., 1995; Riemann et al., 1999; Russell et al., 1996; Scholzen et al., 1998; Wallengren, 1999). However, DPPIV/CD26 activity expressed by the same cellular populations was unaffected by these factors; instead, it is upregulated by IL-1. This enzyme catalyzes the removal of glycine-proline dipeptides from N-termini of small peptides. Native peptide targets for this enzyme are RANTES and eotaxin (Hoffmann et al., 1993; Mentlein, 1999; Proost et al., 1998, 2000; Saison et al., 1983). Thus, fibroblasts play an important role in tissues by regulating the function of neuropeptides (Scholzen et al., 2001).

The expression of APN/CD13 by fibroblasts is not restricted to human skin. Atherton et al. (1992, 1994), in studies of developing human breast tissue, found that APN/CD13 expressing fibroblasts were intimately associated with developing glandular epithelial structures. In contrast, interstitial stromal

fibroblasts did not express this antigen. In human skin, immunohistochemical and histochemical evidence places APN/CD13 primarily at the dermal–epidermal junction (Sorrell et al., 2003a). This suggests that APN/CD13 plays a significant role in regulating epithelial/mesenchymal interactions.

9. FIBROBLASTS IN AGING

Much of our information regarding the cellular role in the aging process is derived from skin fibroblasts. This is due to the ready accessibility of these cells and to ease by which they can be cultured. Furthermore, human skin is a primary indicator of aging; aged skin tends to become roughened and wrinkled and displays laxity and uneven discoloration (Fisher et al., 2008). However, skin, because of its exterior location, is susceptible to two types of aging (Gilchrest, 1996), intrinsic or chronological aging and extrinsic or environmentally induced aging. Both of these aging processes have a direct functional impact on dermal fibroblasts.

Normal human skin from variously aged donors contains fibroblasts which display variability in culture with respect to their replicative longevity (Bayreuther et al., 1988, 1991; Rodemann et al., 1989). The presence of these diverse subpopulations raises the issue as to what extent this might be due to intrinsic aging. In other words, does the percentage of fibroblasts with shorter replicative lifespans increase with advancing chronological aging? Some studies, such as the ones by the Rodemann group (Nolte et al., 2008) suggest that there are an increased proportion of nonreplicative fibroblasts due to chronological aging. Cristofalo et al. (1998) addressed this issue by measuring the maximum number of population doubling for fibroblasts obtained from donors of different ages. The fibroblasts used in their study were obtained from the Baltimore Longitudinal Study of Aging where all donors were medically examined and declared healthy with respect to the study protocol. Further the cells used for comparison were obtained from the same anatomic site. They found diversity in replicative lifespan of fibroblasts in all donor samples, irregardless of donor age. More significantly, they found no increase in the percentage of populations that exhibited shortened replicative lifespans as a function of donor age. The question then becomes whether assays of replicative lifespans are the best marker of aging. Recent studies (Clark, 2008) have shown that environmental factors in which cells are exposed to oxidative stress can induce replicative senescence. Consequently, analyses of aging that rely exclusively on this phenomenon may not provide the best assay for aging.

Borlon et al. (2008) sought to find a method to identify age-specific markers in fibroblasts and simultaneously to disassociate these from chronological aging markers. They incorporated human dermal fibroblasts from

different aged donors into three-dimensional collagen gels and exposed one set of gels to repeated UVB exposure. Comparison of global gene array results of UVB- and nonexposed cultures led to their identification of five transcripts that were upregulated from chronologically older donors: TGF- β 1, transgelin, dermatopontin, glutathione peroxidase, and TNF receptor superfamily 1A. Genes affected by UVB exposure were identified as MMP-3 (upregulated), COL3A1, COL1A1, connective tissue growth factor, and fibromodulin (latter all downregulated). The upregulation of proteinases and downregulation of ECM molecules have been observed in other studies of aging skin (Ashcroft et al., 1997a,b; Varani et al., 2006). Varani and his group (Fisher et al., 2009; Varani et al., 2004, 2006) proposed that the consequences of ECM changes affected fibroblast phenotypic behavior in the dermis. They asserted that fibroblasts situated in a damaged matrix were no longer subjected to mechanical stretching via integrin-collagen interactions. Since stretching of fibroblasts results in a more metabolically active cell (Grinnell, 2003), ECM damage that surround fibroblasts may have profound effect on their behavior in skin. However, it is not clear how this might affect the behavior of these cells once they have been removed from the skin for culture. The dermis of individuals of advanced age becomes thinner than that of younger individuals (Ashcroft et al., 1997a; Gilchrist, 1996). This implies that physiological changes, such as in ECM metabolism, of fibroblasts may be a part of chronological aging *in vivo*. However, it is not clear to what extent these manifestations are reflected in fibroblasts that are isolated and cultured from aging tissues.

Extrinsic aging of skin is a major issue in those regions that are chronically exposed to UV irradiation (Fisher et al., 2008). Acute UV irradiation induces the formation of “sunburn” cells in both the epidermis and dermis (Bernerd and Asselineau, 1997). These cells become apoptotic and disappear. Nearby fibroblasts may be influenced by “sunburn cells.” Bernerd and Asselineau (1997, 1998), using a skin equivalent model, demonstrated that fibroblasts at the bottom of UV-exposed skin equivalents began to proliferate and migrated upwards. Also, increased levels of MMP-1 were detected in exposed samples. Increased proteinase activity at chronic UV-exposed sites of skin has been noted in other studies. One consequence of degradative activity by dermal cells is the loss of structural elements, which results in increased laxity and wrinkle formation. An example of degradative effects is shown in Fig. 4.9. This figure compares human skin taken from a sun-protected site (postauricular skin) with skin taken from a nearby chronically sun-exposed site (preauricular skin). Dermal architecture near the dermal/epidermal junction region is stabilized by an elaborate network of microfibrillar structures that insert into the basal aspect of the epidermis (Watson et al., 1999; Zimmermann et al., 1994). One of the components of these microfilaments is the large chondroitin sulfate proteoglycan versican. Another component of these microfilaments is fibrillin-1. In sun-exposed

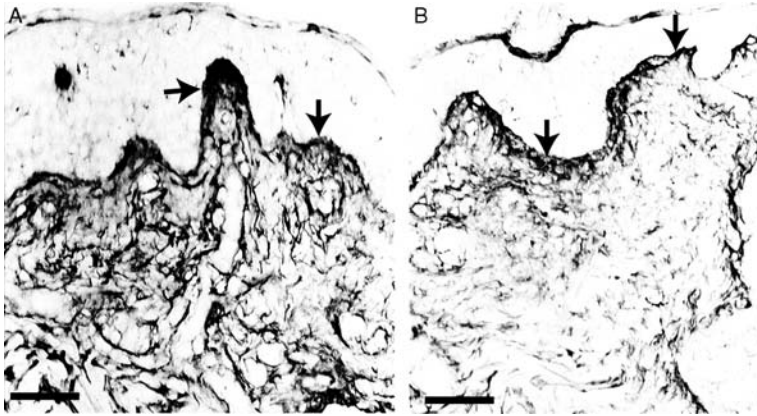


Figure 4.9 Extrinsic aging of human skin. Dermal fibroblasts play a role in the aging of human skin (Fisher et al., 2008, 2009; Varani et al., 2004, 2006). (A) In sun-protected postauricular human skin, amorphous deposits of the large proteoglycan versican (antibody 2B1, Seikagaku America, Falmouth, MA) appear at the DEJ-region (arrows). In addition, versican is organized into a complex array of microfilaments in the papillary dermis. (B) In sun-exposed preauricular skin from the same individual, these versican containing microfilaments have disappeared; however, amorphous deposits of versican remain (arrows). Bars = 100 μm .

sites, this network of microfilaments is absent. This implies that adjacent dermal fibroblasts release proteolytic enzymes that degrade structural elements other than collagens. In other words, fibroblasts, in addition to building ECM, also play a prominent role in the deconstruction of ECM. In order to effectively understand the aging process in skin, it is necessary to better understand the biology of fibroblasts and their responses to environmental factors. The consequences of environmental exposure may also influence the phenotypes of fibroblasts cultured from the skin.

Dermal fibroblasts play a central role in the etiology of nonhealing chronic wounds. Fibroblasts taken from nonhealing chronic wound sites exhibit characteristics of the senescent phenotype whereas dermal fibroblasts taken from nearby normal skin do not display this characteristic (Ågren and Werthén, 2007; Hasan et al., 1997). Wall et al. (2008) performed comparative global gene array analyses on senescent dermal fibroblasts from chronic wound sites and normal adjacent fibroblasts. They found that the expression of genes involved in cellular aging/cell-cycle regulation, oxidative stress, and cytoskeletal genes was significantly modified in the chronic wound fibroblasts. Phenotypic characteristics of senescent fibroblasts include large, epithelioid size and shape, highly expressed cytoplasmic filaments, poor migration characteristics, and inability to divide. The gene profiles appeared to account for these characteristics. More interesting was the evidence of genes associated with oxidative stress. Oxidative stress was compared for chronic wound fibroblasts and normal fibroblasts in a cytochrome *c*

reduction assay for superoxide radical generation over a 10-day period. This assay demonstrated elevated levels of radical generation for chronic wound fibroblasts. They also noted that the exposure of cells to superoxide radicals could induce the senescent phenotype for cells. They proposed that fibroblasts in chronic wound sites are exposed to infectious agents that might increase the population of “aged” cells through the release of oxidation factors. Thus, aging in this respect may be, at least partially, due to localized environmental factors. Understanding the role of the fibroblast in this healing process will hasten our understanding of this increasingly important area of health maintenance.

A manifestation of aging is the formation of advanced glycation end products (AGEs) that result from the nonenzymatic reaction between reducing sugars and amino groups of proteins based upon the Maillard reaction (Jeanmaire et al., 2001). AGEs constitute a heterogeneous group of structures that accumulate with advancing age both in ECM and inside cells (Bucciarelli et al., 2002). Thus, the accumulation of AGEs has the potential of modifying cellular physiology. Intracellular AGEs induce oxidative stress, activate NF- κ B, and produce lipid peroxidation products (Kasper and Funk, 2001). Kueper et al. (2007) demonstrated that the FSP-1 vimentin was a target of intracellular AGE modification. This resulted in the retention and redistribution of defective vimentin which may contribute to the loss of cellular contraction and migration capabilities of the affected cells. Thus, there is now substantive evidence that fibroblasts are targets for both intrinsic and extrinsic aging events. This feature needs to be taken into account in any *in vitro* study of fibroblasts and fibroblast subpopulations.

Aging of adult human dermal fibroblasts may affect selected subpopulations. In consequence, the influence of aging on site-matched papillary and reticular dermal fibroblasts was studied by Mine et al. (2008). They found that papillary dermal fibroblasts were more affected by aging than were reticular fibroblasts. With advancing age papillary dermal fibroblasts became more heterogeneous in their size profile, grew in culture at a slightly slower rate. Aging papillary dermal fibroblasts produced increased amounts of KG-1 and VEGF-A in contrast to reticular fibroblasts which did not differ in the production of these factors. Papillary fibroblasts also upregulated their production of the MMPs-1, -2, and -3, as well as, increases in the levels of tissue inhibitors of metalloproteinases-1 and -2 in comparison to reticular fibroblasts from the same piece of skin. Reticular fibroblast interactions with epidermal cells in the bilayered skin equivalents resulted in a slightly thinner epidermis that was less well differentiated. Thus, the loss of the papillary fibroblast phenotype in aged skin might account for the characteristic thinning of the epidermis and loss of rete ridges (Montagna and Carlisle, 1979). This suggests that analyses of nonselected fibroblast populations, as has been performed in most studies, might miss salient functional changes that occur during fibroblast aging.

10. CONCLUDING REMARKS

Fibroblast diversity is a natural and pervasive feature that complicates our understanding of how these cells function. Although our understanding of fibroblast physiology is still limited, it is now clear that they play two essential roles: communication with other cells and the production and organization of ECM. Both of these properties position fibroblasts to have a central role in the advancing field of tissue engineering. In addition, fibroblasts play a role in tissue fibrosis and they are a critical component of tumors. Finally, fibroblasts are a barometer for aging. Taken together, these characteristics underline the central role of fibroblasts in tissue biology.

ACKNOWLEDGMENTS

We wish to acknowledge the support of L'Oréal Life Sciences and NIH Grant AG021542 for portions of this work.

REFERENCES

- Adany, R., Heimer, R., Caterson, B., Sorrell, J.M., Iozzo, R.V., 1990. Altered expression of chondroitin sulfate proteoglycan in the stroma of human colon carcinoma. *J. Biol. Chem.* 265, 11389–11396.
- Adzick, N.S., Lorenz, H.P., 1994. Cells, matrix, growth factors, and the surgeon. The biology of scarless fetal wound repair. *Ann. Surg.* 220, 10–18.
- Ågren, M.S., Werthén, M., 2007. The extracellular matrix in wound healing: a closer look at therapeutics for chronic wounds. *Int. J. Low. Extrem. Wounds* 6, 82–97.
- Akagi, A., Tajima, S., Ishibashi, A., Yamaguchi, N., Nagai, Y., 1999. Expression of type XVI collagen in human skin fibroblasts: enhanced expression in fibrotic skin diseases. *J. Invest. Dermatol.* 113, 246–250.
- Amadeu, T.P., Coulomb, B., Desmoulière, A., Costa, A.M.A., 2003. Cutaneous wound healing: myofibroblastic differentiation and *in vitro* methods. *Int. J. Low. Extrem. Wounds* 2, 60–68.
- Angel, P., Szabowski, A., 2002. Function of AP-1 target genes in mesenchymal–epithelial cross-talk in skin. *Biochem. Pharmacol.* 64, 949–956.
- Ashcroft, G.S., Horan, M.A., Ferguson, M.W.J., 1997a. Aging is associated with reduced deposition of specific extracellular matrix components, an upregulation of angiogenesis, and an altered inflammatory response in a murine incisional wound healing model. *J. Invest. Dermatol.* 108, 430–437.
- Ashcroft, G.S., Horan, M.A., Herrick, S.E., Tamuzzer, R.W., Schultz, G.S., Ferguson, M. W.J., 1997b. Age-related differences in the temporal and spatial regulation of matrix metalloproteinases (mmps) in normal skin and acute cutaneous wounds of healthy humans. *Cell Tissue Res.* 290, 581–591.
- Asselineau, D., Bernard, B.A., Bailly, C., Darmon, M., Prunieras, M., 1986. Human epidermis reconstructed by culture: is it “normal”? *J. Invest. Dermatol.* 86, 181–186.

- Atherton, A.J., Monaghan, P., Warburton, M.J., Gusterson, B.A., 1992. Immunocytochemical localization of the ectoenzyme aminopeptidase N in the human breast. *J. Histochem. Cytochem.* 40, 705–710.
- Atherton, A.J., Anbazhagan, R., Monaghan, P., Bartek, J., Gusterson, B.A., 1994. Immunolocalisation of cell surface peptidases in the developing human breast. *Differentiation* 56, 101–106.
- Aumailley, M., Rousselle, P., 1999. Laminins of the dermo-epidermal junction. *Matrix Biol.* 18, 19–28.
- Azzarone, B., Macieira-Coelho, A., 1982. Heterogeneity of the kinetics of proliferation within human skin fibroblastic cell populations. *J. Cell Sci.* 57, 177–187.
- Badiavas, E.V., Abedi, M., Butmarc, J., Falanga, V., Quesenberry, P., 2003. Participation of bone marrow derived cells in cutaneous wound healing. *J. Cell. Physiol.* 196, 245–250.
- Bahar, M.A., Bauer, B., Tredget, E.E., Ghahary, A., 2004. Dermal fibroblasts from different layers of human skin are heterogeneous in expression of collagenase and types I and III procollagen mma. *Wound Repair Regen.* 12, 175–182.
- Balin, A.K., Fisher, A.J., Anzelone, M., Leong, I., Allen, R.G., 2002. Effects of establishing cell cultures and cell culture conditions on the proliferative life span of human fibroblasts isolated from different tissues and donors of different ages. *Exp. Cell Res.* 274, 275–287.
- Ballard, V.L.T., Sharma, A., Duignan, I., Holm, J.M., Chin, A., Choi, R., et al., 2006. Vascular tenascin-C regulates cardiac endothelial phenotype and neovascularization. *FASEB J.* 20, 717–719.
- Barker, T.H., Pallero, M.A., MacEwen, M.W., Tilden, S.G., Woods, A., Murphy-Ullrich, J.E., et al., 2004. Thrombospondin-1-induced focal adhesion disassembly in fibroblasts requires Thy-1 surface expression, lipid raft integrity, and Src activation. *J. Biol. Chem.* 279, 23510–23516.
- Bayreuther, K., Rodmann, H.P., Francz, P.I., Maier, K., 1988. Differentiation of fibroblast stem cells. *J. Cell Sci.* 10, 115–130.
- Bayreuther, K., Francz, P.I., Gogol, J., Hapke, C., Maier, M., Meinrath, H.G., 1991. Differentiation of primary and secondary fibroblasts in cell culture systems. *Mutat. Res.* 256, 233–242.
- Bell, E., Ivarsson, B., Merrill, C., 1979. Production of a tissue-like structure by contraction of collagen lattices by human fibroblasts of different proliferative potential *in vitro*. *Proc. Natl. Acad. Sci. USA* 76, 1274–1278.
- Bell, E., Sher, S., Hull, B., Merrill, C., Rosen, S., Chamson, A., et al., 1983. The reconstitution of living skin. *J. Invest. Dermatol.* 81, 2s–10s.
- Bernerd, F., Asselineau, D., 1997. Successive alteration and recovery of epidermal differentiation and morphogenesis after specific UVB-damages in skin reconstructed *in vitro*. *Dev. Biol.* 183, 123–138.
- Bernerd, F., Asselineau, D., 1998. UVA exposure of human skin reconstructed *in vitro* induces apoptosis of dermal fibroblasts: subsequent connective tissue repair and implications in photoaging. *Cell Death Differ.* 5, 792–802.
- Berthod, F., Germain, L., Guignard, R., Lethias, C., Garrone, R., Damour, O., et al., 1997. Differential expression of collagens XII and XIV in human skin and in reconstructed skin. *J. Invest. Dermatol.* 108, 737–742.
- Bianco, P., Riminucci, M., Gronthos, S., Robey, P.G., 2001. Bone marrow stromal stem cells: nature, biology, and potential applications. *Stem Cells* 19, 180–192.
- Bishop, E.T., Bell, G.T., Bloor, S., Broom, I.J., Hendry, N.F.K., Wheatley, D.N., 1999. An *in vitro* model of angiogenesis: basic features. *Angiogenesis* 3, 335–344.
- Bissell, M.J., Radisky, D.C., Rizki, A., Weaver, V.M., Peterson, O.W., 2002. The organizing principal: microenvironmental influences in the normal and malignant breast. *Differentiation* 70, 537–546.

- Black, A.F., Berthod, F., L'Heureux, N., Germain, L., Auger, F.A., 1999. *In vitro* reconstruction of a human capillary-like network in a tissue-engineered skin equivalent. *FASEB J.* 12, 1331–1340.
- Blomme, E.A.G., Sugimoto, Y., Lin, Y.C., Capen, C.C., Rosol, T.J., 1999a. Parathyroid hormone-related protein is a positive regulator of keratinocyte growth factor expression by normal dermal fibroblasts. *Mol. Cell. Endocrinol.* 152, 189–197.
- Blomme, E.A.G., Zhou, H., Kartsogiannis, V., Capen, C.C., Rosol, T.J., 1999b. Spatial and temporal expression of parathyroid hormone-related protein during wound healing. *J. Invest. Dermatol.* 112, 788–795.
- Borlon, C., Weemaels, G., Godard, P., Debacq, F., Lemaire, P., Deroanne, C., et al., 2008. Expression profiling of senescent-associated genes in human dermis from young and old donors. Proof-of-concept study. *Biogerontology* 9, 197–208.
- Borrello, M.A., Phipps, R.P., 1996. Differential Thy-1 expression by splenic fibroblasts defines functionally distinct subsets. *Cell. Immunol.* 173, 198–206.
- Botchkarev, V.A., 2003. Bone morphogenetic proteins and their antagonists in skin and hair follicle biology. *J. Invest. Dermatol.* 120, 35–47.
- Boyce, S.T., 1996. Cultured skin substitutes: a review. *Tissue Eng.* 2, 255–266.
- Boyce, S.T., Warden, G.D., 2002. Principles and practices for treatment of cutaneous wounds with cultured skin substitutes. *Am. J. Surg.* 183, 445–456.
- Bucciarelli, L.G., Wendt, T., Rong, L., Lalla, E., Hofmann, M.A., Goova, M.T., et al., 2002. RAGE is a multiligand receptor of the immunoglobulin superfamily: implications for homeostasis and chronic disease. *Cell. Mol. Life Sci.* 59, 1117–1128.
- Burgeson, R.E., Christiano, A.M., 1997. The dermal–epidermal junction. *Curr. Opin. Cell Biol.* 9, 651–658.
- Cao, H.J., Wang, H.S., Zang, Y., Lin, H.Y., Phipps, R.T., Smith, T.J., 1998. Activation of human orbital fibroblasts through CD40 engagement results in a dramatic induction of hyaluronan synthesis and prostaglandin endoperoxide H synthase-2 expression. *J. Biol. Chem.* 273, 29615–29625.
- Caplan, A.I., 2005. Mesenchymal stem cells. In: R. Lanza, J. Gearhart, B. Hogan, D. Melton, R. Pedersen, J. Thomason, (Eds.), *Essentials of Stem Cell Biology*, Elsevier Academic Press, Burlington, MA, pp. 205–210.
- Caplan, A.I., 2007. Adult mesenchymal stem cells for tissue engineering versus regenerative medicine. *J. Cell. Physiol.* 213, 341–347.
- Carrino, D.A., Sorrell, J.M., Caplan, A.I., 2000. Age-related changes in the proteoglycans of human skin. *Arch. Biochem. Biophys.* 373, 91–101.
- Carrino, D.A., Onnerfjord, P.I., Sandy, J.D., Cs-Szabo, G., Scott, P.G., Sorrell, J.M., et al., 2003. Age-related changes in the proteoglycans of human skin. Specific cleavage of decorin to yield a major catabolic fragment in adult skin. *J. Biol. Chem.* 278, 17566–17772.
- Chang, H.Y., Chi, J.T., Dudoit, S., Bondre, C., van de Rijn, M., Botstein, D., et al., 2002. Diversity, topographic differentiation, and positional memory in human fibroblasts. *Proc. Natl. Acad. Sci. USA* 99, 12877–12882.
- Chesney, J., Bacher, M., Bender, A., Bucala, R., 1997. The peripheral blood fibrocyte is a potent antigen-presenting cell capable of priming naive T cells *in situ*. *Proc. Natl. Acad. Sci. USA* 94, 6307–6312.
- Chinnathambi, S., Tomanek-Chalkley, A., Ludwig, N., King, E., DeWaard, R., Johnson, G., et al., 2003. Recapitulation of oral mucosal tissues in long-term organotypic culture. *Anat. Rec.* 270A, 162–174.
- Christ, B., Scaal, M., 2009. Formation and differentiation of avian somite derivatives. *Adv. Exp. Med. Biol.* 638, 1–29.
- Clark, R.A.F., 2008. Oxidative stress and “senescent” fibroblasts in non-healing wounds as potential therapeutic targets. *J. Invest. Dermatol.* 128, 2361–2364.

- Clark, R.A., Kupper, T.S., 2007. IL-15 and dermal fibroblasts induce proliferation of natural regulatory T cells isolated from human skin. *Blood* 109, 194–202.
- Clark, R.A., Chong, B.F., Mirchandani, N., Yamanaka, K.I., Murphy, G.F., Dowgiert, R. K., et al., 2006. A novel method for the isolation of skin resident T cells from normal and diseased human skin. *J. Invest. Dermatol.* 126, 1059–1070.
- Conrad, G.W., Hamilton, C., Haynes, E., 1977a. Differences in glycosaminoglycans synthesized by fibroblast-like cells from chick cornea, heart, and skin. *J. Biol. Chem.* 252, 6861–6870.
- Conrad, G.W., Hart, G.W., Chen, Y., 1977b. Differences *in vitro* between fibroblast-like cells from cornea, heart, and skin of embryonic chicks. *J. Cell Sci.* 26, 119–137.
- Contard, P., Bartel, R.L., Jacobs, L. II, Perlish, J.S., Macdonald, E.D. II, Handler, L., et al., 1993. Culturing keratinocytes and fibroblasts in a three-dimensional mesh results in epidermal differentiation and formation of a basal lamina-anchoring zone. *J. Invest. Dermatol.* 100, 35–39.
- Cormack, D.H., 1987. The integumentary system. In: Ham's Histology, ninth ed. J.B. Lippincott Company, Philadelphia, PA, pp. 450–474.
- Costea, D.E., Loro, L.L., Dimba, E.A.D., Vintermyr, O.K., Johannessen, A.C., 2003. Crucial effects of fibroblasts and keratinocyte growth factor on morphogenesis of reconstituted human oral epithelium. *J. Invest. Dermatol.* 121, 1479–1486.
- Couchman, J.R., 1986. Rat hair follicle dermal papillae have an extracellular matrix containing basement membrane components. *J. Invest. Dermatol.* 87, 762–767.
- Covas, D.T., Panepucci, R.A., Fontes, A.M., Silva, W.A., Orellana, M.D., Freitas, M.C.C., et al., 2008. Multipotent mesenchymal stromal cells obtained from diverse human sites share functional properties and gene-expression profile with CD146⁺ perivascular cells and fibroblasts. *Exp. Hematol.* 36, 642–654.
- Cristofalo, V.J., Allen, R.G., Pignolo, R.J., Martin, B.G., Beck, J.C., 1998. Relationship between donor age and the replicative lifespan of human cells in culture: a reevaluation. *Proc. Natl. Acad. Sci. USA* 95, 10614–10619.
- Danielson, K.G., Baribault, H., Holmes, D.F., Graham, H., Kadler, K.E., Iozzo, R.V., 1997. Targeted disruption of decorin leads to abnormal collagen fibril morphology and skin fragility. *J. Cell Biol.* 136, 729–743.
- Darby, I.A., Hewitson, T.D., 2007. Fibroblast differentiation in wound healing and fibrosis. *Int. Rev. Cytol.* 257, 143–179.
- Davie, N.J., Gerasimovskaya, E.V., Hofmeister, S.E., Richman, A.P., Jones, P.L., Reeves, J.T., et al., 2006. Pulmonary artery adventitial fibroblasts cooperate with vasa vasorum endothelial cells to regulate vasa vasorum neovascularization. A process mediated by hypoxia and endothelin-1. *Am. J. Pathol.* 168, 1793–1807.
- Démarchez, M., Hartmann, D.J., Regnier, M., Asselineau, D., 1992. The role of fibroblasts in dermal vascularization and remodeling of reconstructed human skin after transplantation onto the nude mouse. *Transplantation* 54, 317–326.
- De Meester, I., Korom, S., van Damme, J., Scharpe, S., 1999. CD26, let it cut or cut it down. *Immunol. Today* 20, 367–375.
- Desmoulière, A., Rubbia-Brandt, L., Abdiu, A., Walz, T., Macieira-Coelho, A., Gabbiani, G., 1992. α -Smooth muscle actin is expressed in a subpopulation of cultured and cloned fibroblasts and is modulated by α -interferon. *Exp. Cell Res.* 201, 64–73.
- Detmar, M., 2000. The role of VEGF and thrombospondins in skin angiogenesis. *J. Dermatol. Sci.* 24, S78–S84.
- Dhouailly, D., 1973. Dermo-epidermal interactions between birds and mammals: differentiation of cutaneous appendages. *J. Embryol. Exp. Morphol.* 30, 587–603.
- Dicker, A.J., Serewko, M.M., Russell, T., Rothnagel, J.A., Strutton, G.M., Dahler, A.L., et al., 2002. Isolation (from a basal cell carcinoma) of a functionally distinct fibroblast-like cell type that overexpresses Ptch. *J. Invest. Dermatol.* 118, 859–865.

- Dimiri, G.P., Lee, X., Basile, G., Acosta, M., Scott, G., Roskelley, C., et al., 1995. A biomarker that identifies senescent human cells in culture and in aging skin *in vivo*. *Proc. Natl. Acad. Sci. USA* 92, 9363–9367.
- Doane, K.J., Birk, D.E., 1991. Fibroblasts retain their tissue phenotype when grown in three-dimensional collagen gels. *Exp. Cell Res.* 195, 432–442.
- Dudas, J., Mansuroglu, T., Batusic, D., Saile, B., Ramadori, G., 2007. Thy-1 is an *in vivo* and *in vitro* marker of liver myofibroblasts. *Cell Tissue Res.* 329, 503–514.
- Enoch, S., Moseley, R., Stephens, P., Thomas, D.W., 2008. The oral mucosa: a model of wound healing with reduced scarring. *Oral Surg.* 1, 11–21.
- Falanga, V., Zhou, L.H., Takagi, H., Murata, H., Ochoa, S., Martin, T.A., et al., 1995. Human dermal fibroblast clones derived from single cells are heterogeneous in the production of mRNAs for $\alpha 1(I)$ procollagen and transforming growth factor- $\alpha 1$. *J. Invest. Dermatol.* 105, 27–31.
- Fisher, G.J., Varani, J., Voorhees, J.J., 2008. Looking older. Fibroblast collapse and therapeutic implications. *Arch. Dermatol.* 144, 666–672.
- Fisher, G.J., Quan, T., Purohit, T., Shao, Y., Cho, M.K., He, T., et al., 2009. Collagen fragmentation promotes oxidative stress and elevates matrix metalloproteinase-1 in fibroblasts in aged human skin. *Am. J. Pathol.* 174, 101–114.
- Fleischmajer, R., MacDonald, E.D. II, Contard, P., Perlish, J.S., 1993. Immunocytochemistry of a keratinocyte-fibroblast co-culture model for reconstruction of human skin. *J. Histochem. Cytochem.* 41, 1359–1366.
- Fleischmajer, R., Schechter, A., Bruns, M., Perlish, J.S., MacDonald, E.D., Pan, T.-C., Timpl, R., Chu, M.-L., 1995. Skin fibroblasts are the only source of nidogen during early basal lamina formation *in vitro*. *J. Invest. Dermatol.* 105, 597–601.
- Fries, K.M., Blieden, T., Looney, R.J., Sempowski, G.D., Silvera, M.R., Willis, R.A., et al., 1994. Evidence of fibroblast heterogeneity and the role of fibroblast subpopulations in fibrosis. *Clin. Immunol. Immunopathol.* 72, 283–292.
- Fries, K.M., Sempowski, G.D., Gaspari, A.A., Blieden, T., Looney, R.J., Phipps, R.P., 1995. CD40 expression by human fibroblasts. *Clin. Immunol. Immunopathol.* 77, 42–51.
- Fritsch, C., Orian-Rousseau, V., Lefebvre, O., Simon-Assmann, P., Reimund, J.M., Duclos, B., et al., 1999. Characterization of human intestinal stromal cell lines: response to cytokines and interactions with epithelial cells. *Exp. Cell Res.* 248, 391–406.
- Gabbiani, G., 2003. The myofibroblast in wound healing and fibrocontractive diseases. *J. Pathol.* 200, 500–503.
- Garrett, D.M., Conrad, G.W., 1979. Fibroblast-like cells from embryonic chick cornea, heart, and skin are antigenically distinct. *Dev. Biol.* 70, 50–70.
- Geesin, J.C., Brown, L.J., Gordon, J.S., Berg, R.A., 1993. Regulation of collagen synthesis in human dermal fibroblasts in contracted collagen gels by ascorbic acid, growth factors, and inhibitors of lipid peroxidation. *Exp. Cell Res.* 206, 283–290.
- Germain, L., Jean, A., Auger, F.A., Garrel, D.R., 1994. Human wound healing fibroblasts have greater contractile properties than dermal fibroblasts. *J. Surg. Res.* 57, 268–273.
- Ghahary, A., Ghaffari, A., 2007. Role of keratinocyte-fibroblast cross-talk in development of hypertrophic scar. *Wound Repair Regen.* 15, S46–S53.
- Ghahary, A., Karimi-Busheri, F., Marcoux, Y., Li, Y., Tredget, E.E., Kilani, R.T., et al., 2004. Keratinocyte-releasable stratifin functions as a potent collagenase-stimulating factor in fibroblasts. *J. Invest. Dermatol.* 122, 1188–1197.
- Gilchrist, B.A., 1996. A review of skin ageing and its medical therapy. *Br. J. Dermatol.* 135, 867–873.
- Grässel, S., Unsöld, C., Schäcke, H., Bruckner-Tuderman, L., Bruckner, P., 1999. Collagen XVI is expressed by human dermal fibroblasts and keratinocytes and is associated with the microfibrillar apparatus in the upper papillary dermis. *Matrix Biol.* 18, 309–317.

- Grinnell, F., 1994. Fibroblasts, myofibroblasts, and wound contraction. *J. Cell Biol.* 124, 401–404.
- Grinnell, F., 2003. Fibroblast biology in three-dimensional collagen matrices. *Trends Cell Biol.* 13, 264–269.
- Grøn, B., Stoltze, K., Andersson, A., Dabelsteen, E., 2002. Oral fibroblasts produce more HGF and KGF than skin fibroblasts in response to co-culture with keratinocytes. *APMIS* 110, 892–898.
- Guilak, F., Lott, K.E., Awad, H.A., Cao, Q., Hicok, K.C., Fermor, B., et al., 2006. Clonal analysis of the differentiation potential of human adipose-derived adult stem cells. *J. Cell. Physiol.* 206, 229–237.
- Gupta, K., Ramakrishnan, S., Browne, P.V., Solovey, A., Hebbel, R.P., 1997. A novel technique for culture of human dermal microvascular endothelial cells under either serum-free or serum-supplemented conditions: isolation by panning and stimulation with vascular endothelial growth factor. *Exp. Cell Res.* 230, 244–251.
- Hagood, J.S., Prabhakaran, P., Kumbla, P., Salazar, L., Macewen, M.W., Barker, T.H., et al., 2005. Loss of fibroblast thy-1 expression correlates with lung fibrogenesis. *Am. J. Pathol.* 167, 365–379.
- Harper, R.A., Grove, G., 1979. Human skin fibroblasts derived from papillary and reticular dermis: differences in growth potential *in vitro*. *Science* 204, 526–527.
- Hasan, A., Murata, H., Falabella, A., Ochoa, S., Zhou, L., Badiavas, E., et al., 1997. Dermal fibroblasts from venous ulcers are unresponsive to the action of transforming growth factor- β 1. *J. Dermatol. Sci.* 16, 59–66.
- Heinegård, D., Oldberg, A., 1993. Glycosylated matrix proteins. In: P.M. Royce B. Steinmann, (Eds.), *Connective Tissue and Its Heritable Disorders*, Wiley-Liss, New York, NY, pp. 189–209.
- Helmbold, P., Nayak, R.C., Marsch, W.C., Herman, I.M., 2001. Isolation and *in vitro* characterization of human dermal microvascular pericytes. *Microvasc. Res.* 61, 160–165.
- Hoffmann, T., Faust, J., Nuebert, K., Ansoorge, S., 1993. Dipeptidyl peptidase IV (CD 26) and aminopeptidase N (CD 13) catalyzed hydrolysis of cytokines and peptides with N-terminal cytokine sequences. *FEBS Lett.* 336, 61–64.
- Holbrook, K.A., Minami, S.I., 1991. Hair follicle embryogenesis in the human. Characterization of events *in vivo* and *in vitro*. *Ann. N. Y. Acad. Sci.* 642, 167–196.
- Houzelstein, D., Cheraud, Y., Auda-Boucher, G., Fontaine-Perus, J., 2000. The expression of the homeobox gene *Msx1* reveals two populations of dermal progenitor cells originating from the somites. *Development* 127, 2155–2164.
- Hudon, V., Berthod, F., Black, A.F., Damour, O., Germain, L., Auger, F.A., 2003. A tissue-engineered endothelialized dermis to study the modulation of angiogenic and angiostatic molecules on capillary-like tube formation *in vitro*. *Br. J. Dermatol.* 148, 1094–1104.
- Hughes, M.W., Chuong, C.M., 2003. A mouthful of epithelial–mesenchymal interactions. *J. Invest. Dermatol.* 121, vii–viii.
- Igarashi, M., Finch, P.W., Aaronson, S.A., 1996. Characterization of recombinant human fibroblast growth factor (FGF)-10 reveals functional similarities with keratinocyte growth factor (FGF-7). *J. Biol. Chem.* 273, 13230–13235.
- Iozzo, R.V., 1997. The family of the small leucine-rich proteoglycans: key regulators of matrix assembly and cellular growth. *Crit. Rev. Biochem. Mol. Biol.* 32, 141–174.
- Iozzo, R.V., 1998. Matrix proteoglycans: from molecular design to cellular function. *Annu. Rev. Biochem.* 67, 609–652.
- Iozzo, R.V., 1999. The biology of the small leucine-rich proteoglycans. *J. Biol. Chem.* 274, 18843–18846.
- Iozzo, R.V., 2005. Basement membrane proteoglycans: from cellar to ceiling. *Nat. Rev. Mol. Cell Biol.* 6, 646–656.
- Itami, S., Kurata, S., Sonoda, T., Takayasu, S., 1995. Interaction between dermal papilla cells and follicular epithelial cells *in vitro*: effect of androgen. *Br. J. Dermatol.* 132, 527–532.

- Jahoda, C.A.B., Reynolds, A.J., 2001. Hair follicle dermal sheath cells: unsung participants in wound healing. *Lancet* 358, 1445–1448.
- Jahoda, C.A.B., Reynolds, A.J., Chaponnier, C., Forester, J.C., Gabbiani, G., 1991. Smooth muscle α -actin is a marker for hair follicle dermis *in vivo* and *in vitro*. *J. Cell Sci.* 99, 627–636.
- Jain, R.K., 2003. Molecular regulation of vessel maturation. *Nat. Med.* 9, 685–693.
- Jeanmaire, C., Danoux, L., Pauly, G., 2001. Glycation during human dermal intrinsic and actinic ageing: an *in vivo* and *in vitro* model study. *Br. J. Dermatol.* 145, 10–18.
- Kahler, C.M., Sitte, B.A., Reinisch, N., Wiedermann, C.J., 1993. Stimulation of the chemotactic migration of human fibroblasts by substance P. *Eur. J. Pharmacol.* 249, 281–286.
- Kalluri, R., Zeisberg, M., 2006. Fibroblasts in cancer. *Nat. Rev. Cancer* 6, 392–401.
- Kanayama, N., Kajiwar, Y., Goto, J., Elmaradny, E., Maehara, K., Andou, K., et al., 1995. Inactivation of interleukin-8 by aminopeptidase N (CD13). *J. Leukoc. Biol.* 57, 129–134.
- Kasper, M., Funk, R.H., 2001. Age-related changes in cells and tissues due to advanced glycation end products (ages). *Arch. Gerontol. Geriatr.* 32, 233–243.
- Kletsas, D., Caselgrandi, E., Barbieri, D., Stathakos, D., Franceschi, C., Ottaviani, E., 1998. Neutral endopeptidase-24.11 (NEP) activity in human fibroblasts during development and ageing. *Mech. Ageing Dev.* 102, 15–23.
- Ko, S.D., Page, R.C., Narayanan, A.S., 1977. Fibroblast heterogeneity and prostaglandin regulation of subpopulations. *Proc. Natl. Acad. Sci. USA* 74, 3429–3432.
- König, A., Bruckner-Tuderman, L., 1991. Epithelial-mesenchymal interactions enhance expression of collagen VII *in vitro*. *J. Invest. Dermatol.* 96, 803–808.
- König, A., Bruckner-Tuderman, L., 1994. Transforming growth factor- β promotes deposition of collagen VII in a modified organotypic skin model. *Lab. Invest.* 70, 203–209.
- Kopf, A.W., 1957. The distribution of alkaline phosphatase in normal and pathologic human skin. *Arch. Dermatol.* 75, 1–37.
- Korn, J.H., Torres, D., Downie, E., 1984. Clonal heterogeneity in the fibroblast response to mononuclear cell derived mediators. *Arthritis Rheum.* 27, 174–179.
- Koumas, L., King, A.E., Kelly, R.W., Phipps, R.P., 2001. Existence of functionally distinct Thy 1 + and Thy 1 – human female reproductive tract fibroblasts. *Am. J. Pathol.* 159, 925–935.
- Koumas, L., Smith, T.J., Feldon, S., Blumberg, N., Phipps, R.P., 2003. Thy-1 expression in human fibroblast subsets defines myofibroblastic or lipofibroblastic phenotypes. *Am. J. Pathol.* 163, 1291–1300.
- Kraling, B.M., Jimenez, S.A., Sorger, T., Maul, G.C., 1994. Isolation and characterization of microvascular endothelial cells from the adult human dermis and from skin biopsies of patients with systemic sclerosis. *Lab. Invest.* 71, 745–754.
- Kueper, T., Grune, T., Prah, S., Lenz, H., Welge, V., Biernoth, T., et al., 2007. Vimentin is the specific target in skin glycation. Structural prerequisites, functional consequences, and role in skin aging. *J. Biol. Chem.* 282, 23427–23436.
- Lacina, L., Smetana, K., Dvorankova, B., Pytlik, R., Kideryova, L., Plzakova, Z., et al., 2007. Stromal fibroblasts from basal cell carcinoma affect phenotype of normal keratinocytes. *Br. J. Dermatol.* 156, 819–829.
- Le Lièvre, C.S., Le Douarin, N.M., 1975. Mesenchymal derivatives of the neural crest: analysis of chimaeric quail and chick embryos. *J. Embryol. Exp. Morphol.* 34, 125–154.
- Lennon, D.P., Haynesworth, S.E., Arm, D.M., Baber, M.A., Caplan, A.I., 2000. Dilution of human mesenchymal stem cells with dermal fibroblasts and the effects on *in vitro* and *in vivo* osteochondrogenesis. *Dev. Dyn.* 219(50), 2000.
- Lethias, C., Descollonges, Y., Boutillon, M.M., Garrone, R., 1996. Flexilin: a new extracellular matrix glycoprotein localized on collagen fibers. *Matrix Biol.* 15, 11–19.

- Lightner, V.A., Gumkowski, F., Bigner, D.D., Erickson, H.P., 1993. Tenascin/hexabronchion in human skin: biochemical identification and localization by light and electron microscopy. *J. Cell Biol.* 108, 2483–2493.
- Lim, I.J., Phan, T.T., Bay, B.H., Qi, R., Huynh, H., Tan, W.T.L., et al., 2002. Fibroblasts cocultured with keloid keratinocytes: normal fibroblasts secrete collagen in a keloidlike manner. *Am. J. Physiol.* 283, C212–C222.
- Limeback, H., Sodek, J., Aubin, J.E., 1982. Variation in collagen expression by cloned periodontal ligament cells. *J. Periodont. Res.* 18, 242–248.
- Maas-Szabowski, N., Fusenig, N.E., 1996. Interleukin-1-induced growth factor expression in postmitotic and resting fibroblasts. *J. Invest. Dermatol.* 107, 849–855.
- Maas-Szabowski, N., Szabowski, A., Stark, H.-J., Andrecht, S., Kolbus, A., Schorpp-Kistner, M., et al., 2001. Organotypic cocultures with genetically modified mouse fibroblasts as a tool to dissect molecular mechanisms regulating keratinocyte growth and differentiation. *J. Invest. Dermatol.* 116, 816–820.
- Malgoures, S., Thibaut, S., Bernard, B.A., 2008. Proteoglycan expression patterns in human hair follicle. *Br. J. Dermatol.* 158, 234–242.
- Malmström, E., Sennström, M., Holmberg, A., Frielingsdor, H., Eklund, E., Malmström, L., et al., 2007. The importance of fibroblasts in remodelling of the human uterine cervix during pregnancy and parturition. *Mol. Hum. Reprod.* 13, 333–341.
- Marinkovich, M.P., Keene, D.R., Rimberg, C.S., Burgeson, R.E., 1993. Cellular origin of the dermal-epidermal basement membrane. *Dev. Dyn.* 197, 255–267.
- Martin, T.A., Harding, K.G., Jiang, W.G., 1999. Regulation of angiogenesis and endothelial cell motility by matrix-bound fibroblasts. *Angiogenesis* 3, 69–76.
- Meigel, W.N., Gay, S., Weber, L., 1977. Dermal architecture and collagen type distribution. *Arch. Dermatol. Res.* 259(18), 1–10.
- Mentlein, R., 1999. Dipeptidyl-peptidase IV (CD26)—role in the inactivation of regulatory peptides. *Regul. Pept.* 85, 9–24.
- Metcalfe, A.D., Ferguson, M.W.J., 2007. Bioengineering skin using mechanisms of regeneration and repair. *Biomaterials* 28, 5100–5113.
- Millar, S.E., 2002. Molecular mechanisms regulating hair follicle development. *J. Invest. Dermatol.* 118, 216–225.
- Mine, S., Fortunel, N.O., Pageon, H., Asselineau, D., 2008. Aging alters functionally human dermal papillary fibroblasts but not reticular fibroblasts: a new view of skin morphogenesis and aging. *PLoS ONE* 3, e4066, doi:10.1372/journal.pone.00004066.
- Monical, P.L., Kefalides, N.A., 1994. Coculture modulates laminin synthesis and mRNA levels in epidermal keratinocytes and dermal fibroblasts. *Exp. Cell Res.* 210, 154–159.
- Montagna, W., Carlisle, K., 1979. Structural changes in aging human skin. *J. Invest. Dermatol.* 73, 47–53.
- Montesano, R., Pepper, M.S., Orci, L., 1993. Paracrine induction of angiogenesis *in vitro* by Swiss 3T3 fibroblasts. *J. Cell Sci.* 105, 1013–1024.
- Moulin, V., Auger, F.A., Garrel, D., Germain, L., 2000. Role of wound healing myofibroblasts on re-epithelialization of human skin. *Burns* 26, 3–12.
- Moulin, V., Tam, B.Y.Y., Castilloux, G., Auger, F.A., O'Connor-McCourt, M.D., Philip, A., et al., 2001. Fetal and adult human skin fibroblasts display intrinsic differences in contractile capacity. *J. Cell. Physiol.* 188, 211–222.
- Nilsson, J., von Euler, A.M., Dalsgaard, C.J., 1985. Stimulation of connective tissue cell growth by substance P and substance K. *Nature* 315, 61–63.
- Nolte, S.V., Xu, W., Rennekamp, H.O., 2008. Diversity of fibroblasts—a review on implications for skin tissue engineering. *Cells Tissues Organs* 187, 165–176.
- Nowinski, D., Lysheden, A.S., Gardner, H., Rubin, K., Gerdin, B., Ivarsson, M., 2004. Analysis of gene expression in fibroblasts in response to keratinocyte-derived factors

- in vitro*: potential implications for the wound healing process. *J. Invest. Dermatol.* 122, 216–221.
- Olerud, J.E., Usui, M.L., Seckin, D., Chiu, D.S., Haycox, C.L., Song, I.S., et al., 1999. Neutral endopeptidase expression and distribution in human skin and wounds. *J. Invest. Dermatol.* 112, 873–881.
- Park, J.E., Lenter, M.C., Zimmermann, R.N., Garin-Chesa, P., Old, L.J., Rettig, W.J., 1999. Fibroblast activation protein, a dual specificity serine protease expressed in reactive human tumor stromal fibroblasts. *J. Biol. Chem.* 274, 36505–36512.
- Parker, R.C., 1932. The functional characteristics of nine races of fibroblasts. *Science* 76, 219–220.
- Parsonage, G., Filer, A.D., Haworth, O., Nash, G.B., Rainger, G.E., Salmon, M., et al., 2005. A stromal address code defined by fibroblasts. *Trends Immunol.* 26, 150–156.
- Paus, R., Botchkarev, V.A., Botchkareva, N.V., Mecklenburg, L., Luger, T., Slominski, A., 1999. The skin POMC system (SPS). Leads and lessons from the hair follicle. *Ann. N. Y. Acad. Sci.* 885, 350–363.
- Penney, D.P., Keng, P.C., Derdak, S., Phipps, R.P., 1992. Morphologic and functional characteristics of subpopulations of murine lung fibroblasts grown *in vitro*. *Anat. Rec.* 232, 432–443.
- Peters, E.M.J., Ericson, M.E., Hosoi, J., Seiffert, K., Hordinsky, M.K., Ansel, J.C., et al., 2006. Neuropeptide control mechanisms in cutaneous biology: physiological and clinical significance. *J. Invest. Dermatol.* 126, 1937–1947.
- Piela-Smith, T.H., Korn, J.H., 1995. Aminopeptidase N: a constitutive cell-surface protein on human dermal fibroblasts. *Cell. Immunol.* 162, 42–48.
- Pinney, E., Liu, K., Sheeman, B., Mansbridge, J., 2000. Human three-dimensional fibroblast cultures express angiogenic activity. *J. Cell. Physiol.* 183, 74–82.
- Proost, P., De Meester, I., Schols, D., Struyf, S., Lambeir, A.M., Wuyts, A., et al., 1998. Amino-terminal truncation of chemokines by CD26/dipeptidyl-peptidase IV: conversion of RANTES into a potent inhibitor of monocyte chemotaxis and HIV-1-infection. *J. Biol. Chem.* 273, 7222–7227.
- Proost, P., Menten, P., Struyf, S., Schutyser, E., De Meester, I., Van Damme, J., 2000. Cleavage by CD26/dipeptidyl peptidase IV converts the chemokine LD78 β into a most efficient monocytes attractant and CCR1 agonist. *Blood* 96, 1674–1680.
- Pugliese, P.T., 2007. The pathogenesis of cellulite: a new concept. *J. Cosmet. Dermatol.* 6, 140–142.
- Puolakkainen, P.A., Bradshaw, A.D., Brekken, R.A., Ree, M.J., Kyriakides, T., Funk, S.E., et al., 2005. SPARC-thrombospondin-2-double-null mice exhibit enhanced cutaneous wound healing and increased fibrovascular invasion of subcutaneous polyvinyl alcohol sponges. *J. Histochem. Cytochem.* 53, 571–581.
- Quan, T.E., Cowper, S., Wu, S.P., Bockenstedt, L.K., Bucala, R., 2004. Circulating fibrocytes: collagen-secreting cells of the peripheral blood. *Int. J. Biochem. Cell Biol.* 36, 598–606.
- Ramirez, F., Rifkin, D.B., 2003. Cell signaling events: a view from the matrix. *Matrix Biol.* 22, 101–107.
- Raynaud, F., Bauvois, B., Berbaoud, P., Evian-Brion, D., 1992. Characterization of specific proteases associated with the surface of human skin fibroblasts, and their modulation in pathology. *J. Cell. Physiol.* 151, 378–385.
- Rege, T.A., Hagood, J.S., 2006. Thy-1 as a regulator of cell-cell and cell-matrix interactions in axon regeneration, apoptosis, adhesion, migration, cancer, and fibrosis. *FASEB J.* 20, 1045–1054.
- Rheinwald, J.G., Green, H., 1975. Serial cultivation of strains of human epidermal keratinocytes: the formation of keratinizing colonies from single cells. *Cell* 6, 331–344.

- Richard, L., Velasco, P., Detmar, M., 1998. A simple immunomagnetic protocol for the selective isolation and long-term culture of human dermal microvascular endothelial cells. *Exp. Cell Res.* 240, 1–6.
- Riemann, D., Kehlen, A., Langner, J., 1999. CD13—not just a marker in leukemia typing. *Immunol. Today* 20, 83–88.
- Rinn, J.L., Bondre, C., Gladstone, H.B., Brown, P.O., Chang, H.Y., 2006. Anatomic demarcation by positional variation in fibroblast gene expression programs. *PLoS Genet.* 2, 1084–1096.
- Rinn, J.L., Wang, J.K., Liu, H., Montgomery, K., van de Rijn, M., Chang, H.Y., 2008. A systems biology approach to anatomic diversity of skin. *J. Invest. Dermatol.* 128, 776–782.
- Rodemann, H.P., Bayreuther, K., Francz, P.I., Dittmann, K., Albiez, M., 1989. Selective enrichment and biochemical characterization of seven human skin fibroblasts cell types *in vitro*. *Exp. Cell Res.* 180, 84–93.
- Ronnov-Jessen, L., Petersen, O.W., Koteliansky, V.E., Bissell, M.J., 1995. The origin of the myofibroblasts in breast cancer. Recapitulation of tumor environment in culture unravels diversity and implicates converted fibroblasts and recruited smooth muscle cells. *J. Clin. Invest.* 95, 859–873.
- Ronnov-Jessen, L., Petersen, O.W., Bissell, M.J., 1996. Cellular changes involved in conversion of normal to malignant breast: importance of the stromal reaction. *Physiol. Rev.* 76, 69–125.
- Rubin, J.S., Bottaro, D.P., Chedid, M., Miki, T., Ron, D., Cheon, G., et al., 1995. Keratinocyte growth factor. *Cell Biol. Int.* 19, 399–411.
- Ruhrberg, C., Gerhardt, H., Golding, M., Watson, R., Ioannidou, S., Fujisawa, H., et al., 2002. Spatially restricted patterning cues provided by heparin-binding VEGF-A control blood vessel branching morphogenesis. *Genes Dev.* 16, 2684–2698.
- Russell, J.S., Chi, H., Lantry, L.E., Stephens, R.E., Ward, P.E., 1996. Substance P and neurokinin A metabolism by cultured human skeletal muscle myocytes and fibroblasts. *Peptides* 17, 1397–1403.
- Saalbach, A., Anderegg, U., Bruns, M., Schnabel, E., Hermann, K., Hausteine, U.F., 1996. Novel fibroblast-specific monoclonal antibodies: properties and specificities. *J. Invest. Dermatol.* 106, 1314–1319.
- Saalbach, A., Aust, G., Hausteine, U.F., Herrmann, K., Anderegg, U., 1997. The fibroblast-specific monoclonal antibody AS02: a novel tool for detection and elimination of human fibroblasts. *Cell Tissue Res.* 290, 593–599.
- Saalbach, A., Kraft, R., Herrmann, K., Hausteine, U.F., Anderegg, U., 1998. The monoclonal antibody AS02 recognizes a protein on human fibroblasts being highly homologous to Thy-1. *Arch. Dermatol. Res.* 290, 360–366.
- Saison, M., Verlinden, J., Van Leuven, F., Cassiman, J.J., Van den Berghe, H., 1983. Identification of cell surface dipeptidyl peptidase IV EC-3.4.14.5 in human fibroblasts. *Biochem. J.* 216, 177–184.
- Sandy, J.D., Westling, J., Kenagy, R.D., Iruela, M.L., Verscharen, C., Rodriguez, J.C., et al., 2001. Versican v1 proteolysis in human aorta *in vivo* occurs at the glu441-ala442 bond, a site that is cleaved by recombinant ADAMTS-1 and ADAMTS-4. *J. Biol. Chem.* 276, 13372–13378.
- Scaal, M., Christ, B., 2004. Formation and differentiation of the avian dermomyotome. *Anat. Embryol.* 208, 411–424.
- Schafer, I.A., Pandey, M., Ferguson, R., Davis, B.R., 1985. Comparative observation of fibroblasts derived from the papillary and reticular dermis of infants and adults: growth kinetics, packing density at confluence and surface morphology. *Mech. Ageing Dev.* 31, 275–293.

- Scholzen, T., Armstrong, C.A., Bunnett, N.W., Luger, T.A., Olerud, J.E., Ansel, J.C., 1998. Neuropeptides in the skin: interactions between the neuroendocrine and the skin immune systems. *Exp. Dermatol.* 7, 81–96.
- Scholzen, T.E., Steinhoff, M., Bonaccorsi, P., Klein, R., Amadesi, S., Geppetti, P., et al., 2001. Neutral endopeptidase terminates substance P-induced inflammation in allergic contact dermatitis. *J. Immunol.* 166, 1285–1291.
- Schönherr, E., Beavan, L.A., Hausser, H., Kresse, H., Culp, L.A., 1993. Differences in decorin expression by papillary and reticular fibroblasts *in vivo* and *in vitro*. *Biochem. J.* 290, 893–899.
- Sempowski, G.D., Borrello, M.A., Blieden, T.M., Barth, R.K., Phipps, R.P., 1995. Fibroblast heterogeneity in the healing wound. *Wound Repair Regen.* 3, 120–131.
- Sempowski, G.D., Derdak, S., Phipps, R.P., 1996. Interleukin-4 and interferon- γ discordantly regulate collagen biosynthesis by functionally distinct lung fibroblast subsets. *J. Cell. Physiol.* 167, 290–296.
- Serini, G., Bochaton-Piallat, M.L., Ropraz, P., Geinoz, A., Borsi, L., Zardi, L., et al., 1998. The fibronectin domain ED-A is crucial for myofibroblastic phenotype induction by transforming growth factor- β 1. *J. Cell Biol.* 142, 873–881.
- Shannon, D.B., McKeown, S.T.W., Lundy, F.T., Irwin, C.R., 2006. Phenotypic differences between oral and skin fibroblasts in wound contraction and growth factor expression. *Wound Repair Regen.* 14, 172–178.
- Silvera, M.R., Sempowski, G.D., Phipps, R.P., 1994. Expression of TGF- β isoforms by Thy-1⁺ and Thy-1⁻ pulmonary fibroblast subsets; evidence for TGF- β as a regulator of IL-1-dependent stimulation of IL-6. *Lymphokine Cytokine Res.* 13, 277–285.
- Silzle, T., Randolph, G.J., Kreutz, M., Kunz-Schughart, L.A., 2004. The fibroblast: sentinel cell and local immune modulator in tumor tissue. *Int. J. Cancer* 108, 173–180.
- Singer, A.J., Clark, R.A.F., 1999. Cutaneous wound healing. *N. Engl. J. Med.* 341, 738–746.
- Smith, J.R., Hayflick, L., 1974. Variation in the life-span of clones derived from human diploid cell strains. *J. Cell Biol.* 62, 48–53.
- Smith, L.T., Holbrook, K.A., 1986. Embryogenesis of the dermis in human skin. *Pediatr. Dermatol.* 3, 271–280.
- Smith, R.S., Smith, T.J., Blieden, T.M., Phipps, R.P., 1997. Fibroblasts as sentinel cells. Synthesis of chemokines and regulation of inflammation. *Am. J. Pathol.* 151, 317–322.
- Smola, H., Thiekötter, G., Fusenig, N.E., 1993. Mutual induction of growth factor gene expression by epidermal-dermal cell interaction. *J. Cell Biol.* 122, 417–429.
- Smola, H., Stark, H.-J., Thiekötter, G., Mirancea, N., Krieg, T., Fusenig, N.E., 1998. Dynamics of basement membrane formation by keratinocyte-fibroblast interactions in organotypic skin culture. *Exp. Cell Res.* 239, 399–410.
- Sorrell, J.M., Caplan, A.I., 2004. Fibroblast heterogeneity: more than skin deep. *J. Cell Sci.* 117, 667–675.
- Sorrell, J.M., Mahmoodian, F., Schafer, I.A., Davis, B., Caterson, B., 1990. Identification of monoclonal antibodies that recognize novel epitopes in native chondroitin/dermatan sulfate glycosaminoglycan chains: their use in mapping functionally distinct domains of human skin. *J. Histochem. Cytochem.* 38, 393–402.
- Sorrell, J.M., Carrino, D.A., Baber, M.A., Asselineau, D., Caplan, A.I., 1999a. A monoclonal antibody which recognizes a glycosaminoglycan epitope in both dermatan sulphate and chondroitin sulphate proteoglycans of human skin. *Histochem. J.* 31, 549–559.
- Sorrell, J.M., Carrino, D.A., Baber, M.A., Caplan, A.I., 1999b. Versican in human fetal skin development. *Anat. Embryol.* 199, 45–56.
- Sorrell, J.M., Baber, M.A., Brinon, L., Carrino, D.A., Seavolt, M., Asselineau, D., et al., 2003a. Production of a monoclonal antibody, DF-5, that identifies cells at the epithelial-

- mesenchymal interface in normal human skin. APN/CD13 is an epithelial–mesenchymal marker in skin. *Exp. Dermatol.* 12, 315–323.
- Sorrell, J.M., Brinon, L., Baber, M.A., Caplan, A.I., 2003b. Cytokines and glucocorticoids differentially regulate APN/CD13 and DPPIV/CD26 enzyme activities in cultured human dermal fibroblasts. *Arch. Dermatol. Res.* 295, 160–168.
- Sorrell, J.M., Baber, M.A., Caplan, A.I., 2004. Site-matched papillary and reticular human dermal fibroblasts differ in their release of specific growth factors/cytokines and in their interaction with keratinocytes. *J. Cell. Physiol.* 200, 134–145.
- Sorrell, J.M., Baber, M.A., Caplan, A.I., 2007a. Clonal characterization of fibroblasts in the superficial layer of the adult human dermis. *Cell Tissue Res.* 327, 499–510.
- Sorrell, J.M., Baber, M.A., Caplan, A.I., 2007b. A self-assembled fibroblast–endothelial cell co-culture system that supports *in vitro* vasculogenesis by both human umbilical vein endothelial cells and human dermal microvascular endothelial cells. *Cells Tissues Organs* 186, 157–168.
- Sorrell, J.M., Baber, M.A., Caplan, A.I., 2008. Human dermal fibroblast subpopulations; differential interactions with vascular endothelial cells in coculture: nonsoluble factors in the extracellular matrix influence interactions. *Wound Repair Regen.* 16, 300–309.
- Sorrell, J.M., Baber, M.A., Caplan, A.I., 2009. Influence of adult mesenchymal stem cells on *in vitro* vascular formation. *Tissue Eng.* 15, in press, doi: 10.1089/ten.tea.2008.0254.
- Sottile, J., 2004. Regulation of angiogenesis by extracellular matrix. *Biochim. Biophys. Acta* 1654, 13–22.
- Stefanović, V., Vlahović, P., Mitić-Zlatković, M., 1998. Receptor-mediated induction of human dermal fibroblast ectoaminopeptidase N by glucocorticoids. *Cell. Mol. Life Sci.* 54, 614–617.
- Stenmark, K.R., Davie, N., Frid, M., Gerasimovskaya, M., Das, M., 2006. The role of the adventitia in pulmonary vascular remodeling. *Physiology* 21, 134–145.
- Strutz, F., Okada, H., Lo, C.W., Danoff, T., Carone, R.L., Tomaszewski, J., et al., 1995. Identification and characterization of a fibroblast marker: FSP1. *J. Cell Biol.* 130, 393–405.
- Supp, D.M., Wilson-Landy, K., Boyce, S.T., 2002. Human dermal microvascular endothelial cells form vascular analogs in cultured skin substitutes after grafting to athymic mice. *FASEB J.* 16, 797–804.
- Szabowski, A., Maas-Szabowski, N., Andrecht, S., Kolbus, A., Schorpp-Kristner, M., Fusenig, N.E., et al., 2000. C-Jun and junb antagonistically control cytokine-regulated mesenchymal-epidermal interaction in skin. *Cell* 103, 745–755.
- Tajima, S., Izumi, T., 1996. Differential *in vitro* responses of elastin expression to basic fibroblast growth factor and transforming growth factor $\beta 1$ in upper middle, and lower dermal fibroblasts. *Arch. Dermatol. Res.* 288, 753–756.
- Tajima, S., Pinnell, S.R., 1981. Collagen synthesis by human skin fibroblasts in culture: studies of fibroblasts explanted from papillary and reticular dermis. *J. Invest. Dermatol.* 77, 410–412.
- Tremblay, P.L., Hudon, V., Berthod, F., Germain, L., Auger, F.A., 2005. Inoculation of tissue-engineered capillaries with the host's vasculature in a reconstructed skin transplanted on mice. *Am. J. Transplant.* 5, 1002–1010.
- Varani, J., Schuger, L., Dame, M.K., Leonard, C., Fligiel, S.E.G., Kang, S., et al., 2004. Reduced fibroblast interaction with intact collagen as a mechanism for depressed collagen synthesis in photodamaged skin. *J. Invest. Dermatol.* 122, 1471–1479.
- Varani, J., Dame, M.K., Rittie, L., Fligiel, S.E.G., Kang, S., Fisher, G.J., et al., 2006. Decreased collagen production in chronologically aged skin. *Am. J. Pathol.* 168, 1861–1868.
- Velazquez, O.M., Snyder, R., Liu, Z.J., Fairman, R.M., Herlyn, M., 2002. Fibroblast-dependent differentiation of human microvascular endothelial cells into capillary-like, three-dimensional networks. *FASEB J.* 16, 1316–1318.

- Wälchli, C., Koch, M., Chiquet, M., Odermatt, B.F., Trueb, B., 1994. Tissue-specific expression of the fibril-associated collagens XII and XIV. *J. Cell Sci.* 107, 669–681.
- Wall, I.B., Moseley, R., Baird, D.M., Kipling, D., Giles, P., Laffafian, I., et al., 2008. Fibroblast dysfunction is a key factor in the non-healing of chronic venous leg ulcers. *J. Invest. Dermatol.* 128, 2526–2540.
- Wallengren, J., 1999. Neuropeptides: their significance in the skin. *Drug News Perspect.* 12, 401–411.
- Wang, H., van Blitterswijk, C.A., Bertrand-De Haas, M., Schuurman, A.H., Lamme, E.N., 2004. Improved enzymatic isolation of fibroblasts for the creation of autologous skin substitutes. *In Vitro Cell. Dev. Biol.* 40A, 268–277.
- Wang, J.F., Jiao, H., Stewart, T.L., Shankowsky, H.A., Scott, P.G., Tredget, E.E., 2006. Fibrocytes from burn patients regulate the activities of fibroblasts. *Wound Repair Regen.* 15, 113–121.
- Wang, J., Dodd, C., Shankowsky, H.A., Scott, P.G., Tredget, E.E., 2008. Deep dermal fibroblasts contribute to hypertrophic scarring. *Lab. Invest.* 88, 1278–1290.
- Watson, R.E.B., Griffiths, C., Craven, N., Shuttleworth, A., Kielty, C.M., 1999. Fibrillin-rich microfibrils are reduced in photoaged skin. Distribution at the dermal–epidermal junction. *J. Invest. Dermatol.* 112, 782–787.
- Werner, S., 1998. Keratinocyte growth factor: a unique player in epithelial repair processes. *Cytokine Growth Factor Rev.* 9, 153–165.
- Werner, S., Smola, H., 2001. Paracrine regulation of keratinocyte proliferation and differentiation. *Trends Cell Biol.* 11, 143–146.
- Werner, S., Krieg, T., Smola, H., 2007. Keratinocyte-fibroblast interactions in wound healing. *J. Invest. Dermatol.* 127, 998–1008.
- Yamaguchi, Y., Itami, S., Tarutani, M., Hosokawa, K., Miura, H., Yoshikawa, K., 1999. Regulation of keratin 9 in nonpalmoplantar keratinocytes by palmoplantar fibroblasts through epithelial–mesenchymal interactions. *J. Invest. Dermatol.* 112, 483–488.
- Yang, L., Scott, P.G., Dodd, C., Medina, A., Jiao, H., Shankowsky, H.A., et al., 2005. Identification of fibrocytes in postburn hypertrophic scar. *Wound Repair Regen.* 13, 398–404.
- Zhou, Y., Hagood, J.S., Murphy-Ullrich, J.E., 2004. Thy-1 expression regulates the ability of rat lung fibroblasts to activate transforming growth factor- α in response to fibrogenic stimuli. *Am. J. Pathol.* 165, 659–669.
- Zimmermann, D.R., Dours-Zimmermann, M.T., Schubert, M., Bruckner-Tuderman, L., 1994. Versican is expressed in the proliferating zone in the epidermis and in association with the elastic network of the dermis. *J. Cell Biol.* 124, 817–825.

IMPRINTING AND EXTRAEMBRYONIC TISSUES—MOM TAKES CONTROL

Kamelia Miri *and* Susannah Varmuza

Contents

1. Introduction	216
2. Genomic Imprinting—What is It?	217
2.1. Genomic imprinting phenomena—Mammals	217
2.2. Genomic imprinting phenomena—Plants and insects	219
3. Genomic Imprinting as a Maternal Effect	220
3.1. Active remodeling of paternal but not maternal pronucleus	220
3.2. Familial hydatidiform moles caused by maternal effect mutations	221
3.3. Maternal effect phenotypes associated with DNA methyltransferase mutations	222
3.4. Other maternal effect mutations affecting imprinting	223
3.5. Mother Knows Best model of genomic imprinting	224
4. Placenta as Target of Imprinting	225
4.1. Placentation	226
4.2. Imprinted gene function in development	228
4.3. PrE in development	239
4.4. Tetraploid rescue experiments and their potential for exploring imprinted gene function	241
5. Conclusions	246
Acknowledgments	246
References	247

Abstract

Genomic imprinting is an epigenetic mechanism that silences one parental allele of a small subset of genes. Many imprinted genes exhibit this property only in extraembryonic tissues—placenta and yolk sac. This has led to the idea that imprinting in mammals coevolved with some aspect of placentation. Nevertheless, many studies of imprinting have ignored the extraembryonic tissues, the yolk sac and its precursor, the primitive endoderm, in particular. The primitive endoderm is involved in very early signaling events during a critical

Department of Cell and Systems Biology, University of Toronto, Toronto, Ont., Canada M5S 3G5

International Review of Cell and Molecular Biology, Volume 276
ISSN 1937-6448, DOI: 10.1016/S1937-6448(09)76005-8

© 2009 Elsevier Inc.
All rights reserved.

stage in development, gastrulation, during which body plan axes and head process neuroectoderm are established. Improper signaling from primitive endoderm as a result of abnormal expression of imprinted genes has the capacity to effect long-term defects in embryonic/fetal tissues that might hitherto have been overlooked. We discuss these gaps in the knowledge, propose a mechanism for genomic imprinting based on current data, and suggest a line of investigation that will expand our understanding of this unique regulatory mechanism and its impact on development.

Key Words: Genomic imprinting, Placenta, Yolk sac, Primitive endoderm, Maternal effect. © 2009 Elsevier Inc.

1. INTRODUCTION

Reproduction is a perilous journey for women. Until the twentieth century, maternal death due to pregnancy complications was a common occurrence, and still is in parts of the world with poor healthcare infrastructure. In developed countries, maternal health during pregnancy is monitored more rigorously, but the risks still remain high. Mammalian reproduction has often been described as parasitic, in large part because of the intimate relationship between fetal and maternal tissues at their interface, the placenta. Indeed, there is evidence that fetal cells from the placenta remain in the maternal circulation for long periods of time, and they may contribute to autoimmune diseases in later life (Bianchi, 2000; Waldorf and Nelson, 2008).

Reproduction is also a risky venture for the child. In humans, it is extraordinarily inefficient, with up to an estimated 70% of conceptions being wasted, often before pregnancy is detected. Of documented pregnancies, 31% end in spontaneous abortion. While miscarriage is also often associated with abnormal placentation, it is unclear which came first, a dead embryo or a malfunctioning placenta (Jauniaux and Burton, 2005). Recent evidence has indicated that the placenta can have a more profound effect on fetal development than originally thought, and has led to the “Developmental Origins Hypothesis” of adult disease (Barker, 2004; Godfrey, 2002; Red-Horse et al., 2004), which posits that events occurring during development can have life-long effects. Certainly, the impact of placenta function on fetal growth is evident from studies of intrauterine growth retardation (IUGR) (Chaddha et al., 2004; Gluckman and Hanson, 2004; Monk and Moore, 2004; Ross and Beall, 2008), a major negative health predictor for newborns and children (Bamberg and Kalache, 2004; Victora et al., 2008).

One significant factor involved in both placental and fetal development is genomic imprinting, in which subsets of genes are monoallelically expressed in a parent-of-origin fashion. Much of the research in this area has focussed mainly on fetal growth, overlooking some critical features of

gene regulation during development, including important signaling roles played by extraembryonic tissues in establishing body axes and inducing specification of tissues such as the neuroectoderm and the germline.

In this chapter, we will describe genomic imprinting, discuss a model of genomic imprinting-based evidence of a maternal effect mechanism, outline the results of targeted mutagenesis studies in mice, and propose some avenues of research that will enlighten our understanding of both genomic imprinting and the function of extraembryonic tissues during development. Much of the chapter will focus on imprinting in mice because the bulk of experimental data derives from murine studies. Links to studies of human imprinted genes and parent-of-origin effects can be found at the Otago imprinting Web site (<http://igc.otago.ac.nz/home.html>).

2. GENOMIC IMPRINTING—WHAT IS IT?

Genomic imprinting is an epigenetic gene silencing mechanism that distinguishes alleles in a parent-of-origin fashion. One subset of genes is expressed only from the maternal allele, while a different subset of genes is expressed only from the paternal allele. There have been numerous excellent reviews of genomic imprinting written over the past several years (Bourc'his and Proudhon, 2008; Hore et al., 2007; Sha, 2008; Wan and Bartolomei, 2008).

2.1. Genomic imprinting phenomena—Mammals

Genomic imprinting in mammals was discovered in 1984 following experiments in which maternal or paternal pronuclei were microsurgically transplanted between zygotes to create embryos with two paternal genomes (androgenotes), two maternal genomes (gynogenotes/parthenotes), or normal controls (Barton et al., 1984; McGrath and Solter, 1984). Androgenotes fail to develop past early postimplantation stages, and typically have poorly developed embryo components, but hyperplastic trophoblast. Parthenotes also fail to develop past early postimplantation stages, and have almost nonexistent trophoblast, but well developed if small embryos. The interpretation of these observations, since borne out by extensive research, was that some genes are expressed exclusively from one parental allele. There is a growing list of imprinted genes that display parent-of-origin monoallelic expression (<http://www.mgu.har.mrc.ac.uk/research/imprinting>, <http://igc.otago.ac.nz/home.html>).

The discovery of genomic imprinting also provided an explanation for the failure to recover certain combinations of reciprocal translocation offspring (Cattanach, 1986). In these experiments, Robertsonian or reciprocal

translocation chromosomes were transmitted, in a small number of cases resulting from nondisjunction events in both parents, in such a way as to generate offspring with cytologically balanced chromosome complements in which whole chromosomes or parts of chromosomes were inherited from only one parent. Certain combinations proved to be either lethal, in which none of the expected nondisjunction offspring was observed, or developmentally catastrophic, in which the affected offspring displayed recognizable abnormalities. For example, maternal duplication/paternal deletion (matDp/patDel) of proximal Chr 11 causes fetal and placental growth restriction, while the reciprocal patDp/matDel causes fetal/placental overgrowth. This led to the generation of an imprinting map, based on lethality or abnormal phenotypes observed in mice with uniparental inheritance of particular chromosomal regions. This imprint map is *a priori* highly parsimonious; there may be imprinted genes/domains that result in either no or a highly subtle phenotype that would have been missed by the nondisjunction studies. The imprint map can be found at the Harwell Web site (<http://www.mgu.har.mrc.ac.uk/research/imprinting>).

Since the discovery of genomic imprinting, close to 90 genes have been identified in the mouse that exhibit monoallelic expression. Studies aimed at identifying imprinted genes have relied on comparisons of transcriptomes between normal and abnormal embryos, cells, or tissues (Kuzmin et al., 2008; Miyoshi et al., 1998; Mizuno et al., 2002; Nikaïdo et al., 2003; Piras et al., 2000; Schultz et al., 2006). Recently, high throughput sequence analysis of *M. castaneus* × *M. domesticus* F1 embryos made use of single-nucleotide polymorphism (SNP) representation to reveal monoallelic transcripts in the whole transcriptome. Several newly identified imprinted genes were revealed with this methodology (Babak et al., 2008). The analysis of the placenta transcriptome will be an extremely useful resource when it is completed.

What distinguishes the two parental alleles such that one is silent and the other active? This is still an open question, although progress has been made in understanding the molecular underpinning of genomic imprinting. One of the earliest features to be examined was the state of methylation of the genomic DNA surrounding imprinted alleles. Many, although not all, imprinted genes are methylated on the inactive allele. Also, as additional imprinted genes were identified, it became clear that most are clustered together in chromosomal domains. This observation inspired extensive research into the *cis* regulatory controls governing imprinting, and led to the discovery that all of the genes within imprinted domains, in general, are controlled by a single element, called a germline differentially methylated region (DMR) or imprint control region (ICR). Several recent reviews describe this research in greater detail (Edwards and Ferguson-Smith, 2007; Wood and Oakey, 2006).

While imprinting has been observed in a number of different mammalian species, exhaustive searches in nonmammalian vertebrates have been fruitless.

Marsupials display a limited repertoire of imprinted genes, probably because the analysis in these species is still ongoing. Monotremes appear to have dispensed with imprinting altogether suggesting that in mammals imprinting arose after the divergence of metatheria (placental mammals, marsupials) from prototheria (monotremes) (Hore et al., 2007). This coincides with the evolution of the placenta (see below), leading many investigators to speculate that some aspect of placentation benefits from genomic imprinting (Charalambous et al., 2007; Coan et al., 2005; Hall, 1990; Kaneko-Ishino et al., 2003; Renfree et al., 2008; Varmuza and Mann, 1994; Wagschal and Feil, 2006).

2.2. Genomic imprinting phenomena—Plants and insects

Parent-of-origin phenomena have been observed in angiosperm plants and various arthropods, such as Sciarids and Coccids. Indeed, the term “imprinting” was coined in reference to the unusual cytological behavior of paternal chromosomes in Sciarids by Crouse (1960), although a less confusing term, “chromosome conditioning,” was originally used by White as early as the 1945 edition of his book *Animal Cytology and Evolution* in reference to the paternal genome elimination in Coccids (White, 1945, 1973).

Imprinting in plants is confined to the endosperm, the part of the seed that can be loosely equated with the mammalian placenta, in part because it is embryonic rather than maternal. The ovule consists of a haploid oocyte and a diploid central cell, surrounded by the maternal cells of the seed coat. Double fertilization, with one pollen cell joining the oocyte and the other entering the central cell, generates two distinct products, the embryo and the endosperm, respectively. The endosperm nuclei undergo several rounds of endoreduplication before migrating to the periphery of the central cell and engaging in cellularization, in a fashion reminiscent of early *Drosophila* blastoderm nuclear divisions. The endosperm is sensitive to imbalance in the dose of maternal and paternal genomes; excess of maternal genomes results in premature cellularization and a small endosperm, while excess paternal genomes leads to delayed cellularization and overgrown endosperm. Both situations are in general lethal and lead to seed abortion (Scott et al., 1998).

So far only 10 imprinted plant genes have been identified (Huh et al., 2007). Of these, eight are maternally expressed and two, *Pheres* and *peg 1*, are paternally expressed. Imprinted expression of several of these genes has been demonstrated to depend on differential methylation and regulation by *Medea*, itself an imprinted polycomb group (PcG) gene. The emerging theme in plants indicates that the differential methylation is achieved by active demethylation of one allele in the endosperm by maternally inherited proteins such as DME (Gehring et al., 2006) or by inhibition of methylation by an Rb complex during female gametophyte development (Jullien et al., 2008), indicating that methylation is the default state.

Various arthropods make use of differential chromosome marks to drive sex determination. The general theme involves heterochromatinization of paternal chromosomes followed by nondisjunctional loss during some phase of early embryonic development, or sequestration of heterochromatinized chromosomes into inactive sites. In Coccids (mealybugs), haploid embryos develop as males while diploid embryos develop as females. Haploidy is achieved by either wholesale elimination or functional inactivation of the paternal genome (Bongiorni and Prantera, 2003; White, 1973). In Sciarids, which have a sex chromosome sex determination mechanism similar to nematodes, the situation is more complicated, with subsets of the paternal genome being eliminated during development, including X chromosomes prior to sex determination. The number of paternal X chromosomes eliminated will determine whether the embryo becomes a female (one of three lost) or a male (two of three lost) (Goday and Esteban, 2001). Interestingly, there is evidence that sex determination in coccids and sciarids is controlled by maternal factors inherited in the oocyte, probably so that populations can respond to shifting environmental needs (Nelson-Rees, 1960; White, 1973). Similar phenomena have been described in other arthropods harboring endosymbiotic *Wolbachia* proteobacteria (Werren et al., 2008).

3. GENOMIC IMPRINTING AS A MATERNAL EFFECT

What is becoming clear from a growing body of evidence is that the mechanism by which genes become imprinted is a maternal effect. The mechanisms of genomic imprinting in plants and arthropods appear to be regulated by maternal factors in the oocyte or female gametophyte. In mammals, evidence is also accumulating that genomic imprinting is a maternal effect regulated by oocyte proteins, and acting in part during the long first cell cycle that precedes cleavage divisions.

3.1. Active remodeling of paternal but not maternal pronucleus

By 1994, differential methylation of maternal and paternal genomes had been demonstrated to be extensive, and not restricted to imprinted genes. This is not surprising in cells of such profoundly different nature (egg and sperm) (Sanford et al., 1987). Global demethylation had been shown to occur after fertilization; this was believed to be mostly passive demethylation. Recently, the nature of the global demethylation was revealed to be highly selective, with the paternal genome undergoing extensive active demethylation a few hours after fertilization. Immunohistochemistry with

an antibody directed against 5-methyl cytosine revealed a positive signal on both maternal and paternal pronuclei at 3 h after fertilization, but a positive signal on only the maternal pronucleus at 8 h after fertilization (Morgan et al., 2005; Santos et al., 2002). Either the paternal genome brings its own demethylating activity with it, or the two pronuclei have different trafficking capabilities, such that a demethylase and possibly other chromatin modifying activities have ready access to the paternal genome, but are blocked from entering the maternal pronucleus. Such a scenario makes intuitive sense given the state of the paternal genome at fertilization; it is highly condensed and associated with protamines that must be stripped off and replaced by histones. On the other hand, the maternal genome is poised for development, as is evident by the capacity of parthenogenetic embryos to recapitulate early events with ease. Other chromatin remodeling events that discriminate the two parental pronuclei have also been observed (Santos et al., 2005; Yoshida et al., 2007). Interestingly, somatic nuclei transplanted into enucleated oocytes do not follow a pattern that is like either pronucleus, suggesting that there is something idiosyncratic about somatic nuclei that causes them to respond differently to the oocyte environment (Yoshida et al., 2007).

3.2. Familial hydatidiform moles caused by maternal effect mutations

Hydatidiform moles are relatively rare, but potentially deadly (to the mother) conceptuses that possess two paternal genomes but no maternal genome. The trophoblast is hyperplastic and can aggressively metastasize if left untreated. Most molar pregnancies are spontaneous. However, there are several rare families presenting with Familial Biparental Complete Hydatidiform Moles (BiCHM) (Slim et al., 2005). In these families, affected women have recurring molar pregnancies as a result of one or more recessive mutations. Analysis of the methylation pattern of molar tissues from one of these families revealed that the maternal genome had taken on a paternal-like methylation pattern at several imprinted genes (Judson et al., 2002).

These data are consistent with two alternative hypotheses: (1) the maternal genome adopts a paternal-like epigenetic pattern during oogenesis, or (2) the maternal pronucleus loses its ability to block access to demethylating and chromatin modifying activities after fertilization.

These two hypotheses can only be resolved by examining the epigenetic state of maternal genomes in oocytes of affected females. Identification of mouse models will be extremely useful in this regard, bypassing difficult and invasive experiments in humans.

Recently, one of the loci associated with Familial BiCHM has been identified as the *Nalp7* gene (Murdoch et al., 2006). NALP7 is likely a multifunctional protein, and possesses several domains, one of which, the LRR domain, is present on Ran GAP polypeptides, and is required for

functional nuclear trafficking by these proteins (Haberland and Gerke, 1999). Indeed, the related mouse *Nalp5* protein, product of the *Mater* locus, has been shown to be associated with nuclear pores, among other things (Tong et al., 2004). Mice do not have a *Nalp7* orthologue, although the *Nalp* family of genes is quite large; however, *Nalp5* is 37% identical and 22% strongly similar to human NALP7. Loss of function mutations of *Mater/Nalp5* causes arrest at the two-cell stage. It should be remembered that the *NALP7* mutations associated with BiCHM are not null mutations. Two are splice site mutations, one of which must be a hypomorphic allele since there were at least two live births recorded from a patient homozygous for the mutation. The second splice site mutation is in intron 7, and would generate a protein missing the last 99 (10%) amino acids. The other four mutations were all nonsynonymous substitutions. *Mater*, on the other hand, is a null mutation in *Nalp5* and would be expected to produce the most severe phenotype. Analysis of imprinting defects in *Nalp5/Mater* mutant mice, and other *Nalp* mutations that have a maternal effect phenotype, may provide some insight into the function of NALP7 in human BiCHM.

3.3. Maternal effect phenotypes associated with DNA methyltransferase mutations

The association of differential methylation with genomic imprinting naturally led investigators to look at DNA methyltransferases. Mammals possess several genes that potentially encode DNA methyltransferases: *Dnmt1*, *Dnmt3A*, *Dnmt3B*, and *Dnmt3L*. Targeted mutations have been made in all of these genes.

Dnmt1 is the major maintenance methylase, and is required to maintain both imprinted and nonimprinted methylation patterns (Li et al., 1992). There are two isoforms of *Dnmt1*: the somatic isoform which is required for embryonic development beyond about day 7 and which maintains both imprinted and nonimprinted methylation patterns, and the oocyte isoform (*Dnmt1o*) which is required strictly for imprinted gene methylation maintenance (Howell et al., 2001). Loss of *Dnmt1o* leads to loss of imprinted methylation on both maternal and paternal alleles, and is a classic maternal effect mutation; that is, the effect is observed in the embryos of *Dnmt1o*^{-/-} mothers, regardless of the genotype of the embryos. In addition, immunostaining experiments on oocytes and preimplantation embryos with zona pellucida-induced conditional knockout of *Dnmt1* confirm this maintenance methylase to be exclusively maternal up to the blastocyst stage (Hirasawa et al., 2008).

Dnmt3L is also a maternal effect methyltransferase required for imprinted gene methylation in embryos of affected mothers (Bourc'his et al., 2001; Hata et al., 2002). Loss of maternal *Dnmt3L* leads to death of heterozygous embryos at midgestation with particularly severe effects on the placenta.

Interestingly, parthenogenetic embryos derived from Dnmt3L homozygous mothers display the same phenotype as fertilized embryos from *Dnmt3L*^{-/-} mothers, which suggest that the paternal genome is a passive participant, up to this stage of development, in these embryos (Tim Bestor, personal communication). Paternal loss of *Dnmt3L* causes male infertility through disruption of meiosis.

Dnmt3A and Dnmt3B are homozygous lethal. However, the role of these proteins in both oogenesis and spermatogenesis was examined in conditional knockout mice, where the genes were mutated in germ cells only (Kaneda et al., 2004). Loss of maternal *Dnmt3A* produces the same phenotype as maternal loss of *Dnmt3L*—embryos die at midgestation and lose maternal methylation imprints. Similarly, paternal loss of *Dnmt3A* also causes meiotic failure and male infertility. Germ cell knockout of *Dnmt3B* has no effect. Interestingly, Dnmt3L interacts with Dnmt3A in co-IP experiments of transfected COS-1 cells (Hata et al., 2002). Furthermore, zona pellucida-induced conditional knockout of Dnmt3a identifies it solely of maternal origin up to the blastocyst stage (Hirasawa et al., 2008).

3.4. Other maternal effect mutations affecting imprinting

The *Stella/PGC7* null mutation and a dominant negative *Ranbp5* transgene separately generate the same phenotype—a maternal effect postfertilization loss of imprinting (LOI) of both maternal and paternal targets (Nakamura et al., 2007). These experiments were interesting in that the authors examined the “methylation imprints” of maternally methylated DMRs and found that they were established normally during gametogenesis, but were lost in the wave of demethylation observed after fertilization. Indeed, the maternal pronuclei were demethylated along with the paternal pronuclei in these mutants. One interpretation that is consistent with all of these observations is the idea that genomic imprinting is in part a function of protection of the maternal genome from a zygotic wave of “remodeling” that is necessary to prepare the paternal genome for development. Selective protection could be achieved by differential pronuclear trafficking. In this regard, it is interesting to note that *Ranbp5* is a known component in nuclear trafficking machinery.

Genetic evidence from elegant studies with *Peromyscus* hybrids has revealed that some of the components of the imprinting machinery behave like maternal effect mutations. *Peromyscus* (deer mice) range across North America. However, there is a clear boundary between the ranges of two major species, with *P. maniculatus* (BW) residing in most of North America, except the southwest United States, which is inhabited by *P. polionotus* (PO) (Loschiavo et al., 2006). Reciprocal crosses between BW and PO generate two different kinds of offspring—small but viable (BW × PO) or large and dysmorphic/lethal (PO × BW), with particularly severe effects on placental

development and function, suggesting an incompatibility associated with imprinting. Indeed, LOI has been observed in the lethal cross for several imprinted genes (Vrana *et al.*, 1998). Genetic analysis of backcross progeny has revealed that the LOI phenotype is in part a function of several maternal effect loci (Duselis *et al.*, 2005). Molecular identification of these genes will be an important addition to our understanding of the process.

3.5. Mother Knows Best model of genomic imprinting

The evidence that has accumulated over the past several years allows us to propose a model of genomic imprinting that accounts for the disparate observations made in both wild-type and manipulated embryos. We refer to this as the Mother Knows Best mechanism of genomic imprinting (Fig. 5.1). The main supposition is that the paternal genome is a passive participant in a process that is part of the initial phase of oocyte activation. This includes the remodeling of the paternal genome that occurs just after fertilization and involves the replacement of protamines by histones. The maternal genome does not need to be remodeled, and so is protected from

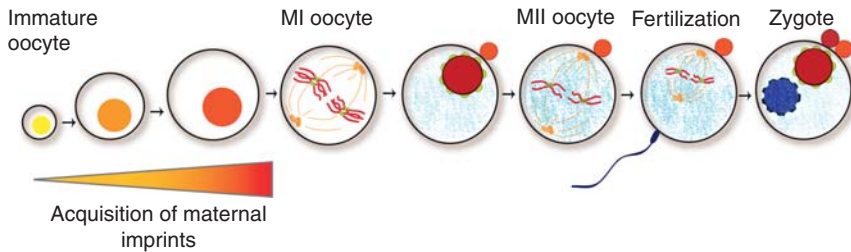


Figure 5.1 Mother Knows Best model of genomic imprinting. Immature oocytes are naive with respect to imprinting (yellow nucleus). As they mature, they acquire maternal methylation imprints (progression from yellow to dark red). At the same time, the oocyte cytoplasm is expanding, and components of the remodeling system necessary for paternal genome epigenetic establishment are deposited (blue dots). To shield the maternal genome from this remodeling, the maternal nuclear envelope nuclear/cytoplasmic trafficking highway is modified to exclude enzymes such as demethylases. Some of these nuclear envelope modifying components (green dots) may become associated with the maternal metaphase spindle, and reform after fertilization on the maternal pronucleus. The paternal pronucleus (dark blue sphere), which does not contain the nuclear envelope modifying components, is porous with respect to the remodeling components in the oocyte cytoplasm, and allows ready access to components such as DNA demethylase. This model would explain the results of Kono *et al.* (2002) in which parthenogenetic embryos derived from a combination of immature or nongrowing (ng) (yellow nucleus, no protection) and fully grown (fg) (dark red, fully protected) pronuclei were able to develop to much later stages than “normal” parthenogenetic embryos, which mostly die before or at gastrulation (Varmuza *et al.*, 1993). The ng pronuclei would have behaved like the paternal pronucleus and allowed free passage to remodeling components.

much of this activity by factors that accumulate during the maturation process, some of which associate with the nuclear envelope and regulate trafficking in and out of the pronucleus. It is well known that nuclear-pore proteins such as nucleoporins associate with the kinetochore during mitosis, and drive reassembly of nuclear pore complexes after cell division (Antonin et al., 2008); maternal pronuclear components would be associated with the second meiotic spindle in ovulated oocytes. Somatic nuclei, with their own distinctive nuclear envelopes, would respond to the oocyte cytoplasm in an idiosyncratic fashion, which might explain the restricted ability of cloned embryos to proceed through development. Tissue-specific components of the nuclear trafficking machinery are not a novel idea (D'Angelo and Hetzer, 2008). Some of the difference could also be mediated by differential posttranslational modification; the MII oocyte form of NPM2, a nuclear chaperone, is phosphorylated but becomes partially dephosphorylated in zygotes and progressively less phosphorylated through early development (Vitale et al., 2007).

This model would also explain the remarkable survival of parthenogenetic embryos created by transplanting one immature (ng) and one mature (fg) maternal “pronucleus” into activated oocytes (Kono et al., 1996, 2002); the “ng” pronucleus would be comparable to a paternal pronucleus in its accessibility to oocyte remodeling machinery. It is also consistent with the observation that most germline DMRs are methylated on the maternal allele. There are three paternally methylated DMRs—the *H19* DMR, the *Dlk1* locus IG-DMR, and the *Rasgf1* DMR. Methylation of the *H19* DMR may be the default state; loss of oocyte CTCF protein results in methylation of the maternal *H19* DMR, suggesting that it is protected from methylation by the binding of CTCF (Fedoriw et al., 2004). A similar situation may exist for the *Dlk1* locus IG-DMR, although CTCF protein is not involved (Edwards and Ferguson-Smith, 2007). Deletion of the unmethylated maternal IG-DMR leads to paternalization of the locus, including methylation of secondary sites that are normally differentially methylated on the paternal allele (Lin et al., 2003). This “paternalized” state is similar to the nonimprinted (default) state of the marsupial *Dlk1* locus (Edwards et al., 2008).

4. PLACENTA AS TARGET OF IMPRINTING

While the necessity of remodeling the paternal genome following fertilization seems intuitive, the outcome in which a subset of genes is differentially silenced does not. One rationale for imprinting in mammals is protection of mothers from aggressive or ectopic placentation (Hall, 1990; Varmuza and Mann, 1994). Regulation of placental growth and function is

also critical for survival of offspring, as both overgrowth (large offspring syndrome—LOS) and growth retardation (intrauterine growth restriction—IUGR) are pathological conditions (Ross and Beall, 2008; Young et al., 1998). A maternally controlled mechanism that regulates extraembryonic tissues would ensure survival of females and offspring during pregnancy. Interest in the placental connection to genomic imprinting has enjoyed a recent surge (Charalambous et al., 2007; Coan et al., 2005; Kaneko-Ishino et al., 2003; Renfree et al., 2008; Wagschal and Feil, 2006), especially following the realization that for a number of genes, the imprint exists only in the extraembryonic tissues. It is therefore useful to review our knowledge of the development and evolutionary relationships of fetal membranes, and to examine the role played by imprinted genes in development of extraembryonic tissues.

4.1. Placentation

Imprinting has been most extensively studied in mice and humans, although a growing interest in evolutionary origins of biological systems has expanded the field of study to include other mammals, including marsupials, and to a lesser extent, monotremes. The latter two taxa have informed our understanding of genomic imprinting largely because of the differences in placentation among the three branches of mammals—monotremes (egg laying), marsupials (mostly yolk sac placenta, but sometimes chorioallantoic with invasive trophoblast), and eutherians (variable types and combinations of chorioallantoic and yolk sac placentas). Yolk sac placentation is the more basal type, and can be found in some nonmammalian vertebrates such as viviparous fish and reptiles (Mossman, 1987). Imprinting has so far not been found in any nonmammalian species and appears to be restricted to marsupial and eutherian mammals. This raises questions about the selective pressures that might have led to imprinting in mammals. Coevolution of some aspects of placentation and genomic imprinting is a logical interpretation.

In eutherians, the function of the placenta is to provide a safe place for interchange between maternal and fetal vascular systems. The two bloods do not mix. Instead, blood vessels from both are remodeled such that between them lies a series of trophoblastic endothelial-like cells that allow nutrient and gas exchange. Fetal placental vessels project villi into maternal vascular spaces that are lined with trophoblast cells. The whole structure is designed to maximize surface area exchange, and is tightly regulated by physiological cues coming from both the placenta and the maternal homeostasis system (Cross et al., 2003; Georgiades et al., 2002; Mossman, 1987; Red-Horse et al., 2004; Rossant and Cross, 2001). Dysregulation of placentation can be catastrophic for both mother and child; excessive growth can lead to invasive, malignant trophoblast disease in the mother (Hui et al., 2005),

while hypoplastic growth is associated with maternal hypertension (pre-eclampsia) and fetal growth retardation (IUGR) (Cross, 2003; Fisher, 2004).

Most of the mechanistic details of extraembryonic tissue development in mammals have been generated by developmental and genetic studies of mice. The first differentiation event in murine embryos is the formation of the trophoblast, the outer layer of epithelial cells that initially pump fluid into the interior of the embryo to form a blastocyst. In murine embryos, FGF4 signaling from the inner cell mass, the prospective fetus, prevents the trophoblast cells in close proximity (polar trophoctoderm) from differentiating into giant cells (Rossant and Cross, 2001). The cells that receive insufficient FGF4 signals on the opposite side of the blastocyst (mural trophoctoderm) differentiate into primary trophoblast giant cells. These will later interact with the uterine epithelium to mediate attachment and invasion of the embryo into the endometrium.

A second differentiation event involves delamination of primitive endoderm (PrE) cells from the inner cell mass. These cells initially line the blastocoel cavity and are destined to form a layer of cells in direct apposition to the epiblast that are critical in signaling positional cues required for the establishment of embryonic axes and specification of embryonic tissues such as neuroectoderm and germline (the AVE, see section on PrE below). PrE derivatives also form part of the yolk sac, likely reflecting one of the ancient roles played by these extraembryonic cells. Recent evidence indicates that, similar to the situation with several nonmammalian vertebrates (Mossman, 1987), PrE cells are subsumed by the embryo proper and end up populating part of the gut (Kwon et al., 2008).

Following implantation, the polar trophoctoderm expands into two subpopulations—the ectoplacental cone (epc) and the extraembryonic ectoderm (eee). Trophoblast cells migrate out of the epc and invade the maternal spiral arteries to remodel the interior and create large vessels or vascular sinuses. Other trophoblast cells migrate from the epc into the maternal decidua, while those remaining behind proliferate to create a spongiotrophoblast layer. The eee starts out as a cylinder, which widens and flattens eventually creating a tri-layered structure called the labyrinth that, following fusion with the allantois, an extraembryonic mesoderm derivative, undergoes branching morphogenesis to form villi-like projections into maternal blood spaces. A similar, although not identical, process yields the human placenta. Many of the genes involved in the various aspects of placental development have been identified through targeted mutagenesis in the mouse, or through expression analyses in human placenta (Cross et al., 2003; Red-Horse et al., 2004; Rossant and Cross, 2001).

Prior to elaboration of the vascularized placenta, the embryo depends on sustenance from the yolk sac, which develops from the PrE and extraembryonic mesoderm that migrates out of the posterior end of the primitive streak. The extraembryonic mesoderm generates the vascular components

of the yolk sac placenta, while the PrE layer plays a supporting role, both structurally and molecularly. Many eutherians retain yolk sac placentas throughout pregnancy, and most marsupials use only yolk sac placentas; an exception to the latter are the bandicoots (Peramelidae), which occupy a basal position in the phylogeny of Australian marsupials, but not of all marsupials (Asher et al., 2004) (Fig. 5.2). Chorioallantoic placentas develop in bandicoots (Freyer et al., 2003; Mossman, 1987). The phylogenetic relationship of bandicoots within the Marsupial family tree suggests that chorioallantoic placentation either arose independently twice—once in the lineage leading to modern eutherians and a second time in the marsupial branch leading to Australian bandicoots, or it arose once in the eutherian/marsupial common ancestor and has been silenced in most modern marsupials. Imprinting has been demonstrated for some genes in marsupials, but not in monotremes (Hore et al., 2007), suggesting that some aspect of marsupial/eutherian development, such as chorioallantoic placentation, has coevolved with genomic imprinting. Another feature that may have coevolved with imprinting is invasive trophoblast. Invasiveness is a feature that comes and goes, both in marsupials and eutherians, possibly because it is suppressed in some species more than in others (Freyer et al., 2003). Coevolution of imprinting and invasive trophoblast is consistent with maternal control of reproduction in mammals.

4.2. Imprinted gene function in development

The most informative experiments regarding the role of genomic imprinting in development are the studies of targeted mutations in mice. Table 5.1 lists the knockout models that have been studied to date. Forty imprinted genes have been knocked out (KO) by targeted mutagenesis and display a variety of phenotypes. Reports for 19 of these genes did not examine the

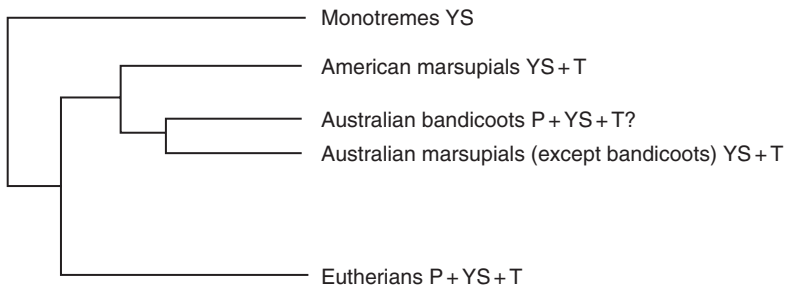


Figure 5.2 Phylogeny of mammals. This cladogram illustrates the evolutionary relationships of the mammals. All have yolk sac placentas (YS), whereas only eutherians and bandicoots also have chorioallantoic placentas (P). Invasive trophoblast (T) is widespread throughout the therian lineage.

Table 5.1 Targeted mutations in imprinted genes

Gene	Exp. Ex.	Exp. Som.	KO placenta	KO embryo	References
<i>Ascl2</i>	M (pl)	Bi	Reduced labyrinth, expanded giant cell	Lethal at e10	Guillemot et al. (1994)
<i>Calcr</i>	Bi (pl)	M (br)	Not examined	Lethal (recessive)	Dacquain et al. (2004)
<i>Cd81</i>	M (pl)	Bi	Not examined; assumed normal	Impaired antibody response (recessive)	Maecker and Levy (1997)
<i>Cdkn1c</i>	M	M	Hyperplastic spongio and labyrinthine layers with reduced trophoblast invasion of maternal vessels leading to preeclampsia	Multiple defects including overgrowth and neonatal lethality	Kanayama et al. (2002), Takahashi et al. (2000)
<i>Cited</i>	M (pl)	Bi (X-linked)	Abnormal; enlarged maternal sinuses	Growth restricted; perinatal lethal	Rodriguez et al. (2004)
<i>Commf1</i>	U	M (br)	Failed vascularization (recessive)	Embryonic lethal (recessive)	van de Sluis et al. (2007)
<i>Dlk1</i>	P (pl)	P	Not examined	High levels pre and perinatal lethality; growth retardation	Moon et al. (2002)
<i>Gnas</i>	U	M (fat)	Not examined	Edema; mild effects on metabolism	Yu et al. (2000), Skinner et al. (2002)

(continued)

Table 5.1 (continued)

Gene	Exp. Ex.	Exp. Som.	KO placenta	KO embryo	References
<i>Gnasxl</i>	U	P	Not examined	Hypoactive, thin; postnatal lethality	Plagge et al. (2004)
<i>Nesp</i>	U	M	Not examined	Mild behavioral defects	Plagge et al. (2005)
<i>Grb10</i>	M	M	Slight overgrowth	30% overgrowth	Charalambous et al. (2003)
<i>Gtl2</i>	M (pl)	M in some	Not examined	Partial lethality, overgrowth; both subject to genetic modifier effects	Steshina et al. (2006)
<i>H19</i>	M	M	No phenotype	No phenotype	Leighton et al. (1995a)
<i>Htr2a</i>	U	M (br, ovary, eye)	Not examined; presumed normal	Behavior (recessive)	Weisstaub et al. (2006)
<i>Igf2</i>	P (pl, ys)	P; Bi (br)	Abnormal, reduced	Growth retardation	DeChiara et al. (1991)
<i>Igf2P0</i>	P	Not expressed	Reduced labyrinth	Growth retardation	Constância et al. (2002)
<i>Igf2r</i>	M	M; Bi in some neural tissues	Placentomegaly	Overgrowth, dysmorphic, some embryonic lethality	Wang et al. (1994)
<i>Igf2ras/Air</i>	P	P	Normal weight	Reduced weight	Wutz et al. (2001)
<i>Ins2</i>	P (ys at e14)	Bi (pancreas)	Not reported	No phenotype	Duvillié et al. (1997)

<i>Ipl</i>	M (pl, ys)	M in most	Abnormal; enlarged spongiotrophoblast layer	Normal, viable	Frank et al. (2002)
<i>Kcnk9</i>	U	M (parts of br)	Not examined	Mild brain defects (recessive)	Mulkey et al. (2007)
<i>Kcnq1</i>	M (pl)	M in some	Not examined	Deafness (recessive)	Casimiro et al. (2001)
<i>Kcnq1ot1</i>	P (pl, ys)	P	Reduced weight	Growth retardation	Shin et al. (2008)
<i>Magel2</i>	U	P (br)	Normal weight	Circadian defects	Kozlov et al. (2007)
<i>Mas1</i>	P (ys); Bi (pl)	P (br)	Normal	Mild behavior (recessive?)	Walther et al. (1998)
<i>Mest</i>	P (pl, ys)	P (most)	Growth retardation	Growth retardation; some perinatal and postnatal lethality; all phenotypes subject to genetic modifier effects (Lefebvre, personal communication)	Lefebvre et al. (1998)
<i>Ndn</i>	U (expressed in pl)	P (br)	Not examined	Results differ from no phenotype to perinatal lethality	Tsai et al. (1999), Gérard et al. (1999), Muscatelli et al. (2000)

(continued)

Table 5.1 (continued)

Gene	Exp. Ex.	Exp. Som.	KO placenta	KO embryo	References
<i>Peg3/Pw1</i>	U	P	Growth retardation	Growth retardation; some perinatal lethality; poor “mothering” in females	Curley et al. (2004)
<i>Peg10</i>	P	P (br, vertebrae)	Severely reduced trophoblast	Embryonic lethal	Ono et al. (2006)
<i>Plagl1</i>	P	P	Normal weight and histopathology	Dysmorphology; early postnatal lethality	Varrault et al. (2006)
<i>Pon2</i>	M (pl, ys)	Bi (br)	Not examined, assumed normal	Altered serum LDL	Ng et al. (2006)
<i>Pwrc1</i>	U	P (br)	Normal	Mild postnatal growth deficiency	Ding et al. (2008)
<i>Rasgrf1</i>	U	P (br)	Unkown	Long-term memory deficit	Brambilla et al. (1997)
<i>Rtl1</i> <i>PatKO</i>	P	P	Degeneration of fetal endothelial layer in labyrinth	Pre and perinatal lethality; growth retardation of survivors	Sekita et al. (2008)
<i>Rtl1</i> <i>MatKO</i>	P	P	Overexpression of <i>Rtl1</i> through loss of <i>Rtl1as</i> leads to placentomegaly	Growth retardation	Sekita et al. (2008)

<i>Sgce</i>	P (pl, ys)	P	Not examined	Myoclonus dystrophy	Yokoi et al. (2005, 2006)
<i>Slc22a2</i>	M (pl)	Bi	Not examined, assumed normal	Viable, fertile; bred as $-/-$	Jonker et al. (2003)
<i>Slc22a3</i>	M (pl)	Bi	Reduced uptake-2	Viable, fertile; bred as $-/-$	Zwart et al. (2001b)
<i>Snrpn/ Snurf</i>	P	P	Not examined; assumed normal	No phenotype	Yang et al. (1998)
<i>U2af1-rs1</i>	P	P	Not examined; assumed normal	No reported phenotype	Sunahara et al. (2000)
<i>Ube3a</i>	U (expressed in pl)	M (br)	Not examined	Similar to Angelman Syndrome	Jiang et al. (1998), Albrecht et al. (1997)

Exp. Ex, expression in extraembryonic tissues; Exp. Som., expression in somatic tissues; P, paternal; M, maternal; Bi, biallelic; U, unknown; br, brain; pl, placenta; ys, yolk sac.

placenta at all, even though 8 display problems at birth, including perinatal lethality, usually an indication of developmental abnormalities originating during the fetal period. Sixteen mutations affect placental development, although in some cases, the description was limited to analysis of size. In many cases where placental phenotypes were examined in detail, loss of a maternally expressed gene led to hypertrophy or abnormal differentiation, while loss of a paternally expressed gene led to reduced placental size. However, the placental size effects were not always reflected in the size of the fetus. Most studies of imprinted gene function focus on growth regulation, even though evidence indicates that control of cell differentiation pathways is probably a more critical factor in the effect of loss or gain of function of these gene products. This limited approach to phenotypic evaluation has hampered our understanding of the role of imprinting in development by restricting analysis of placental function to either none or only cursory examination of size.

Several targeted mutations of imprinted genes result in no phenotype at all or recessive phenotypes only, indicating probable biallelic expression in the primary site of action. These genes could be classified as “innocent bystanders”, whose monoallelic expression is a function of proximity to a germline DMR/ICR, but whose imprinted regulation is not germane to their function. A good example of this scenario is the *Igf2r* domain, which consists of *Igf2r*, the regulatory *Air* transcript within the *Igf2r* second intron, and two neighboring genes—*Slc22a2* and *Slc22a3*. Loss of *Igf2r* leads to sublethality and dysmorphology, while its overexpression causes weight reduction. However, loss of both *Slc22a2* and *Slc22a3* is without consequence. Thus, the primary target of the *Igf2r* domain is likely *Igf2r*, while *Slc22a2* and *Slc22a3* are innocent bystanders. Nevertheless, all three genes are imprinted in placenta while only *Igf2r* retains imprinting in somatic tissues. Is *Igf2r* a target because of its imprinted expression in extraembryonic tissues? Is it possible to exclude any known imprinted domains as having primary targets that operate in the extraembryonic tissues?

There are 25 domains that have been identified in the mouse (Fig. 5.3; Table 5.2). Of these, 11 are single gene domains. We have recently discovered a new imprinted domain in mice that consists of a single gene, *Sfmbt2*, that is imprinted only in extraembryonic tissues, where it is expressed at high levels (Kuzmin et al., 2008; Varmuza, unpublished). Seventeen domains have at least one extraembryonically imprinted gene target and six have not been thoroughly examined, even though five of these contain genes known to be expressed in extraembryonic tissues. One domain, *Inpp5f_v2/v3*, is a single gene domain that is not expressed in extraembryonic tissues. *Inpp5f_v2/v3* is a complex gene that has acquired imprinted differential promoter usage associated with insertion of a retrotransposon (Wood et al., 2007). The newly identified *Zbdf2* gene on Chr 1 is biallelic in placenta (Kobayashi et al., 2009); a wider survey of the genes in the

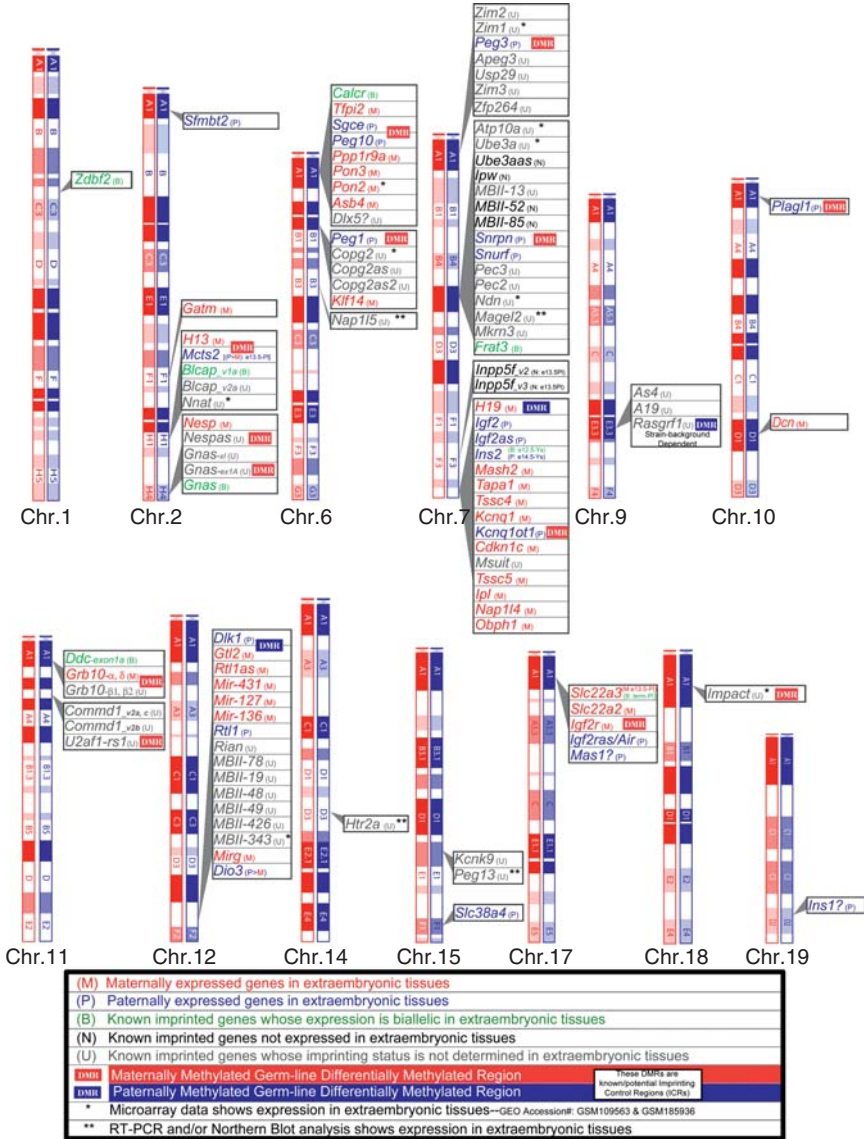


Figure 5.3 Status of imprinted genes in the extraembryonic tissues and their chromosomal location. Parent-of-origin expression in extraembryonic tissues (placenta and yolk sac) is indicated with colored font (blue, paternal; red, maternal; green, biallelic; gray, unknown; black, not expressed). Germline DMRs are indicated by red (maternal methylation) and blue (paternal methylation) background.

Table 5.2 References for genes illustrated in Fig. 5.3

Gene	References
<i>A19</i>	de la Puente et al. (2002)
<i>Apeg3</i>	Choo et al. (2008)
<i>As4</i>	Nomura et al. (2008)
<i>Asb4</i>	Monk et al. (2008), Mizuno et al. (2002)
<i>Atp10a</i>	Kashiwagi et al. (2003), Kayashima et al. (2003a,b)
<i>Blcap_v1a, v2a</i>	Schulz et al. (2009)
<i>Calcr</i>	Hoshiya et al. (2003)
<i>Cdkn1c</i>	Hatada and Mukai (1995), Umlauf et al. (2004)
<i>Commd1_v2a, b, c</i>	Schulz et al. (2009), Wang et al. (2004), Zhang et al. (2006)
<i>Copg2</i>	Lee et al. (2000b)
<i>Copg2as</i>	Lee et al. (2000b)
<i>Copg2as2/Mit1</i>	Lee et al. (2000b)
<i>Dcn</i>	Mizuno et al. (2002)
<i>Ddc-exon1a</i>	Menhennott et al. (2008)
<i>Dio3</i>	Hernandez et al. (2002), Tsai et al. (2002), Yevtodiyyenko et al. (2002)
<i>Dlk1/Pref1</i>	Kobayashi et al. (2000), Schmidt et al. (2000), Takada et al. (2000)
<i>Dlx5</i>	Horike et al. (2005), Kimura et al. (2004), Monk et al. (2008), Schüle et al. (2007)
<i>Frat3/Peg12</i>	Chai et al. (2001), Kobayashi et al. (2002)
<i>Gatm</i>	Sandell et al. (2003)
<i>Gnas</i>	Peters et al. (1999), Williamson et al. (2004, 2006)
<i>Gnas-exon1A</i>	Peters et al. (1999), Williamson et al. (2004, 2006)
<i>Gnasxl</i>	Peters et al. (1999)
<i>Grb10-α and δ</i>	Arnaud et al. (2003), Charalambous et al. (2003), Miyoshi et al. (1998)
<i>Grb10-β1 and β2</i>	Arnaud et al. (2003)
<i>Gtl2/Meg3</i>	Miyoshi et al. (2000), Schmidt et al. (2000)
<i>H13</i>	Wood et al. (2007)
<i>H19</i>	Bartolomei et al. (1991), Leighton et al. (1995b)
<i>Htr2a</i>	Kato et al. (1998)
<i>Igf2</i>	DeChiara et al. (1991), Leighton et al. (1995a,b)
<i>Igf2as</i>	Moore et al. (1997)
<i>Igf2r</i>	Barlow et al. (1991), Hu et al. (1998), Nagano et al. (2008), Stöger et al. (1993)
<i>Igf2ras/Air</i>	Nagano et al. (2008), Sleutels et al. (2003), Wutz et al. (1997)
<i>Impact</i>	Hagiwara et al. (1997)
<i>Impp5f_v2, v3</i>	Choi et al. (2005), Wood et al. (2007, 2008)
<i>Ins1</i>	Deltour et al. (1995, 2004), Giddings et al. (1994)

Table 5.2 (continued)

Gene	References
<i>Ins2</i>	Deltour et al. (1995, 2004)
<i>Ipl/Tssc3/Phlda2</i>	Frank et al. (2002), Qian et al. (1997)
<i>Ipw</i>	Landers et al. (2004), Le Meur et al. (2005), Wevrick and Francke (1997)
<i>Kcnk9</i>	Ruf et al. (2007)
<i>Kcnq1/Kvlqt1</i>	Caspary et al. (1998), Gould and Pfeifer (1998), Paulsen et al. (1998), Umlauf et al. (2004)
<i>Kcnq1ot1/Kvlqt1as</i>	Fitzpatrick et al. (2002), Lewis et al. (2004), Umlauf et al. (2004)
<i>Klf14</i>	Parker-Katirae et al. (2007)
<i>Magel2</i>	Boccaccio et al. (1999), Lee et al. (2000a)
<i>Mas1</i>	Lyle et al. (2000), Schweifer et al. (1997), Villar and Pedersen (1994)
<i>Mash2/Ascl2</i>	Caspary et al. (1998), Guillemot et al. (1995)
<i>MBII-13, 19, 48, 49, 78, 343, 426</i>	Cavaillé et al. (2000)
<i>MBII-52</i>	Cavaillé et al. (2002), Le Meur et al. (2005)
<i>MBII-85/Pwcr1</i>	Cavaillé et al. (2000), de los Santos et al. (2000), Le Meur et al. (2005)
<i>Mcts2</i>	Wood et al. (2007)
<i>Mest/Peg1</i>	Kaneko-Ishino et al. (1995), Reule et al. (1998)
<i>Mir-127, 136, 431</i>	Davis et al. (2005), Seitz et al. (2003)
<i>Mirg</i>	Seitz et al. (2003), Tierling et al. (2006)
<i>Mkm3/Zfp127</i>	Jong et al. (1999)
<i>Msuit</i>	Onyango et al. (2000)
<i>Nap114</i>	Engemann et al. (2000), Paulsen et al. (1998), Umlauf et al. (2004)
<i>Nap115</i>	Smith et al. (2003), Wood et al. (2007)
<i>Ndn</i>	MacDonald and Wevrick (1997), Watrin et al. (1997)
<i>Nesp</i>	Li et al. (2000), Peters et al. (1999)
<i>Nespas</i>	Li et al. (2000)
<i>Nnat</i>	Kagitani et al. (1997), Kikyo et al. (1997)
<i>Obph1/Osbp15</i>	Clark et al. (2002), Engemann et al. (2000)
<i>Pec2, 3</i>	Buettner et al. (2005)
<i>Peg10</i>	Monk et al. (2008), Ono et al. (2001, 2003, 2006)
<i>Peg13</i>	Davies et al. (2004), Smith et al. (2003)
<i>Peg3/Pw1</i>	Curley et al. (2004), Kaneko-Ishino et al. (1995), Kuroiwa et al. (1996)
<i>Plagl1/Zac1</i>	Piras et al. (2000), Smith et al. (2002), Varrault et al. (2006)
<i>Pon2</i>	Monk et al. (2008), Ono et al. (2003)

(continued)

Table 5.2 (continued)

Gene	References
<i>Pon3</i>	Monk et al. (2008), Ono et al. (2003)
<i>Ppp1r9a</i> (<i>Neurabin</i>)	Monk et al. (2008), Ono et al. (2003)
<i>Rasgrf1</i>	de la Puente et al. (2002), Pearsall et al. (1999), Plass et al. (1996), Yoon et al. (2002)
<i>Rian</i>	Cavaillé et al. (2002), Hatada et al. (2001), Shimoda et al. (2002), Seitz et al. (2004)
<i>Rtl1/Peg11</i>	Davis et al. (2005), Sekita et al. (2008), Seitz et al. (2003)
<i>Rtl1as/Antipeg11</i>	Charlier et al. (2001), Davis et al. (2005)
<i>Sfmbt2</i>	Kuzmin et al. (2008)
<i>Sgce</i>	Monk et al. (2008), Piras et al. (2000)
<i>Slc22a2</i>	Nagano et al. (2008), Zwart et al. (2001a)
<i>Slc22a3</i>	Nagano et al. (2008), Zwart et al. (2001a)
<i>Slc38a4/Ata3</i>	Mizuno et al. (2002), Smith et al. (2003)
<i>Snrpn</i>	Gray et al. (1999), Landers et al. (2004), Leff et al. (1992), Le Meur et al. (2005)
<i>Snufr</i>	Gray et al. (1999), Landers et al. (2004), Leff et al. (1992), Le Meur et al. (2005)
<i>Tapa1/Cd81</i>	Caspary et al. (1998), Lewis et al. (2004), Umlauf et al. (2004)
<i>Tfpi2</i>	Monk et al. (2008)
<i>Tssc4</i>	Paulsen et al. (2000), Umlauf et al. (2004)
<i>Tssc5/Slc22a11</i>	Cooper et al. (1998), Dao et al. (1998), Morisaki et al. (1998)
<i>U2af1-rs1</i>	Hatada et al. (1993), Hayashizaki et al. (1994), Shibata et al. (1997), Wang et al. (2004)
<i>Ube3a</i>	Albrecht et al. (1997)
<i>Ube3aas</i>	Chamberlain and Brannan (2001), Landers et al. (2004), Le Meur et al. (2005), Rougeulle et al. (1998)
<i>Usp</i>	Kim et al. (2000)
<i>Zdbf2</i>	Kobayashi et al. (2009)
<i>Zfp264</i>	Kim et al. (2001)
<i>Zim1</i>	Kim et al. (1999)
<i>Zim2</i>	Kim et al. (2004)
<i>Zim3</i>	Kim et al. (2001)

neighborhood will determine whether any are imprinted in extraembryonic tissues. Thus, for the majority of imprinted domains, an extraembryonic target has been demonstrated and for several others the possibility still remains to be assessed.

Several imprinted genes have been shown to play major roles in placentation. Loss of function mutations in *Ascl2* (*Mash2*), *Cdkn1c* (*p57KIP2*), *Cited*, *Ipl*, *Peg10*, and *Rtl1* all result in severely dysmorphic placentae. *Cdkn1c* is interesting because mutations in this gene have been found to be associated with preeclampsia-like symptoms in mice. This is the only mutation that has been examined for maternal pathology, in spite of the severe risks associated with abnormal placentation in humans. Interestingly, the lethal hybrid crosses in *Peromyscus* described earlier are associated with extensive maternal morbidity that cannot be attributed to the excessive size of the fetuses in all cases, suggesting that some other pregnancy related pathology is responsible for the maternal deaths (Duselis et al., 2005).

Many imprinted genes appear to play roles in brain development or function, although these tend to be mild, and in some cases recessive. Almost completely missing is any analysis of the yolk sac. This organ is a critical site of fetal hematopoiesis. Perhaps more germane to this review, however, is the fact that the yolk sac contains derivatives of the PrE in sufficient quantity for molecular analysis. Future analyses of imprinted gene function, including allelic expression, would benefit greatly from addition of the yolk sac to the collection of tissues assayed. An examination of the role played by the PrE in development may provide readers with a clearer rationale for this kind of follow-up.

4.3. PrE in development

Until now we have focussed mainly on the placenta and to a lesser extent the yolk sac as targets of imprinted gene function. One tissue that has been ignored, perhaps because of its transient nature, is the very early primitive endoderm (PrE) that plays a key role during gastrulation. Gastrulation is a critical period during early development in which a naïve sheet of cells, the epiblast, acquires landmarks that determine where the anterior and posterior, left and right, and dorsal and ventral axes of the fetus will develop. Much of this activity is mediated by a structure called the node, and by the PrE.

PrE is old. Other vertebrates make use of a similar transient tissue for establishment of body axes through signaling to the epiblast during gastrulation. Teleost fish, for example, generate an extraembryonic epithelium called the syncytial yolk layer (SYL) that signals to the epiblast at the time of node formation. A similar tissue in birds and reptiles, the hypoblast, is required for axis formation. In other nonmammalian vertebrates, parts of the yolk sac endoderm, a derivative of PrE, are incorporated into the gut (Mossman, 1987).

Much of our understanding of PrE in mammalian development comes again from studies with mice. Extensive analyses using both genetic and

embryological tools have allowed investigators to build a detailed picture of early axis formation and signaling during gastrulation (Tam et al., 2006). The three tissues involved in these early patterning events—the cup-shaped epiblast, the adjacent extraembryonic ectoderm (eee, which eventually forms the chorion), and the overlying PrE—communicate with each other through a complex series of overlapping signaling pathways prior to and during gastrulation to generate the primitive streak, which establishes the anterior/posterior body axis and the three definitive germ layers of the embryo proper (Perea-Gomez et al., 2001; Takaoka et al., 2007; Tam et al., 2006). In addition, the PrE derivative, the anterior visceral endoderm (AVE), signals to the overlying epiblast to form the neuroectoderm and head process (Acampora et al., 1998; Ding et al., 1998; Dufort et al., 1998; Rhinn et al., 1998; Shawlot et al., 1999; Thomas and Beddington, 1996; Varlet et al., 1997). Often, expression of genes required for neuroectoderm development displays a two-step pattern, starting first in the PrE and then following in the developing head process. A good example of this two-step process is the *Otx2* gene, whose expression pattern is progressively restricted during gastrulation to the anterior end and finally the neuroectoderm. Early expression in PrE is required for appropriate signaling to the overlying ectoderm in the head region; wild-type PrE can rescue early neuroectoderm development in *Otx2*^{-/-} embryos and mutant PrE induces classic *Otx2* mutant phenotype in wild-type embryos; however, later stages of neural development are not rescued, indicating a cell/tissue autonomous role for *Otx2* within that tissue (Rhinn et al., 1998).

A recent study of PrE cells labeled with GFP or RFP transgenes driven by PrE specific promoters (*Afp* and *Ttr*) has revealed that extraembryonic cells become incorporated into the embryonic gut through intercalation of definitive endoderm cells from the primitive streak with PrE cells overlying the distal epiblast (Kwon et al., 2008). Interestingly, these cells retain their “extraembryonic” character in that, in female embryos, the imprinted paternal X-inactivation is maintained. The authors were able to follow the fate of these extraembryonic cells in the embryonic gut up to the beginning of organogenesis; activation of the *Afp* and *Ttr* genes (and hence the fluorescent protein transgenes) in embryonic tissues at later stages prevented them from distinguishing PrE derived from epiblast derived cells after e9.5. It will be interesting to see whether PrE-derived cells find their way into other embryonic/fetal tissues.

Thus, both trophoblast and PrE play major roles in early development during gastrulation and neuroectoderm patterning that have long-term consequences. Their later roles in embryo nutrition through formation of both the yolk sac placenta and the chorioallantoic placenta are of great importance, but may not always be the major site of action of imprinted genes expressed in these extraembryonic tissues.

4.4. Tetraploid rescue experiments and their potential for exploring imprinted gene function

The distinctive signaling role played by the PrE in axis formation and neuroectoderm patterning has been established through the aegis of tetraploid rescue experiments. Tetraploid embryos, created by electrofusion of the two blastomeres of the two-cell embryo, are capable of development up to implantation, but fail to proceed through postimplantation development (Eakin et al., 2005). However, when combined with either diploid embryos or embryonic stem (ES) cells, tetraploid embryos are capable of generating all of the extraembryonic tissues, including the placenta and yolk sac. These experiments, pioneered by Tarkowski et al. (1977, 2001), were greatly enhanced by the introduction of fluorescent tags that allowed live imaging of chimeric embryos (Hadjantonakis et al., 2002). The ability to combine ES cells with tetraploid embryos has allowed investigators to quickly assess phenotypic consequences of embryonic lethal mutations using ES cells harboring homozygous null alleles. One drawback to these experiments, however, is the later lethality that may be a consequence of some aspect of ES cell epigenetic modification, or possibly some role played by diploid extraembryonic cells that has still not been clarified (see below, discussion of *Erk2*). Nevertheless, many mutations have been assessed with this technology, and have revealed that some genes appear to act solely in the extraembryonic tissues, while many others have early effects mediated by either placental or PrE function, and later effects arising from dysfunction in the embryo proper. Table 5.3 lists a number of mutations that have been tested in tetraploid rescue experiments.

Erk2 is a very interesting case. *Erk2* knockout is lethal at early postimplantation stages. This lethality can be completely rescued by aggregation with wild-type tetraploid embryos (Hatano et al., 2003). However, a conditional knockout using a *Wnt1-Cre* transgene causes neural crest-derived craniofacial defects (Newbern et al., 2008). This phenotype would seem odd, given the total rescue of mutants by tetraploid embryos, except that *Wnt-1* is also expressed at the blastocyst stage in a small subset of cells near the location of the PrE (Kemp et al., 2005). If the PrE in the conditional mutants is also mutant for *Erk2*, then it may be causing the craniofacial defects through either impaired signaling to the neuroectoderm (the precursor of the neural crest) or perhaps following incorporation of PrE cells into the neuroectoderm in a manner similar to the endoderm, as described recently by Kwon et al. (2008).

These experiments highlight the utility of performing tetraploid aggregation to test the function of imprinted genes in extraembryonic tissues. Some of the presumed embryonic phenotypes may in fact be a consequence of early signaling events during development, either from the

Table 5.3 Tetraploid rescue

Gene	Tissue expression	KO phenotype	Rescued phenotype	Likely rescuing tissue	Notes	References
Partial rescue ^a Alk2 (2)	Widely	Arrest at gastrulation	Arrest at limb bud stage	PrE?	Reverse combination causes early defect	Mishina et al. (1999)
Arnt	Ubiquitous	Arrest at early postimplantation with severe defects in placental and yolk sac development	Partial rescue of placental vascularization; no rescue of yolk sac vascularization defects	Trophoblast		Adelman et al. (2000)
Cdx2	Early—extraembryonic; later—multiple tissues	Preimplantation lethal	Early somite stage; failed development of extraembryonic mesoderm	Trophoblast; PrE?		Chawengsaksophak et al. (2004)
Dsp (13)	Early—trophoblast; later—multiple tissues	Pregastrulation arrest	Postgastrulation arrest	Trophoblast	Desmoplakin required for epithelial integrity	Gallicano et al. (2001)
Flt1	Placental and maternal endothelial cells	Endothelial cell morphogenesis defects	Mutant placenta rescued by wt ES cells		Reverse combination; embryonic mesoderm required for placental vasculature	Hirashima et al. (2003)
Gata4	Extraembryonic; heart, spinal cord, somites	Early loss of ventral patterning	Partial rescue of patterning revealed later role in cardiac development	PrE ^b		Watt et al. (2004)

Hand1	Extraembryonic tissues; heart; lateral plate mesoderm	Early postimplantation lethal	Partial rescue of placental defects	Trophoblast	Later cardiac defects uncovered	Riley et al. (1998)
Hnf3 β	AVE; node	Gastrulation defects	Partial rescue past gastrulation	PrE	Later gut and asymmetry defects	Dufort et al. (1998)
Hnf4	Extraembryonic; gut, liver	Gastrulation defects	Partial rescue of gastrulation	PrE	Later hepatic defects uncovered by tetraploid rescue	Duncan et al. (1997), Li et al. (2000)
JunB	Ubiquitous	Early postimplantation lethal due to placenta and yolk sac defects	Partial (?) rescue to midgestation	Trophoblast and PrE	Later defects not assessed	Schorpp-Kistner et al. (1999)
Notch2	Trophoblast (transient); variable	Impaired vasculogenesis in placenta	Partial rescue of placental vasculogenesis defects	Trophoblast		Hamada et al. (2007)
NR5a2	PrE; definitive endoderm	Impaired gastrulation	Gastrulation defects rescued	PrE	Experiment did not go beyond e9.0	Labelle-Dumais et al. (2006)
Sall4-1a	Ubiquitous	Gastrulation	Partial rescue of promodistal (PD) patterning	Extraembryonic ectoderm or PrE		Uez et al. (2008)
Smad4	Ubiquitous	Gastrulation	Partial rescue to head fold stage	PrE	Smad2 ^{-/-} EEE causes defects in wt epiblast	Sirard et al. (1998), Waldrip et al. (1998)
Tcf2	PrE, pancreas	Gastrulation arrest	Partial rescue to organogenesis	PrE	Chimeras displayed pancreas defects uncovered by early rescue	Haumaitre et al. (2005)
TM	Endothelial cells; trophoblast	Arrest shortly after gastrulation	Partial rescue to midgestation	Trophoblast		Isermann et al. (2001)
TRAP220	Ubiquitous	Midgestation lethality	Partial rescue to later stage	Placenta and PrE?	Mutant placentas appear normal; yolk sac not examined	Landles et al. (2003)

(continued)

Table 5.3 (continued)

Gene	Tissue expression	KO phenotype	Rescued phenotype	Likely rescuing tissue	Notes	References
VEGF	PrE, trophoblast; endothelial cells	Early postimplantation lethal; compromised vasculogenesis	Yolk sac vasculogenesis rescued	PrE	Reverse experiment indicates yolk sac mesoderm adversely affected by mutant PrE	Damert et al. (2002)
vHNF1	PrE; liver, lung, pancreas	Peri-implantation lethal	Partial rescue to organogenesis stage	PrE		Barbacci et al. (1999)
Complete rescue						
Chm (X)	Ubiquitous	Male arrest at early somite; female arrest at early limb bud	Viable fertile	PrE and trophoblast?	Genetic background effects	Shi et al. (2004)
Eed	Widespread	Compound heterozygotes midgestation lethality; ballooning pericardial sac, kinky neural tube, growth retardation	At least one rescued to birth	Trophoblast secondary giant cells; PrE?		Wang et al. (2002)
Egfr (11)	Early—trophoblast; later—multiple tissues	Placental defects on 129; brain defects on all	Live born but with brain defects	Placenta	Genetic background effects	Sibilia et al. (1998)
Erk2 (16)	Ubiquitous	Labyrinthine layer defects	Viable, fertile	Placental trophoblast		Hatano et al. (2003)
Err β	Trophoblast	Reduced chorion, diploid trophoblast	Indistinguishable from wt	Placental trophoblast		Luo et al. (1997)
Ets2	Early—trophoblast; later—multiple tissues	Defective gastrula; abnormal extraembryonic tissues	Viable, fertile, wavy fur	Extraembryonic tissues		Yamamoto et al. (1998)
Mash2 ^c	Trophoblast	Reduced Spongiotrophoblast	Rescued	Spongiotrophoblast	Diploid chimeras	Tanaka et al. (1997)

Peg10 ^c	Placenta, yolk sac, brain	Severely reduced placenta; embryonic lethal	Rescued, viable	Trophoblast		Ono et al. (2006)
PLCδ1/δ3	Widely expressed	Impaired placental development	Placental defects rescued	Trophoblast	Single KO have minor or no phenotype	Nakamura et al. (2005)
PPARγ	Trophoblast; interscapular fat pad (PrE not assayed)	Impaired placenta and heart; postnatal pathologies	Placental and cardiac defects rescued; postnatal defects not rescued	Trophoblast and PrE?	Heart defects a function of premature differentiation of cardiac cells/tissue	Barak et al. (1999)
Rb	Ubiquitous	Neurologic and hematopoietic defects, embryonic lethal	Embryonic lethality, including neurologic and erythropoietic defects, rescued to term	Trophoblast and PrE?	Rescued pups die at birth	Wu et al. (2003)
SOCS3	Trophoblast; several tissues	Midgestation lethal with erythrocytosis	Rescue to term	Placenta and PrE?		Takahashi et al. (2003)
No rescue Brca1	Ubiquitous	Arrest at gastrulation with both embryonic and extraembryonic defects	Not rescued			Hakem et al. (1996)
Fatp4	Ubiquitous	Skin abnormality leading to perinatal lethality	No rescue; placenta expression redundant			Moulson et al. (2007)
LBP1a	Ubiquitous	Failure of placental and yolk sac vasculogenesis	Not rescued			Parekh et al. (2004)
Man1	Ubiquitous	Impaired yolk sac vasculogenesis	Not rescued			Cohen et al. (2007)

^a Some tetraploid experiments were done with mutant ES cells. While it is possible to generate live mice that are wholly ES derived by aggregation with tetraploid embryos, this tends to be cell line specific; many ES cell lines are not capable of full term development by this route, for reasons that remain a mystery (see, e.g., Barbacci et al., 1999).

^b PrE: primitive endoderm.

^c Imprinted genes.

PrE?: The role of PrE may not have been carefully examined in some cases.

extraembryonic ectoderm or the PrE. By focussing solely on phenotypes such as growth, often in the small subset of embryos/pups that survive, important gene activities may be overlooked. The distinctive role played by PrE in early patterning of the neuroectoderm in particular makes analysis of imprinted genes with neural functions especially appealing. For example, *Sgce*, which is known to be imprinted in both placenta and yolk sac, results in myoclonus dystrophy, a defect of the central nervous system, when mutated. Survival of pups to adulthood suggests that placentation is normal in these mutants. However, PrE function may not be normal; tetraploid rescue would clearly establish whether there is an early signaling function that has been overlooked. Another gene that warrants closer attention is *Igf2r*. Mutants are dysmorphic, and often contain tail kinks, a sign of abnormal notochord function. Notochord is one of the earliest axial structures made during gastrulation. Indeed, all of the imprinted gene knockout models should be tested with tetraploid rescue. These experiments would tell us whether extraembryonic function, rather than size, is the critical feature that is controlled by genomic imprinting. More careful analysis of phenotypes will provide us with a better understanding of the development and function of the extraembryonic tissues, including the placenta, and may provide insight into placental pathologies such as preeclampsia.



5. CONCLUSIONS

Genomic imprinting is a unique gene regulatory mechanism seen only in mammals, the endosperm of angiosperm plants, and some arthropods. The similar functions played by placenta and endosperm have led investigators to question whether imprinting arose in these two very distant taxa for similar reasons—regulation of placental and endosperm development and function. Widening the scope of investigation of imprinted gene activity to include earlier signaling functions of extraembryonic tissues may yield a better understanding of the unique interactions between both mother and child and extraembryonic and fetal tissues. This may lead to a more comprehensive picture of disease processes that start early in life.

ACKNOWLEDGMENTS

We thank our many colleagues for helpful discussions and Dr. Mellissa Mann, in particular, for critical evaluation of the manuscript.

REFERENCES

- Acampora, D., Avantaggiato, V., Tuorto, F., Briata, P., Corte, G., Simeone, A., 1998. Visceral endoderm-restricted translation of Otx1 mediates recovery of Otx2 requirements for specification of anterior neural plate and normal gastrulation. *Development* 125, 5091–5104.
- Adelman, D., Gertsenstein, M., Nagy, A., Simon, M., Maltepe, E., 2000. Placental cell fates are regulated *in vivo* by HIF-mediated hypoxia responses. *Genes Dev.* 14, 3191–3203.
- Albrecht, U., Sutcliffe, J.S., Cattanach, B.M., Beechey, C.V., Armstrong, D., Eichele, G., et al., 1997. Imprinted expression of the murine Angelman syndrome gene, Ube3a, in hippocampal and Purkinje neurons. *Nat. Genet.* 17, 75–78.
- Antonin, W., Ellenberg, J., Dultz, E., 2008. Nuclear pore complex assembly through the cell cycle: regulation and membrane organization. *FEBS Lett.* 582, 2004–2016.
- Arnaud, P., Monk, D., Hitchins, M., Gordon, E., Dean, W., Beechey, C.V., et al., 2003. Conserved methylation imprints in the human and mouse GRB10 genes with divergent allelic expression suggests differential reading of the same mark. *Hum. Mol. Genet.* 12, 1005–1019.
- Asher, R., Horovitz, I., Sánchez-Villagra, M., 2004. First combined cladistic analysis of marsupial mammal interrelationships. *Mol. Phylogenet. Evol.* 33, 240–250.
- Bamberg, C., Kalache, K., 2004. Prenatal diagnosis of fetal growth restriction. *Semin. Fetal Neonatal Med.* 9, 387–394.
- Babak, T., Deveale, B., Armour, C., Raymond, C., Cleary, M., van der Kooy, D., et al., 2008. Global survey of genomic imprinting by transcriptome sequencing. *Curr. Biol.* 18, 1735–1741.
- Barak, Y., Nelson, M., Ong, E., Jones, Y., Ruiz-Lozano, P., Chien, K., et al., 1999. PPAR γ is required for placental, cardiac, and adipose tissue development. *Mol. Cell* 4, 585–595.
- Barbacci, E., Reber, M., Ott, M.O., Breillat, C., Huetz, F., Cereghini, S., 1999. Variant hepatocyte nuclear factor 1 is required for visceral endoderm specification. *Development* 126, 4795–4805.
- Barker, D., 2004. Developmental origins of adult health and disease. *J. Epidemiol. Community Health* 58, 114–115.
- Barlow, D.P., Stöger, R., Herrmann, B.G., Saito, K., Schweifer, N., 1991. The mouse insulin-like growth factor type-2 receptor is imprinted and closely linked to the Tme locus. *Nature* 349, 84–87.
- Bartolomei, M.S., Zemel, S., Tilghman, S.M., 1991. Parental imprinting of the mouse H19 gene. *Nature* 351, 153–155.
- Barton, S., Surani, M.A., Norris, M., 1984. Role of paternal and maternal genomes in mouse development. *Nature* 311, 374–376.
- Bianchi, D., 2000. Fetal cells in the mother: from genetic diagnosis to diseases associated with fetal cell microchimerism. *Eur. J. Obstet. Gynecol. Reprod. Biol.* 92, 103–108.
- Boccaccio, I., Glatt-Deeley, H., Watrin, F., Roëckel, N., Lalande, M., Muscatelli, F., 1999. The human MAGEL2 gene and its mouse homologue are paternally expressed and mapped to the Prader-Willi region. *Hum. Mol. Genet.* 8, 2497–2505.
- Bongiorni, S., Prantera, G., 2003. Imprinted facultative heterochromatization in mealybugs. *Genetica* 117, 271–279.
- Bourc'his, D., Proudhon, C., 2008. Sexual dimorphism in parental imprint ontogeny and contribution to embryonic development. *Mol. Cell Endocrinol.* 282, 87–94.
- Bourc'his, D., Xu, G.L., Lin, C.S., Bollman, B., Bestor, T., 2001. Dnmt3L and the establishment of maternal genomic imprints. *Science* 294, 2536–2539.
- Brambilla, R., Gnesutta, N., Minichiello, L., Whitek, G., Roylance, A., Herron, C., et al., 1997. A role for the Ras signalling pathway in synaptic transmission and long-term memory. *Nature* 390, 281–286.

- Buettner, V.L., Walker, A.M., Singer-Sam, J., 2005. Novel paternally expressed intergenic transcripts at the mouse Prader-Willi/Angelman syndrome locus. *Mamm. Genome* 16, 219–227.
- Casimiro, M., Knollmann, B., Ebert, S., Vary, J., Greene, A., Franz, M., et al., 2001. Targeted disruption of the *Kcnq1* gene produces a mouse model of Jervell and Lange-Nielsen syndrome. *Proc. Natl. Acad. Sci.* 98, 2526–2531.
- Casparly, T., Cleary, M.A., Baker, C.C., Guan, X.J., Tilghman, S.M., 1998. Multiple mechanisms regulate imprinting of the mouse distal chromosome 7 gene cluster. *Mol. Cell. Biol.* 18, 3466–3474.
- Cattanach, B., 1986. Parental origin effects in mice. *J. Embryol. Exp. Morphol.* 97 (Suppl.), 137–150.
- Cavaillé, J., Buiting, K., Kieffmann, M., Lalonde, M., Brannan, C.I., Horsthemke, B., et al., 2000. Identification of brain-specific and imprinted small nucleolar RNA genes exhibiting an unusual genomic organization. *Proc. Natl. Acad. Sci. USA* 97, 14311–14316.
- Cavaillé, J., Seitz, H., Paulsen, M., Ferguson-Smith, A.C., Bachelier, J.P., 2002. Identification of tandemly-repeated C/D snoRNA genes at the imprinted human 14q32 domain reminiscent of those at the Prader-Willi/Angelman syndrome region. *Hum. Mol. Genet.* 11, 1527–1538.
- Chaddha, V., Viero, S., Huppertz, B., Kingdom, J., 2004. Developmental biology of the placenta and the origins of placental insufficiency. *Semin. Fetal Neonatal Med.* 9, 357–369.
- Chai, J.H., Locke, D.P., Ohta, T., Grealley, J.M., Nicholls, R.D., 2001. Retrotransposed genes such as *Frat3* in the mouse chromosome 7C Prader-Willi syndrome region acquire the imprinted status of their insertion site. *Mamm. Genome* 12, 813–821.
- Chamberlain, S.J., Brannan, C.I., 2001. The Prader-Willi syndrome imprinting center activates the paternally expressed murine *Ube3a* antisense transcript but represses paternal *Ube3a*. *Genomics* 73, 316–322.
- Charalambous, M., Smith, F.M., Bennett, W.R., Crew, T.E., Mackenzie, F., Ward, A., 2003. Disruption of the imprinted *Grb10* gene leads to disproportionate overgrowth by an *Igf2*-independent mechanism. *Proc. Natl. Acad. Sci.* 100, 8292–8297.
- Charalambous, M., da Rocha, S.T., Ferguson-Smith, A.C., 2007. Genomic imprinting, growth control and the allocation of nutritional resources: consequences for postnatal life. *Curr. Opin. Endocrinol. Diabetes Obes.* 14, 3–12.
- Charlier, C., Segers, K., Wagenaar, D., Karim, L., Berghmans, S., Jaillon, O., et al., 2001. Human-ovine comparative sequencing of a 250-kb imprinted domain encompassing the callipyge (*clpg*) locus and identification of six imprinted transcripts: *DLK1*, *DAT*, *GTL2*, *PEG11*, *antiPEG11*, and *MEG8*. *Genome Res.* 11, 850–862.
- Chawengsaksophak, K., de Graaff, W., Rossant, J., Deschamps, J., Beck, F., 2004. *Cdx2* is essential for axial elongation in mouse development. *Proc. Natl. Acad. Sci.* 101, 7641–7645.
- Choi, J.D., Underkoffler, L.A., Wood, A.J., Collins, J.N., Williams, P.T., Golden, J.A., et al., 2005. A novel variant of *Inpp5f* is imprinted in brain, and its expression is correlated with differential methylation of an internal CpG island. *Mol. Cell. Biol.* 25, 5514–5522.
- Choo, J.H., Kim, J.D., Kim, J., 2008. Imprinting of an evolutionarily conserved antisense transcript gene *APeg3*. *Gene* 409, 28–33.
- Clark, L., Wei, M., Cattoretti, G., Mendelsohn, C., Tycko, B., 2002. The *Tnfrh1* (*Tnfrsf23*) gene is weakly imprinted in several organs and expressed at the trophoblast-decidua interface. *BMC Genet.* 3, 11–21.
- Coan, P., Burton, G., Ferguson-Smith, A., 2005. Imprinted genes in the placenta—a review. *Placenta* 26 (Suppl. A), S10–S20.
- Cohen, T., Kostı, O., Stewart, C., 2007. The nuclear envelope protein *MAN1* regulates TGF signaling and vasculogenesis in the embryonic yolk sac. *Development* 134, 1385–1395.

- Constância, M., Hemberger, M., Hughes, J., Dean, W., Ferguson-Smith, A., Fundele, R., et al., 2002. Placental-specific IGF-II is a major modulator of placental and fetal growth. *Nature* 417, 945–948.
- Cooper, P.R., Smilnich, N.J., Day, C.D., Nowak, N.J., Reid, L.H., Pearsall, R.S., et al., 1998. Divergently transcribed overlapping genes expressed in liver and kidney and located in the 11p15.5 imprinted domain. *Genomics* 49, 38–51.
- Cross, J., 2003. The genetics of pre-eclampsia: a feto-placental or maternal problem? *Clin. Genetics* 64, 96–103.
- Cross, J., Baczyk, D., Dobric, N., Hemberger, M., Hughes, M., Simmons, D., et al., 2003. Genes, development and evolution of the placenta. *Placenta* 24, 123–130.
- Crouse, H.V., 1960. The nature of the influence of X-translocation on sex of progeny in *Sciara coprophila*. *Chromosoma* 18, 230–235.
- Curley, J., Barton, S., Surani, A., Keverne, E., 2004. Coadaptation in mother and infant regulated by paternally expressed imprinted gene. *Proc. Biol. Sci.* 271, 1303–1309.
- Dacquin, R., Davey, R., Laplace, C., Levasseur, R., Morris, H., Goldring, S., et al., 2004. Amylin inhibits bone resorption while the calcitonin receptor controls bone formation *in vivo*. *J. Cell Biol.* 164, 509–514.
- Damert, A., Miquerol, L., Gertsenstein, M., Risau, W., Nagy, A., 2002. Insufficient VEGFA activity in yolk sac endoderm compromises haematopoietic and endothelial differentiation. *Development* 129, 1881–1892.
- D'Angelo, M., Hetzer, M., 2008. Structure, dynamics and function of nuclear pore complexes. *Trends Cell Biol.* 18, 456–466.
- Dao, D., Frank, D., Qian, N., O'Keefe, D., Vosatka, R.J., Walsh, C.P., et al., 1998. IMPT1, an imprinted gene similar to polyspecific transporter and multi-drug resistance genes. *Hum. Mol. Genet.* 7, 597–608.
- Davies, W., Smith, R.J., Kelsey, G., Wilkinson, L.S., 2004. Expression patterns of the novel imprinted genes *Nap115* and *Peg13* and their non-imprinted host genes in the adult mouse brain. *Gene Expr. Patterns* 4, 741–747.
- Davis, E., Caiment, F., Tordoier, X., Cavallé, J., Ferguson-Smith, A., Cockett, N., et al., 2005. RNAi-mediated allelic trans-interaction at the imprinted *Rtl1/Peg11* locus. *Curr Biol.* 15, 743–749. Erratum in: *Curr. Biol.* 2005 May 10, 15 (9), 884.
- de la Puente, A., Hall, J., Wu, Y.Z., Leone, G., Peters, J., Yoon, B.J., et al., 2002. Structural characterization of *Rasgrfl* and a novel linked imprinted locus. *Gene* 291, 287–297.
- de los Santos, T., Schweizer, J., Rees, C.A., Francke, U., 2000. Small evolutionarily conserved RNA, resembling C/D box small nucleolar RNA, is transcribed from *PWCR1*, a novel imprinted gene in the Prader–Willi deletion region, which is highly expressed in brain. *Am. J. Hum. Genet.* 67, 1067–1082.
- DeChiara, T.M., Robertson, E.J., Efstratiadis, A., 1991. Parental imprinting of the mouse insulin-like growth factor II gene. *Cell* 64, 849–859.
- Deltour, L., Montagutelli, X., Guenet, J.L., Jami, J., Páldi, A., 1995. Tissue- and developmental stage-specific imprinting of the mouse proinsulin gene, *Ins2*. *Dev. Biol.* 168, 686–688.
- Deltour, L., Vandamme, J., Jouvenot, Y., Duvillié, B., Kelemen, K., Schaerly, P., et al., 2004. Differential expression and imprinting status of *Ins1* and *Ins2* genes in extraembryonic tissues of laboratory mice. *Gene Expr. Patterns* 5, 297–300.
- Ding, J., Yang, L., Yan, Y., Chen, A., Desai, N., Wynshaw-Boris, A., et al., 1998. *Cripto* is required for correct orientation of the anteriorposterior axis in the mouse embryo. *Nature* 395, 702–707.
- Ding, F., Li, H.H., Zhang, S., Solomon, N.M., Camper, S.A., Cohen, P., et al., 2008. *SnoRNA Snord116 (Pwcr1/MBII-85)* deletion causes growth deficiency and hyperphagia in mice. *PLoS ONE* 3 (3), e1709. doi:10.1371/journal.pone.0001709.

- Dufort, D., Schwartz, L., Harpal, K., Rossant, J., 1998. The transcription factor HNF3b is required in visceral endoderm for normal primitive streak morphogenesis. *Development* 125, 3015–3025.
- Duncan, S., Nagy, A., Chan, W., 1997. Murine gastrulation requires HNF-4 regulated gene expression in the visceral endoderm: tetraploid rescue of *Hnf-4^{-/-}* embryos. *Development* 124, 279–287.
- Duselis, A., Wiley, C., O'Neill, M., Vrana, P., 2005. Genetic evidence for a maternal effect locus controlling genomic imprinting and growth. *Genesis* 43, 155–165.
- Duvill  , B., Cordonnier, N., Deltour, L., Dandoy-Dron, F., Itier, J.M., Monthieux, E., et al., 1997. Phenotypic alterations in insulin-deficient mutant mice. *Proc. Natl. Acad. Sci.* 94, 5137–5140.
- Eakin, G., Hadjantonakis, A., Papaioannou, V., Behringer, R., 2005. Developmental potential and behavior of tetraploid cells in the mouse embryo. *Dev. Biol.* 288, 150–159.
- Edwards, C., Ferguson-Smith, A., 2007. Mechanisms regulating imprinted genes in clusters. *Curr. Opin. Cell Biol.* 19, 281–289.
- Edwards, C.A., Mungall, A.J., Matthews, L., Ryder, E., Gray, D.J., Pask, A., et al., 2008. The evolution of the DLK1-DIO3 imprinted domain in mammals. *PLoS Biol.* 6 (6), e135. doi:10.1371/journal.pbio.0060135.
- Engemann, S., Str  dicke, M., Paulsen, M., Franck, O., Reinhardt, R., Lane, N., et al., 2000. Sequence and functional comparison in the Beckwith-Wiedemann region: implications for a novel imprinting centre and extended imprinting. *Hum. Mol. Genet.* 9, 2691–2706.
- Fedoriw, A.M., Stein, P., Svoboda, P., Schultz, R.M., Bartolomei, M.S., 2004. Transgenic RNAi reveals essential function for CTCF in H19 gene imprinting. *Science* 303, 238–240.
- Fisher, S., 2004. The placental problem: linking abnormal cytotrophoblast differentiation to the maternal symptoms of preeclampsia. *Reprod. Biol. Endocrinol.* 2, 53–56.
- Fitzpatrick, G.V., Soloway, P.D., Higgins, M.J., 2002. Regional loss of imprinting and growth deficiency in mice with a targeted deletion of *KvDMR1*. *Nat. Genet.* 32, 426–431.
- Frank, D., Fortino, W., Clark, L., Musalo, R., Wang, W., Saxena, A., et al., 2002. Placental overgrowth in mice lacking the imprinted gene *Ipl*. *Proc. Natl. Acad. Sci.* 99, 7490–7495.
- Freyer, C., Zeller, U., Renfree, M., 2003. The marsupial placenta: a phylogenetic analysis. *J. Exp. Zool. A Comp. Exp. Biol.* 299A, 59–77.
- Gallicano, G., Bauer, C., Fuchs, E., 2001. Rescuing desmoplakin function in extra-embryonic ectoderm reveals the importance of this protein in embryonic heart, neuroepithelium, skin and vasculature. *Development* 128, 929–941.
- Gehring, M., Huh, J., Hsieh, T.F., Penterman, J., Choi, Y., Harada, J., et al., 2006. DEMETER DNA glycosylase establishes MEDEA polycomb gene self-imprinting by allele-specific demethylation. *Cell* 124, 495–506.
- Georgiades, P., Ferguson-Smith, A., Burton, G., 2002. Comparative developmental anatomy of the murine and human definitive placentae. *Placenta* 23, 3–19.
- G  rard, M., Hernandez, L., Wevrick, R., Stewart, C., 1999. Disruption of the mouse *neccdin* gene results in early post-natal lethality. *Nat. Genet.* 23, 199–202.
- Giddings, S.J., King, C.D., Harman, K.W., Flood, J.F., Carnaghi, L.R., 1994. Allele specific inactivation of insulin 1 and 2, in the mouse yolk sac, indicates imprinting. *Nat. Genet.* 6, 310–313.
- Gluckman, P., Hanson, M., 2004. Maternal constraint of fetal growth and its consequences. *Semin. Fetal Neonatal Med.* 9, 419–425.
- Goday, C., Esteban, M., 2001. Chromosome elimination in sciarid flies. *Bioessays* 23, 242–250.

- Godfrey, K.M., 2002. The role of the placenta in fetal programming—a review. *Placenta* 23 (Suppl. A), S20–S27.
- Gould, T.D., Pfeifer, K., 1998. Imprinting of mouse *Kvlqt1* is developmentally regulated. *Hum. Mol. Genet.* 7, 483–487.
- Gray, T.A., Saitoh, S., Nicholls, R.D., 1999. An imprinted, mammalian bicistronic transcript encodes two independent proteins. *Proc. Natl. Acad. Sci. USA* 96, 5616–5621.
- Guillemot, F., Nagy, A., Auerbach, A., Rossant, J., Joyner, A., 1994. Essential role of *Mash-2* in extraembryonic development. *Nature* 371, 333–336.
- Guillemot, F., Caspary, T., Tilghman, S.M., Copeland, N.G., Gilbert, D.J., Jenkins, N.A., et al., 1995. Genomic imprinting of *Mash2*, a mouse gene required for trophoblast development. *Nat. Genet.* 9, 235–242.
- Haberland, J., Gerke, V., 1999. Conserved charged residues in the leucine-rich repeat domain of the Ran GTPase activating protein are required for Ran binding and GTPase activation. *Biochem. J.* 343, 653–662.
- Hadjantonakis, A.K., Macmaster, S., Nagy, A., 2002. Embryonic stem cells and mice expressing different GFP variants for multiple non-invasive reporter usage within a single animal. *BMC Biotechnol.* 2, 11–19.
- Hagiwara, Y., Hirai, M., Nishiyama, K., Kanazawa, I., Ueda, T., Sakaki, Y., et al., 1997. Screening for imprinted genes by allelic message display: identification of a paternally expressed gene impact on mouse chromosome 18. *Proc. Natl. Acad. Sci. USA* 94, 9249–9254.
- Hakem, R., de la Pompa, J., Sirard, C., Mo, R., Woo, M., Hakem, A., et al., 1996. The tumor suppressor gene *brca1* is required for embryonic cellular proliferation in the mouse. *Cell* 85, 1009–1023.
- Hall, J.G., 1990. Genomic imprinting: review and relevance to human diseases. *Am. J. Hum. Genet.* 46, 857–873.
- Hamada, Y., Hiroe, T., Suzuki, Y., Oda, M., Tsujimoto, Y., Coleman, R., et al., 2007. *Notch2* is required for formation of the placental circulatory system, but not for cell-type specification in the developing mouse placenta. *Differentiation* 75, 268–278.
- Hata, K., Okano, M., Lei, H., Li, E., 2002. *Dnmt3L* cooperates with the *Dnmt3* family of de novo DNA methyltransferases to establish maternal imprints in mice. *Development* 129, 1983–1993.
- Hatada, I., Sugama, T., Mukai, T., 1993. A new imprinted gene cloned by a methylation-sensitive genome scanning method. *Nucleic Acids Res.* 21, 5577–5582.
- Hatada, I., Mukai, T., 1995. Genomic imprinting of *p57KIP2*, a cyclin-dependent kinase inhibitor, in mouse. *Nat. Genet.* 11, 204–206.
- Hatada, I., Morita, S., Obata, Y., Sotomaru, Y., Shimoda, M., Kono, T., 2001. Identification of a new imprinted gene, *Rian*, on mouse chromosome 12 by fluorescent differential display screening. *J. Biochem.* 130, 187–190.
- Hatano, N., Mori, Y., Oh-hora, M., Kosugi, A., Fujikawa, T., Nakai, N., et al., 2003. Essential role for ERK2 mitogen-activated protein kinase in placental development. *Genes Cells* 8, 847–856.
- Haumaitre, C., Barbacci, E., Jenny, M., Ott, M., Gradwohl, G., Cereghini, S., 2005. Lack of *TCF2vHNF1* in mice leads to pancreas agenesis. *Proc. Natl. Acad. Sci.* 102, 1490–1495.
- Hayashizaki, Y., Shibata, H., Hirotsune, S., Sugino, H., Okazaki, Y., Sasaki, N., et al., 1994. Identification of an imprinted *U2af* binding protein related sequence on mouse chromosome 11 using the RLGs method. *Nat. Genet.* 6, 33–40.
- Hernandez, A., Fiering, S., Martinez, E., Galton, V.A., St Germain, D., 2002. The gene locus encoding iodothyronine deiodinase type 3 (*Dio3*) is imprinted in the fetus and expresses antisense transcripts. *Endocrinology* 143, 4483–4486.

- Hirasawa, R., Chiba, H., Kaneda, M., Tajima, S., Li, E., Jaenisch, R., et al., 2008. Maternal and zygotic *Dnmt1* are necessary and sufficient for the maintenance of DNA methylation imprints during preimplantation development. *Genes Dev.* 22, 1607–1616.
- Hirashima, M., Lu, Y., Byers, L., Rossant, J., 2003. Trophoblast expression of *fms*-like tyrosine kinase 1 is not required for the establishment of the maternal–fetal interface in the mouse placenta. *Proc. Natl. Acad. Sci.* 100, 15637–15642.
- Hore, T., Rapkins, R.W., Graves, J.A., 2007. Construction and evolution of imprinted loci in mammals. *Trends Genet.* 23, 440–448.
- Horike, S., Cai, S., Miyano, M., Cheng, J.F., Kohwi-Shigematsu, T., 2005. Loss of silent-chromatin looping and impaired imprinting of *DLX5* in Rett syndrome. *Nat. Genet.* 37, 31–40.
- Hoshiya, H., Meguro, M., Kashiwagi, A., Okita, C., Oshimura, M., 2003. *Calcr*, a brain-specific imprinted mouse calcitonin receptor gene in the imprinted cluster of the proximal region of chromosome 6. *J. Hum. Genet.* 48, 208–211.
- Howell, C., Bestor, T., Ding, F., Latham, K., Mertineit, C., Trasler, J., et al., 2001. Genomic imprinting disrupted by a maternal effect mutation in the *Dnmt1* gene. *Cell* 104, 829–838.
- Hu, J.F., Oruganti, H., Vu, T.H., Hoffman, A.R., 1998. Tissue-specific imprinting of the mouse insulin-like growth factor II receptor gene correlates with differential allele-specific DNA methylation. *Mol. Endocrinol.* 12, 220–232.
- Huh, J., Bauer, M., Hsieh, T.F., Fischer, R., 2007. Endosperm gene imprinting and seed development. *Curr. Opin. Genet. Dev.* 17, 480–485.
- Hui, P., Martel, M., Parkash, V., 2005. Gestational trophoblastic diseases: recent advances in histopathologic diagnosis and related genetic aspects. *Adv. Anat. Pathol.* 12, 116–125.
- Isermann, B., Hendrickson, S., Hutley, K., Wing, M., Weiler, H., 2001. Tissue-restricted expression of thrombomodulin in the placenta rescues thrombomodulin-deficient mice from early lethality and reveals a secondary developmental block. *Development* 128, 827–838.
- Jauniaux, E., Burton, G.J., 2005. Pathophysiology of histological changes in early pregnancy loss. *Placenta* 26, 114–123.
- Jiang, Y.H., Armstrong, D., Albrecht, U., Atkins, C., Noebels, J., Eichele, G., et al., 1998. Mutation of the Angelman ubiquitin ligase in mice causes increased cytoplasmic p53 and deficits of contextual learning and long-term potentiation. *Neuron* 21, 799–811.
- Jong, M.T., Carey, A.H., Caldwell, K.A., Lau, M.H., Handel, M.A., Driscoll, D.J., et al., 1999. Imprinting of a RING zinc-finger encoding gene in the mouse chromosome region homologous to the Prader–Willi syndrome genetic region. *Hum. Mol. Genet.* 8, 795–803.
- Jonker, J., Wagenaar, E., van Eijl, S., Schinkel, A., 2003. Deficiency in the organic cation transporters 1 and 2 (*Oct1/Oct2* [*Slc22a1/Slc22a2*]) in mice abolishes renal secretion of organic cations. *Mol. Cell. Biol.* 23, 7902–7908.
- Judson, H., Hayward, B., Sheridan, E., Bonthron, D., 2002. A global disorder of imprinting in the human female germ line. *Nature* 416, 539–542.
- Jullien, P.E., Mosquna, A., Ingouff, M., Sakata, T., Ohad, N., Frédéric, B., 2008. Retinoblastoma and its binding partner *MSI1* control imprinting in Arabidopsis. *PLoS Biol.* 6 (8), e194. doi:10.1371/journal.pbio.0060194.
- Kagitani, F., Kuroiwa, Y., Wakana, S., Shiroishi, T., Miyoshi, N., Kobayashi, S., et al., 1997. *Peg5/Neuronatin* is an imprinted gene located on sub-distal chromosome 2 in the mouse. *Nucleic Acids Res.* 25, 3428–3432.
- Kanayama, N., Takahashi, K., Matsuura, T., Sugimura, M., Kobayashi, T., Moniwa, N., et al., 2002. Deficiency in *p57Kip2* expression induces preeclampsia-like symptoms in mice. *Mol. Hum. Reprod.* 8, 1129–1135.

- Kaneda, M., Okano, M., Hata, K., Sado, T., Tsujimoto, N., Li, E., et al., 2004. Essential role for *de novo* DNA methyltransferase Dnmt3a in paternal and maternal imprinting. *Nature* 429, 900–903.
- Kaneko-Ishino, T., Kuroiwa, Y., Miyoshi, N., Kohda, T., Suzuki, R., Yokoyama, M., et al., 1995. Peg1/Mest imprinted gene on chromosome 6 identified by cDNA subtraction hybridization. *Nat. Genet.* 11, 52–59.
- Kaneko-Ishino, T., Kohda, T., Ishino, F., 2003. The regulation and biological significance of genomic imprinting in mammals. *J. Biochem.* 133, 699–711.
- Kashiwagi, A., Meguro, M., Hoshiya, H., Haruta, M., Ishino, F., Shibahara, T., et al., 2003. Predominant maternal expression of the mouse Atp10c in hippocampus and olfactory bulb. *J. Hum. Genet.* 48, 194–198.
- Kato, M.V., Ikawa, Y., Hayashizaki, Y., Shibata, H., 1998. Paternal imprinting of mouse serotonin receptor 2A gene Htr2 in embryonic eye: a conserved imprinting regulation on the RB/Rb locus. *Genomics* 47, 146–148.
- Kayashima, T., Yamasaki, K., Joh, K., Yamada, T., Ohta, T., Yoshiura, K., et al., 2003a. Atp10a, the mouse ortholog of the human imprinted ATP10A gene, escapes genomic imprinting. *Genomics* 81, 644–647.
- Kayashima, T., Ohta, T., Niikawa, N., Kishino, T., 2003b. On the conflicting reports of imprinting status of mouse ATP10a in the adult brain: strain-background-dependent imprinting? *J. Hum. Genet.* 48, 492–493.
- Kemp, C., Willems, E., Abdo, S., Lambiv, L., Leyns, L., 2005. Expression of all Wnt genes and their secreted antagonists during mouse blastocyst and postimplantation development. *Dev. Dyn.* 233, 1064–1075.
- Kikyo, N., Williamson, C.M., John, R.M., Barton, S.C., Beechey, C.V., Ball, S.T., et al., 1997. Genetic and functional analysis of neuronatin in mice with maternal or paternal duplication of distal Chr 2. *Dev. Biol.* 190, 66–77.
- Kim, J., Lu, X., Stubbs, L., 1999. Zim1, a maternally expressed mouse Kruppel-type zinc-finger gene located in proximal chromosome 7. *Hum. Mol. Genet.* 8, 847–854.
- Kim, J., Noskov, V.N., Lu, X., Bergmann, A., Ren, X., Warth, T., et al., 2000. Discovery of a novel, paternally expressed ubiquitin-specific processing protease gene through comparative analysis of an imprinted region of mouse chromosome 7 and human chromosome 19q13.4. *Genome Res.* 10, 1138–1147.
- Kim, J., Bergmann, A., Wehri, E., Lu, X., Stubbs, L., 2001. Imprinting and evolution of two Kruppel-type zinc-finger genes, ZIM3 and ZNF264, located in the PEG3/USP29 imprinted domain. *Genomics* 77, 91–98.
- Kim, J., Bergmann, A., Lucas, S., Stone, R., Stubbs, L., 2004. Lineage-specific imprinting and evolution of the zinc-finger gene ZIM2. *Genomics* 84, 47–58.
- Kimura, M.I., Kazuki, Y., Kashiwagi, A., Kai, Y., Abe, S., Barbieri, O., et al., 2004. Dlx5, the mouse homologue of the human-imprinted DLX5 gene, is biallelically expressed in the mouse brain. *J. Hum. Genet.* 49, 273–277.
- Kobayashi, S., Wagatsuma, H., Ono, R., Ichikawa, H., Yamazaki, M., Tashiro, H., et al., 2000. Mouse Peg9/Dlk1 and human PEG9/DLK1 are paternally expressed imprinted genes closely located to the maternally expressed imprinted genes: mouse Meg3/Gtl2 and human MEG3. *Genes Cells* 5, 1029–1037.
- Kobayashi, S., Kohda, T., Ichikawa, H., Ogura, A., Ohki, M., Kaneko-Ishino, T., et al., 2002. Paternal expression of a novel imprinted gene, Peg12/Frat3, in the mouse 7C region homologous to the Prader–Willi syndrome region. *Biochem. Biophys. Res. Commun.* 290, 403–408.
- Kobayashi, H., Yamada, K., Morita, S., Hiura, H., Fukuda, A., Kagami, M., et al., 2009. Identification of the mouse paternally expressed imprinted gene Zdbf2 on chromosome 1 and its imprinted human homolog ZDBF2 on chromosome 2. *Genomics* 93 (5), 461–472.

- Kono, T., Obata, Y., Yoshimzu, T., Nakahara, T., Carroll, J., 1996. Epigenetic modifications during oocyte growth correlates with extended parthenogenetic development in the mouse. *Nat. Genet.* 13, 91–94.
- Kono, T., Sotomaru, Y., Katsuzawa, Y., Dandolo, L., 2002. Mouse parthenogenetic embryos with monoallelic H19 expression can develop to day 17.5 of gestation. *Dev. Biol.* 243, 294–300.
- Kozlov, S., Bogenpohl, J., Howell, M., Wevrick, R., Panda, S., Hogenesch, J., et al., 2007. The imprinted gene *Mage12* regulates normal circadian output. *Nat. Genet.* 39, 1266–1272.
- Kuroiwa, Y., Kaneko-Ishino, T., Kagitani, F., Kohda, T., Li, L.L., Tada, M., et al., 1996. *Peg3* imprinted gene on proximal chromosome 7 encodes for a zinc finger protein. *Nat. Genet.* 12, 186–190.
- Kuzmin, A., Han, Z., Golding, M., Mann, M., Latham, K., Varmuza, S., 2008. The PcG gene *Sfnbt2* is paternally expressed in extraembryonic tissues. *Gene Expr. Patterns* 8, 107–116.
- Kwon, G., Viotti, M., Hadjantonakis, A.K., 2008. The endoderm of the mouse embryo arises by dynamic widespread intercalation of embryonic and extraembryonic lineages. *Dev. Cell* 15, 509–520.
- Labelle-Dumais, C., Jacob-Wagner, M., Paré, J.F., Bélanger, L., Dufort, D., 2006. Nuclear receptor NR5A2 is required for proper primitive streak morphogenesis. *Dev. Dyn.* 235, 3359–3369.
- Landers, M., Bancescu, D.L., Le Meur, E., Rougeulle, C., Glatt-Deeley, H., Brannan, C., et al., 2004. Regulation of the large (approximately 1000 kb) imprinted murine *Ube3a* antisense transcript by alternative exons upstream of *Snurf/Snrpn*. *Nucleic Acids Res.* 32, 3480–3492.
- Landes, C., Chalk, S., Steel, J., Rosewell, I., Spencer-Dene, B., Lalani, E., et al., 2003. The thyroid hormone receptor-associated protein TRAP220 is required at distinct embryonic stages in placental, cardiac, and hepatic development. *Mol. Endocrinol.* 17, 2418–2435.
- Le Meur, E., Watrin, F., Landers, M., Stumy, R., Lalande, M., Muscatelli, F., 2005. Dynamic developmental regulation of the large non-coding RNA associated with the mouse 7C imprinted chromosomal region. *Dev. Biol.* 286, 587–600.
- Lee, S., Kozlov, S., Hernandez, L., Chamberlain, S.J., Brannan, C.I., Stewart, C.L., et al., 2000a. Expression and imprinting of *MAGEL2* suggest a role in Prader–Willi syndrome and the homologous murine imprinting phenotype. *Hum. Mol. Genet.* 9, 1813–1819.
- Lee, Y.J., Park, C.W., Hahn, Y., Park, J., Lee, J., Yun, J.H., et al., 2000b. *Mit1/Lb9* and *Copg2*, new members of mouse imprinted genes closely linked to *Peg1/Mest(1)*. *FEBS Lett.* 472, 230–234.
- Lefebvre, L., Viville, S., Barton, S., Ishino, F., Keverne, E., Surani, M., 1998. Abnormal maternal behaviour and growth retardation associated with loss of the imprinted gene *Mest*. *Nat. Genet.* 20, 163–169.
- Leff, S.E., Brannan, C.I., Reed, M.L., Ozcelik, T., Francke, U., Copeland, N.G., et al., 1992. Maternal imprinting of the mouse *Snrpn* gene and conserved linkage homology with the human Prader–Willi syndrome region. *Nat. Genet.* 2, 259–264.
- Leighton, P., Ingram, R., Eggenschwiller, J., Efstratiadis, A., Tilghman, S., 1995a. Disruption of imprinting caused by deletion of the H19 gene region in mice. *Nature* 375, 34–39.
- Leighton, P.A., Saam, J.R., Ingram, R.S., Stewart, C.L., Tilghman, S.M., 1995b. An enhancer deletion affects both H19 and *Igf2* expression. *Genes Dev.* 9, 2079–2089.
- Lewis, A., Mitsuya, K., Umlauf, D., Smith, P., Dean, W., Walter, J., et al., 2004. Imprinting on distal chromosome 7 in the placenta involves repressive histone methylation independent of DNA methylation. *Nat. Genet.* 36, 1291–1295.

- Li, E., Bestor, T.H., Jaenisch, R., 1992. Targeted mutation of the DNA methyltransferase gene results in embryonic lethality. *Cell* 69, 915–926.
- Li, J., Ning, G., Duncan, S., 2000. Mammalian hepatocyte differentiation requires the transcription factor HNF-4 α . *Genes Dev.* 14, 464–474.
- Lin, S.P., Youngson, N., Takada, S., Seitz, H., Reik, W., Paulsen, M., et al., 2003. Asymmetric regulation of imprinting on the maternal and paternal chromosomes at the Dlk1-Gtl2 imprinted cluster on mouse chromosome 12. *Nat. Genet.* 35, 97–102.
- Loschiavo, M., Nguyen, Q., Duselis, A., Vrana, P., 2006. Mapping and identification of candidate loci responsible for *Peromyscus* hybrid overgrowth. *Mamm. Genome* 18, 75–85.
- Luo, J., Sladek, R., Bader, J., Matthyssen, A., Rossant, J., Giguere, V., 1997. Placental abnormalities in mouse embryos lacking the orphan nuclear receptor ERR- β . *Nature* 388, 778–782.
- Lyle, R., Watanabe, D., te Vruchte, D., Lerchner, W., Smrzka, O.W., Wutz, A., et al., 2000. The imprinted antisense RNA at the *Igf2r* locus overlaps but does not imprint *Mas1*. *Nat. Genet.* 25, 19–21.
- MacDonald, H.R., Wevrick, R., 1997. The *necdin* gene is deleted in Prader-Willi syndrome and is imprinted in human and mouse. *Hum. Mol. Genet.* 6, 1873–1878.
- Maecker, H., Levy, S., 1997. Normal lymphocyte development but delayed humoral immune response in CD81-null mice. *J. Exp. Med.* 185, 1505–1510.
- McGrath, J., Solter, D., 1984. Completion of mouse embryogenesis requires both the maternal and paternal genomes. *Cell* 37, 179–183.
- Menhenniott, T.R., Woodfine, K., Schulz, R., Wood, A.J., Monk, D., Giraud, A.S., et al., 2008. Genomic imprinting of Dopa decarboxylase in heart and reciprocal allelic expression with neighboring *Grb10*. *Mol. Cell. Biol.* 28, 386–396.
- Miyoshi, N., Kuroiwa, Y., Kohda, T., Shitara, H., Yonekawa, H., Kawabe, T., et al., 1998. Identification of the *Meg1/Grb10* imprinted gene on mouse proximal chromosome 11, a candidate for the Silver–Russell syndrome gene. *Proc. Natl. Acad. Sci.* 95, 1102–1107.
- Miyoshi, N., Wagatsuma, H., Wakana, S., Shiroishi, T., Nomura, M., Aisaka, K., et al., 2000. Identification of an imprinted gene, *Meg3/Gtl2* and its human homologue *MEG3*, first mapped on mouse distal chromosome 12 and human chromosome 14q. *Genes Cells* 5, 211–220.
- Mishina, Y., Crombie, R., Bradley, A., Behringer, R., 1999. Multiple roles for activin-like kinase-2 signaling during mouse embryogenesis. *Dev. Biol.* 213, 314–326.
- Mizuno, Y., Sotomaru, Y., Katsuzawa, Y., Kono, T., Meguro, M., Oshimura, M., et al., 2002. *Asb4*, *Ata3* and *Dcn* are novel imprinted genes identified by high throughput screening using RIKEN cDNA microarray. *Biochem. Biophys. Res. Commun.* 290, 1499–1505.
- Monk, D., Moore, G., 2004. Intrauterine growth restriction—genetic causes and consequences. *Semin. Fetal Neonatal Med.* 9, 371–378.
- Monk, D., Wagschal, A., Arnaud, P., Müller, P.S., Parker-Katirae, L., Bourc’his, D., et al., 2008. Comparative analysis of human chromosome 7q21 and mouse proximal chromosome 6 reveals a placental-specific imprinted gene, *TFPI2/Tfpi2*, which requires *EHMT2* and *EED* for allelic-silencing. *Genome Res.* 18, 1270–1281.
- Moon, Y., Smas, C., Lee, K., Villena, J., Kim, K.H., Yun, E., et al., 2002. Mice lacking paternally expressed *Pref-1/Dlk1* display growth retardation and accelerated adiposity. *Mol. Cell. Biol.* 22, 5585–5592.
- Moore, T., Constancia, M., Zubair, M., Bailleul, B., Feil, R., Sasaki, H., et al., 1997. Multiple imprinted sense and antisense transcripts, differential methylation and tandem repeats in a putative imprinting control region upstream of mouse *Igf2*. *Proc. Natl. Acad. Sci. USA* 94, 12509–12514.
- Morgan, H., Santos, F., Green, K., Dean, W., Reik, W., 2005. Epigenetic reprogramming in mammals. *Hum. Mol. Genet.* 14, R47–R58.

- Morisaki, H., Hatada, I., Morisaki, T., Mukai, T., 1998. A novel gene, ITM, located between p57KIP2 and IPL, is imprinted in mice. *DNA Res.* 5, 235–240.
- Mossman, H., 1987. *Vertebrate Fetal Membranes*. Rutgers University Press, New Brunswick, New Jersey.
- Moulson, C., Lin, M.H., White, J., Newberry, E., Davidson, N., Miner, J., 2007. Keratinocyte-specific expression of fatty acid transport protein 4 rescues the wrinkle-free phenotype in *Slc27a4/Fatp4* mutant mice. *J. Biol. Chem.* 282, 15912–15920.
- Mulkey, D., Talley, E., Stornetta, R., Siegel, A., West, G., Chen, X., et al., 2007. TASK channels determine pH sensitivity in select respiratory neurons but do not contribute to central respiratory chemosensitivity. *J. Neurosci.* 27, 14049–14058.
- Murdoch, S., Djuric, U., Mazhar, B., Seoud, M., Khan, R., Kuick, R., et al., 2006. Mutations in *Nalp7* cause recurrent hydatidiform moles and reproductive wastage in humans. *Nat. Genet.* 38, 300–302.
- Muscатели, F., Abrous, D., Massacrier, A., Boccaccio, I., Le Moal, M., Cau, P., et al., 2000. Disruption of the mouse *Necdin* gene results in hypothalamic and behavioural alterations reminiscent of the human Prader–Willi syndrome. *Hum. Mol. Genet.* 9, 3101–3110.
- Nagano, T., Mitchell, J.A., Sanz, L.A., Pauler, F.M., Ferguson-Smith, A.C., Feil, R., et al., 2008. The Air noncoding RNA epigenetically silences transcription by targeting G9a to chromatin. *Science* 322, 1717–1720.
- Nakamura, Y., Hamada, Y., Fujiwara, T., Enomoto, H., Hiroe, T., Tanaka, S., et al., 2005. Phospholipase C-1 and -3 are essential in the trophoblast for placental development. *Mol. Cell. Biol.* 25, 10979–10988.
- Nakamura, T., Arai, Y., Umehara, H., Masuhara, M., Kimura, T., Taniguchi, H., et al., 2007. PGC7/Stella protects against DNA demethylation in early embryogenesis. *Nat. Cell. Biol.* 9, 64–71.
- Nelson-Rees, W., 1960. A study of sex predetermination in the mealy bug *Planococcus citri* (Risso). *J. Exp. Zool.* 144, 111–137.
- Newbern, J., Zhong, J., Wickramasinghe, S., Li, X., Wu, Y., Samuels, I., et al., 2008. Mouse and human phenotypes indicate a critical conserved role for ERK2 signaling in neural crest development. *Proc. Natl. Acad. Sci.* 105, 17115–17120.
- Nikaido, I., Saito, C., Mizuno, Y., Meguro, M., Bono, H., Kadomura, M., et al., 2003. Discovery of imprinted transcripts in the mouse transcriptome using large-scale expression profiling. *Genome Res.* 13, 1402–1409.
- Ng, C., Bourquard, N., Grijalva, V., Hama, S., Shih, D., Navab, M., et al., 2006. Paraoxonase-2 deficiency aggravates atherosclerosis in mice despite lower apolipoprotein-B-containing lipoproteins. *J. Biol. Chem.* 281, 29491–29500.
- Nomura, T., Kimura, M., Horii, T., Morita, S., Soejima, H., Kudo, S., et al., 2008. MeCP2-dependent repression of an imprinted miR-184 released by depolarization. *Hum. Mol. Genet.* 17, 1192–1199.
- Ono, R., Kobayashi, S., Wagatsuma, H., Aisaka, K., Kohda, T., Kaneko-Ishino, T., et al., 2001. A retrotransposon-derived gene, PEG10, is a novel imprinted gene located on human chromosome 7q21. *Genomics* 73, 232–237.
- Ono, R., Shiura, H., Aburatani, H., Kohda, T., Kaneko-Ishino, T., Ishino, F., 2003. Identification of a large novel imprinted gene cluster on mouse proximal chromosome 6. *Genome Res.* 13, 1696–1705.
- Ono, R., Nakamura, K., Inoue, K., Naruse, M., Usami, T., Wakisaka-Saito, N., et al., 2006. Deletion of Peg10, an imprinted gene acquired from a retrotransposon, causes early embryonic lethality. *Nat. Genet.* 38, 101–106.
- Onyango, P., Miller, W., Lehoczy, J., Leung, C.T., Birren, B., Wheelan, S., et al., 2000. Sequence and comparative analysis of the mouse 1-megabase region orthologous to the human 11p15 imprinted domain. *Genome Res.* 10, 1697–1710. Erratum in: *Genome Res.* 2001 Feb, 11 (2), 308.

- Parekh, V., McEwen, A., Barbour, V., Takahashi, Y., Rehg, J., Jane, S., et al., 2004. Defective extraembryonic angiogenesis in mice lacking LBP-1a, a member of the grainyhead family of transcription factors. *Mol. Cell. Biol.* 24, 7113–7129.
- Parker-Katiraei, L., Carson, A.R., Yamada, T., Arnaud, P., Feil, R., Abu-Amero, S.N., et al., 2007. Identification of the imprinted KLF14 transcription factor undergoing human-specific accelerated evolution. *PLoS Genet.* 3, e65. doi:10.1371/journal.pgen.0030065.
- Paulsen, M., Davies, K.R., Bowden, L.M., Villar, A.J., Franck, O., Fuermann, M., et al., 1998. Syntenic organization of the mouse distal chromosome 7 imprinting cluster and the Beckwith–Wiedemann syndrome region in chromosome 11p15.5. *Hum. Mol. Genet.* 7, 1149–1159.
- Paulsen, M., El-Maarri, O., Engemann, S., Strödicke, M., Franck, O., Davies, K., et al., 2000. Sequence conservation and variability of imprinting in the Beckwith–Wiedemann syndrome gene cluster in human and mouse. *Hum. Mol. Genet.* 9, 1829–1841.
- Pearsall, R.S., Plass, C., Romano, M.A., Garrick, M.D., Shibata, H., Hayashizaki, Y., et al., 1999. A direct repeat sequence at the Rasgrf1 locus and imprinted expression. *Genomics* 55, 194–201.
- Perea-Gomez, A., Rhinn, M., Ang, S.L., 2001. Role of the anterior visceral endoderm in restricting posterior signals in the mouse embryo. *Int. J. Dev. Biol.* 45, 311–320.
- Peters, J., Wroe, S.F., Wells, C.A., Miller, H.J., Bodle, D., Beechey, C.V., et al., 1999. A cluster of oppositely imprinted transcripts at the Gnas locus in the distal imprinting region of mouse chromosome 2. *Proc. Natl. Acad. Sci. USA* 96, 3830–3835.
- Piras, G., el Kharroubi, A., Kozlov, S., Escalante-Alcalde, A., Hernandez, L., Copeland, N., et al., 2000. Zac1 (Lot1), a potential tumor suppressor gene, and the gene for epsilon-sarcoglycan are maternally imprinted genes: identification by a subtractive screen of novel uniparental fibroblast lines. *Mol. Cell. Biol.* 20, 3308–3315.
- Plagge, A., Gordon, E., Dean, W., Boiani, R., Cinti, S., Peters, J., et al., 2004. The imprinted signaling protein XL α s is required for postnatal adaptation to feeding. *Nat. Genet.* 36, 818–826.
- Plagge, A., Isles, A., Gordon, E., Humby, T., Dean, W., Gritsch, S., et al., 2005. Imprinted Nesp55 influences behavioral reactivity to novel environments. *Mol. Cell. Biol.* 25, 3019–3026.
- Plass, C., Shibata, H., Kalcheva, I., Mullins, L., Kotelevtseva, N., Mullins, J., et al., 1996. Identification of Grf1 on mouse chromosome 9 as an imprinted gene by RLGS-M. *Nat. Genet.* 14, 106–109.
- Qian, N., Frank, D., O’Keefe, D., Dao, D., Zhao, L., Yuan, L., et al., 1997. The IPL gene on chromosome 11p15.5 is imprinted in humans and mice and is similar to TDAG51, implicated in Fas expression and apoptosis. *Hum. Mol. Genet.* 6, 2021–2029.
- Red-Horse, K., Zhou, Y., Genbacev, O., Prakobphol, A., Foulk, R., McMaster, M., et al., 2004. Trophoblast differentiation during embryo implantation and formation of the maternal–fetal interface. *J. Clin. Invest.* 114, 744–754.
- Renfree, M.B., Ager, E.I., Shaw, G., Pask, A.J., 2008. Genomic imprinting in marsupial placentation. *Reproduction* 136, 523–531.
- Reule, M., Krause, R., Hemberger, M., Fundele, R., 1998. Analysis of Peg1/Mest imprinting in the mouse. *Dev. Genes Evol.* 208, 161–163.
- Rhinn, M., Dierich, A., Shawlot, W., Behringer, R., Le Meur, M., Ang, S.L., 1998. Sequential roles for *Otx2* in visceral endoderm and neuroectoderm for forebrain and midbrain induction and specification. *Development* 125, 845–856.
- Riley, P., Anson-Cartwright, L., Cross, J., 1998. The Hand1 bHLH transcription factor is essential for placental and cardiac morphogenesis. *Nat. Genet.* 18, 271–275.
- Rodriguez, T.A., Sparrow, D.B., Scott, A.N., Withington, S.L., Preis, J.I., Michalick, J., et al., 2004. Cited1 is required in trophoblasts for placental development and for embryo growth and survival. *Mol. Cell. Biol.* 24, 228–244.

- Ross, M., Beall, M., 2008. Adult sequelae of intrauterine growth restriction. *Semin. Perinatol.* 32, 213–218.
- Rossant, J., Cross, J., 2001. Placental development: lessons from mouse mutants. *Nat. Rev. Genet.* 2, 538–548.
- Rougeulle, C., Cardoso, C., Fontés, M., Colleaux, L., Lalonde, M., 1998. An imprinted antisense RNA overlaps UBE3A and a second maternally expressed transcript. *Nat. Genet.* 19, 15–16.
- Ruf, N., Bähring, S., Galetzka, D., Pliushch, G., Luft, F.C., Nürnberg, P., et al., 2007. Sequence-based bioinformatic prediction and QUASEP identify genomic imprinting of the KCNK9 potassium channel gene in mouse and human. *Hum. Mol. Genet.* 16, 2591–2599.
- Sandell, L.L., Guan, X.J., Ingram, R., Tilghman, S.M., 2003. Gattm, a creatine synthesis enzyme, is imprinted in mouse placenta. *Proc. Natl. Acad. Sci. USA* 100, 4622–4627.
- Sanford, J.P., Clark, H.J., Chapman, V.M., Rossant, J., 1987. Differences in DNA methylation during oogenesis and spermatogenesis and their persistence during early embryogenesis in the mouse. *Genes Dev.* 10, 1039–1046.
- Santos, F., Hendrich, B., Reik, W., Dean, W., 2002. Dynamic reprogramming of DNA methylation in the early mouse embryo. *Dev. Biol.* 241, 172–182.
- Santos, F., Peters, A., Otte, A., Reik, W., Dean, W., 2005. Dynamic chromatin modifications characterise the first cell cycle in mouse embryos. *Dev. Biol.* 280, 225–236.
- Schmidt, J.V., Matteson, P.G., Jones, B.K., Guan, X.J., Tilghman, S.M., 2000. The Dlk1 and Gtl2 genes are linked and reciprocally imprinted. *Genes Dev.* 14, 1997–2002.
- Schorpp-Kistner, M., Wang, Z.Q., Angel, P., Wagner, E., 1999. JunB is essential for mammalian placentation. *EMBO J.* 18, 934–948.
- Schüle, B., Li, H.H., Fisch-Kohl, C., Purmann, C., Francke, U., 2007. DLX5 and DLX6 expression is biallelic and not modulated by MeCP2 deficiency. *Am. J. Hum. Genet.* 81, 492–506.
- Schulz, R., McCole, R.B., Woodfine, K., Wood, A.J., Chahal, M., Monk, D., et al., 2009. Transcript- and tissue-specific imprinting of a tumour suppressor gene. *Hum. Mol. Genet.* 18, 118–127.
- Schultz, R., Menhenniott, T., Woodfine, K., Wood, A., Choi, J., Oakey, R., 2006. Chromosome-wide identification of novel imprinted genes using microarrays and uniparental disomies. *Nucleic Acids Res.* 34, e88.
- Schweifer, N., Valk, P.J., Delwel, R., Cox, R., Francis, F., Meier-Ewert, S., et al., 1997. Characterization of the C3 YAC contig from proximal mouse chromosome 17 and analysis of allelic expression of genes flanking the imprinted Igf2r gene. *Genomics* 43, 285–297.
- Scott, R., Spielman, M., Bailey, J., Dickinson, H., 1998. Parent-of-origin effects on seed development in *Arabidopsis thaliana*. *Development* 125, 3329–3341.
- Seitz, H., Youngson, N., Lin, S.P., Dalbert, S., Paulsen, M., Bachellerie, J.P., et al., 2003. Imprinted microRNA genes transcribed antisense to a reciprocally imprinted retrotransposon-like gene. *Nat. Genet.* 34, 261–262.
- Seitz, H., Royo, H., Bortolin, M.L., Lin, S.P., Ferguson-Smith, A.C., Cavallé, J., 2004. A large imprinted microRNA gene cluster at the mouse Dlk1-Gtl2 domain. *Genome Res.* 14, 1741–1748.
- Sekita, Y., Wagatsuma, H., Nakamura, K., Ono, R., Kagami, M., Wakisaka, N., et al., 2008. Role of retrotransposon-derived imprinted gene, Rtl1, in the feto-maternal interface of mouse placenta. *Nat. Genet.* 40, 243–248.
- Sha, K., 2008. A mechanistic view of genomic imprinting. *Annu. Rev. Genomics Hum. Genet.* 9, 197–216.
- Shawlot, W., Behringer, R.R., 1995. Requirement for Lim1 in head-organizer function. *Nature* 374, 425–430.

- Shi, W., van den Hurk, J., Alamo-Bethencourt, V., Mayer, W., Winkens, H., Ropers, H.H., et al., 2004. Choroideremia gene product affects trophoblast development and vascularization in mouse extra-embryonic tissues. *Dev. Biol.* 272, 53–65.
- Shibata, H., Ueda, T., Kamiya, M., Yoshiki, A., Kusakabe, M., Plass, C., et al., 1997. An oocyte-specific methylation imprint center in the mouse U2afbp-rs/U2af1-rs1 gene marks the establishment of allele-specific methylation during preimplantation development. *Genomics* 44, 171–178.
- Shimoda, M., Morita, S., Obata, Y., Sotomaru, Y., Kono, T., Hatada, I., 2002. Imprinting of a small nucleolar RNA gene on mouse chromosome 12. *Genomics* 79, 483–486.
- Shin, J.Y., Fitzpatrick, G., Higgins, M., 2008. Two distinct mechanisms of silencing by the KvDMR1 imprinting control region. *EMBO J.* 27, 168–178.
- Sibilia, M., Steinbach, J., Stingl, L., Aguzzi, A., Wagner, E., 1998. A strain-independent postnatal neurodegeneration in mice lacking the EGF receptor. *EMBO J.* 17, 719–731.
- Sirard, C., de la Pompa, J., Elia, A., Itie, A., Mirtsos, C., Cheung, A., et al., 1998. The tumor suppressor gene *Smad4/Dpc4* is required for gastrulation and later for anterior development of the mouse embryo. *Genes Dev.* 12, 107–119.
- Skinner, J., Cattanch, B., Peters, J., 2002. The imprinted oedematous-small mutation on mouse chromosome 2 identifies new roles for *Gnas* and *Gnasxl* in development. *Genomics* 80, 373–375.
- Sleutels, F., Tjon, G., Ludwig, T., Barlow, D.P., 2003. Imprinted silencing of *Slc22a2* and *Slc22a3* does not need transcriptional overlap between *Igf2r* and *Air*. *EMBO J.* 22, 3696–3704.
- Slim, R., Fallahianb, M., Rivière, J.B., Zalid, M., 2005. Evidence of a genetic heterogeneity of familial hydatidiform moles. *Placenta* 26, 5–9.
- Smith, R.J., Arnaud, P., Konfortova, G., Dean, W.L., Beechey, C.V., Kelsey, G., 2002. The mouse *Zac1* locus: basis for imprinting and comparison with human *ZAC*. *Gene* 292, 101–112.
- Smith, R.J., Dean, W., Konfortova, G., Kelsey, G., 2003. Identification of novel imprinted genes in a genome-wide screen for maternal methylation. *Genome Res.* 13, 558–569.
- Steshina, E., Carr, M., Glick, E., Yevtodiynenko, A., Appelbe, O., Schmidt, J., 2006. Loss of imprinting at the *Dlk1-Gtl2* locus caused by insertional mutagenesis in the *Gtl2* 5' region. *BMC Genet.* doi:10.1186/1471-2156-7-44.
- Stöger, R., Kubicka, P., Liu, C.G., Kafri, T., Razin, A., Cedar, H., et al., 1993. Maternal-specific methylation of the imprinted mouse *Igf2r* locus identifies the expressed locus as carrying the imprinting signal. *Cell* 73, 61–71.
- Sunahara, S., Nakamura, K., Nakao, K., Gondo, Y., Nagata, Y., Katsuki, M., 2000. The oocyte-specific methylated region of the *U2afbp-rs/U2af1-rs1* gene is dispensable for its imprinted methylation. *Biochem. Biophys. Res. Commun.* 268, 590–595.
- Takada, S., Tevendale, M., Baker, J., Georgiades, P., Campbell, E., Freeman, T., et al., 2000. Delta-like and *gtl2* are reciprocally expressed, differentially methylated linked imprinted genes on mouse chromosome 12. *Curr. Biol.* 10, 1135–1138.
- Takahashi, K., Kobayashi, T., Kanayama, N., 2000. p57KIP2 regulates the proper development of labyrinthine and spongiotrophoblasts. *Mol. Hum. Reprod.* 6, 1019–1025.
- Takahashi, Y., Carpino, N., Cross, J., Torres, M., Parganas, E., Ihle, J., 2003. SOCS3: an essential regulator of LIF receptor signaling in trophoblast giant cell differentiation. *EMBO J.* 22, 372–384.
- Takaoka, K., Yamamoto, M., Hamada, H., 2007. Origin of body axes in the mouse embryo. *Curr. Opin. Genet. Dev.* 17, 344–350.
- Tam, P., Loebel, D., Tanaka, S., 2006. Building the mouse gastrula: signals, asymmetry and lineages. *Curr. Opin. Genet. Dev.* 16, 419–425.
- Tanaka, M., Gertsenstein, M., Rossant, J., Nagy, A., 1997. *Mash2* acts cell autonomously in mouse spongiotrophoblast development. *Dev. Biol.* 190, 55–65.

- Tarkowski, A., Witkowska, A., Opas, J., 1977. Development of cytochalasin B-induced tetraploid and diploid/tetraploid mosaic mouse embryos. *J. Embryol. Exp. Morphol.* 41, 47–64.
- Tarkowski, A., Ozdzenski, W., Czolowska, R., 2001. Mouse singletons and twins developed from isolated diploid blastomeres supported with tetraploid blastomeres. *Int. J. Dev. Biol.* 45, 591–596.
- Thomas, P., Beddington, R., 1996. Anterior primitive endoderm may be responsible for patterning the anterior neural plate in the mouse embryo. *Curr. Biol.* 6, 1487–1496.
- Tierling, S., Dalbert, S., Schoppenhorst, S., Tsai, C.E., Oliger, S., Ferguson-Smith, A.C., et al., 2006. High-resolution map and imprinting analysis of the Gtl2-Dnchc1 domain on mouse chromosome 12. *Genomics* 87, 225–235.
- Tong, Z.B., Gold, L., de Pol, A., Vanevski, K., Dorward, H., Sena, P., et al., 2004. Developmental expression and subcellular localization of mouse MATER, an oocyte-specific protein essential for early development. *Endocrinology* 145, 1427–1434.
- Tsai, T.F., Armstrong, D., Beaudet, A., 1999. Necdin-deficient mice do not show lethality or the obesity and infertility of Prader–Willi syndrome. *Nat. Genet.* 22, 15–16.
- Tsai, C.E., Lin, S.P., Ito, M., Takagi, N., Takada, S., Ferguson-Smith, A.C., 2002. Genomic imprinting contributes to thyroid hormone metabolism in the mouse embryo. *Curr. Biol.* 12, 1221–1226.
- Uez, N., Lickert, H., Kohlhase, J., Hrabe de Angelis, M., Kühn, R., Wurst, W., et al., 2008. Sall4 isoforms act during proximal–distal and anterior–posterior axis formation in the mouse embryo. *Genesis* 46, 463–477.
- Umlauf, D., Goto, Y., Cao, R., Cerqueira, F., Wagschal, A., Zhang, Y., et al., 2004. Imprinting along the Kcnq1 domain on mouse chromosome 7 involves repressive histone methylation and recruitment of Polycomb group complexes. *Nat. Genet.* 36, 1296–1300.
- van de Sluis, B., Muller, P., Duran, K., Chen, A., Groot, A., Klomp, L., et al., 2007. Increased activity of hypoxia-inducible factor 1 is associated with early embryonic lethality in *Commd1* null mice. *Mol. Cell. Biol.* 27, 4142–4156.
- Varlet, I., Collignon, J., Robertson, E., 1997. *Nodal* expression in the primitive endoderm is required for specification of the anterior axis during mouse gastrulation. *Development* 124, 1033–1044.
- Varmuza, S., Mann, M., Rogers, I., 1993. Site of action of imprinted genes revealed by phenotypic analysis of parthenogenetic embryos. *Dev. Genet.* 14, 239–248.
- Varmuza, S., Mann, M., 1994. Genomic imprinting—defusing the ovarian time bomb. *Trends Genet.* 10, 118–123.
- Varrault, A., Gueydan, C., Delalbre, A., Bellmann, A., Houssami, S., Aknin, C., et al., 2006. *Zac1* regulates an imprinted gene network critically involved in the control of embryonic growth. *Dev. Cell* 11, 711–722.
- Victoria, C., Adair, L., Fall, C., Hallal, P., Martorell, R., Richter, L., Maternal and Child Undernutrition Study Group, 2008. Maternal and child undernutrition: consequences for adult health and human capital. *Lancet* 371, 340–357.
- Villar, A.J., Pedersen, R.A., 1994. Parental imprinting of the *Mas* protooncogene in mouse. *Nat. Genet.* 8, 373–379.
- Vitale, A., Calvert, M., Mallavarapu, M., Yurttas, P., Perlin, J., Herr, J., et al., 2007. Proteomic profiling of murine oocyte maturation. *Mol. Reprod. Dev.* 74, 608–616.
- Vrana, P., Guan, X.J., Ingram, R., Tilghman, S., 1998. Genomic imprinting is disrupted in interspecific *Peromyscus* hybrids. *Nat. Genet.* 20, 362–365.
- Wagschal, A., Feil, R., 2006. Genomic imprinting in the placenta. *Cytogenet. Genome Res.* 113, 1–4.
- Waldorf, K.M., Nelson, J.L., 2008. Autoimmune disease during pregnancy and the micro-chimerism legacy of pregnancy. *Immunol. Invest.* 37, 631–644.

- Waldrip, W., Bikoff, E., Hoodless, P., Wrana, J., Robertson, E., 1998. Smad2 signaling in extraembryonic tissues determines anterior-posterior polarity of the early mouse embryo. *Cell* 92, 797–808.
- Walther, T., Balschun, D., Voigt, J., Finki, H., Zuschratter, W., Birchmeier, C., et al., 1998. Sustained long term potentiation and anxiety in mice lacking the Mas protooncogene. *J. Biol. Chem.* 273, 11867–11873.
- Wan, L., Bartolomei, M., 2008. Regulation of imprinting in clusters: non-coding RNAs versus insulators. *Adv. Genet.* 61, 207–223.
- Wang, Z.Q., Fung, M., Barlow, D., Wagner, E., 1994. Regulation of embryonic growth and lysosomal targeting by the imprinted *Igf2/Mpr* gene. *Nature* 372, 464–467.
- Wang, J., Mager, J., Schneider, E., Magnuson, T., 2002. The mouse *PcG* gene *eed* is required for *Hox* gene repression and extraembryonic development. *Mamm. Genome* 13, 493–503.
- Wang, Y., Joh, K., Masuko, S., Yatsuki, H., Soejima, H., Nabetani, A., et al., 2004. The mouse *Murr1* gene is imprinted in the adult brain, presumably due to transcriptional interference by the antisense-oriented *U2af1-rs1* gene. *Mol. Cell. Biol.* 24, 270–279.
- Watt, A., Battle, M., Li, J., Duncan, S., 2004. *GATA4* is essential for formation of the proepicardium and regulates cardiogenesis. *Proc. Natl. Acad. Sci.* 101, 12573–12578.
- Watrif, F., Roëckel, N., Lacroix, L., Mignon, C., Mattei, M.G., Disteche, C., et al., 1997. The mouse *Necdin* gene is expressed from the paternal allele only and lies in the 7C region of the mouse chromosome 7, a region of conserved synteny to the human Prader-Willi syndrome region. *Eur. J. Hum. Genet.* 5, 324–332.
- Weisstaub, N., Zhou, M., Lira, A., Lambe, E., González-Maeso, J., Homung, J.P., et al., 2006. Cortical 5-HT_{2A} receptor signaling modulates anxiety-like behaviors in mice. *Science* 313, 536–540.
- Werren, J., Baldo, L., Clark, M., 2008. Wolbachia: master manipulators of invertebrate biology. *Nat. Rev. Microbiol.* 6, 741–751.
- Wevrick, R., Francke, U., 1997. An imprinted mouse transcript homologous to the human imprinted in Prader-Willi syndrome (IPW) gene. *Hum. Mol. Genet.* 6, 325–332.
- White, M.J.D., 1945, 1973. *Animal Cytology and Evolution*. Cambridge University Press, Cambridge, UK.
- Williamson, C.M., Ball, S.T., Nottingham, W.T., Skinner, J.A., Plagge, A., Turner, M.D., et al., 2004. A cis-acting control region is required exclusively for the tissue-specific imprinting of *Gnas*. *Nat. Genet.* 36, 894–899.
- Williamson, C.M., Turner, M.D., Ball, S.T., Nottingham, W.T., Glenister, P., Fray, M., et al., 2006. Identification of an imprinting control region affecting the expression of all transcripts in the *Gnas* cluster. *Nat. Genet.* 38, 350–355.
- Wood, A.J., Oakey, R.J., 2006. Genomic imprinting in mammals: emerging themes and established theories. *PLoS Genet.* 2 (11), e147. doi:10.1371/journal.pgen.0020147.
- Wood, A.J., Roberts, R.G., Monk, D., Moore, G.E., Schulz, R., Oakey, R.J., 2007. A screen for retrotransposed imprinted genes reveals an association between X chromosome homology and maternal germ-line methylation. *PLoS Genet.* 3, e20. doi:10.1371/journal.pgen.0030020.
- Wood, A., Bourc'his, D., Bestor, T., Oakey, R., 2008. Allele-specific demethylation at an imprinted mammalian promoter. *Nucleic Acids Res.* 35, 7031–7039.
- Wu, L., de Bruin, A., Saavedra, H., Starovic, M., Trimboli, A., Yang, Y., et al., 2003. Extraembryonic function of *Rb* is essential for embryonic development and viability. *Nature* 421, 942–947.
- Wutz, A., Smrzka, O.W., Schweifer, N., Schellander, K., Wagner, E.F., Barlow, D.P., 1997. Imprinted expression of the *Igf2r* gene depends on an intronic CpG island. *Nature* 389, 745–749.

- Wutz, A., Theussl, H., Dausman, J., Jaenisch, R., Barlow, D., Wagner, E., 2001. Non-imprinted *Igf2r* expression decreases growth and rescues the T^{me} mutation in mice. *Development* 128, 1881–1887.
- Yang, T., Adamson, T., Resnick, J., Leff, S., Wevrick, R., Francke, U., et al., 1998. A mouse model for Prader–Willi syndrome imprinting–centre mutations. *Nat. Genet.* 19, 25–31.
- Yamamoto, H., Flannery, M., Kupriyanov, S., Pearce, J., McKercher, S., Henkel, G., et al., 1998. Defective trophoblast function in mice with a targeted mutation of *Ets2*. *Genes Dev.* 12, 315–326.
- Yevtodiyyenko, A., Carr, M.S., Patel, N., Schmidt, J.V., 2002. Analysis of candidate imprinted genes linked to *Dlk1-Gtl2* using a congenic mouse line. *Mamm. Genome* 13, 633–638.
- Yokoi, F., Dang, M.T., Mitsui, S., Li, Y., 2005. Exclusive paternal expression and novel alternatively spliced variants of epsilon-sarcoglycan mRNA in mouse brain. *FEBS Lett.* 579, 4822–4828.
- Yokoi, F., Dang, M.T., Mitsui, S., Li, Y., 2006. Myoclonus, motor deficits, alterations in emotional responses and monoamine metabolism in ϵ -sarcoglycan deficient mice. *J. Biochem.* 140, 141–146.
- Yoon, B.J., Herman, H., Sikora, A., Smith, L.T., Plass, C., Soloway, P.D., 2002. Regulation of DNA methylation of *Rasgrf1*. *Nat. Genet.* 30, 92–96.
- Yoshida, N., Brahmajosyula, M., Shoji, S., Amanai, M., Perry, A., 2007. Epigenetic discrimination by mouse metaphase II oocytes mediates asymmetric chromatin remodeling independently of meiotic exit. *Dev. Biol.* 301, 464–477.
- Young, L., Sinclair, K., Wilmut, I., 1998. Large offspring syndrome in cattle and sheep. *Rev. Reprod.* 3, 155–163.
- Yu, S., Gavrilova, O., Chen, H., Lee, R., Liu, J., Pacak, K., et al., 2000. Paternal versus maternal transmission of a stimulatory G-protein α subunit knockout produces opposite effects on energy metabolism. *J. Clin. Invest.* 105, 615–623.
- Zhang, Z., Joh, K., Yatsuki, H., Wang, Y., Arai, Y., Soejima, H., et al., 2006. Comparative analyses of genomic imprinting and CpG island-methylation in mouse *Murr1* and human *MURR1* loci revealed a putative imprinting control region in mice. *Gene* 366, 77–86.
- Zwart, R., Sleutels, F., Wutz, A., Schinkel, A.H., Barlow, D.P., 2001a. Bidirectional action of the *Igf2r* imprint control element on upstream and downstream imprinted genes. *Genes Dev.* 15, 2361–2366.
- Zwart, R., Verhaagh, S., Buitelaar, M., Popp-Snijders, C., Barlow, D., 2001b. Impaired activity of the extraneuronal monoamine transporter system known as uptake-2 in *Orct3/Slc22a3*-deficient mice. *Mol. Cell. Biol.* 21, 4188–4196.

CELL AND MOLECULAR BIOLOGY OF ATP-BINDING CASSETTE PROTEINS IN PLANTS

Kazufumi Yazaki, Nobukazu Shitan, Akifumi Sugiyama,
and Kojiro Takanashi

Contents

1. Introduction	264
2. ABC Proteins Localized to Plasma Membranes	265
2.1. Functions at leaf and shoot epidermis	265
2.2. Functions at shoot and root apical meristems	275
2.3. Other functions in roots and rhizomes	280
2.4. Functions in seeds and flowers	283
3. ABC Proteins Localized to Other Organelles	283
3.1. Vacuoles	283
3.2. Plastids	286
3.3. Mitochondria	287
3.4. Peroxisomes	289
4. Soluble-Type ABC Proteins in Plants	290
5. Conclusion	291
References	292

Abstract

ATP-binding cassette (ABC) proteins constitute a large and diverse superfamily of membrane-bound and soluble proteins, which are involved in a wide range of biological processes in all organisms from prokaryotes to eukaryotes. Genome analyses of model plants, for example, *Arabidopsis* and rice, have revealed that plants have more than double numbers of this family member in their genomes compared to animals and insects. In recent years, various biochemical and physiological functions of ABC proteins in plants have been reported. Some are relevant for the defense mechanisms to biotic and abiotic stresses, whereas others are involved in the basic functions necessary for maintaining the plant life. Here, we

provide an updated inventory of plant ABC proteins and summarize their tissue specificities, membrane localizations, and physiological functions.

Key Words: ATP-binding cassette protein, Channel regulation, Cell organelles, Primary transport, Stress tolerance, Tissue specificity. © 2009 Elsevier Inc.

1. INTRODUCTION

ATP-binding cassette (ABC) proteins are a large and diverse superfamily of mainly membrane-bound proteins and soluble proteins, ubiquitous in all organisms. ABC proteins are characterized by a highly conserved amino acid domain for the ATP-binding cassette, also known as the nucleotide-binding domain (NBD) or nucleotide-binding fold (NBF). This domain contains conserved motifs called Walker A, Walker B, ABC signature, H loop, and Q loop (Higgins and Linton, 2004). Many ABC proteins in plants contain transmembrane domains (TMDs) consisting of 5–6 α -helices. The core unit of ABC proteins is one TMD and one NBD. “Half-size” ABC proteins have only one core unit while “full-size” ABC proteins have two or more in tandem. It is generally accepted that full-size ABC proteins function as transporters, while half-size ABC proteins must form homo- or heterodimers to become functional transporters. In prokaryotes, these domains are encoded by separate genes but associate to form an ABC transporter complex involved in the import or export of substances. In higher plants, along with the membrane-bound full-size and half-size ABC proteins, there are bacteria-type soluble ABC proteins. Because some members seem to function as an ATP sensor or a molecular switch and are not directly involved in transport, the name ABC protein is often used to define this family.

Completion of the genome-sequencing projects for Arabidopsis and rice, which are models of dicots and monocots, respectively revealed that plants are rich sources of ABC proteins, that is, more than 120 ABC protein genes were found in both plants. The model legume plant *Lotus japonicus* possesses a similar number of ABC proteins in the genome (Sugiyama et al., 2006), a number more than double of that in the human genome. It is presumed that the large size of this family is related to the sessile nature of plants and the extensive metabolism and the photosynthesis that occur in plants, since plants need to detoxify both xenobiotics from the environment and endogenous toxic metabolites, and that ABC proteins play important roles in protection against biotic and abiotic stress.

As transporters, ABC proteins are classified into primary transporters, which are directly energized by ATP hydrolysis to transport substances. Thus, transport activity is independent of membrane potential and/or proton gradients across the membrane. In recent years, it has been

demonstrated that ABC proteins are involved in the transport of phytohormones, heavy metals, lipids, chlorophyll catabolites, secondary metabolites, and xenobiotics. Moreover, some members are relevant for integrated functions, such as stomatal movement and plant–pathogen interactions. In this review, we have categorized plant ABC proteins according to the membrane in which they occur, that is, plasma membrane, vacuolar membrane, and membranes of other organelles, which may aid understanding of the subcellular and intercellular functions of ABC proteins in the plant body. The nomenclature used in this review is in compliance with the unified nomenclature proposed by plant ABC protein researchers (Verrier et al., 2008).

2. ABC PROTEINS LOCALIZED TO PLASMA MEMBRANES

2.1. Functions at leaf and shoot epidermis

The aerial parts of plants are covered with a waxy cuticle, which serves as a protective barrier against dryness and also prevents the loss of compounds from plant cells. The cuticle layer, therefore, acts as an interface between the plant and surrounding environment. The plant cuticle is composed of cutin, an insoluble lipid-derived polymeric structural component, which is embedded in wax. The wax layer is formed from very long chain fatty acids and their derivatives, which are synthesized in the epidermal cells and exported to the plant surface. An ABC protein was reported to function in the wax load at the plasma membrane of epidermal cells. Among *cer* (*eceriferum*) mutants unable to form a cuticle, the *cer5* mutant had a central vacuole with large protrusions of the cytoplasm in the epidermis (Pighin et al., 2004). The total fatty acid profiles and total amount of epidermal wax of the *cer5* mutant did not differ from those of wild-type plants, but the amount of wax components on the surface was reduced, indicating that the wax components were produced but not transported. The *CER5* gene was found to encode a half-size ABC protein belonging to the ABCG/White–Brown Complex (WBC) subfamily, and is now designated AtABCG12 (Verrier et al., 2008).

Recently, the authors have reported another member of the ABCG subfamily of Arabidopsis, AtABCG11 (AtWBC11), which is also involved in cuticular lipid secretion (Bird et al., 2007). They revealed that the expression of *AtABCG11* was most strongly correlated with the expression of *AtABCG12* within the ABCG subfamily, which consists of 29 half-size proteins. Knockout mutants of AtABCG11 showed reduced alkanes of surface waxes and cutin load on the plant surface. They also showed postgenital organ fusion and stunted growth, which was, however, not found in the *cer5* mutant, suggesting that AtABCG11 plays important roles in the normal growth of plants.

Shortly after this publication, three different groups independently reported similar observations for AtABCG11 functions (Luo et al., 2007; Panikashvili et al., 2007; Ukitsu et al., 2007). Luo et al. used T-DNA insertion lines of AtABCG11 to analyze the function of this protein. The knockout mutants showed organ fusion and stunted growth, and the amount of wax crystals on the stem surface of the mutants was reduced (Luo et al., 2007). Promoter::GFP-ABCG11 transformants showed epidermis-specific fluorescence in leaves, stems, and siliques, although promoter::GUS transformants showed GUS activity in subepidermal cells as well as the epidermis, suggesting an unknown regulatory mechanism for the cell-type specific expression of this membrane protein. As both AtABCG11 and AtABCG12 occur in plasma membranes (Table 6.1), and are involved presumably in the transport of wax components, there is a possibility that they form a heterodimer. It is, however, also possible that AtABCG11 forms a homodimer or a heterodimer with another ABCG protein to function in the formation of cutin for normal plant growth, because the knockout of this gene markedly altered the phenotype, unlike in the *abcg12* mutant (Fig. 6.1).

Two mutants, named *cof1-1* and *cof1-2* (cuticular defect and organ fusion), established from transposon-tagged lines, show organ fusion of rosette leaves and sterility (Ukitsu et al., 2007). Both mutants had a transposon inserted in the *AtABCG11* gene. Scanning electron microscopy revealed a lower density of wax crystals on stems in the *cof1-1* mutant than wild-type plants. In this mutant, the amount of C29 alkane recovered from the stem surface was reduced, while that extracted intracellularly was increased, suggesting that AtABCG11 mediates the secretion of C29 alkane across the plasma membrane. Another report came from analyses of RNAi lines of *AtABCG11*, designated as *DSO* (DESPERADO) (Panikashvili et al., 2007). The *DSO* mutants displayed retarded growth, organ fusion in rosette leaves, and less root branching. They also used T-DNA insertion lines to analyze the contents of wax and cutin monomers, and confirmed that the load of C29 alkanes and cutin monomers (alkan-1-oic acids, 2-hydroxy acids, ω -hydroxy acids, and α , ω -dicarboxylic acids) was reduced in the mutants. Arabidopsis possesses 29 half-size ABCG proteins, most of which have not been characterized yet. As half-size ABC proteins are thought to function as a dimer in transportation, the detailed characterization of heterodimerization or homodimerization is of interest, and the discovery of additional wax transporters within the ABCG subfamily is also expected. AtABCG11 of Arabidopsis is the closest homologue of GhWBC1 of cotton, which was highly expressed in developing fiber cells (Zhu et al., 2003).

As plants are sessile, they have developed highly sophisticated defense mechanisms to cope with both abiotic and biotic stress. Some full-size transporters of the ABCG subfamily, also called pleiotropic drug resistance

Table 6.1 Plant ABC proteins

Gene name	Subfamily	Protein-type	Tissue expression	Subcellular localization	Function	Substrate	Plant spp.
ABC proteins localized to plasma membranes							
<i>AtPGP1</i> (<i>AtABCB1</i>)	B	F	Hypocotyl, root tip	PM (MF&WB, IP)	Auxin transport	IAA	Arabidopsis
<i>AtPGP4/</i> <i>AtMDR4</i> (<i>AtABCB4</i>)	B	F	Root	PM (MF&WB)	Auxin transport	IAA	Arabidopsis
<i>AtPGP19/</i> <i>AtMDR1</i> (<i>AtABCB19</i>)	B	F	Hypocotyl, root, flower	PM (IP)	Auxin transport	IAA	Arabidopsis
<i>Brachytic2</i>	B	F	–	–	Auxin transport?	IAA?	<i>Zea mays</i>
<i>Dwarf3</i>	B	F	–	–	Auxin transport?	IAA?	Sorghum
<i>AtABCB14</i>	B	F	Leaf, flower, silique, stem	PM (GFP, MF&WB for HA)	Stomata regulation	Malate	Arabidopsis
<i>CjMDR1</i>	B	F	Rhizome, petiole, peduncle, bud, flower	PM (MF&WB)	Berberine transport	Berberine	<i>Coptis japonica</i>
<i>TaMDR1</i>	B	F	Root		Al stress response	–	<i>Triticum aestivum</i>
<i>AtMRP4</i> (<i>AtABCC4</i>)	C	F	Leaf, flower, silique, stem, root	PM (GFP, MF&WB for GFP)	Stomata regulation	–	Arabidopsis
<i>AtMRP5</i> (<i>AtABCC5</i>)	C	F	Leaf, flower, silique, root	PM (GFP)	Stomata regulation	–	Arabidopsis
<i>NpPDR1</i>	G	F	Leaf	PM (MF&WB)	Sclareol secretion	Sclareolide	<i>Nicotiana plumbaginifolia</i>

(continued)

Table 6.1 (continued)

Gene name	Subfamily	Protein-type	Tissue expression	Subcellular localization	Function	Substrate	Plant spp.
<i>NtPDR1</i>	G	F	–	–	Defense response	–	<i>Nicotiana tabacum</i>
<i>NtPDR3</i>	G	F	–	–	Response to iron deficiency	–	<i>Nicotiana tabacum</i>
<i>OsPDR9</i>	G	F	Leaf, root	–	Stress response	–	<i>Oryza sativa</i>
<i>GmPDR12</i>	G	F	–	–	Defense response	–	<i>Glycine max</i>
<i>SpTUR2</i>	G	F	Frond	PM (MF&WB)	Sclareol secretion	Sclareol?	<i>Spirodela polyrrhiza</i>
<i>AtPDR8/PEN3</i> (<i>AtABCG36</i>)	G	F	Leaf, silique, stem, root	PM (GFP, MF&WB)	Nonhost resistance, Cd detoxification	Cd	Arabidopsis
<i>AtPDR9</i> (<i>AtABCG37</i>)	G	F	Root	PM (MF&WB)	Herbicide tolerance	Auxinic herbicides?	Arabidopsis
<i>AtPDR12</i> (<i>AtABCG40</i>)	G	F	Leaf, flower, silique, stem, root	PM (GFP)	Defense response, Pb detoxification	Pb?	Arabidopsis
<i>AtWBC11/COF1/DSO</i> (<i>AtABCG11</i>)	G	H	Leaf, flower, silique, stem	PM (GFP, YFP)	Wax component transport	Wax component?	Arabidopsis
<i>CER5</i> (<i>AtABCG12</i>)	G	H	Leaf, flower, silique, stem, root	PM (GFP)	Wax component transport	Wax component?	Arabidopsis
<i>GhWBC1</i>	G	H	Cotton fiber	PM (GFP)	–	–	<i>Gossypium hirsutum</i>
<i>NtWBC1</i>	G	H	Stigma, anther	–	–	–	<i>Nicotiana tabacum</i>
<i>ALS3</i> (<i>AtABCI16</i>)	I	T	Leaf, flower, stem, root	PM (IS)	Al tolerance	–	Arabidopsis

ABC proteins localized to vacuolar membranes							
<i>ALS1/AtTAP2</i> (<i>AtABCB27</i>)	B	H	Leaf, flower, stem, root	VM (GFP)	Al tolerance	Chelated Al (?)	Arabidopsis
<i>IDI7</i> (TAP homolog)	B	H	Root	VM (GFP)	Response to iron deficiency	–	<i>Hordeum vulgare</i>
<i>AtMRP1</i> (<i>AtABCC1</i>)	C	F	Leaf, flower, stem, root	VM (GFP, MF&WB)	Detoxification	GS conjugate	Arabidopsis
<i>AtMRP2</i> (<i>AtABCC2</i>)	C	F	Leaf, flower, stem, root	VM (MF&WB)	Detoxification, senescence	GS conjugate, chlorophyll catabolite	Arabidopsis
<i>ZmMRP3</i>	C	F	Husk, leaf, developing tassel	VM (GFP)	Anthocyanin transport	Cyanidin 3- glucoside	<i>Zea mays</i>
<i>AtWBC19</i> (<i>AtABCG19</i>)	G	H	–	VM (GFP)	Kanamycin resistance	Kanamycin (?)	Arabidopsis
ABC proteins localized to plastids							
<i>AtNAP6</i> (<i>AtABCI6</i>)	I	S	–	Plastid (YFP)	Fe/S cluster biogenesis	–	Arabidopsis
<i>AtNAP7</i> (<i>AtABCI7</i>)	I	S	Embryo, meristem, flower	Plastid (YFP)	Fe/S cluster biogenesis	–	Arabidopsis
<i>Laf6/AtNAP1/ AtABC1</i> (<i>AtABCGI8</i>)	I	S	–	Plastid (GFP)	Fe/S cluster biogenesis	–	Arabidopsis
<i>TGD3</i> (<i>AtABCI13</i>)	I	S	–	Plastid (GFP, <i>in vitro</i> transport)	Lipid biosynthesis	Phosphatidic acid (?)	Arabidopsis
<i>TGD1</i> (<i>AtABCI14</i>)	I	T	–	Plastid (GFP, OF&WB, <i>in vitro</i> transport)	Lipid biosynthesis	Phosphatidic acid (?)	Arabidopsis
<i>TGD2</i> (<i>AtABCI15</i>)	I	T	–	Plastid (GFP)	Lipid biosynthesis	Phosphatidic acid (?)	Arabidopsis

(continued)

Table 6.1 (continued)

Gene name	Subfamily	Protein-type	Tissue expression	Subcellular localization	Function	Substrate	Plant spp.
ABC proteins localized to mitochondria							
<i>AtATM1</i> (<i>AtABCB24</i>)	B	H	Leaf, flower, silique, stem, root	Mit (GFP)	Fe/S cluster biogenesis	Fe/S center (?)	Arabidopsis
<i>AtATM2</i> (<i>AtABCB23</i>)	B	H	Leaf, flower, stem, root	Mit (GFP)	–	–	Arabidopsis
<i>AtATM3</i> (<i>AtABCB25</i>)	B	H	Leaf, flower, silique, stem, root	Mit (GFP)	Fe/S cluster biogenesis, Cd tolerance	Fe/S center (?)	Arabidopsis
<i>CrCDS1</i>	B	H	–	Mit (IS)	Cd tolerance	–	<i>Chlamydomonas reinhardtii</i>
<i>AtCCMA</i> (<i>AtABCI1</i>)	I	S	–	Mit (OF&WB)	Cytochrome <i>c</i> maturation	–	Arabidopsis
<i>AtCCMB</i> (<i>AtABCI2</i>)	I	T	–	Mit (EMG)	Cytochrome <i>c</i> maturation	–	Arabidopsis
ABC proteins localized to peroxisomes							
<i>CTS/PED3/</i> <i>PXA1</i> (<i>AtABCD1</i>)	D	F	–	Per (MF&WB)	Fatty acid transport	Acyl-CoA	Arabidopsis
Soluble ABC proteins							
<i>AtRLI2</i> (<i>AtABCE2</i>)	E	S	Leaf, flower, silique, stem, root	–	Suppressor of RNA silencing	–	Arabidopsis

Notes: Protein-type: F, full-size; H, half-size; S, soluble; T, transmembrane.

Subcellular localization: PM, plasma membrane; VM, vacuolar membrane; Mit, mitochondria; Per, peroxisome; MF, microsomal fractionation; OF, organelle fraction; WB, Western blot; IP, immunoprecipitation; IS, immunostaining; EMG, encoded in the mitochondrial genome.

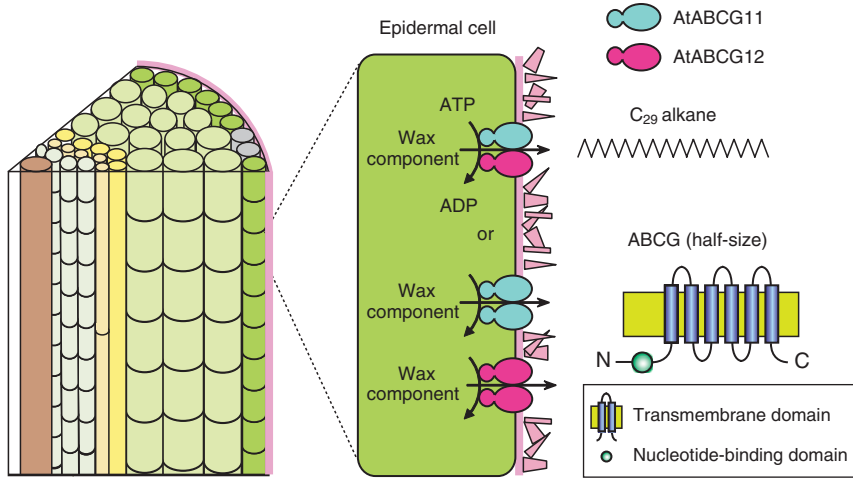


Figure 6.1 AtABCG11 and AtABCG12 function in wax secretion at the plasma membrane of stem cells.

(PDR), are involved in defense mechanisms against pathogens. In tobacco plants (e.g., *Nicotiana plumbaginifolia*), an antifungal diterpene compound, sclareol, is biosynthesized and excreted at the leaf surface. NpPDR1, previously called NpABC1, was reported to be responsible for the secretion of sclareol (Jasinski et al., 2001), and in fact the suppression of NpPDR1 by RNAi made transgenic tobacco plants more susceptible to fungal attack (*Botrytis cinerea*) (Stukkens et al., 2005). As an orthologue of this ABC transporter, an elicitor-inducible PDR gene was isolated from bright yellow (BY)-2 cells of *Nicotiana tabacum* (Sasabe et al., 2002). This gene, named *NtPDR1*, is homologous to NpPDR1, and was strongly induced by methyl jasmonate, yeast extract, and flagellin. A rice orthologue *OsPDR9*, which also showed high similarity to NpPDR1, was isolated as a polyethylene glycol-induced gene from RNA differential display (Moons, 2003). This gene was also highly induced by heavy metals and hypoxic stress. An orthologue reported in legume, *GmPDR12*, was identified as a salicylic acid-induced gene from soybean cell cultures (Eichhorn et al., 2006), and its expression was induced by methyl jasmonate in a similar manner to other plant orthologues. This suggests that the defense mechanism via full-size ABCG members is well conserved from monocots to dicots in terms of the inducibility of gene expression by various chemicals and biotic stress, though substrates have not been fully characterized (Fig. 6.2).

SpTUR2 was the first PDR protein to be isolated from a water plant, *Spirodela polyrrhiza* (Smart and Fleming, 1996). Its expression was induced by abscisic acid (ABA) and also by abiotic environmental stress like low temperature and high salt. These authors later reported that the

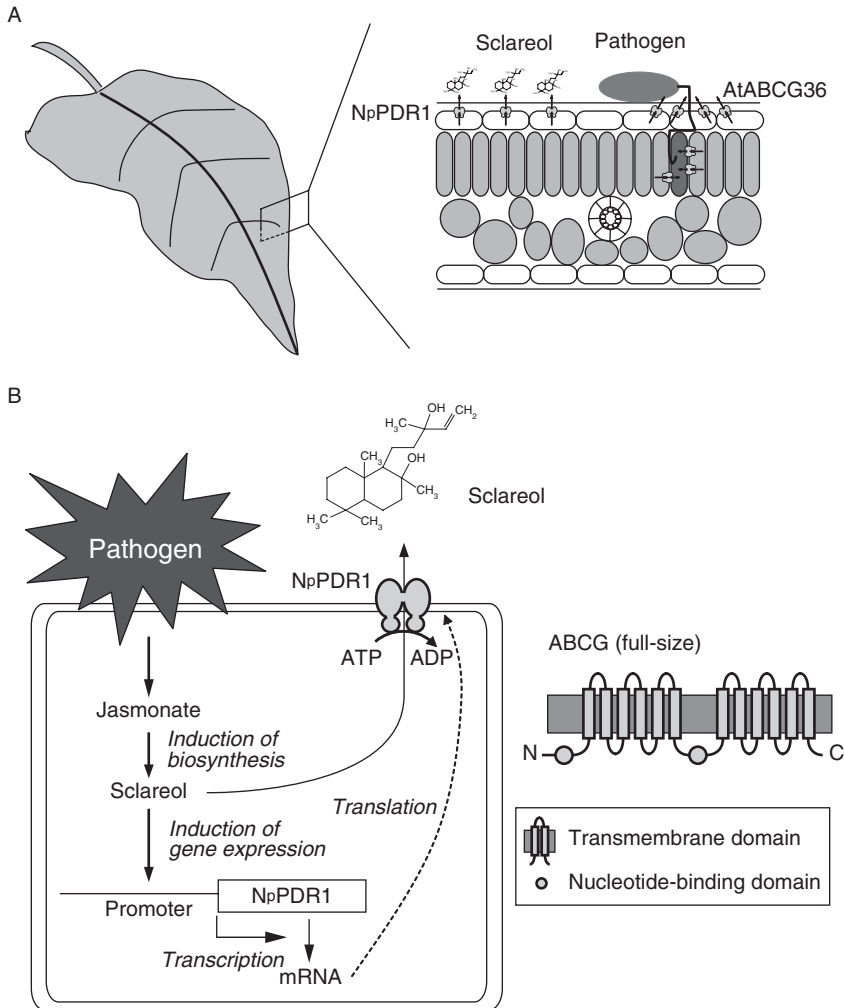


Figure 6.2 A model of the function of full-size ABCG proteins in defense. (A) NpPDR1 secretes sclareol at the leaf surface. AtABCG36 functions in nonhost resistance. (B) Induction of NpPDR1 gene expression by pathogen attack.

overexpression of SpTUR2 in *Arabidopsis* conferred tolerance to sclareol, and that this diterpene was actually present in *S. polyrhiza* (van den Brule et al., 2002). Interestingly, transgenic *Arabidopsis* plants showed tolerance only to sclareol among 19 compounds evaluated in root elongation assays, suggesting that SpTUR2 has a relatively high level of specificity, unlike the PDR5 protein of *Saccharomyces cerevisiae*, which recognizes more than 300 compounds as substrates. Although a direct study with this full-size ABCG protein has not been conducted yet, one possible physiological function of

SpTUR2 in *S. polyrrhiza* is the transport of sclareol or related diterpenes to resist pathogens.

In the Arabidopsis genome, there are 15 full-size ABCG (PDR) proteins (van den Brule and Smart, 2002). *AtABCG40* (*AtPDR12*), a homologue of *NpPDR1*, was identified as a gene induced by the inoculation of a fungal pathogen of Arabidopsis, *Alternaria brassicicola* (Campbell et al., 2003). This gene was induced to express by salicylic acid, methyl jasmonate, ethylene, and both compatible and incompatible pathogens, suggesting its relevance to defense. Cell-type specific expression is reported for *AtABCG36* (*AtPDR8*), which is constitutively expressed in the stomata and hydathode (Kobae et al., 2006), but its gene expression was strongly induced in leaf blades on infection by both virulent and avirulent bacterial pathogens. In the *pdr8* knockout mutant infected with *Pseudomonas syringae*, a virulent bacterial pathogen causing chlorotic lesions and cell death in leaves, bacterial growth was suppressed, presumably because yet unidentified toxic substances were produced by the attack and accumulated in the mutant to trigger hypersensitive cell death (Kobae et al., 2006). Shortly after the publication of this report, another study screened mutants deficient in nonhost resistance. One of the Arabidopsis mutants deficient in nonhost resistance (*pen3*) was identified as being a mutant of the same gene, *AtABCG36* (Stein et al., 2006). Microscopic observation with promoter::PEN3-GFP transgenic plants showed that PEN3 localized to the penetration site upon attack, leading to the hypothesis that this ABC transporter exports toxic metabolites to the apoplast at the site of invasion (Fig. 6.2).

Due to the waxy cuticle surrounding a plant, water and carbon dioxides are not freely permeable and thus the uptake of CO₂ and transpiration are controlled via stomata mostly on the underside of leaves. Stomata are pores formed by a pair of specialized cells called guard cells, which regulate the opening and closure of the pore. ABC proteins are also involved in the movement of stomata. The movement of stomata is controlled by environmental factors such as light, temperature, humidity, and CO₂ concentration. The opening of stomata results from osmotic swelling of the guard cells through the uptake of K⁺ by inward K⁺ channels, uptake of Cl⁻, and production of organic solutes, whereas the closure of stomata is mediated by the release of K⁺ and anions from guard cells (Hetherington and Woodward, 2003). ABCC5 of Arabidopsis (*AtMRP5*) was first reported as being involved in the movement of stomata (Gaedeke et al., 2001) (Fig. 6.3), that is, knockout mutants of *AtABCC5* did not open their stomata on treatment with a sulfonylurea, glybenclamide, which normally induces stomatal opening in wild-type plants (Leonhardt et al., 1997). It was later shown by another group that *AtABCC5* binds to glybenclamide when expressed in HEK293 cells (Lee et al., 2004). A detailed investigation of *mrp5* mutant plants revealed a reduction in stomatal aperture under light, and that the guard cells did not respond to external calcium or abscisic acid under

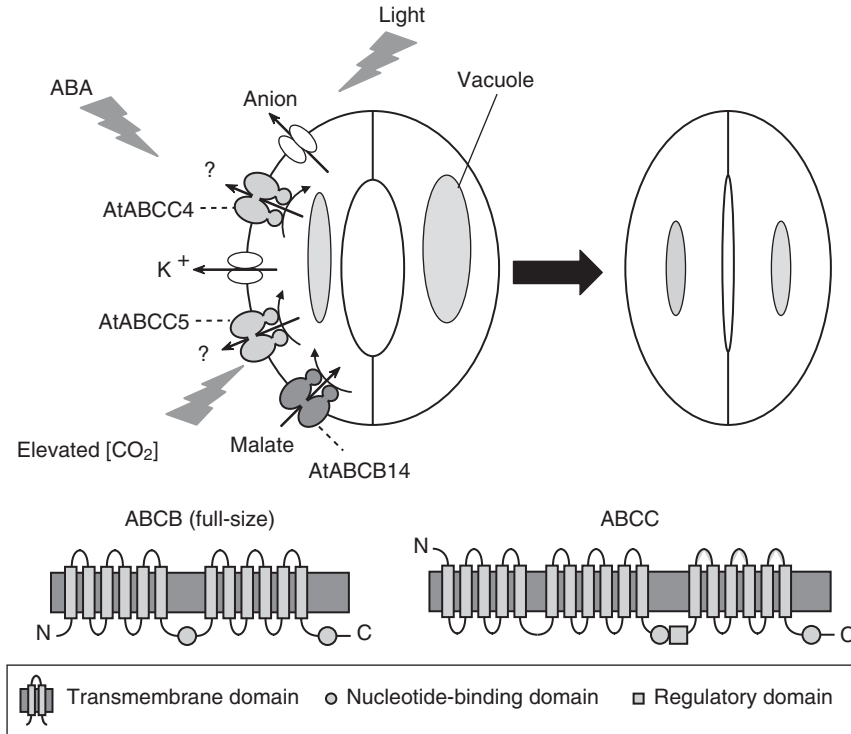


Figure 6.3 ABC proteins are involved in the regulation of stomata.

illumination, which reduced the stomatal aperture in wild-type plants (Klein et al., 2003). Interestingly, *mrp5* mutant plants showed more efficient usage of water than the wild-type plants, and thus survived much longer without water. An electrophysiological study revealed that the activation of slow anion channels by abscisic acid or calcium ion was blocked in guard cells of *mrp5* mutants, suggesting that AtABCC5 is a central regulator of the ion channels of guard cells (Suh et al., 2007). Another ABCC protein, ABCC4 (MRP4) of Arabidopsis, is also involved in the functions of stomata (Fig. 6.3). The stomatal aperture of the *mrp4* mutant was larger than that of the wild type both under illumination and in the dark (Klein et al., 2004), and the mutants wilted earlier than wild-type plants under drought stress. When expressed in yeast, AtABCC4 transported methotrexate, an antifolate drug identified as a substrate of mammalian ABCC transporters, and the application of methotrexate reduced the stomatal aperture in wild-type plants under light but not in *mrp4* mutants. Recently, a member of a different subfamily, ABCB14 of Arabidopsis, was also reported to function in guard cells, this full-size ABC protein transporting malate from the apoplast into the guard cells (Lee et al., 2008). Malate in apoplasts activates the anion channels of

guard cells, leading to the release of anions to the apoplast and closure of stomata (Hedrich et al., 2001). AtABCB14 imports malate into guard cells, and thereby acts as an osmoticum and reduces the speed of stomatal closure (Fig. 6.3).

2.2. Functions at shoot and root apical meristems

A variety of metabolites are involved in the development and maintenance of shoot apical meristems and root apical meristems, which govern the plant body plan and contribute to the plant architecture. A representative of such signaling molecules in plants is auxin (indole-3-acetic acid (IAA)), a phytohormone that regulates plant growth and development in a highly sophisticated manner. In particular, auxin functions by a strictly regulated polar movement leading to a concentration gradient throughout the vertical axis of plants. This polar transport is mediated by cell-to-cell movement generated by a chemiosmotic model (Raven, 1975; Rubery and Sheldrak, 1974) where the existence of carrier proteins localized to the plasma membrane and responsible for IAA uptake and efflux out of the cell is proposed. The model is rationalized by the asymmetric distribution of the efflux carriers to one side of the cell, which determines the direction of the intercellular movement of IAA in plants. In the current model, polar IAA transport is mediated by several different classes of transporter molecules; that is, AUXIN/LIKE-AUXIN (AUX/LAX) permeases (Kramer and Bennett, 2006), PIN-FORMED (PIN) efflux carriers (Teale et al., 2006; Vieten et al., 2007), and the ABCB subfamily of ABC proteins (Geisler and Murphy, 2006) (Fig. 6.4).

2.2.1. ABC proteins mediating the transport of auxin in hypocotyls and stem

AtABCB1 (AtPGP1) and AtABCB19 (AtPGP19/AtMDR1) are the most intensively characterized plant ABC proteins involved in the transport of auxin. *AtABCB1* was originally cloned in order to isolate the proteins that function in broad-spectrum herbicide resistance (Dudler and Hertig, 1992), but later was suggested to be an auxin transporter based on observations that the hypocotyls of *AtABCB1*-overexpressing transformants were elongated under dim light conditions, whereas those of antisense transformants showed reduced elongation (Sidler et al., 1998). *AtABCB1* is specifically expressed in root and shoot meristems. Its paralogue *AtABCB19* was first isolated as an orthologue of the *Brassica napus* gene, which was upregulated by treatment with an anion channel inhibitor, 5-nitro-2-(3-phenylpropylamino)-benzoic acid. *AtABCB19* expression was observed in whole plants including flowers. The insertion of T-DNA in *AtABCB19* resulted in partial dwarfism (Noh et al., 2001). A detailed analysis of two mutants, *atabcb1* and *atabcb19*, showed reduced auxin loading in apical tissue, hypersensitivity to far-red, red, and blue-light inhibition of hypocotyl elongation,

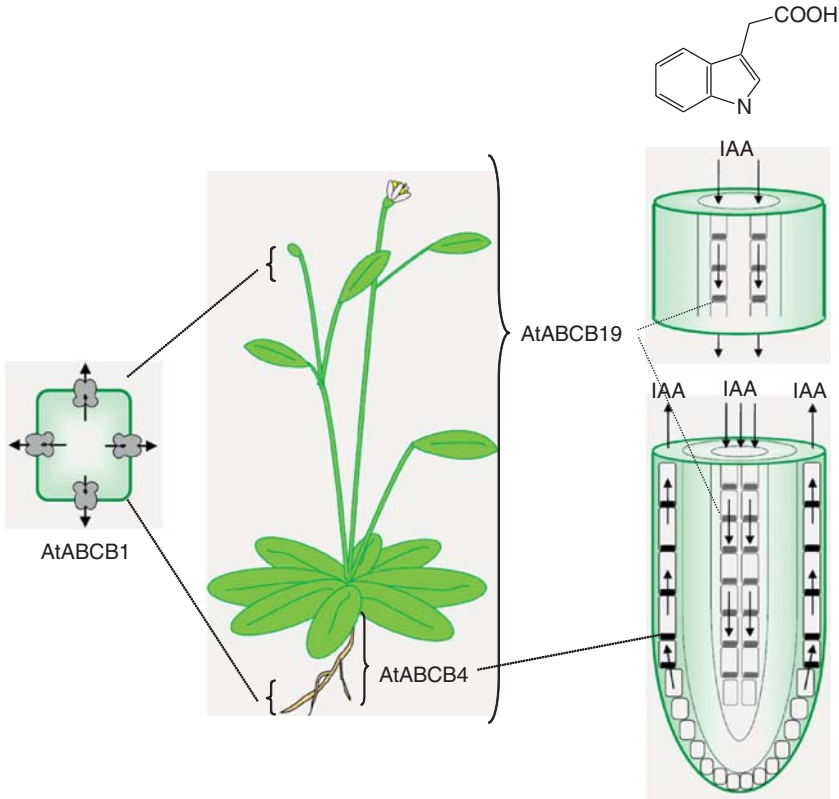


Figure 6.4 Current model of ABCB-mediated IAA transport. AtABCB1 is mainly expressed in shoot and root apices, whereas AtABCB19 is highly expressed throughout the plant. AtABCB4 is a root-specific ABC transporter.

reduced chlorophyll and anthocyanin accumulation, and the abnormal expression of several light-responsive genes. These phenotypes were more apparent in *atabcb19* than *atabcb1* and became marked when both *atabcb1* and *atabcb19* were knocked out, suggesting overlapping functions (Geisler et al., 2005; Lewis et al., 2007; Lin and Wang, 2005; Noh et al., 2003). AtABCB19 is also a target of Gravacin, which inhibits gravitropism and the trafficking of protein to the tonoplast in Arabidopsis. Gravacin binds to AtABCB19 and affects gravitropism to inhibit its subcellular localization (Rojas-Pierce et al., 2007; Surpin et al., 2005). Recent study revealed that *AtABCB19* expression was suppressed by phytochromes and cryptochromes (Nagashima et al., 2008). Other ABCBs involved in the transport of IAA were identified from a maize *brachytic2* mutant and a sorghum *dwarf3* mutant, which exhibited the inhibition of stalk elongation and basipetal IAA transport (Multani et al., 2003). A GUS reporter gene assay and *in situ* hybridization analysis showed *AtABCB1* expression only at hypocotyls

and the root tip (Sidler et al., 1998). Its subcellular localization at the plasma membrane was confirmed by both histochemical analysis and membrane fractionation using anti-AtABCB1 (Sidler et al., 1998). The plasma membrane localization of AtABCB19 was observed in a NPA (1-*N*-naphthylphthalamic acid) binding activity assay (Noh et al., 2001).

In several studies with whole plants, protoplasts, and heterologous expression systems, AtABCB1 and AtABCB19 showed the direct efflux of IAA, the synthetic auxin 1-NAA, and IAA oxidative break down products (Bouchard et al., 2006; Geisler et al., 2003, 2005; Noh et al., 2001). It is noteworthy that when AtABCB1 protein is expressed in heterologous systems alone, ABCB1-mediated auxin transport exhibited reduced substrate specificity for auxin, suggesting that the coexistence of other factors is necessary to reproduce polar auxin transport with ABCB members *in planta*. Indeed, when ABCB1 or ABCB19 is coexpressed with PIN1 protein, substrate specificity and also sensitivity to NPA is apparently increased (Blakeslee et al., 2007). Recently, several effectors have been also reported as modulators of polar auxin transport via ABCB (see Section 2.2.3).

2.2.2. ABC proteins mediating auxin transport in root tissues

Both AtABCB1 and AtABCB19 are also involved in the transport of auxin in roots. Expression analyses of *AtABCB1* with the GUS reporter and GFP showed an apolar localization at the root tip, compared to the polar localization in mature cortical and endodermal cells (upper side) (Geisler et al., 2005; Sidler et al., 1998). The expression of *AtABCB19* was observed in the lower end of cells in the epidermis, cortex, stele, and pericycle derivatives beginning at an early stage of primodium development (Blakeslee et al., 2007; Wu et al., 2007). Both the *atabcb1* and *atabcb19* mutants showed fewer lateral roots than the wild-type plants and the *atabcb1/atabcb19* double mutant revealed further reduced lateral root formation (Bouchard et al., 2006; Lin and Wang, 2005; Wu et al., 2007).

Another ABCB member, *AtABCB4* (*AtPGP4/AtMDR4*), was characterized as involved in early lateral root initiation (Santelia et al., 2005). This full-size ABCB protein is an Arabidopsis homologue of *CjMDR1*, a berberine influx carrier isolated from a ranunculaceous herb, *Coptis japonica* (Shitan et al., 2003; Terasaka et al., 2005). *AtABCB4* showed a characteristic expression pattern; that is, it is specifically expressed in the roots, in particular in the epidermis and the root cap. A specific peptide antibody against AtABCB4 revealed subcellular polarity in the elongated epidermal cells in the root (Terasaka et al., 2005). Analysis of a T-DNA insertion mutant of *AtABCB4* showed light-dependent change in lateral root numbers, root hair elongation, reduced basipetal auxin transport, and decreased NPA growth inhibition. These findings suggested the direct involvement of ABCB4 in the transport of auxin in the root epidermis (Cho et al., 2007; Santelia et al., 2005; Terasaka et al., 2005).

The auxin-transporting function of ABCB4 has been characterized by several groups. AtABCB4-expressing yeast strains exhibited severe hypersensitivity to IAA and a cytotoxic auxin analog, 5-fluoroindole (Santelia et al., 2005). Another heterologous expression system using mammalian HeLa cells showed IAA-uptake activity of AtABCB4, which was clearly inhibited by NPA (Terasaka et al., 2005). This transport occurs in the opposite direction to that of AtABCB1 and AtABCB19 evaluated with those assay systems. However, a recent study using Arabidopsis root hair cells and tobacco suspension cell cultures has suggested that AtABCB4 functions as an auxin efflux transporter. Cho et al. demonstrated that the specific overexpression of AtABCB4 in root hair cells decreased root hair elongation in a similar manner as that of auxin efflux transporters, AtABCB1, AtABCB19, and PIN3 (Lee and Cho, 2006), whereas overexpression of the influx transporter AUXIN-RESISTANT1 (Yang et al., 2006) enhanced root hair length. Furthermore, AtABCB4-overexpressing tobacco suspension cells showed an increase in the efflux of a synthetic auxin, NAA (Cho et al., 2007). These results suggested that coexisting proteins or other factors influence the direction of transport as observed in different assay systems. Another possibility is that AtABCB4 behaves differently toward NAA than toward the natural auxin IAA, because NAA is a “new compound” for the transporter despite having the same equivalent activity as auxin. Evidence that AtABCB4 transports auxin in different directions depending on its PIN partner in HeLa cells (Blakeslee et al., 2007) may resolve this issue (see Section 2.2.3).

Most recently, a new member of the Arabidopsis ABCB family, AtABCB21 (AtPGP21), has been characterized and shown as another auxin transporter. AtABCB21 was identified as most similar to AtABCB4 with 79% amino acid sequence identity. *Atabc21* RNAi mutants showed a slight reduction in root length and strong decrease in lateral root numbers, accompanied by the generation of adventitious roots from the shoot/root transition zone. A gene expression analysis with the GUS reporter gene assay indicated that *AtABCB21* is specifically expressed in the pericycle cells, with especially strong expression in the cells adjacent to the xylem parenchyma. The transport of IAA was investigated with a yeast transformant, which showed transport activity in an inward direction to accumulate more IAA than the control (Y. Kamimoto and K. Yazaki, unpublished data). However, in the Arabidopsis protoplast assay, IAA efflux activity of AtABCB21 was suggested. A possible mechanism for regulating the direction of transport by ABCB proteins is summarized in the next section.

2.2.3. Effectors of ABCB-mediated auxin transport

The existence of several regulators or modulators of the transport function of ABCB proteins has been suggested in biochemical experiments. Endogenous flavonoids such as quercetin, kaempferol, and flavonoid aglycones have been shown to inhibit the polar transport and enhance the local

accumulation of auxin (Peer and Murphy, 2007; Taylor and Grotewold, 2005). *Arabidopsis transparent testa* mutants, which lack biosynthetic activities of the flavonoid pathway, exhibited altered lateral root numbers, root lengths, and also auxin polar transport (Brown et al., 2001; Murphy et al., 2000; Peer et al., 2004). In fact, flavonoids inhibited cellular auxin transport in some assay systems using *Arabidopsis* mesophyll protoplasts and also in heterologous expression systems with yeast and HeLa cells (Bouchard et al., 2006; Geisler et al., 2005; Terasaka et al., 2005). It is proposed that these inhibitory effects on the transport of auxin are due to the ability of flavonoids to bind ABCB protein and compete with NPA at the binding site of the transporter (Bernasconi et al., 1996; Jacobs and Rubery, 1988; Murphy et al., 2000). The precise mechanisms of the inhibition were not clear, but recent study has revealed that flavonoids negatively modulate auxin transport via interaction between ABCB and the immunophilin-like FKBP42, TWISTED DWARF1 (TWD1), which can bind to ABCB as well as NPA (Bailey et al., 2008) (Fig. 6.5).

TWD1 belongs to the FKBP (FK506-binding protein)-type family of PPIases (peptidyl-prolyl *cis-trans* isomerases), most of which catalyze the *cis-trans* isomerization of *cis*-prolyl bonds. Mutation in TWD1 in *Arabidopsis* resulted in a twisted dwarf phenotype and reduced auxin transport, comparable to the *abc1/abc19* double mutant (Geisler et al., 2003). Direct interaction between TWD1 and AtABCB1/19 was demonstrated with the

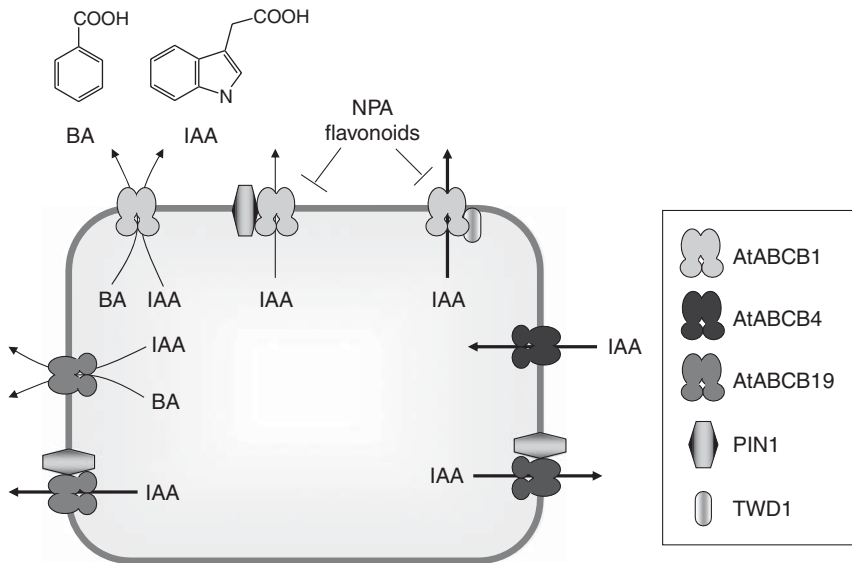


Figure 6.5 Effector molecules of ABCBs. Interactions of effector molecules with ABCB are drawn. The interactions of ABCB protein with PIN, and the effect of NPA and flavonoids are also pictured with ABCB1 as representative.

yeast two-hybrid system. An *in vitro* examination revealed that TWD1 binds, via its N-terminal FK506-binding domain, to the C-terminal nucleotide-binding domain of AtABCB1 and AtABCB19. In this way, TWD1 acts *in planta* as a positive regulator of AtABCB1- and AtABCB19-mediated auxin efflux by means of protein-protein interaction (Bouchard et al., 2006; Geisler et al., 2003). TWD1 can in this manner modulate the movement of auxin out of apical regions, to contribute positively to the long-range transport of auxin at the cellular level (Bouchard et al., 2006; Lewis et al., 2007). Recently, Bailly et al. have demonstrated using a yeast bioluminescence resonance energy transfer system that NPA and flavonoids interrupt TWD1-AtABCB1 binding. They verified that NPA binds to both ABCB1 and TWD1 but not to the TWD1-AtABCB1 complex in a yeast expression system and that auxin flux and gravitropism in *twd1* roots showed less sensitivity to NPA treatment (Bailly et al., 2008).

PIN proteins, representative of auxin efflux carriers, are also involved in the regulation of ABCBs. PINs are members of the membrane protein family with a predicted membrane topology similar to that of ion-coupled transporters, the major facilitator superfamily (MFS) (Muller et al., 1998). PIN proteins activate auxin transport in both plant and also in heterologous cell expression systems (Chen et al., 1998; Luschnig et al., 1998; Petrasek et al., 2006). The protein-protein interaction between PIN and ABCB was first suggested from the disruption of the basal localization of PIN1 in hypocotyls of *abc19* mutant plants (Noh et al., 2003). Further analysis revealed specific PIN-ABCB interactions in yeast two-hybrid and coimmunoprecipitation assays (Blakeslee et al., 2007). In heterologous coexpression systems, PIN-ABCB interactions appeared to enhance transport activity and substrate/inhibitor specificity. Moreover, when ABCB4 was coexpressed with PIN1, its direction of transport of IAA was altered from influx to efflux in the HeLa cells. Colocalization of PINs and ABCBs is one of the key regulatory mechanisms of IAA transport in plant cells, but usually only one gene is expressed in heterologous systems, which may explain the findings for some ABCB members mentioned above. Blakeslee et al. further confirmed that AtABCB1 and AtABCB19 colocalized with PIN1 at the shoot apex, whereas they colocalized with PIN1 and PIN2 in root tissues in Arabidopsis. Another map of the distribution of PINs and ABCBs in plant tissues was provided by Bandyopadhyay et al. (2007). A recent study indicated ABCB19 stabilized PIN1's localization at the plasma membrane in discrete cellular subdomains where PIN1 and ABCB19 expression overlapped (Titapiwatanakun et al., 2009).

2.3. Other functions in roots and rhizomes

Plant roots have two primary functions, that is, the absorption of water and minerals and anchoring the plant body in the soil. Many transporters responsible for the absorption of nutrients have been studied, but there

has been no report on ABC proteins that function in the uptake of nutrients in roots, except for a candidate in tobacco, the iron-deficiency inducible transporter NtPDR3, identified in BY-2 cells (Ducos et al., 2005). The promoter region of NtPDR3 contained an iron-deficiency element-1 (IDE-1) box that is found in many iron-deficiency inducible gene promoters (Kobayashi et al., 2003). Although its expression was not analyzed in intact plants, this report suggested that NtPDR3 plays a role in the uptake of iron from the soil, or in the long-distance transport of iron in the plant body, such as the xylem loading of iron in root tissues.

While plant roots absorb water and minerals from the soil, they in turn secrete large amounts of root exudates, which consist of amino acids, organic acids, sugars, secondary metabolites, and proteins (Bais et al., 2006). These organic compounds provide not only a source of nutrients for encroaching microorganisms but also mediate interactions between plants and other organisms. One of the most well-characterized plant-microbe interactions in the rhizosphere is that between legume plants and rhizobium. Legume plants are known to secrete signal molecules such as flavonoids to attract rhizobium and induce the expression of its *nod* genes. In soybean, the isoflavonoid genistein has been identified as a signal molecule for *Bradyrhizobium japonicum* (Kosslak et al., 1987), and biochemical transport analyses using plasma membrane vesicles suggested the involvement of an ABC-type transporter in the secretion of genistein from soybean roots (Sugiyama et al., 2007). The involvement of ABC proteins in root exudates was demonstrated in comprehensive analyses with T-DNA knockout mutants of several ABC proteins (Badri et al., 2008). As a strategy, these authors chose ABC protein genes that were exclusively or highly expressed in the root endodermis and endodermis-cortex region, atrichoblast, and lateral root cap cells. Profiles of root exudates of several mutants differed from those of the wild type, suggesting that the secretion of organic compounds from roots is at least partially controlled by ABC proteins.

A perennial medicinal plant, *C. japonica*, contains a yellow isoquinoline alkaloid, berberine. Berberine, which is widely used as an antibacterial and antimalarial drug as well as bitter stomachic in many countries, is biosynthesized in root cells of *C. japonica* and translocated to the rhizome, where it accumulates in the vacuole (Iwasa et al., 1998; Yamamoto et al., 1993). An ABCB-type transporter, CjMDR1, is involved in the uptake of berberine into rhizome cells (Shitan et al., 2003), whereas proton antiporter mediates the transport of berberine into vacuoles (Otani et al., 2005). Such an alkaloid proton antiporter in the tonoplast has been recently reported in tobacco plants (Morita et al., 2009) (Fig. 6.6).

Soil is often contaminated with xenobiotic compounds and toxic metals such as Al, Pb, Cd, Hg, and As. Aluminum is the most abundant metal in the earth's crust. Although the majority of aluminum forms harmless aluminosilicates, solubilized aluminum in the form of Al^{3+} is highly toxic to plants

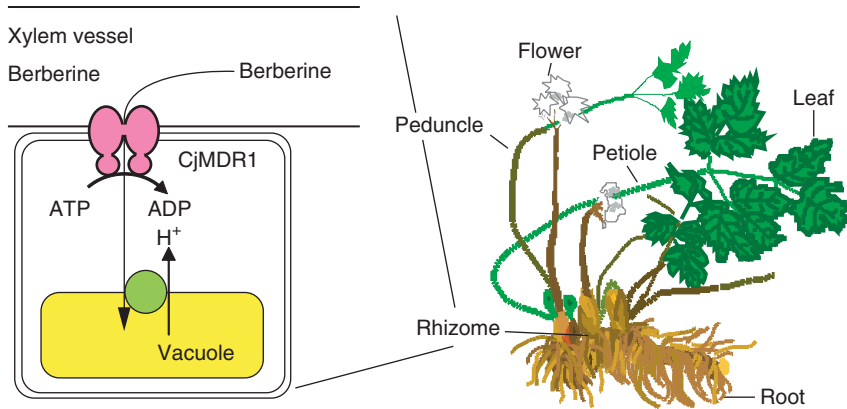


Figure 6.6 A model of the function of CjMDR1 in *C. japonica*. Berberine biosynthesized in roots is translocated to the rhizome. CjMDR1 imports berberine into rhizome cells at the plasma membrane and a proton antiporter mediates the uptake of berberine at the vacuolar membrane.

(Ma and Furukawa, 2003). An aluminum-inducible ABCB-type transporter (TaMDR1) was first identified from barley (Sasaki et al., 2002). Its expression was also inducible by calcium channel inhibitors and calcium deficiency, suggesting a disruption of calcium homeostasis, one of the initial events in aluminum toxicity, and this is the signal for the expression of *TaMDR1*. In Arabidopsis, a molecular genetic approach has been employed to identify genes that are involved in aluminum tolerance. Map-based cloning of loss-of-function mutants has identified two ABC protein genes, *ALS1* and *ALS3* (Larsen et al., 2005, 2007). *ALS1* belongs to the half-size ABCB subfamily, previously called Transporter associated with Antigen Processing (TAP), and localized to tonoplasts (see below), while *ALS3* (AtABC116), which has a transmembrane domain but lacks nucleotide-binding domains, localized to the plasma membrane as shown by immunofluorescence analysis. *ALS3* has high amino acid similarity (63%) with ybbM, a possible metal resistance ABC transporter-like protein of *Escherichia coli*. *ALS3* is primarily expressed in the root epidermis and cortex as well as in leaf hydathodes and the phloem, and has functions in aluminum tolerance probably by mediating the transport of aluminum or aluminum-chelating compounds.

Several full-size ABCG members have been reported to function in heavy metal tolerance. AtABCG40 (AtPDR12) was induced by lead treatment. Overexpression of AtAGCG40 in Arabidopsis conferred improved tolerance to lead but not to cadmium or other heavy metals, whereas the knockout mutants were more susceptible to lead (Lee et al., 2005). These authors suggested that AtABCG40 functions as an exporter of lead at the plasma membrane. They also reported that the expression of AtABCG36 (AtPDR8) was upregulated by treatment with cadmium or lead (Kim et al., 2007).

RNAi knockdown and T-DNA knockout of AtABCG36 resulted in increased sensitivity to cadmium and lead, whereas the overexpression of AtABCG36 improved tolerance. They also performed cadmium uptake assays using protoplasts of wild-type and transgenic plants, and showed that the cadmium content was increased in RNAi plants and decreased in overexpressors. AtABCG37 (AtPDR9) was reported to be involved in the export of organic xenobiotics (Ito and Gray, 2006). Ito and Gray showed that a gain-of-function mutant of AtABCG37 exhibited increased tolerance to 2,4-dichlorophenoxyacetic acid (2,4-D) and another auxin-related compound, whereas a loss-of-function mutant was more susceptible to these compounds. As a single amino acid change in AtABCG37 conferred resistance to 2,4-D, these authors suggested using this mutated protein as a plant-derived marker for selection by 2,4-D.

2.4. Functions in seeds and flowers

Proteomic and transcriptome studies have revealed that a variety of genes and proteins are involved in flower and seed development in plant species, while few ABCs have been identified as preferentially expressed in flowers or seeds (Becker et al., 2003; Honys and Twell, 2003). From cotton plants (*Gossypium hirsutum*), a half-size ABCG protein gene, *GhWBC1*, was cloned in an effort to obtain genes highly expressed in ovules. *GhWBC1* was in fact highly expressed in developing fiber cells of the wild type and weakly in a *li* (*ligon-lintless*) mutant. The substrates and physiological role of this half-size ABC protein are still unknown. Short siliques with decreased seed numbers were observed when *GhWBC1* cDNA driven by a 35S promoter was introduced into Arabidopsis (Zhu et al., 2003). Another half-size ABCG, *NtWBC1*, was cloned from tobacco (*N. tabacum*) as the first example of an ABC protein preferentially expressed in plant reproductive organs. *In situ* hybridization revealed the regulated expression of *NtWBC1* in the stigmatic secretory zone and anthers (Otsu et al., 2004).

AtABCA1 is the largest ABC protein in Arabidopsis that consisting of 1882 amino acid residues. Recently, the cDNA has been cloned and characterized as a gene expressed in vascular tissues and most strongly in pollen grains (C. Forestier and K. Yazaki, unpublished data). The function of ABCA1 is still under investigation.

3. ABC PROTEINS LOCALIZED TO OTHER ORGANELLES

3.1. Vacuoles

The plant vacuole is the most important organelle in terms of the detoxification of xenobiotics such as herbicides. Detoxification generally proceeds in three steps in animals, fungi, and plants (Ishikawa, 1992). The first step

(Phase I) is the modification of xenobiotics by enzymes such as cytochrome P450-dependent monooxygenases. The second step (Phase II) is conjugation with a hydrophilic molecule like glutathione, glucose, or glucuronate via respective transferases to form hydrophilic conjugates. As the third step (Phase III), the modified and conjugated compounds are excreted from the cytosol. This excretion is mediated by specific transporters, previously known as GS-X pumps. In mammals, these GS-X pumps are plasma membrane-localized ABCC-type ABC proteins which excrete xenobiotics outside of the cell. Contrary to animals, plants can often deposit these compounds in vacuoles, and the involvement of ABC proteins in the vacuolar transport of xenobiotics was suggested (Martinoia et al., 1993). To date, several tonoplast-localized ABC proteins have been characterized in plants. It has been demonstrated in a heterologous expression system that Arabidopsis AtABCC1–5 are able to transport glutathione conjugates (Klein et al., 2006). Whereas AtABCC4 and 5 are localized to the plasma membrane and implicated in stomatal movement (Gaedeke et al., 2001; Klein et al., 2003, 2004), AtABCC1 and 2 are localized to the tonoplast (Geisler et al., 2004; Liu et al., 2001) and suggested to be responsible for the deposition of xenobiotics in the vacuoles. AtABCC2 seemed to show a broader substrate specificity than AtABCC1, and was able to transport *B. napus* chlorophyll catabolite 1 (Bn-NCC-1), an endogenous toxic compound produced during senescence (Lu et al., 1998). This observation suggested that AtABCC2 is relevant for leaf senescence *in vivo*. Indeed, reduced senescence was demonstrated in T-DNA knockout lines of *Atabcc2* (Frelet-Barrand et al., 2008). Interestingly, TWD1 occurs not only in the plasma membrane where it regulates AtABCB1 and AtABCB19 activity (see Section 2.2.3), but also in tonoplasts where it regulates the transport activity of AtABCC1 and 2 (Geisler et al., 2004). Similarly, in monocots like wheat and maize, some ABCC-type ABC proteins are induced by treatments with herbicide safeners and prooxidants (Swarbreck et al., 2003; Theodoulou et al., 2003). The wheat ABCC protein is at least localized to the tonoplast. These ABCC proteins are expected to function in the vacuolar deposition of xenobiotics in a similar way to AtABCC1 and 2 in Arabidopsis (Fig. 6.7).

The detoxification process via vacuolar transport is useful not only for organic compounds but also for heavy metals. AtABCB27 (ALS1 or AtTAP2) is a half-size transporter that belongs to the ABCB subfamily. The *als1-1* mutant line was found by screening strong root growth inhibition by aluminum (Al). This gene is expressed in roots, leaves, stems, and flowers independent of Al treatment. The main expression site is the root tip and the vasculature throughout the plant. ALS1-GFP revealed the tonoplast localization of this ABC protein. Although the substrate of this protein is not yet determined, the deposition of some substrates, possibly chelated Al, is suggested (Larsen et al., 2007). An ABC protein related to iron depletion was identified in barley. The gene, designated *IDI7* (iron-deficiency induced

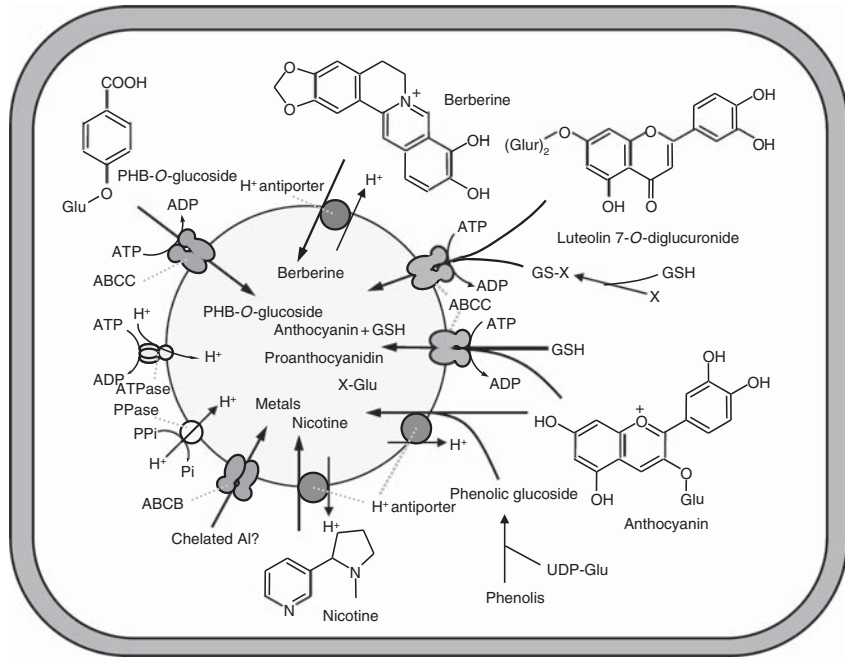


Figure 6.7 ABC proteins involved in vacuolar transport in plant cells. Glur, glucuronide; GS, glutathione; PHB, *p*-hydroxybenzoic acid; UDP-Glu, UDP-glucose; X, xenobiotics.

gene 7), was specifically induced in root tissue under iron (Fe) deficiency, but treatment with an excess of heavy metals such as copper, manganese, and zinc did not affect the gene expression. *IDI7* also belongs to the half-size ABCB subfamily, and the GFP-fused form showed a tonoplast localization (Yamaguchi et al., 2002), while the substrate and physiological function of *IDI7* are not known.

The vacuole also acts as the site of accumulation of various endogenous secondary metabolites such as alkaloids and phenol glycosides. An ABCC-type ABC protein was reported to be responsible for the transport of anthocyanins into the vacuoles of maize. A maize mutant named *bronze-2* (*bz2*), whose gene product was glutathione *S*-transferase (GST), was defective in the accumulation of anthocyanins in the vacuoles (Marrs et al., 1995). Since glutathione conjugates are in general preferred as substrates by ABCC-type transporters, the involvement of an ABCC member in the vacuolar transport of anthocyanin was presumed. Also in dicots, such as petunia (Alfenito et al., 1998), Arabidopsis (Kitamura et al., 2004), and carnation (Larsen et al., 2003), similar results were obtained, that is, GST was relevant to the accumulation of anthocyanins despite that the responsible ABCC gene was not identified in dicot plants. Strong evidence for the

involvement of an ABCC-type ABC protein in the vacuolar accumulation of anthocyanin was obtained in a reverse genetic study in maize (Goodman et al., 2004). ZmMRP3 is located in the tonoplast, and is required for the accumulation of anthocyanins process.

Proton gradient-dependent transport also contributes to the vacuolar accumulation of secondary metabolites including anthocyanins. The Arabidopsis TT12, a multidrug and toxic compound extrusion (MATE) transporter, was shown to transport cyanidin-3-O-glucoside (Marinova et al., 2007). Analysis of a *tt12* knockout line suggested that TT12 was also involved in the deposition of proanthocyanidin in vacuoles of seed endothelial cells (Debeaujon et al., 2001). Biochemical evidence of the involvement of proton antiporters in vacuolar sequestration was recently obtained also for alkaloids. Nt-JAT1, a MATE transporter, is responsible for the accumulation of nicotine in leaf vacuoles (Morita et al., 2009). Although the gene has not been identified yet, berberine alkaloid is also transported into the vacuole by a putative proton/berberine antiporter in *C. japonica* cells (Otani et al., 2005).

Some ABC protein might have commercial uses. Overexpression of AtABCG19 (AtWBC19) confers resistance to kanamycin in transgenic plants (Mentewab and Stewart, 2005). Since AtABCG19 was found to be present in the tonoplast using GFP-fused protein and some ABCG proteins are known to have broad substrate specificity in animals, it is speculated that these proteins efflux xenobiotics like kanamycin from the cytosol to the vacuole. For the preparation of plant transformants, selectable markers like antibiotic resistance from bacteria are general tools, but there is a risk of horizontal gene transfer from transgenic plants to bacteria or other organism surrounding the plants. The use of an endogenous ABC protein gene from plants might be utilized as an alternative marker in transformation. Another possibility for molecular breeding with ABC protein genes is proposed in cereal grains and oilseed. They contain phytic acid, which has, however, negative effects on animal nutrition and the environment. Interestingly, suppression of ABCC proteins in maize and soybean generated low-phytic-acid seeds, whereas the seed dry weight or germination rate was not affected (Shi et al., 2007). Although the transport function and localization of this ABCC protein are not clear, one possible explanation is that an ABCC protein plays a role in the accumulation of phytic acid in protein storage vacuoles, and this ABCC protein gene might be useful for the creation of agriculturally desirable crops.

3.2. Plastids

Plastids play a central role in photosynthesis in green plants. Plastidic ABC protein was first characterized from the study of light signaling via phytochromes. Møller et al. characterized the Arabidopsis mutant *laf* (long after far-red (FR) light) 6, and found that its hypocotyl elongation was less inhibited than wild type under FR light (Møller et al., 2001). The disrupted

gene encoded AtABC18 (AtNAP1, AtABC1, or LAF6), a soluble ABC protein without a transmembrane domain. This protein is encoded in the nucleus, contains a transit peptide in N-terminus and actually localized to the plastid. In the *laf6* mutant, the chlorophyll precursor protoporphyrin IX is increased accompanied by a decrease in chlorophyll content. It is thus presumed that AtABC18 is involved in the transport of protoporphyrin IX from the chloroplast envelope into the stroma, by forming an ABC protein complex with an unidentified TMD (Møller et al., 2001), which usually occurs in prokaryotes. Further characterization of AtABC18 was recently reported by the same group with two similar ABC proteins of soluble type AtABC16 (AtNAP6) and AtABC17 (AtNAP7). Iron–sulfur (Fe–S) cluster are important cofactors of Fe–S protein, and its biogenesis and maintenance occur in both plastids and mitochondria (for the biogenesis in mitochondria, see Section 3.3), and in bacteria. SUF (mobilization of sulfur) is one of the Fe–S biogenesis systems and encoded in the *suf* operon (*sufABCDSE*). AtABC18 is a SufB homologue and can complement SufB deficiency in *E. coli* during oxidative stress. Moreover, AtABC17, a SufC homologue, partially rescued the growth defect of an *E. coli* SufC mutant, and also interacted with AtABC18 and AtABC16, a SufD homologue. It was demonstrated that all these soluble ABC proteins were localized to the plastid. Because the other homologues such as SfuA, SufS, and SufE were predicted to be located in the plastid in Arabidopsis, the complete SUF system can be found in plastids, which may be involved in the plastidic Fe–S cluster’s maintenance and repair (Xu and Møller, 2004; Xu et al., 2005b).

Plastidic ABC proteins also play an important role in the biosynthesis of membrane lipids such as galactolipid in the thylakoid membrane. The *trigalactosyldiacylglycerol* (*tgd*) mutants *tgd1*, *tgd2*, and *tgd3* were isolated based on the high accumulation of oligogalactolipids (Awai et al., 2006; Lu et al., 2007; Xu et al., 2003, 2005a). Thus far three genes have been identified whose gene products are similar to the components of the bacteria-type ABC protein complex. AtABC14 (TGD1) encodes a membrane protein homologous to the bacterial-type ABC permease domain, AtABC15 (TGD2) codes for a phosphatidic acid-binding protein similar to the periplasmic binding protein of bacteria, and AtABC13 (TGD3, AtNAP11) is a soluble ABC domain. These three proteins are suggested to be located in the inner plastid envelope, and function as phosphatidic acid transporters. These proteins were revealed to be necessary for the import of phosphatidic acid from the ER to plastid, and plastidic galactoglycerol biosynthetic machinery.

3.3. Mitochondria

The first characterized plant mitochondrial ABC protein was AtABC25 (previously called AtATM3 or STA1). The gene was identified in the Arabidopsis mutant *starik* (Russian for “old man”), which showed dwarfism, chlorosis, thick leaves, and at the cellular level, larger nuclei than the

wild type (Kushnir et al., 2001). AtABCB25 is an ABCB-type half-size ABC protein with sequence similarity to the mitochondrial ABC protein ATM1 of *S. cerevisiae* and human ABC7. The yeast ATM1 is localized to the mitochondrial inner membrane with its ABC domain facing the mitochondrial matrix. This protein is suggested to mediate the formation of Fe/S proteins by transporting Fe/S centers from the mitochondrial matrix to the cytosol. The yeast *atm1* mutant exhibited slow growth and extensive accumulation of Fe in the mitochondria. Similarly, the Arabidopsis *stark* showed greater accumulation of nonheme, nonprotein Fe in mitochondria than did the wild type. AtABCB25 was also localized to mitochondria, and able to complement the phenotype of the yeast *atm1* mutant, suggesting that AtABCB25 is a functional orthologue of yeast ATM1. In the Arabidopsis genome, three ATM1 homologues exist, that is, AtABCB23 (AtATM1, STA2), AtABCB24 (AtATM2), and AtABCB25. All these proteins are located in the mitochondria. AtABCB23 was able to weakly complement the phenotype of yeast *atm1*, and also the Arabidopsis *stark* phenotype when it was overexpressed, whereas AtABCB24 showed less complementation and was rather toxic to yeast cells. These findings suggest that at least two proteins, AtABCB23 and 25, are involved in the Fe/S cluster's biosynthesis in plants like yeasts (Chen et al., 2007) (Fig. 6.8).

Interestingly, AtABCB25 is also involved in heavy metal resistance. AtABCB25 expression is induced when plants are treated with cadmium [Cd(II)] or lead. Transgenic plants overexpressing AtABCB25 exhibited enhanced resistance to Cd, whereas knockout *atabcb25* plants showed increased sensitivity to Cd. These findings indicate that AtABCB25 has the ability to detoxify heavy metals (Kim et al., 2006). A similar detoxifying function of ABCB was observed in other organisms, that is, CrCDS1 was identified as a cadmium tolerance protein in *Chlamydomonas reinhardtii* (Hanikenne et al., 2005). Although it is still unclear whether or not these proteins directly transport Cd (-complex) or the Cd tolerance is an indirect effect, mitochondrial ABC proteins might generally play an important role in cellular heavy metal tolerance.

Mitochondrial ABC proteins are also involved in cytochrome *c* maturation (Ccm). In bacteria, for example, *E. coli* proteins in the Ccm complex are encoded by an operon starting with CcmA, which is the NBF domain of an ABC transporter complex. CcmB and CcmC are membrane proteins consisting of six transmembrane helices that function as the TMD of the ABC transporter assembly. These NBF and TMD proteins form a complex, which is indispensable for the maturation of cytochrome *c*. Plant genomes have several genes coding for proteins showing high similarity with these bacterial Ccm proteins. One representative is AtABC11 (AtCCMA), a soluble protein previously designated as NAP10 (nonintrinsic ABC protein 10). AtCCMA is localized to the matrix side of the mitochondrial inner membrane as a membrane-bound protein. This protein shows ATPase

activity and interacts with AtABCI2 (AtCcmB), a homologue of bacterial CcmB. Since other Ccm proteins (AtCCMC, AtCCME, and AtCCMH) are also found in the genome, a similar maturation system of cytochrome *c* is thought to exist in plant mitochondria where ABC proteins of separate type (AtCCMA and AtCCMB) are involved (Rayapuram et al., 2007) (Fig. 6.8).

3.4. Peroxisomes

The ABCD subfamily is suggested to be peroxisomal ABC proteins involved in peroxisomal function. In humans, four ABCD members, all half-size types having a forward orientation, are characterized; Adrenoleukodystrophy protein (ALDP, ABCD1), Adrenoleukodystrophy-related protein (ALDRP, ABCD2), peroxisomal membrane protein (PMP70, ABCD3), and PMP69 (ABCD4). These proteins homodimerize or heterodimerize, and function as transporters in the peroxisome to import fatty acids CoA, which are subjected to beta-oxidation in the peroxisome. Defects in these proteins in humans cause severe diseases such as X-linked Adrenoleukodystrophy (X-ALD). By contrast, Arabidopsis has only one half-size and one full-size ABCD protein. AtABCD1 is the full-size ABC protein and was first identified by three different groups almost simultaneously. Thus, this protein has three names, that is, COMATOSE (CTS), Peroxisome defective3 (PED3), and Peroxisomal ABC transporter1 (PXA1) (Footitt et al., 2002; Hayashi et al., 2002; Zolman et al., 2001). The *ped3/pxa1* mutants were identified in the screening of resistance for 2,4-dichlorophenoxybutyrate (2,4-DB) and indole butyric acid (IBA), which provide auxin when they are transported as their CoA esters into peroxisomes followed by the beta-oxidation of these compounds. This mutant also shows impaired fatty acid catabolism, and addition of sucrose to the growth medium is necessary for normal development. The *cts* mutant was isolated in a study of dormancy, that is, *cts* seeds are not able to germinate without sucrose supplementation (Footitt et al., 2006; Russell et al., 2000). CTS was later characterized in more detail and suggested to function in acetate metabolism (Hooks et al., 2007), jasmonate production (Theodoulou et al., 2005), full fertility in both pollen and female tissues (Footitt et al., 2007), and phase II of germination (Carrera et al., 2007). Taken together, it is proposed that this protein is responsible for the transport of acyl-CoA into the peroxisomal matrix. The function of AtABCD2, a half-size transporter, is still unclear. In an early computer analysis, this protein had been presumed to be located at the peroxisome due to a conserved sequence for peroxisomal proteins (Sanchez-Fernandez et al., 2001), but later it was found that the amino acid sequence of AtABCD2 contains a putative chloroplast transit peptide, suggesting that this protein is not localized to the peroxisome, but probably to plastids

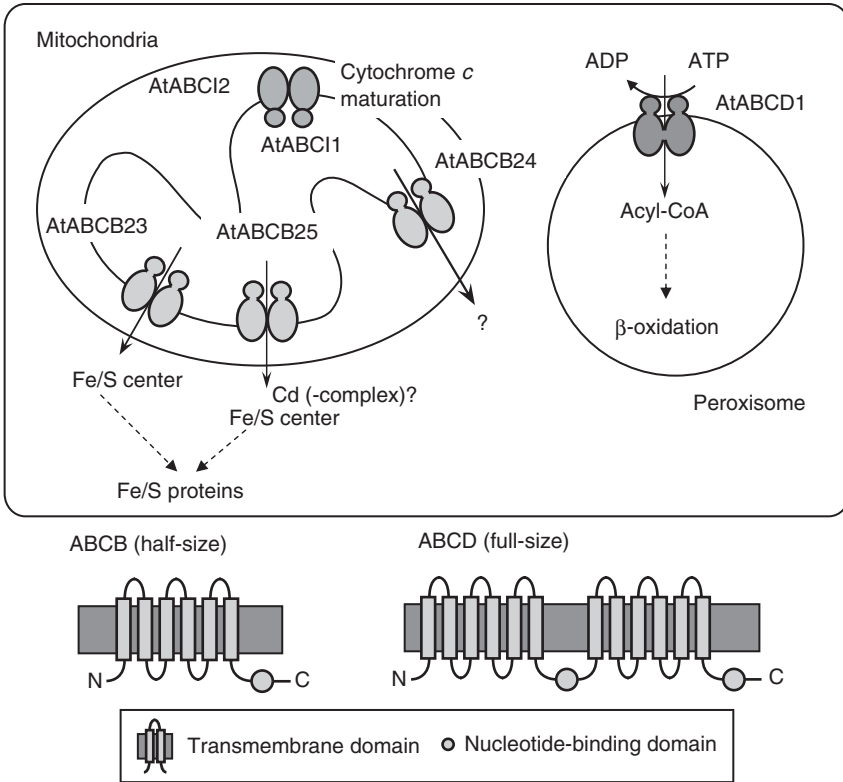


Figure 6.8 ABC proteins located in mitochondria and peroxisomes.

(Theodoulou et al., 2006). If this presumption is correct, only one ABC protein is responsible in Arabidopsis for the membrane transport of all acyl-CoA into the peroxisome (Fig. 6.8).

4. SOLUBLE-TYPE ABC PROTEINS IN PLANTS

Some soluble-type ABC proteins are described above, for example, AtABC16–8 (plastid), ABC113 (plastid), and AtABC11 (mitochondria), all of which belong to the ABC1 subfamily, and are known as nonintrinsic ABC proteins (NAP). These proteins have only one nucleotide-binding fold and are suggested to function as a catalytic (ATPase) subunit of the ABC transporter complex by assembling with identified or unidentified TMDs.

Other soluble ABC proteins reported so far include ABCE, which has two ABC domains in a polypeptide but no TMD in its protein sequence. ABCE belongs to the RNase L inhibitor (RLI) family, which is conserved among eukaryotes and archaea. The function of family members is presumed to be relevant for RNA silencing or RNA interference. Actually, *AtABCE2* (*AtRLI2*) is ubiquitously expressed in all plant organs and suppresses RNA silencing at the local and at the systemic level (Braz et al., 2004; Sarmiento et al., 2006), though its mechanism of action is still to be clarified.

Another soluble ABC protein having two NBFs is the ABCF family. In the *Arabidopsis* genome, five ABCF (*AtABCF1*–*5*) proteins are found. This family was previously called GCN (general control nonrepressible) after the name of yeast orthologues. These proteins are clearly distinguishable from the ABCE family due to low sequence similarity. Although their physiological functions are not yet characterized, the tissue-specific expression pattern was analyzed in *Arabidopsis* transformants with promoter–GUS fusion constructs by Dr. Tomohiko Kato of Oji Paper Company (personal communication). In brief, three members, *AtABCF1* (*GCN1*), *AtABCF4* (*GCN4*), and *AtABCF5* (*GCN5*), are highly expressed in leaves, and also in siliques and roots, whereas *AtABCF2* (*GCN2*) is specifically expressed in anthers and pollen. *AtABCF3* (*GCN3*) shows also strong expression in anthers and pollen, but its expression was observed at the root tip as well. Further functional characterization is expected in this subfamily.



5. CONCLUSION

ABC proteins were originally known by intensive studies in the field of cancer research, because some members exhibit a very broad specificity toward wide range of anticancer drugs, which causes multidrug resistance in animal cancer cells. In recent years, however, it has turned out that some members are involved in various important biological events by transporting endogenous metabolites or protecting the organism from chemical stresses. Especially in plants, many findings show that ABC proteins play crucial and characteristic roles in different tissues and cell types, where in some cases physiological substrates are also identified. As primary transporters that can recognize organic compounds, ABC proteins will draw the further interest of plant biologists. Moreover, novel functions as channel regulators or molecular switches are also attractive aspects of ABC proteins. It is expected that interdisciplinary combinations of research specialities among cell biology, biochemistry, and molecular genetics will contribute to the development of ABC protein-implicated plant biology.

REFERENCES

- Alfenito, M.R., Souer, E., Goodman, C.D., Buell, R., Mol, J., Koes, R., et al., 1998. Functional complementation of anthocyanin sequestration in the vacuole by widely divergent glutathione *S*-transferases. *Plant Cell* 10, 1135–1149.
- Awai, K., Xu, C., Tamot, B., Benning, C., 2006. A phosphatidic acid-binding protein of the chloroplast inner envelope membrane involved in lipid trafficking. *Proc. Natl. Acad. Sci. USA* 103, 10817–10822.
- Badri, D.V., Loyola-Vargas, V.M., Broeckling, C.D., De-la-Pena, C., Jasinski, M., Santelia, D., et al., 2008. Altered profile of secondary metabolites in the root exudates of *Arabidopsis* ATP-binding cassette transporter mutants. *Plant Physiol.* 146, 762–771.
- Bailly, A., Sovero, V., Vincenzetti, V., Santelia, D., Bartnik, D., Koenig, B.W., et al., 2008. Modulation of P-glycoproteins by auxin transport inhibitors is mediated by interaction with immunophilins. *J. Biol. Chem.* 283, 21817–21826.
- Bais, H.P., Weir, T.L., Perry, L.G., Gilroy, S., Vivanco, J.M., 2006. The role of root exudates in rhizosphere interactions with plants and other organisms. *Annu. Rev. Plant Biol.* 57, 233–266.
- Bandyopadhyay, A., Blakeslee, J.J., Lee, O.R., Mravec, J., Sauer, M., Titapiwatanakun, B., et al., 2007. Interactions of PIN and PGP auxin transport mechanisms. *Biochem. Soc. Trans.* 35, 137–141.
- Becker, J.D., Boavida, L.C., Carneiro, J., Haury, M., Feijo, J.A., 2003. Transcriptional profiling of *Arabidopsis* tissues reveals the unique characteristics of the pollen transcriptome. *Plant Physiol.* 133, 713–725.
- Bernasconi, P., Patel, B.C., Reagan, J.D., Subramanian, M.V., 1996. The *N*-1-naphthylphthalamic acid-binding protein is an integral membrane protein. *Plant Physiol.* 111, 427–432.
- Bird, D., Beisson, F., Brigham, A., Shin, J., Greer, S., Jetter, R., et al., 2007. Characterization of *Arabidopsis* ABCG11/WBC11, an ATP binding cassette (ABC) transporter that is required for cuticular lipid secretion. *Plant J.* 52, 485–498.
- Blakeslee, J.J., Bandyopadhyay, A., Lee, O.R., Mravec, J., Titapiwatanakun, B., Sauer, M., et al., 2007. Interactions among PIN-FORMED and P-glycoprotein auxin transporters in *Arabidopsis*. *Plant Cell* 19, 131–147.
- Bouchard, R., Bailly, A., Blakeslee, J.J., Vincenzetti, V., Paponov, I., Palme, K., et al., 2006. Immunophilin-like TWISTED DWARF1 modulates auxin efflux activities of *Arabidopsis* P-glycoproteins. *J. Biol. Chem.* 281, 30603–30612.
- Braz, A.S., Finnegan, J., Waterhouse, P., Margis, R., 2004. A plant orthologue of RNMase L inhibitor (RLI) is induced in plants showing RNA interference. *J. Mol. Evol.* 59, 20–30.
- Brown, D.E., Rashotte, A.M., Murphy, A.S., Normanly, J., Tague, B.W., Peer, W.A., et al., 2001. Flavonoids act as negative regulators of auxin transport *in vivo* in *Arabidopsis*. *Plant Physiol.* 126, 524–535.
- Campbell, E.J., Schenk, P.M., Kazan, K., Penninckx, I.A., Anderson, J.P., Maclean, D.J., et al., 2003. Pathogen-responsive expression of a putative ATP-binding cassette transporter gene conferring resistance to the diterpenoid sclareol is regulated by multiple defense signaling pathways in *Arabidopsis*. *Plant Physiol.* 133, 1272–1284.
- Carrera, E., Holman, T., Medhurst, A., Peer, W., Schmuths, H., Footitt, S., et al., 2007. Gene expression profiling reveals defined functions of the ATP-binding cassette transporter COMATOSE late in phase II of germination. *Plant Physiol.* 143, 1669–1679.
- Chen, R., Hilson, P., Sedbrook, J., Rosen, E., Caspar, T., Masson, P.H., 1998. The *Arabidopsis thaliana* AGRAVITROPIC 1 gene encodes a component of the polar-auxin-transport efflux carrier. *Proc. Natl. Acad. Sci. USA* 95, 15112–15117.
- Chen, S., Sanchez-Fernandez, R., Lyver, E.R., Dancis, A., Rea, P.A., 2007. Functional characterization of AtATM1, AtATM2, and AtATM3, a subfamily of *Arabidopsis*

- half-molecule ATP-binding cassette transporters implicated in iron homeostasis. *J. Biol. Chem.* 282, 21561–21571.
- Cho, M., Lee, S.H., Cho, H.T., 2007. P-glycoprotein4 displays auxin efflux transporter-like action in Arabidopsis root hair cells and tobacco cells. *Plant Cell* 19, 3930–3943.
- Debeaujon, I., Peeters, A.J., Leon-Kloosterziel, K.M., Koornneef, M., 2001. The *TRANS-PARENT TESTA12* gene of Arabidopsis encodes a multidrug secondary transporter-like protein required for flavonoid sequestration in vacuoles of the seed coat endothelium. *Plant Cell* 13, 853–871.
- Ducos, E., Fraysse, S., Boutry, M., 2005. NtPDR3, an iron-deficiency inducible ABC transporter in *Nicotiana tabacum*. *FEBS Lett.* 579, 6791–6795.
- Dudler, R., Hertig, C., 1992. Structure of an *mdr*-like gene from *Arabidopsis thaliana*. Evolutionary implications. *J. Biol. Chem.* 267, 5882–5888.
- Eichhorn, H., Klinghammer, M., Becht, P., Tenhaken, R., 2006. Isolation of a novel ABC-transporter gene from soybean induced by salicylic acid. *J. Exp. Bot.* 57, 2193–2201.
- Footitt, S., Slocombe, S.P., Larner, V., Kurup, S., Wu, Y., Larson, T., et al., 2002. Control of germination and lipid mobilization by COMATOSE, the Arabidopsis homologue of human ALDP. *EMBO J.* 21, 2912–2922.
- Footitt, S., Marquez, J., Schmutz, H., Baker, A., Theodoulou, F.L., Holdsworth, M., 2006. Analysis of the role of COMATOSE and peroxisomal beta-oxidation in the determination of germination potential in Arabidopsis. *J. Exp. Bot.* 57, 2805–2814.
- Footitt, S., Dietrich, D., Fait, A., Fernie, A.R., Holdsworth, M.J., Baker, A., et al., 2007. The COMATOSE ATP-binding cassette transporter is required for full fertility in Arabidopsis. *Plant Physiol.* 144, 1467–1480.
- Frelet-Barrand, A., Kolukisaoglu, H.U., Plaza, S., Ruffer, M., Azevedo, L., Hortensteiner, S., et al., 2008. Comparative mutant analysis of Arabidopsis ABC-type ABC transporters: AtMRP2 contributes to detoxification, vacuolar organic anion transport and chlorophyll degradation. *Plant Cell Physiol.* 49, 557–569.
- Gaedeke, N., Klein, M., Kolukisaoglu, U., Forestier, C., Muller, A., Ansoerge, M., et al., 2001. The *Arabidopsis thaliana* ABC transporter AtMRP5 controls root development and stomata movement. *EMBO J.* 20, 1875–1887.
- Geisler, M., Murphy, A.S., 2006. The ABC of auxin transport: the role of P-glycoproteins in plant development. *FEBS Lett.* 580, 1094–1102.
- Geisler, M., Kolukisaoglu, H.U., Bouchard, R., Billion, K., Berger, J., Saal, B., et al., 2003. TWISTED DWARF1, a unique plasma membrane-anchored immunophilin-like protein, interacts with Arabidopsis multidrug resistance-like transporters AtPGP1 and AtPGP19. *Mol. Biol. Cell* 14, 4238–4249.
- Geisler, M., Girin, M., Brandt, S., Vincenzetti, V., Plaza, S., Paris, N., et al., 2004. Arabidopsis immunophilin-like TWD1 functionally interacts with vacuolar ABC transporters. *Mol. Biol. Cell* 15, 3393–3405.
- Geisler, M., Blakeslee, J.J., Bouchard, R., Lee, O.R., Vincenzetti, V., Bandyopadhyay, A., et al., 2005. Cellular efflux of auxin catalyzed by the Arabidopsis MDR/PGP transporter AtPGP1. *Plant J.* 44, 179–194.
- Goodman, C.D., Casati, P., Walbot, V., 2004. A multidrug resistance-associated protein involved in anthocyanin transport in *Zea mays*. *Plant Cell* 16, 1812–1826.
- Hanikenne, M., Motte, P., Wu, M.C.S., Wang, T., Loppes, R., Matagne, R.F., 2005. A mitochondrial half-size ABC transporter is involved in cadmium tolerance in *Chlamydomonas reinhardtii*. *Plant Cell Environ.* 28, 863–873.
- Hayashi, M., Nito, K., Takei-Hoshi, R., Yagi, M., Kondo, M., Suenaga, A., et al., 2002. Ped3p is a peroxisomal ATP-binding cassette transporter that might supply substrates for fatty acid beta-oxidation. *Plant Cell Physiol.* 43, 1–11.
- Hedrich, R., Neimanis, S., Savchenko, G., Felle, H.H., Kaiser, W.M., Heber, U., 2001. Changes in apoplastic pH and membrane potential in leaves in relation to stomatal

- responses to CO₂, malate, abscisic acid or interruption of water supply. *Planta* 213, 594–601.
- Hetherington, A.M., Woodward, F.I., 2003. The role of stomata in sensing and driving environmental change. *Nature* 424, 901–908.
- Higgins, C.F., Linton, K.J., 2004. The ATP switch model for ABC transporters. *Nat. Struct. Mol. Biol.* 11, 918–926.
- Honys, D., Twell, D., 2003. Comparative analysis of the Arabidopsis pollen transcriptome. *Plant Physiol.* 132, 640–652.
- Hooks, M.A., Turner, J.E., Murphy, E.C., Johnston, K.A., Burr, S., Jaroslowski, S., 2007. The Arabidopsis ALDP protein homologue COMATOSE is instrumental in peroxisomal acetate metabolism. *Biochem. J.* 406, 399–406.
- Ishikawa, T., 1992. The ATP-dependent glutathione S-conjugate export pump. *Trends Biochem. Sci.* 17, 463–468.
- Ito, H., Gray, W.M., 2006. A gain-of-function mutation in the Arabidopsis pleiotropic drug resistance transporter PDR9 confers resistance to auxinic herbicides. *Plant Physiol.* 142, 63–74.
- Iwasa, K., Nanba, H., Lee, D.U., Kang, S.I., 1998. Structure–activity relationships of protoberberines having antimicrobial activity. *Planta Med.* 64, 748–751.
- Jacobs, M., Rubery, P.H., 1988. Naturally occurring auxin transport regulators. *Science* 241, 346–349.
- Jasinski, M., Stukkens, Y., Degand, H., Purnelle, B., Marchand-Brynaert, J., Boutry, M., 2001. A plant plasma membrane ATP binding cassette-type transporter is involved in antifungal terpenoid secretion. *Plant Cell* 13, 1095–1107.
- Kim, D.Y., Bovet, L., Kushnir, S., Noh, E.W., Martinoia, E., Lee, Y., 2006. AtATM3 is involved in heavy metal resistance in Arabidopsis. *Plant Physiol.* 140, 922–932.
- Kim, D.Y., Bovet, L., Maeshima, M., Martinoia, E., Lee, Y., 2007. The ABC transporter AtPDR8 is a cadmium extrusion pump conferring heavy metal resistance. *Plant J.* 50, 207–218.
- Kitamura, S., Shikazono, N., Tanaka, A., 2004. TRANSPARENT TESTA 19 is involved in the accumulation of both anthocyanins and proanthocyanidins in Arabidopsis. *Plant J.* 37, 104–114.
- Klein, M., Perfus-Barbeoch, L., Frelet, A., Gaedeke, N., Reinhardt, D., Mueller-Roeber, B., et al., 2003. The plant multidrug resistance ABC transporter AtMRP5 is involved in guard cell hormonal signalling and water use. *Plant J.* 33, 119–129.
- Klein, M., Geisler, M., Suh, S.J., Kolukisaoglu, H.U., Azevedo, L., Plaza, S., et al., 2004. Disruption of AtMRP4, a guard cell plasma membrane ABCC-type ABC transporter, leads to deregulation of stomatal opening and increased drought susceptibility. *Plant J.* 39, 219–236.
- Klein, M., Burla, B., Martinoia, E., 2006. The multidrug resistance-associated protein (MRP/ABCC) subfamily of ATP-binding cassette transporters in plants. *FEBS Lett.* 580, 1112–1122.
- Kobae, Y., Sekino, T., Yoshioka, H., Nakagawa, T., Martinoia, E., Maeshima, M., 2006. Loss of AtPDR8, a plasma membrane ABC transporter of *Arabidopsis thaliana*, causes hypersensitive cell death upon pathogen infection. *Plant Cell Physiol.* 47, 309–318.
- Kobayashi, T., Nakayama, Y., Itai, R.N., Nakanishi, H., Yoshihara, T., Mori, S., et al., 2003. Identification of novel *ds*-acting elements, IDE1 and IDE2, of the barley IDS2 gene promoter conferring iron-deficiency-inducible, root-specific expression in heterogeneous tobacco plants. *Plant J.* 36, 780–793.
- Kosslak, R.M., Bookland, R., Barkei, J., Paaren, H.E., Appelbaum, E.R., 1987. Induction of *Bradyrhizobium japonicum* common nod genes by isoflavones isolated from *Glycine max*. *Proc. Natl. Acad. Sci. USA* 84, 7428–7432.

- Kramer, E.M., Bennett, M.J., 2006. Auxin transport: a field in flux. *Trends Plant Sci.* 11, 382–386.
- Kushnir, S., Babiychuk, E., Storozhenko, S., Davey, M.W., Papenbrock, J., De Rycke, R., et al., 2001. A mutation of the mitochondrial ABC transporter *Sta1* leads to dwarfism and chlorosis in the *Arabidopsis* mutant *starik*. *Plant Cell* 13, 89–100.
- Larsen, E.S., Alfenito, M.R., Briggs, W.R., Walbot, V., 2003. A carnation anthocyanin mutant is complemented by the glutathione *S*-transferases encoded by maize *Bz2* and petunia *An9*. *Plant Cell Rep.* 21, 900–904.
- Larsen, P.B., Geisler, M.J., Jones, C.A., Williams, K.M., Cancel, J.D., 2005. *ALS3* encodes a phloem-localized ABC transporter-like protein that is required for aluminum tolerance in *Arabidopsis*. *Plant J.* 41, 353–363.
- Larsen, P.B., Cancel, J., Rounds, M., Ochoa, V., 2007. *Arabidopsis ALS1* encodes a root tip and stele localized half type ABC transporter required for root growth in an aluminum toxic environment. *Planta* 225, 1447–1458.
- Lee, S.H., Cho, H.T., 2006. *PINOID* positively regulates auxin efflux in *Arabidopsis* root hair cells and tobacco cells. *Plant Cell* 18, 1604–1616.
- Lee, E.K., Kwon, M., Ko, J.H., Yi, H., Hwang, M.G., Chang, S., et al., 2004. Binding of sulfonylurea by *AtMRP5*, an *Arabidopsis* multidrug resistance-related protein that functions in salt tolerance. *Plant Physiol.* 134, 528–538.
- Lee, M., Lee, K., Lee, J., Noh, E.W., Lee, Y., 2005. *AtPDR12* contributes to lead resistance in *Arabidopsis*. *Plant Physiol.* 138, 827–836.
- Lee, M., Choi, Y., Burla, B., Kim, Y.Y., Jeon, B., Maeshima, M., et al., 2008. The ABC transporter *AtABCB14* is a malate importer and modulates stomatal response to CO₂. *Nat. Cell Biol.* 10, 1217–1223.
- Leonhardt, N., Marin, E., Vavasseur, A., Forestier, C., 1997. Evidence for the existence of a sulfonylurea-receptor-like protein in plants: modulation of stomatal movements and guard cell potassium channels by sulfonylureas and potassium channel openers. *Proc. Natl. Acad. Sci. USA* 94, 14156–14161.
- Lewis, D.R., Miller, N.D., Splitt, B.L., Wu, G., Spalding, E.P., 2007. Separating the roles of acropetal and basipetal auxin transport on gravitropism with mutations in two *Arabidopsis* multidrug resistance-like ABC transporter genes. *Plant Cell* 19, 1838–1850.
- Lin, R., Wang, H., 2005. Two homologous ATP-binding cassette transporter proteins, *AtMDR1* and *AtPGP1*, regulate *Arabidopsis* photomorphogenesis and root development by mediating polar auxin transport. *Plant Physiol.* 138, 949–964.
- Liu, G., Sanchez-Fernandez, R., Li, Z.S., Rea, P.A., 2001. Enhanced multispecificity of *Arabidopsis* vacuolar multidrug resistance-associated protein-type ATP-binding cassette transporter, *AtMRP2*. *J. Biol. Chem.* 276, 8648–8656.
- Lu, Y.P., Li, Z.S., Drozdowicz, Y.M., Hortensteiner, S., Martinoia, E., Rea, P.A., 1998. *AtMRP2*, an *Arabidopsis* ATP binding cassette transporter able to transport glutathione *S*-conjugates and chlorophyll catabolites: functional comparisons with *AtMRP1*. *Plant Cell* 10, 267–282.
- Lu, B., Xu, C., Awai, K., Jones, A.D., Benning, C., 2007. A small ATPase protein of *Arabidopsis*, *TGD3*, involved in chloroplast lipid import. *J. Biol. Chem.* 282, 35945–35953.
- Luo, B., Xue, X.Y., Hu, W.L., Wang, L.J., Chen, X.Y., 2007. An ABC transporter gene of *Arabidopsis thaliana*, *AtWBC11*, is involved in cuticle development and prevention of organ fusion. *Plant Cell Physiol.* 48, 1790–1802.
- Luschign, C., Gaxiola, R.A., Grisafi, P., Fink, G.R., 1998. *EIR1*, a root-specific protein involved in auxin transport, is required for gravitropism in *Arabidopsis thaliana*. *Genes Dev.* 12, 2175–2187.
- Ma, J.F., Furukawa, J., 2003. Recent progress in the research of external Al detoxification in higher plants: a mini review. *J. Inorg. Biochem.* 97, 46–51.

- Marinova, K., Pourcel, L., Weder, B., Schwarz, M., Barron, D., Routaboul, J.M., et al., 2007. The Arabidopsis MATE transporter TT12 acts as a vacuolar flavonoid/H⁺-antiporter active in proanthocyanidin-accumulating cells of the seed coat. *Plant Cell* 19, 2023–2038.
- Martinoia, E., Grill, E., Tommasini, R., Kreuz, K., Amrhein, N., 1993. ATP-dependent glutathione S-conjugate 'export' pump in the vacuolar membrane of plants. *Nature* 364, 247–249.
- Mars, K.A., Alfenito, M.R., Lloyd, A.M., Walbot, V., 1995. A glutathione S-transferase involved in vacuolar transfer encoded by the maize gene Bronze-2. *Nature* 375, 397–400.
- Mentewab, A., Stewart, C.N. Jr., 2005. Overexpression of an *Arabidopsis thaliana* ABC transporter confers kanamycin resistance to transgenic plants. *Nat. Biotechnol.* 23, 1177–1180.
- Møller, S.G., Kunkel, T., Chua, N.H., 2001. A plastidic ABC protein involved in inter-compartmental communication of light signaling. *Genes Dev.* 15, 90–103.
- Moons, A., 2003. Ospdr9, which encodes a PDR-type ABC transporter, is induced by heavy metals, hypoxic stress and redox perturbations in rice roots. *FEBS Lett.* 553, 370–376.
- Morita, M., Shitan, N., Sawada, K., Van Montagu, M.C., Inze, D., Rischer, H., et al., 2009. Vacuolar transport of nicotine is mediated by a multidrug and toxic compound extrusion (MATE) transporter in *Nicotiana tabacum*. *Proc. Natl. Acad. Sci. USA* 106, 2447–2452.
- Muller, A., Guan, C., Galweiler, L., Tanzler, P., Huijser, P., Marchant, A., et al., 1998. AtPIN2 defines a locus of Arabidopsis for root gravitropism control. *EMBO J.* 17, 6903–6911.
- Multani, D.S., Briggs, S.P., Chamberlin, M.A., Blakeslee, J.J., Murphy, A.S., Johal, G.S., 2003. Loss of an MDR transporter in compact stalks of maize br2 and sorghum dw3 mutants. *Science* 302, 81–84.
- Murphy, A., Peer, W.A., Taiz, L., 2000. Regulation of auxin transport by aminopeptidases and endogenous flavonoids. *Planta* 211, 315–324.
- Nagashima, A., Suzuki, G., Uehara, Y., Saji, K., Furukawa, T., Koshihara, T., et al., 2008. Phytochromes and cryptochromes regulate the differential growth of Arabidopsis hypocotyls in both a PGP19-dependent and a PGP19-independent manner. *Plant J.* 53, 516–529.
- Noh, B., Murphy, A.S., Spalding, E.P., 2001. Multidrug resistance-like genes of Arabidopsis required for auxin transport and auxin-mediated development. *Plant Cell* 13, 2441–2454.
- Noh, B., Bandyopadhyay, A., Peer, W.A., Spalding, E.P., Murphy, A.S., 2003. Enhanced gravi- and phototropism in plant mdr mutants mislocalizing the auxin efflux protein PIN1. *Nature* 423, 999–1002.
- Otani, M., Shitan, N., Sakai, K., Martinoia, E., Sato, F., Yazaki, K., 2005. Characterization of vacuolar transport of the endogenous alkaloid berberine in *Coptis japonica*. *Plant Physiol.* 138, 1939–1946.
- Otsu, C.T., daSilva, I., de Molfetta, J.B., da Silva, L.R., de Almeida-Engler, J., Engler, G., et al., 2004. NtWBC1, an ABC transporter gene specifically expressed in tobacco reproductive organs. *J. Exp. Bot.* 55, 1643–1654.
- Panikashvili, D., Savaldi-Goldstein, S., Mandel, T., Yifhar, T., Franke, R.B., Hofer, R., et al., 2007. The Arabidopsis DESPERADO/AtWBC11 transporter is required for cutin and wax secretion. *Plant Physiol.* 145, 1345–1360.
- Peer, W.A., Murphy, A.S., 2007. Flavonoids and auxin transport: modulators or regulators? *Trends Plant Sci.* 12, 556–563.
- Peer, W.A., Bandyopadhyay, A., Blakeslee, J.J., Makam, S.N., Chen, R.J., Masson, P.H., et al., 2004. Variation in expression and protein localization of the PIN family of auxin

- efflux facilitator proteins in flavonoid mutants with altered auxin transport in *Arabidopsis thaliana*. *Plant Cell* 16, 1898–1911.
- Petrasek, J., Mravec, J., Bouchard, R., Blakeslee, J.J., Abas, M., Seifertova, D., et al., 2006. PIN proteins perform a rate-limiting function in cellular auxin efflux. *Science* 312, 914–918.
- Pighin, J.A., Zheng, H., Balakshin, L.J., Goodman, I.P., Western, T.L., Jetter, R., et al., 2004. Plant cuticular lipid export requires an ABC transporter. *Science* 306, 702–704.
- Raven, J.A., 1975. Transport of indoleacetic-acid in plant-cells in relation to pH and electrical potential gradients, and its significance for polar IAA transport. *New Phytol.* 74, 163–172.
- Rayapuram, N., Hagenmuller, J., Grienenberger, J.M., Giege, P., Bonnard, G., 2007. AtCCMA interacts with AtCCMB to form a novel mitochondrial ABC transporter involved in cytochrome *c* maturation in *Arabidopsis*. *J. Biol. Chem.* 282, 21015–21023.
- Rojas-Pierce, M., Titapiwatanakun, B., Sohn, E.J., Fang, F., Larive, C.K., Blakeslee, J., et al., 2007. *Arabidopsis* P-glycoprotein19 participates in the inhibition of gravitropism by gravacin. *Chem. Biol.* 14, 1366–1376.
- Rubery, P.H., Sheldrak, R., 1974. Carrier-mediated auxin transport. *Planta* 118, 101–121.
- Russell, L., Larner, V., Kurup, S., Bougourd, S., Holdsworth, M., 2000. The *Arabidopsis* COMATOSE locus regulates germination potential. *Development* 127, 3759–3767.
- Sanchez-Fernandez, R., Davies, T.G., Coleman, J.O., Rea, P.A., 2001. The *Arabidopsis thaliana* ABC protein superfamily, a complete inventory. *J. Biol. Chem.* 276, 30231–30244.
- Santelia, D., Vincenzetti, V., Azzarello, E., Bovet, L., Fukao, Y., Duchtig, P., et al., 2005. MDR-like ABC transporter AtPGP4 is involved in auxin-mediated lateral root and root hair development. *FEBS Lett.* 579, 5399–5406.
- Sarmiento, C., Nigul, L., Kazantseva, J., Buschmann, M., Truve, E., 2006. AtRLI2 is an endogenous suppressor of RNA silencing. *Plant Mol. Biol.* 61, 153–163.
- Sasabe, M., Toyoda, K., Shiraishi, T., Inagaki, Y., Ichinose, Y., 2002. cDNA cloning and characterization of tobacco ABC transporter: NtPDR1 is a novel elicitor-responsive gene. *FEBS Lett.* 518, 164–168.
- Sasaki, T., Ezaki, B., Matsumoto, H., 2002. A gene encoding multidrug resistance (MDR)-like protein is induced by aluminum and inhibitors of calcium flux in wheat. *Plant Cell Physiol.* 43, 177–185.
- Shi, J., Wang, H., Schellin, K., Li, B., Faller, M., Stoop, J.M., et al., 2007. Embryo-specific silencing of a transporter reduces phytic acid content of maize and soybean seeds. *Nat. Biotechnol.* 25, 930–937.
- Shitan, N., Bazin, I., Dan, K., Obata, K., Kigawa, K., Ueda, K., et al., 2003. Involvement of CjMDR1, a plant multidrug-resistance-type ATP-binding cassette protein, in alkaloid transport in *Coptis japonica*. *Proc. Natl. Acad. Sci. USA* 100, 751–756.
- Sidler, M., Hassa, P., Hasan, S., Ringli, C., Dudler, R., 1998. Involvement of an ABC transporter in a developmental pathway regulating hypocotyl cell elongation in the light. *Plant Cell* 10, 1623–1636.
- Smart, C.C., Fleming, A.J., 1996. Hormonal and environmental regulation of a plant PDR5-like ABC transporter. *J. Biol. Chem.* 271, 19351–19357.
- Stein, M., Dittgen, J., Sanchez-Rodriguez, C., Hou, B.H., Molina, A., Schulze-Lefert, P., et al., 2006. *Arabidopsis* PEN3/PDR8, an ATP binding cassette transporter, contributes to nonhost resistance to inappropriate pathogens that enter by direct penetration. *Plant Cell* 18, 731–746.
- Stukkens, Y., Bultreys, A., Grec, S., Trombik, T., Vanham, D., Boutry, M., 2005. NpPDR1, a pleiotropic drug resistance-type ATP-binding cassette transporter from *Nicotiana plumbaginifolia*, plays a major role in plant pathogen defense. *Plant Physiol.* 139, 341–352.

- Sugiyama, A., Shitan, N., Sato, S., Nakamura, Y., Tabata, S., Yazaki, K., 2006. Genome-wide analysis of ATP-binding cassette (ABC) proteins in a model legume plant, *Lotus japonicus*: comparison with Arabidopsis ABC protein family. *DNA Res.* 13, 205–228.
- Sugiyama, A., Shitan, N., Yazaki, K., 2007. Involvement of a soybean ATP-binding cassette-type transporter in the secretion of genistein, a signal flavonoid in legume-Rhizobium symbiosis. *Plant Physiol.* 144, 2000–2008.
- Suh, S.J., Wang, Y.F., Frelet, A., Leonhardt, N., Klein, M., Forestier, C., et al., 2007. The ATP binding cassette transporter AtMRP5 modulates anion and calcium channel activities in Arabidopsis guard cells. *J. Biol. Chem.* 282, 1916–1924.
- Surpin, M., Rojas-Pierce, M., Carter, C., Hicks, G.R., Vasquez, J., Raikhel, N.V., 2005. The power of chemical genomics to study the link between endomembrane system components and the gravitropic response. *Proc. Natl. Acad. Sci. USA* 102, 4902–4907.
- Swarbreck, D., Ripoll, P.J., Brown, D.A., Edwards, K.J., Theodoulou, F., 2003. Isolation and characterisation of two multidrug resistance associated protein genes from maize. *Gene* 315, 153–164.
- Taylor, L.P., Grotewold, E., 2005. Flavonoids as developmental regulators. *Curr. Opin. Plant Biol.* 8, 317–323.
- Teale, W.D., Paponov, I.A., Palme, K., 2006. Auxin in action: signalling, transport and the control of plant growth and development. *Nat. Rev. Mol. Cell Biol.* 7, 847–859.
- Terasaka, K., Blakeslee, J.J., Titapiwatanakun, B., Peer, W.A., Bandyopadhyay, A., Makam, S.N., et al., 2005. PGP4, an ATP binding cassette P-glycoprotein, catalyzes auxin transport in *Arabidopsis thaliana* roots. *Plant Cell* 17, 2922–2939.
- Theodoulou, F.L., Clark, I.M., He, X.L., Pallett, K.E., Cole, D.J., Hallahan, D.L., 2003. Co-induction of glutathione-S-transferases and multidrug resistance associated protein by xenobiotics in wheat. *Pest Manag. Sci.* 59, 202–214.
- Theodoulou, F.L., Job, K., Slocombe, S.P., Footitt, S., Holdsworth, M., Baker, A., et al., 2005. Jasmonic acid levels are reduced in COMATOSE ATP-binding cassette transporter mutants. Implications for transport of jasmonate precursors into peroxisomes. *Plant Physiol.* 137, 835–840.
- Theodoulou, F.L., Holdsworth, M., Baker, A., 2006. Peroxisomal ABC transporters. *FEBS Lett.* 580, 1139–1155.
- Titapiwatanakun, B., Blakeslee, J.J., Bandyopadhyay, A., Yang, H., Mravec, J., Sauer, M., et al., 2009. ABCB19/PGP19 stabilises PIN1 in membrane microdomains in Arabidopsis. *Plant J.* 57, 27–44.
- Ukitsu, H., Kuromori, T., Toyooka, K., Goto, Y., Matsuoka, K., Sakuradani, E., et al., 2007. Cytological and biochemical analysis of COF1, an Arabidopsis mutant of an ABC transporter gene. *Plant Cell Physiol.* 48, 1524–1533.
- van den Brule, S., Smart, C.C., 2002. The plant PDR family of ABC transporters. *Planta* 216, 95–106.
- van den Brule, S., Muller, A., Fleming, A.J., Smart, C.C., 2002. The ABC transporter SpTUR2 confers resistance to the antifungal diterpene sclareol. *Plant J.* 30, 649–662.
- Verrier, P.J., Bird, D., Burla, B., Dassa, E., Forestier, C., Geisler, M., et al., 2008. Plant ABC proteins—a unified nomenclature and updated inventory. *Trends Plant Sci.* 13, 151–159.
- Vieten, A., Sauer, M., Brewer, P.B., Friml, J., 2007. Molecular and cellular aspects of auxin-transport-mediated development. *Trends Plant Sci.* 12, 160–168.
- Wu, G., Lewis, D.R., Spalding, E.P., 2007. Mutations in Arabidopsis multidrug resistance-like ABC transporters separate the roles of acropetal and basipetal auxin transport in lateral root development. *Plant Cell* 19, 1826–1837.
- Xu, X.M., Moller, S.G., 2004. AtNAP7 is a plastidic SufC-like ATP-binding cassette/ATPase essential for Arabidopsis embryogenesis. *Proc. Natl. Acad. Sci. USA* 101, 9143–9148.
- Xu, C., Fan, J., Riekhof, W., Froehlich, J.E., Benning, C., 2003. A permease-like protein involved in ER to thylakoid lipid transfer in Arabidopsis. *EMBO J.* 22, 2370–2379.

- Xu, C., Fan, J., Froehlich, J.E., Awai, K., Benning, C., 2005a. Mutation of the TGD1 chloroplast envelope protein affects phosphatidate metabolism in *Arabidopsis*. *Plant Cell* 17, 3094–3110.
- Xu, X.M., Adams, S., Chua, N.H., Moller, S.G., 2005b. AtNAP1 represents an atypical SufB protein in *Arabidopsis* plastids. *J. Biol. Chem.* 280, 6648–6654.
- Yamaguchi, H., Nishizawa, N.K., Nakanishi, H., Mori, S., 2002. IDI7, a new iron-regulated ABC transporter from barley roots, localizes to the tonoplast. *J. Exp. Bot.* 53, 727–735.
- Yamamoto, K., Takase, H., Abe, K., Saito, Y., Suzuki, A., 1993. Pharmacological studies on antidiarrheal effects of a preparation containing berberine and geranii herba. *Nippon Yakurigaku Zasshi* 101, 169–175.
- Yang, Y., Hammes, U.Z., Taylor, C.G., Schachtman, D.P., Nielsen, E., 2006. High-affinity auxin transport by the AUX1 influx carrier protein. *Curr. Biol.* 16, 1123–1127.
- Zhu, Y.Q., Xu, K.X., Luo, B., Wang, J.W., Chen, X.Y., 2003. An ATP-binding cassette transporter GhWBC1 from elongating cotton fibers. *Plant Physiol.* 133, 580–588.
- Zolman, B.K., Silva, I.D., Bartel, B., 2001. The *Arabidopsis* pxa1 mutant is defective in an ATP-binding cassette transporter-like protein required for peroxisomal fatty acid beta-oxidation. *Plant Physiol.* 127, 1266–1278.

CELL AND MOLECULAR BIOLOGY OF THE FASTEST MYOSINS

Sugie Higashi-Fujime *and* Akio Nakamura

Contents

1. Introduction	302
2. <i>In Vitro</i> Motility	303
2.1. Dark-field microscopy	304
2.2. Direct observation of protein at a molecular level	304
3. Myosins in Plants	305
3.1. Extraction of myosin from plant cells	305
3.2. The fastest myosin from Characean cells	306
3.3. Biochemical properties of Chara myosin	306
3.4. Distinct properties of Chara myosin	307
4. Molecular Structure of Plant Myosins	311
4.1. Plant myosin belonging to class XI	312
4.2. Molecular structure of Chara myosin	312
4.3. Neck region of Chara myosin	314
4.4. Myosin tail	317
5. Three-Dimensional Structure of Chara Myosin	321
5.1. Interface between actin and myosin in the complex	322
5.2. Structural aspects of interaction between myosin and cleaved actin	325
5.3. Structural aspects of tropomyosin effect	327
6. Mechanism of Chara Myosin Motility	328
6.1. Processivity of Chara myosin	329
6.2. Step size	332
6.3. Mechanism of fast movement of Chara myosin	334
6.4. Functional states of Chara myosin in the cell	335
7. Concluding Remarks	336
Acknowledgments	338
References	338

Department of Molecular and Cellular Pharmacology, Faculty of Medicine, Gunma University Graduate School of Medicine, Maebashi, Gunma 371-8511, Japan

International Review of Cell and Molecular Biology, Volume 276
ISSN 1937-6448, DOI: 10.1016/S1937-6448(09)76007-1

© 2009 Elsevier Inc.
All rights reserved.

Abstract

Chara myosin is a class XI plant myosin in green algae *Chara corallina* and responsible for fast cytoplasmic streaming. The Chara myosin exhibits the fastest sliding movement of F-actin at 60 $\mu\text{m/s}$ as observed so far, 10-fold of the shortening speed of muscle. It has some distinct properties differing from those of muscle myosin.

Although knowledge about Chara myosin is very limited at present, we have tried to elucidate functional bases of its characteristics by comparing with those of other myosins. In particular, we have built the putative atomic model of Chara myosin by using the homology-based modeling system and databases. Based on the putative structure of Chara myosin obtained, we have analyzed the relationship between structure and function of Chara myosin to understand its distinct properties from various aspects by referring to the accumulated knowledge on mechanochemical and structural properties of other classes of myosin, particularly animal and fungal myosin V. We will also discuss the functional significance of Chara myosin in a living cell.

Key Words: Chara myosin, Class XI myosin, Cytoplasmic streaming, Processive myosin, Molecular modeling, Tropomyosin, Cleaved actin.

© 2009 Elsevier Inc.

1. INTRODUCTION

Several decades ago, only a few scientists had an idea that cytoplasmic streaming in plant cells would be caused by motile proteins of actin and myosin like animal muscle cells. In 1966, actin was purified for the first time from plant, plasmodium of *Physarum polycephalum* (Hatano and Oosawa, 1966), and myosin was also purified from *Physarum* plasmodium (Hatano and Tazawa, 1968; Kohama and Kendrick-Jones, 1986). This myosin was class II type and could polymerize into filaments. In *Physarum* plasmodium, the sol of the cytoplasm streams vigorously in the bidirectional way and this streaming is thought to be caused by the repeated contraction and relaxation of the gel of the cytoplasm in plasmodium (Kamiya, 1981). Therefore, cytoplasmic streaming itself in *Physarum* plasmodium is very fast, but passive flow.

In giant cells of Characeae, *Nitella* or *Chara*, the cytoplasm streams very fast rotationally along array of chloroplasts just beneath the cell wall. Kamiya and Kuroda (1956) found that the motive force for cytoplasmic streaming was produced at the interface between streaming endoplasm and stationary ectoplasm. At this interface, many subcortical fibrils connected chloroplasts and small vesicles moved along the fibrils. The fibrils squeezed out of the cell slid very fast on the glass surface in an artificial medium (Higashi-Fujime, 1980). Various pharmacological examinations gave us evidences supporting the idea that cortical fibrils consisted of actin filaments and myosin in the endoplasm

were implicated in generation of motive force for streaming (Kuroda, 1990; Tazawa and Shimmen, 1987). Electron microscopy revealed that the fibrils were actually composed of bundles of actin filaments, since fibrils formed arrowheads when decorated with muscle HMM (Higashi-Fujime, 1980; Palevitz et al., 1974). The arrowheads pointed to the direction opposite to the direction of cytoplasmic streaming, suggesting that myosin existed in the streaming cytoplasm and generated force for streaming in the same way as myosin in muscle (Kersey et al., 1976). In the electron micrograph of ultrathin sectioning, vesicles were attached to the cortical fibrils via crossbridges, which might probably be myosin associated with vesicles (Nagai and Hayama, 1979).

As described above, fast cytoplasmic streaming in *Physarum* is passive flow produced by contraction of plasmodia. On the other hand, in Characean cells, cytoplasmic streaming is thought to take place by interaction between actin cables of cortical fibrils and myosin in the streaming endoplasm. If this is the case, the speed of streaming must be equal to the sliding speed of the myosin molecule, and it is interesting to know the mechanism of this fast myosin and its structure. It was a long way to purify myosin from Characean cells, as homogenizing the cells did not work for purification owing to the endogenous strong proteases. Squeezing the cytoplasm out of the cell with fingers was the effective way to obtain an active myosin from Characean cells (Higashi-Fujime et al., 1995). As described in the next section, technical developments of direct observation of protein molecules and the *in vitro* motility assay were great help for purification and discovery of the motor proteins.

In a couple of decades, the techniques of observation of protein molecules and laser trap nanometry have greatly developed. Molecular biology techniques now become popular and especially X-ray crystallography of protein has provided us with a lot of knowledge on structures of actin and myosin. Now, we know that myosin comprises a superfamily consisting of 24 classes (Foth et al., 2006; Goodson and Dawson, 2006; Richards and Cavalier-Smith, 2005). Unfortunately, knowledge about fast myosin responsible for cytoplasmic streaming in Characean cells, that is Chara myosin, is quite limited. But in this chapter, in addition to the review of studies on Chara myosin, we will try to foresee its function and structure by referring the accumulated results of studies on other various myosins, particularly myosin V.

2. *IN VITRO* MOTILITY

The development of the *in vitro* motility assay (Higashi-Fujime, 1991; Kron and Spudich, 1986; Toyoshima et al., 1987) was indispensable for purification of myosin from Characean cells, because endogenous ATPase contaminated in the crude extract was too high to distinguish the myosin ATPase activity. By using this assay method, the motor activity can be followed

even in a crude extract and with a small amount of specimen (Higashi-Fujime et al., 1995). The motor activity of a certain protein, even if it is an unknown motor protein, can be assayed by introducing the actin filaments or microtubules in a solution containing ATP into the flow cell, on the surface of which certain motor protein tested is adsorbed. When a single F-actin filament or a single microtubule is observed under a microscope, we can see movement of the filaments and assay its motility. This *in vitro* motility assay is now a routine method. But its development was triggered by the observation of movement of actin cables isolated from *Nitella* on the glass surface (Higashi-Fujime, 1980).

2.1. Dark-field microscopy

Huxley and Niedergark (1954) obtained conclusive evidence that muscle contraction was the sliding between thick and thin filaments, by observing muscle contraction with an interference microscope improved by themselves. Based on this observation, the famous sliding theory was proposed for muscle contraction (Huxley, 1957). Summer and Gibbons (1971) demonstrated that surprisingly a single microtubule could be observed sliding out of the trypsin-treated axoneme of sea urchin sperm with a dark-field microscope and showed dynein was a microtubule-based motor protein.

When the cytoplasm of the *Nitella* cell was squeezed out of the cell, endoplasm was enclosed by membrane to form droplets, in which chloroplasts rotation and polygonal fibrils moving were observed (Kuroda, 1990). To this extract, when the medium containing ATP and EGTA was added, the membrane was disrupted and chloroplast chains connected by fibrils were observable moving freely in the medium (Higashi-Fujime, 1980). After washing out a number of chloroplasts by perfusion with the medium containing ATP and EGTA into the flow cell, dark-field microscopy revealed that the fibrils were sliding or rotating very fast on the glass surface. Fibrils continued moving even under vigorous flow of the medium, indicating that the moving fibrils were interacting with probably myosin attached on the glass surface (Higashi-Fujime, 1980). Thus, observations by light microscopy impressed with a great impact of seeing the biological molecules. As the moving fibrils were confirmed to be the bundles of actin filaments which formed arrowheads when decorated with HMM, the motor protein attached on the glass surface would be myosin (Higashi-Fujime, 1985).

2.2. Direct observation of protein at a molecular level

Purified muscle actomyosin exhibits so-called “superprecipitation” by adding ATP at low ionic strength. This phenomenon was thought to be a model of muscle contraction (Szent Györgyi, 1951). In fact, under a

dark-field microscope actin and myosin filaments showed vigorous sliding movement until ATP in the medium was exhausted (Higashi-Fujime, 1982). Unfortunately, the single actin filament is so thin that it cannot be seen directly under the dark-field microscope. But the single myosin filaments can be seen to be sliding along bundles of F-actin (Higashi-Fujime, 1985). The single actin filament became visible under epifluorescence microscope if an F-actin was labeled fluorescently with Rhodamine-phalloidin (Yanagida et al., 1984). Based on this direct observation of a single actin filament, the *in vitro* motility assay method was devised and improved (Higashi-Fujime, 1991; Kron et al., 1986; Toyoshima et al., 1987). Myosin belonging to various classes or a modified myosin adsorbed on the glass surface, which was usually coated with nitrocellulose, moved F-actin filaments at a velocity intrinsic to myosin adsorbed. By using this *in vitro* motility assay method, Chara myosin could be purified by following the motor activity. This technique could be applied to the assay of the microtubule-dependent motor protein. This was also helpful to identify a new motor protein. Myosin VI was verified to be only the minus end-directed myosin with *in vitro* motility assay (Wells et al., 1999), and the minus-directed microtubule motor protein of kinesin was discovered (Vale et al., 1985).

3. MYOSINS IN PLANTS

Plant myosin was first purified from *Physarum* plasmodia and its biochemical properties were extensively examined (Nakamura and Kohama, 1999). But this myosin belongs to conventional class II myosin. In pollen tubes of *Lilium longiflorum* and *Nicotiana glauca*, myosins I, II, and V were found by immunofluorescence microscopy (Miller et al., 1995), but they were not reported to be purified.

3.1. Extraction of myosin from plant cells

It is very difficult to prepare proteins from the homogenates of plant cells, because of degradation by strong proteases, especially in case of Characean cells. There were some exceptions and myosins were purified from lily pollen tube and tobacco bright yellow-2 (BY-2) cells. Myosin purified from lily pollen tubes (Kohno et al., 1992) was the mixture of myosin with molecular mass of heavy chains 110, 120, and 140 kDa and slid muscle F-actin at about $2 \mu\text{m/s}$. But these were the degraded ones of myosin with the molecular mass of 170 kDa which slid F-actin at $7.7 \mu\text{m/s}$ (Yokota and Shimmen, 1994).

Two kinds of myosins were purified from tobacco BY-2 cells (Yokota et al., 1999). One was 170 kDa myosin which slid F-actin at $4 \mu\text{m/s}$ and the other was 175 kDa myosin which slid F-actin at $9 \mu\text{m/s}$. These two myosins were not originally the same, and did not crossreact immunologically with each other. Interestingly, sliding velocities of these plant myosins are similar to or even faster than muscle myosin. As we will describe later, 175 kDa myosin is reported to be a processive motor (Tominaga et al., 2003).

3.2. The fastest myosin from Characean cells

The vesicle movement in Characean cells was found to be ATP dependent (Kachar, 1985; Williamson, 1975), and the presence of myosin in the endoplasm was suggested by differential treatment of the endoplasm with N-ethyl maleimide (NEM) (Chen and Kamiya, 1975). Isolated myosin from Characean cells, Chara myosin, slid F-actin at $\sim 60 \mu\text{m/s}$ with the *in vitro* motility assay (Higashi-Fujime et al., 1995; Rivolta et al., 1995). For extraction of myosin, strong proteases in the homogenate were not effectively inhibited by protease inhibitors even at high concentrations. As the cytoplasm squeezed into the medium containing ATP and EGTA showed active movement of endogenous actin cables (Higashi-Fujime, 1980), squeezing the cytoplasm with fingers was a good procedure for preparation. Further myosin purification by F-actin binding was one of the routine methods. But without ATP in the medium, Chara myosin immediately lost its activity, therefore addition of 50% glycerol was necessary to protect Chara myosin from denaturation to form rigor complex with F-actin (Higashi-Fujime et al., 1995). Chara myosin had a large molecular mass of 225 kDa estimated from SDS-PAGE, but soluble at low ionic strength indicating that Chara myosin did not polymerize into filaments. The velocity of cytoplasmic streaming in Chara cells was $30\text{--}60 \mu\text{m/s}$, but purified Chara myosin slid F-actin at $15\text{--}30 \mu\text{m/s}$ *in vitro*, probably due to damage by proteolyses and/or dissociation of light chain(s).

3.3. Biochemical properties of Chara myosin

Acanthamoeba myosin I is active form when its heavy chain is phosphorylated (Albanesi et al., 1984) at the TEDS site (Bement and Mooseker, 1995). Its basic ATPase of 0.25 s^{-1} was activated by actin up to 60-fold (Albanesi et al., 1983). The site corresponding to this phosphorylation site, Thr or Ser, is replaced by the negatively charged residue in vertebrate myosin I. The actin activated ATPase activity of myosin V was $\sim 15 \text{ s}^{-1}$ (De La Cruz et al., 2000a). The activities of these myosins were similar to that of muscle myosin II. From the motility assay, however, myosin I and myosin V slid F-actin at 0.2 (Zot et al., 1992) and $0.4 \mu\text{m/s}$ (Cheney et al., 1993), respectively. These velocities were much slower than the velocity $6 \mu\text{m/s}$ of

muscle myosin, but their ATPase activities did not differ so much with each other. We will discuss the sliding velocity in the later section.

In plant myosins, lily pollen tube myosin (170 kDa) was activated by actin up to 60-fold, and the actin activated ATPase activity (V_{\max}) of 175 kDa myosin from tobacco BY-2 cells was 77 s^{-1} (Tominaga et al., 2003). The ATPase of Chara myosin in the crude extract was activated by actin up to 120-fold (Higashi-Fujime et al., 1995). Column purified Chara myosin showed the actin activated ATPase activity of 24 s^{-1} when it was measured in solution and 57 s^{-1} when the activity was measured by using flow cells, the surface of which myosin was attached (Sumiyoshi et al., 2007). Thus, purified plant myosins have considerably high ATPase activities.

Chimeric myosin construct with the Chara myosin motor domain and the neck and tail of *Dictyostelium* myosin II had ATPase activity comparable to that of muscle myosin (Kashiyama et al., 2001) and similar chimeric Chara myosin with artificial neck of α -actinin and with the neck of myosin V had ATPase activities of 500 and 390 s^{-1} , respectively (Ito et al., 2003, 2007).

3.4. Distinct properties of Chara myosin

Actin is a ubiquitous protein functioning in various cells of animals and plants. The polymerized actin filament provides myosin with a polarized track to produce various types of movements in a cell. For regulation of such movements, actin has various interacting proteins, more than 50 kinds of the actin binding proteins (ABPs) (Pollard and Cooper, 1986). Tropomyosin is one of the important ABPs acting widely in various cells. In striated muscle, tropomyosin acts as an on-off switch of actin-myosin interaction by forming a complex with troponin which receives a signal of change in the intracellular Ca^{2+} concentration (Ebashi, 1991). In smooth muscle and nonmuscle cells, tropomyosin also plays an important role in structural and functional regulation for the cytoskeleton containing actin and myosin. In Characean cells, there has been no report about tropomyosin, but *Arabidopsis thaliana* has a gene encoding tropomyosin related protein.

It will be fruitful for understanding the nature of Chara myosin to compare it with that of other classes of myosin with regard to the mechanochemical properties such as effects of tropomyosin. Modification of actin such as limited cleavage by enzyme is another good tool to investigate the molecular pattern of interaction between actin and myosin. Distinct properties of Chara myosin will be described more specifically in the following sections.

3.4.1. Motility of cleaved actin on Chara myosin

Limited cleavage of G-actin by trypsin produced the 33 kDa core fragment. This cleaved actin could not polymerize into F-actin by adding salt (Konno, 1987; Mornet and Ue, 1984), or even in the presence of phalloidin (Jacobson and Rosenbusch, 1976). Subtilisin cleaved actin at the site between

Met47 and Gly48 in 40–50 loop called DNase I loop, and produced 35 kDa core and 9 kDa fragments. This actin cleaved by subtilisin (sub-actin) could polymerize into F-actin and formed arrowheads when bound with HMM (Schwyter et al., 1989). Electron micrographs of filaments of sub-actin and its arrowhead structure formed when bound with HMM seemed to morphologically be normal. The maximum rate of myosin ATPase activated by sub-actin was almost the same as that of intact F-actin (12.5 s^{-1}) but affinity was quite low (200 vs. $33 \mu\text{M}$) (Schwyter et al., 1990).

Proteinase K also cut G-actin at the site between Met47 and Gly48 and produced 35 kDa core fragment, but did not produce 9 kDa fragment, indicating that proteinase K cleaved additionally in the N-terminal side. Actually, this actin cleaved by proteinase K (proK-actin) did not polymerize by adding salts. However, in the presence of phalloidin, it could polymerize into F-actin. Electron micrographs of the filament of proK-actin and its arrowhead structure when bound with HMM showed features as good as those of intact actin (Higashi-Fujime et al., 1992).

These cleaved actins retained motile activities. With the *in vitro* motility assay on the surface on which HMM was adsorbed, intact actin filaments slid at $6.0 \mu\text{m/s}$, whereas sub-actin filaments slid at $2.4 \mu\text{m/s}$, and proK-actin filaments slid only at $0.4 \mu\text{m/s}$ (Higashi-Fujime et al., 1992). Surprisingly, on Chara myosin, these actins, that is intact, sub-actin, and proK-actin, all slid at very similar speed of $\sim 60 \mu\text{m/s}$ (Higashi-Fujime et al., 1995). In accordance with this similarity of the velocity, the Chara myosin ATPase activities activated by sub-actin and proK-actin were also very similar, 77% and 86% of that activated by intact actin, respectively (Higashi-Fujime et al., 1995). Interestingly, myosin V also slid sub-actin filaments as fast as intact actin filaments (personal communication with Kubota and Ishiwata in Waseda University, Tokyo).

Subtilisin cleaves actin at the site between Gly42 and Val43 following cleavage at the site between Met47 and Gly48. Removal of penta-peptides between these cleavage sites lost polymerizability by adding salts (Kiessling et al., 1995). But sub-actin removed penta-peptides could polymerize by the aid of phalloidin, but the arrowhead structure was not as clear as that seen for the native actin filament (Kiessling et al., 1995).

How could Chara myosin move cleaved actin, sub-actin, and proK-actin, at the velocity very similar to that of intact actin, despite strong impairment of motility on muscle myosin? ProK-actin slid on Chara myosin 150 times as fast as on HMM. We will discuss this issue from the structural aspects in the later section.

3.4.2. Regulatory effect of tropomyosin

In various kinds of cell motility based on actin–myosin interaction, its regulatory system is rich in variety. Calcium-regulation by the complex of tropomyosin and troponin (native tropomyosin) is the regulatory system

specifically evolved for contraction of striated muscle (Ebashi and Endo, 1968). Since tropomyosin is a long molecule consisting of the α -helical coiled-coil of two polypeptides, it binds seven actin monomers in a protofilament of an actin filament (Brown et al., 2005; Phillips et al., 1986). The mechanism of Ca^{2+} -regulation in muscle contraction is understood by the idea as follows. Upon elevation of the intracellular calcium concentration, Ca^{2+} binds to troponin, and it induces displacement of the binding position of tropomyosin from the outer surface of the actin filament in the inhibited state to the inner surface of actin subdomains 3 and 4 in the activated state (Haselgrove, 1972; Huxley H., 1972). As a consequence, the myosin binding site blocked by tropomyosin becomes open to interact with myosin.

This steric hindrance model is now modified as the three-state model: blocked, closed, and open states (McKillop and Geeves, 1993; Vibert et al., 1997). In the thin filament, that is, the actin filament bound with native tropomyosin, when Ca^{2+} binds to troponin, myosin can first interact with actin in the weak binding state and then advances to the strong binding state, which induces further displacement of tropomyosin (the open state). Concomitantly, the thin filament becomes fully active. Thus, the images of these three states related to the native tropomyosin can be depicted as three distinct positions of tropomyosin on the actin filament (Craig and Lehman, 2001). The binding position of tropomyosin without troponin on the actin filament is reported to coincide with the position of tropomyosin in the open state of the thin filament (Brown et al., 2005; Holthauzen et al., 2004).

With the *in vitro* motility assay on HMM, the sliding velocity of actin filaments increased from 6.0 to 7.1 and 7.7 $\mu\text{m/s}$, when actin bound with tropomyosin, and native tropomyosin in the presence of Ca^{2+} , respectively. Actin cleaved by subtilisin, sub-actin, slid at a speed of 2.2 $\mu\text{m/s}$ on HMM, and sub-actin bound with tropomyosin and native tropomyosin slid at 2.2 and 4.8 $\mu\text{m/s}$, respectively (Higashi-Fujime and Hozumi, 1997). The sliding speed of the regulated sub-actin filament was 2.2-fold of that of the unregulated sub-actin filament. Native tropomyosin seemed to greatly compensate the damage by cleavage at 40–50 loop. Although recovery of the sliding speed of regulated sub-actin filaments was yet about a half of that of the regulated intact actin filaments, calcium sensitivities of the sliding speed of both regulated intact actin and regulated sub-actin filaments were almost the same, indicating that 40–50 loop did not directly take part in the regulatory mechanism (Pavlov et al., 2003).

In case of proK-actin, the sliding speed increased from 0.5 to 1.4 $\mu\text{m/s}$ by adding tropomyosin and to 3.0 $\mu\text{m/s}$ by adding native tropomyosin (Higashi-Fujime et al., 1992). As the cleavage site by subtilisin is in 40–50 loop and the site cleaved by proteinase K is the same and additionally the N-terminal side from 40 to 50 loop. These are located in the outer domain

(subdomains 1 and 2) containing myosin binding sites, but do not seem to be the binding site of tropomyosin and native tropomyosin at the open state. The reason is unknown why tropomyosin and particularly native tropomyosin compensate the damage in actin effectively, but it should be emphasized that owing to tropomyosin and particularly native tropomyosin, myosin communicates properly with the actin filament and produces force more efficiently at the open state, in spite of the damage in the close vicinity of the myosin binding domain of 40–50 loop.

3.4.3. Inhibitory effect of tropomyosin on Chara myosin

Smooth muscle myosin is regulated by phosphorylation of its regulatory light chain (Somlyo and Somlyo, 2003). Tropomyosin augments its mechanochemical activity. For instance, with the *in vitro* motility assay on phosphorylated smooth muscle myosin, the sliding speed of the actin filament increased from 0.36 to 0.76 $\mu\text{m/s}$ (2.1-fold) upon addition of tropomyosin (Okagaki et al., 1991). On the other hand, motility on brush border myosin I was inhibited by tropomyosin (Collins et al., 1990; Fanning et al., 1994). In nonmuscle cells, tropomyosin has two isoforms, one is a high molecular weight isoform which is 40 nm long and binds seven protomers on the actin protofilament, and another is a low molecular weight isoform which is 34 nm long and binds six protomers (Lees-Miller and Helfman, 1991). Tropomyosin of both isoforms completely inhibited motility of actin filaments on myosin I (Fanning et al., 1994).

There is an idea to explain this inhibitory effect of tropomyosin on brush border myosin 1b (Lieto-Trivedi et al., 2007). Myosin 1b has long loop 4 consisting of eight amino acid residues, which is longer than those of other myosins (Fig. 7.1). Due to this long loop 4, tropomyosin may hinder the interaction between actin and myosin. This idea was tested by examination as follows: myosin 1b was mutated by replacing its loop 4 with the sequence of myosin II and also another mutant was produced by deletion of four amino acid residues from loop 4 of myosin 1b, and motilities of these mutants were not affected by tropomyosin (Lieto-Trivedi et al., 2007). Thus, long loop 4 of myosin 1b might block the binding of myosin to the actin filament bound with tropomyosin.

Like myosin 1b, Chara myosin motility and its actin activated ATPase were completely inhibited by tropomyosin, and by native tropomyosin in the presence of Ca^{2+} (Higashi-Fujime et al., 2000). Consistently with the idea that long loop 4 causes inhibitory effect by tropomyosin, loop 4 of Chara myosin is short by only one amino acid residue when compared with myosin 1b, as shown in Fig. 7.1. As loop 4 of myosin V is short by two amino acid residues, motility and actin activated ATPase of myosin V can be expected to be inhibited by tropomyosin. But, so far, there has been no report about the effect of tropomyosin on myosin V. Beads coated with myosin V moved along *Limulus* acrosomal process at $\sim 0.5 \mu\text{m/s}$,

Myo1b	VLEVVAAVLKLGNIEFKPESRMNGLDESKIKDKNELKEICELTSIDQVV	319
Chara	IFRTIAAVLHLGNIEFDGSDAS-EVSTESKSFHLKAAAEMLMCDEQM	370
MyoVa 190p	IFRILAGILHLGNVEFASRSDS--SCAIPPKHDPTAAQKVCHLMGINVT	381
skMyo Gal	IYKLTGAVMHYGNLKFQKQKQ----REEQAEPDGTVEADKAAAYLMGLNSA	396
smMyo Gal	ILRVVSSVLQLGNIVFKKER----NTDQASMPDNTAAQKVCHLMGINVT	395
skMyo rab	IYKLTGAVMHYGNMKFKQKQKQ----REEQAEPDGTVEADKAGYLMGLNSA	395

Figure 7.1 Sequence alignment of myosin loop 4. The sequence alignment of myosins shows the length difference in loop 4. Eight amino acid residues shaded by dark color is loop 4 of myosin 1b. The number of amino acid residue of the last sequence represented is shown in the right. Abbreviations of myosins are as follows: Myo1b, brush border myosin 1b; Chara, Chara myosin; MyoVa 190p, chicken myosin Va; skMyo Gal, chicken skeletal muscle myosin; smMyo Gal, chicken smooth muscle myosin; skMyo rab, rabbit skeletal muscle myosin. When myosin has long loop 4, its interaction with actin might be inhibited by tropomyosin.

irrespective of presence or absence of tropomyosin (Wolenski et al., 1995), but in this case the concentration of tropomyosin used was very low (1 nM tropomyosin to actin 600 nM). Tropomyosin effect on myosin Va should be examined more intensively by changing the concentration of tropomyosin.

Curiously enough, tropomyosin affected mechanochemical properties of myosin oppositely depending on the myosin classes, activation for myosin II and inhibition for myosins I and XI. We can understand the biological significance of inhibition by tropomyosin on myosin I as the phenomenon that tropomyosin probably excludes myosin I in a specific area of actin cytoskeleton in a living cell by working together with other ABP(s) (Lieto-Trivedi et al., 2007). Primary structure of brush border myosin 1b has high similarity to that of Chara myosin (40% identity and 59% similarity). So, it may be understandable that both myosin 1b and Chara myosin are inhibited by tropomyosin, but its biological significance for Chara myosin is unknown.

Another possibility to explain the inhibitory effect of tropomyosin on actin–myosin interaction is steric hindrance via cardiomyopathy loop (CM-loop). This subject will be discussed in the later section.

4. MOLECULAR STRUCTURE OF PLANT MYOSINS

Myosin superfamily now consists of 24 classes identified according to homology of the motor domain of the head (Foth et al., 2006; Richards and Cavalier-Smith, 2005). Among them, classes VIII, XI, and XIII are plant

myosins. Class XI myosins purified from *Chara corallina*, Chara myosin, and Nt 175-kDa myosin from tobacco BY-2 cells (*Nicotiana tabacum*) have extensively been studied on mechanochemical properties (Higashi-Fujime, 2003; Shimmen, 2007; Shimmen and Yokota, 2004). In contrast, *Arabidopsis* contains 13 subclasses of myosin XI, but none of them has been purified from the cells. Its biochemical and histochemical studies have just begun. In this section, molecular structure of plant myosins will be discussed mainly from the view point on the primary structure of Chara myosin.

4.1. Plant myosin belonging to class XI

Class VIII plant myosin from *A. thaliana* was first identified (Knight and Kendrick-jones, 1993), and finding of class XI myosin in *Arabidopsis* was followed (Kinkema and Schiefelbein, 1994). Molecular structure of Chara myosin was determined from cDNA cloned with antibody against Chara myosin (Kashiyama et al., 2000; Morimatsu et al., 2000). The primary structure of class XI myosin from tobacco BY-2 cells was also determined (Tominaga et al., 2003). Class XI myosin has the N-terminal motor domain followed by six IQ motifs for binding of CaM or the CaM-related protein as light chains. After six IQ motifs, there is the coiled-coil region to form a dimer and followed by the C-terminal globular tail. This molecular feature is very similar to those of animal and fungal myosin V, but the molecular length varies greatly from myosin to myosin.

Mouse dilute myosin and fungal myosin V, myo2p, are composed of 1852 and 1574 amino acid residues, respectively. Class XI myosins of MYA1, Nt 175-kDa myosin, and Chara myosin are composed of 1520, 1362, and 2167 amino acid residues, respectively. In particular, the heavy chain of Chara myosin is very long because of the long rod and the large globular tail.

4.2. Molecular structure of Chara myosin

Properties of two distinct domains of the Chara myosin structure will be specifically described here, one is loop 2 in the motor domain and the second is the coiled-coil rod domain. Other structural characteristics, especially IQ sequences of the neck and the structure of the globular tail, will be described in the later sections.

4.2.1. Loop 2 of Chara myosin

In the motor domain of Class XI myosin, not only Chara myosin but also MYA1 and Nt 175-kDa myosin, loop 2 is extremely short compared with myosin of other classes. For instance, loop 2 consists of 26 amino acid residues in skeletal muscle myosin, 43 residues in myosin V, but only 14 residues in Chara myosin. Class XI myosin is often considered to be very

similar to myosin V from various aspects, but concerning the length of loop 2, these two myosins are the extremes. Contrarily, myosin E of class I has loop 2 consisting of 15 residues, which is only one amino acid residue longer than that of Chara myosin.

Loop 2 is the junction between 50 and 20 kDa domains in the head of skeletal muscle myosin. Many charged residues reside in loop 2 of myosin II and the net charge is positive. This positive charge must be important to bind with actin at the N-terminal negatively charged region (Sutoh, 1983). In case of myosin V, this net charge is important for the affinity to actin at the weak binding state, and the run length of the processive movement depends on this cluster of charged residues (Trybus et al., 1997). In loop 2 of Chara myosin, there are four charged residues but no net charge. The other class XI myosin, for instance, processive Nt 175-kDa myosin also has no net charge. Electrostatic interaction between loop 2 and the N-terminal domain of actin is thought to be important for the trailing head to execute the next forward stepping of the weak binding state, before the leading head dissociates. How does the class XI myosin, if it is a processive motor, attain the long run without net charge in loop 2? The functional reason of short loop 2 is unknown at present. It is interesting if short loop 2 without net charge might reflect the structural requirement for the high-speed processive movement of class XI myosin.

4.2.2. Rod structure of Chara myosin

It should be noted that Chara myosin has a very long rod from Arg885 to Val1635. The first 191 residues from Arg885 to Lys1075 are very similar to the rod sequence of MYA1 (55% homology). The rest of the rod (560 residues from Gln1076 to Val1635) is the tandem repeats of the sequence of 33 amino acid residues. This sequence repeats 12 times but the tandem repeat is interrupted by insertion of 53 amino acid residues, 3 times. This insertion contains the sequence to disrupt the coiled-coil structure (18 aa residues). These repeat sequences have no similarities to any other proteins found so far.

The role of the rod domain is not merely the stalk to dimerize by the coiled-coil structure. Smooth and nonmuscle myosin is regulated by phosphorylation of the regulatory light chain. Monomeric S-1 without the rod domain was constitutively active irrespective of phosphorylation or dephosphorylation of the light chain, but the regulatory function resumed depending on the length of rod (Trybus, 1994).

Myosin V was found to have a compact inhibited conformation in which the tail bound with the head, in a solution containing EGTA, but it took the extended form in the presence of Ca^{2+} , instead (Krementsov et al., 2004; Li et al., 2004; Wang et al., 2004). Myosin V lost this Ca^{2+} -dependent regulation when the globular tail domain was truncated (Homma et al., 2000; Wang et al., 2000). The coiled-coil structure of the

rod of myosin V is disrupted four times and divided into five parts. Interestingly, the globular tail bound with the C-terminal portion of the first coiled-coil rod, and this binding was critical for inhibition by binding of the tail to the head (Li et al., 2006). There has been no evidence about the inhibited compact form of Chara myosin but the area where the coiled-coil is broken may possibly have some biological significance. For instance, this area may take some role to associate with regulatory protein(s).

4.3. Neck region of Chara myosin

Myosins V and XI have the long neck consisting of tandem repeat of six IQ motifs with the consensus sequence for calmodulin target of IQXXXRGXXXXR where the letter X denotes any amino acid (Bähler and Rhoads, 2002). Calmodulin (CaM) or the CaM-like light chain binds to the IQ motif and regulates motor activity and also binding of CaM or the CaM-like light chain to the IQ motif makes the neck rigid. Thereby, the neck plays the vital role to act as a lever arm (Uyeda et al., 1996) and amplifies the displacement produced by small conformational change in the head, and produces effective movement. Mouse myosin Va binds only CaM as light chains, whereas chicken myosin V contains an essential light chain in addition to CaM (Espindola et al., 2000). Little is known about the neck of myosin XI. Contrariwise, extensive investigations into the neck of myosin V have been performed.

4.3.1. IQ motif and the light chain

The amino acid sequence in the IQ motif must be important for binding of the specific light chain. The sequences of IQ motifs of Chara myosin widely vary from its typical sequence, such as IQ sequences of myosin Va. For instance, IQ is often replaced by FQ or VQ, and the arginine residue in the consensus sequence is replaced by other noncharged residue, and charged residues are much fewer in the neck of Chara myosin than in myosin Va and net charge of each IQ motif of Chara myosin is very small. Chara myosin was very labile in solution and the ATPase activity or motility decreased considerably in a few hours. This inactivation might partly be due to dissociation of the light chain from the neck. However, the addition of bovine CaM or even Chara CaM did not protect Chara myosin from inactivation, and not resume the activity (Higashi-Fujime, unpublished data). Chara myosin construct did not exhibit its activity when CaM was coexpressed together as light chains (Kashiyama et al., 2001). Therefore, the light chain of Chara myosin may not be CaM, but the CaM-related protein(s). It is unknown whether the Chara myosin light chain can bind Ca^{2+} , but with the *in vitro* motility assay the sliding movement is not inhibited by Ca^{2+} at all (Higashi-Fujime et al., 1995).

We can evaluate the provability of CaM target to the IQ motif of Chara myosin, according to “Calmodulin Target Database” (Yap et al., 2000). The results of such search are shown in Fig. 7.2. As expected, CaM perfectly hits all IQ sequences of mouse myosin V. On the other hand, judging from this result obtained, it is seemingly hopeless to expect that calmodulin binds IQ motifs of Chara myosin, except IQ6. The calmodulin target search suggests the light chains of Chara myosin greatly differ from calmodulin. Identification and sequencing of Chara myosin light chains remain to be solved in the near future.

4.3.2. Regulation by Ca²⁺ and calmodulin

The activity of myosin V is regulated by Ca²⁺ and CaM (Cheney et al., 1993; Reck-Peterson et al., 2000; Taylor, 2007). Although the mechanism of the Ca²⁺ regulation of myosin V remained elusive for many years, two paradoxical problems on the Ca²⁺ regulation were clarified, recently.

A Chara myosin IQ motifs	B Myosin Va (mouse) IQ motifs
746 AVKIQHVMVQSFLMRRDYERMKRA 0000000000000111222344	770 CIRIQKTIRGWLLRKRKRYLCMQRA 9999999999999999999000
769 SLLVQAYWRGTMARMEFRFLREQVS 444444444443322211000011	793 AITVQRYVRGYQARCYAKFLRRTKA 999999999999999999900000
794 AVCFQRYIRGYLAQKNYFEMRQA 2333344555555678876545	818 ATTIQKYWRMYVRRRYKIRRAA 99999999999999999990000
817 AIRIQSAIRSLAARRVLCVLQDNHA 554322222221111111000000	841 TIVIQSYLRGYLTRNRYRKILREYK 999999999999999999900000
842 ATQIQSKWRSYVAFRSYDELLRS 0011123444445555567899	866 AVIIQKRVRGWLARTHVKRTMKA 99999999999999999990000
865 CKVFQGAWRCKEARSEIKLRQAARE 99999888877777766544321111	889 IVYLQCCFRMMMAKRELKCLKIEAR 999999999999999999900000

Figure 7.2 IQ motifs fitting to calmodulin binding. The IQ motifs from IQ1 to IQ6 of Chara myosin and those of mouse myosin Va are shown in the left and the right panel, respectively. In each IQ motif, amino acid sequence and its score obtained by the calmodulin target search (Yap et al., 2000) are shown in the upper and lower lines, respectively. The highest score “9” indicates best fitting of calmodulin to the IQ sequence. It is quite natural that all IQ motifs of mouse myosin Va have the highest score because all IQ motifs have calmodulin as light chains in the neck. On the other hand, Chara myosin obtained very low score for each IQ motif except IQ6, indicating that Chara myosin would have its own specific light chains but not calmodulin. The sequence number of the first amino acid in each line is indicated in the left.

The first problem was that the actin activated ATPase of tissue purified myosin V was greatly activated by Ca^{2+} , whereas its motility was inhibited completely by Ca^{2+} . This motility inhibition by Ca^{2+} was understood by the idea that the high concentration of Ca^{2+} caused dissociation of the calmodulin light chain from the neck (Homma et al., 2000; Nascimento et al., 1996; Nguyen and Higuchi, 2005). The definite evidence was obtained by examination using the CaM mutant (Krementsov et al., 2004). When myosin V bound the mutated CaM construct, which was deficient in Ca^{2+} binding at a high affinity site, elevation of the Ca^{2+} concentration up to 100 μM did not induce dissociation of this mutated CaM, and motility was not inhibited even in the presence of Ca^{2+} at a high concentration. Among six IQ motifs, dissociation of the light chain occurs usually at the site of IQ2 in case of myosin Va (Koide et al., 2006; Krementsov et al., 2004; Martin and Bayley, 2004).

When Chara myosin was extracted in the medium for purification, Chara myosin moved F-actin usually at 15–30 $\mu\text{m/s}$ with the *in vitro* motility assay, despite the high speed of $\sim 60 \mu\text{m/s}$ of cytoplasmic streaming in a cell. The *in vitro* motility of Chara myosin was not affected by Ca^{2+} , even in the presence of 1 mM Ca^{2+} (Higashi-Fujime et al., 1995). The reduction of sliding velocity is thought to be due to degradation of myosin by endogenous strong proteases. In addition, the light chain(s) may dissociate from the neck during purification and the naked neck may cause the defect in power stroke of the neck and in motility, because myosin V inserted alanine residues in the middle of the neck results in a short step size (Sakamoto et al., 2003).

4.3.3. The inhibited state and activation by Ca^{2+}

About the activity of myosin V, the first question was why Ca^{2+} inhibited motility while it activated ATPase. The answer to this question was that Ca^{2+} binding to the CaM light chain induced dissociation of CaM from the neck and then CaM dissociation caused loss of motility (Cheney et al., 1993). Conversely, the second long-standing question about the activity of myosin V was that the actin activated ATPase inhibited in the presence of EGTA, whereas motility of myosin V was very active in the presence of EGTA. At low concentration of Ca^{2+} , however, only tissue purified myosin V or full length construct of myosin V was inhibited in its actin activated ATPase, but constructs of S1 and HMM were constitutively active (Krementsov et al., 2004; Li et al., 2004; Wang et al., 2004).

A clue to solve this problem at low calcium concentration was obtained by analytical centrifugation experiments. The sedimentation coefficient of myosin V was 14s in a solution containing EGTA indicating a globular conformation, whereas in the presence of 10 μM Ca^{2+} it was 10s (Krementsov et al., 2004; Li et al., 2004; Wang et al., 2004). Electron microscopic observations revealed that 10s myosin V of the active form

exhibited an extended conformation and 14s myosin V exhibited the triangular shape of the folded configuration, where the stalk of the rod bent at the neck–rod junction and the globular tail bound with the head (Liu et al., 2006; Thirumurugan et al., 2006). This folded form could bind F-actin with only one head weakly (Taylor, 2007). Thus, myosin V will release the cargo after it reaches the destination in the cell periphery, and takes the folded form of inhibited state in order to be recruited to the initial place without much consumption of ATP. The similar folded conformation to inhibit the motor activity had been found in regulation of kinesin (Hackney and Stock, 2000) and in the dephosphorylated state of smooth muscle myosin II (Onishi and Wakabayashi, 1982; Wendt et al., 2001).

4.4. Myosin tail

Myosin has a conserved ATPase motor domain in the N-terminal domain, but the rest of the C-terminal domain varies from myosin to myosin and characterizes its own specific function in the cell. One of the important functions of myosin V of animals and yeast fungi and myosin XI of plants is translocation of cargos to their destinations according to the temporal and spatial requirement in a cell. The cargo binds to the C-terminal globular tail of myosin V, but we do not know much about the tail of myosin XI. It will be expected that there may be some similarity in the tail between myosins V and XI. Comparative studies must be useful for better understanding about the properties of the myosin tail of class XI.

4.4.1. Tail structure of Chara myosin

Although the tail structure of myosin V had long been unsolved, despite the importance of its knowledge, the crystal structure of myo2p tail was recently solved (Pashkova et al., 2006). In the crystal, the tail comprised 15 α -helices, whose axes were arranged almost in parallel forming an oblong shape. It was divided into two domains, N-terminal subdomain I (SDI) and C-terminal subdomain II (SDII). These domains corresponded to subdomains obtained by limited cleavage of the tail by trypsin (Pashkova et al., 2005). Subdomains I and II bind vacuoles and secretory vesicles (Pashkova et al., 2005), respectively. The binding sites of these cargos were located nearly in the center of both subdomains and in the opposite surface of the globular tail with each other (Pashkova et al., 2006).

There is considerable diversity in the amino acid sequence of the globular tail between *Arabidopsis* myosin XI, MYA1, and *Saccharomyces* myo2p. However, Li and Nebenführ managed to depict the 3D structure of the MYA1 tail domain based on the crystal structure of myo2p using the homology-based modeling system (Li and Nebenführ, 2007). The 3D structure of the MYA1 tail extremely resembled the molecular architecture of the myo2p tail. Moreover, the functional similarities of SDI and SDII of

MYA1 to those of myo2p were verified by yeast two-hybrid and biomolecular fluorescence complementation assays (Li and Nebenführ, 2007). Separately expressed SDI and SDII could bind tightly and were associated with cargos to function properly in a cell. In case of MYA1, these subdomains needed the coiled-coil rod portion prior to the globular tail domain, probably because the tail was required to dimerize for functioning properly (Li and Nebenführ, 2008).

The fastest Chara myosin is highly similar to MYA1 in the head (53% identical and 70% homology) and also in about two-thirds of C-terminal side of the globular tail domain (59% identical and 73% homology), as shown in Fig. 7.3. Consequently, we tried to figure out the putative tail structure of Chara myosin by using Swiss Model System (Arnold et al., 2006). Its 3D molecular architecture predicted was actually very similar to that of myo2p tail as shown in Fig. 7.4, indicating that the Chara myosin tail was also expected to have specific binding sites for vacuole and secretory vesicle in the similar way to those of myo2p and MYA1.

As described above, in the sequence of Chara myosin the coiled-coil rod portion ends at the amino acid Val1635. The following sequence from Val1636 to the C-terminal end Ala2167 must be the globular tail. However, as shown in Fig. 7.3, Chara myosin tail from Gln1722 to the C-terminal end is homologous to the tail of MYA1 and that of myo2p. The rest of the tail of Chara myosin, 86 amino acid residues from Val1636 to Gln1721, has unique sequence and has no similarity to any other known proteins. This segment probably might have additional function as a tail such as association with certain cargo other than vacuoles and secretory vesicles or binding regulatory protein(s), or as a site for modification of the activity.

4.4.2. Adaptor protein for cargo binding

Vesicles are transported by motor proteins, myosin, kinesin, and dynein. How can the motor protein recognize a specific cargo which has to be transported to the specific destination? As we have at present no experimental data about specific cargo binding with Chara myosin, we will briefly overview results of the cargo binding with other class myosins to speculate upon the feature of vesicle binding for Chara myosin.

Single headed myosin I of *Acanthamoeba* could bind directly with phospholipids at very basic TH1 (tail homology 1) region in the tail (Doberstein and Pollard, 1992; Lee et al., 1999). By the *in vitro* motility assay, this myosin could bind to the surface coated with phospholipids as well as with nitrocellulose and slid F-actin (Zot et al., 1992). Myosin 1a (brush border myosin I) was found to localize in plasma membrane of brush border and its TH1 domain was critical for membrane binding (Tyska and Mooseker, 2002; Tyska et al., 2005). But it is unclear if there is an adaptor protein additionally for membrane binding of myosin 1a.

		H1	H2				
MYA1	1019	<u>DRPQKSLNQK</u>	<u>QQ-ENQELLL</u>	<u>KSISED</u>	---	-----	--GFSEGKPV
Chara	1722	<u>QKKSMMMPDK</u>	<u>LQ-SDQEALL</u>	<u>DCLMODV</u>	---	-----	--GFSKDHVP
Myo2p	1152	<u>NATQINEELY</u>	<u>RLLLEDTEILN</u>	<u>QEITEGLLKG</u>			FEVPDAGVAI <u>QLSKRDVVYP</u>
		H3		H4			
MYA1	1125	<u>AACLIYKCLI</u>	<u>HWR</u> S-FEVER	<u>TSIFNRIIET</u>	<u>IASAIEM</u>	---	<u>Q-ENSDVLC-</u>
Chara	1783	<u>AAVVIIFKCLL</u>	<u>QWHS-FEAER</u>	<u>TDVFDRIISA</u>	<u>IQKATIES</u>	---	<u>HSNDNDVLA-</u>
Myo2p	1202	<u>ARILLIIVLSE</u>	<u>MWRFG</u> LTKOS	<u>ESFLA</u> QVLTT	<u>IQKVVT</u> QLKG		<u>N-DLIPSGV-</u>
		H5		H5a		H5b	
MYA1	1169	<u>YWLSNSATLL</u>	<u>MFLQRTLKAG</u>	<u>ATGSITTPRR</u>	<u>RGMPSSLF</u>	GR	<u>VSQ</u> SFRGSPQ
Chara	1828	<u>YWLSNTSTLL</u>	<u>HLLQRTLKTG</u>	<u>GGGG-TTPRR</u>	<u>RRQ-ATL</u> FGR		<u>MTQRF--SSQ</u>
Myo2p	1250	<u>FWLANVRELY</u>	<u>SFVV</u> FALNSI	<u>LTEET</u>	----	-----	-----
		H6					
MYA1	1219	<u>SAGFPFMTGR</u>	<u>AIGGGLDEL</u> R	<u>QVEAKYPALL</u>	<u>FKQQLTAFLE</u>		<u>KIYGMIRDKM</u>
Chara	1874	<u>QENYPNGMGP</u>	V---GLDNVR	<u>QVEAKYPALL</u>	<u>FKQQLSAYVE</u>		<u>KIYGMIRDL</u>
Myo2p	1312	-----MTDE	<u>EYKEYVSLVT</u>	<u>ELKDDFEALS</u>	<u>YNIYNIWLKK</u>		<u>LOKQLOKKA</u>
		H6a		H7			
MYA1	1269	<u>KKEISPLLAS</u>	<u>CIQVP</u> RTPRS	<u>GLVKGRS</u> QNT	<u>QNNV</u> VAPKPM		<u>I AHWQNI</u> VTIC
Chara	1921	<u>KKEITPLLGS</u>	<u>CIQAP</u> RAPRH	<u>QLVRKLSLTP</u>	<u>AQOVL</u> S----		<u>SHWGS</u> IINS
Myo2p	1323	<u>NAVVIS</u> ESLP	<u>G</u> FSA-----	-----	-----		<u>YETMDD</u> ILTF
		H8					
MYA1	1319	<u>LNGHLRTMRA</u>	<u>NYVPS</u> LLISK	<u>VFGQIF</u> SFIN	<u>VQLFNS</u> LLLR		<u>RECCS</u> FSNGE
Chara	1966	<u>LLTLLNALRG</u>	<u>NKVP</u> PLYVRN	<u>IFTQIF</u> SFIN	<u>VQLVNS</u> LLLR		<u>RECCS</u> FSNGE
Myo2p	1362	<u>FNSIY</u> WCMKS	<u>FHIENE</u> VFHA	<u>VVTLLN</u> YVD	<u>AICF</u> NELIMK		<u>RNFLS</u> WKRGL
		H9		H10		H11	
MYA1	1369	<u>YVKTGLAELE</u>	<u>KWCH</u> DATEEF	<u>VGSAW</u> DELKH	<u>IRQAV</u> GFLVI		<u>HQKPK</u> SLKE
Chara	2016	<u>YIKAG</u> LAQLE	<u>HWIYE</u> AGEEY	<u>AGDSW</u> EELRY	<u>IRQAV</u> GFLVI		<u>HQKPK</u> SLDE
Myo2p	1412	<u>QLNYN</u> VTRLE	<u>EWCK</u> THG---	<u>LTDG</u> TECLQH	<u>LIQTA</u> KLQV		<u>-RKYT</u> IEDID
		H12		H13			
MYA1	1419	<u>ITTEL</u> CPVLS	<u>IQQLY</u> RISTM	<u>YWDDK</u> YGTHS	<u>VSTEVI</u> ATMR		<u>AEVSD</u> VSKSA
Chara	2066	<u>IINDL</u> CPALS	<u>OMQLY</u> RISTM	<u>YWDDK</u> YGTHT	<u>VAPEVI</u> QNM		<u>ILMTE</u> YSYNA
2f6hX	1458	<u>ILRGI</u> CYSLT	<u>PAQLO</u> KLISQ	<u>YQVAD</u> YES-P	<u>IPQEI</u> LRVVA		<u>DI</u> VKKEAALS
		H14		H15			
MYA1	1469	---ISNSFLL	<u>DDSS</u> IPFSL	<u>DDISK</u> SMQNV	<u>EVAE</u> VDPPPL		<u>IRQNS</u> FMFL
Chara	2116	---GNSFLL	<u>DDSG</u> IPFSV	<u>DDISK</u> SMPDV	<u>DLSQ</u> VDPPPL		<u>LKNR</u> PSFRFL
Myo2p	1508	<u>SSGS</u> FITPE	<u>TGF</u> PTDPFSL	<u>IKTRK</u> FDQVE	<u>AYIP</u> AWLSLP		<u>STKR</u> IVDLVA
MYA1	1516	LERSD					
Chara	2163	QPGKA					
Myo2p	1568	QQVV					

Figure 7.3 Sequence alignment in the tail region of myosins V and XI. The underlines show the α -helical portion according to the crystal structure of the myo2p tail (PDB 2F6H), and according to the results on the MYA1 tail reported by Li and Nebenführ (2007), and the result on the Chara myosin tail analyzed by using “Swiss Model System” (Arnold et al., 2006). Wavy underlines for the Chara myosin sequence indicate α -helical regions obtained by using “Chou and Fasman” program (Chou and Fasman, 1978).

Microvilli in the apical surface of the brush border are composed of polarized bundles of actin filaments, which are crosslinked by myosin 1a with the plasma membrane. The membrane moved toward the apical tip in

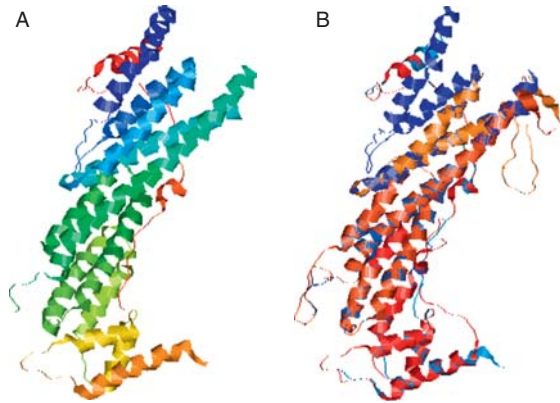


Figure 7.4 Putative 3D structure of the Chara myosin tail. The predicted structure of the Chara myosin tail was constructed according to Swiss Model System (Arnold et al., 2006) based on the crystal structure of the myo2p tail (PDB 2F6H) (Pashkova et al., 2006). The structure of Chara myosin globular tail is very similar to the crystal structure of myo2p tail or the structure of MYA1 tail, indicating that Chara myosin may have specific binding sites for vesicles and vacuoles.

an ATP-dependent fashion and this shedding of microvilli via membrane translocation took place vesiculation at the apical tip (McConnell and Tyska, 2007). The speed of this membrane moving was ~ 20 nm/s, corresponding to the speed of myosin 1a measured by the *in vitro* motility assay (McConnell and Tyska, 2007). For comparison, *Acanthamoeba* myosin I slid F-actin at ~ 0.2 $\mu\text{m/s}$ on phospholipids- or nitrocellulose-coated surface, when activated by heavy chain phosphorylation (Ostap and Pollard, 1996), and *Dictyostelium* myosin I (MyoD) slid F-actin very fast at a velocity of 1.78 $\mu\text{m/s}$ (Fujita-Becker et al., 2005). Thus, the sliding velocities of myosin I isoforms exhibited quite large variations probably depending on the cellular function.

There are a variety of features of binding between myosin V and cargos. For instance, in melanocyte, melanophilin mediates between myosin Va and rab27 GTPase located on the melanosome membrane surface (Fukuda et al., 2002; Hume et al., 2007; Wu et al., 2002). In yeast cells, myo2p binds Vac17p and Vac8p which act as an intermediary for vacuole binding (Ishikawa et al., 2003; Wang et al., 2001).

Little is known about specific localization of cargo in plants and whether myosin XI binds directly with cargo or with the adaptor protein in the membrane. Immunofluorescence staining with antibody raised against Chara myosin (Morimatsu et al., 2000) or antibody against myosin XI from Tobacco BY-2 cells (Yokota et al., 1999) showed localization of myosin XI on vesicles, but the cargo was not specified yet. Antibody against MYA2, one of myosin XI in *A. thaliana* was found to bind peroxisomes

(Jedd and Chua, 2002). Reisen and Hanson (2007) examined the localization of 6 isoforms out of 13 isoforms of class XI myosin in *Arabidopsis* by expressing the YFP-tail fusion protein and they confirmed particular localization in peroxisome, vacuole, Golgi, and mitochondria. Importantly, the coiled-coil region was required for proper localization of myosin XI (Reisen and Hanson, 2007). Overexpression of the tail might result in the dominant negative effect, but the plant organelles remained motile. Deletion of MYA2 did not show discernible deficiency (Hashimoto et al., 2005). These results indicate that 13 isoforms of myosin XI of *A. thaliana* have considerable redundancy in function. Recently, small G proteins were found to bind with the myosin XI tail (Hashimoto et al., 2008). The specific role of myosin XI and adaptor proteins to support specific cargo binding will be elucidated soon.

Class XI myosins in *A. thaliana* bound their own specific cargos with their tails, as described above. Chara myosin was reported to bind lipid directly (Yamamoto et al., 1994), but it would not work mainly in a cell. The similarity of 3D structural model of the Chara myosin tail to the tail structure of MYA1 and of myo2p, as shown in Fig. 7.4, strongly suggests that Chara myosin has specific binding sites for various cargos, including vacuoles and secretory vesicles.

5. THREE-DIMENSIONAL STRUCTURE OF CHARA MYOSIN

For understanding of the protein function, it is indispensable to obtain information about the atomic structure of the protein at high resolution. X-ray crystallography is a means to meet such requirement. It was a very difficult task to crystallize muscle proteins, actin and myosin. Although actin is a globular protein, it polymerizes into filamentous structure instead of forming crystals. Crystallization of actin was succeeded by preventing actin from polymerization by using the complex of actin and DNase I (Kabsch et al., 1990), actin and profilin (Schutt et al., 1993), or actin and gelsolin (McLaughlin et al., 1993).

Muscle myosin has a unique feature with a long rod and polymerizes into a bipolar filament in the physiological condition. Even a proteolytic fragment of S1, the globular head with the motor activity, did not crystallize so easily. Methylation of almost all lysine and arginine residues in the myosin head resulted in crystallization of the myosin molecule, and X-ray crystallography revealed the atomic structure of the myosin head (Rayment et al., 1993b). Then, atomic structures of myosins associated with various nucleotide analogs or in the nucleotide-free state were analyzed. It was found that the neck bound with light chains would act as a lever arm, since

the lever arm pointed to different angles relative to the head depending on the binding nucleotide analogs (Coureux et al., 2004; Dominguez et al., 1998; Fisher et al., 1995; Houdusse et al., 1999). These results supported the power stroke model (Howard, 1997) for sliding movement between actin and myosin.

Since the sliding velocity of plant myosin of class XI is faster than any other myosins observed so far, it is very interesting to know its atomic structure. Unfortunately, its 3D structure has not been solved yet. The knowledge accumulated so far about atomic structures of various myosins foresee the atomic model of a certain myosin based on its amino acid sequence. We obtained the reliable predicted atomic model of Chara myosin according to its amino acid sequence by using Swiss Model System (Arnold et al., 2006), as shown in Fig. 7.5. This atomic model of Chara myosin, the backbone of which is shown with green color in Fig. 7.5, was constructed based on the structure of chicken myosin Va at the nucleotide-free state (PDB 1oe9) (Coureux et al., 2003), which is shown with yellow color in Fig. 7.5.

Chara myosin has 42% sequence identity to myosin Va (one of the highest). Chara myosin showed considerably high duty ratio (0.49) (Sumiyoshi et al., 2007) similar to the processive motor of myosin Va (Mehta et al., 1999), and motilities of both myosins are not inhibited by cleavage of actin, as described in the previous section. These similarities may be expected to come from the similarity of the 3D structure of the head. We will speculate the structural grounds of unique mechanochemical properties of Chara myosin more specifically in the following sections.

5.1. Interface between actin and myosin in the complex

Chara myosin expressed its distinct properties during interaction with actin. Therefore, in order to investigate the structural bases of such properties, we need structural information about the interface between actin and myosin in the complex. However, the complex of actin and myosin has not been crystallized yet. On the basis of crystal structures of actin and myosin obtained by X-ray crystallography, the models of the rigor complex of F-actin and skeletal myosin were built up by combining the results on the F-actin structure obtained by X-ray diffraction of fiber gels (Holmes et al., 1990) or the data obtained by cryoelectron microscopy of the complex of F-actin and myosin (Rayment et al., 1993a; Schröder et al., 1993).

According to these models, the interface between F-actin and chicken skeletal myosin in the rigor state reported (Milligan, 1996; Rayment et al., 1993a) are summarized in the first and the second columns in Table 7.1. Myosin has contacts with actin in five domains: (1) loop 2, (2) the contact with “90–100 loop” of actin, (3) CM-loop located at the tip portion of upper 50 K of myosin, (4) the domain characterized as hydrophobic

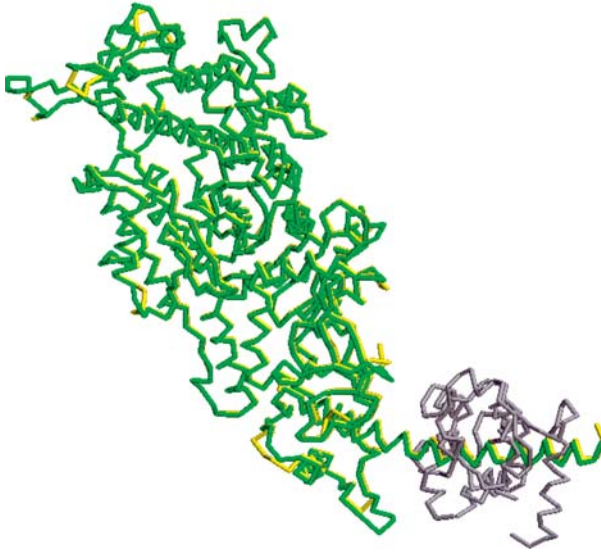


Figure 7.5 The atomic model of Chara myosin. The three-dimensional atomic model of Chara myosin was constructed according to Swiss Model System (Arnold et al., 2006) based on the crystal structure of myosin V at the nucleotide-free state (PDB 1oe9). The backbone of the most probable molecular structure of Chara myosin obtained is shown in color with green and the crystal structure of myosin V (PDB 1oe9) is shown with yellow. The light chain of myosin V is shown in color with gray.

interaction, and (5) the domain interacting with “40–50 (DNase I-binding) loop” of actin which is the adjacent actin monomer next to the barbed end side.

From the sequence homology between skeletal myosin and myosin Va, the corresponding contact domains of myosin V were determined, as shown in the third column in Table 7.1. Likewise, the contact domains of other myosins, *Dictyostelium* myosin II, *Dictyostelium* MyoE (class I myosin), and Chara myosin were determined from the sequence homology as shown in Table 7.1. Loop 2 is the junction between 50 and 20 kDa domain of the myosin head of S1. Loop 2 of skeletal myosin is rich in positively charged lysine residues and this domain is postulated to interact with actin at the N-terminal region in which many negatively charged residues reside. Not only the amino acid sequence but also the length of loop 2 varies from myosin to myosin, as shown in Table 7.1. Loop 2 of myosin V is very long and positively charged, but loop 2 of Chara myosin is extremely short and notably has few charged residues and no net charge. The structure of loop 2 is very interesting to know. The structure of loop 2, however, was mobile in the crystalline state and its atomic structure could not be determined. According to the data shown in Table 7.1, we will investigate the structural bases of the characteristics specific to Chara myosin, in the next section.

Table 7.1 Actin–myosin contact domains in the rigor complex

Myosin contact	Myosin II	Myosin Va	Myosin E (class I)	Dictyo mhca	Chara myosin
Loop 2	F624–T649 (26)	F593–T635 (43)	F547–E561 (15)	F612–T629 (18)	F594–S607 (14)
90–100 loop	K567–H578	K540–A547	S490–C502	E560–E568	K541–A548
Hydrophobic	P529–P543	K502–P516	P452–A466	P522–P536	P504–P518
CM-loop	P404–K415	R378–K389	R323–V338	P396–Q407	R378–K390
40–50 loop	N552–K561	Q525–K534	D475–K483	T545–K554	R527–N535

In the rigor complex, the contact domains between actin and skeletal muscle myosin were reported (Milligan, 1996; Rayment et al., 1993a). Five contact domains are named in the first column and those of skeletal muscle myosin are summarized in the second column with one letter expression of amino acid and its sequence number. The sequences corresponding to respective contact domains of myosin V, which are determined by sequence homology search between skeletal muscle myosin and myosin V, are described in the third column. Similarly, according to the sequence homology, corresponding contact domains of myosin 1E, *Dictyostelium* myosin mhca and of Chara myosin are determined and described in the fourth, fifth, and sixth column, respectively. In the second row, the number in the bracket indicates the number of amino acid residues contained in loop 2, to show the large difference between the lengths of loop 2 of myosin belonging to different classes.

5.2. Structural aspects of interaction between myosin and cleaved actin

The features of the contacts between actin and skeletal myosin, which are summarized in Table 7.1, are depicted in Fig. 7.6A (PDB 1alm). In Fig. 7.6, the predicted atomic model of Chara myosin (green backbone) is superimposed with the atomic model of skeletal myosin (yellow backbone), under the condition that the “hydrophobic” contact (colored with blue) and the “40–50 loop” contact (colored with orange) are exactly superimposed. As a result, the “CM-loop” contact and the “90–100 loop” contact are not able to be imposed at all. The contact “90–100 loop” of skeletal myosin (colored with black) is much longer than that of Chara myosin and its location is totally different from that of Chara myosin (colored with cyan). Moreover, the “90–100 loop” contact domain of skeletal myosin does not seem to be in close vicinity to 90–100 loop of actin. Contrary to this, the “90–100 loop” contact domain of Chara myosin is much closer to 90–100 loop of actin. Particularly, the side chains of Lys543 (blue) and Phe544 (cyan) (for myosin V Arg542 instead of Lys) residues of Chara myosin extend toward 90–100 loop as shown in Fig. 7.6A, and they face Asn92 and Arg95 of actin. This feature suggests the strong interaction between actin and myosin at this location of the “90–100” contact domain in case of Chara myosin, but not in muscle myosin.

Thus, in Chara myosin the “40–50 loop” contact and “90–100 loop” contact domains sandwich the cleavage site of subtilisin in 40–50 loop of actin between Met47 and Gly48 (indicated by an arrow in Fig. 7.6A). This situation in case of Chara myosin will make the actin–myosin interaction strong, and the mechanochemical cycle in interaction between cleaved actin and Chara myosin will advance more smoothly than that between cleaved actin and muscle myosin. This must be the reason why Chara myosin can slide actin filaments at the same speed irrespective of cleavage at 40–50 loop by subtilisin. Cleaved actin, in which pentapeptide from Val43 to Met47 in the loop was removed, retained polymerizability but had no motility (Kiessling et al. 1995). Our idea explains this result reasonably since the pentapeptide removed is exactly the portion of the actin–myosin contact of 40–50 loop, as shown in Fig. 7.6A. This result indicates that without the 40–50 loop contact myosin cannot communicate properly with actin and fails to produce force for movement.

The atomic model of Chara myosin is constructed based on the 3D structure of myosin Va in the nucleotide-free state (PDB 1oe9), which is the best fit structure as far as searched. The structures of myosin V in the ADP binding state, ADPBeFx binding state, and the state of nucleotide-free differ from each other. However, actin contact domains of “hydrophobic” “40–50 loop” and “90–100 loop” domains are exactly superimposed irrespective of nucleotide binding states of myosin. The “40–50 loop” and

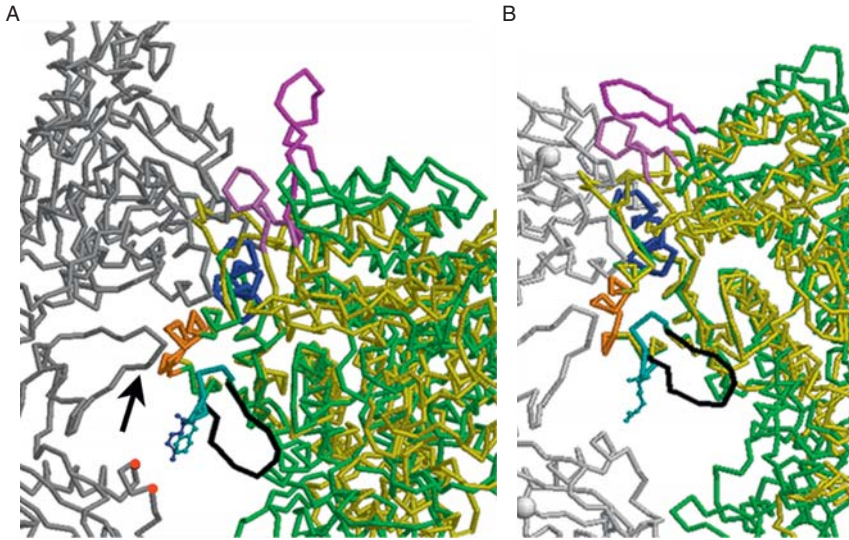


Figure 7.6 Actin–myosin contact domains in the atomic model. (A) Location of 90–100 loop contacts. The backbone of actin, skeletal muscle myosin (nucleotide-free), and Chara myosin (nucleotide-free) molecules are depicted in color with gray, yellow, and green, respectively. Actin–myosin contact domains described in Table 7.1 are shown in different colors: hydrophobic, blue; 40–50 loop, orange; CM-loop, violet for skeletal myosin and magenta for Chara myosin; 90–100 loop, black for skeletal myosin and cyan for Chara myosin. The hydrophobic contact and 40–50 loop domains of skeletal myosin and Chara myosin can be superimposed, exactly. The location of 90–100 loop of skeletal myosin (black) completely differs from that of Chara myosin (cyan). In the contact domain of 90–100 loop of Chara myosin, not only the loop but also the side chains Lys543 (blue) and Phe544 (cyan) extends toward 90–100 loop of actin as shown in the figure. The residues 92Asn and 95Arg of actin are indicated with small red dots. An arrow points to the cleavage site by subtilisin between 47Met and 48Gly of actin. These situations of 90–100 loop contacts may important for understanding the mechanochemical properties of Chara myosin interacting with cleaved actin (see text). The structure of actin and skeletal myosin complex is from PDB 1alm. (B) Change of CM-loop location during chemical cycle. The illustration of actin and myosin molecules is the same as in (A), except that Chara myosin was replaced by myosin V with nucleotide ADP-AlFx (green) (PDB 1w7j), to imitate the prestroke state of Chara myosin. As the structure of nucleotide-free state of Chara myosin is almost exactly the same as that of myosin V as shown in Fig. 7.5, the prestroke state of Chara myosin is assumed to be very similar to that of myosin V. When the hydrophobic and 40–50 loop contacts of the two myosin molecules of skeletal myosin and myosin V are superimposed, location of CM-loop of Chara myosin (myosin V) is clearly shown to be changed during chemical cycle. Closure location of CM-loop of Chara myosin to the actin molecule might cause the inhibition of binding with actin by tropomyosin.

“hydrophobic” domains of chicken skeletal myosin are exactly superimposed not only with those of myosin V but also with those of *Dictyostelium* myosin II, and *Dictyostelium* class I myosin. This fact indicates that these two

contact domains do not change conformation and relative location, and play the key role for communication between actin and myosin during mechanochemical cycle to generate force for movement. Since the 3D structural model of Chara myosin is based on the atomic structure of myosin V at the nucleotide-free state, the same discussion as mentioned above for Chara myosin will be applicable to understand the property of myosin V, that cleavage at 40–50 loop does not affect the sliding velocity of myosin V.

As myosin I also shows the structural feature similar to that of Chara myosin, particularly on the conformation and location of the “40–50 loop” and “90–100 loop” contacts, it is expected for myosin I to slide actin filaments of sub-actin at the speeds very similar to that of intact actin filaments. But there has been no report about motility of cleaved actin on myosin I.

5.3. Structural aspects of tropomyosin effect

Tropomyosin inhibited the actin activated ATPase and motility of Chara myosin completely (Higashi-Fujime et al., 2000). Brush border myosin I was also inhibited by tropomyosin (Fanning et al., 1994; Lieto-Trivedi et al., 2007). As described in the previous section, loop 4 of myosin I is longer than those of other myosins (Fig. 7.1), and this long loop 4 of myosin I may inhibit contact of myosin with actin in the presence of tropomyosin (Lieto-Trivedi et al., 2007). Loop 4 is not usually considered to contact directly to actin, but Chara myosin also has long loop 4, and this might be one of the reasons why Chara myosin is sterically hindered from interaction with actin by tropomyosin.

As addressed in the previous section, CM-loop can be another candidate, which may compete or bump against tropomyosin when myosin binds to actin. To test this idea, atomic models of skeletal myosin and Chara myosin are compared with each other by superimposing their structures in the same way as described in the previous section (Fig. 7.6A and B). The configuration or location of CM-loop of myosin II does not change when the binding substrate changes, that is, binding analogs of ATP or ADP-Pi or even nucleotide-free. CM-loop of myosin V, however, changes its configuration or location greatly when the bound nucleotide changes, because CM-loop is in the tip of the upper 50-K and this domain rotates considerably relative to the lower 50-K domain depending on the binding nucleotide. In consequence, CM-loop of myosin V moves upward and as shown in Fig. 7.6A and B, CM-loop of skeletal myosin (violet) and that of Chara myosin (magenta) are found in different locations. The structural model of Chara myosin is based on the structure of myosin V at the nucleotide-free state. When myosin V binds nucleotide analog ADP-BeFx, CM-loop changes its location as shown in Fig. 7.6B, and the top of CM-loop becomes more vicinity to the surface of the actin filament. If Chara myosin takes the

conformation at the nucleotide binding state very similar to that of myosin V, the CM-loop location may crucially be interfered with binding to actin by tropomyosin.

Myosin I also shows location of CM-loop differing from that of skeletal myosin but similar to those of myosin V and Chara myosin when it binds with actin. Therefore, not only Chara myosin but also myosin I and myosin V will be inhibited by tropomyosin, though there has been no report about inhibition of motility of myosin V by tropomyosin. As described in the previous section, tropomyosin binds with the actin filament on the inner surface of actin subdomains 3 and 4. These locations of tropomyosin are postulated to be the same as that in the open state of the thin filament. However, the structure of the actin filament-bound tropomyosin or native tropomyosin (thin filament) is still elusive.

We have no evidence about the contact of loop 2 with actin, despite the fact that this contact is very important on actin–myosin interaction. Loop 2 of skeletal muscle myosin was protected by binding with actin from proteolytic cleavage. Contrary to this, loop 2 of cardiac myosin was not protected by binding with actin from cleavage by an enzyme (Ajtai et al., 2001). These facts may imply that loop 2 will possibly change its conformation of the actin contact domain dramatically during the mechanochemical cycle. Without precise structural information about loop 2, we may not discuss further the structural aspect of distinct properties of Chara myosin.

6. MECHANISM OF CHARA MYOSIN MOTILITY

In muscle cells, we see the organized crystalline-like structure consisting of actin and myosin filaments in electron micrographs. The smallest repeating unit is a half sarcomer composed of the actin filament and a half of the bipolar filament of myosin II and both filaments slide relatively at $\sim 6 \mu\text{m/s}$ under no load. In a melanocyte, myosin V bearing a cargo moves along an actin filament to transport meranosome to its destination at $\sim 0.5 \mu\text{m/s}$ (Cheney et al., 1993). However, the actin activated ATPase activities of both myosin II and myosin V were very similar, 20 s^{-1} (Toyoshima et al., 1987) and 15 s^{-1} (De La Cruz et al., 1999), respectively. Chara myosin does not polymerize into a filament and is thought to transport vesicles like myosin V, but little is known about its sliding mechanism. The mechanism of myosin V motility has been extensively investigated (Sellers and Veigel, 2006; Vale, 2003). This accumulated knowledge about myosin V will be helpful for us to understand the mechanism of sliding movement of Chara myosin, though the speed of Chara myosin ($30\text{--}60 \mu\text{m/s}$) (Higashi-Fujime et al., 1995) differs by two order from the speed of myosin V.

6.1. Processivity of Chara myosin

Myosin V is a two-headed myosin and a processive molecular motor which is thought to walk along an actin filament (Mehta et al., 1999; Rief et al., 2000; Veigel et al., 2002). To perform this walking, either head should not dissociate from actin before the other head advances its step to the next binding site ahead, otherwise the molecule dissociates from the actin filament and cannot continue movement. To assure this process, ADP release from the actin–myosin–ADP complex must be the rate-limiting step of the actomyosin ATPase cycle, unlike the rate limiting of Pi release in muscle actomyosin. In fact, myosin V was strongly inhibited by ADP (De La Cruz et al., 2000a). In addition, to walk in a long distance by continuing many successive steps more than 10–60 steps (Baker et al., 2004; Sakamoto et al., 2003; Uemura et al., 2004), myosin heads should communicate with each other via strain in the neck and thereby, ADP dissociation from the trailing head was 2–3 times faster and that from the leading head was 50 times slower, than that from single headed myosin (Rosenfeld and Sweeney, 2004).

At very low ATP concentration of $\sim 1 \mu\text{M}$, electron microscopy actually revealed that both heads of a myosin V molecule as well as its one head bound to the actin filament in various features as if they represent some certain shots during walking (Walker et al., 2000).

In the meantime, the walking style of myosin V was verified to be in the hand-over-hand fashion by single molecule observation with the TIRF (total internal reflection fluorescence) microscope (Sakamoto et al., 2005; Snyder et al., 2004; Warshaw et al., 2005; Yieldiz et al., 2003), since advancement of 72 nm steps (double of single step size) was observed when only one head or one CaM light chain of a molecule was fluorescently labeled. Furthermore, it was visualized that ADP release occurred favorably in the trailing head (Sakamoto et al., 2008).

6.1.1. Key factors to determine the specific velocity of myosin

To understand the mechanism of sliding movement, it is important to clarify the factors which determine the sliding velocity. Three factors are essential: (1) the cycle rate of actin activated myosin ATPase, $\nu(\text{ATP})$; (2) the step size, d , which is the displacement of myosin during one chemical cycle produced by rotational movement of the lever arm of the neck; and (3) the duty ratio, f , which is the fraction of duration time at the strong binding state of myosin with actin against the cycle time of chemical reaction (Howard, 1997). The value of the duty ratio, f , can be from 0 to 1. The reciprocal of the duty ratio, $1/f$, is the minimum number of myosin head interacting with an actin filament during one cycle time in order to give rise to continuous sliding movement of an actin filament. Thus, the sliding velocity, V , is calculated as follows:

$$V = v(\text{ATP}) \times d \times \frac{1}{f} \quad (1)$$

For instance, the duty ratio of skeletal myosin is 0.05 (Uyeda et al., 1990), so that 20 heads are required to interact consecutively with an actin filament in a cycle time for continuous sliding. As the myosin head drives the actin filament by one step at each cycle, the lower the duty ratio, the faster the sliding velocity. The step size of skeletal myosin was determined to be 5–15 nm by using the optical tweezers (Molloy et al., 1995; Saito et al., 1994; Veigel et al., 1998), and maximum ATPase activity is $\sim 20 \text{ s}^{-1}$ (Toyoshima et al., 1987). Thus, the velocity is calculated to be $\sim 4 (20 \text{ s}^{-1} \times \sim 10 \text{ nm} \times 1/0.05) \mu\text{m/s}$ and this velocity is very similar to the shortening speed of muscle under no load. In case of myosin V, its duty ratio was close to 1, the ATPase activity was $\sim 15 \text{ s}^{-1}$, and the step size was 35 nm. Then, the velocity is calculated to be $\sim 0.5 \mu\text{m/s}$.

6.1.2. Duty ratio of Chara myosin

The actin activated ATPase and motility of Chara myosin were strongly inhibited by ADP, indicating that the rate-limiting step of actin activated Chara myosin ATPase was ADP release (Sumiyoshi et al., 2007). Therefore, the processivity of Chara myosin is expected to be substantially high. The duty ratio of Chara myosin can be estimated by measuring sliding velocities at various surface density of Chara myosin with the conventional *in vitro* motility assay.

The velocity profile against the surface density of myosin gives a tool to estimate the duty ratio according to the following equation (Howard, 1997):

$$V(\rho) = V_{\max}[1 - (1 - f)^{\rho A}] \quad (2)$$

where ρ is the surface density of myosin, $V(\rho)$ is the sliding velocity at the surface density of ρ , V_{\max} is the maximum sliding velocity. A is the area that an actin filament can interact with myosin, and it is estimated by doubling the approximate distance that a myosin head can reach, and “ f ” is the duty ratio.

Another way to estimate the duty ratio is based on the measurement of the landing rate of actin filaments by varying the surface density of myosin. The duty ratio can be estimated according to the following equation (Hancock and Howard, 1998):

$$L(\rho) = Z(1 - \exp^{-\rho A})^n \quad (3)$$

where $L(\rho)$ is the landing rate as a function of the surface density of myosin of ρ , A is the same definition as in Eq. (2), n is the minimum number of myosin molecules on the surface required for continuous sliding of the actin filament, and then the reciprocal of n is equal to the duty ratio, $n = 1/f$.

The duty ratio of Chara myosin was 0.49 which was the result obtained by analyzing the velocity profile against the surface density, and 0.34 from the landing rate measurement (Sumiyoshi et al., 2007). The landing rate measurement was technically difficult and estimation from the velocity profile was more reliable than that from the landing rate. The duty ratio of 0.49 means considerably high processivity.

Plant myosin class XI in tobacco BY-2 cells, Nt 175-kDa myosin, is postulated to be responsible for cytoplasmic streaming (Shimmen and Yokota, 2004). This myosin slid actin filaments at $7 \mu\text{m/s}$, more than 10-fold faster than the processive motor of myosin V. But by optical trap nanometry, Nt 175-kDa myosin was a processive motor with a step size of 35 nm (Tominaga et al., 2003). The molecular feature of Nt 175-kDa myosin was very similar to that of myosin V in electron micrographs (Tominaga et al., 2003). From the optical trap nanometry, Chara myosin was reported to be nonprocessive (Kimura et al., 2003), but this should be reexamined by using purified myosin. The duty ratio of Chara myosin was reported to be smaller than 0.05 of the duty ratio of muscle myosin or to be <0.3 from kinetic analysis using the Chimeric construct of Chara myosin having an artificial neck (Ito et al., 2007).

Yeast class V myosin, myo2p, and myo4p were nonprocessive motors based on the landing rate measurement (Reck-Peterson et al., 2001). The sliding velocity of myo2p was $2.8 \mu\text{m/s}$ and its duty ratio was 0.2. However, the chimeric construct, consisting of the motor domain of myo4p with the neck and the rod of mouse myosin V, was processive and surprisingly its run length was much longer than that of mouse myosin V at the low ionic strength (Krementsova et al., 2006). The run length of this chimeric myo4p showed dependence on ionic strength. The net charge in loop 2 seems to be important for processivity, since loop 2 binds with the N-terminal acidic domain of actin at the weak binding state (Volkman et al., 2005). This might explain the dependence on the ionic strength for the processivity of chimeric myo4p. It is very interesting to know whether myo4p and myo2p purified from cells, not chimeric myosin, move processively at the low ionic strength.

Intramolecular strain between the lever arms leads both heads to coordinate consecutive stepping via communication between trailing and leading heads (Rosenfeld and Sweeney, 2004). Loop 2 of myosin V is positively charged and this charged loop 2 induces the detached rear head to a new leading site and stabilizes the contact (Volkman et al., 2005). When this net charge was changed by adding or reducing three positively charged residues, the run length changed in parallel with the value of the net change, despite of unchanging the velocity (Hodges et al., 2007).

Loop 2 of myosin V consists of 43 amino acid residues, whereas that of *Chara* myosin is extremely short consisting of only 14 residues and besides it has few charged residues and no net charge. Similarly, Nt 175-kDa myosin has 16 amino acid residues and no net charge in its loop 2. *Chara* myosin was not proved to be a processive motor but showed considerably high duty ratio (Sumiyoshi et al., 2007), and Nt 175-kDa myosin was a processive motor (Tominaga et al., 2003). Myo4p has seven positively charged residues in the loop 2 but no net charge. How can chimeric myo4p and Nt 175-kDa myosin move processively with short loop 2 and no net charge? The determinant of processivity may contain not only the charge in loop 2 but also other factor(s) may contribute, and it must be clarified.

Some accessory protein might assist processivity of *Chara* myosin in a cell, in a way similar to that dynactin increases processivity of dynein (King and Schroer, 2000) and kinesin (Berezuk and Schroer, 2007).

6.2. Step size

Huxley (1957) proposed the sliding theory of muscle contraction and estimated the displacement of the active myosin head in muscle to be ~ 10 nm from the physiological aspects. At present, the step size can be measured by laser trap nanometry. The step size is not merely the stride of double headed myosin, but it has biological significance we will discuss here.

6.2.1. Correlation between the step size and the neck length

As we have described in the previous section, the velocity of sliding between myosin and an actin filament is thought to be determined by three factors, the ATPase cycle rate, the step size, and the duty ratio. From analyses of data obtained by the *in vitro* motility assay, Uyeda obtained the step size to be about 20 nm and the duty ration of 0.05 for muscle myosin (Uyeda et al., 1990). Myosin V having a long neck of ~ 24 nm long consisting of six IQ motifs as a lever arm was confirmed to move processively by stepping with 36 nm step size by optical trap nanometry (Mehta et al., 1999) or by electron microscopy (Walker et al., 2000).

If we obtain constructs of myosin having the same motor domain but different length of the neck, we may certify the lever arm rotation model by the *in vitro* motility assay, because the sliding velocity must be proportional to the neck length. *Dictyostelium* myosins composed of the motor domain of the head having different neck lengths, that is no light chain, one, two (wild type), and three light chains, were constructed. These constructs showed clearly linear relationship between sliding velocity and the neck length (Uyeda et al., 1996). Similar constructs of myosin V with various neck lengths of two, four, six, and eight IQ motifs stepped with a stride proportional to the neck length (Purcell et al., 2002; Sakamoto et al., 2003, 2005).

Thus, the neck length is one of the essential factors to determine the step size. However, lever arm rotation caused by the conformational change in the head varies from myosin to myosin. The step size of rat myosin 1b (Myo1d) was also proportional to the neck length, but much longer than that of *Dictyostelium discoideum* myosin II if compared with myosins having the same neck length (Köhler et al., 2003). The difference of rotational angle of the lever arm (90° of myo1b vs. $\sim 30^\circ$ of *D. discoideum* myosin II) (Ruff et al., 2001) accounted for this difference of the step size. Actually, in the crystal structure of *Dictyostelium* myo IE, the lever arm position at the prepower stroke state extended $\sim 30^\circ$ more than in myosin II, and it located in almost 100° apart from the position at the nucleotide-free state (Kollmar et al., 2002).

6.2.2. Step size of Chara myosin

The step size of Chara myosin was measured with optical trap nanometry to be 19 nm (Kimura et al., 2003). Myosin V having a long neck of six IQ motifs walks processively with a step size of ~ 35 nm (Mehta et al., 1999) and class XI Nt 175-kDa myosin having a long neck of six IQ motifs also walks with a step size of ~ 35 nm (Tominaga et al., 2003). It is quite rational to expect that Chara myosin having a long neck composed of six IQ motifs will advance with a step size of ~ 35 nm.

As described in the previous section about the result of analysis of velocity profile against the myosin density to estimate the duty ratio of Chara myosin, best fit of the experimental data gave the value of 0.077 for the parameter A , which indicated double of the distance that the myosin head could reach (Sumiyoshi et al., 2007). Therefore, the step size is suggested to be approximately the half of this value, that is, $0.038 \mu\text{m} = 38$ nm, very similar to that of myosin V.

The fact that this step size is equal to the length of a half pitch of double stranded helix of an actin filament is very important and has the biological significance for myosin to function in a cell. Chara myosin is postulated to produce force for cytoplasmic streaming by interacting with actin cables connecting chloroplasts arrays and transport vesicles along these actin cables. For vesicle transport high processivity is requisite, because Chara myosin does not polymerize. Myosin cannot play a role for cargo transport if myosin bound with a cargo dissociates from the actin cable at every stepping and diffuses into the cytoplasm. If the step size of processive myosin is much smaller than 36 nm of the half pitch of the actin filament, myosin rotates around an actin filament during movement. Thereby the actin cable will be disrupted, or myosin dissociates from the actin filament after advancement of one or two steps. Thus, the processive motor with the step size of the half pitch of the actin filament will be the necessary condition for Chara myosin to transport cargos along actin cables and produce cytoplasmic streaming.

6.3. Mechanism of fast movement of Chara myosin

Chara myosin is unique for its fast sliding movement ($\sim 60 \mu\text{m/s}$). The mechanism remains to be solved for many years as a puzzle how Chara myosin moves so fast. Cooperation of many myosin molecules like in muscle, that is low duty ratio, seems to give a solution to this question (Uyeda, 1996). According to this idea, the duty ratio was reported to be 0.05 (Awata et al., 2003), and the ATPase activity was measured by using constructs with an artificial neck of α -actinin to be 500 s^{-1} (Ito et al., 2003). By applying these values to Eq. (1), the velocity of Chara myosin can be calculated, but the value is too large to account for the velocity of Chara myosin.

In the streaming endoplasm, there is no organized structure like a myosin filament in muscle and purified Chara myosin does not polymerize. Since the Chara myosin molecule may be bound to some organelles (Morimatsu et al., 2002) and endoplasmic reticulum (ER) (Higashi-Fujime, 1988, 1991) or may be freely floating in the streaming endoplasm, it may not act by cooperating with many myosin molecules like in muscle but individually functioning for vesicle transport and formation of the ER network. So, in a living cell, Chara myosin is functionally expected to have a property of high processivity. Actually, pivot movement was observed on Chara myosin suggesting high processivity (Higashi-Fujime, 2003; Sumiyoshi, et al., 2007). The experimental value of the duty ratio of 0.49 may reflect the real nature of Chara myosin.

According to Eq. (1), the velocity is calculated to be $\sim 2.2 \mu\text{m/s}$ ($57.6 \text{ s}^{-1} \times 19 \text{ nm} \times 1/0.49$) by adopting the step size of 19 nm (Kimura et al., 2003), or $4.2 \mu\text{m/s}$ even if the step size of the expected value 36 nm is adopted (Sumiyoshi et al., 2007). This calculated velocity is yet much slower than the real speed *in vivo*. Purified Chara myosin is so labile that the ATPase activity and its step size measurements should be reexamined. In this case, it must be important to confirm that each myosin head retains light chains fully in the neck without dissociation. As described in the previous section, the sequences of six IQ motifs of Chara myosin do not conform to the standard CaM binding structure. Therefore, Chara myosin has its specific light chains and some of them may probably dissociate from the neck during purification. If this is the case, the Chara myosin neck cannot fully perform the stroke for movement, and the velocity inevitably becomes slower. This would probably be one of the reasons why the velocity of Chara myosin *in vitro* is slower than that *in vivo*.

Tanaka et al. (2002) reported that the myosin V construct with a short neck of one IQ moved processively with a long step size of 36 nm. The authors asserted that a myosin head could slide consecutively on the actin protomers of the actin filament to the proximity of the next binding site of the partner head. The single head of skeletal myosin of S1 was observed to move along an actin filament by several steps with 5.3-nm step size in a single chemical cycle (Kitamura et al., 1999).

Along the microtubule, diffusional movements of motor proteins in a long distance were observed. The microtubule-based motor, dynein, moved in a manner of one-dimensional diffusion along a microtubule at the weak binding state of the complex of microtubule, dynein and ADP-VO₄ of an analog of ADP-Pi (Vale et al., 1989). A microtubule bound to a single dynein molecule on the glass surface moved back and forth more than 1 μm long by thermal diffusion. Another microtubule-based motor protein kinesin also showed diffusional movement along microtubule (Helenius, et al., 2006; Okada and Hirokawa, 1999). Amazingly, actin-based motor protein myosin V bound with microtubule and exhibited diffusional movement on microtubule without consuming ATP hydrolysis energy (Ali et al., 2007; Ross et al., 2008). Fluorescently labeled myosin Va could be observed to move back and forth in a few micrometers long on microtubule for ~ 50 s before dissociation. The speed of this diffusional movement was 5.3 $\mu\text{m/s}$, almost one order faster than the speed of active movement.

This finding by Ali et al. (2007) gave a clear image to the scenario about the way how myosin V searches kinesin-bound cargo. Vesicles are transported by kinesin along microtubule from the cell center to near the cell periphery, where actin meshworks reside and kinesin has to hand the cargo to myosin V (Ali et al., 2008; Hammer and Wu, 2007). Myosin V diffusing on microtubules can meet the cargos at a probability much higher than that to meet them by diffusing in the 3D space. Electrostatic interaction between microtubule and myosin V seemed to play an important role in this diffusional motion, because on a microtubule consisting of tubulin lacking its E-hook myosin V did not exhibit such thermal motion (Ali et al., 2007). It is very interesting to know whether any other myosin can slide on microtubule-like myosin V. These diffusional sliding movements on microtubule or on the actin filament may be important nature of the biological motor protein.

6.4. Functional states of Chara myosin in the cell

Some of plant myosins will certainly participate in cargo transport and ER network formation. In the cytoplasm extracted from *Chara* cells, small vesicles move on the muscle actin filaments added (Morimatsu et al., 2002). In a Characean cell, small vesicles moved along actin cables at the same speed of endoplasmic streaming, but active movement of tiny vesicles would not be enough to produce streaming of the entire endoplasm. The hydrodynamic model suggested that viscous coupling between ER network in the cytoplasm and myosin would drive streaming (Nothnagel and Webb, 1982). Actually, in the crude extract, the network of ER was observable to change the network pattern vividly by forming projections and their elongation on the glass surface under a dark-field microscope, when F-actin was added (Higashi-Fujime, 1988, 1991). In the droplet of the endoplasm squeezed out of the cell, rings composed of bundles of actin filaments

rotated vigorously and repeated formation and destruction, indicating that the actin concentration was high and F-actin meshwork was formed in the endoplasmic droplet. Therefore, this actin network may participate in viscous coupling together with the ER network for producing streaming of the entire endoplasm.

The myosin concentration was estimated to be $\sim 0.2 \mu\text{M}$ in the endoplasm (Yamamoto et al., 2006). Myosin producing directional force for streaming is only myosin molecules interacting with cortical fibrils of actin cables. Rest of a majority of Chara myosin molecules in the endoplasm should stay in the inhibited form. If myosin molecules are all fully active, ATP in the cytoplasm will be exhausted in several minutes, because as mentioned above the actin concentration must be high in the endoplasm. Myosin V takes the inhibited form of the triangular shape that the globular tail binds to the head of the motor domain (Taylor, 2007), but such inhibited form has not been found for Chara myosin.

Protein phosphorylation was the regulatory mechanism of Chara myosin (Morimatsu et al., 2002). In *Xenopus* egg extract, $\text{Ca}^{2+}/\text{CaM}$ -dependent protein kinase phosphorylated Myosin V at the tail region and phosphorylated myosin V dissociated from its bearing cargo (Karcher et al., 2001). In Characean cells, $\text{Ca}^{2+}/\text{CaM}$ -dependent kinase was associated with the actin cable (McCurdy and Harmon, 1992). If the similar downregulation mechanism of myosin V in the *Xenopus* oocytes works in Characean cells, $\text{Ca}^{2+}/\text{CaM}$ -dependent kinase is activated by Ca^{2+} which enters into the cell due to the external stimulus and then phosphorylates Chara myosin. Phosphorylated Chara myosin will dissociate vesicles and ER, and at the same time its activity must be inhibited (Morimatsu et al., 2002). This will result in cessation of cytoplasmic streaming. The cell may, however, have another strategy to keep Chara myosin in the inhibited state in the endoplasm in order to pool myosin in reserve.

There were some reports that myosin V was activated by phosphorylation. For instance, in adipocytes, myosin Va was activated by phosphorylation by Akt2 and facilitated GLUT vesicles translocation (Yoshizaki et al., 2007). In mitotic *Xenopus* oocyte extract myosin V was phosphorylated and activated network formation of ER in an F-actin-dependent manner (Wollert et al., 2002). There is no evidence for activation of Chara myosin by phosphorylation, but Chara myosin may be regulated in many ways by coordinating with various cellular activities.

7. CONCLUDING REMARKS

The mechanism of fast sliding of Chara myosin remains to be a puzzle, yet. The step size of 38 nm and the duty ratio of 0.49 were obtained from the analyses of sliding phenomena with *in vitro* motility assay

(Sumiyoshi et al., 2007). The actin activated ATPase activity of 57 s^{-1} (Sumiyoshi et al., 2007) resulted in the calculated sliding velocity slower than the real speed of Chara myosin. Chara myosin did not polymerize into filaments, and it transported vesicles (Morimatsu et al., 2002) and elongated ER in F-actin-dependent manner (Higashi-Fujime, 1991). As discussed previously according to the biological view point, Chara myosin is expected to be a processive motor walking by the step size of a half pitch of the actin filament along the cable.

Myosin with the duty ratio of 0.5 can be estimated to walk 3.4 steps on average (Veigel et al., 2002). Single myosin V molecule could walk along F-actin by $2.4 \mu\text{m}$ long (Sakamoto et al., 2000) which corresponded to successive 70 steps on average. From this result myosin V was calculated to have the duty ratio of ~ 0.9 (Veigel et al., 2002). Under the physiological condition in a living cell, Chara myosin might be expected to increase processivity by binding with a certain regulatory protein such that dynactin increases processivity of dynein (King and Schroer, 2000) and also increases processivity of kinesin (Berezuk and Schroer, 2007).

Loop 2 plays an important role in actin–myosin interaction. But not only its length but also the net charge in loop 2 greatly varies from myosin to myosin. The net charge in loop 2 might be a determinant of run length of processive movement in case of myosin V. Loop 2 of plant myosin including Chara myosin, however, is extremely short and has no net charge as shown in Table 7.1. How is loop 2 reacting with actin during actin–myosin interaction? This mechanism must be a difficult problem to be solved, but its solution is important for understanding the specific way of interaction between individual myosin and actin.

In general, sliding speed and actin activated ATPase activity of plant myosins are very high compared with those of animal myosins: Nt 175-kDa myosin, $7.7 \mu\text{m/s}$ and 76 s^{-1} (Tominaga et al., 2003); Chara myosin, $30\text{--}60 \mu\text{m/s}$ and 57 s^{-1} (Sumiyoshi et al., 2007). The ATPase activity of Chara myosin might be estimated lower than the real value, because some molecules may be damaged by endogenous protease(s) or lose one or some of the light chains by dissociation from the neck. Because sequences of IQ motifs of Chara myosin are very unique as described, the light chains of Chara myosin must be highly specific for each IQ sequence and inevitably the light chain(s) might dissociate during purification of myosin unless it has the extremely high affinity.

Chara myosin constructs with an artificial neck of α -actinin repeats and myosin V neck exhibited very high ATPase activity of 500 s^{-1} (Ito et al., 2003) and 390 s^{-1} (Ito et al., 2007), respectively. But constructs of myosin V having light chains from other kind of myosin changed its biochemical characteristics substantially (De La Cruz et al., 2000b). When the loop 2 sequence was substituted with that of other myosin, the actin activated ATPase activity does not necessarily change in parallel with its motility

(Uyeda et al., 1994). As it is very difficult to purify Chara myosin from the living cells, we will need recombinant Chara myosin for further investigation to elucidate the mechanism of the fast sliding movement, but it has to be the authentic myosin. To do so, knowledge about the light chains of Chara myosin is indispensable. At present, we have only two plant myosins purified from living cells and investigated extensively. The studies on Chara myosin and Nt 175-kDa myosin will progress in future and give us information indispensable to understand the properties of other plant myosins.

Under the situation that we have very limited information about Chara myosin, we have shown that the comparative investigation of Chara myosin with other myosin, such as myosin V and myosin I, is very important to extend our basic knowledge on its mechanochemical and functional aspects. In this review, we have also performed a lot about molecular modeling and target searching by using Swiss Model System and fitting search together with databases. As a result, we have been able to foresee some features of structure and function of Chara myosin and understand more about the mechanism of its mechanochemical properties from the results obtained.

ACKNOWLEDGMENTS

The authors express their thanks to Dr. Oosawa in Aichi Institute of Technology for his encouragement and suggestions. They also thank Dr. Kohama and Dr. Yoshiyama in Gunma University for their encouragement and technical support, respectively.

REFERENCES

- Ajtai, K., Garamszegi, S.P., Park, S., Velazquez Dones, A.L., Burghardt, T.P., 2001. Structural characterization of beta-cardiac myosin subfragment 1 in solution. *Biochemistry* 40, 12078–12093.
- Albanesi, J.P., Hammer III, J.A., Korn, E.D., 1983. The interaction of F-actin with phosphorylated and unphosphorylated myosins IA and IB from *Acanthamoeba castellanii*. *J. Biol. Chem.* 258, 10176–10181.
- Albanesi, J.P., Fujisaki, H., Korn, E.D., 1984. Localization of the active site and phosphorylation site of *Acanthamoeba* myosins IA and IB. *J. Biol. Chem.* 259, 14184–14189.
- Ali, M.Y., Kremntsova, E.B., Kennedy, G.G., Mahaffy, R., Pollard, T.D., Trybus, K.M., et al., 2007. Myosin Va maneuvers through actin intersections and diffuses along microtubules. *Proc. Natl. Acad. Sci. USA* 104, 4332–4336.
- Ali, M.Y., Lu, H., Bookwalter, C.S., Warshaw, D.M., Trybus, K.M., 2008. Myosin V and kinesin act as tethers to enhance each others' processivity. *Proc. Natl. Acad. Sci. USA* 105, 4691–4696.
- Arnold, K., Bordoli, L., Kopp, J., Schwede, T., 2006. The SWISS-MODEL Workspace: a web-based environment for protein structure homology modelling. *Bioinformatics* 22, 195–201.
- Awata, J.Y., Kashiyama, T., Ito, K., Yamamoto, K., 2003. Some motile properties of fast characean myosin. *J. Mol. Biol.* 326, 659–663.

- Bähler, M., Rhoads, A., 2002. Calmodulin signaling via the IQ motif. *FEBS Lett.* 513, 107–113.
- Baker, J.E., Krementsova, E.B., Kennedy, G.G., Armstrong, A., Trybus, K.M., Warsaw, D.M., 2004. Myosin V processivity: multiple kinetic pathways for head-to-head coordination. *Proc. Natl. Acad. Sci. USA* 101, 5542–5546.
- Bement, W.M., Mooseker, M.S., 1995. TEDS rule: a molecular rationale for differential regulation of myosins by phosphorylation of the heavy chain head. *Cell Motil. Cytoskeleton* 31, 87–92.
- Berezuk, M.A., Schroer, T.A., 2007. Dynactin enhances the processivity of kinesin-2. *Traffic* 8, 124–129.
- Brown, J.H., Zhou, Z., Reshetnikova, L., Robinson, H., Yammani, R.D., Tobacman, L.S., et al., 2005. Structure of the mid-region of tropomyosin: bending and binding sites for actin. *Proc. Natl. Acad. Sci. USA* 102, 18878–18883.
- Chen, J.C.W., Kamiya, N., 1975. Localization of myosin in the intermodal cell of *Nitella* as suggested by differential treatment with *N*-ethylmaleimide. *Cell Struct. Funct.* 1, 1–9.
- Cheney, R.E., O’Shea, M.K., Heuser, J.E., Coelho, M.V., Wolenski, J.S., Espreafico, E.M., et al., 1993. Brain myosin-V is a two-headed unconventional myosin with motor activity. *Cell* 75, 13–23.
- Chou, P.Y., Fasman, G.D., 1978. Prediction of the secondary structure of proteins from their amino acid sequence. *Adv. Enzymol. Relat. Areas Mol. Biol.* 47, 145–148.
- Collins, K., Sellers, J.R., Matsudaira, P., 1990. Calmodulin dissociation regulates brush border myosin I (110-kd-calmodulin) mechanochemical activity *in vitro*. *J. Cell Biol.* 110, 1137–1147.
- Coureux, P.D., Wells, A.L., Menetrey, J., Yengo, C.M., Morris, C.A., Sweeney, H.L., et al., 2003. A structural state of the myosin V motor without bound nucleotide. *Nature* 425, 419–423.
- Coureux, P.D., Sweeney, H.L., Houdusse, A., 2004. Three myosin V structures delineate essential features of chemo-mechanical transduction. *EMBO J.* 23, 4527–4537.
- Craig, R., Lehman, W., 2001. Crossbridge and tropomyosin positions observed in native, interacting thick and thin filaments. *J. Mol. Biol.* 311, 1027–1036.
- De La Cruz, E.M., Wells, A.L., Rosenfeld, S.S., Ostap, E.M., Sweeney, H.L., 1999. The kinetic mechanism of myosin V. *Proc. Natl. Acad. Sci. USA* 96, 13726–13731.
- De La Cruz, E.M., Wells, A.L., Sweeney, H.L., Ostap, E.M., 2000a. Actin and light chain isoform dependence of myosin V kinetics. *Biochemistry* 39, 14196–14202.
- De La Cruz, E.M., Sweeney, H.L., Ostap, E.M., 2000b. ADP inhibition of myosin V ATPase activity. *Biophys. J.* 79, 1524–1529.
- Doberstein, S.K., Pollard, T.D., 1992. Localization and specificity of the phospholipid and actin binding sites on the tail of *Acanthamoeba* myosin IC. *J. Cell Biol.* 117, 1241–1249.
- Dominguez, R., Freyzon, Y., Trybus, K.M., Cohen, C., 1998. Crystal structure of a vertebrate smooth muscle myosin motor domain and its complex with the essential light chain: visualization of the pre-power stroke state. *Cell* 94, 559–571.
- Ebashi, S., 1991. Excitation-contraction coupling and the mechanism of muscle contraction. *Annu. Rev. Physiol.* 53, 1–16.
- Ebashi, S., Endo, M., 1968. Calcium ion and muscle contraction. *Prog. Biophys. Mol. Biol.* 18, 123–183.
- Espindola, F.S., Suter, D.M., Partata, L.B., Cao, T., Wolenski, J.S., Cheney, R.E., et al., 2000. The light chain composition of chicken brain myosin-Va: calmodulin, myosin-II essential light chains, and 8-kda dynein light chain/PIN. *Cell Motil. Cytoskeleton* 47, 269–281.
- Fanning, A.S., Wolenski, J.S., Mooseker, M.S., Izant, J.G., 1994. Differential regulation of skeletal muscle myosin-II and brush border myosin-I enzymology and mechanochemistry by bacterially produced tropomyosin isoforms. *Cell Motil. Cytoskeleton* 29, 29–45.

- Fisher, A.J., Smith, C.A., Thoden, J.B., Smith, R., Sutoh, K., Holden, H.M., et al., 1995. X-ray structures of the myosin motor domain of *Dictyostelium discoideum* complexed with mgadp.befx and mgadp.alf4-. *Biochemistry* 34, 8960–8972.
- Foth, B.J., Goedecke, M.C., Soldati, D., 2006. New insights into myosin evolution and classification. *Proc. Natl. Acad. Sci. USA* 103, 3681–3686.
- Fujita-Becker, S., Dürrwang, U., Erent, M., Clark, R.J., Geeves, M.A., Manstein, D.J., 2005. Changes in Mg²⁺ ion concentration and heavy chain phosphorylation regulate the motor activity of a class I myosin. *J. Biol. Chem.* 280, 6064–6071.
- Fukuda, M., Kuroda, T.S., Mikoshiba, K., 2002. Slac2-a/melanophilin, the missing link between Rab27 and myosin Va: implications of a tripartite protein complex for melanosome transport. *J. Biol. Chem.* 277, 12432–12436.
- Goodson, H.V., Dawson, S.C., 2006. Multiplying myosins. *Proc. Natl. Acad. Sci. USA* 103, 3498–3499.
- Hackney, D.D., Stock, M.F., 2000. Kinesin's IAK tail domain inhibits initial microtubule-stimulated ADP release. *Nat. Cell Biol.* 2, 257–260.
- Hammer III, J.A., Wu, X., 2007. Slip sliding away with myosin V. *Proc. Natl. Acad. Sci. USA* 104, 5255–5256.
- Hancock, W.O., Howard, J., 1998. Processivity of the motor protein kinesin requires two heads. *J. Cell Biol.* 140, 1395–1405.
- Haselgrove, J.C., 1972. X-ray evidence for a conformational change in the actin-containing filaments of vertebrate striated muscle. *Cold Spring Harb. Symp. Quant. Biol.* 37, 341–352.
- Hashimoto, K., Igarashi, H., Mano, S., Nishimura, M., Shimmen, T., Yokota, E., 2005. Peroxisomal localization of a myosin XI isoform in *Arabidopsis thaliana*. *Plant Cell Physiol.* 46, 782–789.
- Hashimoto, K., Igarashi, H., Mano, S., Takenaka, C., Shiina, T., Yamaguchi, M., et al., 2008. An isoform of *Arabidopsis* myosin XI interacts with small gtpases in its C-terminal tail region. *J. Exp. Bot.* 59, 3523–3531.
- Hatano, S., Oosawa, F., 1966. Isolation and characterization of plasmodium actin. *Biochim. Biophys. Acta* 127, 488–498.
- Hatano, S., Tazawa, M., 1968. Isolation, purification and characterization of myosin B from myxomycete plasmodium. *Biochim. Biophys. Acta* 154, 507–519.
- Helenius, J., Brouhard, G., Kalaidzidis, Y., Diez, S., Howard, J., 2006. The depolymerizing kinesin MCAK uses lattice diffusion to rapidly target microtubule ends. *Nature* 441, 115–119.
- Higashi-Fujime, S., 1980. Active movement *in vitro* of bundle of microfilaments isolated from *Nitella* cell. *J. Cell Biol.* 87, 569–578.
- Higashi-Fujime, S., 1982. Active movement of bundles of actin and myosin filaments from muscle: a simple model for cell motility. *Cold Spring Harb. Symp. Quant. Biol.* 46 (Pt. 1), 69–75.
- Higashi-Fujime, S., 1985. Unidirectional sliding of myosin filaments along the bundle of F-actin filaments spontaneously formed during superprecipitation. *J. Cell Biol.* 101, 2335–2344.
- Higashi-Fujime, S., 1988. Actin-induced elongation of fibers composed of cytoplasmic membrane from *Nitella*. *Protoplasma* (Suppl. 2), 27–36.
- Higashi-Fujime, S., 1991. Reconstitution of active movement *in vitro* based on the actin-myosin interaction. *Int. Rev. Cytol.* 125, 95–138.
- Higashi-Fujime, S., 2003. The fastest myosin from green algae *Chara corallina*: its sliding mechanism. *Recent Res. Dev. Biophys. Biochem.* 3, 801–814.
- Higashi-Fujime, S., Hozumi, T., 1997. Restoration of defective mechanochemical properties of cleaved actins by native tropomyosin: involvement of the 40–50 loop in subdomain 2 of actin in interaction with myosin and tropomyosin. *Biochem. Biophys. Res. Commun.* 237, 121–125.

- Higashi-Fujime, S., Suzuki, M., Titani, K., Hozumi, T., 1992. Muscle actin cleaved by proteinase K: its polymerization and *in vitro* motility. *J. Biochem. (Tokyo)* 112, 568–572.
- Higashi-Fujime, S., Ishikawa, R., Iwasawa, H., Kagami, O., Kurimoto, E., Kohama, K., et al., 1995. The fastest actin-based motor protein from the green algae, Chara, and its distinct mode of interaction with actin. *FEBS Lett.* 375, 151–154.
- Higashi-Fujime, S., Morimatsu, M., Hirakawa, N., 2000. Inhibitory effect of tropomyosin on Chara myosin motility. *Proc. Jpn. Acad.* 76 (Ser. B), 118–122.
- Hodges, A.R., Kremontsova, E.B., Trybus, K.M., 2007. Engineering the processive run length of Myosin V. *J. Biol. Chem.* 282, 27192–27197.
- Holmes, K.C., Popp, D., Gebhard, W., Kabsch, W., 1990. Atomic model of the actin filament. *Nature* 347, 44–49.
- Holthauzen, L.M., Corrêa, F., Farah, C.S., 2004. Ca²⁺-induced rolling of tropomyosin in muscle thin filaments: the alpha- and beta-band hypothesis revisited. *J. Biol. Chem.* 279, 15204–15213.
- Homma, K., Saito, J., Ikebe, R., Ikebe, M., 2000. Ca(2+)-dependent regulation of the motor activity of myosin V. *J. Biol. Chem.* 275, 34766–34771.
- Houdusse, A., Kalabokis, V.N., Himmel, D., Szent-Györgyi, A.G., Cohen, C., 1999. Atomic structure of scallop myosin subfragment S1 complexed with mgadp: a novel conformation of the myosin head. *Cell* 97, 459–470.
- Howard, J., 1997. Molecular motors: structural adaptations to cellular functions. *Nature* 389, 561–567.
- Hume, A.N., Ushakov, D.S., Tarafder, A.K., Ferenczi, M.A., Seabra, M.C., 2007. Rab27a and myoVa are the primary Mlph interactors regulating melanosome transport in melanocytes. *J. Cell Sci.* 120, 3111–3122.
- Huxley, A.F., 1957. Muscle structure and theories of contraction. *Prog. Biophys. Biophys. Chem.* 7, 255–318.
- Huxley, H.E., 1972. Structural changes in the actin- and myosin-containing filaments during contraction. *Cold Spring Harb. Symp. Quant. Biol.* 37, 361–376.
- Huxley, A.F., Niedergerke, R., 1954. Structural changes in muscle during contraction; Interference microscopy of living muscle fibres. *Nature* 173, 971–973.
- Ishikawa, K., Catlett, N.L., Novak, J.L., Tang, F., Nau, J.J., Weisman, L.S., 2003. Identification of an organelle-specific myosin V receptor. *J. Cell Biol.* 160, 887–897.
- Ito, K., Kashiyama, T., Shimada, K., Yamaguchi, A., Awata, J., Hachikubo, Y., et al., 2003. Recombinant motor domain constructs of *Chara corallina* myosin display fast motility and high atpase activity. *Biochem. Biophys. Res. Commun.* 312, 958–964.
- Ito, K., Ikebe, M., Kashiyama, T., Mogami, T., Kon, T., Yamamoto, K., 2007. Kinetic mechanism of the fastest motor protein, Chara myosin. *J. Biol. Chem.* 282, 19534–19545.
- Jacobson, G.R., Rosenbusch, J.P., 1976. ATP binding to a protease-resistant core of actin. *Proc. Natl. Acad. Sci. USA* 73, 2742–2746.
- Jedd, G., Chua, N.H., 2002. Visualization of peroxisomes in living plant cells reveals actomyosin-dependent cytoplasmic streaming and peroxisome budding. *Plant Cell Physiol.* 43, 384–392.
- Kabsch, W., Mannherz, H.G., Suck, D., Pai, E.F., Holmes, K.C., 1990. Atomic structure of the actin:DNase I complex. *Nature* 347, 37–44.
- Kachar, B., 1985. Direct visualization of organelle movement along actin filaments dissociated from characean algae. *Science* 227, 1355–1357.
- Kamiya, N., 1981. Physical and chemical basis of cytoplasmic streaming. *Ann. Rev. Plant Physiol.* 32, 201–236.
- Kamiya, N., Kuroda, K., 1956. Velocity distribution of the protoplasmic streaming in *Nitella* cells. *Bot. Mag. (Tokyo)* 69, 544–554.

- Karcher, R.L., Roland, J.T., Zappacosta, F., Huddleston, M.J., Annan, R.S., Carr, S.A., et al., 2001. Cell cycle regulation of myosin-V by calcium/calmodulin-dependent protein kinase II. *Science* 293, 1317–1320.
- Kashiyama, T., Kimura, N., Mimura, T., Yamamoto, K., 2000. Cloning and characterization of a myosin from characean alga, the fastest motor protein in the world. *J. Biochem. (Tokyo)* 127, 1065–1070.
- Kashiyama, T., Ito, K., Yamamoto, K., 2001. Functional expression of a chimeric myosin-containing motor domain of Chara myosin and neck and tail domains of *Dictyostelium* myosin II. *J. Mol. Biol.* 311, 461–466.
- Kersey, Y.M., Hepler, P.K., Palevitz, B.A., Wessells, N.K., 1976. Polarity of actin filaments in Characean algae. *Proc. Natl. Acad. Sci. USA* 73, 165–167.
- Kiessling, P., Jahn, W., Maier, G., Polzar, B., Mannherz, H.G., 1995. Purification and characterization of subtilisin cleaved actin lacking the segment of residues 43–47 in the dnase I binding loop. *Biochemistry* 34, 14834–14842.
- Kimura, Y., Toyoshima, N., Hirakawa, N., Okamoto, K., Ishijima, A., 2003. A kinetic mechanism for the fast movement of Chara myosin. *J. Mol. Biol.* 328, 939–950.
- King, S.J., Schroer, T.A., 2000. Dynactin increases the processivity of the cytoplasmic dynein motor. *Nat. Cell Biol.* 2, 20–24.
- Kinkema, M., Schiefelbein, J., 1994. A myosin from a higher plant has structural similarities to class V myosins. *J. Mol. Biol.* 239, 591–597.
- Kitamura, K., Tokunaga, M., Iwane, A.H., Yanagida, T., 1999. A single myosin head moves along an actin filament with regular steps of 5.3 nanometres. *Nature* 397, 129–134.
- Knight, A.E., Kendrick-Jones, J., 1993. A myosin-like protein from a higher plant. *J. Mol. Biol.* 231, 148–154.
- Kohama, K., Kendrick-Jones, J., 1986. The inhibitory Ca^{2+} -regulation of the actin-activated Mg-atpase activity of myosin from *Physarum polycephalum* plasmodia. *J. Biochem. (Tokyo)* 99, 1433–1446.
- Köhler, D., Ruff, C., Meyhöfer, E., Bähler, M., 2003. Different degrees of lever arm rotation control myosin step size. *J. Cell Biol.* 161, 237–241.
- Kohno, T., Ishikawa, R., Nagata, T., Kohama, K., Shimmen, T., 1992. Partial purification of myosin from lily pollen tubes by monitoring with *in vitro* motility assay. *Protoplasma* 170, 77–85.
- Koide, H., Kinoshita, T., Tanaka, Y., Tanaka, S., Nagura, N., Meyer zu Hörste, G., et al., 2006. Identification of the single specific IQ motif of myosin V from which calmodulin dissociates in the presence of Ca^{2+} . *Biochemistry* 45, 11598–11604.
- Kollmar, M., Dürrwang, U., Kliche, W., Manstein, D.J., Kull, F.J., 2002. Crystal structure of the motor domain of a class-I myosin. *EMBO J.* 21, 2517–2525.
- Konno, K., 1987. Functional, chymotryptically split actin and its interaction with myosin subfragment 1. *Biochemistry* 26, 3582–3589.
- Krementsov, D.N., Kremntsova, E.B., Trybus, K.M., 2004. Myosin V: regulation by calcium, calmodulin, and the tail domain. *J. Cell Biol.* 164, 877–886.
- Kremntsova, E.B., Hodges, A.R., Lu, H., Trybus, K.M., 2006. Processivity of chimeric class V myosins. *J. Biol. Chem.* 281, 6079–6086.
- Kron, S.J., Spudich, J.A., 1986. Fluorescent actin filaments move on myosin fixed to a glass surface. *Proc. Natl. Acad. Sci. USA* 83, 6272–6276.
- Kuroda, K., 1990. Cytoplasmic streaming in plant cells. *Int. Rev. Cytol.* 121, 267–307.
- Lee, W.L., Ostap, E.M., Zot, H.G., Pollard, T.D., 1999. Organization and ligand binding properties of the tail of *Acanthamoeba* myosin-IA. Identification of an actin-binding site in the basic (tail homology-1) domain. *J. Biol. Chem.* 274, 35159–35171.
- Lees-Miller, J.P., Helfman, D.M., 1991. The molecular basis for tropomyosin isoform diversity. *Bioessay* 13, 429–437.

- Li, J.F., Nebenführ, A., 2007. Organelle targeting of myosin XI is mediated by two globular tail subdomains with separate cargo binding sites. *J. Biol. Chem.* 282, 20593–20602.
- Li, J.F., Nebenführ, A., 2008. Inter-dependence of dimerization and organelle binding in myosin XI. *Plant J.* 55, 478–490.
- Li, X.D., Mabuchi, K., Ikebe, R., Ikebe, M., 2004. Ca^{2+} -induced activation of atpase activity of myosin Va is accompanied with a large conformational change. *Biochem. Biophys. Res. Commun.* 315, 538–545.
- Li, X.D., Jung, H.S., Mabuchi, K., Craig, R., Ikebe, M., 2006. The globular tail domain of myosin Va functions as an inhibitor of the myosin Va motor. *J. Biol. Chem.* 281, 21789–21798.
- Lieto-Trivedi, A., Dash, S., Coluccio, L.M., 2007. Myosin surface loop 4 modulates inhibition of actomyosin 1b atpase activity by tropomyosin. *Biochemistry* 46, 2779–2786.
- Liu, J., Taylor, D.W., Kremntsova, E.B., Trybus, K.M., Taylor, K.A., 2006. Three-dimensional structure of the myosin V inhibited state by cryoelectron tomography. *Nature* 442, 208–211.
- Martin, S.R., Bayley, P.M., 2004. Calmodulin bridging of IQ motifs in myosin-V. *FEBS Lett.* 567, 166–170.
- McConnell, R.E., Tyska, M.J., 2007. Myosin-1a powers the sliding of apical membrane along microvillar actin bundles. *J. Cell Biol.* 177, 671–681.
- McCurdy, D.W., Harmon, A.C., 1992. Calcium-dependent protein kinase in the green alga *Chara*. *Planta* 188, 54–61.
- McKillop, D.F., Geeves, M.A., 1993. Regulation of the interaction between actin and myosin subfragment 1: evidence for three states of the thin filament. *Biophys. J.* 65, 693–701.
- McLaughlin, P.J., Gooch, J.T., Mannherz, H.G., Weeds, A.G., 1993. Structure of gelsolin segment 1-actin complex and the mechanism of filament severing. *Nature* 364, 685–692.
- Mehta, A.D., Rock, R.S., Rief, M., Spudich, J.A., Mooseker, M.S., Cheney, R.E., 1999. Myosin-V is a processive actin-based motor. *Nature* 400, 590–593.
- Miller, D.D., Scordilis, S.P., Hepler, P.K., 1995. Identification and localization of three classes of myosins in pollen tubes of *Lilium longiflorum* and *Nicotiana glauca*. *J. Cell Sci.* 108, 2549–2563.
- Milligan, R.A., 1996. Protein-protein interactions in the rigor actomyosin complex. *Proc. Natl. Acad. Sci. USA* 93, 21–26.
- Molloy, J.E., Burns, J.E., Sparrow, J.C., Tregear, R.T., Kendrick-Jones, J., White, D.C., 1995. Single-molecule mechanics of heavy meromyosin and S1 interacting with rabbit or *Drosophila* actins using optical tweezers. *Biophys. J.* 68, 298S–303S; 303S–305S.
- Morimatsu, M., Nakamura, A., Sumiyoshi, H., Sakaba, N., Taniguchi, H., Kohama, K., et al., 2000. The molecular structure of the fastest myosin from green algae, *Chara*. *Biochem. Biophys. Res. Commun.* 270, 147–152.
- Morimatsu, M., Hasegawa, S., Higashi-Fujime, S., 2002. Protein phosphorylation regulates actomyosin-driven vesicle movement in cell extracts isolated from the green algae, *Chara corallina*. *Cell Motil. Cytoskeleton* 53, 66–76.
- Momet, D., Ue, K., 1984. Proteolysis and structure of skeletal muscle actin. *Proc. Natl. Acad. Sci. USA* 81, 3680–3684.
- Nagai, R., Hayama, T., 1979. Ultrastructure of the endoplasmic factor responsible for cytoplasmic streaming in *Chara* internodal cells. *J. Cell Sci.* 36, 121–136.
- Nakamura, A., Kohama, K., 1999. Calcium regulation of the actin-myosin interaction of *Physarum polycephalum*. *Int. Rev. Cytol.* 191, 53–98.
- Nascimento, A.A., Cheney, R.E., Tauhata, S.B., Larson, R.E., Mooseker, M.S., 1996. Enzymatic characterization and functional domain mapping of brain myosin-V. *J. Biol. Chem.* 271, 17561–17569.

- Nguyen, H., Higuchi, H., 2005. Motility of myosin V regulated by the dissociation of single calmodulin. *Nat. Struct. Mol. Biol.* 12, 127–132.
- Nothnagel, E.A., Webb, W.W., 1982. Hydrodynamic models of viscous coupling between motile myosin and endoplasm in characean algae. *J. Cell Biol.* 94, 444–454.
- Okada, Y., Hirokawa, N., 1999. A processive single-headed motor: kinesin superfamily protein KIF1A. *Science* 283, 1152–1157.
- Okagaki, T., Higashi-Fujime, S., Ishikawa, R., Takano-Ohmuro, H., Kohama, K., 1991. *In vitro* movement of actin filaments on gizzard smooth muscle myosin: requirement of phosphorylation of myosin light chain and effects of tropomyosin and caldesmon. *J. Biochem. (Tokyo)* 109, 858–866.
- Onishi, H., Wakabayashi, T., 1982. Electron microscopic studies of myosin molecules from chicken gizzard muscle I: the formation of the intramolecular loop in the myosin tail. *J. Biochem. (Tokyo)* 92, 871–879.
- Ostap, E.M., Pollard, T.D., 1996. Biochemical kinetic characterization of the *Acanthamoeba* myosin-I atpase. *J. Cell Biol.* 132, 1053–1060.
- Palevitz, B.A., Ash, J.F., Hepler, P.K., 1974. Actin in the green alga, *Nitella*. *Proc. Natl. Acad. Sci. USA* 71, 363–366.
- Pashkova, N., Catlett, N.L., Novak, J.L., Wu, G., Lu, R., Cohen, R.E., et al., 2005. Myosin V attachment to cargo requires the tight association of two functional subdomains. *J. Cell Biol.* 168, 359–364.
- Pashkova, N., Jin, Y., Ramaswamy, S., Weisman, L.S., 2006. Structural basis for myosin V discrimination between distinct cargoes. *EMBO J.* 25, 693–700.
- Pavlov, D., Gerson, J.H., Yu, T., Tobacman, L.S., Homsher, E., Reisler, E., 2003. The regulation of subtilisin-cleaved actin by tropomyosin/troponin. *J. Biol. Chem.* 278, 5517–5522.
- Phillips Jr., G.N., Fillers, J.P., Cohen, C., 1986. Tropomyosin crystal structure and muscle regulation. *J. Mol. Biol.* 192, 111–131.
- Pollard, T.D., Cooper, J.A., 1986. Actin and actin-binding proteins. A critical evaluation of mechanisms and functions. *Annu. Rev. Biochem.* 55, 987–1035.
- Purcell, T.J., Morris, C., Spudich, J.A., Sweeney, H.L., 2002. Role of the lever arm in the processive stepping of myosin V. *Proc. Natl. Acad. Sci. USA* 99, 14159–14164.
- Rayment, I., Holden, H.M., Whittaker, M., Yohn, C.B., Lorenz, M., Holmes, K.C., et al., 1993a. Structure of the actin–myosin complex and its implications for muscle contraction. *Science* 261, 58–65.
- Rayment, I., Rypniewski, W.R., Schmidt-Bäse, K., Smith, R., Tomchick, D.R., Benning, M.M., et al., 1993b. Three-dimensional structure of myosin subfragment-1: a molecular motor. *Science* 261, 50–58.
- Reck-Peterson, S.L., Provance Jr., D.W., Mooseker, M.S., Mercer, J.A., 2000. Class V myosins. *Biochim. Biophys. Acta* 1496, 36–51.
- Reck-Peterson, S.L., Tyska, M.J., Novick, P.J., Mooseker, M.S., 2001. The yeast class V myosins, Myo2p and Myo4p, are nonprocessive actin-based motors. *J. Cell Biol.* 153, 1121–1126.
- Reisen, D., Hanson, M.R., 2007. Association of six YFP-myosin XI-tail fusions with mobile plant cell organelles. *BMC Plant Biol.* 7, 6.
- Richards, T.A., Cavalier-Smith, T., 2005. Myosin domain evolution and the primary divergence of eukaryotes. *Nature* 436, 1113–1118.
- Rief, M., Rock, R.S., Mehta, A.D., Mooseker, M.S., Cheney, R.E., Spudich, J.A., 2000. Myosin-V stepping kinetics: a molecular model for processivity. *Proc. Natl. Acad. Sci. USA* 97, 9482–9486.
- Rivolta, M.N., Urrutia, R., Kachar, B., 1995. A soluble motor from the alga *Nitella* supports fast movement of actin filaments *in vitro*. *Biochim. Biophys. Acta* 1232, 1–4.
- Rosenfeld, S.S., Sweeney, H.L., 2004. A model of myosin V processivity. *J. Biol. Chem.* 279, 40100–40111.

- Ross, J.L., Ali, M.Y., Warshaw, D.M., 2008. Cargo transport: molecular motors navigate a complex cytoskeleton. *Curr. Opin. Cell Biol.* 20, 41–47.
- Ruff, C., Furch, M., Brenner, B., Manstein, D.J., Meyhöfer, E., 2001. Single-molecule tracking of myosins with genetically engineered amplifier domains. *Nat. Struct. Biol.* 8, 226–229.
- Saito, K., Aoki, T., Yanagida, T., 1994. Movement of single myosin filaments and myosin step size on an actin filament suspended in solution by a laser trap. *Biophys. J.* 66, 769–777.
- Sakamoto, T., Amitani, I., Yokota, E., Ando, T., 2000. Direct observation of processive movement by individual myosin V molecules. *Biochem. Biophys. Res. Commun.* 272, 586–590.
- Sakamoto, T., Wang, F., Schmitz, S., Xu, Y., Xu, Q., Molloy, J.E., et al., 2003. Neck length and processivity of myosin V. *J. Biol. Chem.* 278, 29201–29207.
- Sakamoto, T., Yildez, A., Selvin, P.R., Sellers, J.R., 2005. Step-size is determined by neck length in myosin V. *Biochemistry* 44, 16203–16210.
- Sakamoto, T., Webb, M.R., Forgacs, E., White, H.D., Sellers, J.R., 2008. Direct observation of the mechanochemical coupling in myosin Va during processive movement. *Nature* 455, 128–132.
- Schröder, R.R., Manstein, D.J., Jahn, W., Holden, H., Rayment, I., Holmes, K.C., et al., 1993. Three-dimensional atomic model of F-actin decorated with *Dictyostelium* myosin S1. *Nature* 364, 171–174.
- Schutt, C.E., Myslik, J.C., Rozycki, M.D., Goonesekere, N.C., Lindberg, U., 1993. The structure of crystalline profilin-beta-actin. *Nature* 365, 810–816.
- Schwytter, D., Phillips, M., Reisler, E., 1989. Subtilisin-cleaved actin: polymerization and interaction with myosin subfragment 1. *Biochemistry* 28, 5889–5895.
- Schwytter, D.H., Kron, S.J., Toyoshima, Y.Y., Spudich, J.A., Reisler, E., 1990. Subtilisin cleavage of actin inhibits *in vitro* sliding movement of actin filaments over myosin. *J. Cell Biol.* 111, 465–470.
- Sellers, J.R., Veigel, C., 2006. Walking with myosin V. *Curr. Opin. Cell Biol.* 18, 68–73.
- Shimmen, T., 2007. The sliding theory of cytoplasmic streaming: fifty years of progress. *J. Plant Res.* 120, 31–43.
- Shimmen, T., Yokota, E., 2004. Cytoplasmic streaming in plants. *Curr. Opin. Cell Biol.* 16, 68–72.
- Snyder, G.E., Sakamoto, T., Hammer III, J.A., Sellers, J.R., Selvin, P.R., 2004. Nanometer localization of single green fluorescent proteins: evidence that myosin V walks hand-over-hand via telemark configuration. *Biophys. J.* 87, 1776–1783.
- Somlyo, A.P., Somlyo, A.V., 2003. Ca^{2+} sensitivity of smooth muscle and nonmuscle myosin II: modulated by G proteins, kinases, and myosin phosphatase. *Physiol. Rev.* 83, 1325–1358.
- Sumiyoshi, H., Ooguchi, M., Ooi, A., Okagaki, T., Higashi-Fujime, S., 2007. Insight into the mechanism of fast movement of myosin from *Chara corallina*. *Cell Motil. Cytoskeleton* 64, 131–142.
- Summers, K.E., Gibbons, I.R., 1971. Adenosine triphosphate-induced sliding of tubules in trypsin-treated flagella of sea-urchin sperm. *Proc. Natl. Acad. Sci. USA* 68, 3092–3096.
- Sutoh, K., 1983. Mapping of actin-binding sites on the heavy chain of myosin subfragment 1. *Biochemistry* 22, 1579–1585.
- Szent-Györgyi, A., 1951. Actomyosin. In: *Chemistry in Muscle Contraction*, second ed. Academic Press, New York, pp. 72–82.
- Tanaka, H., Homma, K., Iwane, A.H., Katayama, E., Ikebe, R., Saito, J., et al., 2002. The motor domain determines the large step of myosin-V. *Nature* 415, 192–195.
- Taylor, K.A., 2007. Regulation and recycling of myosin V. *Curr. Opin. Cell Biol.* 19, 67–74.

- Tazawa, M., Shimmen, T., 1987. Cell motility and ionic relations in Characean cells as revealed by internal perfusion and cell models. *Int. Rev. Cytol.* 109, 259–312.
- Thirumurugan, K., Sakamoto, T., Hammer III, J.A., Sellers, J.R., Knight, P.J., 2006. The cargo-binding domain regulates structure and activity of myosin 5. *Nature* 442, 212–215.
- Tominaga, M., Kojima, H., Yokota, E., Orii, H., Nakamori, R., Katayama, E., et al., 2003. Higher plant myosin XI moves processively on actin with 35 nm steps at high velocity. *EMBO J.* 22, 1263–1272.
- Toyoshima, Y.Y., Kron, S.J., McNally, E.M., Niebling, K.R., Toyoshima, C., Spudich, J.A., 1987. Myosin subfragment-1 is sufficient to move actin filaments *in vitro*. *Nature* 328, 536–539.
- Trybus, K.M., 1994. Regulation of expressed truncated smooth muscle myosins. Role of the essential light chain and tail length. *J. Biol. Chem.* 269, 20819–20822.
- Trybus, K.M., Freyzon, Y., Faust, L.Z., Sweeney, H.L., 1997. Spare the rod, spoil the regulation: necessity for a myosin rod. *Proc. Natl. Acad. Sci. USA* 94, 48–52.
- Tyska, M.J., Mooseker, M.S., 2002. MYO1A (brush border myosin I) dynamics in the brush border of LLC-PK1-CL4 cells. *Biophys. J.* 82, 1869–1883.
- Tyska, M.J., Mackey, A.T., Huang, J.D., Copeland, N.G., Jenkins, N.A., Mooseker, M.S., 2005. Myosin-1a is critical for normal brush border structure and composition. *Mol. Biol. Cell* 16, 2443–2457.
- Uemura, S., Higuch, H., Olivares, A.O., De La Cruz, E.M., Ishiwata, S., 2004. Mechanochemical coupling of two substeps in a single myosin V motor. *Nat. Struct. Mol. Biol.* 11, 877–883.
- Uyeda, T.Q., 1996. Ultra-fast Chara myosin: a test case for the swinging lever arm model for force production by myosin. *J. Plant Res.* 109, 231–239.
- Uyeda, T.Q., Kron, S.J., Spudich, J.A., 1990. Myosin step size. Estimation from slow sliding movement of actin over low densities of heavy meromyosin. *J. Mol. Biol.* 214, 699–710.
- Uyeda, T.Q., Ruppel, K.M., Spudich, J.A., 1994. Enzymatic activities correlate with chimaeric substitutions at the actin-binding face of myosin. *Nature* 368, 567–569.
- Uyeda, T.Q., Abramson, P.D., Spudich, J.A., 1996. The neck region of the myosin motor domain acts as a lever arm to generate movement. *Proc. Natl. Acad. Sci. USA* 93, 4459–4464.
- Vale, R.D., 2003. Myosin V motor proteins: marching stepwise towards a mechanism. *J. Cell Biol.* 163, 445–450.
- Vale, R.D., Reese, T.S., Sheetz, M.P., 1985. Identification of a novel force-generating protein, kinesin, involved in microtubule-based motility. *Cell* 42, 39–50.
- Vale, R.D., Soll, D.R., Gibbons, I.R., 1989. One-dimensional diffusion of microtubules bound to flagellar dynein. *Cell* 59, 915–925.
- Veigel, C., Bartoo, M.L., White, D.C., Sparrow, J.C., Molloy, J.E., 1998. The stiffness of rabbit skeletal actomyosin cross-bridges determined with an optical tweezers transducer. *Biophys. J.* 75, 1424–1438.
- Veigel, C., Wang, F., Bartoo, M.L., Sellers, J.R., Molloy, J.E., 2002. The gated gait of the processive molecular motor, myosin V. *Nat. Cell Biol.* 4, 59–65.
- Vibert, P., Craig, R., Lehman, W., 1997. Steric-model for activation of muscle thin filaments. *J. Mol. Biol.* 266, 8–14.
- Volkman, N., Liu, H., Hazelwood, L., Kremensova, E.B., Lowey, S., Trybus, K.M., et al., 2005. The structural basis of myosin V processive movement as revealed by electron cryomicroscopy. *Mol. Cell* 19, 595–605.
- Walker, M.L., Burgess, S.A., Sellers, J.R., Wang, F., Hammer III, J.A., Trinick, J., et al., 2000. Two-headed binding of a processive myosin to F-actin. *Nature* 405, 804–807.
- Wang, F., Chen, L., Arcucci, O., Harvey, E.V., Bowers, B., Xu, Y., et al., 2000. Effect of ADP and ionic strength on the kinetic and motile properties of recombinant mouse myosin V. *J. Biol. Chem.* 275, 4329–4335.

- Wang, Y.X., Kauffman, E.J., Duex, J.E., Weisman, L.S., 2001. Fusion of docked membranes requires the armadillo repeat protein Vac8p. *J. Biol. Chem.* 276, 35133–35140.
- Wang, F., Thirumurugan, K., Stafford, W.F., Hammer III, J.A., Knight, P.J., Sellers, J.R., 2004. Regulated conformation of myosin V. *J. Biol. Chem.* 279, 2333–2336.
- Warshaw, D.M., Kennedy, G.G., Work, S.S., Kremontsova, E.B., Beck, S., Trybus, K.M., 2005. Differential labeling of myosin V heads with quantum dots allows direct visualization of hand-over-hand processivity. *Biophys. J.* 88, L30–L32.
- Wells, A.L., Lin, A.W., Chen, L.Q., Safer, D., Cain, S.M., Hasson, T., et al., 1999. Myosin VI is an actin-based motor that moves backwards. *Nature* 401, 505–508.
- Wendt, T., Taylor, D., Trybus, K.M., Taylor, K., 2001. Three-dimensional image reconstruction of dephosphorylated smooth muscle heavy meromyosin reveals asymmetry in the interaction between myosin heads and placement of subfragment 2. *Proc. Natl. Acad. Sci. USA* 98, 4361–4366.
- Williamson, R.E., 1975. Cytoplasmic streaming in *Chara*: a cell model activated by ATP and inhibited by cytochalasin B. *J. Cell Sci.* 17, 655–668.
- Wolenski, J.S., Cheney, R.E., Mooseker, M.S., Forscher, P., 1995. *In vitro* motility of immunoadsorbed brain myosin-V using a Limulus acrosomal process and optical tweezer-based assay. *J. Cell Sci.* 108, 1489–1496.
- Wollert, T., Weiss, D.G., Gerdes, H.H., Kuznetsov, S.A., 2002. Activation of myosin V-based motility and F-actin-dependent network formation of endoplasmic reticulum during mitosis. *J. Cell Biol.* 159, 571–577.
- Wu, X.S., Rao, K., Zhang, H., Wang, F., Sellers, J.R., Matesic, L.E., et al., 2002. Identification of an organelle receptor for myosin-Va. *Nat. Cell Biol.* 4, 271–278.
- Yamamoto, K., Kikuyama, M., Sutoh-Yamamoto, N., Kamitubo, E., 1994. Purification of actin based motor protein from *Chara corallina*. *Proc. Jpn. Acad.* 70 (Ser. B), 175–180.
- Yamamoto, K., Shimada, K., Ito, K., Hamada, S., Ishijima, A., Tsuchiya, T., et al., 2006. Chara myosin and the energy of cytoplasmic streaming. *Plant Cell Physiol.* 47, 1427–1431.
- Yanagida, T., Nakase, M., Nishiyama, K., Oosawa, F., 1984. Direct observation of motion of single F-actin filaments in the presence of myosin. *Nature* 307, 58–60.
- Yap, K.L., Kim, J., Truong, K., Sherman, M., Yuan, T., Ikura, M., 2000. Calmodulin target database. *J. Struct. Funct. Genomics* 1, 8–14.
- Yildiz, A., Forkey, J.N., McKinney, S.A., Ha, T., Goldman, Y.E., Selvin, P.R., 2003. Myosin V walks hand-over-hand: single fluorophore imaging with 1.5-nm localization. *Science* 300, 2061–2065.
- Yokota, E., Shimmen, T., 1994. Isolation and characterization of plant myosin from pollen tube of lily. *Protoplasma* 177, 153–162.
- Yokota, E., Yukawa, C., Muto, S., Sonobe, S., Shimmen, T., 1999. Biochemical and immunocytochemical characterization of two types of myosins in cultured tobacco bright yellow-2 cells. *Plant Physiol.* 121, 525–534.
- Yoshizaki, T., Imamura, T., Babendure, J.L., Lu, J.C., Sonoda, N., Olefsky, J.M., 2007. Myosin 5a is an insulin-stimulated Akt2 (protein kinase Bbeta) substrate modulating GLUT4 vesicle translocation. *Mol. Cell Biol.* 27, 5172–5183.
- Zot, H.G., Doberstein, S.K., Pollard, T.D., 1992. Myosin-I moves actin filaments on a phospholipid substrate: implications for membrane targeting. *J. Cell Biol.* 116, 367–376.

Index

A

- AAV. *See* Adeno-associated virus
- A β . *See* Amyloid β peptides
- ABA. *See* Abscisic acid
- ABC. *See* ATP-binding cassette
- ABCB-mediated auxin transport, effectors, 278–280. *See also* Shoot apical meristems
- ABPs. *See* Actin binding proteins
- Abscisic acid, 271
- β 1,4-linked *N*-acetylgalactosamine, 111
- α 1,4-linked *N*-acetylglucosamine, 111
- Actin and myosin, in Chara myosin, 322–324.
See also Chara myosin
- Actin binding proteins, 307
- Activin A and keratinocytes, 180. *See also* Keratinocytes and fibroblasts interactions
- Acute and organotypic slices, differences, 71–72
- Adeno-associated virus, 75
- Advanced glycation end products, 201
- AGEs. *See* Advanced glycation end products
- Aging, fibroblasts in, 198–201.
See also Fibroblasts
- Agurin HSPGs, 108–109. *See also* Heparan sulfate (HS)
- AHK3 expression, 27
- AHKs. *See* *Arabidopsis* histidine kinases
- AHPs. *See* *Arabidopsis* phosphotransfer proteins
- Alder (*Alnus glutinosa*), 37
- Alfalfa (*Medicago sativa*), 36
- ALS. *See* Amyotrophic lateral sclerosis
- ALS1 gene, 282
- ALS3 gene, 282
- Alternaria brassicicola*, 273
- Alzheimer's disease (AD), 51, 136–138
- Aminopeptidase N/CD13, 176
- Amyloid β peptides, 57
- Amyloid diseases, HS in, 136–139
- Amyloid precursor protein, 60
- Amyotrophic lateral sclerosis, 51
- Androgen receptors, in dermal papilla fibroblasts, 176. *See also* Fibroblasts
- Anterior visceral endoderm, 240
- APN/CD13. *See* Aminopeptidase N/CD13
- APP. *See* Amyloid precursor protein
- Arabidopsis*
- ABCC4 protein, 274
 - AtABCB19 protein, 276
 - AtAGCG40 expression, 282
 - CRE-family receptors, properties of, 9
 - cytokinins
 - identification, 2–4
 - receptors, 4–5
 - differentiation zone, 26
 - Hpts, properties, 12
 - lateral root formation, 32–36
 - primary vascular development, 28–29
 - root nodulation, 36–38
 - secondary vascular development, 31–32
 - SpTUR2 protein, 272
 - type-A ARRs, properties, 15–16
 - type-B ARRs, properties, 17
- Arabidopsis* histidine kinases, 4–5, 10
- Arabidopsis* phosphotransfer proteins, 4
- Arabidopsis* response regulator, 4, 20
- ARR7 and 15, in root meristem formation, 23–24
- ARR6 gene, 7
- ARRs. *See* *Arabidopsis* response regulator
- AtABCB4, activity, 278
- AtABCB4, lateral root initiation, 277
- AtABCB21, pericycle cells, 278
- AtABCB25 protein, expression, 287–288
- AtABCB1 protein, role, 275
- AtABCB19 protein, role, 275
- AtABCG36 gene, 273, 282–283
- AtABCG11, role, 265–266
- AtABC114, role, 287
- ATP-binding cassette
 - functions, 264–265
 - in mitochondria, 287–289
 - in peroxisomes, 289–290
 - in plasma membranes
 - leaf and shoot epidermis, 265–266, 271–275
 - roots and rhizomes, 280–283
 - seeds and flowers, 283
 - shoot and root apical meristems, 275–280
 - in plastids, 286–287
 - soluble-type in plants, 290–291
 - in vacuoles, 283–286
- AtPUP1 gene, 3
- Aux/IAA proteins, role, 28
- Auxin. *See also* Root apical meristems
 - hypocotyls and stem, 275–277
 - root tissues, 277–278
- AUXIN/LIKE-AUXIN, 275
- AUXINRESISTANT1, expression, 278
- AUX/LAX. *See* AUXIN/LIKE-AUXIN

AVE. *See* Anterior visceral endoderm
 Axonal transport of mitochondria,
 organelle-specific dyes, 68

B

BDA. *See* Biotinylated dextrane amine
 BFP. *See* Blue fluorescent protein
 BiCHM. *See* Biparental Complete Hydatidiform
 Moles
 BiFC. *See* Bimolecular fluorescence
 complementation
 Bimolecular fluorescence complementation, 59–61
 Biotinylated dextrane amine, 83
 Biparental Complete Hydatidiform Moles, 221
 Blue fluorescent protein, 87
 Bone marrow, fibroblast-related cells, 168–169.
See also Fibroblasts
Bradyrhizobium japonicum, 281
 Bright yellow (BY), 271
Bronze-2, 285
Bz2. *See* *Bronze-2*

C

Caenorhabditis elegans, 4, 84
 Ca²⁺, in myosin V activity, 315–317.
See also Myosins
 Calcium imaging, application, 62
 CALI. *See* Chromophore-assisted laser inactivation
 Calmodulin (CaM), 314
 Cambial development, cytokinins, 31–32
Catharanthus roseus, 13
 Cell surface markers, fibroblast separation, 175.
See also Fibroblasts
 CER5 gene, 265
 CFP. *See* Cyan fluorescent protein
 Characean cells, myosin, 306. *See also* Myosins
Chara corallina, 312
 Chara myosin. *See also* Myosins
 biochemical properties, 306–307
 mechanism, 328
 in cells, 335–336
 fast movement of, 334–335
 processivity of, 329–332
 step size, 332–333
 molecular structure, 312–314
 neck region, 314–317
 properties, 307–311
 structure, 321–322
 actin and myosin, 322–324
 myosin and cleaved actin, 325–327
 tropomyosin effect, 327–328
 tail of
 atomic model of, 322, 323
 structure of, 317–318, 320
Chlamydomonas reinhardtii, 288
 Chromophore-assisted laser inactivation, 69
 CJD. *See* Creutzfeld–Jacob disease

CjMDR1 transporter, in rhizome cells, 281
 CKX genes, 3
 CLEM. *See* Correlative light–electron microscopy
 Clone C20, role, 177. *See also* Fibroblasts
 Collagen fiber bundles, in papillary dermis, 191
 COMATOSE (CTS), 289
 Connective tissues, constituents, 163
Coptis japonica, 277
 Correlative light–electron microscopy, 93
 Cortical cell proliferation, cytokinin-induced
 stimulation, 36–37
 Cortical spreading depression, 88
 CrCDS1 protein, *C. reinhardtii*, 288
 cre1. *See* Cytokinin response 1
 CRE1 gene, 5, 10
 Creutzfeld–Jacob disease, 51
 CRF. *See* Cytokinin response factors
cf target genes and type-B *arr* mutants,
 comparison, 21
 CSD. *See* Cortical spreading depression
 C-terminal subdomain II (SDII), 317
 Cyan fluorescent protein, 58
 Cytochrome c maturation (Ccm), 288
 Cytokinin binding site, mapping, 10
 Cytokinin oxidases, identification, 3
 Cytokinin phytohormones(ck).
See also Arabidopsis
 function and synthesis, 2–3
 signaling in developmental pathways
 primary vascular development, 28–31
 root architecture regulation, 32–36
 root meristem size, 24–28
 root nodulation control, 36–38
 root stem cell niche, 22–24
 secondary vascular development, 31–32
 signal transduction pathway, 4–5
 HPTs in, 11, 13
 receptors of, 5–11
 target genes, transcriptional control of,
 14, 18–22
 Cytokinin response 1, 4
 Cytokinin response factors, 5, 7–8
 Cytoskeletal polymer movement visualization,
 FSM for, 68. *See also* Neurodegenerative
 disease

D

2,4-D. *See* 2,4-dichlorophenoxyacetic acid
 2,4-DB. *See* 2,4-dichlorophenoxybutyrate
 Decorin, function, 191
 Dermal fibroblasts, 164. *See also* Fibroblasts
 role, 200
 subpopulations, 171–174
 Dermatome, role, 173
 Diabetic nephropathy, HS in, 138
 2,4-Dichlorophenoxyacetic acid, 283
 2,4-Dichlorophenoxybutyrate, 289

Dictyostelium discoideum, 333
 Differentially methylated region, 218
 Differentiation zone (DZ), 26
 DiI. *See* 1,1'-dioctadecyl-3,3,3',3'-tetramethylindocarbocyanine perchlorate
 DiO. *See* 3,3'-dioladecyloxcarbocyanine perchlorate
 1,1'-Dioctadecyl-3,3,3',3'-tetramethylindocarbocyanine perchlorate, 74
 3,3'-Dioladecyloxcarbocyanine perchlorate, 74
 Dipeptidylpeptidase IV, 168
 DMR. *See* Differentially methylated region
 DNA methyltransferases mutations, 222–223.
See also Genomic imprinting
 Dnmt1, isoforms of, 222. *See also* Genomic imprinting
 Dnmt3L gene, 222–223
 DPPIV. *See* Dipeptidylpeptidase IV
Drosophila melanogaster, 4, 84–86

E

ECM. *See* Extracellular matrix
 ECM production, fibroblasts in, 189–192.
See also Fibroblasts
 EDTA. *See* Ethylenediaminetetraacetic acid
 EGFP. *See* Enhanced green fluorescent protein
 EGFP-tagged Rab3A protein, 61
 Electrophysiology and live-cell imaging, in neural networks study, 93
 Embryogenesis, cytokinin signaling in, 22
 Embryonic stem (ES) cells, 241
 Enhanced green fluorescent protein, 56
 Enhanced yellow-fluorescent protein, 81–82
 Epidermal cell differentiation, fibroblasts in, 183–184. *See also* Fibroblasts
 Epithelial cells and fibroblasts. *See also* Fibroblasts
 basement membrane formation, 182–183
 epidermal cell differentiation, 183–184
 hair follicle epithelium, 184–185
 keratinocytes, 179–182
 vascular endothelial cells, 185–189
 ERF. *See* Ethylene response factor
 ERK. *See* Extracellular signal related kinase
Escherichia coli, 7
 Ethylenediaminetetraacetic acid, 170
 Ethylene response factor, 21
 Eukaryotic genome sequence, role, 4
 Evanescent wave microscopy. *See* Total internal reflection fluorescence microscopy
 Exogenous cytokinin, application, 34
 Explant culture method, in fibroblast cultures, 170–171. *See also* Fibroblasts
Ext1 gene, 132
 Extracellular matrix, 162
 Extracellular signal related kinase, 80
 EYFP. *See* Enhanced yellow-fluorescent protein

F

F-actin binding, myosin purification, 306
 FALI. *See* Fluorophore-assisted light inactivation
 Familial hydatidiform moles, 221–222.
See also Genomic imprinting
 FAP. *See* Fibroblast activation protein
 FCCS. *See* Fluorescence cross-correlation spectroscopy
 FCS. *See* Fluorescence correlation spectroscopy
 Fetal dermal fibroblasts, 165. *See also* Fibroblasts
 FGF1. *See* Fibroblast growth factor 1
 FGFR1. *See* Fibroblast growth factor receptor 1
 FGF4 signal, murine embryos, 227
 Fibrillin-1, 199
 Fibroblast activation protein, 168
 Fibroblast cultures, methods, 170–171. *See also* Fibroblasts
 Fibroblast growth factor 1, 122
 Fibroblast growth factor receptor 1, 122
 Fibroblasts
 in aging, 198–201
 characteristics, 163–165
 bone marrow origin and, 168–169
 fibroblast-related populations, 165–168
 diversity, 169–170
 cell surface markers in, 175
 dermal fibroblast subpopulations, 171–174
 establishment of fibroblast cultures, 170–171
 phenotypic markers, 175–176
 ECM production and, 189–192
 epithelial cells and
 basement membrane formation, 182–183
 epidermal cell differentiation, 183–184
 hair follicle epithelium, 184–185
 keratinocytes, 179–182
 vascular endothelial cells, 185–189
 heterogeneity, 176–179
 immunocompetent cells and, 196
 regulation of neuropeptides, 196–198
 role, 162–163
 Thy-1⁺ and Thy-1⁻ subpopulations, 194–195
 tissue engineering and, 192–194
 Fibroblast-specific protein-1, 165, 175
 Fibrocytes, definition, 165
 FLIM. *See* Fluorescence lifetime imaging microscopy
 FLIP. *See* Fluorescence loss in photobleaching
 Flowers, ABC proteins, 283. *See also* ATP-binding cassette
 Fluorescence correlation spectroscopy. *See also* Neurodegenerative disease
 for membrane binding study, 67
 for molecular dynamics study, 58
 Fluorescence cross-correlation spectroscopy, 58
 Fluorescence lifetime imaging microscopy, 58
 Fluorescence loss in photobleaching, 57

Fluorescence protein tracking.
See also Neurodegenerative disease
 for neurite outgrowth and granules transport,
 55–56
 organelle transport in hippocampal neurons,
 65–66

Fluorescence recovery after photobleaching,
 56–57

Fluorescent speckle microscopy, 68

Fluorophore-assisted light inactivation, 69

FMRP. *See* Fragile X mental retardation protein

Förster resonance energy transfer, 58

Fragile X mental retardation protein, 55–56

FRAP. *See* Fluorescence recovery after
 photobleaching

FRET. *See* Förster resonance energy transfer

FSM. *See* Fluorescent speckle microscopy

FSP-1. *See* Fibroblast-specific protein-1

G

GAG. *See* Glycosaminoglycan

GAGosome concept, application, 118–120

GalNAc. *See* β 1,4-linked *N*-acetylgalactosamine

GCN. *See* General control nonrepressible

GeBP. *See* GLABOROUS1 ENHANCER
 BINDING PROTEIN

GeBP-like proteins, 21

General control nonrepressible, 291

Genomic imprinting

mammals, 217–219

maternal effect

DNA methyltransferases mutations,
 222–223

familial hydatidiform moles, 221–222

imprinting, 223–224

Mother Knows Best mechanism, 224–225

remodeling of paternal, 220–221

in plants and insects, 219–220

GFP. *See* Green fluorescent protein

GhWBC1 gene, 283

Gingival fibroblasts, features, 184

GLABOROUS1 ENHANCER BINDING
 PROTEIN, 21

GlcNAc. *See* α 1,4-linked *N*-acetylglucosamine

Glutathione *S*-transferase, 285

Glycogen synthase kinase 3 β , 60

Glycosaminoglycan, 109

Glycosylphosphatidylinositol, 108

Glypican (Gpc) HSPGs, 108. *See also* Heparan
 sulfate (HS)

GM-CSF. *See* Granulocyte/macrophage
 colony-stimulating factor

GPI. *See* Glycosylphosphatidylinositol

GPLs. *See* GeBP-like proteins

Granulocyte/macrophage colony-stimulating
 factor, 178, 180

Gravacin and AtABC19 protein, 276

Green fluorescent protein, 54

GSK3 β . *See* Glycogen synthase kinase 3 β

GST. *See* Glutathione *S*-transferase

GTPase. *See* Guanosine triphosphatase

Guanosine triphosphatase, 80

H

Hair follicle epithelium, fibroblasts, 184–185.

See also Epithelial cells and fibroblasts

Hair follicles and fibroblast, 167–168. *See also*
 Fibroblasts

Heparan sulfate (HS), 106

and amyloidosis, 136–139

in development and homeostasis, 129–134

and infection, 141–142

inflammatory and repair process, 140–141

and protein interactions, 120–121

functional significance, 123–126

protein-binding domains topology, 122

specificity in, 126–129

proteoglycans

glypican, 108

perlecan and agrin, 108–109

syndecan, 107–108

structure and biosynthesis, 109–111

chain assembly and modification, 115–117

linkage region formation, 111, 115

regulation of, 117–120

sulfation code for, 134–136

tumor development and metastasis, 139–140

Hepatocyte growth factor/scatter factor, 177

Hereditary multiple exostoses, 140

Herpes simplex virus, 55

HGF/SF. *See* Hepatocyte growth factor/scatter
 factor

Histidine-containing phosphotransfer protein, 4

Histidine kinase activity, of AHK4, 5

Histidine protein kinase (HK), 4

hit1 mutant. *See hyperinfected1* mutant

HME. *See* Hereditary multiple exostoses

HPt. *See* Histidine-containing phosphotransfer
 protein

HSV. *See* Herpes simplex virus

HSV-mediated gene transfer, usage, 65

Human dermal fibroblasts, in tissue engineering,
 192–194. *See also* Fibroblasts

Human umbilical vein endothelial cells, 186–187

Huntington's disease (HD), 51

HUVECs. *See* Human umbilical vein endothelial
 cells

hyperinfected1 mutant, 37

Hypocotyls and stem, auxin, 275–277. *See also*
 ATP-binding cassette

I

IAA. *See* Indole-3-acetic acid

IAPP. *See* Islet amyloid polypeptide

IBA. *See* Indole butyric acid

- ICR. *See* Imprint control region
- IDE-1. *See* Iron-deficiency element-1
- IDI1. *See* Iron-deficiency induced gene 7
- IGF-1. *See* Insulin-like growth factor-1
- Immunocompetent cells and fibroblast interaction, 196. *See also* Fibroblasts
- Imprint control region, 218
- Imprinting and placenta, 225–226
 imprinted gene function, 228, 234–239
 placentation, 226–228
 PrE in development, 239–240
 tetraploid rescue experiments, 241–246
- Indole-3-acetic acid, 275
- Indole butyric acid, 289
- Ipp5f_v2/v3* gene, 234
- Insects, genomic imprinting, 219–220.
See also Genomic imprinting
- Insulin-like growth factor-1, 180
- Intracellular calcium levels, determination, 69–70
- Intrauterine growth retardation, 216
- Ion-sensitive dyes. *See also* Neurodegenerative disease
 for neuronal Ca^{2+} homeostasis imaging, 69–70
 neuronal function study, 81–82
 for neuronal function study, 62–63
- IPT* genes, 3, 34
- IQ motifs, of Chara myosin, 314–315.
See also Myosins
- Iron-deficiency element-1, 281
- Iron-deficiency induced gene 7, 284–285
- Iset amyloid polypeptide, 138
- IUGR. *See* Intrauterine growth retardation
- K**
- Keratinocyte growth factor-1, 178
- Keratinocytes and fibroblasts interactions, 179–182. *See also* Fibroblasts
- KGF-1. *See* Keratinocyte growth factor-1
- L**
- LaHK1* gene, 38
- Large offspring syndrome, 226
- Laser scanning microscopy, 94
- Lateral root primordia, 32
- Leaf and shoot epidermis, ABC proteins, 265–266, 271–275. *See also* ATP-binding cassette
 regulation of stomata, 274
- Lentivirus-mediated gene transfer, usage, 65
- Lilium longiflorum*, 305
- Lily pollen tube myosin, role, 307
- Live-cell imaging, in neurodegenerative disease of animals
 advantage and limitation, 90–91
 cell function study, 87–90
 network development and degeneration, 86–87
 transgenic animals, 84–86
 for cell lines
 advantage and limitation, 63
 cell membrane vesicles study, 61
 cultures and gene delivery, 54–55
 mitochondrial mobility study, 61–62
 molecular dynamics study, 58
 molecular interactions study, 58–59
 neurite outgrowth and granules transport study, 55–56
 neuronal function study, 62–63
 protein aggregation and mobility study, 56–57
 protein interactions analysis, 59–61
 CLEM and electrophysiology, 93
 FRET in, 58
 and matrix-assisted laser desorption/ionization, 92
 multiphoton and one-photon microscopy, 91–92
 for organotypic cultures
 advantage and limitation of, 83–84
 axonal outgrowth and developmental alteration study, 82–83
 cultures and gene delivery in, 71–75
 molecular dynamics study, 79–81
 neuronal connectivity study, 77–78
 neuronal function study, 81–82
 neuron imaging, 76–77
 RNA translation, live imaging of, 83
 for primary neurons
 advantage and limitation, 70–71
 axonal transport of mitochondria, determination, 68
 axonal vesicle transport study, 65–66
 cell motility study, 69
 cultures and gene delivery, 64–65
 cytoskeletal polymer movement study, 68
 membrane binding study, 67
 neuronal Ca^{2+} homeostasis imaging, 69–70
 protein diffusion analysis, 66–67
- LOG* gene, 3
- LOS. *See* Large offspring syndrome
- Loss of imprinting (LOI), 223
- Lotus japonicus*, 35, 264
- LRP. *See* Lateral root primordia
- LSM. *See* Laser scanning microscopy
- M**
- Major facilitator superfamily, 280
- MALDI. *See* Matrix-assisted laser desorption/ionization
- Mammalian HS biosynthesis, enzymes, 112–114
- Mammals, genomic imprinting in, 217–219. *See also* Genomic imprinting
- MAPs. *See* Microtubule-associated protein
- MAP tau in axon growth, CALI in, 69

- MARK. *See* Microtubule affinity regulating kinase
- MATE. *See* Multidrug and toxic compound extrusion
- Matrix-assisted laser desorption/ionization, 92
- Matrix metalloproteinase-1, 180
- MEA. *See* Multielectrode array
- Medicago truncatula*, 35
- mEGFP. *See* Monomeric enhanced green fluorescent protein
- α -Melanocyte-stimulating hormone, 130
- Membrane anchored enhanced GFP, 79
- Membrane interface culture method, for tissue, 72–73
- Mesenchymal stem cells, 165
- MFS. *See* Major facilitator superfamily
- mGFP. *See* Membrane anchored enhanced GFP
- Microtubule affinity regulating kinase, 68
- Microtubule-associated protein, 62
- Mitochondria, ABC proteins in, 287–289. *See also* ATP-binding cassette
- Mitochondria mobility tracking, organelle-specific dyes for, 61–62. *See also* Neurodegenerative disease
- Mitochondria-specific staining, usage, 62
- MMP-1. *See* Matrix metalloproteinase-1
- Molecular interaction study, FLIM, FRET and FCCS in, 58–59. *See also* Neurodegenerative disease
- Monomeric enhanced green fluorescent protein, 80
- Monomeric red fluorescent proteins, 80
- Mother Knows Best mechanism, of genomic imprinting, 224–225. *See also* Genomic imprinting
- mRFPs. *See* Monomeric red fluorescent proteins
- MSCs. *See* Mesenchymal stem cells
- MSH. *See* α -Melanocyte-stimulating hormone
- Msx-1* gene, 164
- Multicolor BiFC approach, application, 59–60
- Multidrug and toxic compound extrusion, 286
- Multielectrode array, 73
- Multiple sclerosis (MS), 51
- Multiple triple mutant combinations, analysis, 31
- Mutations, in imprinted genes, 229–233
- Myofibroblasts, characteristics, 165–167. *See also* Fibroblasts
- Myosins
- molecular structure, of plant, 311–312
 - Chara myosin, 312–314
 - class XI, 312
 - myosin tail, 317–321
 - neck region of Chara myosin, 314–317
 - in plants
 - characean cells, 306
 - Chara myosin, 306–311
 - extraction of, 305–306
 - in vitro* motility, 303–304
 - dark-field microscopy, 304
 - protein at molecular level, 304–305
- Myosin V, role, 329
- ## N
- NALP7 protein, role, 221–222
- NAP. *See* Nonintrinsic ABC proteins
- NBD. *See* Nucleotide-binding domain
- NBF. *See* Nucleotide-binding fold
- NDST enzymes, role, 115–116
- NEM. *See* N-ethyl maleimide
- Nerve growth factor, 55
- N-ethyl maleimide, 306
- Neurite outgrowth and granules transport, study, 55–56
- Neurodegenerative disease, 51
- cell lines, live imaging
 - advantage and limitation, 63
 - cell membrane vesicles study, 61
 - cultures and gene delivery, 54–55
 - mitochondrial mobility study, 61–62
 - molecular dynamics study, 58
 - molecular interactions study, 58–59
 - neurite outgrowth and granules transport study, 55–56
 - neuronal function study, 62–63
 - protein aggregation and mobility study, 56–57
 - protein interactions analysis, 59–61
 - CLEM and electrophysiology, 93
 - live imaging of animals
 - advantage and limitation, 90–91
 - cell function study, 87–90
 - network development and degeneration, 86–87
 - transgenic animals, 84–86
 - and matrix-assisted laser desorption/ionization, 92
 - multiphoton and one-photon microscopy, 91–92
 - organotypic cultures, live imaging of
 - advantage and limitation of, 83–84
 - axonal outgrowth and developmental alteration study, 82–83
 - cultures and gene delivery in, 71–75
 - molecular dynamics study, 79–81
 - neuronal connectivity study, 77–78
 - neuronal function study, 81–82
 - neuron imaging, 76–77
 - RNA translation, live imaging of, 83
 - primary neurons, live imaging
 - advantage and limitation, 70–71
 - axonal transport of mitochondria, determination, 68
 - axonal vesicle transport study, 65–66
 - cell motility study, 69
 - cultures and gene delivery, 64–65

cytoskeletal polymer movement study, 68
 membrane binding study, 67
 neuronal Ca^{2+} homeostasis imaging, 69–70
 protein diffusion analysis, 66–67
 symptoms and cellular mechanisms, 52–53
 Neuronal Ca^{2+} homeostasis imaging,
 ion-sensitive dyes, 69–70
 Neuronal function study, ion-sensitive dyes,
 62–63
 Neuropeptides, fibroblast regulation, 196–198.
See also Fibroblasts
 NGF. *See* Nerve growth factor
Nicotiana glauca, 305
Nicotiana tabacum, BY cells, 271
 NMDARs. *See* N-methyl-D-aspartate receptors
 N-methyl-D-aspartate receptors, 79–80
 Nodule formation and LR initiation, relationship,
 38
 Nonintrinsic ABC proteins, 290
NpPDR1 gene, 273
 N-terminal subdomain I (SDI), 317
 Nt-JAT1, role, 286
 NtPDR3, role, 281. *See also* ATP-binding cassette
 Nucleotide-binding domain, 264
 Nucleotide-binding fold, 264

O

Organelle-specific dyes
 in axonal transport of mitochondria, 68
 for mitochondria mobility tracking, 61–62
 Organelle transport in axon, fluorescence protein
 tracking and time-lapse microscopy, 65–66
Oryza sativa, 35
Otx2 gene, 240

P

Papillary dermal fibroblasts, 180. *See also* Fibroblasts
 Parkinson's disease (PD), 51
 PC12 cell line, application, 55
 PC12 cell proteins interaction, analysis, 59
 PDR. *See* Pleiotropic drug resistance
 Pea (*Pisum sativum*), 36
 PED3. *See* Peroxisome defective3
 Perlecan HSPGs, 108–109. *See also* Heparan
 sulfate (HS)
 Peroxisomal ABC transporter1, 289
 Peroxisome defective3, 289
 Peroxisomes, ABC proteins, 289–290.
See also ATP-binding cassette
 PET. *See* Positron emission tomography
 2pFLIM. *See* Two photon fluorescence lifetime
 imaging
 Phenotypic markers, for fibroblasts, 175–176.
See also Fibroblasts
 Phosphorelay
 components, 8
 mechanism, 6

Photoactivation and photobleaching.
See also Neurodegenerative disease
 molecular dynamics study, 79–81
 for protein diffusion analysis, 66–67
 in protein misfolding and aggregation study,
 56–57
Physarum polycephalum, 302
 PIN-FORMED (PIN), 275
 PIN proteins and ABCBs interactions, 280
 Placenta and imprinting, 225–226
 imprinted gene function, 228, 234–239
 placentation, 226–228
 PrE in development, 239–240
 tetraploid rescue experiments, 241–246
 Plant ABC proteins, 267–270
 Plant cuticle, role, 265
 Plant myosins, molecular structure, 311–312.
See also Myosins
 Chara myosin, 312–317
 class XI myosin, 312
 myosin tail, 317–321
 Plants
 genomic imprinting, 219–220
 (*see also* Genomic imprinting)
 root anatomy, 25
 soluble-type ABC proteins, 290–291
 (*see also* ATP-binding cassette)
 Plasma membrane cellular processes analysis,
 TIRFM in, 61. *See also* Neurodegenerative
 disease
 Plastids, ABC proteins, 286–287.
See also ATP-binding cassette
 Pleiotropic drug resistance, 266, 271
 Polar trophectoderm, subpopulation, 227
 Polycomb group (PcG) gene, 219
 Polymerase chain reaction (PCR), 169
 Positron emission tomography, 54
 Primary neuronal cultures, advantage and
 disadvantage, 70
 Primary vascular development, cytokinin
 signaling, 28–31. *See also* Cytokinin
 phytohormones (ck)
 Promoter::GFP-ABCG11 transformants,
 function, 266
 Protein aggregation and mobility study,
 photobleaching/photoactivation in, 56–57
 Protein and heparan sulfate, interactions, 120–121
 functional significance, 123–126
 protein-binding domains topology, 122
 specificity in, 126–129
 Protein diffusion analysis, photobleaching/
 photoactivation for, 66–67
 Protein interactions analysis, BiFC in, 29–61.
See also Neurodegenerative disease
 Protein misfolding and aggregation, photobleaching
 and photoactivation in, 56–57
 Proteoglycans, role, 189–190. *See also* Fibroblasts
 PXA1. *See* Peroxisomal ABC transporter1

Q

Quiescent centre (QC), 22

R

- Ras-binding domain, 80
 RBD. *See* Ras-binding domain
 Response regulator (RR), 4
 Rhizomes, ABC proteins, 280–283.
 See also ATP-binding cassette
 RLI. *See* RNase L inhibitor
 RNAi. *See* RNA interference
 RNA interference, 13
 RNase L inhibitor, 291
 Roller drum technique, 72
 Root, ABC proteins, 280–283.
 See also ATP-binding cassette
 Root apical meristems, ABC proteins.
 See also ATP-binding cassette
 ABC-mediated auxin transport, 278–280
 auxin in root tissues, 277–278
 in hypocotyls and stem, 275–277
 Root, cytokinin role. *See also* Cytokinin
 phytohormones (ck)
 apical meristem development, 22–24
 architecture, 32–36
 elongation, 34
 growth phases, 28
 meristem size determination, 24–28
 nodulation process, 36–38
 Root tissues, auxin, 277–278.
 See also ATP-binding cassette

S

- S100A4. *See* Fibroblast-specific protein-1
 SAA. *See* Serum amyloid A
Saccharomyces cerevisiae, PDR5 protein in, 272
 Secondary vascular development, cytokinin,
 31–32. *See also* Cytokinin phytohormones
 (ck)
 Seeds, ABC proteins, 283. *See also* ATP-binding
 cassette
 Semliki forest virus, 65
 Serum amyloid A, 138
 SFV. *See* Semliki forest virus
 Shoot apical meristems, ABC proteins.
 See also ATP-binding cassette
 ABC-mediated auxin transport, 278–280
 auxin in root tissues, 277–278
 in hypocotyls and stem, 275–277
 SHY2 overexpression, effects, 28
 Single-nucleotide polymorphism (SNP), 218
 Skin basement membrane formation, 182–183.
 See also Fibroblasts
snf2 mutant. *See* *spontaneous nodule formation2*
 mutant
Spirodela polyrhiza, SpTUR2 protein in, 271

- spontaneous nodule formation2* mutant, 37
 SpTUR2 protein, 271
 STED. *See* Stimulated emission depletion
 microscopy
 Stem cells, AtABCG11 and AtABCG12
 functions, 266, 271. *See also* ATP-binding
 cassette
 Stimulated emission depletion microscopy, 78
stunted plant1 mutant, identification of, 26–27
 SYL. *See* Syncytial yolk layer
 Syncytial yolk layer, 239
 Syndecan (Sdc) cell-surface HSPGs, 107–108.
 See also Heparan sulfate (HS)

T

- TaMDR1 transporter, expression, 282
 TAP. *See* Transporter associated with Antigen
 Processing
 Tetraploid rescue experiments, 241–246.
 See also Imprinting and placenta
 TGF- β 1. *See* Transforming growth factor- β 1
 Thy-1⁺ and Thy-1⁻ subpopulations, of
 fibroblasts, 194–195
 Time-lapse microscopy.
 See also Neurodegenerative disease
 for neurite outgrowth and granules transport,
 55–56
 organelle transport in hippocampal neurons,
 65–66
 TIRFM. *See* Total internal reflection fluorescence
 microscopy
 Tissue engineering, human dermal fibroblasts in,
 192–194. *See also* Fibroblasts
 TMDs. *See* Transmembrane domains
 TNF- α . *See* Tumor necrosis factor- α
 Total internal reflection fluorescence microscopy,
 61, 329
 Transforming growth factor- β 1, 167
 Transition zone (TZ), 26
 Transmembrane domains, 264
 Transporter associated with Antigen Processing,
 282
 Tropomyosin
 aspects, 327–328 (*see also* Chara myosin)
 in Chara myosin, 310–311
 effect, 308–310
 role, 307
 Tumor development and metastasis, HS,
 139–140
 Tumor necrosis factor- α , 177
 Tumor stromal cells, 168. *See also* Fibroblasts
 TWD1. *See* TWISTED DWARF1
 TWISTED DWARF1, 279
 Two-color video microscopy, 66
 Two photon fluorescence lifetime imaging, 80
 Type-A ARRs, cytokinin regulation, 19–21
 Type-B ARRs, in cytokinin signal, 18–19

V

- Vacuoles, ABC proteins, 283–286.
 See also ATP-binding cassette
- Vascular endothelial cells, fibroblast interaction, 185–189. *See also* Epithelial cells and fibroblasts
- Vascular endothelial growth factor-A, 180
- VEGF-A. *See* Vascular endothelial growth factor-A
- Versican, abundance, 190

W

- WBC. *See* White–Brown Complex
- White–Brown Complex, 265
- White clover (*Trifolium repens*), 36

- Wnt1-Cre* transgene, role, 241
- WOL* gene, 5

X

- Xylosyltransferase, 111
- XylT. *See* Xylosyltransferase

Y

- Yellow-fluorescent protein, 58
- YFP. *See* Yellow-fluorescent protein

Z

- Zea mays*, 37
- Zebrafish (*Danio rerio*), 85
- ZmMRP3, role, 286